frontiers | Research Topics

Optimizing fertilizer and irrigation for specialty crops using precision agriculture technologies

Edited by
Amir Ali Khoddamzadeh, Sukhbir Singh and
Maruthi Sridhar Balaji Bhaskar

Published in
Frontiers in Plant Science

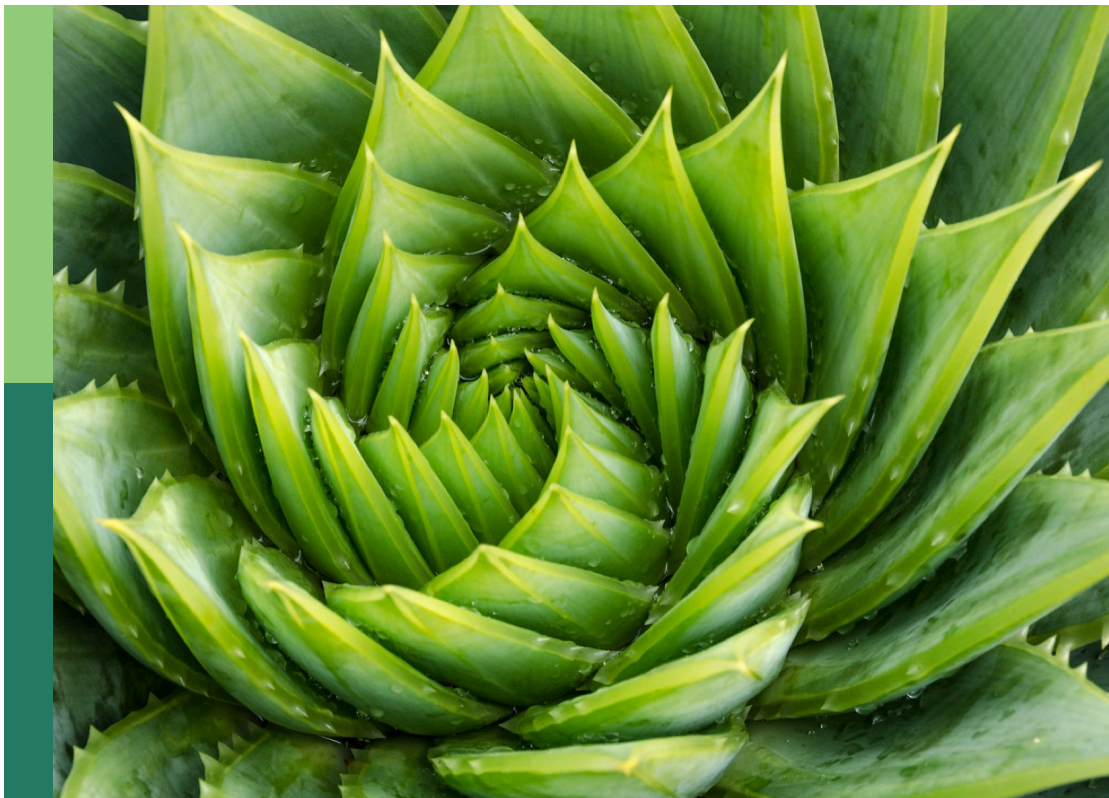

FRONTIERS EBOOK COPYRIGHT STATEMENT

The copyright in the text of individual articles in this ebook is the property of their respective authors or their respective institutions or funders. The copyright in graphics and images within each article may be subject to copyright of other parties. In both cases this is subject to a license granted to Frontiers.

The compilation of articles constituting this ebook is the property of Frontiers.

Each article within this ebook, and the ebook itself, are published under the most recent version of the Creative Commons CC-BY licence. The version current at the date of publication of this ebook is CC-BY 4.0. If the CC-BY licence is updated, the licence granted by Frontiers is automatically updated to the new version.

When exercising any right under the CC-BY licence, Frontiers must be attributed as the original publisher of the article or ebook, as applicable.

Authors have the responsibility of ensuring that any graphics or other materials which are the property of others may be included in the CC-BY licence, but this should be checked before relying on the CC-BY licence to reproduce those materials. Any copyright notices relating to those materials must be complied with.

Copyright and source acknowledgement notices may not be removed and must be displayed in any copy, derivative work or partial copy which includes the elements in question.

All copyright, and all rights therein, are protected by national and international copyright laws. The above represents a summary only. For further information please read Frontiers' Conditions for Website Use and Copyright Statement, and the applicable CC-BY licence.

ISSN 1664-8714
ISBN 978-2-8325-7269-6
DOI 10.3389/978-2-8325-7269-6

Generative AI statement
Any alternative text (Alt text) provided alongside figures in the articles in this ebook has been generated by Frontiers with the support of artificial intelligence and reasonable efforts have been made to ensure accuracy, including review by the authors wherever possible. If you identify any issues, please contact us.

About Frontiers

Frontiers is more than just an open access publisher of scholarly articles: it is a pioneering approach to the world of academia, radically improving the way scholarly research is managed. The grand vision of Frontiers is a world where all people have an equal opportunity to seek, share and generate knowledge. Frontiers provides immediate and permanent online open access to all its publications, but this alone is not enough to realize our grand goals.

Frontiers journal series

The Frontiers journal series is a multi-tier and interdisciplinary set of open-access, online journals, promising a paradigm shift from the current review, selection and dissemination processes in academic publishing. All Frontiers journals are driven by researchers for researchers; therefore, they constitute a service to the scholarly community. At the same time, the *Frontiers journal series* operates on a revolutionary invention, the tiered publishing system, initially addressing specific communities of scholars, and gradually climbing up to broader public understanding, thus serving the interests of the lay society, too.

Dedication to quality

Each Frontiers article is a landmark of the highest quality, thanks to genuinely collaborative interactions between authors and review editors, who include some of the world's best academicians. Research must be certified by peers before entering a stream of knowledge that may eventually reach the public - and shape society; therefore, Frontiers only applies the most rigorous and unbiased reviews. Frontiers revolutionizes research publishing by freely delivering the most outstanding research, evaluated with no bias from both the academic and social point of view. By applying the most advanced information technologies, Frontiers is catapulting scholarly publishing into a new generation.

What are Frontiers Research Topics?

Frontiers Research Topics are very popular trademarks of the *Frontiers journals series*: they are collections of at least ten articles, all centered on a particular subject. With their unique mix of varied contributions from Original Research to Review Articles, Frontiers Research Topics unify the most influential researchers, the latest key findings and historical advances in a hot research area.

Find out more on how to host your own Frontiers Research Topic or contribute to one as an author by contacting the Frontiers editorial office: frontiersin.org/about/contact

Optimizing fertilizer and irrigation for specialty crops using precision agriculture technologies

Topic editors

Amir Ali Khoddamzadeh — Florida International University, United States

Sukhbir Singh — Texas Tech University, United States

Maruthi Sridhar Balaji Bhaskar — Florida International University, United States

Citation

Khoddamzadeh, A. A., Singh, S., Balaji Bhaskar, M. S., eds. (2026). *Optimizing fertilizer and irrigation for specialty crops using precision agriculture technologies*. Lausanne: Frontiers Media SA. doi: 10.3389/978-2-8325-7269-6

Table of contents

05 Editorial: Optimizing fertilizer and irrigation for specialty crops using precision agriculture technologies
Amir Ali Khoddamzadeh, Sukhbir Singh and Maruthi Sridhar Balaji Bhaskar

08 Monitoring canopy SPAD based on UAV and multispectral imaging over fruit tree growth stages and species
Yirui Huang, Dongming Li, Xuan Liu and Zhenhui Ren

25 Application of APSIM model in winter wheat growth monitoring
Yunlong Tan, Enhui Cheng, Xuxiang Feng, Bin Zhao, Junjie Chen, Qiaoyun Xie, Hao Peng, Cunjun Li, Chuang Lu, Yong Li, Bing Zhang and Dailiang Peng

41 Estimation of potato canopy leaf water content in various growth stages using UAV hyperspectral remote sensing and machine learning
Faxu Guo, Quan Feng, Sen Yang and Wanxia Yang

60 The input of organic fertilizer can improve soil physicochemical properties and increase cotton yield in southern Xinjiang
Yupeng Zhao, Qingyong Bian, Zhiduo Dong, Xiaojuan Rao, Zhiguo Wang, Yanbo Fu and Bolang Chen

75 Sensor-controlled fertigation management for higher yield and quality in greenhouse hydroponic strawberries
George Kerrigan Hutchinson, Lan Xuan Nguyen, Zilfina Rubio Ames, Krishna Nemali and Rhuanito Soranz Ferrarezi

89 Data-driven nitrogen application for satinleaf: leveraging optical sensors in urban landscape management
Bárbara Nogueira Souza Costa and Amir Ali Khoddamzadeh

97 Nondestructive estimation of leaf chlorophyll content in banana based on unmanned aerial vehicle hyperspectral images using image feature combination methods
Weiping Kong, Lingling Ma, Huichun Ye, Jingjing Wang, Chaojia Nie, Binbin Chen, Xianfeng Zhou, Wenjiang Huang and Zikun Fan

112 Apparent soil electrical conductivity and gamma-ray spectrometry to map particle size fraction in micro-irrigated citrus orchards in California
Elia Scudiero, Michael P. Schmidt, Todd H. Skaggs, Jorge F. S. Ferreira, Daniele Zaccaria, Alireza Pourreza and Dennis L. Corwin

128 Silkworm excrement organic fertilizer substitution compound fertilizer improves bamboo shoot yield by altering soil properties and bacterial communities of Moso bamboo (*Phyllostachys edulis*) forests in subtropical China
Zhenya Yang, Jiancheng Zhao and Huijing Ni

142 By promoting growth and development, castor bean meal biofertilizer improves the yield and quality of Tartary buckwheat and indirectly improves the growth and development of Tartary buckwheat sprouts
Li Mingjing, Hu Xuemei, Luo Rui, Zhang Chunhua, Hu Ruimei, Xue Guibin, Li Guorui, Di Jianjun, Wang Cheng, Gu Xiaohui, Su Zhimin, Li Ruxin, Zhao Yong and Huang Fenglan

158 Optimal fertilizer rate and sowing density can improve oat quality, yield and N and P comprehensive efficiency in the Loess Plateau of China
Ruochen Zhang, Yue Wang, Kamran Malik, Jianjun Wang, Guiqin Zhao and Chunjie Li

177 High-quality carrots in relation to the superior phloem parenchyma cells and proportion of xylem vessel in coordinated water-fertilizer management
Ying Zhao, Yanchen Gong, Yun Li, Hua Xin, Ruiping Chi and Yanling Chen

195 Organic fertilizer substitution optimizes aroma metabolites in Wuyi Rock tea
Shuping Huang, Yongdong Yu, Jilai Cui, Zhengwei Luo, Lanxin Luo, Chuankui Song and Hong Liao

206 Construction of nitrogen critical dilution curve and differences in nitrogen nutrition characteristics in different organs of maize varieties with contrasting nitrogen efficiencies
Shuqin Bao, Xingying Chai, Linzheng Liao, Xiaoying Li, Lin Shi, Xixi Dong, Sida Long, Huifu Li, Hanyu Wang, Zhenghong Li, Mengting Wang, Yun Ren and Qiang Li

222 Optimization of water and fertilizer management on the intercropping system between maize and mung bean to improve photosynthetic characteristics & water use and to increase plant yield
Mengfan Gao, Xinxin Wang, Renqiang Chen, Huiyan Gao, Xiaoling Wang and Hongquan Liu

239 Effects of irrigation and fertilization management on kiwifruit yield, water use efficiency and quality in China: A meta-analysis
Yuehua Ding, Chunfeng Shang, Long Zhao, Shanshan Jin, Chenyang Li, Shanshan Yin and Golam Jalal Ahammed

254 Meta-analysis reveals that grain quality is improved in ratoon season crop compared with main crop
Xuelian Yang, Zhijie Ruan, Kezhi Chen, Shiting Gu, Yuchao Wang, Qiang Cai, Li-Ang Yao, Mohammad Reza Boorboori, Arafat Yasir, Juthamas Chaiwanon, Kanako Bessho-Uehara, Kihye Shin, Yunfei Wu, Wenfei Wang and Wenxiong Lin

frontiers | Frontiers in Plant Science

TYPE Editorial
PUBLISHED 20 January 2026
DOI 10.3389/fpls.2026.1760142

Check for updates

OPEN ACCESS

EDITED AND REVIEWED BY
Ruslan Kalendar,
University of Helsinki, Finland

*CORRESPONDENCE
Amir Ali Khoddamzadeh
akhoddam@fiu.edu

RECEIVED 03 December 2025
REVISED 07 January 2026
ACCEPTED 08 January 2026
PUBLISHED 20 January 2026

CITATION
Khoddamzadeh AA, Singh S and Balaji Bhaskar MS (2026) Editorial: Optimizing fertilizer and irrigation for specialty crops using precision agriculture technologies. *Front. Plant Sci.* 17:1760142. doi: 10.3389/fpls.2026.1760142

COPYRIGHT
© 2026 Khoddamzadeh, Singh and Balaji Bhaskar. This is an open-access article distributed under the terms of the Creative Commons Attribution License (CC BY). The use, distribution or reproduction in other forums is permitted, provided the original author(s) and the copyright owner(s) are credited and that the original publication in this journal is cited, in accordance with accepted academic practice. No use, distribution or reproduction is permitted which does not comply with these terms.

Editorial: Optimizing fertilizer and irrigation for specialty crops using precision agriculture technologies

Amir Ali Khoddamzadeh[1]*, Sukhbir Singh[2] and Maruthi Sridhar Balaji Bhaskar[1]

[1]Department of Earth and Environment, Institute of Environment, Florida International University, Miami, FL, United States, [2]Department of Plant and Soil Science, College of Agricultural Sciences and Natural Resources, Texas Tech University, Lubbock, TX, United States

KEYWORDS

irrigation management, optical sensors, precision agriculture, remote sensing, specialty crops, fertilizer management

Editorial on the Research Topic
Optimizing fertilizer and irrigation for specialty crops using precision agriculture technologies

Introduction

Global demand for specialty crops continues to grow, driven by consumer preferences for high-quality, diverse produce and by the need to transition toward environmentally sustainable production systems (Vuppalapati, 2023). At the same time, specialty crop agriculture faces mounting constraints: increasing pressure on water and nutrient resources, spatial heterogeneity of soils and microclimates, stricter environmental regulations, and the imperative to improve both yield and quality under variable climatic conditions (Sandhu et al., 2025; Gonzalez et al., 2025). Precision agriculture offers a pathway to address these challenges through site-specific, data-driven management of fertilizer and irrigation. By integrating proximal and remote sensors, advanced analytics, and decision-support tools, precision approaches can enhance resource-use efficiency, reduce nutrient losses, and improve crop performance while safeguarding environmental quality (Munoz Salas et al., 2025; Souza Costa and Khoddamzadeh, 2025).

This Research Topic brings together studies that collectively address three interrelated challenges: (i) how to diagnose crop nutrient and water status at high spatial and temporal resolution; (ii) how to translate these diagnostics into variable-rate management of fertilizers and irrigation; and (iii) how to integrate technological, biological, and modeling approaches into coherent decision-support systems for specialty crops.

Sensor-based and remote sensing approaches for nutrient and water diagnostics

Several contributions demonstrate how proximal and remote sensing technologies enable non-destructive, spatially explicit assessment of crop nutritional and water status. Costa and Khoddamzadeh employ optical sensors (GreenSeeker™, SPAD, and atLEAF) to determine nitrogen requirements for Satinleaf (Chrysophyllum oliviforme), illustrating how sensor indices can guide site-specific nitrogen application in horticultural systems. Kong et al. extend this concept using UAV-based hyperspectral imaging combined with machine-learning models to estimate leaf chlorophyll content in banana, integrating spectral and textural features to map nutrient status across heterogeneous orchards.

Water status monitoring is similarly advanced by Ding et al., who apply UAV hyperspectral imagery and machine learning to estimate potato canopy leaf water content across growth stages, enabling stage-specific irrigation decisions. Huang et al. combine UAV multispectral data with ground-based SPAD measurements to generate spatially explicit nitrogen diagnostic maps for orchard systems. Collectively, these studies show that sensor-driven diagnostics can replace uniform input strategies with real-time, crop-responsive management. Their convergence on data fusion (spectral and structural features) and predictive modeling highlights a broader shift toward operational remote sensing as a core component of precision nutrient and water management.

Soil and geophysical mapping for site-specific management

Understanding within-field variability in soil properties is essential for variable-rate input management. Scudiero et al. integrate apparent soil electrical conductivity with gamma-ray spectrometry to characterize particle-size distribution in micro-irrigated citrus orchards. Their approach enables delineation of management zones based on water-holding capacity and nutrient retention, supporting targeted irrigation and fertilization. This work emphasizes that crop-based sensing must be complemented by soil and geophysical characterization to establish the physical context in which nutrient and water decisions are made. Integrating soil mapping with canopy level diagnostics is key to robust site-specific management.

Organic and bio-based fertilizers in precision nutrient management

A set of studies explores how organic amendments and biofertilizers can be integrated into precision frameworks to reduce reliance on synthetic inputs. Yang et al. report that substituting silkworm excrement in compound fertilizers increases bamboo shoot yield and enhances soil microbial communities in Phyllostachys edulis forests. Mingjing et al. demonstrate that castor bean meal based biofertilizers improve growth, yield, and quality of Tartary buckwheat. Huang et al. show that partial replacement of synthetic nitrogen with organic sources enhances aroma-related metabolites in Wuyi Rock tea, linking nutrient management to product quality. Zhao et al. further document improvements in soil physicochemical properties and cotton yield following organic fertilizer inputs in southern Xinjiang. These studies collectively indicate that organic and bio-based fertilizers can be deployed in precision systems to achieve dual goals: improving soil health while maintaining or enhancing crop performance. Their integration with sensor-based diagnostics offers a promising route toward environmentally sustainable, input efficient specialty crop production.

Optimizing irrigation–fertilization regimes and cropping systems

Several contributions address coordinated management of water and nutrients. Zhang et al. identify optimal fertilizer rates and sowing densities that maximize yield, quality, and nutrient-use efficiency in oats. Gao et al. demonstrate that synchronized irrigation and fertilization in maize mung bean intercropping enhances photosynthetic efficiency, water use, and yield. Hutchinson et al. compare sensor-controlled fertigation with timer-based systems in hydroponic strawberry production, showing that real-time moisture sensing improves resource and energy efficiency. Guo et al. provide a meta-analysis for kiwifruit, quantifying how irrigation and fertilization strategies affect yield, water-use efficiency, and fruit quality across environments. These studies underscore the importance of coupling irrigation and fertilization decisions rather than optimizing them in isolation. Precision management emerges not only as a technological upgrade but as a systems approach to coordinating multiple inputs for maximum agronomic and environmental benefit.

Modeling, meta-analysis, and decision-support tools

Beyond field-level experimentation, modeling and synthesis approaches contribute to scalable decision-making. Tan et al. implement the APSIM crop model to simulate winter wheat growth dynamics, demonstrating the value of "digital twin" frameworks for predicting biomass, phenology, and yield under variable climate and management scenarios. Yang et al. apply meta-analysis to compare ratoon-season and main crop cereals, revealing improvements in grain quality under optimized water nutrient regimes. Modeling and meta-analytic approaches provide the temporal and spatial generalization needed to translate site-

specific findings into broadly applicable management guidelines. When coupled with sensor-derived data streams, these tools form the backbone of adaptive, data driven agronomic decision systems.

Toward integrated precision nutrient water management

Taken together, the contributions in this Research Topic illustrate a transition from isolated technological applications to integrated management frameworks. Sensor networks diagnose crop and soil status; organic and bio-based fertilizers enhance sustainability; coordinated irrigation fertilization regimes optimize resource use; and models synthesize data across scales. The emerging paradigm is one of adaptive precision agriculture, in which real-time diagnostics, biological inputs, and predictive analytics are combined to deliver site-specific, environmentally responsible management. Future progress will depend on: (i) tighter integration of multi-sensor platforms with crop and soil models; (ii) standardization and interoperability of agronomic data; (iii) incorporation of artificial intelligence for real-time optimization; and (iv) development of scalable solutions accessible to both high-tech operations and resource-limited producers.

Conclusions

This Research Topic demonstrates that precision agriculture technologies can substantially improve fertilizer and irrigation management in specialty crops by enhancing resource-use efficiency, crop quality, and environmental performance. By uniting sensor-based diagnostics, soil mapping, organic nutrient strategies, coordinated water-nutrient management, and modeling tools, the collected studies move beyond incremental optimization toward integrated, system-level solutions. Looking ahead, continued innovation in sensor technologies, data analytics, and decision-support systems coupled with close collaboration among researchers, growers, and technology providers will be essential to realize the full potential of precision agriculture. Such integration will ensure that specialty crop production remains productive, profitable, and sustainable under increasingly complex environmental and market conditions.

Author contributions

AK: Writing – original draft, Writing – review & editing. SS: Writing – review & editing. MB: Writing – review & editing.

Acknowledgments

We thank all authors and reviewers for contributing to this Research Topic and for the editorial office's support. Very special thanks to Dr. Ruslan Kalendar for reviewing and editing the editorial.

Conflict of interest

The author(s) declared that this work was conducted in the absence of any commercial or financial relationships that could be construed as a potential conflict of interest.

Generative AI statement

The author(s) declared that generative AI was not used in the creation of this manuscript.

Any alternative text (alt text) provided alongside figures in this article has been generated by Frontiers with the support of artificial intelligence and reasonable efforts have been made to ensure accuracy, including review by the authors wherever possible. If you identify any issues, please contact us.

Publisher's note

All claims expressed in this article are solely those of the authors and do not necessarily represent those of their affiliated organizations, or those of the publisher, the editors and the reviewers. Any product that may be evaluated in this article, or claim that may be made by its manufacturer, is not guaranteed or endorsed by the publisher.

References

Gonzalez, P., Tucker, D., Maruthi, B. B.Sridhar, Nageswara-Rao, R., Balaji Baskar, M. S., Griffith, P., et al. (2025). Enhancing cabbage palm resilience to saltwater stress through silicon applications. *HortScience* 60, 1547–1554. doi: 10.21273/HORTSCI18718-25

Munoz Salas, M., Roddy, A. B., PDastpak, A., Costa, B. N. S., and Khoddamzadeh, A. A. (2025). Ecophysiological adaptations of musa haekkinenii to light intensity and water quality. Special issue: management of artificial light in horticultural crops. *Horticulture* 11, 1188. doi: 10.3390/horticulturae11101188

Sandhu, D., Pudussery, E., Tammar, K., Cendan, L., Khoddamzadeh, A. A., and Ferreira, J. (2025). Decoding the genetic basis of salinity tolerance in tomatoes through ion transport and stress regulation. *ACS Agric. Sci. Technol.* 5, 1817–1826. doi: 10.1021/acsagscitech.5c00209

Souza Costa, B., and Khoddamzadeh, A. A. (2025). Data-driven nitrogen application for Satinleaf: Leveraging optical sensors in urban landscape management. Technical Advances in Plant Science. Special Issue: Optimizing Fertilizer and Irrigation for Specialty Crops Using Precision Agriculture Technologies. *Front. Plant Sci.* 16. doi: 10.3389/fpls.2025.1522662

Vuppalapati, C. (2023). "Specialty crops," in *Specialty crops for climate change adaptation: Strategies for enhanced food security by using machine learning and artificial intelligence* (Springer Nature Switzerland, Cham), 35–197.

frontiers | Frontiers in Plant Science

TYPE Original Research
PUBLISHED 01 August 2024
DOI 10.3389/fpls.2024.1435613

Check for updates

OPEN ACCESS

EDITED BY
Amir Khoddamzadeh,
Florida International University, United States

REVIEWED BY
Juan De Dios Franco-Navarro,
Spanish National Research Council (CSIC), Spain
Bolin Fu,
Guilin University of Technology, China

*CORRESPONDENCE
Zhenhui Ren
renzh68@163.com

RECEIVED 20 May 2024
ACCEPTED 11 July 2024
PUBLISHED 01 August 2024

CITATION
Huang Y, Li D, Liu X and Ren Z (2024) Monitoring canopy SPAD based on UAV and multispectral imaging over fruit tree growth stages and species. *Front. Plant Sci.* 15:1435613. doi: 10.3389/fpls.2024.1435613

COPYRIGHT
© 2024 Huang, Li, Liu and Ren. This is an open-access article distributed under the terms of the Creative Commons Attribution License (CC BY). The use, distribution or reproduction in other forums is permitted, provided the original author(s) and the copyright owner(s) are credited and that the original publication in this journal is cited, in accordance with accepted academic practice. No use, distribution or reproduction is permitted which does not comply with these terms.

Monitoring canopy SPAD based on UAV and multispectral imaging over fruit tree growth stages and species

Yirui Huang[1], Dongming Li[2], Xuan Liu[2] and Zhenhui Ren[2]*

[1]Intelligent Sensor Network Engineering Research Center of Hebei Province, College of Information Engineering, Hebei GEO University, Shijiazhuang, China, [2]College of Mechanical and Electrical Engineering, Hebei Agricultural University, Baoding, China

Chlorophyll monitoring is an important topic in phenotypic research. For fruit trees, chlorophyll content can reflect the real-time photosynthetic capacity, which is a great reference for nutrient status assessment. Traditional *in situ* estimation methods are labor- and time-consuming. Remote sensing spectral imagery has been widely applied in agricultural research. This study aims to explore a transferable model to estimate canopy SPAD across growth stages and tree species. Unmanned aerial vehicle (UAV) system was applied for multispectral images acquisition. The results showed that the univariate model yielded with Green Normalized Difference Vegetation Index (GNDVI) gave valuable prediction results, providing a simple and effective method for chlorophyll monitoring for single species. Reflection features (RF) and texture features (TF) were extracted for multivariate modeling. Gaussian Process Regression (GPR) models yielded better performance for mixed species research than other algorithm models, and the R^2 of the RF+TF+GPR model was approximately 0.7 in both single and mixed species. In addition, this method can also be used to predict canopy SPAD over various growth stages, especially in the third and fourth stages with R^2 higher than 0.6. This paper highlights the importance of using RF+TF for canopy feature expression and deep connection exploration between canopy features with GPR algorithm. This research provides a universal model for canopy SPAD inversion which can promote the growth status monitoring and management of fruit trees.

KEYWORDS

multispectral imaging, canopy SPAD value, vegetation index, reflection feature, texture feature

1 Introduction

Chlorophyll, as an important component of plant cells with the ability to absorb light and convert it into chemical energy, is critical to observe the photosynthetic capacity (Zarco-Tejada et al., 2016) and the nitrogen status of the fruit trees. Under the background of climate change and population growth, limited land resources and water resources make agricultural production face great pressure (Intergovermental Panel on Climate Change, 2022). Chlorophyll content monitoring in fruit trees can help predict yield and optimize plant varieties in biological research (Brewer et al., 2022), thereby increasing agricultural productivity and ensuring food security and sustainable development.

Traditionally, chlorophyll content was measured by chemical method (chromatographic separation), which is time- and labor-consuming. Spectral technology has gained widespread application in the non-destructive detection of chlorophyll content. The development of a portable spectrometer provides much convenience for field spectral collection for its mobility (Crocombe, 2018; Xiao et al., 2024). However, this approach is still labor-intensive and not suitable for large-scale area applications. With the evolvement of science and technology, remote sensing techniques have become popular gradually, promoting the development of high-throughput phenotypic research (Jafarbiglu and Pourreza, 2022). Satellite remote sensing technology helps us with large-scale data analysis. Nevertheless, for precision agriculture in small farms, satellite remote sensing is limited in spatial and temporal resolution. Unmanned aerial vehicle (UAV) remote sensing enables fast data acquisition with highly ground and temporal resolution; its advantages of simple operation and flexible application make it become an important means in agricultural monitoring research (Sankaran et al., 2019; Jafarbiglu and Pourreza, 2022).

Multispectral and hyperspectral sensors are imaging devices, which can simultaneously obtain two-dimensional spatial information and one-dimensional spectral information. The combination of spectral imaging and UAV can effectively facilitate data acquisition for a large area (Zhao et al., 2019). Lao et al. (2024) proposed a parameter/non-parameter combined model for canopy chlorophyll content retrieval of seven typical vegetation communities; high-spatial-resolution images were captured with UAV multispectral device. Wang et al. (2022) used UAV to estimate the percent green cover for high-throughput turfgrass; they found that multispectral images might offer a solution for non-green vegetation which is not captured by RGB images. Fu et al. used multi-platforms including analytical spectral device, UAV, and PlanetScope for water chlorophyll *a* concentration retrieval; the transfer learning methods were proposed for the ASD hyperspectral data to UAV and Planet platforms (Fu et al., 2023). Hyperspectral imagers have high spectral resolution and can detect more spectral information than multispectral cameras, but the processing method is more complicated for hyperspectral images (Hernanda et al., 2023). In addition, a multispectral camera is much cheaper than a hyperspectral camera (Zhang and Zhu, 2023), which is a significant factor considered in our research because economy is an important aspect that determines the possibility of application for a smallholder.

Vegetation index (VI) is calculated with reflectance of different spectral bands intending to select informative and sensitive spectral data and minimize non-informative information. It provides an important contribution to the assessment of plant status and successfully applied for chlorophyll estimation (Haboudane et al., 2008; Li et al., 2018), LAI monitoring (Hunt et al., 2010), and yield prediction (Zhou et al., 2017; Guan et al., 2019). However, previous research was mainly focused on plant evaluation for specific growth stage due to the great influence of phenological changes in biochemical content (Féret et al., 2017; Wang et al., 2018). Obviously, the growth model corresponding to different stages is inconvenient in the evaluation of the whole growing season. Therefore, it is necessary to build an applicable model throughout the growth cycle for chlorophyll retrieval. Moreover, Main et al. (2011) pointed out that for plant species (maize, cabbage, tomato, and several savanna tree species) with different degrees of chlorophyll content, indices using off-chlorophyll absorption center wavebands (690–730 nm) performed the most robust results. Similarly, in fruit tree studies, more research needs to be done to find common indices. More studies should continue to find a universal index for chlorophyll monitoring.

Texture feature, which refers to visual patterns or spatial arrangement of pixels, is another significant characteristic of images. It can provide spatial information on crop growth (Duan et al., 2019; Yogeshwari and Thailambal, 2021). In the rice aboveground biomass monitoring research, Xu et al. found that texture features can help to recognize the emergence of rice panicles, thus avoiding the overestimation at panicle initiation (Xu et al., 2022a). During the tillering stage to the booting stage, the texture features tended to be stable, which helps to the improvement of prediction accuracy (Xu et al., 2022b). Moreover, Li et al. got improved accuracy of nitrogen content models in winter wheat with the fusion of spectral and texture features (Li et al., 2023). Maimaitijiang et al. recognized that canopy texture features could offer canopy subtle structure characteristics which would be beneficial to soybean yield prediction (Maimaitijiang et al., 2020). However, there is a lack of literature on fruit trees about the potential of texture features (TF). Therefore, our research further explored the sensitivity of TF on the chlorophyll content evaluation of fruit trees (Abdelbaki and Udelhoven, 2022).

This study aims to assess the potential of vegetation indices (VIs), reflection features (RF), and TF in estimating the canopy SPAD values of fruit trees, combined with multiple machine learning algorithms. The emphasis focuses on inversion models that can be applied simultaneously to mixed tree species (apple tree and pear tree). The main contributions of this work are given as follows: (1) evaluate the VIs for canopy SPAD monitoring of single and mixed tree species with univariate algorithms, (2) compare the performance of the combined use of the RF and TF in estimating canopy SPAD based on deep learning algorithms, and (3) determine the optimal method for canopy SPAD inversion over various growth stages of mixed tree species.

2 Materials and methods

2.1 Study region

This study was conducted in the city of Baoding, of Hebei province, China, with a temperate and monsoonal climate. The experimental field was an apple orchard (115.37° E, 38.90° N) with an elevation of approximately 25 m and a pear orchard (115.41° E, 38.84° N) with an elevation of approximately 30 m (Figure 1). The two orchards were watered by flowing irrigation, except when rain-fed. The total area size of the apple orchard is approximately 0.2 ha. A total of 91 "Morrissey apple" trees arranged in seven rows were planted in 2009. The apple trees were irrigated four times during the annual period, respectively—earlier during flowering and fruit growth beginning stage, the fruit growth and the volume increase stage, the time after the fruit picking stage, and later during the leaf senescence stage. The average apple tree height is 3.5 m. The pear orchard covers an area of approximately 0.27 ha, and a part of the whole orchard was set as research area, including 96 "Bergamot pear" trees arranged in eight rows and planted in 2015. The pear trees were irrigated four times during the annual period, especially in the time before the flowering stage, later of the flowering stage, the fruit growth and the volume increase stage, and the time after the fruit picking stage. The average pear tree height is 4.2 m. The experimental field was divided into microplots to obtain experimental data separately.

2.2 Field data collection

A chlorophyll meter is a portable device which allows the *in situ* quantification of total leaf chlorophyll by measuring optical densities at two separate wavebands, and the chlorophyll content can be estimated by SPAD values (Shu et al., 2021). In this study, the SPAD value was measured with a chlorophyll meter (TYS-4N Jinkelida Electronics, Beijing, China). The SPAD value was measured at six points and twice for each one; the average was taken as the final value. A comparative experiment between leaf chlorophyll content and SPAD value was carried out, and the results verified that the SPAD value was related to the chlorophyll content at the 0.01 level with a Pearson coefficient of more than 0.9 for both apple and pear tree leaves. For each microplot, the reference canopy SPAD is determined by averaging the SPAD values of 20 sample leaves which are healthy with an intact structure and located at the upper and different directions of the canopy.

We implemented experiments from August 2019 to September 2021 in the apple orchard and from May 2020 to August 2021 in the pear orchard. The experimental date and corresponding growth stages are specified in Table 1. Each experimental day was a sunny day, and the temperature situation is shown in Figure 2. Figure 3 describes the statistical analysis of the canopy SPAD value for fruit trees in different growth stages. It can be concluded that the canopy SPAD value increased from flowering until fruit maturation period and then began to decrease during the annual growth cycle. With

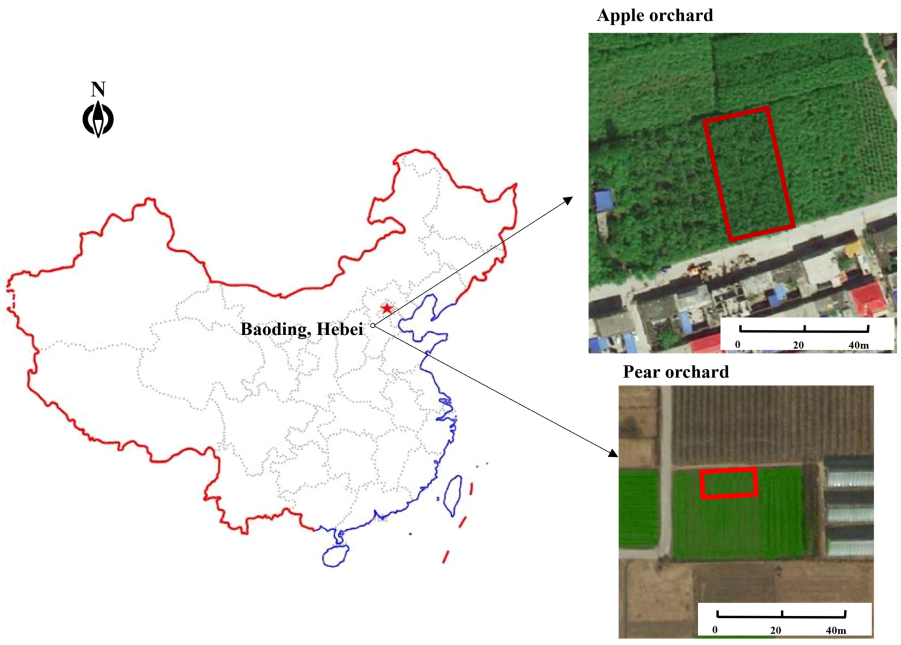

FIGURE 1
Location and satellite pictures of the experimental area.

10.3389/fpls.2024.1435613

TABLE 1 Schedule of experiments in the orchard.

	Experimental date		Growth stage	
For apple tree	2019 year	27 August	Fruit ripe for picking	BBCH 87
		22 September	Leaf senescence	——
	2020 year	11 May	Flowering and fruit growth beginning	BBCH 71
		14 June	Fruit growth and the volume increase	BBCH 72-73
		26 June		
		25 July	Fruit growth and ripening gradually	BBCH 73-87
		8 August		
		22 August	Fruit ripe for picking	BBCH 87
		28 September	Leaf senescence	——
	2021 year	5 May	Flowering and fruit growth beginning	BBCH 71
		14 May		
		5 June	Fruit growth and the volume increase	BBCH 72-73
		2 July	Fruit growth and ripening gradually	BBCH 73-87
		23 July		
		3 August		
		14 August	Fruit ripe for picking	BBCH 87
		21 September	Leaf senescence	——
For pear tree	2020 year	17 May	Flowering and fruit growth beginning	BBCH 71
		20 June	Fruit fall after flowering and size up	BBCH 71-73
		7 July	Fruit growth gradually	BBCH 73-87
		21 July	Fruit ripe for picking	BBCH 87
		20 August	Leaf senescence	——
	2021 year	7 May	Flowering and fruit growth beginning	BBCH 71
		24 May	Fruit fall after flowering and size up	BBCH 71-73
		6 June		
		23 June		
		14 July	Fruit ripe for picking	BBCH 87
		25 August	Leaf senescence	——

the growth and development of tree leaves, the chlorophyll content in the leaves gradually increased, and when the fruits gradually matured, the chlorophyll content in the leaves began to decrease. In our study, the maturity time of pear trees was approximately 20 days earlier than that of apple trees.

2.3 Multispectral image collection

Parrot Sequoia is a small and lightweight multispectral imager designed for agricultural remote sensing, with four spectral sensors and one RGB sensor (Figure 4B). The four spectral bands are situated in green (550 nm), red (660 nm), and near-infrared (790 nm) with bandwidth of 40 nm, respectively, and in red-edge (735 nm) with bandwidth of 10 nm. Furthermore, the imager was equipped with a sunshine sensor to compensate for the variability in sunlight conditions during different campaigns (Figure 4A) and to calibrate the images obtained with a calibration reflectance panel (Figure 4D) under different lighting conditions.

The UAV used in this study was DJI Phantom 3 Advanced (DJI Technology Co., Shenzhen, China), a low-cost quadrotor. Flight paths were generated in DJI GS Pro (https://www.dji.com/cn/

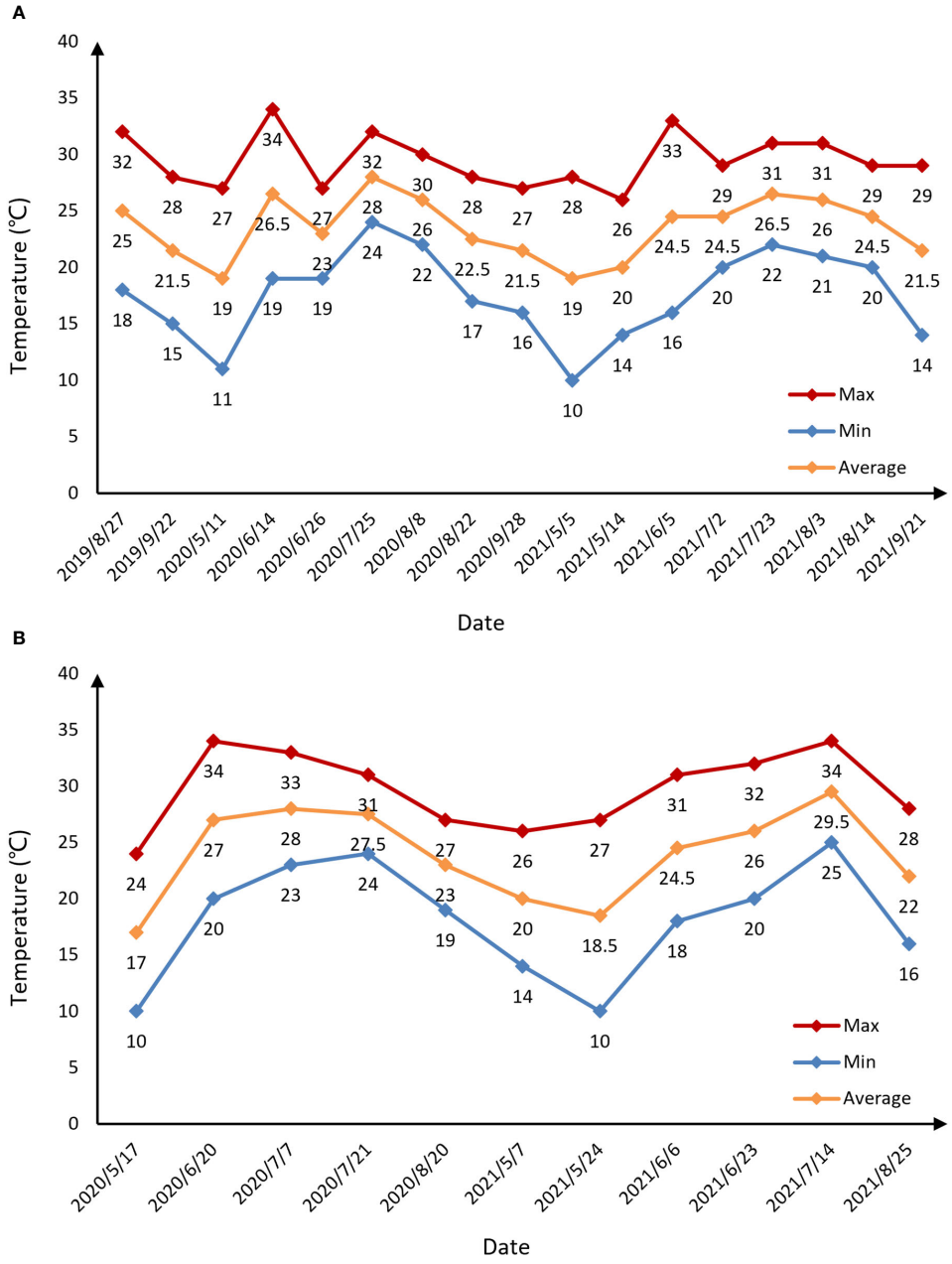

FIGURE 2
Temperature conditions of the experimental days in the apple orchard **(A)** and pear orchard **(B)**. "Max" represents the maximum temperature of the day. "Min" indicates the minimum temperature of the day. "Average" represents the average temperature of the day.

ground-station-pro; DJI Technology Co., Shenzhen, China), ensuring images with 75% forward overlap and 85% side overlap. The drone flew autonomously along the flight path at a speed of 3.5 m/s, a height of 50 m above the ground level of the field. A total of 62 images were collected in the apple orchard, and 98 images were collected in the pear orchard under clear-sky conditions from 10:00 a.m. to 2:00 p.m. on each experiment day. The images have a spatial resolution of approximately 5 cm/pixel. In addition, two to three sets of calibration images were taken for reflectance correction to be applied (Figure 4C).

2.4 Data processing

Machine learning methods were applied for canopy SPAD prediction modeling. The pre-processing of UAV imagery and the extraction of spectral information were computed with Pix4Dmapper software (https://www.pix4d.com.cn/pix4dmapper, Pix4D SA, Switzerland). The commonly used gray level co-occurrence matrix (GLCM) was selected to extract TF from multispectral UAV images. The TF were calculated using ENVI 5.3 software (https://envi.geoscene.cn, ITT Visual Information

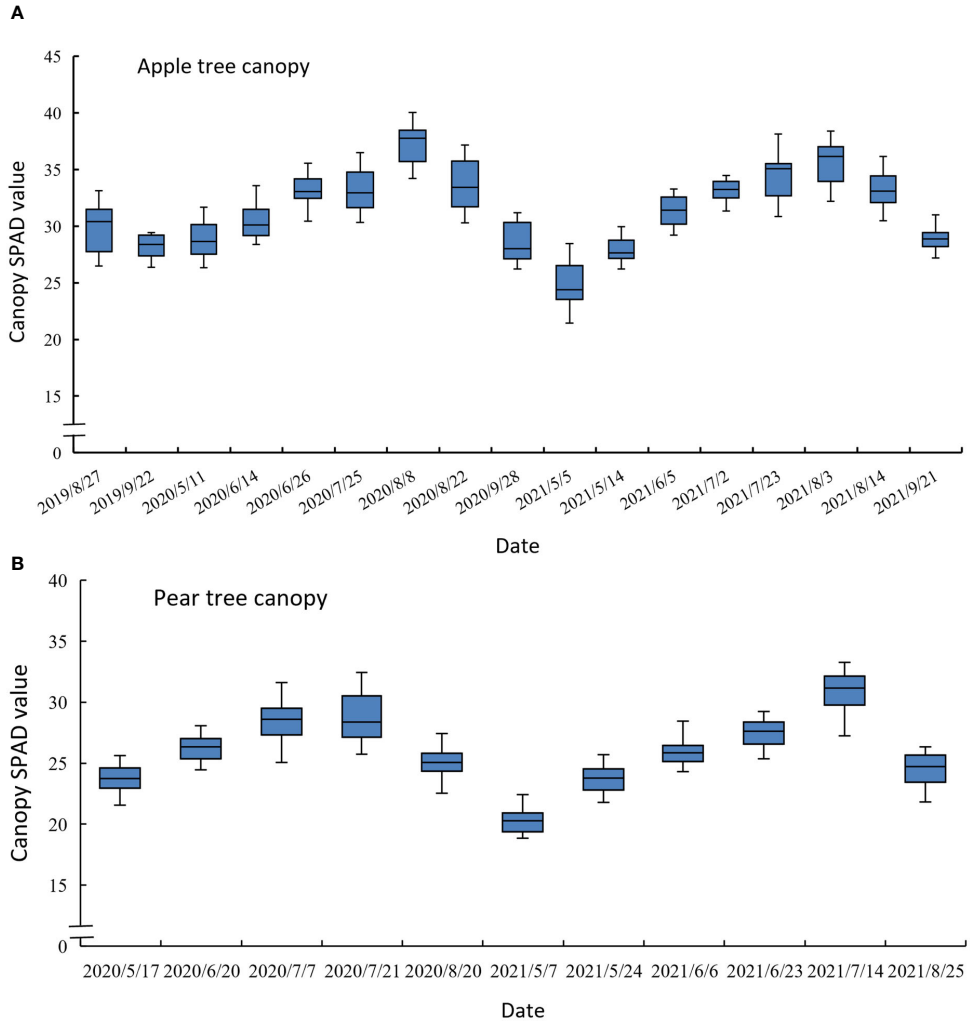

FIGURE 3
Statistical analysis map of canopy SPAD value in different growth stages of the apple tree **(A)** and the pear tree (**B**).

Solutions, USA), including mean, variance, homogeneity, contrast, dissimilarity, entropy, second moment, and correlation. Figure 5 shows the workflow diagram of UAV imagery processing, field data collection, and modeling.

2.5 Univariate regression analysis method

Vegetation index (VI) is the combination of related reflectance and the integration of spectral data from two or more bands after a certain mathematical transformation (Gitelson et al., 2002). Narmilan et al. (2022) constructed different machine learning models with VIs for sugarcane chlorophyll content prediction. Madonsela et al. (2023) proved that the red-edge chlorophyll index and green chlorophyll index, using the red-edge variant centered at 705 nm, were the most useful for estimating maize LAI. In this study, we attempted to explore the utility of univariate methods (linear, exponential, power, and logarithmic regression) for tree canopy chlorophyll estimation with VI. The VIs used in our study for chlorophyll estimation are listed in Table 2. The original bands in the formulation of each VI was replaced by the closest available bands. The univariate regression analysis was implemented in Python environment through the "numpy" and "LinearRegression" packages.

2.6 Multivariate regression analysis method

Previous studies demonstrated that texture information can highlight the structure characteristics of plant and inhibit the saturation of models applied for plants with high heterogeneous features (Lu et al., 2018; Maimaitijiang et al., 2020). In our study, RF and TF were extracted from multispectral images and used for multivariate model inputs. The machine learning methods were linear and non-linear algorithms, as partial least square (PLS), ridge regression (Ridge), support vector regression (SVR), and gaussian process regression (GPR). All the models were trained in Python environment with JetBrains PyCharm (https://www.jetbrains.com/pycharm, JetBrains s.r.o., Prague, CZ).

10.3389/fpls.2024.1435613

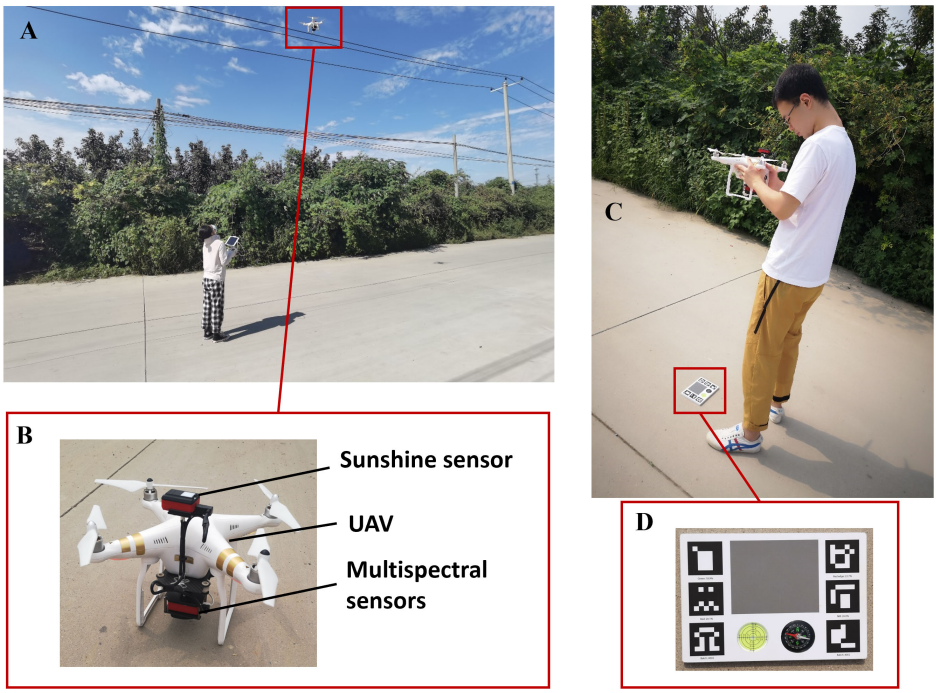

FIGURE 4
Multispectral images and radiometric calibration image collection. **(A)** Diagram of canopy image collection. **(B)** Parrot Sequoia camera and UAV equipment. **(C)** Diagram of radiometric calibration image collection. **(D)** Calibration reflectance panel.

PLS and Ridge methods were used for linear regression modeling. PLS method integrates the characteristics of principal component analysis, canonical correlation analysis, and multiple linear regression analysis, which has been used in bioinformatics, computer vision, and neuroinformatics (Mehmood and Ahmed, 2016). We implement the PLS model through the "PLSRegression" package; the parameter of "n_components" was optimized with "GridSearchCV". Compared with general linear regression, regular terms (L2 norm penalty terms) (Dorugade and Kashid, 2010) are added in the objective function of Ridge models to solve the multicollinearity of independent variables and the overfitting in the training process (Ngo et al., 2003). The Ridge model was achieved with "sklearn.linear_model" package, the "alphas" was set as 0.5, and the "fit_intercept" was set as True.

SVR and GPR methods were used for non-linear regression modeling. Support vector machine (SVM) was used to distinguish

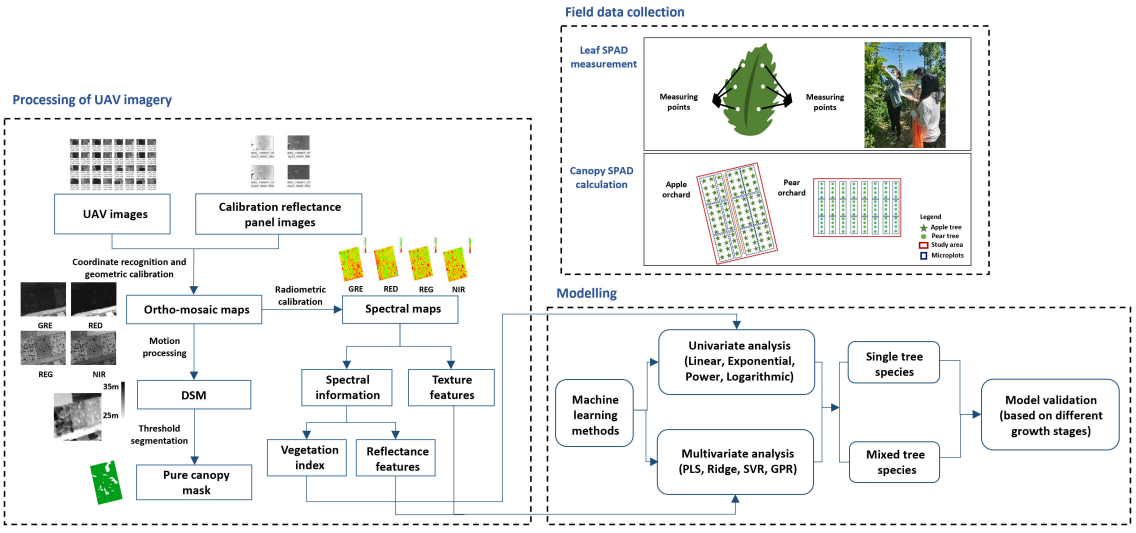

FIGURE 5
Workflow diagram of UAV imagery processing, field data collection, and modeling.

10.3389/fpls.2024.1435613

TABLE 2 VIs selected from the literature.

VI name	VI formulation used in this study	References
NDVI (Normalized Difference Vegetation Index)	$(R_{NIR} - R_{RED})/(R_{NIR} + R_{RED})$	(Gitelson et al., 1996)
GNDVI (Green Normalized Difference Vegetation Index)	$(R_{NIR} - R_{GRE})/(R_{NIR} + R_{GRE})$	
REGNDVI (Red-edge Normalized Difference Vegetation Index)	$(R_{REG} - R_{GRE})/(R_{REG} + R_{GRE})$	
RVI (Ratio Vegetation Index)	R_{NIR}/R_{RED}	(Buschmann and Nagel, 1993; Gitelson and Merzlyak, 1994)
GRVI (Green Ratio Vegetation Index)	R_{NIR}/R_{GRE}	
REGRVI (Reg-edge Ratio Vegetation Index)	R_{REG}/R_{GRE}	
DVI (Difference Vegetation Index)	$R_{NIR} - R_{RED}$	(Tucker, 1979; Cao et al., 2013)
GDVI (Green Difference Vegetation Index)	$R_{NIR} - R_{GRE}$	
REGDVI (Red-Edge Difference Vegetation Index)	$R_{REG} - R_{GRE}$	
TVI (Triangular Vegetation Index)	$0.5 \times [120 \times (R_{NIR} - R_{GRE}) - 200 \times (R_{RED} - R_{GRE})]$	(Broge and Leblanc, 2001; Haboudane et al., 2004, 2008)
MTVI (Modified Triangular Vegetation Index)	$\frac{1.5 \times [1.2 \times (R_{NIR} - R_{GRE}) - 2.5 \times (R_{RED} - R_{GRE})]}{\sqrt{(2 \times R_{NIR} + 1)^2 - (6 \times R_{NIR} - 5 \times \sqrt{R_{NIR}}) - 0.5}}$	
TCI (Triangular Chlorophyll Index)	$1.2 \times \left(\frac{R_{REG}}{R_{GRE}} u\right) - 1.5 \times \left(\frac{R_{RED}}{R_{GRE}}\right) \times \sqrt{\left(\frac{R_{REG}}{R_{RED}}\right)}$	

the feature points with a hyperplane found by maximizing the interval (Dibike et al., 2001). SVR is the development and extension of SVM method (Ansari and Gholami, 2015). Radial basis function was set for the parameter of "kernel". The parameters of "C" and "gamma" were optimized for loops. GPR is a non-parametric regression algorithm based on Bayesian theory (Wang et al., 2017). In the process of parameter adjustment, the posterior distribution on the objective function is defined, and the posterior distribution is constantly updated according to the predicted data until the posterior distribution basically fits the real distribution. GPR models were trained in Python, Matern was selected as "kernel" function, and the "nu" was set as 1.5.

2.7 Statistical analysis

The statistical analysis of original data is listed in Table 3. In single tree species research, the total data sets were divided into calibration set and validation set with the ratio of 3:1. In mixed tree species research, the calibration set included samples for apple, and pear trees were randomly selected from the previous calibration data sets in the same size (n = 150). The validation set was the same as the set in the single tree species studies. To explore the universality of the prediction models, all the canopy SPAD regression models were evaluated on the single tree species validation set of both apple and pear tree species.

In addition, prediction models were evaluated in terms of the coefficient of determination (R^2), the root mean square error (RMSE), and the relative root mean square error (RRMSE) (Sheng et al., 2020; Narmilan et al., 2022). A higher R^2 indicated that the model was more stable, and a lower RMSE or a lower RRMSE indicated great model accuracy. The Equations 1–3 display the formulas of R^2, *RMSE* and *RRMSE*, respectively.

$$R^2 = 1 - \frac{\sum_{i=1}^{n}(Pred_i - Obs_i)^2}{\sum_{i=1}^{n}(\overline{Obs_i} - Obs_i)^2} \quad (1)$$

$$RMSE = \sqrt{\frac{\sum_{i=1}^{n}(Pred_i - Obs_i)^2}{n}} \quad (2)$$

$$RRMSE = \frac{\sqrt{\frac{\sum_{i=1}^{n}(Pred_i - Obs_i)^2}{n}}}{Max(Obs_i) - Min(Obs_i)} \quad (3)$$

where $Pred_i$ are canopy SPAD values predicted with the regression models, Obs_i are canopy SPAD value measurements in the field, $\overline{Obs_i}$is the mean value of the Obs_i, and $n$is the sample size. R_c^2, RMSEC, and RRMSEC are performances of regression models trained on the calibration set, while R_v^2, RMSEV, and RRMSEV are performances of regression models trained on validation set.

3 Results

3. 1 Canopy SPAD estimation with vegetation index

We evaluated the correlations between VI and canopy SPAD value with Pearson correlation coefficient (R) (Table 4). The results showed that GNDVI had the highest correlation with canopy SPAD value with a Pearson coefficient of 0.753 for apple tree and 0.718 for pear tree; GRVI had the second highest Pearson coefficient of 0.646 for apple tree and 0.714 for pear tree. It is worth noting that there are some indicators that are not correlated at the p level.

10.3389/fpls.2024.1435613

TABLE 3 Statistical analysis of the canopy SPAD value.

Data set		Number of data	Max	Min	Mean	SD
Apple tree	All data	204	40.03	21.44	31.34	3.57
	Calibration set	153	40.03	21.44	31.32	3.65
	Validation set	51	39.53	24.42	31.40	3.35
Pear tree	All data	264	33.28	18.85	25.87	3.06
	Calibration set	198	33.28	18.85	25.83	3.12
	Validation set	66	31.62	19.28	26.01	2.90

In single tree species research, we conducted prediction models with VIs correlated with canopy SPAD values. The model results with higher prediction accuracy on the validation set are shown in Table 5. Considering the model results in both apple tree and pear tree, GNDVI was taken as the most potential VI for canopy SPAD evaluation by a simple monistic model, and R^2 was 0.512 and 0.490 on the validation set for apple trees (Figure 6A) and pear trees (Figure 6B), respectively.

In the mixed tree species research, canopy SPAD estimation models were yielded by using GNDVI and GRVI (which were the common VIs in the first three optimal models in single tree species research); the evaluation parameters of the models are listed in Table 6. However, it should be noted that the prediction accuracy of this method was not satisfactory. The model R^2 was 0.2–0.35, which was not reliable enough for canopy SPAD retrieval.

3.2 Canopy SPAD estimation with image features

Multivariate models were established with image features by using PLS, Ridge, SVR, and GPR algorithms; the relevant results are shown in Table 5 and Table 6. For an intuitive comparison of model performance, the R^2 value on the validation data of the models is displayed in Figure 7 (the univariate model results with GNDVI and GRVI were also listed to make a comprehensive comparison between modeling methods).

TABLE 4 Significance test between VI and the canopy SPAD value.

I	NDVI	GNDVI	REGNDVI
R (apple/ pear tree)	0.483**/0.601**	**0.753**/0.718****	0.549**/**0.536****
VI	RVI	GRVI	REGRVI
R (apple/ pear tree)	0.235**/0.613**	**0.646**/0.714****	**0.623**/0.403****
VI	DVI	GDVI	REGDVI
R (apple/ pear tree)	ns /0.324**	0.057/0.488**	−0.027/0.381**
VI	TVI	MTVI	TCI
R (apple/ pear tree)	−0.040/0.248**	0.433**/0.382**	0.545**/0.396**

**, significance at $p < 0.01$; ns, no significance. Bold values: The vegetation index corresponding to the bold values has higher model performances.

In single tree species research, prediction models were implemented with RF firstly. For apple trees, PLS and Ridge were performed equally; the R_v^2 was approximately 0.52, and the GPR model yielded better results with R_v^2 of 0.700 than the SVR model with R_v^2 of 0.585. For pear trees, PLS and Ridge were also performed equally with R_v^2 of 0.55. The R_v^2 of the SVR model was 0.733, and RRMSEV was 12.042%, which were a little superior to the results of the GPR model (R_v^2 = 0.721, RRMSEV = 12.326%). In the latter research, the fusion of RF and TF was set as model inputs; the prediction accuracy of the models obtained by the same algorithm was improved, except by the SVR method. For apple trees, R_v^2 of the PLS and Ridge models were up to 0.70, and R_v^2 of the GPR model was up to 0.788 (Figure 6C). For pear trees, R_v^2 of the PLS and Ridge models were up to 0.73, and R_v^2 of the GPR model was slightly improved to 0.723 (Figure 6D).

In mixed tree species research, when RF were selected as model inputs, the validation performance of the PLS and Ridge models was not reliable, especially for apple trees; R_v^2 was less than 0.1. The GPR model got the best accuracy with R_v^2 of 0.681 for apple trees and 0.707 for pear trees. When RF and TF were mixed for model variables, the validation performance of the PLS and Ridge models were obviously improved, and the Ridge model yielded R_v^2 = 0.476 for apple trees and R_v^2 = 0.614 for pear trees. The GPR model is also the best prediction model with R_v^2 of 0.763 for apple trees and 0.706 for pear trees (Figure 6E).

3.3 Canopy SPAD estimation over the various growth stages

To evaluate the growth periods' prediction performance of the GPR method, the canopy SPAD prediction was carried out at different stages in 2021. Figure 8 shows the accuracy of the models trained with various types of inputs by R^2 metrics over the various growth stages.

In the single tree species inversion, for apple trees, the prediction model yielded well accuracy with only RF during the first stages (flowering and fruit growth beginning) with R^2 of 0.797. In the latter four growth stages, the GPR models got a higher R^2 value with RF+TF than with only RF. It was 0.592 during leaf senescence stage and approximately 0.7 to 0.8 in the remaining

10.3389/fpls.2024.1435613

TABLE 5 Performance of the models yielded in single tree species research.

Tree species	Model type		Calibration			Validation		
			R_c^2	RMSEC	RRMSEC	R_v^2	RMSEV	RRMSEV
For apple tree	GNDVI		0.583	2.350	12.641%	0.512	2.315	15.321%
	REGRVI		0.396	2.827	15.207%	0.359	2.653	17.558%
	GRVI		0.431	2.743	14.755%	0.338	2.697	17.849%
	RF	PLS	0.598	2.305	12.399%	0.519	2.300	15.222%
		Ridge	0.598	2.306	12.405%	0.518	2.302	15.235%
		SVR	0.634	2.201	11.840%	0.585	2.135	14.130%
		GPR	0.883	1.242	6.681%	0.700	1.815	12.012%
	RF + TF	PLS	0.806	1.601	8.612%	0.707	1.795	11.880%
		Ridge	0.832	1.490	8.015%	0.703	1.807	11.960%
		SVR	0.616	2.254	12.125%	0.489	2.368	15.672%
		GPR	0.928	0.975	5.245%	0.788	1.527	10.106%
For pear tree	GNDVI		0.515	2.169	15.031%	0.490	2.056	16.661%
	GRVI		0.524	2.147	14.879%	0.483	2.070	16.775%
	REGNDVI		0.494	2.216	15.357%	0.495	2.045	16.572%
	RF	PLS	0.614	1.934	13.403%	0.550	1.932	15.656%
		Ridge	0.612	1.938	13.430%	0.554	1.921	15.567%
		SVR	0.837	1.257	8.711%	0.733	1.486	12.042%
		GPR	0.834	1.268	8.787%	0.721	1.521	12.326%
	RF + TF	PLS	0.828	1.292	8.954%	0.737	1.475	11.953%
		Ridge	0.828	1.290	8.940%	0.739	1.469	11.904%
		SVR	0.738	1.595	11.053%	0.489	2.057	16.669%
		GPR	0.878	1.089	7.547%	0.723	1.516	12.285%

three stages. For pear trees, the GPR models yielded better results with RF+TR than with only RF during the first four stages; the R^2 value was approximately 0.475–0.765, and the highest accuracy was obtained in the fruit-growth-gradually stage with R^2 = 0.765.

In the mixed tree species inversion, for apple trees, the prediction was that the R^2 values obtained with RF+TF were all greater than those obtained with only RF, which especially increased from 0.492 to 0.695 in the second growth stage and increased from 0.293 to 0.741 in the fourth growth stage. For pear trees, the model results trained with RF+TF got the highest R^2 value of 0.723 in the third growth stages and got an R^2 value between 0.382 and 0.612 in the remaining four stages.

4 Discussion

4.1 Vegetation index for canopy SPAD inversion

Vegetation index has been widely used in agricultural production research, including disease monitoring, biomass detection, etc. The GNDVI was originally developed for chlorophyll concentration measurement in maize leaves (Daughtry et al., 2000). Hunt et al. found that GNDVI was highly relevant with leaf area index and nitrogen status for winter wheat (Hunt et al., 2010). Shanahan et al. found that GNDVI was of great value in predicting corn grain yield (Shanahan et al., 2001). In this paper, prediction models trained with GNDVI yielded an R_v^2 value of 0.512 for apple trees and 0.490 for pear trees in single tree species research. However, the results in mixed tree species research showed that GDVI was not a reliable index for canopy SPAD inversion. In the past studies of chlorophyll retrieval using VIs, researchers found that the sensitivity of vegetation index was greatly affected by the density of the crop canopy (Yang et al., 2022). In our study, apple trees are much older than pear trees, and they have many differences in canopy structure, specifically in canopy volume and canopy density. Therefore, when GNDVI was used for chlorophyll assessment in single tree species, the model yielded relatively reliable results. However, the sensitivity of GNDVI to chlorophyll retrieval decreased under the interference of canopy structure heterogeneity in the research of mixed tree species.

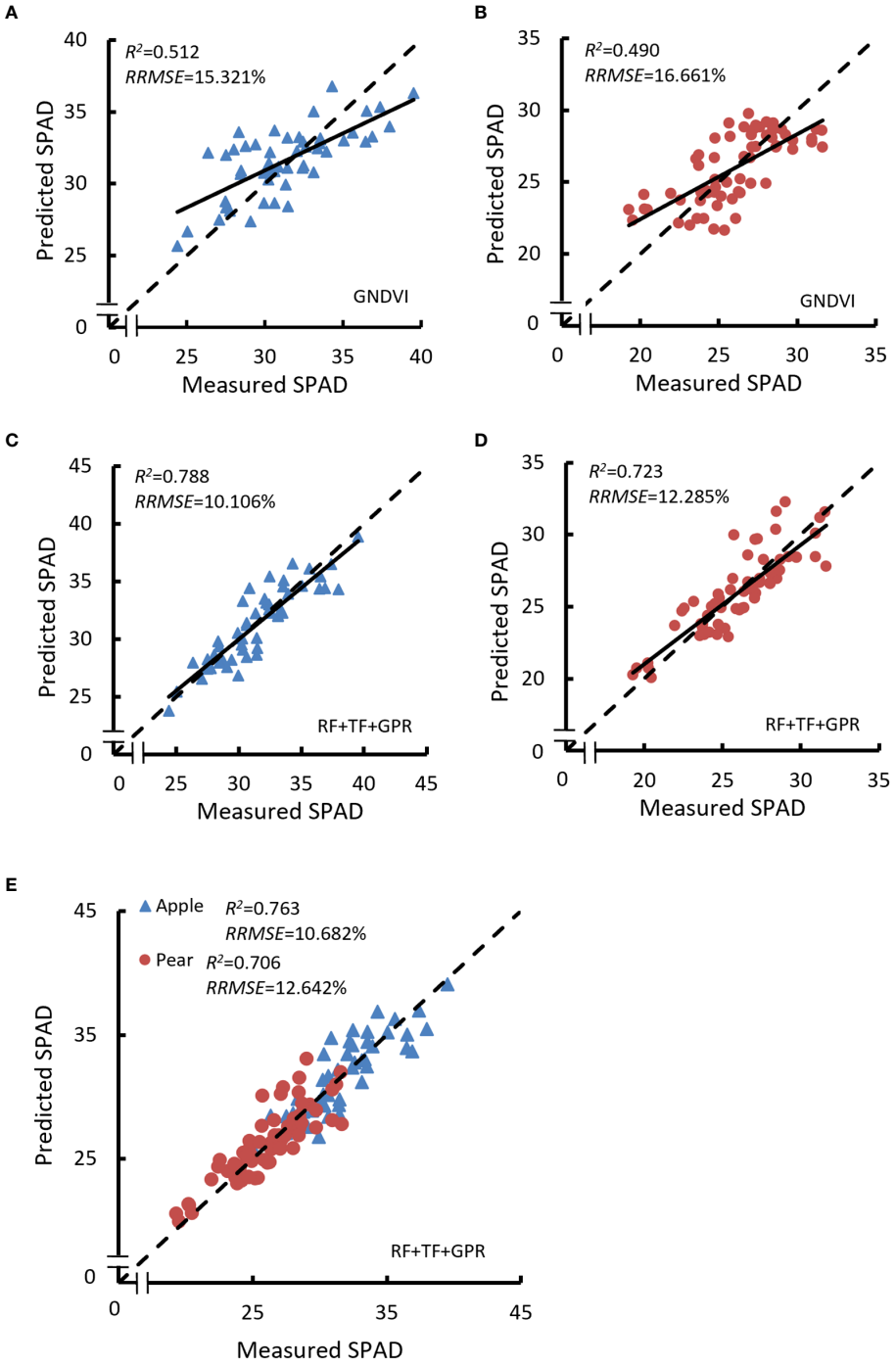

FIGURE 6
Relationship between the predicted and measured SPAD value of canopy SPAD. **(A)** Calculated with GNDVI in single tree species research for apple tree. **(B)** Yielded with GNDVI in single tree species research for apple tree. **(C)** Obtained with RF+TF+GPR in single tree species research for apple tree. **(D)** Trained with RF+TF+GPR in single tree species research for apple tree. **(E)** Done with RF+TF+GPR in mixed tree species research.

4.2 Comparison of modeling methods

Comparing the models' results, the prediction accuracies of the PLS and Ridge models were close, except that the Ridge model performed better than the PLS model with RF+TF in mixed tree species research. However, since that is not a universal phenomenon, the Ridge method cannot be considered superior to the PLS method. SVR models did not do well with the huge distance between the calibration and validation performances, especially in mixed tree species studies. The main factor that caused poor performance may be the several structural parameters, which should be continuously adjusted in model training. Inappropriate parameters would greatly impact prediction performance. From the results of the model based on spectral features or the combination of

TABLE 6 Performance of the models as yielded in mixed tree species research.

Model type		Calibration			Validation (apple tree)			Validation (pear tree)		
		R_c^2	RMSEC	RRMSEC	R_v^2	RMSEV	RRMSEV	R_v^2	RMSEV	RRMSEV
GNDVI		0.566	2.870	13.551%	0.221	2.926	19.365%	0.341	2.337	18.938%
GRVI		0.578	2.830	13.362%	0.262	2.847	18.842%	0.264	2.470	20.016%
RF	PLS	0.454	3.219	15.198%	0.039	3.249	21.502%	0.300	2.412	19.546%
	Ridge	0.516	3.045	14.377%	0.060	3.214	21.271%	0.421	2.190	17.747%
	SVR	0.815	1.874	8.848%	0.556	2.208	14.613%	0.687	1.609	13.039%
	GPR	0.870	1.573	7.427%	0.681	1.873	12.400%	0.707	1.559	12.634%
RF +TF	PLS	0.546	2.936	13.862%	0.253	2.864	18.954%	0.123	2.695	21.840%
	Ridge	0.749	2.181	10.297%	0.476	2.398	15.870%	0.614	1.789	14.498%
	SVR	0.927	1.178	5.562%	0.566	2.183	14.447%	0.322	2.369	19.198%
	GPR	0.943	1.040	4.910%	0.763	1.614	10.682%	0.706	1.560	12.642%

spectral and texture features, we can see that the SVR model yielded robust results when having relatively few variables. It is worth noting that the GPR model has excellent performance in modeling as shown in Figure 7, yielding reliable prediction accuracies on the validation set with the different combinations of variables. In contrast to the non-linear model, the linear model has a weaker ability to explore the deep connections between input features. The results indicated that the more information covered by the inputs contributes to the higher accuracy for linear model, which is in line with the study of Maimaitijiang et al. (2020).

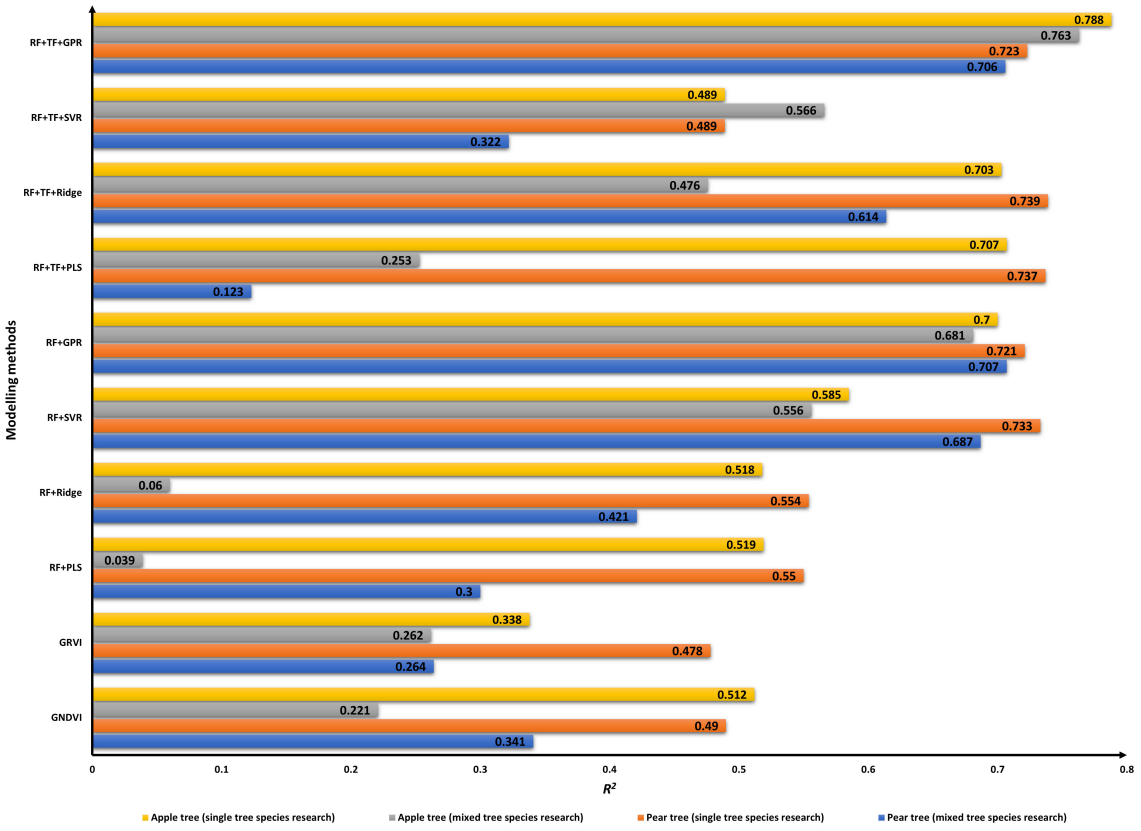

FIGURE 7
Model performance for canopy SPAD estimation.

4.3 Contribution of texture features in canopy SPAD estimation

In our study, we focus on the contribution of TF to the canopy SPAD evaluation over tree species. In single tree species research, compared with the model performances yielded by RF+TF of which were obtained by only RF, the evaluation parameters were generally improved. For apple tree, the linear PLS model had R^2 increased by 36.2%, and the non-linear GPR model had R^2 increased by 12.6%. For pear tree, the R^2 of the linear Ridge model increased from 0.554 to 0.739, an increase of 33.4%. For the non-linear GPR model of pear tree, R^2 had increased by 0.3%. In the mixed tree species research, TF have significant optimization ability for linear Ridge models; the validation R^2 increased from 0.06 to 0.476 for apple tree and from 0.421 to 0.614 for pear tree. In the GPR model results, the validation R^2 increased from 0.681 to 0.763 for apple tree. Although the improvement of the model results for pear tree was slightly smaller than that of apple tree, the importance of texture features in canopy SPAD monitoring research should not be ignored.

For the same tree species, the model results obtained with mixed tree species information were a little weaker than the results obtained with single tree species information, but the reduction

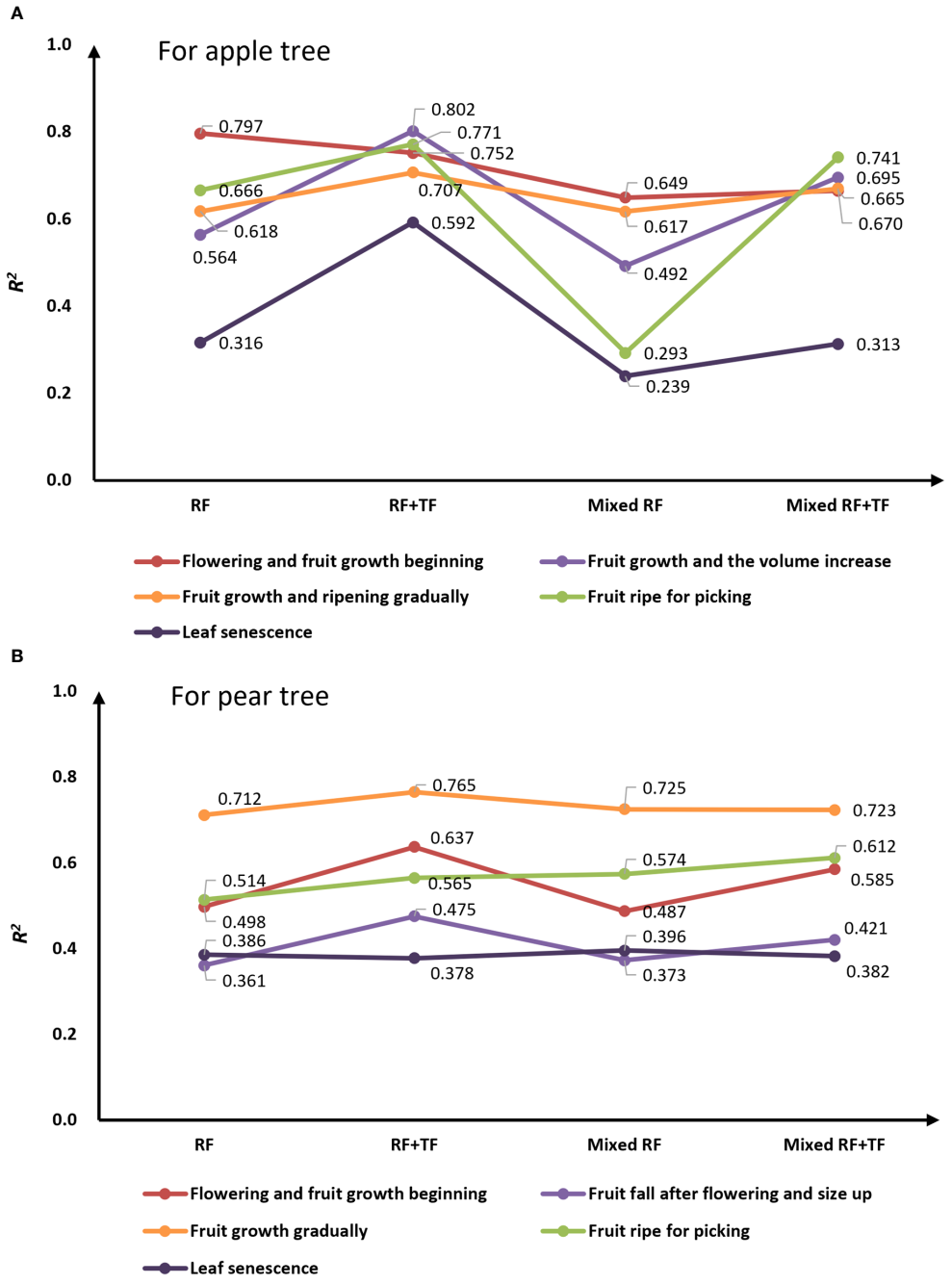

FIGURE 8
Prediction accuracy for the various growth stages of the apple tree **(A)** and the pear tree **(B)**.

was within the expectation considering the effect of tree heterogeneity. Chlorophyll content can be effectively monitored with tree canopy RF, and TF can facilitate the extraction of diversity among tree species, which is beneficial to yield a chlorophyll content assessment model with higher accuracy and more universality ability. In the results obtained by Li et al. (2018) for remote sensing imaging-based canopy chlorophyll estimation, the SVR model with modified NDVI yielded R^2 = 0.667 on the validation set. In this paper, it can be concluded that canopy SPAD would be monitored with the RF+TF+GPR method, R^2 on the validation set in single tree species was 0.788 for apple tree and 0.723 for pear tree, and R^2 on the validation set over different tree species was 0.763 and 0.706 for apple tree and pear tree, respectively. The results go beyond a previous report, successfully getting a higher prediction accuracy on original reflectance and texture data. Nevertheless, it is worth noting that apple trees and pear trees both belong to the wild fruit *Rosaceae* plant resources, which might be one of the reasons supporting the high prediction accuracy in the mixed species study. More research should be carried out to explore the significance of RF+TF for other species with greater canopy differences. Moreover, compared with satellite remote sensing technique, UAV imagery has a wider range of application circumstance as high-throughput phenotyping method, and the UAV images have a higher special resolution which is beneficial to the extraction of TF. These advantages of UAV imagery are conducive to the popularization and application in agriculture.

From the overall trend of the lines in Figure 8, it was noted that the optimization ability of texture features to model prediction accuracy is more prominent for apple orchards than that for pear orchards. Considering the actual planting situation, the high canopy coverage of the apple orchard leads to serious airtight phenomenon and poor light transmittance, resulting in invalid leaves exiting in the canopy which get insufficient illumination. Being different from the apple orchard, the tree rows spacing is regular in the pear

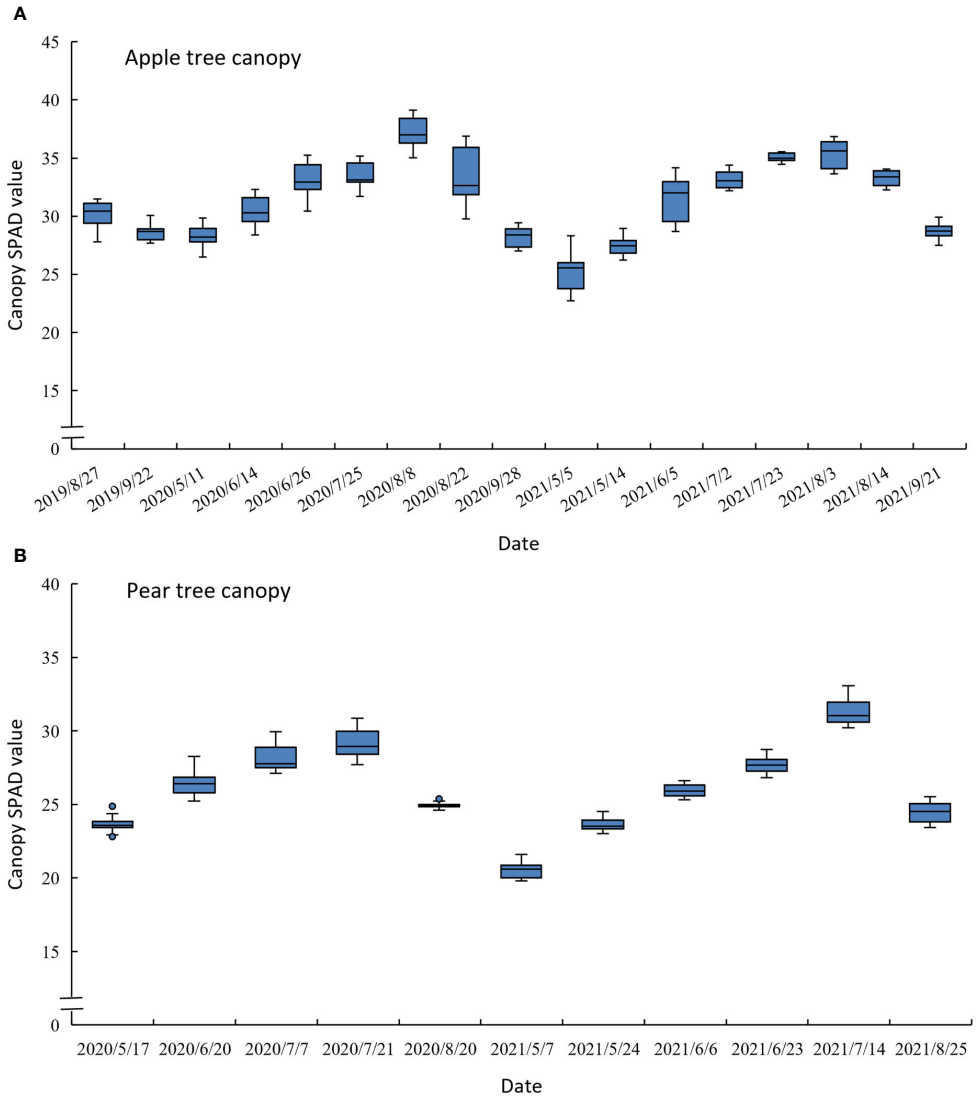

FIGURE 9
Statistical analysis map of the predicted canopy SPAD value (using GPR+RF+TF mixed tree species model) in different growth stages of the apple tree **(A)** and the pear tree (**B**).

orchard, and trees grow in uniform and adequate light conditions. Therefore, the contribution of TF for canopy SPAD inversion for pear orchard was not as prominent as that for the apple orchard. However, the study results of two different tree species indicated that the contribution of TF was still significant.

4.4 Analysis of model performance in different growth stages

By analyzing the model performance obtained with RF+TF in mixed tree species research, it can be found that the models yielded high prediction accuracy during flowering stage to picking stage and the R^2 values between 0.66 and 0.75 for apple trees as well as the R^2 values between 0.58 and 0.73 for pear trees, except at the second stage. This may be attributed to the natural falling of fruits and leaves in the second stage for pear trees. As the leaves fall off, the canopy density will be reduced, and the background effect of canopy gaps will cause the inhomogeneity of the reflectivity scene (Brewer et al., 2022). Hence, the optimal conditions for predicting chlorophyll content are missing in this stage. In addition, the prediction accuracy of the chlorophyll model at the leaf senescence stage was less than 0.4 for both apple and pear trees due to the low chlorophyll content. Leaf senescence is a degenerative process; chlorophyll and its associated proteins break down during this stage, resulting in most bands being absorbed (Guo et al., 2021; Brewer et al., 2022). In total, the RF+TF+GPR model can effectively monitor the canopy SPAD for both apple and pear orchards at different growth stages. More experiment area and tree species need to be developed to improve the model universality and prediction accuracy.

In addition, Figure 9 displays the statistical analysis results of the predicted canopy SPAD at different growth stages by using the mixed tree species model yielded by the GPR+RF+TF method. Compared with Figure 3, which is the analysis results of the measured canopy SPAD value, the predicted results can effectively respond to the change in trend of the canopy chlorophyll content of fruit trees over the various growth periods.

5 Conclusion

In this research, we presented the canopy SPAD evaluation in apple and pear orchards using UAV multispectral imagery. For univariate models, GNDVI was an efficient index in single tree species research, but the same conclusion cannot be supported in mixed tree species research. For multivariate models, GPR algorithm performed better than other machine learning methods; the RF+TF+GPR model yielded R^2 value of 0.788 for apple trees and 0.723 for pear trees in single tree species research and trained R^2 value of 0.763 for apple trees and 0.706 for pear trees in mixed tree species research. Compared with the RF+GPR model results, TF can retrieve more canopy structure information, promoting the prediction accuracy of canopy SPAD. Moreover, the RF+TF+GPR method is suitable for canopy SPAD during the growth-beginning stage to the ripe-for-picking stage, which is beneficial for canopy SPAD monitoring over various stages. The future scope of this work would focus on more fruit tree areas and species using large amounts of data to improve the universality and accuracy of the models.

Data availability statement

The raw data supporting the conclusions of this article will be made available by the authors, without undue reservation.

Author contributions

YH: Conceptualization, Data curation, Methodology, Supervision, Writing – original draft, Writing – review & editing. DL: Conceptualization, Data curation, Writing – original draft, Writing – review & editing. XL: Methodology, Validation, Writing – original draft, Writing – review & editing. ZR: Funding acquisition, Supervision, Writing – original draft, Writing – review & editing.

Funding

The author(s) declare financial support was received for the research, authorship, and/or publication of this article. The authors are grateful for the financial support from the Scientific Research Start-up Foundation for Doctor of Hebei GEO University (BQ2024058) and the Hebei Provincial Department of Science and Technology (Grant number 22327203D).

Conflict of interest

The authors declare that the research was conducted in the absence of any commercial or financial relationships that could be construed as a potential conflict of interest.

Publisher's note

All claims expressed in this article are solely those of the authors and do not necessarily represent those of their affiliated organizations, or those of the publisher, the editors and the reviewers. Any product that may be evaluated in this article, or claim that may be made by its manufacturer, is not guaranteed or endorsed by the publisher.

References

Abdelbaki, A., and Udelhoven, T. (2022). A review of hybrid approaches for quantitative assessment of crop traits using optical remote sensing: research trends and future directions. *Remote Sens.-Basel.* 14, 3515. doi: 10.3390/rs14153515

Ansari, H. R., and Gholami, A. (2015). An improved support vector regression model for estimation of saturation pressure of crude oils. *Fluid Phase Equilibr.* 402, 124–132. doi: 10.1016/j.fluid.2015.05.037

Brewer, K., Clulow, A., Sibanda, M., Gokool, S., Naiken, V., and Mabhaudhi, T. (2022). Predicting the chlorophyll content of maize over phenotyping as a proxy for crop health in smallholder farming systems. *Remote Sens. -Basel.* 14, 518. doi: 10.3390/rs14030518

Broge, N. H., and Leblanc, E. (2001). Comparing prediction power and stability of broadband and hyperspectral vegetation indices for estimation of green leaf area index and canopy chlorophyll density. *Remote Sens. Environ.* 76, 156–172. doi: 10.1016/S0034-4257(00)00197-8

Buschmann, C., and Nagel, E. (1993). *In vivo* spectroscopy and internal optics of leaves as basis for remote sensing of vegetation. *Int. J. Remote Sens.* 14, 711–722. doi: 10.1080/01431169308904370

Cao, Q., Miao, Y., Wang, H., Huang, S., Cheng, S., Khosla, R., et al. (2013). Non-destructive estimation of rice plant nitrogen status with Crop Circle multispectral active canopy sensor. *Field Crop Res.* 154, 133–144. doi: 10.1016/j.fcr.2013.08.005

Crocombe, R. A. (2018). Portable spectroscopy. *Appl. Spectrosc.* 72, 1701–1751. doi: 10.1177/0003702818809719

Daughtry, C. S. T., Walthall, C. L., Kim, M. S., de Colstoun, E. B., and Mcmurtrey, J. E. (2000). Estimating corn leaf chlorophyll concentration from leaf and canopy reflectance. *Remote Sens. Environ.* 74, 229–239. doi: 10.1016/S0034-4257(00)00113-9

Dibike, Y., Velickov, S., Solomatine, D., and Abbott, M. (2001). Model induction with support vector machines: Introduction and applications. *J. Comput. Civil Eng.* 15, 208–216. doi: 10.1061/(ASCE)0887-3801(2001)15:3(208)

Dorugade, A. V., and Kashid, D. N. (2010). Variable selection in linear regression based on ridge estimator. *J. Stat. Comput. Sim.* 80, 1211–1224. doi: 10.1080/00949650903012413

Duan, B., Liu, Y., Gong, Y., Peng, Y., Wu, X., Zhu, R., et al. (2019). Remote estimation of rice LAI based on Fourier spectrum texture from UAV image. *Plant Methods* 15, 124. doi: 10.1186/s13007-019-0507-8

Féret, J. B., Gitelson, A. A., Noble, S. D., and Jacquemoud, S. (2017). PROSPECT-D: Towards modeling leaf optical properties through a complete lifecycle. *Remote Sens. Environ.* 193, 204–215. doi: 10.1016/j.rse.2017.03.004

Fu, B., Li, S., Lao, Z., Yuan, B., Liang, Y., and He, W. (2023). Multi-sensor and multi-platform retrieval of water chlorophyll a concentration in karst wetlands using transfer learning frameworks with ASD, UAV, and Planet CubeSate reflectance data. *Sci. Total Environ* 901, 165963. doi: 10.1016/j.scitotenv.2023.165963

Gitelson, A. A., Kaufman, Y. J., and Merzlyak, M. N. (1996). Use of a green channel in remote sensing of global vegetation from EOS-MODIS. *Remote Sens. Environ.* 58, 289–298. doi: 10.1016/S0034-4257(96)00072-7

Gitelson, A. A., Kaufman, Y. J., Stark, R., and Rundquist, D. (2002). Novel algorithms for remote estimation of vegetation fraction. *Remote Sens. Environ.* 80, 76–87. doi: 10.1016/S0034-4257(01)00289-9

Gitelson, A., and Merzlyak, M. N. (1994). Spectral Reflectance Changes Associated with Autumn Senescence of Aesculus hippocastanum L. and Acer platanoides L. Leaves. Spectral Features and Relation to Chlorophyll Estimation. *J. Plant Physiol.* 143, 286–292. doi: 10.1016/S0176-1617(11)81633-0

Guan, S., Fukami, K., Matsunaka, H., Okami, M., Tanaka, R., Nakano, H., et al. (2019). Assessing correlation of high-resolution NDVI with fertilizer application level and yield of rice and wheat crops using small UAVs. *Remote Sens.-Basel.* 11, 112. doi: 10.3390/rs11020112

Guo, Y., Ren, G., Zhang, K., Li, Z., Miao, Y., and Guo, H. (2021). Leaf senescence: progression, regulation, and application. *Mol. Hortic.* 1, 5. doi: 10.1186/s43897-021-00006-9

Haboudane, D., Miller, J. R., Pattey, E., Zarco-Tejada, P. J., and Strachan, I. B. (2004). Hyperspectral vegetation indices and novel algorithms for predicting green LAI of crop canopies: Modeling and validation in the context of precision agriculture. *Remote Sens. Environ.* 90, 337–352. doi: 10.1016/j.rse.2003.12.013

Haboudane, D., Tremblay, N., Miller, J. R., and Vigneault, P. (2008). Remote estimation of crop chlorophyll content using spectral indices derived from hyperspectral data. *IEEE T. Geosci. Remote.* 46, 423–437. doi: 10.1109/TGRS.2007.904836

Hernanda, R. A. P., Lee, J., and Lee, H. (2023). Spectroscopy imaging techniques as *in vivo* analytical tools to detect plant traits. *Appl. Sci.* 13, 10420. doi: 10.3390/app131810420

Hunt, E. R., Hively, W. D., Fujikawa, S., Linden, D., Daughtry, C. S., and Mccarty, G. (2010). Acquisition of NIR-green-blue digital photographs from unmanned aircraft for crop monitoring. *Remote Sens.-Basel.* 2, 290–305. doi: 10.3390/rs2010290

Intergovermental Panel on Climate Change (2022). *Climate change 2022 mitigation of climate change*. Available online at: https://www.ipcc.ch/report/ar6/wg3.

Jafarbiglu, H., and Pourreza, A. (2022). A comprehensive review of remote sensing platforms, sensors, and applications in nut crops. *Comput. Electron. Agr.* 197, 106844. doi: 10.1016/j.compag.2022.106844

Lao, Z., Fu, B., Wei, Y., Deng, T., He, W., Yang, Y., et al. (2024). Retrieval of chlorophyll content for vegetation communities under different inundation frequencies using UAV images and field measurements. *Ecol. Indic.* 158, 111329. doi: 10.1016/j.ecolind.2023.111329

Li, Z., Zhou, X., Cheng, Q., Fei, S., and Chen, Z. (2023). A machine-learning model based on the fusion of spectral and textural features from UAV multi-sensors to analyse the total nitrogen content in winter wheat. *Remote Sens.-Basel.* 15, 2152. doi: 10.3390/rs15082152

Li, C., Zhu, X., Wei, Y., Cao, S., Guo, X., Yu, X., et al. (2018). Estimating apple tree canopy chlorophyll content based on Sentinel-2A remote sensing imaging. *Sci. Rep.-UK.* 8, 3756. doi: 10.1038/s41598-018-21963-0

Lu, B., He, Y., and Liu, H. H. T. (2018). Mapping vegetation biophysical and biochemical properties using unmanned aerial vehicles-acquired imagery. *Int. J. Remote Sens.* 39, 5265–5287. doi: 10.1080/01431161.2017.1363441

Madonsela, S., Cho, M. A., Naidoo, L., Main, R., and Majozi, N. (2023). Exploring the utility of Sentinel-2 for estimating maize chlorophyll content and leaf area index across different growth stages. *J. Spat. Sci.* 68, 339–351. doi: 10.1080/14498596.2021.2000898

Maimaitijiang, M., Sagan, V., Sidike, P., Hartling, S., and Esposito, F. (2020). and fritschi, F Soybean yield prediction from UAV using multimodal data fusion and deep learning. *B. Remote Sens. Environ.* 237, 111599. doi: 10.1016/j.rse.2019.111599

Main, R., Cho, M. A., Mathieu, R., O Kennedy, M. M., Ramoelo, A., and Koch, S. (2011). An investigation into robust spectral indices for leaf chlorophyll estimation. *ISPRS J. Photogramm.* 66, 751–761. doi: 10.1016/j.isprsjprs.2011.08.001

Mehmood, T. A. B., and Ahmed, B. C. (2016). The diversity in the applications of partial least squares: an overview. *J. Chemometr.* 30, 4–17. doi: 10.1002/cem.2762

Narmilan, A., Gonzalez, F., Salgadoe, A. S. A., Kumarasiri, U. W. L. M., Weerasinghe, H. A. S., and Kulasekara, B. R. (2022). Predicting canopy chlorophyll content in sugarcane crops using machine learning algorithms and spectral vegetation indices derived from UAV multispectral imagery. *Remote Sens.-Basel.* 14, 1140. doi: 10.3390/rs14051140

Ngo, S. H., Kemény, S., and Deák, A. (2003). Performance of the ridge regression method as applied to complex linear and nonlinear models. *Chemometr. Intell. Lab.* 67, 69–78. doi: 10.1016/S0169-7439(03)00062-5

Sankaran, S., Quirós, J. J., and Miklas, P. N. (2019). Unmanned aerial system and satellite-based high resolution imagery for high-throughput phenotyping in dry bean. *Comput. Electron. Agr.* 165, 104965. doi: 10.1016/j.compag.2019.104965

Shanahan, J. F., Schepers, J. S., Francis, D. D., Varvel, G. E., Wilhelm, W. W., Tringe, J. M., et al. (2001). Use of remote-sensing imagery to estimate corn grain yield. *Agron. J.* 93, 583–589. doi: 10.2134/agronj2001.933583x

Sheng, Z., Xie, S. Q., and Pan, C. Y. (2020). *Probability theory and mathematical statistics* (Beijing: Higher Education Press).

Shu, M., Zuo, J., Shen, M., Yin, P., Wang, M., Yang, X., et al. (2021). Improving the estimation accuracy of SPAD values for maize leaves by removing UAV hyperspectral image backgrounds. *Int. J. Remote Sens.* 42, 5862–5881. doi: 10.1080/01431161.2021.1931539

Tucker, C. J. (1979). Red and photographic infrared linear combinations for monitoring vegetation. *Remote Sens. Environ.* 8, 127–150. doi: 10.1016/0034-4257(79)90013-0

Wang, T., Chandra, A., Jung, J., and Chang, A. (2022). UAV remote sensing based estimation of green cover during turfgrass establishment. *Comput. Electron. Agr.* 194, 106721. doi: 10.1016/j.compag.2022.106721

Wang, B., Chen, T., and Xu, A. (2017). Gaussian process regression with functional covariates and multivariate response. *Chemometr. Intell. Lab.* 163, 1–6. doi: 10.1016/j.chemolab.2017.02.001

Wang, K., Li, W., Deng, L., Lyu, Q., Zheng, Y., Yi, S., et al. (2018). Rapid detection of chlorophyll content and distribution in citrus orchards based on low-altitude remote sensing and bio-sensors. *Int. J. Agr. Biol. Eng.* 11, 164–169. doi: 10.25165/j.ijabe.20181102.3189

Xiao, B., Li, S., Dou, S., He, H., Fu, B., Zhang, T., et al. (2024). Comparison of leaf chlorophyll content retrieval performance of citrus using FOD and CWT methods with field-based full-spectrum hyperspectral reflectance data. *Comput. Electron. Agr.* 217, 108559. doi: 10.1016/j.compag.2023.108559

Xu, T., Wang, F., Xie, L., Yao, X., Zheng, J., Li, J., et al. (2022b). Integrating the textural and spectral information of UAV hyperspectral images for the improved estimation of rice aboveground biomass. *Remote Sens.-Basel.* 14, 2534. doi: 10.3390/rs14112534

Xu, L., Zhou, L., Meng, R., Zhao, F., Lv, Z., Xu, B., et al. (2022a). An improved approach to estimate ratoon rice aboveground biomass by integrating UAV-based spectral, textural and structural features. *Precis. Agric.* 23, 1276–1301. doi: 10.1007/s11119-022-09884-5

Yang, H., Hu, Y., Zheng, Z., Qiao, Y., Zhang, K., Guo, T., et al. (2022). Estimation of potato chlorophyll content from UAV multispectral images with stacking ensemble algorithm. *Agron. -Basel.* 12, 2318. doi: 10.3390/agronomy12102318

Yogeshwari, M., and Thailambal, G. (2021). Automatic feature extraction and detection of plant leaf disease using GLCM features and convolutional neural networks. *Materials Today: Proc.* 81, 530–536. doi: 10.1016/j.matpr.2021.03.700

Zarco-Tejada, P. J., González-Dugo, M. V., and Fereres, E. (2016). Seasonal stability of chlorophyll fluorescence quantified from airborne hyperspectral imagery as an indicator of net photosynthesis in the context of precision agriculture. *Remote Sens. Environ.* 179, 89–103. doi: 10.1016/j.rse.2016.03.024

Zhang, Z., and Zhu, L. (2023). A review on unmanned aerial vehicle remote sensing: platforms, sensors, data processing methods, and applications. *Drones (Basel).* 7, 398. doi: 10.3390/drones7060398

Zhao, C., Zhang, Y., Du, J., Guo, X., Wen, W., Gu, S., et al. (2019). Crop phenomics: current status and perspectives. *Front. Plant Sci.* 10. doi: 10.3389/fpls.2019.00714

Zhou, X., Zheng, H. B., Xu, X. Q., He, J. Y., Ge, X. K., Yao, X., et al. (2017). Predicting grain yield in rice using multi-temporal vegetation indices from UAV-based multispectral and digital imagery. *ISPRS J. Photogramm.* 130, 246–255. doi: 10.1016/j.isprsjprs.2017.05.003

frontiers | Frontiers in Plant Science

TYPE Original Research
PUBLISHED 14 November 2024
DOI 10.3389/fpls.2024.1500103

Check for updates

OPEN ACCESS

EDITED BY
Maruthi Sridhar Balaji Bhaskar,
Florida International University, United States

REVIEWED BY
Yahui Guo,
Central China Normal University, China
Wenquan Zhu,
Beijing Normal University, China

*CORRESPONDENCE
Bin Zhao
binzhao@sdau.edu.cn
Dailiang Peng
pengdl@aircas.ac.cn

†These authors share first authorship

RECEIVED 22 September 2024
ACCEPTED 24 October 2024
PUBLISHED 14 November 2024

CITATION
Tan Y, Cheng E, Feng X, Zhao B, Chen J, Xie Q, Peng H, Li C, Lu C, Li Y, Zhang B and Peng D (2024) Application of APSIM model in winter wheat growth monitoring.
Front. Plant Sci. 15:1500103.
doi: 10.3389/fpls.2024.1500103

COPYRIGHT
© 2024 Tan, Cheng, Feng, Zhao, Chen, Xie, Peng, Li, Lu, Li, Zhang and Peng. This is an open-access article distributed under the terms of the Creative Commons Attribution License (CC BY). The use, distribution or reproduction in other forums is permitted, provided the original author(s) and the copyright owner(s) are credited and that the original publication in this journal is cited, in accordance with accepted academic practice. No use, distribution or reproduction is permitted which does not comply with these terms.

Application of APSIM model in winter wheat growth monitoring

Yunlong Tan[1,2†], Enhui Cheng[2,4,5†], Xuxiang Feng[3], Bin Zhao[6*], Junjie Chen[1], Qiaoyun Xie[7], Hao Peng[4,8], Cunjun Li[9], Chuang Lu[9], Yong Li[10], Bing Zhang[3] and Dailiang Peng[2,5*]

[1]School of Surveg and Land Information Engineering, Henan Polytechnic University, Jiaozuo, China, [2]Key Laboratory of Digital Earth Science, Aerospace Information Research Institute, Chinese Academy of Sciences, Beijing, China, [3]Aerospace Information Research Institute, Chinese Academy of Sciences, Beijing, China, [4]College of Resource and Environment, University of Chinese Academy of Sciences, Beijing, China, [5]International Research Center of Big Data for Sustainable Development Goals, Beijing, China, [6]School of Information Science and Engineering, Shandong Agricultural University, Taian, China, [7]School of Engineering, The University of Western Australia, Perth, WA, Australia, [8]Xinjiang Institute of Ecology and Geography, Chinese Academy of Sciences, Urumqi, Xinjiang, China, [9]Information Technology Research Center, Beijing Academy of Agriculture and Forestry Sciences, Beijing, China, [10]National Key Laboratory of Wheat Improvement and College of Agronomy, Shandong Agricultural University, Taian, China

In the past, the use of remote sensing for winter wheat growth monitoring mainly relied on the relative growth assessment of a single vegetation index, such as normalized Vegetation index (NDVI). This study advanced the methodology by integrating field-measured data with Sentinel-2 data. In addition to NDVI, it innovatively incorporated two parameters, aboveground biomass (AGB) and leaf area index (LAI), for a more comprehensive relative growth assessment. Furthermore, the study employed the agricultural production systems simulator (APSIM) model to use LAI and AGB for absolute growth monitoring. The results showed that the simulated LAI and AGB closely match the field-measured values throughout the entire growth period of winter wheat under various conditions (R^2 > 0.9). For relative growth monitoring, NDVI showed significant linear positive correlations (r > 0.74 and P< 0.05) with both LAI and AGB simulated by the APSIM model. Overall, this research shows that LAI and AGB obtained from the APSIM model provide a more detailed and accurate approach to monitoring of winter wheat growth. This improved monitoring capability can support effective land management arable and provide technical guidance to advance precision agriculture practices.

KEYWORDS

winter wheat, vegetation index, remote sensing, growth monitoring, cultivated land management

1 Introduction

In recent years, global climate change and dramatic shifts in land cover have posed significant challenges to the sustainable agricultural development. The increasing risk of food shortages has intensified global concerns about food security (Godfray et al., 2010; Atzberger, 2013; Battude et al., 2016). Wheat, one of the three staple grains, is cultivated worldwide. Its production, marketing, processing and consumption are closely integrated into daily life (Jiang et al., 2021). Providing over 20% of the energy needs for nearly half of the world's population, wheat is a critical food source (Shiferaw et al., 2013). It is cultivated on approximately 30.7% of the global cereal acreage, making it the most widely grown cereals, surpassing corn, rice, and soybeans in cultivation area (Zhao et al., 2018). Timely and accurate assessment of winter wheat growth conditions and yield prediction are essential for shaping agricultural policies, informing market strategies, and ensuring national food security (Jin et al., 2018). As a result, crop growth monitoring is a significant research area, with remote sensing and crop growth simulation being particularly promising fields experiencing for practical application.

Crop growth monitoring encompasses both relative and absolute assessments, providing a scientific basis for monitoring crop growth conditions and forecasting yield by examining various growth parameters and their interrelationships (Wu et al., 2004; Xie et al., 2019). Relative growth monitoring involves comparing the current year's growth with the same period from the previous year, offering insights into how winter wheat growth compares over time (Wu and Yan, 2002; Wu et al., 2004; Shi et al., 2015; Rao et al., 2021). For example, Yin et al. employed multi-source data to compare key growth stages across two years (Yin et al., 2021), highlighting growth trends. Sun et al. leveraged the NDVI difference model to analyze winter wheat growth patterns (Sun et al., 2020). While remote sensing technology allows for broad, macro-level monitoring of crop growth across years, it often lacks the detail needed for within-crop changes (Huang et al., 2019; Lan et al., 2019; Zhang et al., 2021). In contrast, absolute growth monitoring provides a direct assessment of winter wheat's growth status and yield potential by measuring key growth indicators, such as LAI and AGB (A and Xu, 2021; Chang et al., 2023; Wang et al., 2023d). This method is well-suited for in-depth investigations of specific areas or crop types. Although absolute growth monitoring can be highly precise under experimental conditions, it requires substantial labor and financial resources for extensive field data collection, rendering it less feasible for large-scale monitoring efforts (Wang et al., 2022; Ma et al., 2023). Most studies focus on relative growth monitoring (Wu et al., 2017; Wang et al., 2023a; Zhu et al., 2023b), with fewer integrating both relative and absolute growth methods to monitor winter wheat growth.

Crop growth monitoring methods can be primarily categorized into two types: remote sensing data-based methods and growth model simulation-based methods. Remote sensing offers the ability to periodically acquire extensive surface crop data, providing quantitative assessments of crop growth on a regional scale through appropriate inversion methods (Wang et al., 2023b; Hong et al., 2024; Wang et al., 2024). In recent years, remote sensing has been increasingly used for crop classification, nutrient diagnosis, growth assessment, and disease monitoring, offering valuable insights for agricultural management and market decision-making. Compared to traditional information-gathering methods, remote sensing offers distinct advantages in monitoring and characterizing the physiological and biochemical parameters of crops (Chen et al., 2016). Since the 1970s, remote sensing techniques have been employed to monitor crop growth, and today, the technology and methodologies for wheat growth monitoring using satellite remote sensing data have become increasingly advanced. Most wheat growth monitoring via remote sensing primarily relies on the relationship between vegetation indices and agricultural parameters to develop regression models. However, this approach heavily depends on vegetation indices, with limited uses of other growth monitoring parameters, such as LAI and AGB (Luo et al., 2005; Yu et al., 2012; Su et al., 2019; Lu et al., 2020). In contrast, crop growth models use mathematical models to describe the growth and development of crops based on weather, soil, crop variety characteristics, and crop management practices. These models are grounded in principles of material balance and energy conservation, leveraging computer technology to systematically simulate key physiological processes such as photosynthesis, respiration, and transpiration. By establishing mathematical models to simulate crop growth at fixed time intervals, these models offer a robust framework for space-time analysis and continuity. Crop growth modeling can simulate the dynamics of crop growth at a specific point scale and provide mechanistic explanations for variations in crop growth and yield. Currently, over 200 crop models are available globally, with some of the most commonly used being the DSSAT, APSIM, and WOFOST models. The DSSAT model is capable of simulating the growth cycle, maturity process and yield formation of various crops (Yang et al., 2012; Liu et al., 2013; Wang et al., 2023d). The WOFOST (Zhuo et al., 2022a, b, 2023) model is recognized for its focus on soil and climate conditions and its ability to operate under multiple constraints. The APSIM (Briak and Kebede, 2021; He, 2022; Winn et al., 2023) model is extensively utilized and validated, taking into account factors such as soil quality, crop ecological processes, and atmospheric conditions (Wang et al., 2007). Its comprehensive approach makes it particularly suitable for assessing crop growth under various management practices.

Given the limitations of relying solely on relative growth monitoring—such as inadequate capture of detailed crop changes—as well as the current reliance on vegetation indices in most winter wheat monitoring studies, this research integrates the APSIM crop model with Sentinel-2 data. By incorporating AGB and LAI alongside NDVI, this study aims to provide a more comprehensive analysis through relative and absolute growth monitoring. The goal is to enable more detailed and accurate monitoring of winter wheat growth, ensure timely detection of abnormal conditions, optimize management and decision-making processes, ultimately enhancing both ecological and economic outcomes.

2 Materials and methods

2.1 Study areas

As shown in Figure 1, field experiments in our study were conducted from 2021 to 2023 at the Precision Agriculture Demonstration Base of the National Research Center for Agricultural Information Technology, located in Xiaotangshan Township, Changping District, Beijing, China. The region experiences an average annual temperature ranging between 10 and 13 degrees Celsius, with average daily sunshine hours spanning from 6 to 9 hours. Precipitation in the area is distributed unevenly throughout the seasons. The experimental crop was winter wheat, with a growth cycle commencing in late October and concluding with the harvest in mid-June of the following year. The soil type belongs to the widely distributed tidal soil in North China.

2.2 Field experiment design

The experiment was conducted out from 2021 to 2023 at the experimental base in Xiaotangshan, Beijing, with an experimental field area of 240 m×75 m. The experiment was set up in 12 plots, and the specific plot distribution is shown in Figure 1. The test crop in the 2021-2022 test field is winter wheat (Jingdong 18), with a sowing depth of 3 cm and a sowing row spacing of 16.7 cm. The sowing time is October 11, 2021, and the harvest time is June 18, 2022. The seeding rate was set to three treatments: normal sowing D1 (375kg/ha), 50% seeding rate D2 (187.5kg/ha) and 75% seeding rate D3 (281.25kg/ha). Two treatments of normal fertilization (N2) and normal fertilization halved (N1) were used for fertilization. The normal fertilization (N2) was based on the application of the base fertilizer phosphate fertilizer diamine 450 kg/ha (containing N and P_2O_5 accounted for 18% and 46%, respectively) at the time of sowing, and the urea 240 kg/ha (containing N accounted for 46%) was applied when the winter wheat returned to green in the next year as a topdressing. The normal fertilization amount was halved (N1) according to the application of base fertilizer 225kg/ha phosphate diamine (including N and P_2O_5 accounted for 18% and 46%, respectively) at sowing, and urea 120 kg/ha (including N accounted for 46%) was applied as topdressing when winter wheat turned green in the next year. Five tillage methods were adopted: no tillage (T0), subsoiling tillage (T1), plow tillage (T2), rotation (T3) (plow tillage from 2021 to 2022, rotary tillage from 2022 to 2023) and rotary tillage (T4). Other field management conditions were the same in each plot. The measured data acquisition time for 2021-2022 is shown in Table 1.

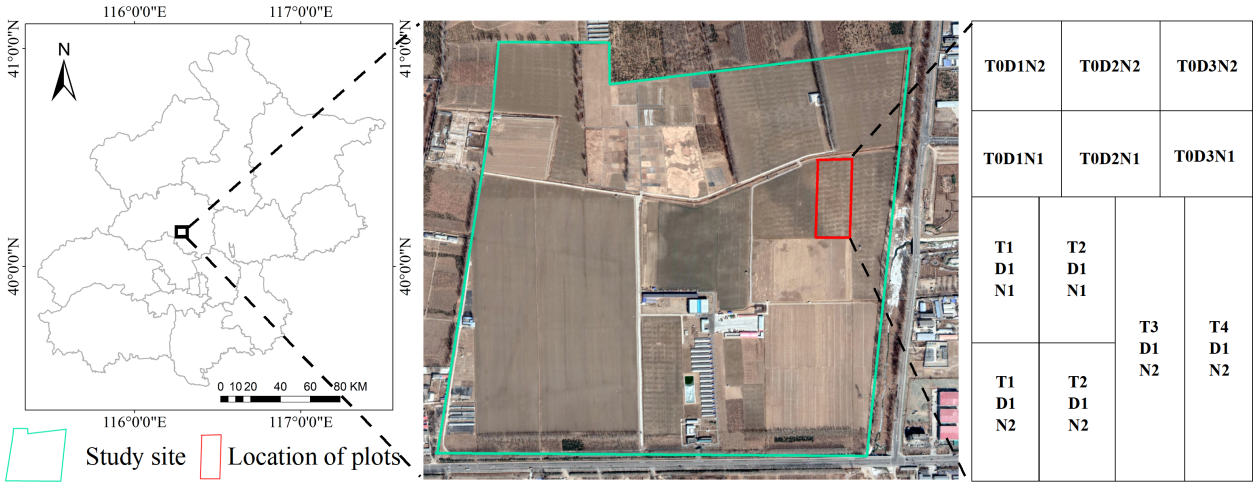

FIGURE 1
Overview of the study area and field trial design in Beijing.

TABLE 1 The collection time of measured data and image data from 2021 to 2023.

Data type	Acquisition time	Data type	Acquisition time	Time interval between measured data and Sentinel-2 image data(day)
	2022/4/08		2022/4/04	4
	2022/4/29		2022/5/02	3
Field measured data	2022/5/20	Sentinel-2	2022/5/22	2
	2023/3/21		2023/3/18	3
	2023/4/08		2023/4/07	1
	2023/5/08		2023/5/07	1

The test crop was winter wheat (Jingdong 18) in the test field from 2022 to 2023, with a sowing depth of 3 cm and a sowing row spacing of 16.7 cm. The sowing time is October 10,2021, and the harvest time is June 15,2022. The sowing amount and fertilization design are the same as those in 2021-2022. In addition to rotation, the same tillage methods as in 2021-2022 are adopted: no-tillage (T0), subsoiling (T1), plow tillage (T2), rotation (T3) (plow tillage in 2021-2022, rotary tillage in 2022-2023) and rotary tillage (T4). The other field management conditions are the same in each plot. The measured data collection time in 2022-2023 is shown in Table 1.

2.3 Data acquisition

2.3.1 Field measured data

The precision of soil parameters directly influences the predictive accuracy of crop growth models, as these parameters are crucial determinants of crop growth and development. In this study, five soil profile parameters were measured across depths of 0 to 20 cm, 20 to 40 cm, 40 to 60 cm, 60 to 80 cm, and 80 to 100 cm, with initial soil water and nutrient values presented in Table 2. Soil parameters and other relevant data for the study area were obtained from the Xiaotangshan Experimental Base and related literature, included measurements of saturated water content, wilting coefficient, and field water holding capacity at various depths. The saturated water content was determined by collecting soil samples from different layers, placing them in containers, and gradually adding water until the soil reached a fully saturated state—indicated by the formation of a layer of free-flowing water on the soil surface. At this point, the soil moisture content was recorded. The wilting coefficient was obtained by place the soil samples in a greenhouse or controlled climate chamber, allowing the soil to dry fully to the permanent wilting point of the plant. The moisture content at this stage represents the wilting coefficient for that specific depth. Field capacity was determined by generating the soil moisture characteristic curve using a measuring instrument and reading the water content corresponding to the field water holding state from the curve. Specific soil parameters are shown in Table 2.

In this study, two methods were employed to calculate and collect LAI: the specific leaf weight method and LAI-2200. The specific leaf weight method is particularly suitable for basic scenarios and standard measurement conditions, while the LAI-2200 is ideal for research and applications requiring higher accuracy and faster measurements. Both methods have their own advantages in different application scenarios. LAI data were obtained by measuring at five different locations within a 100 m^2 plot using the LAI-2200 device, with the average of these measurements calculated to represent the LAI value for the plot. The leaf weight method collects the winter wheat in an area of 0.5m×0.5m and takes the sample of a certain area to randomly select a number of leaf blades and then takes the leaf blades in the width of the narrower more consistent place to cut the length of the small section of 2 or 3 cm. After that, get the width of the blade. Then the area can be calculated. The leaves are dried and weighed. The specific calculations are performed according to the following formula:

$$LAI = \frac{W_1 + W_2}{A * W_1} * S * m \quad (1)$$

where A is the total sample area, m is the number of plants or tillers, S is the selected small part of the sample area, W_1 is the quality of the selected small part of the sample after drying, and W_2 is the quality of the remaining green leaves after drying.

The collection step of aboveground biomass is to select 20 winter wheat plants with uniform growth in the measurement range, separate different plants according to organs (stems, leaves, ears), kill them at 105°C for 30 min, and dry them at 85°C to constant weight. The organs are weighed separately, and the sum is the dry matter weight of the plant, which is recorded as the dry weight of the aboveground part of the plant, and the dry biomass per unit land area is calculated according to the density.

2.3.2 Meteorological data

As shown in Figure 2, APSIM models rely on meteorological data as the basic input for their operation, which include daily average temperature and daily radiation. The climate data of the Xiaotangshan area are derived from the meteorological products provided by the European Centre for Medium-Range Weather Forecasts (https://cds.climate.copernicus.eu/). The spatial resolution is 0.25°×0.25°, and the time resolution is hourly. The daily precipitation (mm), daily radiation (MJ/m^2), daily maximum temperature (°C), daily minimum temperature (°C), and daily potential evaporation (mm) are input into the weather model.

2.3.3 Remote sensing data

This study uses Sentinel-2 data from the GEE cloud platform. The Google Earth Engine (GEE) platform offers Sentinel-2 satellite images in two product types, determined by the level of preprocessing

TABLE 2 Soil parameters.

Depth(cm)	Volume weight of soil ($g \cdot cm^{-3}$)	Saturation capacity ($cm^3 \cdot cm^{-3}$)	Wilting coefficient ($cm^3 \cdot cm^{-3}$)	Field capacity ($cm^3 \cdot cm^{-3}$)
0-20	1.32	0.48	0.10	0.34
20-40	1.43	0.46	0.12	0.33
40-60	1.43	0.46	0.13	0.32
60-80	2.04	0.47	0.15	0.31
80-100	1.93	0.47	0.14	0.31

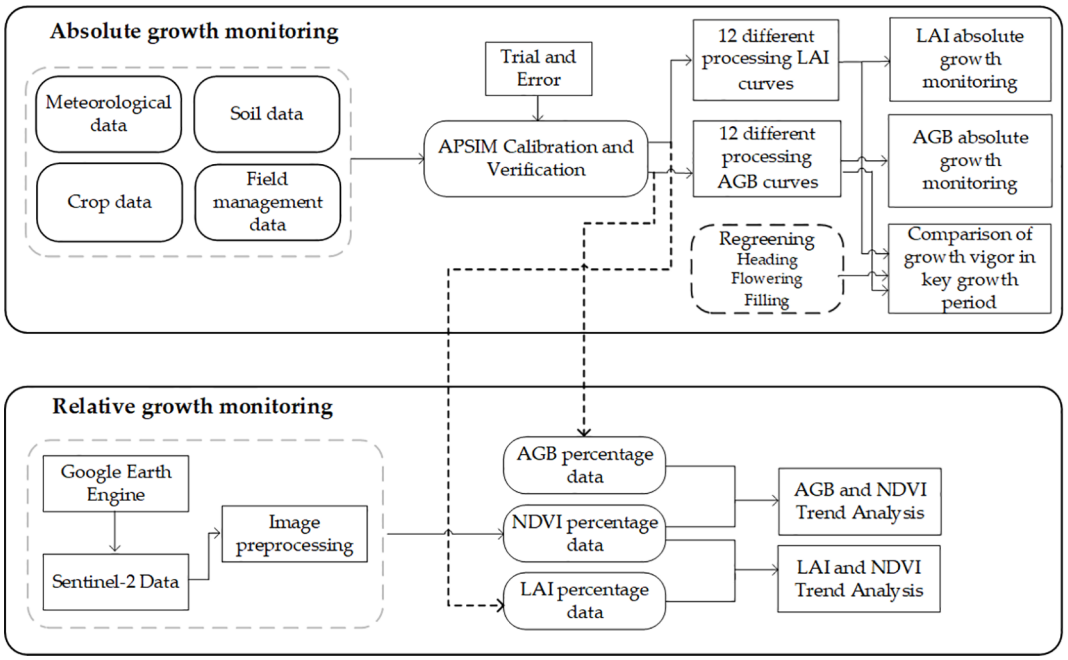

FIGURE 2
Technical route.

applied. Compared with TOA data, SR data have better data consistency and stability in time series. Given the revisit cycle, images were chosen to align as closely as possible with the timing of the field-measured data collection. The acquisition times for both the field measured data and the image data are presented in Table 1.

2.4 APSIM model and calibration

APSIM is a mechanism model that uses a general growth process to simulate the development and growth of crops (Huang et al., 2018; Zhu et al., 2023a). The model integrates various sub-modules—including crop, soil, management, and meteorology—into a modular framework, with meteorological data, crop data, soil data, and field management practices input into their respective sub-modules. Meteorological data, including precipitation, radiation, maximum and minimum temperatures, and potential evaporation, are used to drive the model, and assess crop responses and adaptations to climate change. Crop growth data encompass the phenological development of crops, such as growth stage scales, accumulated temperature calculations, and photosynthesis algorithms, and help the model simulate the entire crop life cycle from sowing to harvest. Soil data, which include the physical and chemical properties of the soil, are crucial for simulating root growth as well as water and nutrient uptake. Field management data, such as sowing time, sowing density, and fertilizer application, this allows the model to analyze the potential impacts of various management strategies on crop growth and yield.

The model must go through a series of debugging and calibration before application (Liu et al., 2023). Therefore, this study selected the data from 2021-2022 to calibrate the model, and verified the model through the data from 2022-2023. In the model calibration, this study went through the following steps. First, basic data such as meteorology, soil, and field management were input to run the model. Secondly, the LAI and AGB and other simulation results of the model operation were compared with the measured data, and the trial and error method, which is currently more common in model calibration, was used to gradually adjust the sensitive parameters until the measured data of different test schemes matched the simulation results (Liang et al., 2016; Chen et al., 2019; Jin et al., 2021; Wang et al., 2023c). Finally, the parameter values were determined to complete the model calibration. Regarding the selection of sensitive parameters, because the sensitive parameters of models in different climate regions are different, this study selected literature with the same or similar distance to the experimental area, and selected parameters that have a greater impact on the model results from the literature. Based on this standard, sensitive parameters were selected, and finally 5 crop parameters that are more sensitive to leaf area index and aboveground biomass were selected (Liu et al., 2011; He and Zhao, 2015; Xing et al., 2017b; Zhang et al., 2023). As shown in Table 3.

2.5 Method

2.5.1 Absolute growth monitoring of winter wheat based on APSIM model

The accuracy of LAI and AGB of winter wheat simulated by the APSIM model was assessed through comparing the simulated values against the measured values. The determination coefficient (R^2), root mean square error (RMSE) and normalized root mean square error

10.3389/fpls.2024.1500103

TABLE 3 Parameters after calibration.

Crop	Parameter	Lower bound	Upper bound	Initial Settings	Parameters after calibration
	vern_sens	0	5	1.5	3.1
	photop_sens	0	5	3.0	3.5
Wheat	Startgf_to_mat(°C/d)	200	900	580	550
	Potential_grain_filling_rate(mg/d)	0.001	0.005	0.0027	0.0029
	grains_per_gram_stem(grain/d)	10	40	27.6	29.5
	max_grain_size(g)	0.02	0.06	0.048	0.046

(NRMSE) were used as the evaluation criteria for the growth results, calculated using Equations 2-4. The absolute growth range of LAI and AGB was compared across four key growth periods. In this paper, the specific growth periods of winter wheat, as determined by both domestic and international literature and experience, are presented in Table 4. The key growth stages selected for the relative growth study include regreening, heading, flowering, and filling. The technical route of this study is shown in Figure 2.

$$R^2 = \frac{\sum_{i=1}^{n}(X_i - \bar{X})^2(Y_i - \bar{Y})^2}{n\sum_{i=1}^{n}(X_i - \bar{X})^2\sum_{i=1}^{n}(Y_i - \bar{Y})^2} \quad (2)$$

$$RMSE = \sqrt{\frac{\sum_{i=1}^{n}(Y_i - X_i)^2}{n}} \quad (3)$$

$$NRMSE = \frac{RMSE}{\bar{X}} \times 100\,\% \quad (4)$$

where n denotes the number of samples, X_i, $\bar{X}$, Y_i, $\bar{Y}$ represent the actual observation data, the actual observation data mean, the model's prediction data, and the model prediction data mean, respectively.

2.5.2 Relative growth monitoring of winter wheat based on APSIM model combined with remote sensing data

To study the relative growth of crops, vegetation indices provide crucial information for monitoring crop growth dynamics. Common vegetation indices include RVI (Gonenc et al., 2019), NDVI (Huang et al., 2021), DVI (Gunathilaka, 2021), and EVI (Shammi and Meng, 2021), etc. Of these, NDVI is the most widely used index for assessing vegetation conditions, as it is particularly sensitive to the growth status of vegetation and can directly reflect its health. The NDVI calculation formula is as follows:

$$NDVI = \frac{NIR - R}{NIR + R} \quad (5)$$

where NIR corresponds to the B8 band of the Sentinel-2 data, and R corresponds to the B4 band of the Sentinel-2 data.

In this paper, Sentinel-2 data is used to monitor the relative growth of winter wheat by using NDVI and APSIM models. We analyzed the correlation between NDVI, LAI, and AGB using Pearson's correlation coefficient. NDVI data for six periods from 2021 to 2023 were obtained from the study area. For each of the three periods in 2022, the corresponding NDVI data from 2023 were subtracted and then divided by the 2022 NDVI data to calculate nine sets of NDVI percentage differences. In addition, the same method was used to calculate the difference percentage data between LAI and AGB output by APSIM model respectively The calculation method is shown in Formula 6. Pearson correlation analysis was then performed using the NDVI percentage difference data along with the percentage difference data for LAI and AGB. Through the Pearson correlation coefficient and P-value, the trends in relative growth in the study area were analyzed. Pearson's correlation coefficient was calculated as shown in Equation 7.

$$X_{\text{percentage data}} = 1 - \frac{2023X_b}{2022X_a} \quad (6)$$

Where X represents NDVI, LAI, or AGB, a represents the three measured data dates in 2022, and b represents the three measured data dates in 2023.

$$r = \frac{\sum_{i=1}^{n}(X_i - \bar{X})(Y_i - \bar{Y})}{\sqrt{\sum_{i=1}^{n}(X_i - \bar{X})^2}\sqrt{\sum_{i=1}^{n}(Y_i - \bar{Y})^2}} \quad (7)$$

where X_i represents the value of remote sensing NDVI of the ith sample, $\bar{X}$ is the average value of remote sensing NDVI sample, Y_i is

TABLE 4 Key growth period of winter wheat.

Item	Phenological phase									
	Emergence	Tillering	Wintering	Regreening	Jointing	Booting	Heading	Flowering	Filling	Maturity
2022/2023	10/16	11/2	1/4	3/18	4/13	4/25	5/5	5/15	5/26	6/10

the model simulation value of LAI or AGB of sample *i*, $\bar{Y}$ is the average value of LAI or AGB model simulation, n is the number of samples.

After calculating the correlation coefficient *r*, it needs to be tested whether it is statistically significant, i.e., whether it is significant or not, and its formula is shown in (8). Consult the t distribution to determine the corresponding P value.

$$t = \frac{r\sqrt{n-2}}{\sqrt{1-r^2}} \quad (8)$$

3 Results

3.1 Absolute growth monitoring of winter wheat based on LAI and AGB model simulation data

3.1.1 Absolute growth monitoring of winter wheat based on LAI model simulation data

Figure 3 shows the dynamic change changes in LAI as the growth index under varying fertilization, sowing, and tillage treatments during in 2021-2022 and 2022-2023 growing seasons. In this study, experimental data from the 2021 to 2022 winter wheat season were used to calibrate the model parameters, while data from the 2022 to 2023 season were employed for model validation. The analysis focused on the LAI growth of winter wheat in Xiaotangshan from 2021 to 2023. As the winter wheat growth period progressed, the LAI remained relatively stable during the overwintering phase. After regreening (about 170 d), winter wheat entered a phase of rapid growth, with LAI peaking towards the end of the growth period (210 d). Following the filling stage, LAI began to decline, approaching zero by the end of the filling period (about 250 d). Although the LAI values in different periods are different under different fertilization rates, seeding rates, and tillage methods, they all have a common growth trend, from regreening to maturity, LAI showed a parabolic trend. From the results of absolute growth monitoring in 2021-2023: (1) Other conditions are consistent, under different fertilization conditions. N2 (normal fertilizer rate) had relatively higher LAI and better growth, and halving the fertilizer rate resulted in relatively smaller leaf area of winter wheat plants, with a reduction of 0.12 to 1.08 in the peak LAI of the model simulation. (2) Other conditions are the same, under different seeding rates. From 2021 to 2022, D1 (normal seeding rate) grew better than D2 (50% seeding rate), and LAI was higher. However, when the fertilizer was halved, from 2021 to 2022, D3 (75% seeding rate) grew better than D1 (normal seeding rate) and D2 (50% seeding rate), and from 2022 to 2023, D3 (75% seeding rate) and D1 (normal seeding rate) grew similarly. The reason may be that the appropriate reduction of seeding rate leads to the improvement of light and nutrient utilization efficiency and thus promotes growth. (3) Other conditions are the same, under different tillage methods, the LAI of winter wheat in 2021-2022 shows T1 > T4 > T2 > T3, and the LAI of winter wheat in 2022-2023 shows T1 > T3 > T4 > T2. Subsoiling tillage showed better growth results than other tillage methods. From 2021 to 2022, the determination coefficient R^2 for growth results using LAI as the growth index under different tillage, fertilization, and sowing treatments ranged from 0.85 to 0.98, with RMSE values between 0.02 and 0.51, and NRMSE values ranging from 1.1% to 18.3%. From 2022 to 2023, the R^2 values ranged from 0.92 to 0.98, RMSE from 0.03 to 0.22, and NRMSE from 1.4% to 15%. The meaning of the field number is shown in Table 5.

As shown in Figure 4, the accuracy results of absolute growth monitoring with LAI as the growth index were given under different fertilization rates, seeding rates, and tillage methods in 2021-2023. The R^2 of simulated LAI in 2021-2023 was 0.943, and the simulated LAI was in good agreement with the measured LAI. The RMSE was 0.291, and the NRMSE was 12.9%.

3.1.2 Absolute growth monitoring of winter wheat based on AGB model simulation data

As shown in Figure 5, the dynamic change results of AGB under different fertilization, seeding amount and tillage methods in 2021-2022 and 2022-2023. Throughout the winter wheat growth period, the APSIM model simulated a general upward trend in AGB, with the growth rate significantly accelerating after the regreening period (about 175 d). The growth rate peaked near the end of the growth period (about 210d), after which it gradually slowed, with biomass accumulation ceasing by the end of the filling stage (about 250 d). 2021-2023, from the results of absolute growth monitoring: (1) Other conditions are consistent, under different fertilization conditions. From 2021 to 2022, the AGB of N2 (normal fertilization) was relatively high and the growth was better. The reason may be that the halving of fertilization amount makes the imbalance of nutrient supply and demand of winter wheat plants and the chlorophyll content of leaves decrease, and the photosynthesis ability decreases, thereby reducing the accumulation of AGB. (2) Other conditions are the same, under different seeding rates. From 2021 to 2022, D1 (normal seeding rate) grew better than D2 (50% seeding rate), but from 2021 to 2023, D3 (75% seeding rate) grew better than D1 (normal seeding rate). (3) Other conditions are the same, under different tillage methods. The AGB of winter wheat in 2021-2022 showed T1 > T4 > T2 > T3, and the AGB of winter wheat in 2022-2023 showed T1 > T3 > T2 > T4. Subsoiling tillage showed better growth results than other tillage methods. From 2021 to 2022, the determination coefficient R^2 for growth results using AGB as the growth index under different tillage, fertilization, and sowing treatments ranged from 0.85 to 0.95, with RMSE values between 0.18 t/ha to 1.75 t/ha, and NRMSE values ranging from 1% to 35.6%. From 2022 to 2023, the R^2 values ranged from 0.9 to 0.97, RMSE from 0.15 t/ha to 0.75 t/ha, and NRMSE from 3% to 9%.

As shown in Figure 6, the absolute growth monitoring accuracy results using AGB as growth index under different fertilization, seeding and tillage methods from 2021 to 2023 were presented. The R^2 of the simulated AGB in 2021-2023 is 0.907, and the simulated AGB is in good agreement with the measured AGB. The RMSE is 0.872 t/ha, and the NRMSE is 20.9%.

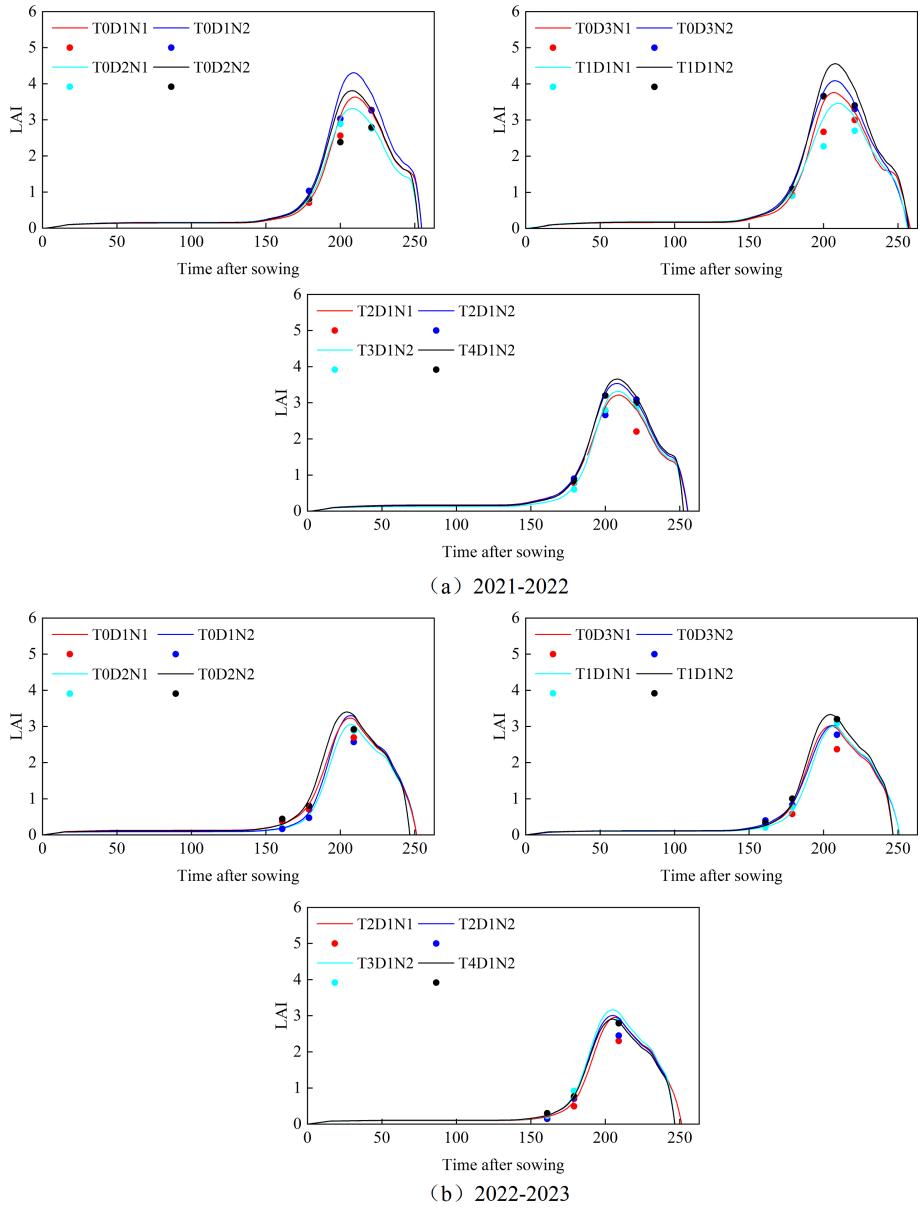

FIGURE 3
(A) Absolute growth monitoring of winter wheat LAI simulated by APSIM model under different tillage methods, fertilization and sowing treatments from 2021 to 2022; **(B)** Absolute growth monitoring of winter wheat LAI simulated by APSIM model under different tillage methods, fertilization and sowing treatments from 2022 to 2023. The curve represents the simulated value, and the point represents the measured value.

3.1.3 Comparison of the absolute growth results of LAI and AGB in the key growth period of winter wheat simulated by the model

As shown in Figure 7, this study compared the variation in LAI and AGB across four key growth stages of winter wheat—regreening, heading, flowering, and filling—over two years and 12 different treatments, using simulations from the APSIM model. The results showed that the changes of LAI and AGB parameters simulated by APSIM model were roughly the same under different treatments in the key growth period of winter wheat. Except for T2D1N2 (normal sowing, plow tillage, and normal fertilization) at the winter wheat regreening stage in 2021-2022 and T0D3N2 (no-tillage, normal sowing, and normal fertilization) at the tasseling, flowering, and irrigating stages of winter wheat in 2022-2023, which did not have the same trend as the neighboring treatments, other treatments showed the results of the same trend of change. The reason for the inconsistent trend of the former may be that winter wheat adjusts its growth to adapt to the environment. Under sufficient fertilization conditions, winter wheat may prioritize root development over leaf growth to adjust to potential nutrient changes. The reason for the inconsistent trend of the latter may be that subsoiling tillage improves soil physical and chemical properties. In contrast, no-tillage may cause soil compaction, hindering root growth and leaf expansion of winter wheat. During key growth stages like heading, flowering, and filling, winter wheat is more sensitive to environmental conditions,

TABLE 5 The specific meaning of field number.

The plot number	Processing mode	The plot number	Processing mode
T0D1N2	No-tillage, normal sowing rate, normal fertilization rate	T1D1N1	Subsoiling tillage, normal sowing rate, half of the amount of fertilizer
T0D2N2	No-tillage, 50% seeding rate, normal fertilizer rate	T1D1N2	Subsoiling tillage, normal sowing rate, normal fertilization rate
T0D3N2	No-tillage, 75% seeding rate, normal fertilizer rate	T2D1N1	Plow tillage, normal seeding rate, half the amount of fertilizer
T0D1N1	No-tillage, normal sowing rate, half of the amount of fertilizer	T2D1N2	Plow tillage, normal sowing amount, normal fertilization amount
T0D2N1	No-tillage, 50% seeding rate, half of the amount of fertilizer	T3D1N2	Rotation tillage, normal sowing rate, normal fertilization rate
T0D3N1	No-tillage, 75% seeding rate, half of the amount of fertilizer	T4D1N2	Rotary tillage, normal sowing rate, normal fertilization rate

making the differences more pronounced. From the perspective of different key growth periods, the regreening stage is characterized by relatively slow growth and recovery due to low temperatures and other limiting factors, resulting in minimal accumulation of LAI and AGB. Consequently, the changes during the regreening period are less noticeable compared to other key growth stages, making it less suitable for distinguishing the effects of different treatments on winter wheat growth.

3.2 Relative growth monitoring of winter wheat based on the combination of model simulation parameters and remote sensing inversion parameters

3.2.1 Trend consistency analysis of LAI and NDVI winter wheat relative growth monitoring by remote sensing

As shown in Figure 8, Sentinel-2 data were selected to calculate the NDVI percentage data and LAI percentage data from 2021-2023 in the research area through GEE platform. These two sets of data were then fitted according to different fertilization rates, seeding rates, and tillage methods to monitor and analyze relative growth. The remote sensing NDVI data from 2021 to 2023 and the simulated LAI data were used as growth indicators for data fitting, and the Pearson correlation analysis was performed. The correlation coefficient r value ranged from 0.759 to 0.948. In the case of T4D1N2, the correlation between LAI percentage data and NDVI percentage data was the best, showing a strong correlation of 0.949 ($p< 0.001$), and T2D1N2 was the worst, showing a strong correlation of 0.759 ($p< 0.05$). Meanwhile, in terms of significance, except for T2D1N2 and T0D3N1, which showed significance ($p< 0.05$), all other cases showed highly significant ($p< 0.01$). Overall, the linear correlation between the two variables was significant, except for T2D1N2 and T0D3N1 which showed a strong correlation, all other cases showed a very strong correlation, all of them had strong linear positive correlation, indicating that it can well reflect the link between LAI and NDVI, and that the fitted correlation between the data in the different cases was better and all of them were significantly positively correlated ($p< 0.05$).

As shown in Figure 9, the correlation coefficient r value of the model simulated LAI percentage data and NDVI percentage data in 2021-2023 was 0.818 ($p< 0.001$), and the simulated LAI percentage data showed a highly significant positive correlation with the NDVI percentage data. In addition, the percentages of NDVI and LAI data, both greater than 0, accounted for about 82%, which suggests that winter wheat growth conditions in 2022 are better than those in 2023.

3.2.2 Trend consistency analysis of AGB and NDVI remote sensing monitoring of relative growth of winter wheat

Using the Sentinel-2 data of GEE platform, NDVI percentage data and AGB percentage data from 2021-2023 in the study area were calculated. These two sets of data were then fitted according to different fertilizer application rates, seeding rates, and tillage

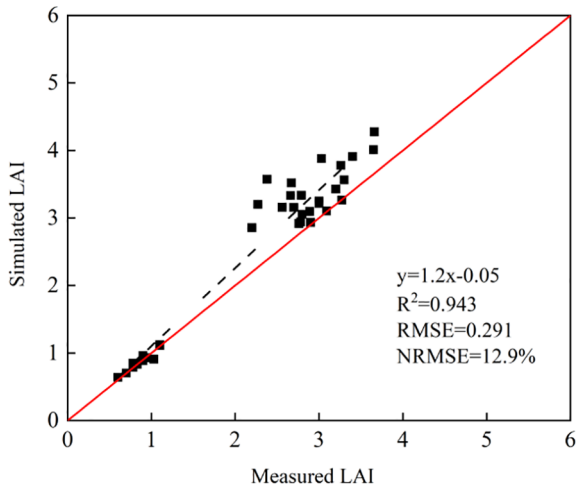

FIGURE 4
Evaluation of LAI growth accuracy from 2021 to 2023.

10.3389/fpls.2024.1500103

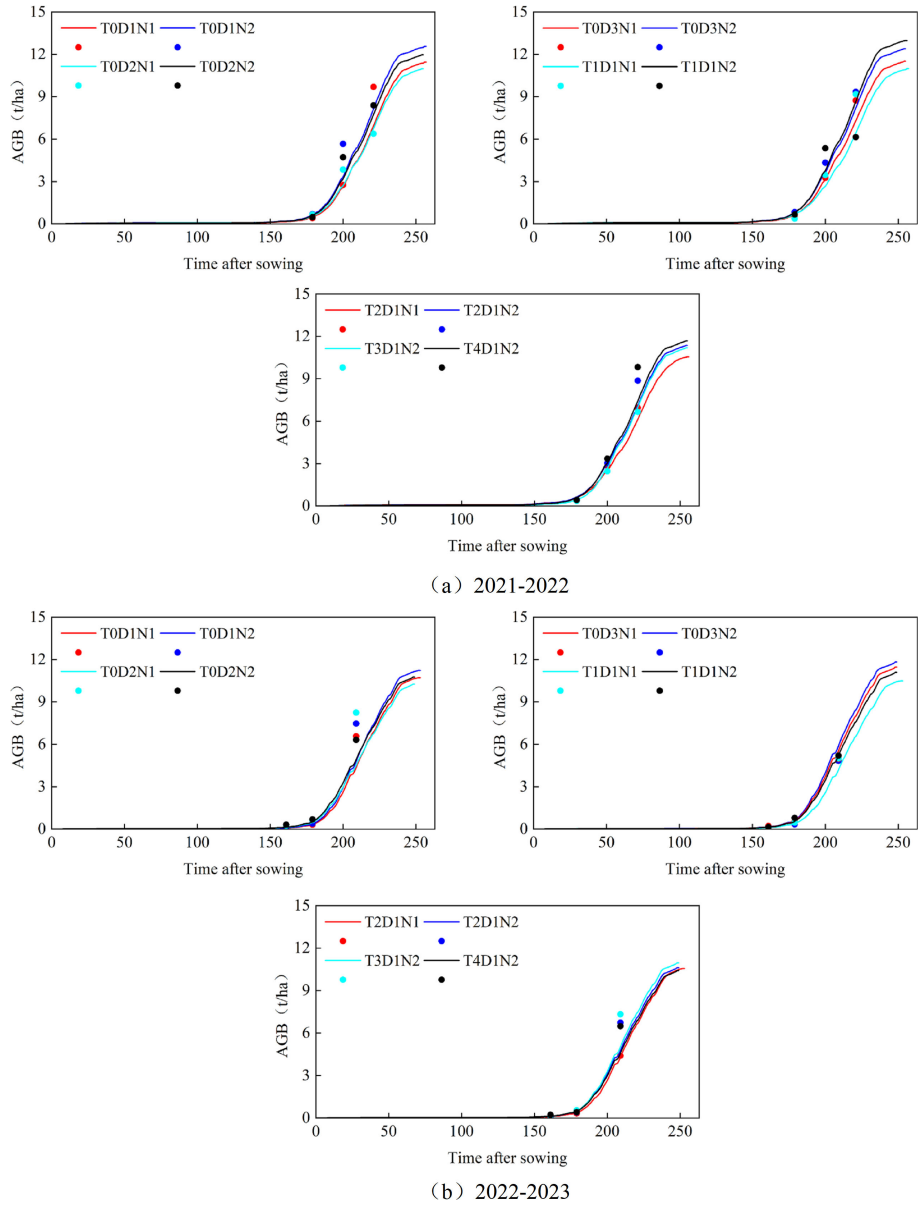

FIGURE 5
(A) Absolute growth monitoring of winter wheat AGB simulated by APSIM model under different tillage methods, fertilization and sowing treatments from 2021 to 2022; **(B)** Absolute growth monitoring of winter wheat AGB simulated by APSIM model under different tillage methods, fertilization and sowing treatments from 2022 to 2023. The curve represents the simulated value, and the point represents the measured value.

practices to perform relative growth monitoring. As shown in Figure 10. The NDVI data based on the remote sensing and model simulated AGB data from 2021-2023 were fitted to the data as a growth indicator, and Pearson correlation analysis was performed, and the r values ranged from 0.741 to 0.927, and the correlation between the data in different cases was good and all of them showed a positive correlation. The best correlation between the AGB percentage data and the NDVI percentage data was found in the case of T4D1N2, which showed a very strong correlation of 0.927 ($p< 0.001$), and the worst in the case of T2D1N1, which showed a strong correlation of 0.741 ($p< 0.05$). Meanwhile, in terms of significance, all cases showed highly significant differences ($p< 0.01$) except for T2D1N1 and T0D3N1, which showed significant differences ($p< 0.05$).

As shown in Figure 11, the correlation coefficient r value was 0.808 ($P< 0.001$) for the simulated AGB difference percentage data and NDVI difference percentage data in 2021-2023, and these data showed highly significant positive correlation. Moreover, the percentage data for which the difference between NDVI and AGB is greater than 0 accounts for about 80%, the AGB results also indicate that the growth conditions for winter wheat in 2022 are better than those in 2023.

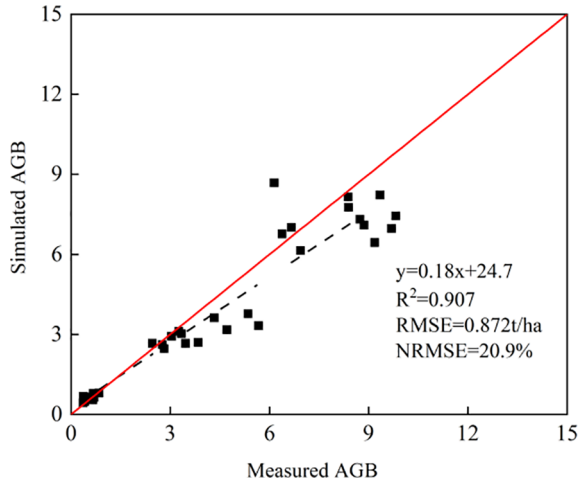

FIGURE 6
Evaluation of AGB growth accuracy from 2021 to 2023.

4 Discussion

4.1 The role of APSIM model in monitoring the growth of winter wheat under different treatments and optimizing field management

Crop model can dynamically monitor the growth process of crops (Ren et al., 2011; Xing et al., 2017a). This study shows that the APSIM model shows significant application prospects for monitoring the growth dynamics of winter wheat. In this study, the growth curves of LAI and AGB of winter wheat were obtained. From the LAI growth curve, we can observe that after the wintering period, as the temperature increases, the plants start to grow rapidly, necessitating a significant amount of nutrients and water. Providing appropriate nutrients from the regreening stage to the jointing stage will greatly benefit the growth of winter wheat. Zhao et al. found that the change in NDVI during these two periods was

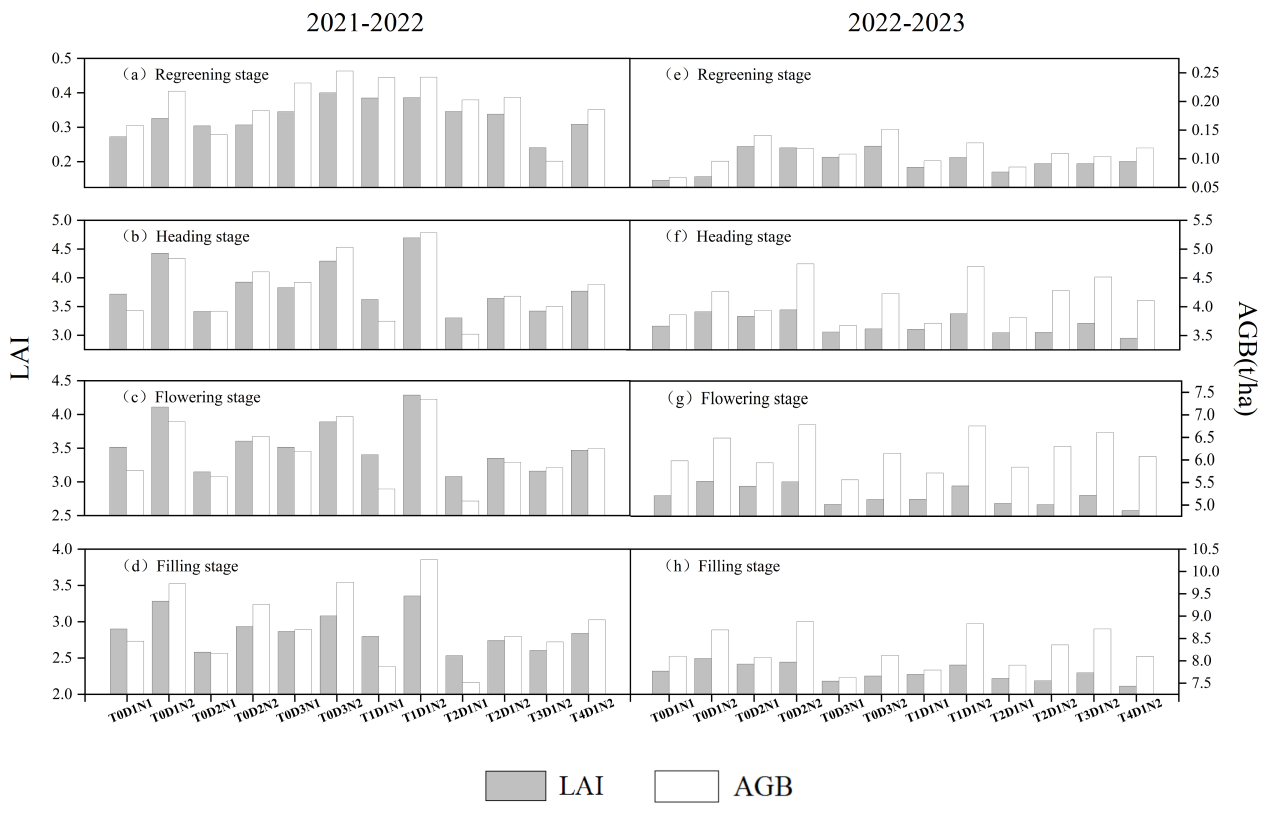

FIGURE 7
APSIM model simulates the changes in LAI and AGB of winter wheat in four key growth periods of 2021-2022 **(A–D)** and 2022-2023 **(E–H)** under different treatments.

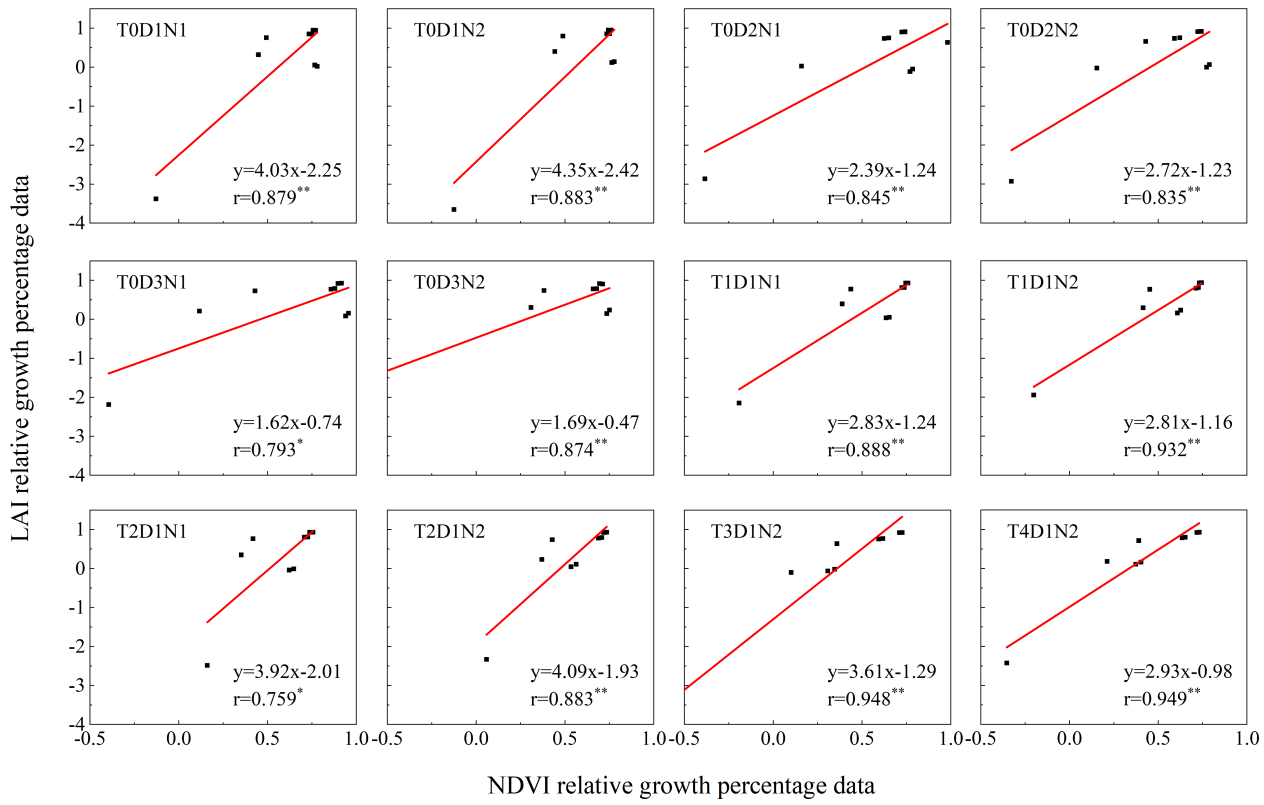

FIGURE 8
Analysis of NDVI and LAI growth in the study area under different tillage methods, fertilization and sowing treatments from 2021 to 2023. Among them, * indicates significance and ** indicates extremely high significance.

relatively large when extracting winter wheat area by NDVI, so they also put forward this view (Zhao et al., 2011). As LAI started to decline, while AGB continued to increase, it was observed that the growth rate slowed down. This suggests that the leaves of winter wheat are approaching saturation, more energy is being directed towards grain formation, and the photosynthetic efficiency is relatively reduced.

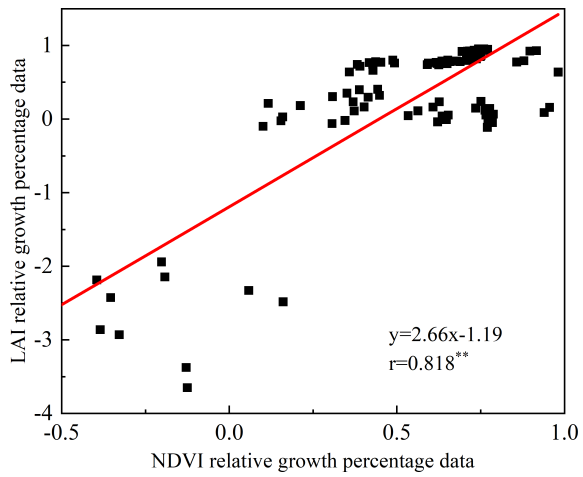

FIGURE 9
Relative growth analysis of NDVI and LAI from 2021 to 2023. Where "**" indicates the significance test result.

In the analysis of different tillage practices, fertilization, and sowing treatments by using the APSIM model, when two gradients of fertilizer application were applied in this study, we found that other conditions were consistent while different fertilizer application rates were applied, the different treatments showed better growth at the normal fertilizer application rate than at the halved fertilizer application rate, which indicated that the reduction of fertilizer application rate in certain cases had a negative impact on the growth and development of the crop, and that the subsequent study could increase the fertilizer application gradient to determine the optimum fertilizer application rate. Among the treatments with the same other conditions but different sowing rates, 75% of the sowing rate in some treatments of LAI and AGB showed better growth than the other sowing rates, indicating that appropriate reduction in sowing rate can promote wheat growth. When studying the effect of sowing density on the growth and yield of wheat, Xiao et al. found that reducing the sowing rate could stimulate wheat plants to produce more tillers and secondary roots, and promote an increase in plant height, suggesting that appropriate growth density can utilize the available resources, such as sunlight, water, and nutrients, in a more efficient manner (Xiao et al., 2021). Among the treatments with the same other conditions but different tillage methods, the growth of winter wheat was relatively better under deep loosening tillage treatment, and the related research of Feng et al. showed that compared with different tillage methods, subsoiling tillage could significantly increase the organic carbon content in the topsoil and enhance the water

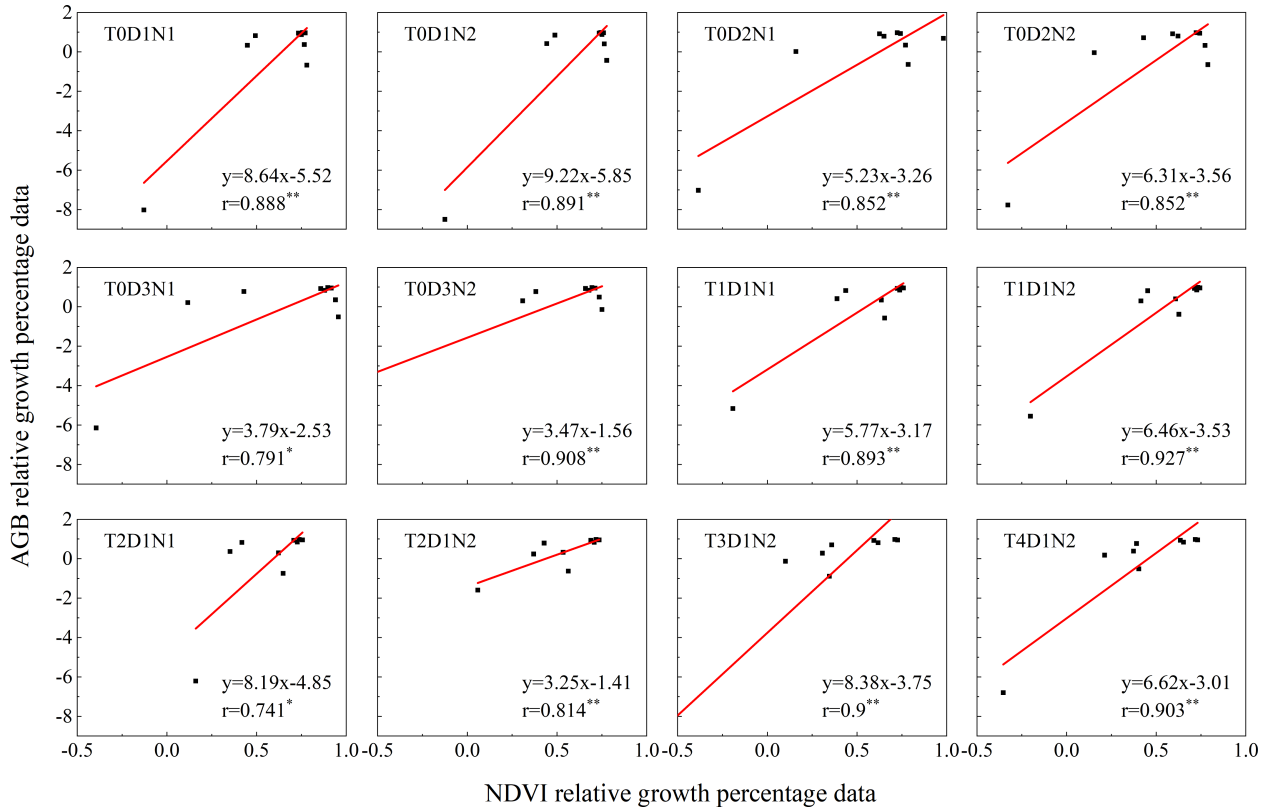

FIGURE 10
Analysis of NDVI and AGB growth in the study area under different tillage methods, fertilization and sowing treatments from 2021 to 2023. Where "*" and "**" represent significant and extremely significant difference results respectively.

holding capacity of the soil, which might be the reason for promoting the growth of winter wheat (Feng et al., 2018). The growth curves of LAI and AGB in different years and under different treatments showed that the growth curves of LAI and AGB in subsoiling tillage, normal sowing, and normal fertilization were better than those in other treatments, and the growth trends of LAI and AGB were significantly greater than those in other treatments, indicating that this treatment may provide more optimized growth conditions, including soil looseness and nutrient supply, etc. these treatments improved the growth environment of plants. Therefore, the most suitable field management methods for winter wheat in these 12 cases are subsoiling tillage, normal sowing, and normal fertilization.

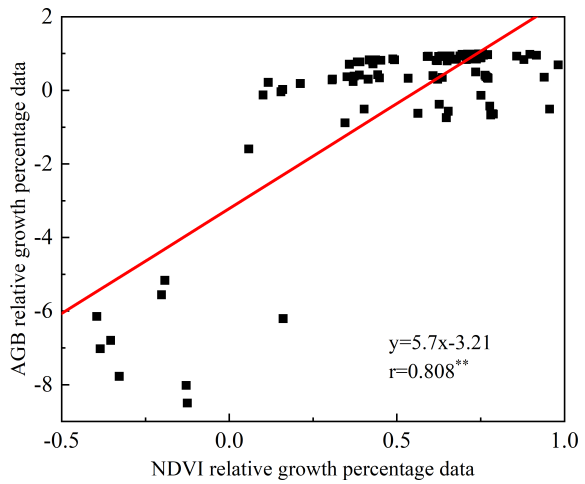

FIGURE 11
Relative growth analysis of NDVI and AGB from 2021 to 2023. Where "**" indicates the significance test result.

4.2 Analysis of correlation results between model simulation parameters and remote sensing inversion parameters

Compared with previous growth monitoring, relative growth remote sensing monitoring relies largely on vegetation indices such as NDVI (Su et al., 2019; Lu et al., 2020) and rarely incorporates other variables. In this study, in addition to NDVI, LAI and AGB are closely related to the growth of winter wheat and are added for trend consistency analysis and are used to comprehensively evaluate the crop's growth status and changes in the growth status from different perspectives (Zheng et al., 2017; Qin et al., 2022). The comparison between NDVI extracted by Sentinel-2 data with 10m spatial resolution and LAI and AGB data simulated by the model showed that the correlation coefficient r value exceeded 0.74, indicating a positive correlation between LAI and AGB data

simulated by NDVI and APSIM models. This is consistent with the obvious positive correlation between NDVI and LAI in different growth periods of winter wheat proposed by Liang et al. (2013) in the inversion of LAI, and the obvious correlation between above-ground biomass and NDVI in the main growth period of winter wheat proposed by Hansen and Schjoerring (2003) in the relevant study. It means that with the increase or decrease of NDVI, LAI and AGB will also increase or decrease to a certain extent.

From the growth consistency results of LAI and AGB and NDVI respectively, the three cases of T1D1N2, T3D1N2, and T4D1N2 showed extremely strong correlation ($r > 0.9$) in LAI and NDVI and AGB and NDVI, and the worst correlation was also the same both for T2D1N1, which also showed strong correlation. In terms of significance, except for T2D1N2 and T0D3N1, which showed significance ($p< 0.05$), all other cases showed highly significant ($p< 0.01$), and the results showed significant correlation, which indicated that correlations due to random factors could be excluded, such as climatic conditions, human activities, and equipment. And it was found that NDVI, AGB and LAI difference percentage data were all greater than 0 accounted for more than 80%, indicating that winter wheat in 2022 under different scenarios grew better than them in 2023. In terms of LAI and AGB structural characteristics, LAI directly reflects the degree of leaf cover and leaf area, leaf density and leaf arrangement of winter wheat plants (Lu et al., 2005), while AGB reflects winter wheat biomass accumulation and plant height, stem thickness, branching status and spike size (Guo et al., 2023). From the results and the structural characteristics of LAI and AGB, the LAI and AGB simulated by the APSIM model can better reflect the growth condition of winter wheat, which is more reliable than relying on NDVI only for relative growth monitoring.

4.3 Limitations of APSIM model in winter wheat growth monitoring

From the results of absolute growth of LAI simulated by the APSIM model, the growth simulated during the regreening period was more accurate, but the results of the simulation in the later part of the growth period were on the high side, which may be due to the inaccurate estimation of the model for the process of the decay of the leaf area in the later part of the growth period, or the possible existence of errors and uncertainties in the measured data, for example, due to errors caused by the measurement method, equipment, or sampling errors (Wang and Wang, 2015). In the later research, parameter sensitivity analysis should be combined to determine which parameters have the greatest impact on the accuracy of simulation results. From the absolute growth results of AGB simulated by APSIM model, it can be seen that at the end of the growth period (about 210 d), some of the simulated values are low. Which may be due to the failure of the model to accurately simulate the changes in soil moisture and nutrients and their effects on plant growth, and the simulated biomass may be low, especially in the final stages of crop growth, the supply of water and nutrients has an important impact on plant biomass accumulation (Guo et al., 2016). In later studies, a more precise division of the growth stages in the model is needed, and the model parameters are adjusted according to the characteristics and needs of each stage in order to better capture the sensitivity to water and nutrients at the end of growth. Precision agriculture and smart agriculture are the main development direction of current and future agriculture (Zhao et al., 2021). In the next step, based on the evaluation of the simulation results and the analysis of the shortcomings, we can further improve the APSIM growth model, especially in simulating the leaf area decaying process in the late growth stage and the effects of soil moisture and nutrients on plant growth, or extend the study to other crops or different environmental conditions to verify the generalizability of the study results. This could help agricultural producers and policy makers to understand the growth requirements and optimal management strategies for different crops.

5 Conclusions

In this study, the APSIM model and Sentinel-2 data were used to monitor both the relative and absolute growth of winter wheat under various tillage methods, fertilization rates, and sowing treatments. In terms of relative growth monitoring, absolute growth was further validated using remote sensing data, and there was a significant linear positive correlation between NDVI based on the Sentinel-2 data and both LAI and AGB data derived from the APSIM model ($r>0.74$, $p<0.05$). It was found that the best correlation with NDVI data ($r>0.9$, $p<0.001$) was obtained in the case of normal sowing, normal fertilizer application and rotary tillage. In terms of absolute growth monitoring, the growth of winter wheat was relatively poor in the area where the amount of fertilizer was halved compared to the area with a standard amount of fertilizer. Properly reducing the sowing rate can help to improve the growth of winter wheat. In the case of only different tillage methods, subsoiling tillage shows better growth than other tillage methods. In this paper, compared with other treatments, the most suitable management methods for winter wheat are subsoiling tillage, normal sowing, and normal fertilization. The results showed that the LAI and AGB indicators simulated by the APSIM model could better reflect the growth condition of winter wheat, and were more reliable than relying only on vegetation indices such as NDVI for relative growth monitoring.

Data availability statement

The original contributions presented in the study are included in the article/supplementary material. Further inquiries can be directed to the corresponding authors.

Ethics statement

Ethical approval was not required for the study involving humans in accordance with the local legislation and institutional requirements. Written informed consent to participate in this study was not required from the participants or the participants' legal guardians/next of kin in accordance with the national legislation and the institutional requirements.

Author contributions

YT: Writing – review & editing, Writing – original draft, Visualization. EC: Writing – review & editing, Supervision, Formal analysis. XF: Writing – review & editing, Supervision. BZ: Writing – review & editing, Supervision, Project administration, Investigation. JC: Writing – review & editing, Supervision, Resources. QX: Writing – review & editing, Supervision, Data curation. HP: Writing – review & editing, Supervision. CJL: Writing – review & editing, Supervision. CL: Writing – review & editing, Supervision. YL: Writing – review & editing, Supervision. BZ: Writing – review & editing, Supervision, Resources, Funding acquisition. DP: Writing – review & editing, Validation, Supervision, Resources, Project administration, Funding acquisition, Conceptualization.

Funding

The author(s) declare financial support was received for the research, authorship, and/or publication of this article. This research was funded by the National Natural Science Foundation of China (42030111, 42401467, 42471372), Natural Science Foundation of Henan Province (242300421363), and Shandong Agricultural University Research Fund(381807).

Conflict of interest

The authors declare that the research was conducted in the absence of any commercial or financial relationships that could be construed as a potential conflict of interest.

Publisher's note

All claims expressed in this article are solely those of the authors and do not necessarily represent those of their affiliated organizations, or those of the publisher, the editors and the reviewers. Any product that may be evaluated in this article, or claim that may be made by its manufacturer, is not guaranteed or endorsed by the publisher.

References

A, L., and Xu, D. (2021). Optimizing biochar and fertilizer application to improve rice production in reclaimed coastal saline soils using the ORYZA_V3 crop model. *J. Irrig. Drain. Div.* 40, 66–71. doi: 10.13522/j.cnki.ggps.2020657

Atzberger, C. (2013). Advances in remote sensing of agriculture: Context description, existing operational monitoring systems and major information needs. *Remote Sens.* 5, 949–981. doi: 10.3390/rs5020949

Battude, M., Al Bitar, A., Morin, D., Cros, J., Huc, M., Sicre, C. M., et al. (2016). Estimating maize biomass and yield over large areas using high spatial and temporal resolution Sentinel-2 like remote sensing data. *Remote Sens Environ.* 184, 668–681. doi: 10.1016/j.rse.2016.07.030

Briak, H., and Kebede, F. (2021). Wheat (Triticum aestivum) adaptability evaluation in a semi-arid region of Central Morocco using APSIM model. *Sci. Rep.* 11, 23173. doi: 10.1038/s41598-021-02668-3

Chang, M., Zhou, Q., and Yin, L. (2023). Research of the effects of different drip irrigation treatments on the growth of summer maize and the adaptability of aquaCrop model. *J. Irrig. Drain. Div.* 42, 32–39. doi: 10.13522/j.cnki.ggps.2022363

Chen, X., Feng, L., Peng, M., and Chen, Y. (2019). Model method establishment ofSugarcane development simulation model based on clock. *Chin. J. Agrometeorol.* 40, 186–194. doi: CNKI:SUN:ZGNY.0.2019-03-006

Chen, Z., Ren, J., Tang, H., Shi, Y., Leng, P., Liu, J., et al. (2016). Progress and perspectives on agricultural remote sensing research andapplications in China. *J. Remote Sens.* 20, 748–767. doi: 10.11834/jrs.20166214

Feng, Q., Han, H., Zhang, Y., Xu, Q., Cao, Y., Wang, S., et al. (2018). Effects of tillage methods on soil carbon sequestration and water holdingcapacity and yield in wheat-maize rotation. *J. Plant Nutr. Fert.* 24, 869–879. doi: 10.11674/ZWYF.17452

Godfray, H. C. J., Beddington, J. R., Crute, I. R., Haddad, L., Lawrence, D., Muir, J. F., et al. (2010). Food security: the challenge of feeding 9 billion people. *Science* 327, 812–818. doi: 10.1126/science.1185383

Gonenc, A., Ozerdem, M. S., and Emrullah, A. (2019). "Comparison of NDVI and RVI vegetation indices using satellite images," in *2019 8th International Conference on Agro-Geoinformatics (Agro-Geoinformatics)*, Istanbul, Turkey, 16-19 July 2019. (IEEE), 1–4. doi: 10.1109/Agro-Geoinformatics.2019.8820225

Gunathilaka, (2021). Modelling the behavior of DVI and IPVI vegetation indices using multi-temporal remotely sensed data. *Int. J. Environ.* 3, 9–16. doi: 10.55151/ijeedu.v3i1.42

Guo, J., Li, C., Zeng, F., Zhang, B., Liu, B., and Guo, Z. (2016). Relationship between root biomass distribution and soil moisture,Nutrient for two desert plant species. *Arid Zone Res.* 33, 166–171. doi: 10.13866/j.azr.2016.01.21

Guo, R., Fu, S., Hou, M., Liu, J., Miao, C., Meng, X., et al. (2023). Remote sensing retrieval of nature grassland biomass in Menyuan County, QinghaiProvince experimental area based on Sentinel-2 data. *Acta Pra. Sin.* 32, 15–29. doi: 10.11686/cyxb2022147

Hansen, P., and Schjoerring, J. (2003). Reflectance measurement of canopy biomass and nitrogen status in wheat crops using normalized difference vegetation indices and partial least squares regression. *Remote Sens Environ.* 86, 542–553. doi: 10.1016/S0034-4257(03)00131-7

He, F. (2022). Estimation of winter wheat yield based on APSIM model and remote sensing data. *Agric. Technol.* 42, 40–45. doi: 10.19754/j.nyjs.20220228111

He, L., and Zhao, G. (2015). Global sensitivity analysis of APSIM-Wheat parameters in different climate zones and yield levels. *Trans. Chin. Soc Agric. Eng.* 31, 148–157. doi: 10.11975/j.issn.1002-6819.2015.14.021

Hong, D., Li, C., and Zhang, B. (2024). Multimodal artificial intelligence foundation models: Unleashing the power of remote sensing big data in earth observation. *Innovation* 2, 100055. doi: 10.59717/j.xinn-geo.2024.100055

Huang, J., Gao, X., Huang, H., Ma, H., Su, W., and Zhu, D. (2019). [amp]]#xFF32; egional winter wheat maturity date prediction based on MODIS and WOFOST model data assimilation. *Trans. Chin. Soc Agric. Mach.* 50, 186–193. doi: 10.6041/j.issn.1000-1298.2019.09.021

Huang, M., Wang, J., Tang, J., Fang, Q., Zhang, J., Bai, H., et al. (2018). Analysis of interaction of sowing date, irrigation and nitrogen applicationon yield of oil sunflower based on APSIM model. *Trans. Chin. Soc Agric. Eng.* 34, 134–143. doi: 10.11975/j.issn.1002-6819.2018.13.016

Huang, S., Tang, L., Hupy, J., Wang, Y., and Shao, G. (2021). A commentary review on the use of normalized difference vegetation index (NDVI) in the era of popular remote sensing. *J. For. Res.* 32, 1–6. doi: 10.1007/s11676-020-01155-1

Jiang, Y., Zhang, L., Xue, P., and Wang, X. (2021). Development status of wheat industry in China andInternational experience for reference. *J. Agric. Sci. Technol.* 23, 1–10. doi: 10.13304/j.nykjdb.2021.0412

Jin, X., Cheng, X., Gong, Z., and Feng, L. (2021). Parameter adjustment and optimization methods for the wheatSM. *J. Agric. Big Data.* 3, 13–22. doi: 10.19788/j.issn.2096-6369.210302

Jin, X., Kumar, L., Li, Z., Feng, H., Xu, X., Yang, G., et al. (2018). A review of data assimilation of remote sensing and crop models. *Eur. J. Agron.* 92, 141–152. doi: 10.1016/j.eja.2017.11.002

Lan, Y., Zheng, X., and Zeng, G. (2019). Advances in diagnosis of crop diseases, pests and weeds by UAV remote sensing. *Smart Agric.* 1, 1. doi: 10.12133/j.smartag.2019.1.2.201904-SA003

Liang, D., Guan, Q., Huang, W., Huang, L., and Yang, G. (2013). Remote sensing inversion of leaf area index based on support vectormachine regression in winter wheat. *Trans. Chin. Soc Agric. Eng.* 29, 117–123. doi: 10.3969/j.issn.1002-6819.2013.07.015

Liang, H., HU, K., and Li, B. (2016). Parameter optimization and sensitivity analysis of soil-crop system model using PEST. *Trans. Chin. Soc Agric. Eng.* 32, 78–85. doi: 10.11975/j.issn.1002-6819.2016.03.012

Liu, J., Chu, J., Wang, G., Chen, G., and Zhang, Y. (2013). Simulating yield gap of winter wheat in response to nitrogen management in North China Plain based on DSSAT model. *Trans. Chin. Soc Agric. Eng.* 29, 124–129. doi: 10.3969/j.issn.1002-6819.2013.23.017

Liu, F., Li, C., Dong, Y., Wang, X., Wang, J., and Huang, W. (2011). Monitoring crop growth based on assimilation of remote sensing data and crop simulation model. *Transactions of the Chinese Society of Agricultural Engineering* 27, 101–106.

Liu, T., Wang, N., Zhang, Z., Wang, X., Sun, S., Liu, Z., et al. (2023). Adaptability of DSSAT crop model to main crops in Lishu County. *Trans. Chin. Soc Agric. Eng.* 42, 1264–1272. doi: 10.13292/j.1000-4890.202305.010

Lu, Y., Li, S., Wang, J., Xie, R., Hang, W., Gao, S., et al. (2005). Spectral and reconqnized method for different plant type wheat cultivars. *Acta Agron. Sin.* 10), 1333–1339. doi: 10.3321/j.issn:0496-3490.2005.10.016

Lu, Z., Luo, M., Tang, C., Xu, F., Liang, S., and Yang, X. (2020). Monitoring and evaluation of winter wheat growth based on analysisof vegetation index changes on remote sensing lmages. *J. Triticeae Crops.* 40, 1257–1264. doi: 10.7606/jissn.1009-10412020.10.13

Luo, Y., Xun, J., and Yue, W. (2005). Research on vegetation indices based on the remote sensing images. *Ecol. Sci.* 01), 75–79. doi: 10.3969/j.issn.1008-8873.2005.01.021

Ma, Y., Wu, S., Yang, P., Cao, H., Tan, J., and Zhao, R. (2023). Research progress and challenges of oil crop yield monitoring by remote sensing. *Smart Agric.* 5, 1. doi: 10.12133/j.smartag.SA202303002

Qin, G.-X., Wu, J., Li, C.-B., Shen, S.-J., Li, H.-H., Yang, D.-H., et al. (2022). Sensitivity analysis of WOFOST model crop parameters in different grassland types. *Acta Pra. Sin.* 31, 13. doi: 10.11686/cyxb2021391

Rao, X., Li, H., Zhang, S., Luo, M., Liu, Z., and Zhang, J. (2021). Suitability analysis of remote sensing monitoring methods for grassland vegetation growth. *Chin. J. Eco-Agric.* 29, 2084–2092. doi: 10.12357/cjea.20210280

Ren, J., Chen, Z., Tang, H., Zhou, Q., and Qin, J. (2011). Regional crop yield simulation based on crop growth model and remote sensing data. *Trans. CSAE.* 27, 257–264. doi: 10.3969/j.issn.1002-6819.2011.08.045

Shammi, S. A., and Meng, Q. (2021). Use time series NDVI and EVI to develop dynamic crop growth metrics for yield modeling. *Ecol. Indic.* 121, 107124. doi: 10.1016/j.ecolind.2020.107124

Shi, Z., Liang, Z., Yang, Y., and Guo, Y. (2015). Status and prospect of agricultural remote sensing. *Trans. Chin. Soc Agric. Mach.* 46, 247–260. doi: 10.1016/j.ecolind.2020.107124

Shiferaw, B., Smale, M., Braun, H.-J., Duveiller, E., Reynolds, M., and Muricho, G. (2013). Crops that feed the world 10. Past successes and future challenges to the role played by wheat in global food security. *Food Secur.* 5, 291–317. doi: 10.1007/s12571-013-0263-y

Su, W., Zhu, D., Su, M., Huang, J., Liu, Z., and Guo, H. (2019). Field-scale corn growth monitoring using time series LAl. *Resour. Sci.* 41, 601–611. doi: 10.6041/j.issn.1000-1298.2015.02.037

Sun, L., Wang, W., Cheng, Y., and Dong, M. (2020). Analysis of winter wheat growth of United States with remote sensing data in 2019. *J. Anhui Agric. Sci.* 48, 241–244. doi: 10.18402/resci.2019.03.17

Wang, X., Cheng, X., Tang, S., and Feng, L. (2023c). Sensitivity analysis and adaptability evaluation of riceSM model. *J. Agric. Big Data.* 5, 97–108. doi: 10.19788/j.issn.2096-6369.230215

Wang, L., Fan, Y., Fan, B., and Wang, Y. (2023a). Monitoring winter wheat growth and analyzing its determinants using high-resolution satellite imagery. *J. Irrig. Drain. Div.* 42, 22–32. doi: 10.13522/j.cnki.ggps.2022268

Wang, S., Han, W., Zhang, X., Li, J., and Wang, L. (2024). Geospatial remote sensing interpretation: From perception to cognition. *Innov. Geo.* 2, 100056–100051-100056-100052. doi: 10.59717/j.xinn-geo.2024.100056

Wang, W., Shi, H., Li, X., Sun, Y., Zheng, Q., Zhang, W., et al. (2022). Effects of tillage modes and soil salinity on regional nitrate nitrogen transport and crop yields using a SWAT model. *Trans. Chin. Soc Agric. Eng.* 38, 55–65. doi: 10.11975/j.issn.1002-6819.2022.03.007

Wang, X., and Wang, C. (2015). Fundamental concepts and field measurement methods of carbon cycling in forestecosystems:a review. *Acta Ecol. Sin.* 35, 4241–4256. doi: 10.5846/stxb201407011359

Wang, Y., Xun, C., Bi, Y., Fan, J., Guo, R., Wang, J., et al. (2023d). Progress of DSSAT-CSM model application in maize planting research. *Chin. J. Agrometeorol.* 44, 492. doi: 10.3969/j.issn.1000-6362.2023.06.004

Wang, L., Zheng, Y., Yu, Y., and Wang, E. (2007). The application of farmland production system model (APSIM) in the management of land, water and fertilizer resources. *Sustain. Dev.* 03), 27–32. doi: 10.3969/j.issn.1005-4944.2007.03.007

Wang, L., Zuo, B., Le, Y., Chen, Y., and Li, J. (2023b). Penetrating remote sensing: Next-generation remote sensing for transparent earth. *Innovation* 4, 100519. doi: 10.1016/j.xinn.2023.100519

Winn, C. A., Archontoulis, S., and Edwards, J. (2023). Calibration of a crop growth model in APSIM for 15 publicly available corn hybrids in North America. *Crop Sci.* 63, 511–534. doi: 10.1002/csc2.20857

Wu, L., Bai, J., Xiao, Q., Du, Y., Liu, Q., and Xu, L. (2017). Research progress and prospeet on combining crop growth models withparameters derived from quantitative remote sensing. *Trans. Chin. Soc Agric. Eng.* 33, 155–166. doi: 10.11975/j.issn.1002-6819.2017.09.020

Wu, J., and Yan, Q. (2002). Crop monitoring and yield estimation using synthetic methods in arid land. *Geogr. Res.* 05), 593–598. doi: 10.3321/j.issn:1000-0585.2002.05.008

Wu, B., Zhang, F., Liu, C., Zhang, L., and Luo, Z. (2004). An integrated method for crop condition monitoring. *J. Remote Sens.* 06), 498–514. doi: 10.3321/j.issn:1007-4619.2004.06.002

Xiao, A., Wang, C., and Jiang, X. (2021). Effects of sowing method and sowing rate on soil moisture, wheat growth and yield in rain-fed area of southern Henan Province. *Bull. Agric. Sci. Technol.* 08), 88–91. doi: 10.3969/j.issn.1000-6400.2021.08.027

Xie, Q., Dash, J., Huete, A., Jiang, A., Yin, G., Ding, Y., et al. (2019). Retrieval of crop biophysical parameters from Sentinel-2 remote sensing imagery. *Int. J. Appl. Earth. Obs.* 80, 187–195. doi: 10.1016/j.jag.2019.04.019

Xing, H., Li, Z., Xu, X., Feng, H., Yang, G., and Chen, Z. (2017a). Multi-assimilation methods based on AquaCrop model andremote sensing data. *Trans. Chin. Soc Agric. Eng.* 33, 183–192. doi: 10.11975/j.issn.1002-6819.2017.13.024

Xing, H., Xiang, S., Xu, X., and Cheng, Y. (2017b). Global sensitivity analysis of aquaC rop crop model parameters based on EFAST method. *Sci. Agric. Sin.* 50, 64–76. doi: 10.3864/j.issn.0578-1752.2017.01.006

Yang, J., Yang, J., Jiang, X., and Zhang, Z. (2012). Progress of crop model research. *J. Jilin Agric. Univ.* 34, 553–561. doi: 10.13327/j.jjlau.2012.05.008

Yin, J., Zhou, L., Li, L., Zhang, Y., Wang, W., Zhang, H., et al. (2021). A comparative study on wheat identificationandGrowthMonitoring based on multi-source remote sensingData. *Remote Sens. Technol. Appl.* 36, 332–341. doi: 10.11873/j.issn.1004-0323.2021.2.0332

Yu, H., Yang, X., Xu, B., Jin, Y., Gao, T., and Li, J. (2012). The progress of remote sensing monitoring for grassland vegetation growth. *Prog. Geogr.* 31, 885–894. doi: 10.11820/dlkxjz.2012.07.007

Zhang, M., Gao, Y., and Zhang, Y. (2023). Sensitivity analysis and calibration of the APSIM next-generation model under different irrigation and sowing density in wheat. *Chin. J. Eco-Agric.* 31, 102–112. doi: 10.12357/cjea.20220384

Zhang, L., Wang, S., Liu, H., Li, Y., Wang, J., Zhu, M., et al. (2021). From spectrum to spectrotemporal : research on time series change detection of remote sensing. *Geomatics Inf. Sci. Wuhan Univ.* 46, 451–468. doi: 10.13203/j.whugis20200666

Zhao, G., Chang, X., Wang, D., Tao, Z., Wang, Y., Yang, Y., et al. (2018). General situation and development of wheat production. *Crops* 04), 1–7. doi: 10.16035/j.issn.1001-7283.2018.04.001

Zhao, L., Li, W., and Du, P. (2011). The area extraction of winter wheat based on multi-temporal HJ remote sensing satellite images. *Remote Sens. Inf.* 2, 41–45. doi: 10.3969/j.issn.1000-3177.2011.02.008

Zhao, X., Li, j., and Feng, X. (2021). 2035 in China development strategy of smart agriculture for. *Strategic. Study. CAE.* 23, 1–9. doi: 10.15302/J-SSCAE-2021.04.001

Zheng, Y., Wu, B., and Zhang, M. (2017). Estimating the above ground biomass of winter wheat using the Sentinel-2 data. *J. Remote Sens.* 21, 318–328. doi: 10.11834/jrs.20176269

Zhu, J., Li, G., Li, Y., and Yang, H. (2023a). Simulation of silage maize yield and sensitivity analysis under differentNitrogen application treatments based on APSlM model. *Crop Res.* 37, 349–353+375. doi: 10.11975/j.issn.1002-6819.202305144

Zhu, X., Yang, Z., Fang, Y., and Dai, J. (2023b). Applying crops yield index in Heilongjiang Province of China. *Trans. Chin. Soc Agric. Eng.* 39, 151–161.

Zhuo, W., Fang, S., Gao, X., Wang, L., Wu, D., Fu, S., et al. (2022a). Crop yield prediction using MODIS LAI, TIGGE weather forecasts and WOFOST model: A case study for winter wheat in Hebei, China during 2009–2013. *Int. J. Appl. Earth. Obs. Geoinf.* 106, 102668. doi: 10.1016/j.jag.2021.102668

Zhuo, W., Huang, H., Gao, X., Li, X., and Huang, J. (2023). An improved approach of winter wheat yield estimation by jointly assimilating remotely sensed leaf area index and soil moisture into the Wofost model. *Remote Sens.* 15, 1825. doi: 10.3390/rs15071825

Zhuo, W., Huang, J., Xiao, X., Huang, H., Bajgain, R., Wu, X., et al. (2022b). Assimilating remote sensing-based VPM GPP into the WOFOST model for improving regional winter wheat yield estimation. *Eur. J. Agron.* 139, 126556. doi: 10.1016/j.eja.2022.126556

frontiers | Frontiers in Plant Science

TYPE Original Research
PUBLISHED 14 November 2024
DOI 10.3389/fpls.2024.1458589

Check for updates

OPEN ACCESS

EDITED BY
Sukhbir Singh,
Texas Tech University, United States

REVIEWED BY
Agustami Sitorus,
National Research and Innovation Agency (BRIN), Indonesia
Atinderpal Singh,
New Mexico State University, United States
Arjun Kafle,
Texas A&M University AgriLife Research and Extension Center at Lubbock, United States

*CORRESPONDENCE
Quan Feng
fquan@gsau.edu.cn

RECEIVED 02 July 2024
ACCEPTED 25 October 2024
PUBLISHED 14 November 2024

CITATION
Guo F, Feng Q, Yang S and Yang W (2024) Estimation of potato canopy leaf water content in various growth stages using UAV hyperspectral remote sensing and machine learning.
Front. Plant Sci. 15:1458589.
doi: 10.3389/fpls.2024.1458589

COPYRIGHT
© 2024 Guo, Feng, Yang and Yang. This is an open-access article distributed under the terms of the Creative Commons Attribution License (CC BY). The use, distribution or reproduction in other forums is permitted, provided the original author(s) and the copyright owner(s) are credited and that the original publication in this journal is cited, in accordance with accepted academic practice. No use, distribution or reproduction is permitted which does not comply with these terms.

Estimation of potato canopy leaf water content in various growth stages using UAV hyperspectral remote sensing and machine learning

Faxu Guo, Quan Feng*, Sen Yang and Wanxia Yang

College of Mechanical and Electrical Engineering, Gansu Agriculture University, Lanzhou, China

To ensure national food security amidst severe water shortages, agricultural irrigation must be reduced through scientific innovation and technological progress. Efficient monitoring is essential for achieving water-saving irrigation and ensuring the sustainable development of agriculture. UAV hyperspectral remote sensing has demonstrated significant potential in monitoring large-scale crop leaf water content (LWC). In this study, hyperspectral and LWC data were collected for potatoes (*Solanum tuberosum*) during the tuber formation, growth, and starch accumulation stage in both 2021 and 2022. The hyperspectral data underwent mathematical transformation by multivariate scatter correction (MSC) and standard normal transformation (SNV). Next, feature spectral bands of LWC were selected using Competitive Adaptive Reweighted Sampling (CARS) and Random Frog (RF). For comparison, both the full-band and feature band were utilized to establish the estimation models of LWC. Modeling methods included partial least squares regression (PLSR), support vector regression (SVR), and BP neural network regression (BP). Results demonstrate that MSC and SNV significantly enhance the correlation between spectral data and LWC. The efficacy of estimation models varied across different growth stages, with optimal models identified as MSC-CARS-SVR (R^2 = 0.81, RMSE = 0.51) for tuber formation, SNV-CARS-PLSR (R^2 = 0.85, RMSE = 0.42) for tuber growth, and MSC-RF-PLSR (R^2 = 0.81, RMSE = 0.55) for starch accumulation. The RPD values of the three optimal models all exceed 2, indicating their excellent predictive performance. Utilizing these optimal models, a spatial distribution map of LWC across the entire potato canopy was generated, offering valuable insights for precise potato irrigation.

KEYWORDS

hyperspectral remote sensing, inversion mapping, machine learning, leaf water content, potato, spectral feature extraction unmanned aerial vehicle

1 Introduction

As global agriculture faces increasing pressure from water scarcity, efficient water management has become more critical than ever. The Food and Agriculture Organization (FAO) of the United Nations projects that by 2050, the world will need to produce 60% more food to meet the demands of a population expected to reach 9.7 billion, all while grappling with increasingly limited water resources (Lakhiar et al., 2024). In this context, precision irrigation emerges as a key strategy to optimize water usage, minimize waste, and ensure sustainable agricultural productivity. Water plays an indispensable role in the growth and development of crops (Féret et al., 2019; Liu et al., 2022; Li et al., 2022a). Crops rely on water for photosynthesis, transpiration, and the synthesis and decomposition of organic matter (Sun et al., 2015; Meiyan et al., 2022). Obtaining crop water information quickly and accurately is vital for timely crop irrigation and yield improvement, especially in regions prone to water scarcity. Efficient water use is critical in agriculture, especially in water-scarce regions. In modern precision agriculture, technologies like UAV hyperspectral remote sensing provide a promising solution for monitoring crop water content in real-time. Among all crop tissues, leaves exhibit the most vigorous metabolism and serve as the primary site for photosynthesis (Zhou et al., 2020; Zhang et al., 2021). Analyzing leaf water content (LWC) is critical for assessing crop moisture status, as LWC level indicate the degree of crop water deficiency. Traditional methods of measuring crop moisture, such as drying and distillation, are accurate but time consuming and energy intensive (Roberto et al., 2018; Wang et al., 2021). Therefore, more efficient monitoring methods are needed for precise agricultural management. When crops suffer from severe water shortages, timely irrigation becomes a challenge.

In the past few decades, satellite-based hyperspectral remote sensing technology has been extensively studied in large-scale regional agricultural monitoring such as crop nitrogen content (Zheng et al., 2022), crop chlorophyll content (Xie and Yang, 2020), and crop biomass (Jia et al., 2019). In China, the cultivated land area of a farmer is usually no more than a few acres. On this scale, the granularity of satellite remote sensing is too rough, and it is difficult for a farmer to obtain remote sensing data in time. As a result, this method cannot provide farmers with timely information on drought conditions and irrigation guidance. In recent years, with the development of technology, the price of unmanned aerial vehicle (UAV) has been becoming cheaper. Chinese farmers have used UAV for many field operations, such as spraying and short-distance transport. Compared with satellites, the remote sensing mode of UAV + hyperspectral sensing has many advantages such as fine granularity, convenience, and flexibility. The combination of the two technologies can make precision agriculture more practical in China and can provide farmers with a scientific basis for precision irrigation based on LWC measurements (Zhang et al., 2021; He et al., 2023). UAV hyperspectral remote sensing offers farmers timely, high-resolution data that can improve precision irrigation strategies. For example, recent studies demonstrated its effectiveness in optimizing water management in crops like maize and wheat, leading to measurable water savings and increased yields (Mohite et al., 2022; Luo et al., 2024).

The widespread adoption of hyperspectral remote sensing technology has enabled its extensive use in monitoring plant water content (Suárez et al., 2009; Raj et al., 2021), and most studies have focused on the infrared region at wavelengths greater than 900 nm. Maes and Steppe (2019) discovered that the vibrational movements of water and other molecules containing O-H groups in plants result in spectral absorption peaks occurring near 970 nm, 1200 nm, 1450 nm, 1940 nm, and 2500 nm in the spectral reflectance of plants. Zhang et al. (2014) investigated the optimal spectral indicators for determining LWC. Their findings demonstrated that the regression model for leaf water content based on the normalized difference spectral index NDSI (R1222, R2264) and the ratio spectral index RSI (R2264, R1321), is closely aligned with the measured and estimated values. Sun et al. (2021) utilized the Fractional Order Savitzky-Golay Derivative (FOSGD) to preprocess the hyperspectral reflectance data of maize leaves spanning from 900 nm to 1700 nm. They employed Variable Importance in Projection (VIP), Competitive Adaptive Reweighted Sampling (CARS), and Random Frog (RF) methods to identify sensitive wavelengths. They established a maize leaf water content estimation model based on Partial Least Squares. The results indicated that the FOSGD-CARS-PLS or FOSGD-RF-PLS model can effectively predict the LWC of maize. Although near-infrared spectra above 900 nm exhibit high reliability in measuring vegetation moisture, the instruments acquiring these spectra are characterized by their high cost, making it unaffordable for the ordinary farmers.

Visible and near-infrared spectroscopy (VIS-NIR) has been extensively employed for estimating leaf water content (LWC) due to its cost-effectiveness and wide accessibility. Previous studies have demonstrated that vegetation indices derived from VIS-NIR reflectance can effectively detect changes in LWC across a variety of crops (Suárez et al., 2008; Kovar et al., 2019). For instance, Ishikawa et al. (2013) found that spectral bands in the 650–690 nm range were strongly correlated with LWC in diverse leaf samples, underscoring the reliability of this method for water content estimation. More recent research by Wang et al. (2023) utilized partial least squares (PLS) models to predict moisture content in fresh tea leaves, integrating spectral data to provide practical applications in real-time monitoring systems. Similarly, Duarte-Carvajalino et al. (2021) applied hyperspectral imaging techniques to predict potato leaf water content, achieving high accuracy under controlled experimental conditions. Nevertheless, these studies predominantly focus on controlled environments, where factors such as temperature, humidity, and lighting are strictly regulated. As a consequence, the models developed may exhibit reduced performance in field conditions, where environmental variability introduces significant challenges.

Additionally, many studies have constructed spectral models specific to particular growth stages, thereby limiting their applicability across the entire crop life cycle (Panigrahi and Das, 2018). Given that crop spectral characteristics evolve with growth stage, health status, and environmental conditions, models developed for a single growth stage may fail to capture the full extent of LWC variation throughout the entire growth period. While some research, such as that by Liu et al. (2015), has

compared models across multiple growth stages, these models often require further validation to ensure their robustness under diverse conditions. Consequently, there remains a critical gap in the development of LWC estimation models that can be reliably applied across multiple growth stages, particularly for crops like potatoes, which exhibit varying water demands at different phenological phases (Sudu et al., 2022).

Potato, along with rice, wheat, and corn, is one of the major food crops globally (Zhang et al., 2017). The vitality and water content of leaf play a crucial role in ensuring a nation's food security (Wijesinha-Bettoni and Mouillé, 2019). Especially in water-scarce regions such as Gansu Province, potatoes, as a key crop, have significant water requirements, making them an ideal subject for research on improving irrigation efficiency. Although numerous studies have applied hyperspectral remote sensing to monitor crop water content, relatively few have specifically focused on potatoes, particularly under real field conditions. Additionally, most existing models are limited to a single growth stage, neglecting the variations in moisture content across different stages of growth. As shown in Table 1, these studies face challenges such as limited spatial coverage, insufficient data acquisition speed, and a lack of validation in real field conditions. This table summarizes the key differences between our research and previous studies, highlighting how our work addresses these limitations. This study aims to address the limitations of previous research by developing and validating a potato LWC estimation model across multiple growth stages using UAV-based hyperspectral remote sensing combined with machine learning algorithms. By focusing on critical growth stages such as tuber formation, growth, and starch accumulation, this research offers valuable insights for optimizing irrigation strategies and advancing precision agriculture techniques in water-scarce regions.

2 Materials and methods

2.1 Overview of the study area

Potato field trials were conducted in Huangyang Town, Liangzhou District, within Wuwei City, from May to October in both 2021 and 2022. Huangyang Town, located in the Hexi Irrigation District of Gansu Province (37°81′49″ *N*, 102°92′38″ *E*) (Figure 1), is a significant area for potato cultivation. The area is situated at an altitude of 1660 m and lies in the eastern part of Hexi Corridor. It has a continental temperate arid climate with a 150-day frost-free period, averaging an annual temperature of 7.2°C and receiving 160 mm of annual precipitation. The soil in this area is grey calcareous with sandy loam texture and is high saline, PH value of 7.82. The main crops cultivated are corn, wheat, and potatoes. The potato variety 'Qingshu9' was planted in both years, courtesy of Gansu Academy of Agricultural Sciences. 'Qingshu 9' is a medium- to late-maturing fresh potato variety, with an average growth period of approximately 115 days from emergence to maturity. This variety is characterized by its high yield, resistance to late blight and scab, and adaptability to local climatic conditions.

Prior to planting, two types of fertilizers were applied: diammonium phosphate (46%P_2O_5, 18%N) at a rate of 400 kg/hm^2, to provide the necessary phosphorus and nitrogen for the early growth stages, and a Western compound fertilizer (15%N, 15% P_2O_5, 15%K2O) at a rate of 750 kg/hm^2, to ensure adequate nutrient supply throughout the reproductive period. Both fertilizers were incorporated into the soil in a single application before sowing. Irrigation was carried out using an under-membrane drip system, with drip pipes buried 6cm deep (Aziz et al., 2021). The irrigation system used drip pipes with a diameter of 16 mm (φ16) and emitters for water delivery, while the branch pipe was a 50 mm diameter (φ50) PE pipe with a pressure resistance of over 0.5MPa. To minimize water evaporation and maintain soil moisture, the soil surface was covered with a black polyethylene film, 90cm wide and 0.012mm thick. Throughout the growth cycle of the potato crop, the total irrigation volume ranged from 2100 to 2300m^3/hm^2. In 2021, irrigation was performed 10 times, while in 2022, it was conducted 11 times, with irrigation intervals of 10–12 days. The irrigation frequency was adjusted according to3the potato2 growth stage and soil moisture levels, with each irrigation delivering between 190 and 250 m/hm. Field management tasks such as sowing, fertilizing, weeding, spraying pesticides, and other farming practices were carried out according to local agricultural practices.

2.2 Hyperspectral image acquisition and processing

Potatoes were planted on May 6, 2021, and May 10, 2022, and harvested on October 3, 2021, and October 8, 2022, respectively. The tuber formation stage began 65 days after planting and lasted for approximately 30 days. The tuber growth phase commenced 95 days after planting and continued for about 25 days, while the starch accumulation phase started 120 days after planting and lasted for around 30 days (Aziz et al., 2021). The study conducted six field trials at three crucial growth stages of potato: July 28, 2021 (S1 - tuber formation stage), August 19 (S2 - tuber growth stage), August 30 (S3 - starch accumulation stage), and August 1, 2022 (S1 - tuber formation stage), August 17 (S2 - tuber growth stage), August 31 (S3 - starch accumulation stage). Hyperspectral images were obtained using the DJI M600 Pro® hexacopter drone, equipped with the Gaia Sky-mini 2® imaging spectrometer (Jiangsu Dualix Spectral Imaging Technology Co., Ltd, China) (Figure 2). The Gaia Sky-mini 2 features a built-in push-scan imaging system with a spectral range of 400 to 1000 nm and a spectral resolution of 3.5 nm. It has a full-frame pixel resolution of 1392×1040 and weighs approximately 1 kg. The device employs a surface-array detector oriented perpendicularly to the direction of movement, allowing it to perform a two-dimensional spatial scan as the motion platform advances. The DJI M600 Pro hexacopter, when unloaded, has a flight time of approximately 35 minutes per battery. Under a maximum load of 6 kg, its battery life is reduced to around 16 minutes. To ensure high-quality hyperspectral images, all six experiments were conducted between 11:00 a.m. and 1:00 p.m. local time, following a fixed flight path on days with stable sunlight

TABLE 1 Overview of hyperspectral remote sensing methods and their limitations in existing studies.

Reference	Cereals	Remote Sensing Platforms	Spectral Range (nm)	Regressors	Limitations	Improvements in This Study
Liu et al. (2022)	Winter Wheat	Ground-Based Platform	350–2500	MLR, SVR, PLSR	Limited spatial coverage	Utilized high-resolution UAV for extensive coverage
Li et al. (2022a)	Winter Wheat	Ground-Based Platform	350–1350	GPR, CART, ANN	Limited spatial coverage	Utilized high-resolution UAV for extensive coverage
Feng et al. (2022)	Winter Wheat	UAV-Based Platform	450–950	MLR, PLSR, RF	Focused only on a single growth stage	Monitored multiple growth stages for potatoes
Li et al. (2022b)	Winter Wheat	UAV-Based Platform	400–1000	SVR, LRR, RF, GPR	Focused only on a single growth stage	Monitored multiple growth stages for potatoes
Sun et al. (2015)	Corn	Ground-Based Platform	900–1700	PLSR, MLR, BP	Not validated in real field conditions	Collected data in actual field conditions
Sun et al. (2021)	Corn	Ground-Based Platform	900–1700	PLSR, MLR	Data collection conditions determined	Collected data in actual field conditions
Ndlovu et al. (2021)	Maize	UAV-Based Platform	475, 560, 668, 717, 840	RF, SVR, PLSR	Focused only on a single growth stage	Monitored multiple growth stages for potatoes
Sudu et al. (2022)	Summer Maize	UAV-Based Platform	450–998	PLSR, RF, XGBoost	Multi-Growth stage mixed modeling	Independent modeling for each growth stage
Tunca et al. (2023)	Sorghum	Ground-Based Platform	325–1075	RF, SVR, XGBoost	Limited spatial coverage	Utilized high-resolution UAV for extensive coverage
Krishna et al. (2019)	Rice	Ground-Based Platform	350–2500	PLSR, MLR, ANN; RF, SVR	Limited spatial coverage	Utilized high-resolution UAV for extensive coverage
Elsherbiny et al. (2021)	Rice	Ground-Based Platform	874–1734	BP, RF, PLSR	Data collection conditions determined	Collected data in actual field conditions
Chen et al. (2020a)	Cotton	UAV-Based Platform	490, 550, 680, 720, 800, 900	MLR	Focused only on a single growth stage	Monitored multiple growth stages for potatoes
Duarte-Carvajalino et al. (2021)	Potato	Ground-Based Platform	400–1000	RF, XGBoost, MLP, CNN, SVR	Limited spatial coverage	Utilized high-resolution UAV for extensive coverage
Suyala et al. (2024)	Potato	Ground-Based Platform	337–2521	PLSR, SVR, BP	Limited spatial coverage	Utilized high-resolution UAV for extensive coverage
Guo et al. (2023)	Potato	UAV-Based Platform	400–1000	PLSR, MLR	Multi-Growth stage mixed modeling	Independent modeling for each growth stage

MLR denotes Multiple Linear Regression, GPR denotes Gaussian Process Regression, CART denotes Classification and Regression Tree, ANN denotes Artificial Neural Network Regression, RF denotes Random Forest Regression, LRR denotes Linear Ridge Regression, and XGBoost denotes Extreme Gradient Boosting Regression.

intensity and clear, cloudless weather. The drone operated at a flight height of 100 m, with a 22° scanning field of view, a high-altitude resolution of 0.039m, 80% lateral overlap, and 60% longitudinal overlap between image data. Before the UAV's departure, the hyperspectral imager underwent radiometric calibration using a whiteboard. The pre-processing of the hyperspectral data primarily involves image correction, stitching, and reflectance extraction (Guo et al., 2023).

2.3 Measurement and statistics of LWC data

Potato leaf sampling and hyperspectral imaging were synchronized. Sampling points were uniformly distributed based on the study and potato planting areas. The center coordinates of each observation were located and recorded using a handheld high-precision GPS sampling device with a positioning accuracy of< 5 cm. Twenty fully expanded and undamaged leaves were collected from each sampling point in the canopy. The collected leaves were sealed, and their fresh weight (W_1, g) was measured in the laboratory using a precision electronic balance (JA3003, Shanghai Hengping Instrument and Meter Co., Ltd., China). Next, the leaves from each sampling point were dried in a laboratory oven at 105°C for 30 min and then further dried at 80°C until a constant weight was achieved (Xu et al., 2022). The dry weight of the leaves (W_2, g) was recorded. The LWC (%) of the potato was calculated by Equation 1:

$$LWC = \frac{W_1 - W_2}{W_1} \times 100\,\% \quad (1)$$

This study measured the potato LWC data at three critical growth stages. At stage S1, 50 samples were collected each year, while at stages S2 and S3, 55 samples were collected each year. A total of 320 samples were collected during the experimental phase.

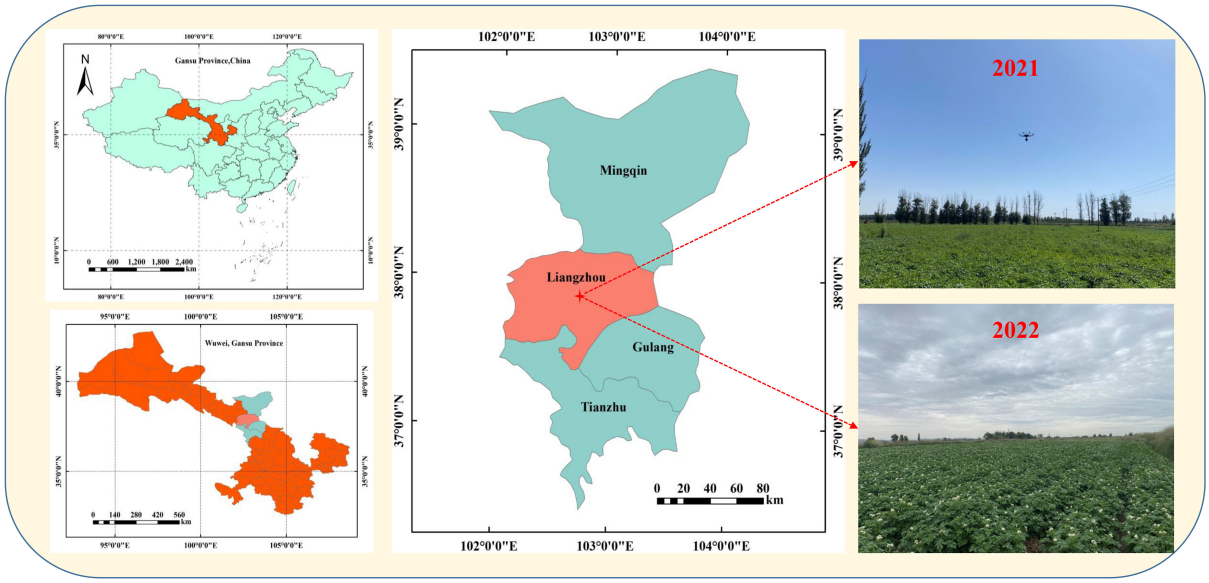

FIGURE 1
Description of the geographic location of the study area.

2.4 Hyperspectral data transformation

During hyperspectral data processing, specific spectral transformations can be used to mitigate the effects of environmental factors and interferences, improve the signal-to-noise ratio, and make spectral forms more sensitive to potato LWC (Yang et al., 2023). In this study, several mathematical transformations were applied to the raw spectra, resulting in six spectral data types: raw reflectance (R), multiple scattering correction (MSC), standard normal variate (SNV), reciprocal transformation (RT), logarithm of the reciprocal [(Lg(1/R)], and first derivative (FD).MSC is a normalization technique that reduces baseline drift, improves the signal-to-noise ratio, and better reveals differences and similarities between samples. It is commonly used to eliminate the effects of scatter on spectral data (Chen et al., 2019; Sun et al., 2020). SNV primarily eliminates the effects of solid particle size, surface scattering, and optical path variations on spectra. Elimination of baseline drift and enhancement spectral signal characteristics contribute to improved accuracy and reliability in spectral analysis (Genkawa et al., 2015; Tao et al., 2020). RT and Lg(1/R) help to enhance features in low reflectance regions, making subtle changes more detectable. Meanwhile, FD highlights minute spectral changes, such as the positions of reflectance peaks and valleys, although it may amplify noise in regions with weaker signals (Sonobe and Hirono, 2022).

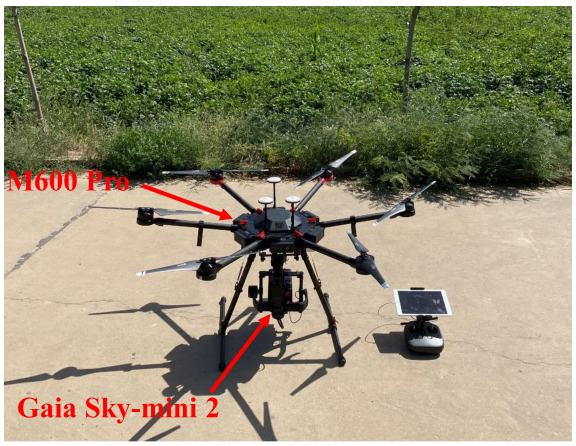

FIGURE 2
UAV imaging hyperspectral system.

2.5 Extraction of hyperspectral feature band

Considering the large number of collected hyperspectral bands, numerous redundant and interfering bands exist. Extracting the feature band related to potato LWC based on the potato hyperspectral reflectance data is crucial. This study utilized two hyperspectral feature band extraction algorithms: CARS and RF.

The CARS algorithm (Sun et al., 2021; Xing et al., 2021) is based on in the evolutionary principle of “survival of the fittest”. It integrates partial least squares (PLS) with CARS technology by using the absolute value percentage of the PLS modeling coefficients as a measure of significance for the target variables. And then it selects wavelengths with substantial coefficients, and discarding those with low weights. The process uses Monte Carlo Sampling (MCS), exponential decay functions, and Adaptive Weighted Sampling (ARS) to acquire an initial subset of wavelengths for further screening. Multiple iterations of the CARS algorithm result in a set of wavelengths closely linked to the target attributes. This produces a high-performance feature wavelength set for regression modeling. The comprehensive approach improves the accuracy and

reliability of spectral analysis, effectively selecting the best modeling wavelength combinations. The RF algorithm (Li et al., 2012; Hu et al., 2015) is a heuristic feature selection algorithm that is highly suitable for spectral data. The RF algorithm mimics the random yet systematic search behavior of a frog 'leaping' between different subsets of features. Each 'leap' represents the algorithm's movement from one potential feature subset to another, selecting subsets based on performance. By continuously performing crossbreeding, mutation, and selection operations, the algorithm gradually optimizes the feature subset to excel in the given task. This method allows the algorithm to explore various feature combinations in the search space to identify the best feature set, thereby improving the model's performance.

2.6 Machine learning modeling

Following the aforementioned processes on the hyperspectral data, three regression algorithms (PLSR, SVR and BP) of machine learning were used to construct a potato LWC estimation models. PLSR (Cheng and Sun, 2017) is a traditional linear regression technique that conducts principal component analysis on the explanatory and response variables to identify a new feature space that optimizes their covariance. This method effectively handles multicollinearity, is suitable for high-dimensional data, and can handle multiple response variables. PLSR ensures that each component is associated with the target, allowing for multi-level regression analysis by retaining different numbers of components to achieve more robust predictions and a deeper understanding of the relationship between independent and dependent variables (Burnett et al., 2021). The model training process involved optimizing the number of principal components, which in this study was varied between two and two-thirds of the total number of features.

SVR (Virnodkar et al., 2020) is based on kernel statistical theory and transforms the sample space into a high-dimensional or infinite-dimensional feature space through nonlinear mapping. This conversion turns the initially nonlinear separable problem in the sample space into a linear separable problem in the feature space. SVR can improve robustness against noise and outliers, exhibits nonlinear modeling capabilities, excels in high-dimensional space, and provides strong generalization performance, making it suitable for various regression problems. In this study, a radial basis function was employed, with the two parameters to be optimized being the penalty coefficient (C) and the kernel function parameter (γ). A grid search approach was utilized to determine the optimal values for these parameters, where the search range for C was from 0.5 to 500, and for γ, from 0.0001 to 0.05.

The Backpropagation (BP) neural network (Li et al., 2016) is widely used for nonlinear modeling and data prediction. It consists of input, output, and intermediate hidden layers. The learning process involves two key steps: forward propagation and backpropagation. During forward propagation, the input data is processed layer by layer, starting with the input layer, then the hidden layer, and finally the output layer. In case of an error between the predicted result of the output layer and the actual data, the backpropagation process is initiated. By using the gradient descent method, the backpropagation algorithm methodically adjusts the weights of each neuron layer by layer, continuing until the error aligns with the predetermined criteria. In the present research, it was necessary to determine the number of hidden layers and the corresponding number of neurons in each layer. Two hidden layers with the same number of neurons were employed. The empirical formula (Equation 2) was applied to define an appropriate range for the number of nodes in the hidden layers. The optimal number of nodes in each hidden layer was then selected using the grid-search method, with 1,000 iterations, a learning rate of 0.01, and a training objective of 1×10^{-6}.

$$q = \sqrt{k+m} + \alpha \tag{2}$$

where q denotes the number of nodes in the hidden layer, k represents the number of input layer units, m indicates the number of output layer units, and α is a constant in the range [1, 10].

2.7 Model evaluation methods

The regression algorithms employed in this research were implemented in the Python 3.6.13 environment using the scikit-learn 0.23.2 or TensorFlow 2.1.0 frameworks. Due to the limited number of samples available for a single growth stage, the constructed models were validated through leave-one-out-cross validation (Wong, 2015). During the cross-validation process, each sample was iteratively used as a test set. Model parameters were determined by a comprehensive comparison of multiple training iterations, providing results that are considered the closest approximation to the expected value derived from training on the entire dataset. We use the coefficient of determination (R^2), root mean square error (RMSE) and relative analytical error (RPD) as evaluation metrics to assess model performance. R^2 (closer to 1) measures how well the model fits the data, while RMSE (closer to 0) quantifies the spread of predicted values around the regression line. A higher R^2 and a lower RMSE indicate greater precision in model estimation. The RPD is used to assess the predictive ability of a model. It is defined as the ratio of the standard deviation of the sample to the RMSE. When RPD< 1.4, the model is considered unable to predict the samples accurately. If 1.4 ≤ RPD< 2, the model is regarded as moderately effective and can be used for rough assessments. For RPD ≥ 2, the model is considered to have excellent predictive capability (Zhu et al., 2020). The calculation of R^2, RMSE, and RPD are shown in Equations 3–5, respectively.

$$R^2 = 1 - \frac{\sum_{i=1}^{n}(y_m - y_p)^2}{\sum_{i=1}^{n}(y_m - \bar{y})^2} \tag{3}$$

$$RMSE = \sqrt{\frac{1}{n}\sum_{i=1}^{n}(y_m - y_p)^2} \tag{4}$$

$$RPD = \frac{S_y}{RMSE} = \frac{\sqrt{\frac{1}{n-1}\sum_{i=1}^{n}(y_{m,i} - \bar{y}_m)^2}}{RMSE} \tag{5}$$

10.3389/fpls.2024.1458589

Where n is the sample size; y_m and y_p are the actual and predicted values of potato LWC, respectively; $\bar{y}$ is the mean value of the actual potato LWC; S_y is the standard deviation of the measured value of potato LWC.

3 Results and analysis

3.1 Mathematical statistics of collection sample

To ensure that the modeling and test data sets better capture the entire dataset's distribution, to mitigate bias from specific data distributions, and to improve the generalizability of the model, we used a random splitting method, allocating 75% of the samples for modeling and 25% for testing. For the potato growth stage S1, 75 samples were selected for the modeling data set and 25 for the test data set. Likewise, for the S2 and S3 growth stages, 83 samples were selected for the modeling data set, and 27 in the test data set. Figure 3 shows the sample distribution in the modeling and test data sets across the three growth stages of potato. As shown in Figure 3, the mean and standard deviation (SD) values of the sample points of the three different growth stages can be obtained. In the S1 stage, the distribution of LWC in the modeling data set ranges from 81.53% to 87.91% (SD = 1.22), while in the test data set, it ranges from 81.70% to 86.62% (SD = 1.19). In the S2 stage, the distribution of LWC in the modeling data set ranges from 79.28% to 83.99% (SD = 1.12), while in the test data set, it ranges from 79.90% to 83.84% (SD = 1.08). In addition, at the S3 stage, the distribution of LWC in the modeling data set ranges from 76.28% to 80.72% (SD = 0.99), while in the test data set, it ranges from 76.40% to 81.58% (SD = 1.27). The mean and standard deviation (SD) values between the modeling and test datasets for the three growth stages show minor variances, indicating a reasonable division of the data set.

3.2 Potato hyperspectral features

3.2.1 Hyperspectral transformation and feature analysis

Figure 4 shows the original spectral curves and their mathematical transformations for the potato samples. As can be seen from Figure 4A, there are obvious differences in the raw reflectance (R) between the samples, and there are phenomena such as baseline shift and tilt between the spectra. These observations can be attributed to light scattering from the potato canopy and changes in the optical path length. After processing with by MSC (Figure 4B) and SNV (Figure 4C), the discrepancies in reflectance are significantly decreased. The spectra show higher concentration and consistent spectral curve characteristics. These results provide the evidence that the two spectral transformation methods can effectively address spectral shifts, eliminate background interference and noise, and enhance spectral features. As a result, feature wavelengths can be identified with greater accuracy and precision. The RT transform (Figure 4D) effectively enhances the spectral features in regions of low reflectance, highlighting subtle changes that are less apparent in the original spectrum. In contrast, the Lg(1/R) transform (Figure 4E) emphasizes spectral variations while preserving the overall trend of the spectrum, making it suitable for analyzing subtle differences. The FD transform (Figure 4F) effectively highlights small changes in the spectrum, such as the positions of reflectance peaks and valleys, thereby reducing background interference and improving the accuracy of feature extraction. However, a burr phenomenon is observed beyond 800 nm in Figure 4F, primarily due to weak signal strength in this spectral region, which results in noise amplification during the derivative transformation process.

3.2.2 Analysis of the correlation between potato canopy reflectance and LWC

Based on the actual measured data of LWC in three critical growth stages of potato, the correlation between the reflectance of each band before and after hyperspectral mathematical transformation with LWC is analyzed during the entire growth period of potato, and the results are shown in Figure 5. It can be observed that the correlation coefficients r for MSC and SNV show an increase compared to R. r between R and LWC ranges from -0.50 to 0.35, while for MSC and LWC, it ranges from -0.84 to 0.73, and for SNV and LWC, it ranges from -0.80 to 0.75. The trend of change in r between the reflectance of each band and LWC before and after spectral transformation remains consistent in the range of 500-725 nm. The absolute value of the negative correlation coefficient r reaches its highest point for each transformation at approximately

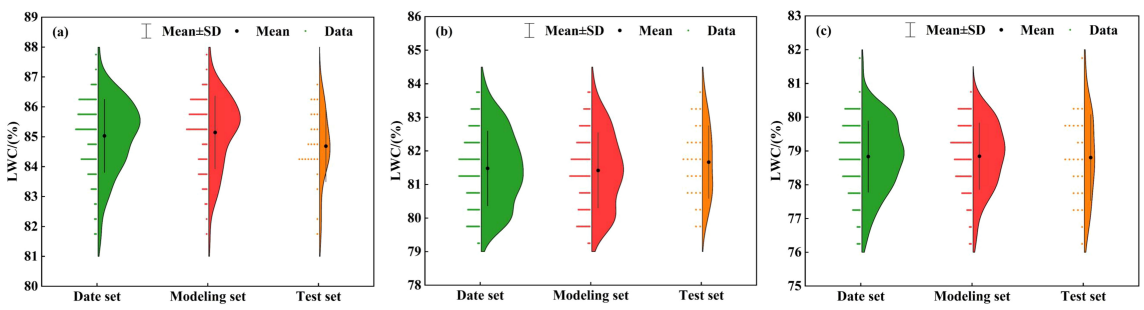

FIGURE 3
Distribution of potato LWC at different growth stages, **(A)** tuber formation stage S1, **(B)** tuber growth stage S2, **(C)** starch accumulation stage S3.

10.3389/fpls.2024.1458589

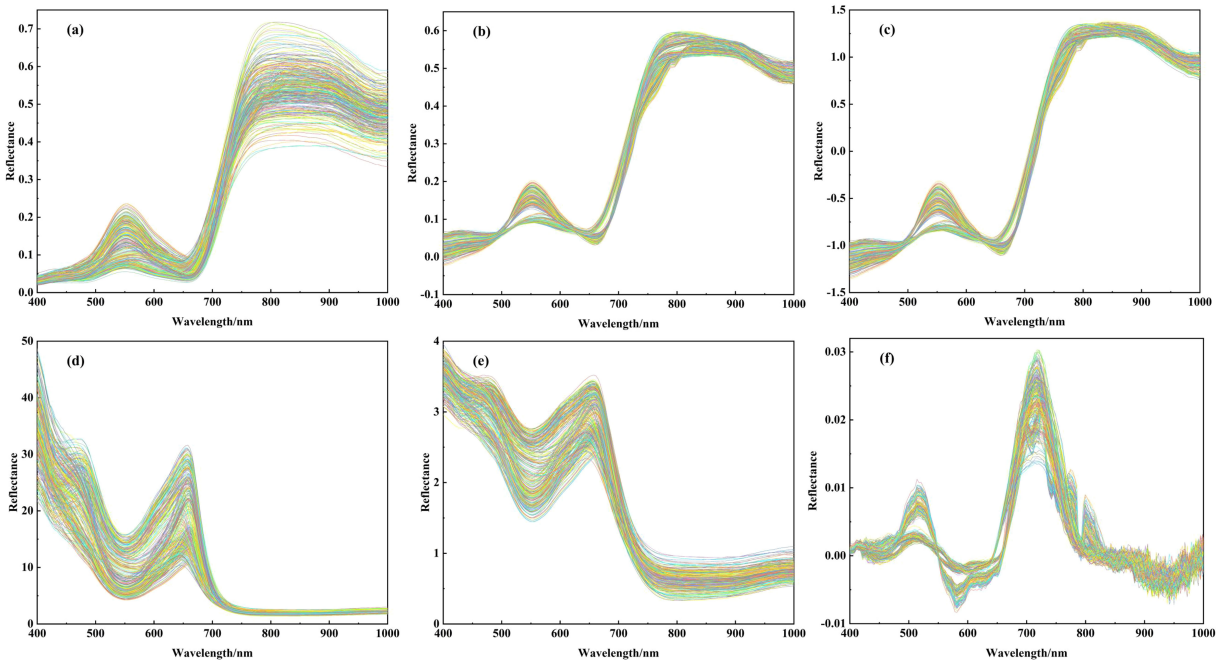

FIGURE 4
Raw and mathematically transformed spectra of potato, **(A)** raw spectra, **(B)** multiple scattering correction transformation spectrum, **(C)** standardized normal variate transformation spectrum, **(D)** inverse transformation spectrum, **(E)** ogarithm of the reciproca transformation spectrum, **(F)** first derivative transformation spectrum.

725 nm, in fact, in this band, all three transformations show the greatest negative correlation with LWC. This suggests that the correlation between spectral features and LWC is better revealed after applying MSC and SNV transformations in this spectral region. In contrast, the correlation curves of RT, Lg(1/R), and FD are smoother, with relatively small fluctuations in the correlation coefficients. Although these transformations provide unique feature information in specific bands (e.g., low reflectance regions), they do not show a significant enhancement in correlation within critical bands (e.g., near 725 nm). This is particularly evident for the FD transform, which shows noise amplification in bands above 800 nm, leading to large fluctuations at high frequencies. As shown in Figure 5, MSC and SNV spectral data are more effective in revealing the relationship between LWC and spectral reflectance. While the RT, Lg(1/R), and FD transforms offer some information gain, their correlation performance is limited in key bands and is more susceptible to noise interference in certain regions. Therefore, R, MSC, and SNV spectral data are selected for subsequent experiments to improve the accuracy of the analysis and the reliability of the model.

3.3 Selection of feature band for potato LWC

The results of band selection processed by CARS and RF are shown in Figure 6, which shows the influence of different selection methods and potato growth stages on the results. Utilizing RF for band selection involves choosing the top 20 bands based on their selection probability, representing 11.36% of all bands. For S1, the feature band identified by the RF band selection methods across in the three types of spectral data was mainly concentrated in the near infrared region of 760-1000 nm, with a smaller distribution in the visible light region of 400-475 nm. For S2, the feature band screened by the RF band selection methods on the three types of spectral data are distributed in both visible light and near-infrared regions, with a more scattered distribution. Fewer feature band selected by RF on the three types of spectra are distributed in the near-infrared region. For S3, the distribution of the feature band selected by RF on the three types of spectra follows the same pattern as in the S2 stage, with a few distributed in the near-infrared region.

For S1, the feature band selected by CARS based on R, MCS, and SNV spectral data are 25, 16, and 22, accounting for 14.20%, 9.09%, and 12.50% of the total bands, respectively. For S2, the feature band screened by the CARS band selection methods on the three types of spectral data are distributed in both visible light and near-infrared regions, with a more scattered distribution. CARS selects 35, 14, and 40 the feature band based on R, MCS, and SNV spectral data, accounting for 19.89%, 7.95%, and 22.73% of the total bands, respectively. For S3, the distribution of the feature band selected by CARS on the three spectra is quite similar, mainly concentrated between 550-830 nm. The feature band selected based on R, MCS, and SNV spectral data are 31, 20, and 31, accounting for 17.61%, 11.36%, and 17.61% of the total bands, respectively. Both band selection methods reduce the spectral dimensions across the three spectral data types, simplifying the model and reducing the computational load.

10.3389/fpls.2024.1458589

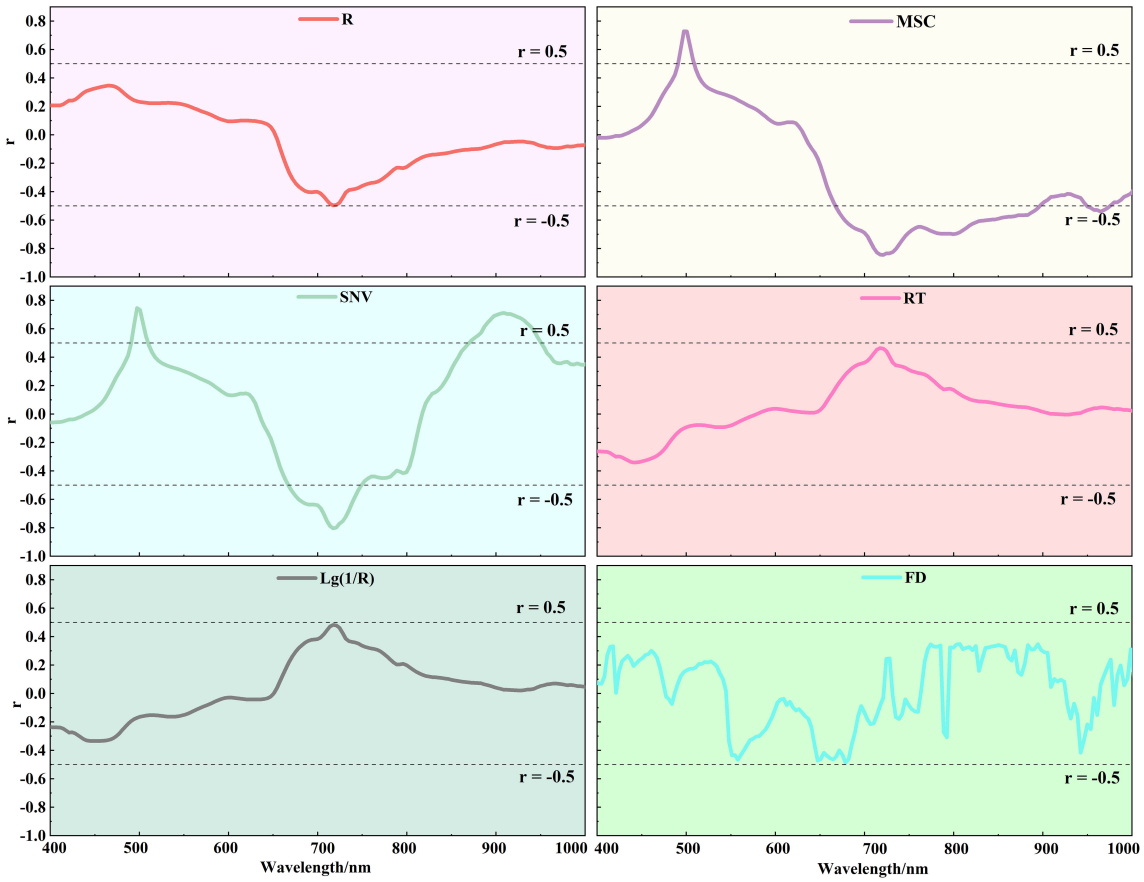

FIGURE 5
Correlation analysis of potato LWC with different transformed spectra.

3.4 Potato LWC estimation models

We used machine learning methods, such as PLSR, SVR, and BP, to develop estimation models for LWC. To achieve more accurate predictions, three different growth stages were modeled independently. In addition, we analyzed the impacts of the full-band and the feature band as variables in the models. 75% of the data is randomly selected to construct the modeling set, and the rest was used as the test set. Figure 7 shows the results of various models on the modeling set.

For S1, the PLSR models show the accuracies ranging from 0.49 to 0.76 for R^2 and 0.60 to 0.87 for RMSE. The MSC-CARS-PLSR model demonstrates the highest R^2 and the smallest RMSE, while the SNV-RF-PLSR model has the lowest R^2 and the largest RMSE. Similarly, the SVR models have accuracies ranging from 0.45 to 0.81 for R^2 and 0.53 to 0.90 for RMSE. The accuracies of the BP models ranged from 0.41 to 0.79 for R^2 and from 0.56 to 0.93 for RMSE. Within this context, the SNV-CARS-BP model demonstrates the highest R^2 and the smallest RMSE, whereas the R-CARS-BP model exhibits the lowest R^2 and the largest RMSE. In the models constructed using raw spectral data R, the full-band models exhibit better modeling performance than the models constructed from selected the feature band. For the models established with spectral data transformed by SNV and MSC, those developed with the feature band selected by CARS outperform the full-band models. However, the performance of the models based on the feature and selected by RF is inferior to that of the full-band models. In addition, after applying SNV and MSC transformations to the original spectral data R, the modeling effect was improved to varying degrees. In particular, the MSC-CARS-SVR model achieves the best modeling effect at the S1 stage.

For S2, the modeling accuracy of the PLSR models ranges from 0.54 to 0.86 for R^2 and from 0.41 to 0.75 for RMSE. Among the models, the SNV-CARS-PLSR model has the highest R^2 and the smallest RMSE, while the R-RF-PLSR model has the lowest R^2 and the highest RMSE. The modeling accuracy of the SVR models ranges from 0.65 to 0.85 for R^2 and 0.42 to 0.65 for RMSE. In this case, the SNV-CARS-SVR model presents the highest R^2 and the smallest RMSE, while the R-RF-SVR model indicates the lowest R^2 and the highest RMSE. Additionally, the modeling accuracy of the BP models ranges from 0.63 to 0.85 for R^2 and 0.42 to 0.67 for RMSE, with the SNV-CARS-BP model achieving the highest R^2 and the smallest RMSE and the R-CARS-BP model recording the lowest R^2 and the highest RMSE. In models established based on the spectral data after MSC transformation, those using the full-band for modeling showed better performance than those using models

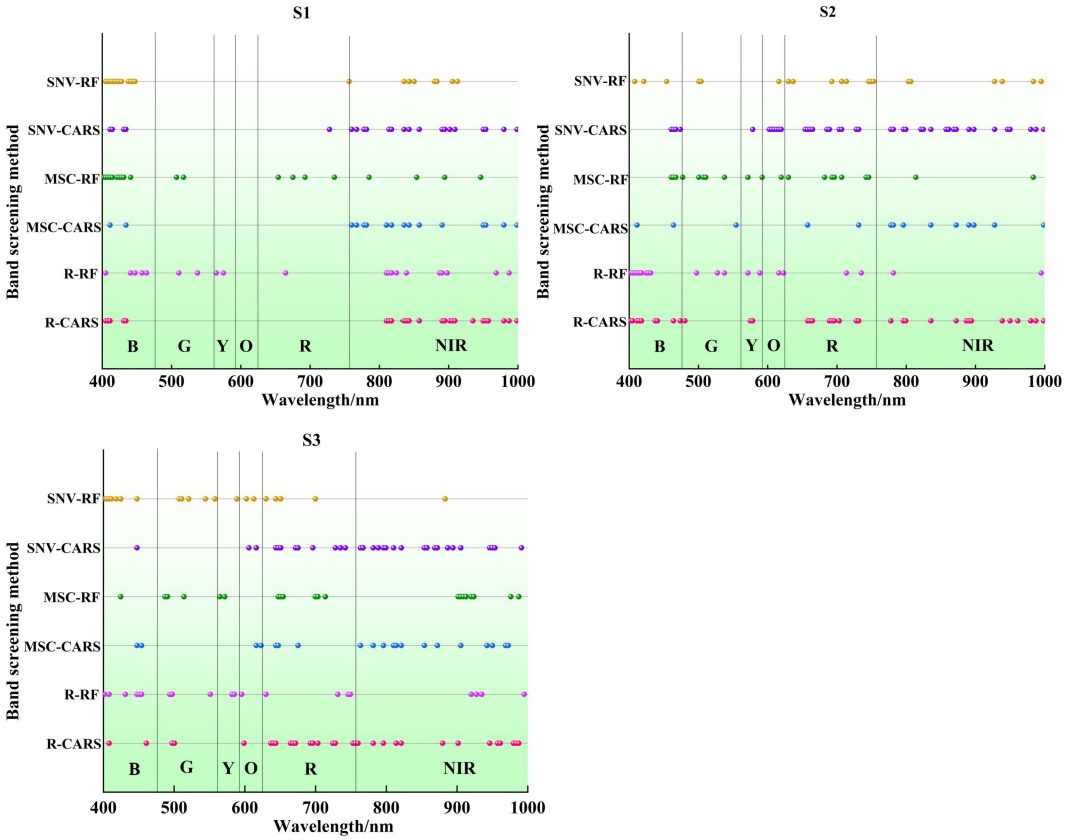

FIGURE 6
Distribution of feature band screened by different feature band screening algorithms.

built with selected the feature band. In the models established based on the original spectral data R and spectra after SNV transformation, models constructed using bands selected by CARS had better performance than those built using the full-band. However, models built with bands selected by RF performed worse than models established with the full-band. Notably, three models established based on data processed by SNV-CARS all achieved optimal predictive performance, with the SNV-CARS-PLSR model emerging as the most accurate at the S2 stage.

For S3, the PLSR model's R^2 modeling accuracy falls between 0.80 and 0.82, with an RMSE ranging from 0.41 to 0.44. Importantly, the MSC-CARS-PLSR model demonstrates the highest R^2 and the smallest RMSE, while the SNV-CARS-PLSR model exhibits the lowest R^2 and the largest RMSE. Likewise, the SVR model's R^2 modeling accuracy spans from 0.81 to 0.87, with an RMSE between 0.36 and 0.43. Once more, the MSC-CARS-SVR model yields the highest R^2 and the smallest RMSE, with the SNV-CARS-SVR model recording the lowest R^2 and the highest RMSE. In the case of the BP models, the R^2 modeling accuracy ranges from 0.80 to 0.86, with an RMSE between 0.37 and 0.44. In this context, the MSC-CARS-BP model demonstrates the highest R^2 and the smallest RMSE, while the R-CARS-BP model exhibits the lowest R^2 and the largest RMSE. Comprehensive analysis reveals that all the models developed during the S3 stage show an R^2 above 0.80 in the prediction set, with minor variations in R^2 and RMSE among the models. Remarkably, three models established based on data processed by MSC-CARS all achieved optimal predictive performance, with the MSC-CARS-SVR model boasting the highest prediction accuracy during the S3 stage.

The potato LWC estimation models should demonstrate high fit universality and repeatability. Accordingly, we further evaluated the accuracy of each growth stage models on the test set. For S1, Figure 8 presents the validation results on the test set for each model. Among them, the nine models based on the R spectrum data show poor test fitting on the test set, with R^2 ranging from 0.25 to 0.63, RMSE ranging from 0.76 to 1.01, and RPD ranging from 1.18 to 1.57. It is noteworthy that, when models being built with the feature band, only the PLSR models surpasses the full-band models. Conversely, the test performances of the SVR and BP models are inferior to the full-band models. In contrast, the nine models based on the MSC spectral data demonstrate good test fitting on the test set, with R^2 ranging from 0.40 to 0.81, RMSE ranging from 0.51 to 0.90, and RPD ranging from 1.32 to 2.33. Models with the feature band selected by CARS demonstrate superior test performance compared to those of the full-band, while models with the feature band selected by RF show inferior test performance. Concerning the nine models based on the SNV spectral data, the test set R^2 ranges from 0.16 to 0.75, RMSE ranges from 0.58 to 1.07, and RPD ranging from 1.11 to 2.05. Models established using the feature band display a test performance similar to that of the MSC spectral data, where

10.3389/fpls.2024.1458589

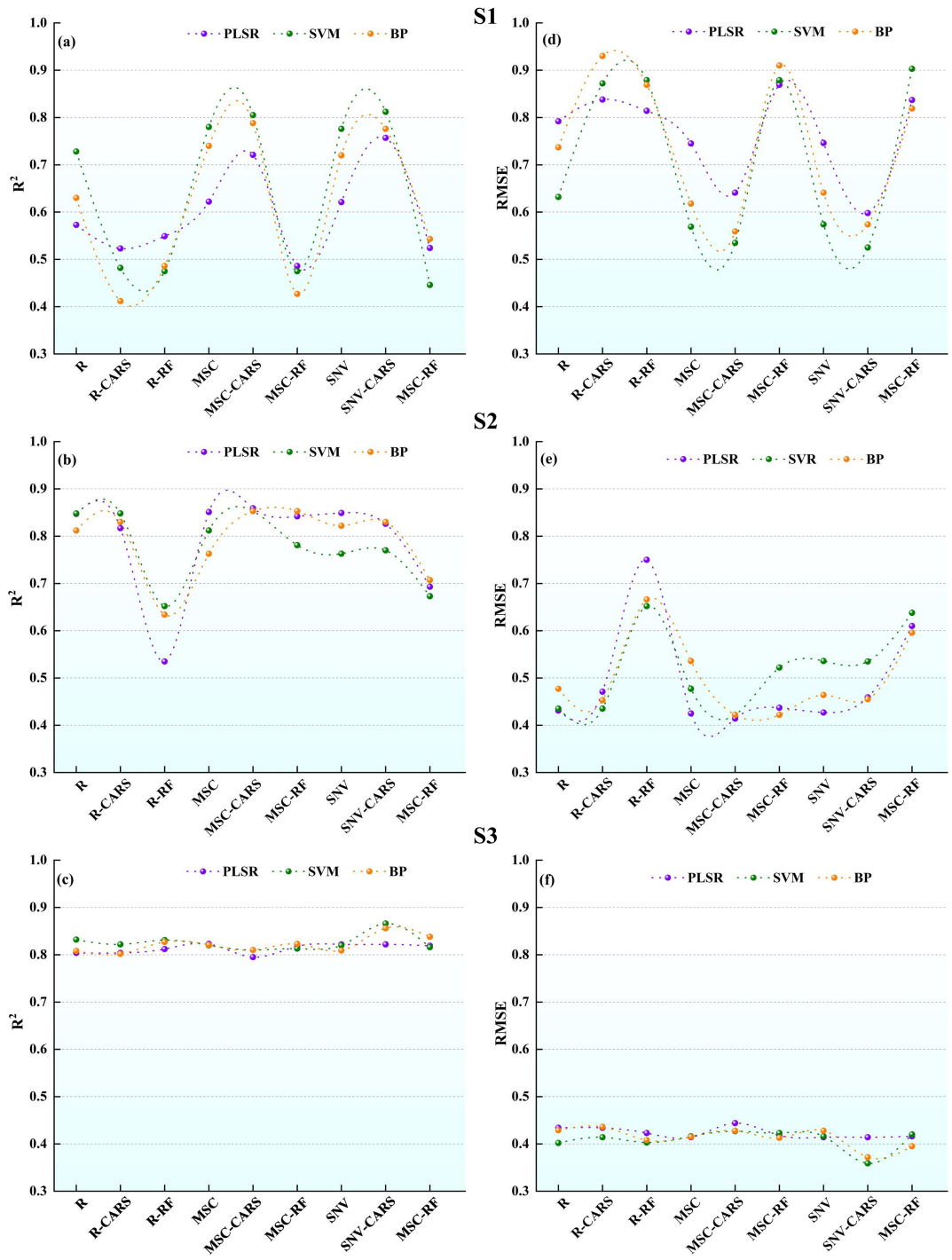

FIGURE 7
Comparison of potato LWC estimation accuracy using three machine learning models: **(A-C)** R^2, **(D-F)** root mean square error (RMSE).

the CARS models demonstrate better test performance than those of the full-band, and the RF models demonstrate inferior test performance. Comparing the test effects of various models for the potato S1 phase, the MSC-CARS-SVR model demonstrates the best test set performance, with R^2 = 0.81, RMSE = 0.51, and RPD=2.33, indicating its potential for potato S1 phase LWC content inversion.

For S2, Figure 9 presents the validation results of the test set samples on each model. In the group of nine models based on the R spectrum data, the test set R^2 ranges from 0.40 to 0.81, with RMSE ranging from 0.47 to 0.82, and RPD ranging from 1.32 to 2.30. Remarkably, the PLSR models with the full-band surpass the those with the feature band in terms of test performance. For the SVR and BP models, the test performance of the models using the feature band selected by the CARS algorithm is superior to the full-band models. Conversely, the RF models demonstrates inferior test performance. Concerning the nine models relying on the MSC

10.3389/fpls.2024.1458589

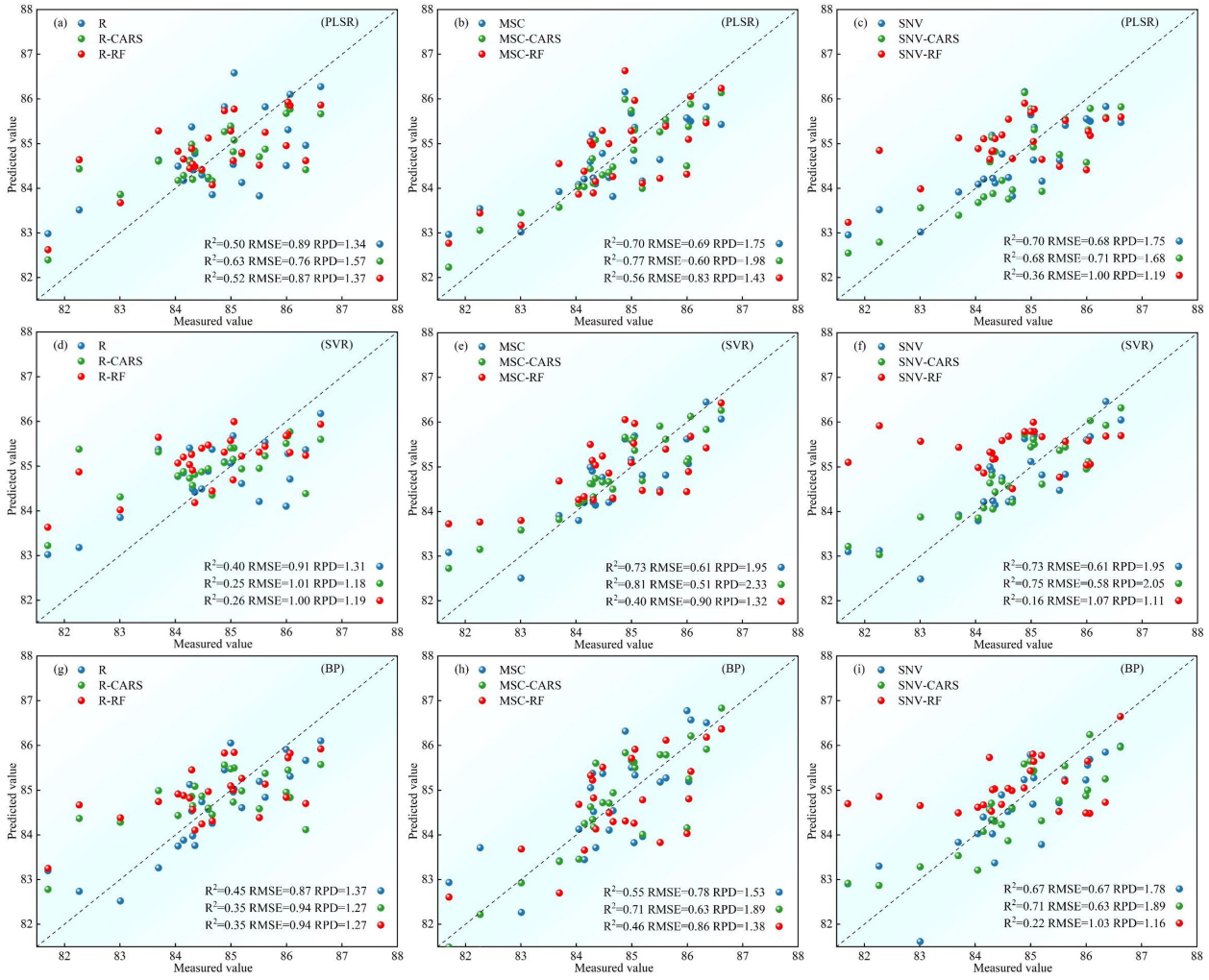

FIGURE 8
Comparison of test set accuracy of potato S1 phase LWC estimation using three machine learning models: **(A-C)** PLSR models, **(D-F)** SVR models, **(G-I)** BP models.

spectral data, the test set R^2 ranges from 0.48 to 0.81, RMSE ranges from 0.47 to 0.77, and RPD ranging from 1.41 to 2.30. Solely the feature band PLSR models outperforms the full-band models in terms of test performance, while the SVR and BP lag behind. Additionally, the nine models based on the SNV spectral data display satisfactory test fitting on the test set, with R^2 ranging from 0.47 to 0.85, RMSE ranging from 0.42 to 0.78, and RPD ranging from 1.39 to 2.58. Specifically, only the SVR models constructed using the feature band selected by CARS exhibits lesser test performance than the full-band models. Conversely, the remaining models using the feature band demonstrate superior test performance. By comparing the test effects of various models for the potato S2 phase, the SNV-CARS-PLSR model emerges with the most optimal test set performance, boasting R^2 = 0.85, RMSE = 0.42, and RPD = 2.58, signifying its effectiveness in inverting the potato S2 phase LWC content.

For S3, Figure 10 presents the validation results of the test set samples on each model. All models exhibit a test set R^2 above 0.70, RMSE below 0.68, and RPD above 1.87. Particularly, among models constructed with the feature band, the test performance of the SVR models, utilizing the feature band selected by CARS, is inferior to the full-band models for the R and MSC spectral data. However, in all other cases, the test performance of the models constructed using the feature band surpasses that of the full-band models. When comparing the test effects of various models for the potato S3 phase, the MSC-RF-PLSR model stands out with the most superior test set performance, boasting an R^2 of 0.81, RMSE of 0.55, and RPD of 2.58. This model effectively monitors the LWC content of potato S3 phase.

Overall, it can be seen that there is no “omnipotent” model to make the most accurate prediction of LWC in different growth stages, so modeling the different growth stages separately is a better choice. For S1, S2 and S3 stages, the most appropriate prediction

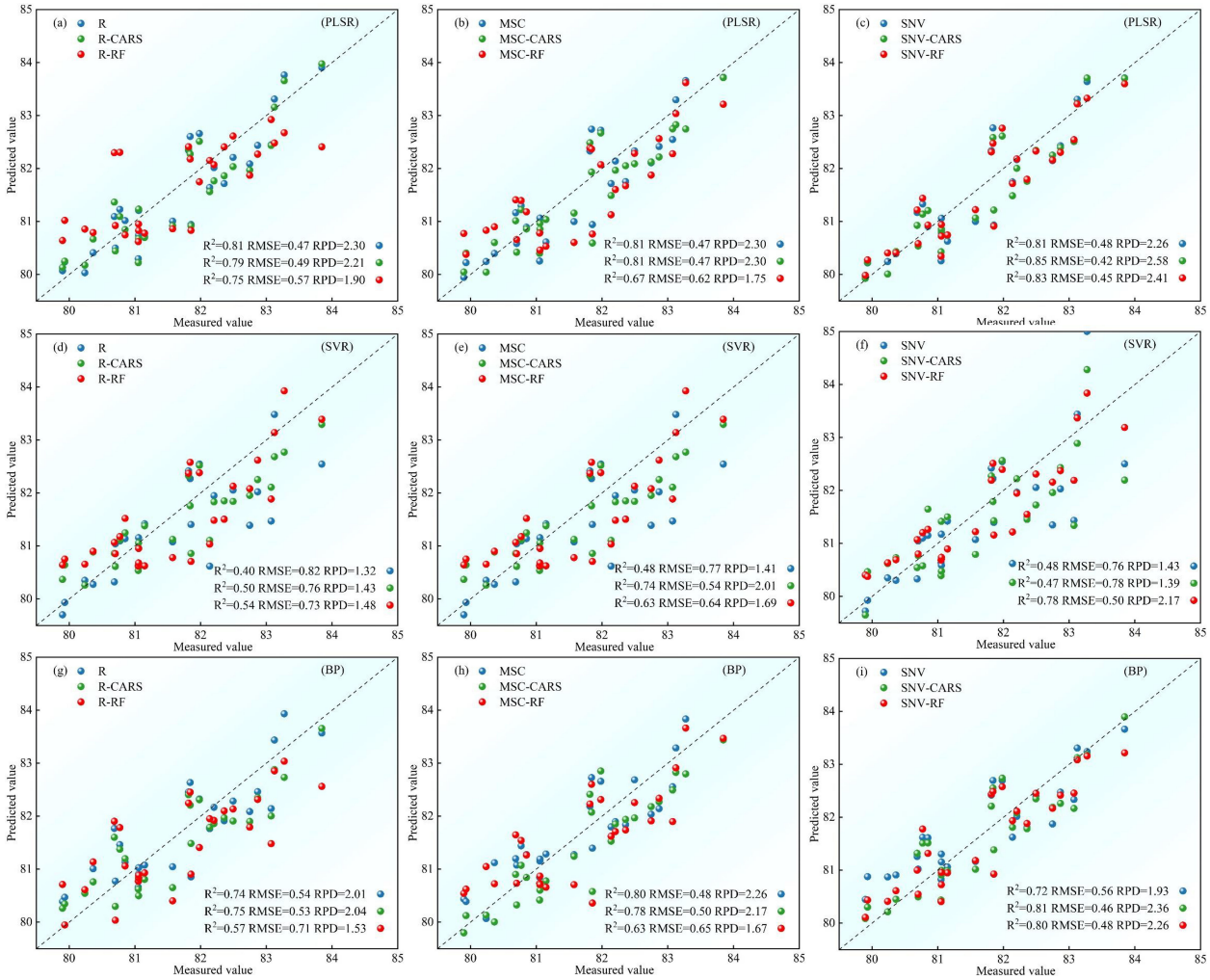

FIGURE 9
Comparison of test set accuracy of potato S2 phase LWC estimation using three machine learning models: **(A-C)** PLSR models, **(D-F)** SVR models, **(G-I)** BP models.

models are MSC-CARS-SVR, SNV-CARS-PLSR and MSC-RF-PLSR respectively.

3.5 Spatial distribution of field potato LWC

Utilizing the best LWC estimation models outlined in Section 3.4, Figure 11 displays the spatial distribution map of LWC for S1, S2, and S3 in 2021 and 2022. Potato LWC levels exhibit notable variations across diverse plots and growth stages, with the S1 stage displaying higher LWC content than the S2 and S3 stages. Additionally, noticeable disparities in potato LWC are observed among different regions within the same plot. Potato plants demonstrate a decrease in LWC during the S3 phase when contrasted with S2. During the S3, the plants prioritize nutrient transfer to the tubers to facilitate tuber growth and starch accumulation. Therefore, foliage may undergo a reduction in water content during this phase to fulfill the nutritional requirements for tuber development. It can be observed that the distribution of LWC in the map is uneven. Some regions, shown in light yellow or orange, indicate higher LWC and may be in vegetation growth and sufficient moisture content. In contrast, dark green regions mean lower LWC and may be under-irrigated. The uneven distribution can indicate which areas should be prioritized for irrigation. By utilizing this map, farmers and managers can pinpoint regions in need of precision irrigation, potentially increasing crop yield achieving the goal of water-saving irrigation.

4 Discussion

4.1 Spectral transformation and feature selection for potato LWC

Mathematical transformation to the original spectrum is essential to improve data quality and modeling accuracy. In our study, we applied MSC and SNV transformations to the potato

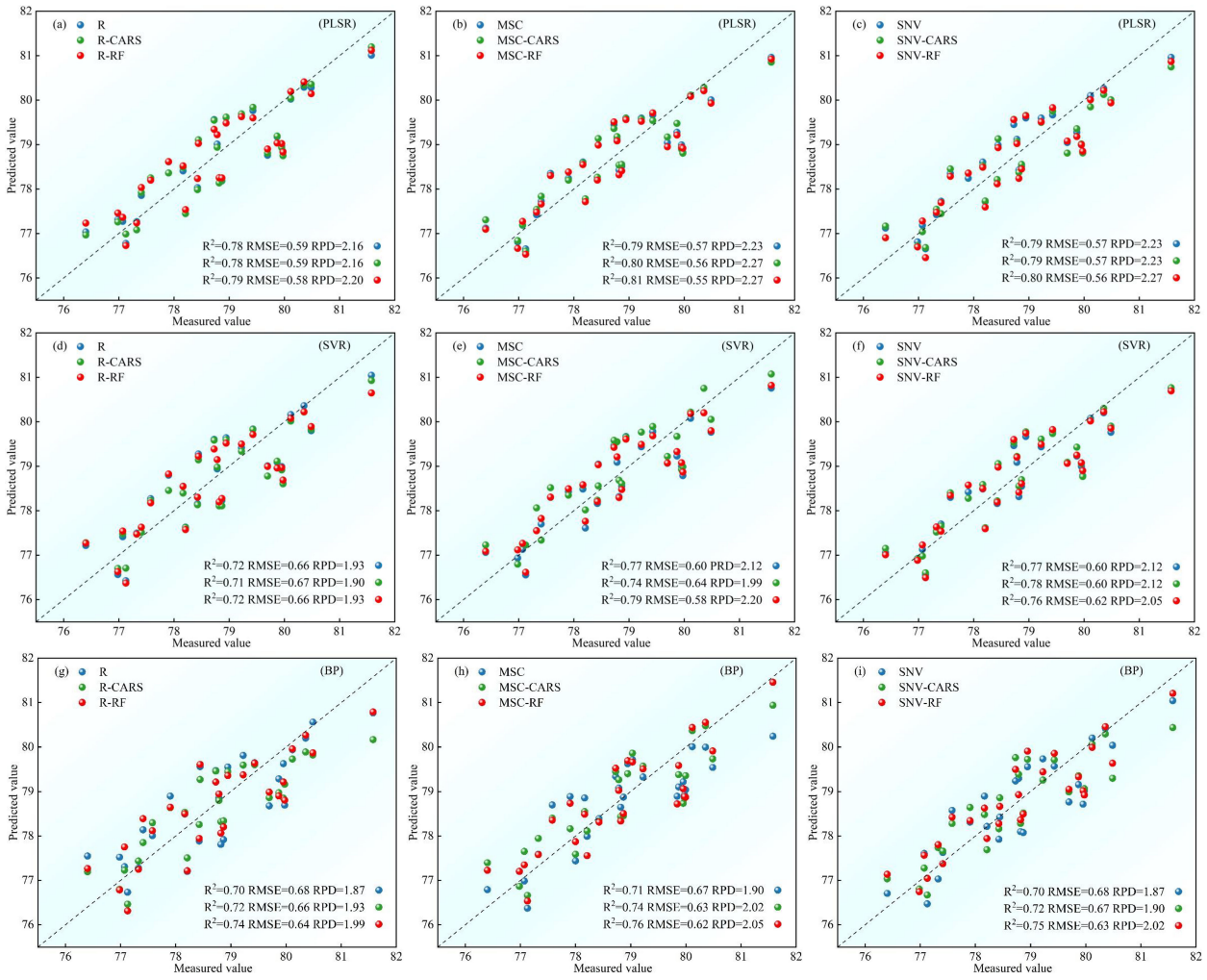

FIGURE 10
Comparison of test set accuracy of potato S3 phase LWC estimation using three machine learning models: **(A-C)** PLSR models, **(D-F)** SVR models, **(G-I)** BP models.

canopy hyperspectral data, which resulted in a significant improvement in the correlation between spectral data and potato LWC. This result is consistent with the research results of Sun et al. (2017) and Chen et al. (2020b), who reported improved correlation values after mathematical transformations of the spectra of purple sweet potatoes and apple leaves. Hyperspectral data contain a significant number of bands, many are irrelevant to potato LWC and make little contribution to the accuracy of the estimation model. Therefore, the full-band modeling is not the best choice. The selection of the feature band handled by CARS and RF helps to reduce data redundancy and improve modeling performance, the result consistent with that of Sudu et al. (2022) and Liu et al. (2020).

4.2 Hyperparameter selection for machine learning models

The performance of machine learning models is heavily influenced by the selection of hyperparameters, and optimizing these hyperparameters directly impacts both the generalization capability and predictive accuracy of the models. To ensure optimal model performance, this study employs grid search and cross-validation to optimize the hyperparameters of PLSR, SVR, and BP. For the PLSR model, the number of principal components is a crucial hyperparameter that influences the model's complexity and generalization ability. Taking the optimization of the number of principal components in the SNV-CARS-PLSR model during the potato S2 stage as an example, Figure 12 demonstrates a clear relationship between the number of principal components and the model's R^2 and RMSE values. As the number of principal components increases from 2 to 20, the R^2 value rises while the RMSE decreases, reaching a peak R^2 of 0.85 at 20 components, with the RMSE minimizing at 0.48. However, beyond 20 components, the R^2 value begins to decline, and the RMSE increases, leading to a decrease in model performance. Therefore, the optimal number of principal components for this model is 20.

For the SVR model, the MSC-CARS-SVR model at the potato S1 stage was used as an example to optimize the hyperparameters C and γ. As shown in Figure 13, the RMSE exhibits a clear trend with varying values of C and γ. When C = 10 and γ = 0.001, the model

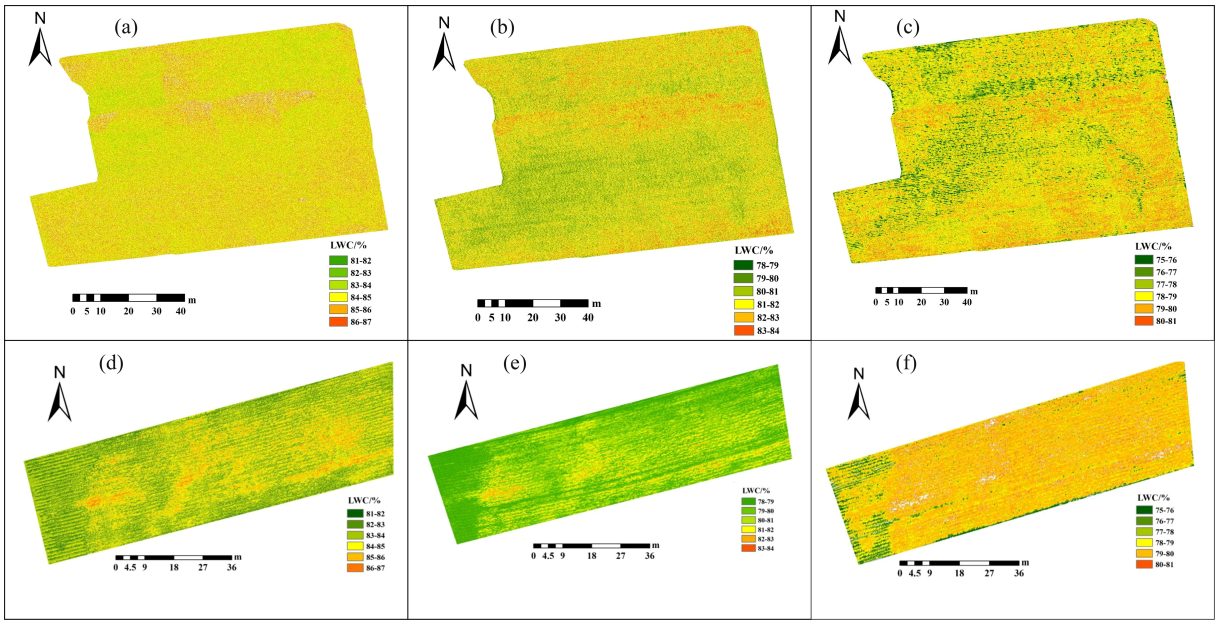

FIGURE 11
Spatial distribution of potato LWC based on the optimal estimation models: **(A-C)** S1-S3 period in 2021, **(D-F)** S1-S3 period in 2022.

achieves the lowest RMSE (0.53), indicating optimal generalization ability. Additionally, Figure 13 illustrates the variation in R^2 values corresponding to different C and γ parameters. Consistent with the RMSE heatmap, the model reaches its highest R^2 value of 0.81 at C = 10 and γ = 0.001, further confirming the best model fit under this parameter combination. Therefore, the optimal parameters for this model are C = 10 and γ = 0.001.

For the BP model, the MSC-CARS-BP model during the potato S3 stage was used as an example, and grid search was employed to identify the optimal constant α. As shown in Table 2, variations in the number of q and the constant α resulted in significant fluctuations in the model's R^2 and RMSE values. Notably, when $q = 7$ and $\alpha = 3$, the model achieved the highest R^2 value of 0.86 and the lowest RMSE of 0.37, indicating optimal model fit. However, an excessive number of

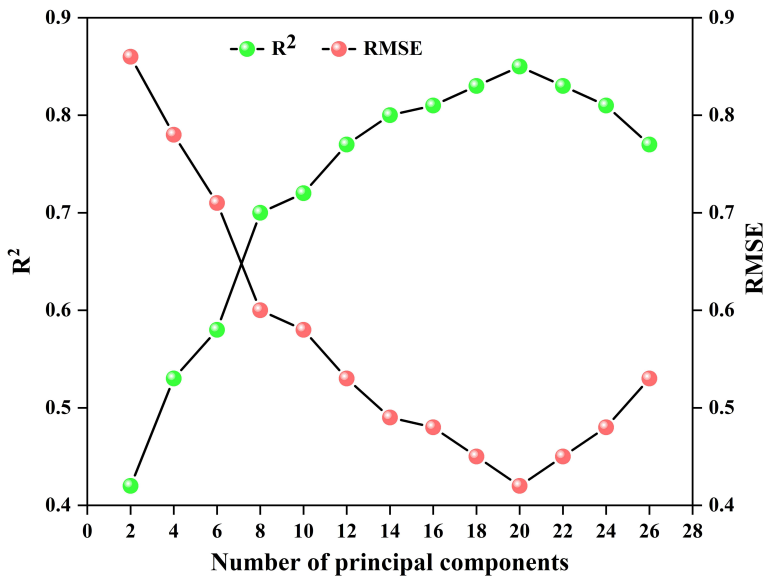

FIGURE 12
Variation of R^2 and RMSE during the optimization of the number of principal components in the SNV-CARS-PLSR model at the potato S2 stage, with 40 input features.

10.3389/fpls.2024.1458589

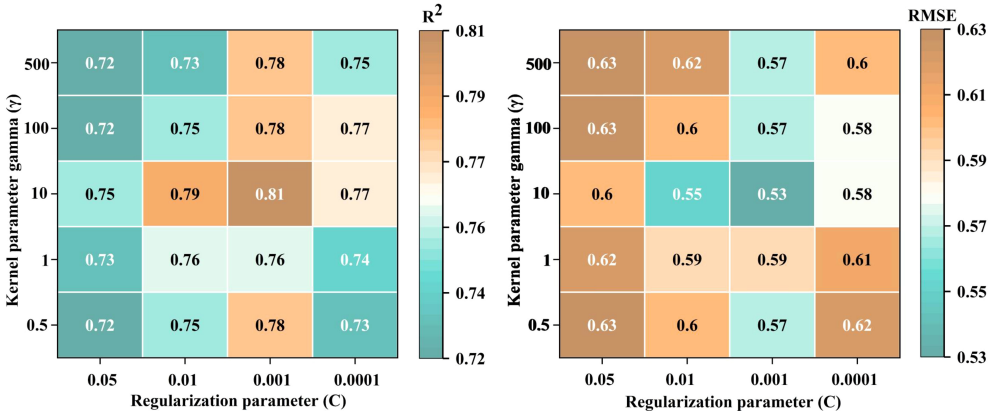

FIGURE 13
Variation of R^2 and RMSE during the optimization of hyperparameters text C and γ in the MSC-CARS-SVR model at the potato S1 stage.

nodes may cause a decrease in R^2 and an increase in RMSE, potentially due to network complexity leading to overfitting. Therefore, the optimal parameters for this model are $q = 10$ and $\alpha = 3$.

By optimizing the hyperparameters of the PLSR, SVR, and BP neural network models, this study successfully enhanced the prediction accuracy and generalization ability of each model. The results demonstrate that proper hyperparameter tuning is crucial for improving model complexity and predictive performance. Future research could explore more complex model structures and optimization algorithms to further enhance model performance.

4.3 Impact of different machine learning algorithms on potato LWC estimation performance

The spectral features of crops are intricately linked to their growth stages, health status, and external environment. These spectral curves undergo distinctive changes across different growth stages (Panigrahi and Das, 2018). A single model can't make accurate predictions for the LWC of the three growth periods. In order to solve this problem, we established LWC estimation models for tuber formation, growth, and starch accumulation stage, respectively - three pivotal growth stages of potatoes. Upon analyzing the potato LWC estimation results for these stages, variations in model accuracy are evident. The model accuracy exhibits a trend of initial increase and subsequent decrease as the growth stages progress, possibly attributed to changes in canopy structure, biomass accumulation, and the distribution of leaf water content as potato growth stages advance, leading to varied predictive performance. Notably, PLSR models emerge as good choice for estimating LWC during the growth and starch accumulation stage. In contrast, SVR models proves better during the tuber formation stage. Primarily, this preference for PLSR is justified by the challenge of multicollinearity among the hyperspectral bands, wherein PLSR demonstrates superior capability in handling multicollinearity compared to SVR and BP algorithms. Additionally, the small sample size of this study suggests that SVR and BP may be susceptible to overfitting. PLSR generally requires less data for small sample sizes, making models established by PLSR more robust than those derived from SVR and BP.

TABLE 2 Variation of R^2 and RMSE during the optimization of BP model hyperparameters C and γ.

q	α	R^2	RMSE
5	1	0.83	0.41
6	2	0.85	0.39
7	3	0.86	0.37
8	4	0.84	0.40
9	5	0.83	0.41
10	6	0.83	0.41
11	7	0.80	0.44
12	8	0.79	0.45
13	9	0.77	0.47
14	10	0.77	0.47

q represents the number of nodes in the hidden layer of the BP neural network, and α is a constant within the range [1, 10]. Using the MSC-CARS-BP model at the potato S3 stage as an example, the number of input features is 20.

4.4 Application of potato LWC distribution maps in adjusting precision irrigation strategies

During potato cultivation, LWC is a key indicator of crop water status and plays a critical role in growth (Suyala et al., 2024; Zununjan et al., 2024). Analysis of LWC data derived from UAV-based hyperspectral inversion shows that the water requirements of potatoes vary significantly at different developmental stages. This finding highlights the importance of developing precise irrigation strategies. The spatial distribution map of LWC can guide irrigation in three main aspects. First, irrigation regulation can be based on LWC variability. As shown in Figure 11, certain regions have low

LWC (e.g., yellow and orange areas), indicating insufficient soil moisture, which may limit crop growth. In these regions, timely increases in irrigation are needed to maintain adequate moisture, promoting root growth and normal tuber development. In contrast, regions with higher LWC (e.g., green areas) should receive reduced irrigation to avoid wasting water and potential soil salinization. Second, precision irrigation can be implemented through zoning management. By using spatial analysis of hyperspectral images, the field can be divided into multiple zones. Each zone can then receive precision drip irrigation based on its LWC levels. The drip irrigation system allows flexible adjustment of water supply according to actual soil moisture needs. This zoning management ensures that each area receives an appropriate water supply during the reproductive period, realizing the principle of 'water supply according to demand.' Finally, irrigation timing should be dynamically adjusted. Time-series analysis of hyperspectral images reveals that potato water demand fluctuates at different growth stages. During S1 and S2 stages, water demand is higher, especially in areas with lower LWC (see Figure 11). In these cases, irrigation frequency and volume should be increased to prevent water shortage. However, during the S3 stage, while water remains important, irrigation should be moderated to prevent excess moisture from inhibiting starch accumulation. Future research will integrate hyperspectral data with soil moisture sensors and meteorological data to further optimize water usage. This will enhance automated irrigation management, contributing to improved potato productivity and quality.

The study aims to develop potato LWC estimation models based on the feature band. Despite achieving impressive accuracy, it faces challenges during training with the machine learning algorithm. This is primarily due to the limited number of test samples, resulting in overfitting and degradation of the model. To overcome this limitation, it is essential to expand the scope of the investigation by increasing the number of sample, period, and potato varieties to validate and enhance the model's applicability. Future research will focus on acquiring more data in more sites, leveraging a larger sample size to enhance the model's robustness and accuracy.

5 Conclusion

The rapid measurement of LWC in the canopy allow farmers know the water distribution of potatoes in the field, so as to formulate water-saving irrigation strategies. In this study, UAV was used as a platform to efficiently collect hyperspectral data of potato canopy at the field scale, and LWCs were actually measured on the ground. After mathematical transformation and the feature band selection, the relationships between LWC and hyperspectral data were analyzed, and the estimation models of LWC were modeled by machine learning. In order to make the model prediction results more accurate, we modeled the LWC of the three main growth stages of potato. The original spectral data underwent two mathematical transformations: MSC and SNV. The methods of the feature band selection contained CARS and RF algorithms. Our modeling approaches included PLSR, SVR, and BP. The investigation yielded the following pivotal findings:

1. Applying MSC and SNV mathematical transformations to the potato canopy hyperspectral data significantly enhanced the correlation between the spectral data and potato LWC. Specifically, the correlation coefficient based on R increased by -0.50 to 0.35 under MSC and by -0.30 to 0.40 under SNV.
2. The band extraction algorithms CARS and RF effectively selected the most relevant bands and reduced data redundancy. Feature band selected by RF represented approximately 11.36% of all bands, while those selected by CARS accounted for 7.95% to 22.73%.
3. The accuracy of the models varied at different stages of potato growth. The optimal models for estimating LWC in stages S1 to S3 were MSC-CARS-SVR, SNV-CARS-PLSR, and MSC-RF-PLSR. These three models consistently provided stable and accurate estimation of potato LWC.

Data availability statement

The raw data supporting the conclusions of this article will be made available by the authors, without undue reservation.

Author contributions

FG: Resources, Formal analysis, Writing – review & editing, Writing – original draft, Visualization, Validation, Software, Methodology, Investigation, Data curation, Conceptualization. QF: Resources, Writing – review & editing, Supervision, Project administration, Funding acquisition, Conceptualization. SY: Writing – review & editing, Validation, Supervision, Investigation. WY: Writing – review & editing, Validation, Supervision, Investigation, Funding acquisition.

Funding

The author(s) declare financial support was received for the research, authorship, and/or publication of this article. This work was supported by the National Natural Science Foundation of China (Grant No. 32160421), the Industrialization Support Project from Education Department of Gansu Province (Grant No.2021CYZC-57), and the Doctoral Foundation of Department of Education of Gansu Provincial (2021QB-033).

Conflict of interest

The authors declare that the research was conducted in the absence of any commercial or financial relationships that could be construed as a potential conflict of interest.

Publisher's note

All claims expressed in this article are solely those of the authors and do not necessarily represent those of their affiliated organizations, or those of the publisher, the editors and the reviewers. Any product that may be evaluated in this article, or claim that may be made by its manufacturer, is not guaranteed or endorsed by the publisher.

References

Aziz, M., Rizvi, S. A., Iqbal, M. A., Syed, S., Ashraf, M., Anwer, S., et al. (2021). A sustainable irrigation system for small landholdings of rainfed Punjab, Pakistan. *Sustainability* 13, 11178.

Burnett, A. C., Jeremiah, A., Davidson, K. J., Ely, K. S., Julien, L., Qianyu, L., et al. (2021). A best-practice guide to predicting plant traits from leaf-level hyperspectral data using partial least squares regression. *J. Exp. Bot.* 72, 6175–6189.

Chen, S., Chen, Y., Chen, J., Zhang, Z., Fu, Q., Bian, J., et al. (2020a). Retrieval of cotton plant water content by uav-based vegetation supply water index (vswi). *Int. J. Remote Sens.* 41, 4389–4407.

Chen, S., Hu, T., Luo, L., He, Q., Zhang, S., Li, M., et al. (2020b). Rapid estimation of leaf nitrogen content in apple-trees based on canopy hyperspectral reflectance using multivariate methods. *Infrared Phys. Technol.* 111, 103542.

Chen, L., Li, Z., Yu, F., Zhang, X., Xue, Y., and Xue, C. (2019). Hyperspectral imaging and chemometrics for nondestructive quantification of total volatile basic nitrogen in pacific oysters (crassostrea gigas). *Food analyt. Methods* 12, 799–810.

Cheng, J.-H., and Sun, D.-W. (2017). Partial least squares regression (plsr) applied to nir and hsi spectral data modeling to predict chemical properties of fish muscle. *Food Eng. Rev.* 9, 36–49.

Duarte-Carvajalino, J. M., Silva-Arero, E. A., Góez-Vinasco, G. A., Torres-Delgado, L. M., Ocampo-Paez, O. D., and Castaño-Marín, A. M. (2021). Estimation of water stress in potato plants using hyperspectral imagery and machine learning algorithms. *Horticulturae* 7, 176.

Elsherbiny, O., Fan, Y., Zhou, L., and Qiu, Z. (2021). Fusion of feature selection methods and regression algorithms for predicting the canopy water content of rice based on hyperspectral data. *Agriculture* 11, 51.

Feng, H., Tao, H., Li, Z., Yang, G., and Zhao, C. (2022). Comparison of uav rgb imagery and hyperspectral remote-sensing data for monitoring winter wheat growth. *Remote Sens.* 14, 3811.

Féret, J.-B., Le Maire, G., Jay, S., Berveiller, D., Bendoula, R., Hmimina, G., et al. (2019). Estimating leaf mass per area and equivalent water thickness based on leaf optical properties: Potential and limitations of physical modeling and machine learning. *Remote Sens. Environ.* 231, 110959.

Genkawa, T., Shinzawa, H., Kato, H., Ishikawa, D., Murayama, K., Komiyama, M., et al. (2015). Baseline correction of diffuse reflection near-infrared spectra using searching region standard normal variate (srsnv). *Appl. Spectrosc.* 69, 1432–1441.

Guo, F., Feng, Q., Yang, S., and Yang, W. (2023). Estimation of potato canopy nitrogen content based on hyperspectral index optimization. *Agronomy* 13, 1693.

He, L., Liu, M.-R., Zhang, S.-H., Guan, H.-W., Wang, C.-Y., Feng, W., et al. (2023). Remote estimation of leaf water concentration in winter wheat under different nitrogen treatments and plant growth stages. *Precis. Agric.* 24, 986–1013.

Hu, M.-H., Dong, Q.-L., Liu, B.-L., Opara, U. L., and Chen, L. (2015). Estimating blueberry mechanical properties based on random frog selected hyperspectral data. *Postharvest Biol. Technol.* 106, 1–10.

Ishikawa, D., Fukuda, S., Arimitsu, S., Ohba, K., Ozaki, Y., and Ishiguro, E. (2013). A case study on evaluation of water contents change in leaves (sudajii) by using chlorophyll absorption band in the 400-1100 nm region. *J. Agric. meteorol.* 69, 201–207.

Jia, M., Li, W., Wang, K., Zhou, C., Cheng, T., Tian, Y., et al. (2019). A newly developed method to extract the optimal hyperspectral feature for monitoring leaf biomass in wheat. *Comput. Electron. Agric.* 165, 104942.

Kovar, M., Brestic, M., Sytar, O., Barek, V., Hauptvogel, P., and Zivcak, M. (2019). Evaluation of hyperspectral reflectance parameters to assess the leaf water content in soybean. *Water* 11, 443.

Krishna, G., Sahoo, R. N., Singh, P., Bajpai, V., Patra, H., Kumar, S., et al. (2019). Comparison of various modelling approaches for water deficit stress monitoring in rice crop through hyperspectral remote sensing. *Agric. Water Manage.* 213, 231–244.

Lakhiar, I. A., Yan, H., Zhang, C., Wang, G., He, B., Hao, B., et al. (2024). A review of precision irrigation water-saving technology under changing climate for enhancing water use efficiency, crop yield, and environmental footprints. *Agriculture* 14, 1141.

Li, Z., Chen, Z., Cheng, Q., Duan, F., Sui, R., Huang, X., et al. (2022b). Uav-based hyperspectral and ensemble machine learning for predicting yield in winter wheat. *Agronomy* 12, 202.

Li, Z., Nie, C., Wei, C., Xu, X., Song, X., and Wang, J. (2016). Comparison of four chemometric techniques for estimating leaf nitrogen concentrations in winter wheat (triticum aestivum) based on hyperspectral features. *J. Appl. Spectrosc.* 83, 240–247.

Li, C., Xiao, Z., Liu, Y., Meng, X., Li, X., Wang, X., et al. (2022a). Hyperspectral estimation of winter wheat leaf water content based on fractional order differentiation and continuous wavelet transform. *Agronomy* 13, 56.

Li, H., Xu, Q., and Frog, Y. L. R. (2012). An efficient reversible jump markov chain monte Carlo-like approach for variable selection with applications to gene selection and disease classification. *Analytica Chimica Acta*. 740, 20–26. doi: 10.1016/j.aca.2012.06.031

Liu, S., Hu, Z., Han, J., Li, Y., and Zhou, T. (2022). Predicting grain yield and protein content of winter wheat at different growth stages by hyperspectral data integrated with growth monitor index. *Comput. Electron. Agric.* 200, 107235.

Liu, S., Peng, Y., Du, W., Le, Y., and Li, L. (2015). Remote estimation of leaf and canopy water content in winter wheat with different vertical distribution of water-related properties. *Remote Sens.* 7, 4626–4650.

Liu, N., Qiao, L., Xing, Z., Li, M., Sun, H., Zhang, J., et al. (2020). Detection of chlorophyll content in growth potato based on spectral variable analysis. *Spectrosc. Lett.* 53, 476–488.

Luo, S., Liu, W., Ren, Q., Wei, H., Wang, C., Xi, X., et al. (2024). Leaf area index estimation in maize and soybean using uav lidar data. *Precis. Agric.*, 1–18.

Maes, W. H., and Steppe, K. (2019). Perspectives for remote sensing with unmanned aerial vehicles in precision agriculture. *Trends Plant Sci.* 24, 152–164.

Meiyan, S., Qizhou, D., ShuaiPeng, F., Xiaohong, Y., Jinyu, Z., Lei, M., et al. (2022). Improved estimation of canopy water status in maize using uav-based digital and hyperspectral images. *Comput. Electron. Agric.* 197, 106982.

Mohite, J., Sawant, S., Agarwal, R., Pandit, A., and Pappula, S. (2022). "Detection of crop water stress in maize using drone-based hyperspectral imaging," in *IGARSS 2022-2022 IEEE International Geoscience and Remote Sensing Symposium*. (IEEE), 5957–5960.

Ndlovu, H. S., Odindi, J., Sibanda, M., Mutanga, O., Clulow, A., Chimonyo, V. G., et al. (2021). A comparative estimation of maize leaf water content using machine learning techniques and unmanned aerial vehicle (uav)-based proximal and remotely sensed data. *Remote Sens.* 13, 4091.

Panigrahi, N., and Das, B. (2018). Canopy spectral reflectance as a predictor of soil water potential in rice. *Water Resour. Res.* 54, 2544–2560.

Raj, R., Walker, J. P., Vinod, V., Pingale, R., Naik, B., and Jagarlapudi, A. (2021). Leaf water content estimation using top-of-canopy airborne hyperspectral data. *Int. J. Appl. Earth Observ. Geoinform.* 102, 102393.

Roberto, C., Lorenzo, B., Michele, M., Micol, R., and Cinzia, P. (2018). "Optical remote sensing of vegetation water content," in *Hyperspectral Indices and Image Classifications for Agriculture and Vegetation* (Boca Raton, FL: CRC Press), 183–200.

Sonobe, R., and Hirono, Y. (2022). Applying variable selection methods and preprocessing techniques to hyperspectral reflectance data to estimate tea cultivar chlorophyll content. *Remote Sens.* 15, 19.

Suárez, L., Zarco-Tejada, P., Berni, J., González-Dugo, V., and Fereres, E. (2009). Modelling pri for water stress detection using radiative transfer models. *Remote Sens. Environ.* 113, 730–744.

Suárez, L., Zarco-Tejada, P. J., Sepulcre-Cantó, G., Pérez-Priego, O., Miller, J., Jiménez-Muñoz, J., et al. (2008). Assessing canopy pri for water stress detection with diurnal airborne imagery. *Remote Sens. Environ.* 112, 560–575.

Sudu, B., Rong, G., Guga, S., Li, K., Zhi, F., Guo, Y., et al. (2022). Retrieving spad values of summer maize using uav hyperspectral data based on multiple machine learning algorithm. *Remote Sens.* 14, 5407.

Sun, Y., Chen, S., Ning, J., Han, W., and Weckler, P. (2015). Prediction of moisture content in corn leaves based on hyperspectral imaging and chemometric analysis. *Trans. ASABE* 58, 531–537.

Sun, Y., Liu, Y., Yu, H., Xie, A., Li, X., Yin, Y., et al. (2017). Non-destructive prediction of moisture content and freezable water content of purple-fleshed sweet potato slices during drying process using hyperspectral imaging technique. *Food Anal. Methods* 10, 1–12.

Sun, J., Yang, W., Zhang, M., Feng, M., Xiao, L., and Ding, G. (2021). Estimation of water content in corn leaves using hyperspectral data based on fractional order savitzky-golay derivation coupled with wavelength selection. *Comput. Electron. Agric.* 182, 105989.

Sun, H., Zhang, L., Rao, Z., and Ji, H. (2020). Determination of moisture content in barley seeds based on hyperspectral imaging technology. *Spectrosc. Lett.* 53, 751–762.

Suyala, Q., Li, Z., Zhang, Z., Jia, L., Fan, M., Sun, Y., et al. (2024). Developing a hyperspectral remote sensing-based algorithm to diagnose potato moisture for water-saving irrigation. *Horticulturae* 10, 811.

Tao, F., Yao, H., Hruska, Z., Liu, Y., Rajasekaran, K., and Bhatnagar, D. (2020). Detection of aflatoxin b1 on corn kernel surfaces using visible-near infrared spectroscopy. *J. Near Infrared Spectrosc.* 28, 59–69.

Tunca, E., Köksal, E. S., Özturk, E., Akay, H., and Çetin Taner, S. (2023). Accurate estimation of sorghum crop water content under different water stress levels using machine learning and hyperspectral data. *Environ. Monit. Assess.* 195, 877.

Virnodkar, S. S., Pachghare, V. K., Patil, V. C., and Jha, S. K. (2020). Remote sensing and machine learning for crop water stress determination in various crops: a critical review. *Precis. Agric.* 21, 1121–1155.

Wang, S., Wu, Z., Cao, C., An, M., Luo, K., Sun, L., et al. (2023). Design and experiment of online detection system for water content of fresh tea leaves after harvesting based on near infra-red spectroscopy. *Sensors* 23, 666.

Wang, F., Yi, Q., Hu, J., Xie, L., Yao, X., Xu, T., et al. (2021). Combining spectral and textural information in uav hyperspectral images to estimate rice grain yield. *Int. J. Appl. Earth Observ. Geoinform.* 102, 102397.

Wijesinha-Bettoni, R., and Mouillé, B. (2019). The contribution of potatoes to global food security, nutrition and healthy diets. *Am. J. Potato Res.* 96, 139–149.

Wong, T.-T. (2015). Performance evaluation of classification algorithms by k-fold and leave-one-out cross validation. *Pattern recogn.* 48, 2839–2846.

Xie, C., and Yang, C. (2020). A review on plant high-throughput phenotyping traits using uav-based sensors. *Comput. Electron. Agric.* 178, 105731.

Xing, Z., Du, C., Shen, Y., Ma, F., and Zhou, J. (2021). A method combining ftir-atr and raman spectroscopy to determine soil organic matter: Improvement of prediction accuracy using competitive adaptive reweighted sampling (cars). *Comput. Electron. Agric.* 191, 106549.

Xu, X., Zhao, T., Ma, J., Song, Q., Wei, Q., and Sun, W. (2022). Application of two-stage variable temperature drying in hot air-drying of paddy rice. *Foods* 11, 888.

Yang, C., Xu, J., Feng, M., Bai, J., Sun, H., Song, L., et al. (2023). Evaluation of hyperspectral monitoring model for aboveground dry biomass of winter wheat by using multiple factors. *Agronomy* 13, 983.

Zhang, H., Fen, X., Yu, W., Hu, H.-h., and Dai, X.-f. (2017). Progress of potato staple food research and industry development in China. *J. Integr. Agric.* 16, 2924–2932.

Zhang, J., Zhang, W., Xiong, S., Song, Z., Tian, W., Shi, L., et al. (2021). Comparison of new hyperspectral index and machine learning models for prediction of winter wheat leaf water content. *Plant Methods* 17, 1–14.

Zhang, L., Zhou, Z., Zhang, G., Meng, Y., Chen, B., and Wang, Y. (2014). Monitoring cotton (gossypium hirsutum l.) leaf ion content and leaf water content in saline soil with hyperspectral reflectance. *Eur. J. Remote Sens.* 47, 593–610.

Zheng, J., Song, X., Yang, G., Du, X., Mei, X., and Yang, X. (2022). Remote sensing monitoring of rice and wheat canopy nitrogen: A review. *Remote Sens.* 14, 5712.

Zhou, X., Sun, J., Tian, Y., Lu, B., Hang, Y., and Chen, Q. (2020). Hyperspectral technique combined with deep learning algorithm for detection of compound heavy metals in lettuce. *Food Chem.* 321, 126503.

Zhu, Z., Li, T., Cui, J., Shi, X., Chen, J., and Wang, H. (2020). Non-destructive estimation of winter wheat leaf moisture content using near-ground hyperspectral imaging technology. *Acta Agricult. Scandinavica Section B—Soil Plant Sci.* 70, 294–306.

Zununjan, Z., Turghan, M. A., Sattar, M., Kasim, N., Emin, B., and Abliz, A. (2024). Combining the fractional order derivative and machine learning for leaf water content estimation of spring wheat using hyper-spectral indices. *Plant Methods* 20, 1–24.

frontiers | Frontiers in Plant Science

TYPE Original Research
PUBLISHED 10 January 2025
DOI 10.3389/fpls.2024.1520272

Check for updates

OPEN ACCESS

EDITED BY
Amir Khoddamzadeh,
Florida International University, United States

REVIEWED BY
Honghai Luo,
Shihezi University, China
Meng Xu,
Chinese Academy of Agricultural Sciences, China

*CORRESPONDENCE
Zhiguo Wang
wangzhiguo@xaas.ac.cn
Yanbo Fu
zxb2023303003@cau.edu.cn

†These authors have contributed equally to this work

RECEIVED 31 October 2024
ACCEPTED 12 December 2024
PUBLISHED 10 January 2025

CITATION
Zhao Y, Bian Q, Dong Z, Rao X, Wang Z, Fu Y and Chen B (2025) The input of organic fertilizer can improve soil physicochemical properties and increase cotton yield in southern Xinjiang. *Front. Plant Sci.* 15:1520272. doi: 10.3389/fpls.2024.1520272

COPYRIGHT
© 2025 Zhao, Bian, Dong, Rao, Wang, Fu and Chen. This is an open-access article distributed under the terms of the Creative Commons Attribution License (CC BY). The use, distribution or reproduction in other forums is permitted, provided the original author(s) and the copyright owner(s) are credited and that the original publication in this journal is cited, in accordance with accepted academic practice. No use, distribution or reproduction is permitted which does not comply with these terms.

The input of organic fertilizer can improve soil physicochemical properties and increase cotton yield in southern Xinjiang

Yupeng Zhao[1,2†], Qingyong Bian[3†], Zhiduo Dong[1], Xiaojuan Rao[4], Zhiguo Wang[1*], Yanbo Fu[1,3*] and Bolang Chen[2]

[1]Institute of Soil Fertilizer and Agricultural Water Conservation, Xinjiang Academy of Agricultural Sciences, Urumqi, Xinjiang, China, [2]College of Resources and Environment, Xinjiang Agricultural University, Urumqi, China, [3]Baicheng Agricultural Experimental Station/National Soil Quality Aksu Observation Experimental Station, Xinjiang Academy of Agricultural Sciences, Aksu/National Soil Quality Observation and Experimental Station, Aksu, Xinjiang, China, [4]Biological Science and Technology College of Xinjiang Agricultural Vocational and Technical University, Urumqi, Xinjiang, China

In this study, the improvement effect of different organic substances on compacted cohesive soil in southern Xinjiang was discussed, with emphasis on the influence of different organic substances on soil chemical properties and microorganisms, so as to determine the best carbon source input and provide theoretical support for the rational utilization of organic materials in southern Xinjiang. Field experiments were conducted to evaluate the effects of farm fertilizer, biochar, commercial organic fertilizer, microbial fertilizer and mineral potassium humate on physical and chemical properties of viscous soil, agronomic properties and yield of cotton, with three gradients for each organic fertilizer. The results showed that: (1) all organic fertilizers improved soil structure, among which farm fertilizer significantly reduced soil bulk density and salinity, increased soil organic matter, total nitrogen and available nutrients, and thus increased cotton height, stem diameter and yield. The optimal application amount was 36000 kg/hm^2. (2) The application of different organic matter increased the contents of organic matter, total nitrogen, hydrolyzed nitrogen, available phosphorus and available potassium in 0-40 cm soil layer, increased the number of bacteria, fungi and actinomyces, and reduced soil salinity; (3) Structural equation model (SEM) was used to investigate the effect mechanism of organic matter input on soil microbial quantity, soil physicochemical properties and cotton yield. The model further confirmed the mechanism: the input of organic matter mainly regulates the number of microorganisms and the richness of microbial species, thereby improving the physical and chemical properties of soil and thereby increasing the cotton yield. The addition of 5 kinds of organic materials can promote the growth and yield of cotton. The comprehensive evaluation shows that the improvement effect is best when the fertilizer dosage is 150% of the recommended amount. In summary, as

an effective soil amendment, farm manure can not only alleviate soil compaction, but also significantly improve the growth potential of cotton, which is in line with the goal of sustainable agricultural development.

KEYWORDS

soil nutrients, cotton, soil physical and chemical properties, soil microorganisms, southern Xinjiang

1 Introduction

Soil is a basic resource for food production and is critical to environmental quality and the health of plants, animals and humans. Soil compaction is an obvious manifestation of soil degradation, which can be caused by a variety of factors such as heavy machinery operations, improper farming practices, soil acidification, and salinization caused by excessive use of fertilizers. These problems can lead to soil structural deterioration and compaction (Głąb, 2014; Han, 2015; Figueiredo et al., 2017), which in turn increases soil hardness and reduces its ability to store, retain and transport water. This compaction leads to decreased soil productivity, weakened water and nutrient storage capacity, and ultimately requires more fertilizer inputs, increasing production costs. In addition, soil compaction interferes with the carbon and nitrogen cycles, inhibits the mineralization of organic matter (De Neve and Hofman, 2000), increases the concentration of carbon dioxide in the soil (Conlin, 2000), and reduces microbial activity (Hamza and Anderson, 2005). Compaction may also cause soil erosion, resulting in nutrient loss and increasing environmental pollution (Du et al., 2022).The southern region of Xinjiang is located in an extremely arid climate, where evaporation is greater than precipitation, which makes the deep saline water in farmland gradually rise to the soil surface with evaporation or plant transpiration, resulting in secondary salinization of farmland soil. Saline-alkali soil contains a large number of sodium ions, chloride ions, these ions have a strong ability to disperse soil particles, resulting in a high degree of dispersion of soil particles, will destroy the soil aggregate structure, make the soil permeability and permeability become poor, the soil wet sticky or dry hard. On the whole, soil compaction leads to a serious decline in cultivated land quality and constraints on comprehensive agricultural production capacity, which directly threatens China's food security and poses challenges to sustainable agricultural development (Figueiredo et al., 2017). Therefore, improving soil quality has become an urgent problem in the current land use and management.

The use of organic materials can reduce the amount of fertilizer used, improve soil fertility, thereby increasing crop yields and improving the ecological environment. Wen et al (Wen et al., 2015). showed that compared with the single application of chemical fertilizer, single application of organic fertilizer or combined application of organic and inorganic fertilizer could significantly improve the level of soil nutrients. The soil organic matter content increased by 95% to 136%, the total nitrogen content increased by 69% to 137%, the available phosphorus content increased by about five times, the available potassium content increased by 81% to 103%, and the pH value decreased by 0.15 to 0.47. The study of Qiu et al (Qiu et al., 2019). showed that different types of organic fertilizer application could effectively improve soil fertility, and the yield of maize in the current season was increased by 48.60% and the economic benefit was increased by 33.75% compared with conventional fertilization. In addition, the application of organic fertilizer not only improves the soil nutrients and microbial quantity, but also enhances the water retention ability (Unger, 1978; Haynes and Naidu, 1998), activates the activity of soil enzymes, and promotes the decomposition and release of organic matter (Stemmer et al., 1998).

Long-term use of organic materials can further improve the nitrogen use efficiency of crops, increase yield, reduce the loss of nitrogen and carbon, and improve the ecological environment. Understanding the characteristics of different types of organic materials and rational use are of great significance for improving soil fertility and crop yield. However, previous studies on the application of organic materials in corn fields (Cheng et al., 2021; Cui et al., 2022; Li et al., 2022) mainly focused on livestock manure, crop straw and biogas residue green manure. In this study, five kinds of organic materials, including organic fertilizer, biochar, microbial fertilizer, commercial organic fertilizer and fulvic acid, were applied in different gradients to investigate their effects on the physical and chemical properties of clay soil, crop agronomic traits and yield.

2 Materials and methods

2.1 Profile of The test area

Field experiments were conducted from April to October 2023 in Kuqa City, Aksu Prefecture, Xinjiang (41°45′N, 83°25′E). Aksu Prefecture is located in the central part of southern Xinjiang, characterized by high terrain in the north and lower elevations in the south. The northern region is marked by numerous peaks, while the southern area features the vast Taklamakan Desert. The central area consists of piedmont gravel fans, alluvial plains, and interspersed gobi and oasis landscapes.

The region exhibits typical characteristics of a warm temperate continental arid climate, with low precipitation and significant seasonal variability. The annual precipitation ranges from 53.2 to 120.6 mm, and there is an abundance of groundwater resources, with water tables ranging from 2 to 7 meters deep. The area experiences many sunny days and long daylight hours, with annual sunlight hours between 2,670 and 3,022 hours, and total solar radiation of 5,340 to 6,220 MJ/m², providing ample light and heat resources. The temperature exhibits a large annual and diurnal range, with an average annual temperature of 7.9 to 13.7°C, and a frost-free period lasting 168 to 225 days. The experimental area utilized drip irrigation, with no winter or spring irrigation.

In March 2023, the physical and chemical properties of the test soil were measured, revealing an organic matter content of 11.7 g/kg, soil moisture content of 12%, bulk density of 1.50 g/cm^3, hydrolyzable nitrogen content of 31.2 mg/kg, available phosphorus content of 12.4 mg/kg, available potassium content of 223.6 mg/kg, and soluble salt content of 11.8 g/kg.The number of soil bacteria was 1.05×108CFU g^{-1}, the number of fungi was 1.0567×108CFU g^{-1}, and the number of actinomyces was 2.4633×108CFU g^{-1}.

2.2 Test materials

The experimental materials included five different organic materials: farmyard manure (N, decomposed cattle manure), biochar (T), microbial fertilizer (J), commercial organic fertilizer (S), and mineral potassium humate (H). The cotton seeds used for testing were the 'Xinluzao 41' variety, purchased from Xinjiang Tianyu Seed Industry Co., Ltd (Kuqa City, Xinjiang). The organic matter and main nutrient contents of each organic material are detailed in Table 1.

2.3 Test design

The experimental site was located in Duntuoktan Town, Kuqa City, Aksu Prefecture. The experiment included five treatments and one control, specifically farmyard manure (N), biochar (T), microbial fertilizer (J), commercial organic fertilizer (S), mineral potassium humate (H), and a control (CK). The application rates for each treatment are shown in Table 2, where the 100% recommended rate was determined based on surveys conducted with local farmers.

Each experimental plot measured 5 m × 6 m, with a total area of 30 m². Each treatment included three application rates: 50% recommended rate (1), 100% recommended rate (2), and 150% recommended rate (3), with three replications for each rate, See Table 2 for specific dosage. Cotton was sown on April 10, 2023, and the organic materials were applied once on April 5, 2023. Following this, the management of the experimental area was carried out by farmers based on their usual farming practices to ensure a high germination rate of the cotton.

2.4 Indicators and methods of project determination

2.4.1 Soil samples

On October 5, 2023, during the cotton harvesting period, soil samples of 0-20 and 20-40cm were randomly taken with soil drill at five points (Wei et al., 2024), and soil pH was adopted by glass electrode method (water and soil mass ratio 1:5). The ratio of soil and deionized water was 1:5, and the mixture was shaken for 0.5 h. After filtration, it was determined by conductivity meter(DDSJ-308F measuring tester). The quality method of soil soluble salt was adopted. The soil alkali-hydrolytic nitrogen content was used by alkali-diffusion method. The content of available phosphorus was extracted by 0.5mol·L-1NaHCO3 colorimetric method. The content of available potassium was determined by ammonium acetate extraction and flame photometer. The content of organic matter was determined by potassium dichromate method. Soil total nitrogen was measured by semi-automatic nitrogen analyzer (DNN-04A) (Bao, 2000).

Equation 1.

$$pd = M/V \quad (1)$$

Where, pd is the bulk density of a soil layer (g/cm3); M is the mass (g); V is the unit volume (cm3).

Equation 2 (Liu, 1982).

$$\text{Soil porosity} = (1 - \text{bulk weight/specific gravity}) \times 100\ \%; \text{The specific gravity of soil is approximately } 2.65\ \text{g/cm}^3 \quad (2)$$

2.4.2 Soil microbial sample

On October 5, 2023, during the early cotton harvest, soil samples were collected from five random points at a depth of 0–40 cm using a soil auger. The quantities of bacteria, fungi, and

TABLE 1 Basic physical and chemical properties of the test materials.

Materials for testing	Organic matter (%)	Nitrogen (%)	Phosphorus (%)	Potassium (%)
Farm manure	77.2	2.27	1.1	2.54
Biochar	65	2.9	2.4	3.5
Biological bacterial fertilizer	60	3.1	1.9	3.7
Commodity organic fertilizer	50	1.7	2.4	2.8
Source of potassium fulvic acid	70	3.3	4.5	2.7

actinomycetes were determined using the dilution plate method. Soil dilution series (dilution levels 10^{-1} to 10^{-6}) were prepared and inoculated onto solid culture media plates, which were then incubated at 28–30°C for 3–6 days. The microbial counts (CFU) in three adjacent dilution levels of the soil solution were recorded, and the number of microorganisms per gram of dry soil was calculated (expressed in CFU/g). The bacterial medium used was beef extract peptone agar; the fungal medium used was Bengal rose agar; and the actinomycete medium used was an improved Gause No. 1 medium (Li et al., 2022).

2.4.3 Plant samples

During the seedling stage of cotton, three plants were randomly sampled from each treatment using a five-point method. Each part of the samples was brought back to the lab to measure plant height and stem diameter, as well as fresh weights of aboveground and underground parts. The samples were then subjected to a killing treatment at 105°C for 30 minutes, followed by drying at 70°C until constant weight was achieved, and the dry weights of the aboveground and underground parts were recorded (Sun et al., 2021).

2.4.4 Yield and yield components

Cotton yield was measured by randomly selecting three representative sampling points within each plot, using either a diagonal method or a five-point star method. To avoid edge effects, a measurement area of 1 m × 2.3 m was selected in the center of each plot to record the number of plants and bolls, allowing for the calculation of harvest density (plants/hm²). From each plot, 15 fully opened cotton bolls were harvested to determine the weight of single-plant bolls and calculate cotton yield (Qu et al., 2021).

2.4.5 Calculation method

Seed cotton yield (kg hm-2) = harvest density (kg hm-2) × average boll number per plant (plant-1) × boll weight per plant (g)/ 1000 × correction coefficient (90%).

2.5 Data processing

Data analysis was conducted using Microsoft Excel 2020, while SPSS 25.0 was used for one-way ANOVA, correlation analysis, and significance testing. Graphs were created using Origin 2018.

3 Results

3.1 Impact of different treatments on soil physical and chemical properties

3.1.1 Impact of different treatments on soil bulk density and porosity

From (Figure 1), it can be observed that with the application of different organic materials, all treatments significantly reduced the bulk density of the 0–40 cm soil layer. This indicates that farmyard manure, biochar, microbial fertilizers, commercial organic fertilizers, and humic acid effectively improved soil structure. Notably, the N2 and T2 treatments in the N and T groups showed particularly pronounced improvements in bulk density. However, with increasing application rates, the N3 and T3 treatments exhibited a rise in soil bulk density, while the bulk density in the J, S, and H groups consistently decreased with higher application rates. Specifically, the T2 treatment achieved the best improvement, with bulk density reductions of 12.78% for the 0–20 cm layer and 10.71% for the 20–40 cm layer compared to the CK treatment.

The application of different organic materials also significantly affected the soil porosity of the 0–40 cm layer. In the 0–20 cm layer, the N2 and T2 treatments resulted in the most notable increases in soil porosity, with increases of 14.97% and 15.22%, respectively, compared to the CK treatment. In the J, S, and H groups, the J3, S3, and H3 treatments showed significant differences from the other gradient treatments, increasing porosity by 17.34%, 18.02%, and 18.14%, respectively, compared to the CK treatment. This indicates that the addition of organic materials can effectively enhance the total porosity of the soil, thereby improving its aeration capacity.

3.1.2 Effects of different treatments on soil nutrients and salinity

From (Figure 2), it can be observed that the application of organic materials led to increases in the content of organic matter, total nitrogen, hydrolyzable nitrogen, available phosphorus, and available potassium in the 0-20 cm soil layer. Compared to the control treatment (CK), there were significant differences in the effects of various treatments on different nutrients. Specifically, the J3 treatment had the most pronounced effect on enhancing organic matter content, while the N1 treatment showed the smallest increase. The T3 treatment exhibited the greatest increase in total nitrogen, whereas the H1 treatment had the smallest increase. For hydrolyzable nitrogen, the J3 treatment again demonstrated the largest increase, while the N1 treatment had the smallest. Regarding available phosphorus and available potassium, the N3 treatment showed the highest increases, while the S1 treatment had the smallest increase in available phosphorus, and the H1 treatment had the smallest increase in available potassium.

In the 20-40 cm soil layer, the treatments also exhibited similar trends regarding the effects on organic matter, total nitrogen, hydrolyzable nitrogen, available phosphorus, and available potassium. The J3 treatment resulted in the greatest increase in organic matter content, while the N1 treatment had the smallest increase, which did not reach significance. The T3 treatment had the largest increase in total nitrogen, while the J1 treatment showed the smallest increase. For hydrolyzable nitrogen, the T1 treatment had the smallest increase, whereas the J3 treatment had the largest. In terms of available phosphorus and available potassium, the H1 treatment had the smallest increase in available phosphorus, the S1 treatment had the smallest increase in available potassium, and the N3 treatment showed the highest increases for both indicators.

Additionally, following the application of organic materials, the pH, electrical conductivity, and water-soluble salt content of the 0-

10.3389/fpls.2024.1520272

TABLE 2 The amount of fertilizer applied in each treatment.

Treatment	Fertilizer application rate		
	50% of the recommended amount	100% of the recommended amount	150% of the recommended amount
Farm manure (Kg HM^{-2})	12000	24000	36000
Biochar (Kg HM^{-2})	15000	30000	45000
Biological bacterial fertilizer (Kg HM^{-2})	3750	7500	11250
Commodity organic fertilizer (Kg HM^{-2})	1500	3000	4500
Source of potassium fulvic acid (Kg HM^{-2})	375	750	1125

40 cm soil exhibited different trends. The N, J, S, and H groups significantly lowered soil pH, electrical conductivity, and water-soluble salt content, whereas the T group increased these indicators, with the T3 treatment showing the most significant changes.

3.1.3 Effects of different treatments on plant agronomic traits and yield

From (Table 3), it can be seen that the effect of different organic material treatments on cotton plant height follows the trend: N group > T group > S group > J group > H group > CK. Among them, the N3 treatment had the most significant effect on plant height and stem diameter, increasing by 20.63% and 35.1%, respectively. Compared to the CK treatment, the N3 treatment showed the greatest improvement in fresh and dry weights, with above-ground fresh and dry weights increasing by 33.86% and 37.59%, respectively, and below-ground fresh and dry weights increasing by 13.59% and 22.23%. Additionally, the N3 treatment also achieved the highest increases in single boll weight

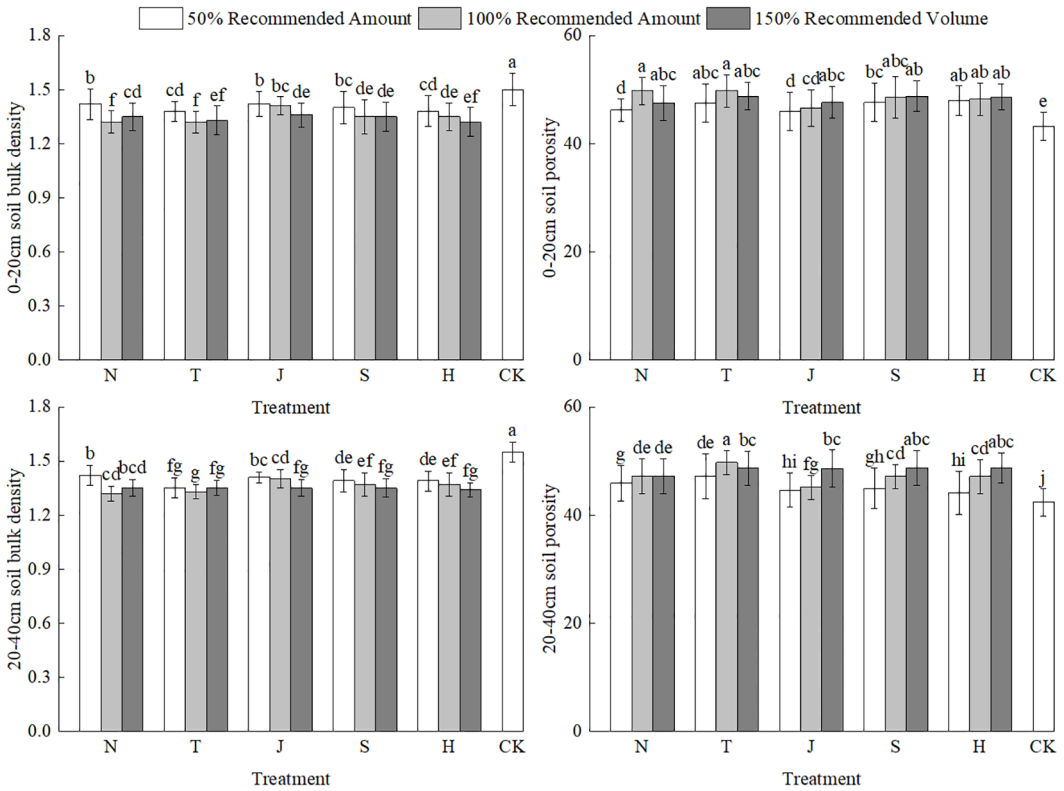

FIGURE 1
Effects of different organic materials on soil bulk density and porosity. Different lowercase letters indicate significant differences at the 0.05 probability level ($P < 0.05$), determined by one-way analysis of variance (ANOVA) and Duncan's *post hoc* test for significance. The vertical bar chart represents the mean ± standard deviation (SD) calculated from three repetitions.N: farm fertilizer, T: biochar, J: biological bacterial fertilizer, S: commercial organic fertilizer, H: mineral source potassium fulvic acid.

10.3389/fpls.2024.1520272

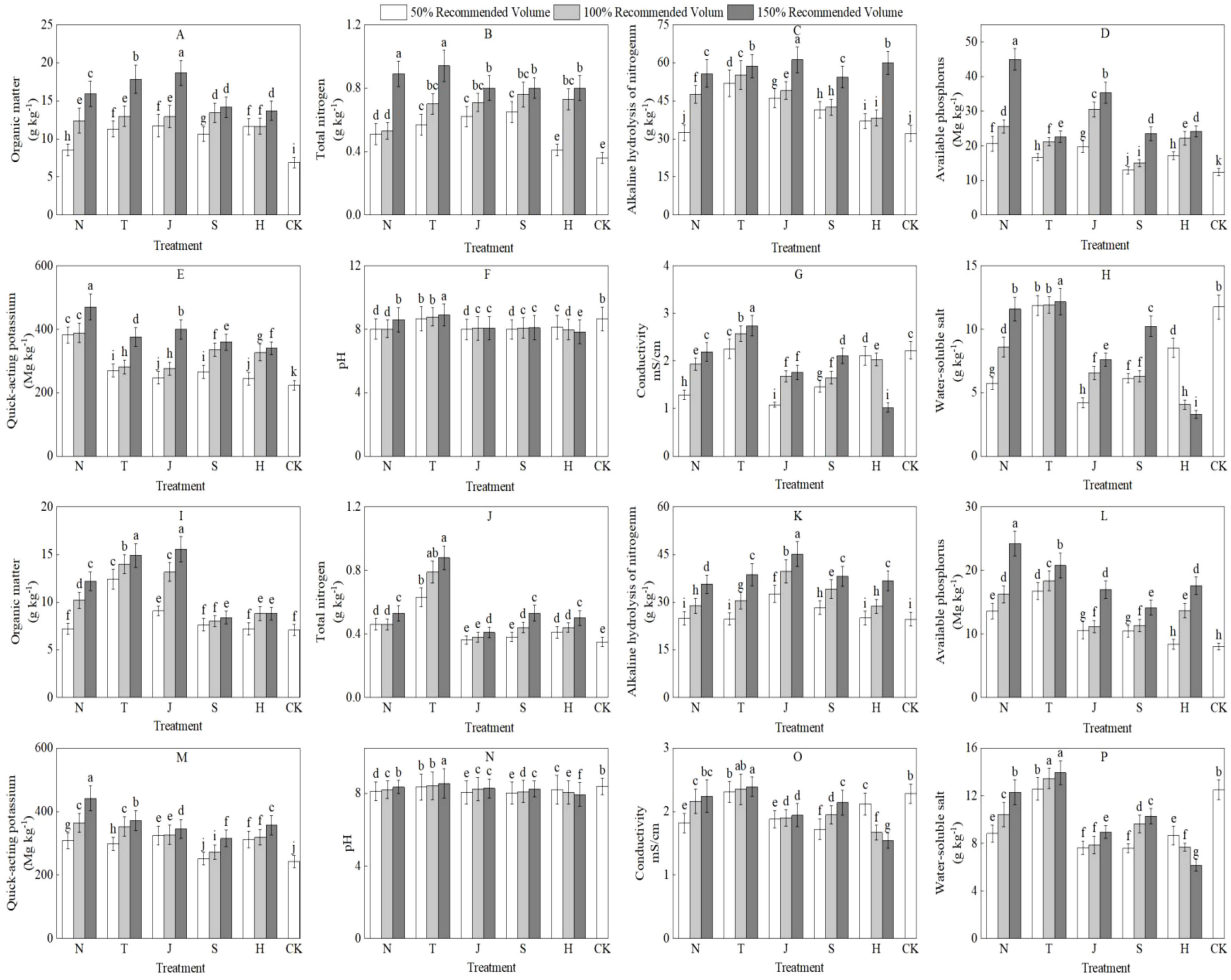

FIGURE 2
Effects of different organic materials on soil nutrients and salinity. Different lowercase letters indicate significant differences at the 0.05 probability level ($P < 0.05$), determined by one-way analysis of variance (ANOVA) and Duncan's *post hoc* test for significance. The vertical bar chart represents the mean ± standard deviation (SD) calculated from three repetitions.N: farm fertilizer, T: biochar, J: biological bacterial fertilizer, S: commercial organic fertilizer, H: mineral source potassium fulvic acid,0-20: **(A–H)**. 20-40: **(I–P)**.

and cotton yield, reaching significant levels compared to other treatment groups.

3.1.4 Impact of different treatments on soil microbial population

From (Figure 3), it is evident that the application of the five types of organic materials significantly increased the numbers of bacteria and actinomycetes in the soil compared to the control (CK) treatment. Except for the N1, J1, and S1 treatments, which did not show significant increases in fungal numbers, the other treatments exhibited notable effects on enhancing fungal populations. As shown in (Figure 3A), the N group had the most significant effect on bacterial counts, with increases ranging from 70.16% to 500.95%, with the N3 treatment achieving the highest bacterial numbers. (Figure 3B) indicates that the T group had the greatest increase in fungal numbers, ranging from 4.41% to 765.27%, with the T3 treatment reaching the peak fungal count. According to (Figure 3C), the N group also showed the most substantial increase in actinomycete counts, with a range of 123.14% to 302.85%, again with the N3 treatment yielding the highest actinomycete numbers.

3.2 Comprehensive evaluation

This study conducted a correlation analysis on 31 indicators related to soil, cotton seedlings, and yield across different treatments (Figure 4). The results indicated a certain degree of discrete correlation among the indicators, albeit with varying levels of correlation. To further explore the relationships between physiological indicators, biplots of principal components were generated (Figures 5, 6), showing a connection between indicator X1 (plant height) and X3 (fresh weight of aerial parts). This information reflects the differences in how various indicators influence the alleviation of soil compaction.

Using SPSS 26.0, a principal component analysis was performed on the 31 indicators, yielding a Kaiser-Meyer-Olkin (KMO) value of 0.789, indicating the data's suitability for this analysis. The cumulative contribution rate of the first three principal

TABLE 3 Effects of different organic materials on agronomic characters and yield of cotton.

Treatment		Height(cm)	Stem Thick(mm)	Fresh Weight above Ground(g)	Underground fresh weight(g)	Dry weight above ground(g)	Dry weight of underground part(g)	Single Bell weight(g)	Output(kg)
N	N1	75.54± 4.78bc	9.6± 0.12c	76.45± 5.15bc	13.875± 0.81ab	36.721± 2.21c	5.698± 0.402cd	6.4124± 1.25b	431.13± 10.45c
	N2	81.22± 4.79b	9.81± 0.16c	83.76± 5.16b	14.008± 0.73a	41.236± 3.24ab	7.003± 0.355a	6.4897± 1.28b	438.93± 10.28b
	N3	89.66± 3.85a	11.2± 0.22a	92.16± 5.27a	14.578± 0.93a	44.878± 3.26a	7.156± 0.311a	6.5521± 1.26a	445.17± 12.44a
T	T1	73.55± 4.35c	9.7± 0.14hc	75.15± 4.15bc	12.972± 0.99b	35.647± 3.19c	5.974± 0.44c	6.0987± 1.31d	422.22± 9.25e
	T2	82.11± 3.44b	9.9± 0.12c	83.92± 4.28b	13.004± 0.81b	40.714± 2.15b	6.213± 0.313bc	6.1152± 1.29d	425.17± 9.55d
	T3	88.49± 3.52a	10.5± 0.29b	90.89± 4.27a	14.185± 0.74a	42.159± 3.16ab	6.634± 0.411b	6.2731± 1.25c	435.97± 10.04b
J	J1	72.15± 4.41c	9.22± 0.17d	75.15± 5.13bc	12.824± 0.88bc	32.105± 4.21d	5.096± 0.405d	6.1423± 1.28d	420.14± 9.88e
	J2	77.88± 4.34bc	10.11± 0.18bc	78.98± 5.15bc	13.2470.97 ± b	34.109± 3.23cd	5.197± 0.313d	6.2116± 1.24c	428.97± 10.01c
	J3	86.89± 3.36a	10.19± 0.26bc	88.29± 4.29ab	13.995± 0.86a	35.708± 2.29c	5.753± 0.407cd	6.2145± 1.31c	440.17± 11.27a
S	S1	69.8± 3.06d	9.7± 0.15c	72.17± 4.14c	12.578± 0.74c	34.189± 4.19cd	5.933± 0.258c	6.0932± 1.34d	423.69± 9.36d
	S2	76.9± 3.25bc	9.85± 0.19c	78.77± 4.27bc	12.989± 0.90b	36.751± 3.16c	6.023± 0.205c	6.2301± 1.24c	432.11± 10.08c
	S3	84.6± 4.28ab	10.5± 0.22b	86.48± 5.21ab	13.887± 0.83ab	39.716± 4.26b	6.412± 0.212b	6.2477± 1.26c	438.19± 10.11b
H	H1	68.6± 4.06d	9.06± 0.13de	69.97± 5.18d	12.851± 0.99bc	28.112± 2.22e	4.511± 0.411e	5.8997± 1.29e	420.66± 9.69e
	H2	74.5± 3.23d	9.15± 0.17d	76.18± 5.13bc	13.013± 0.79b	33.098± 3.21d	4.687± 0.509e	5.9714± 1.05e	426.73± 9.83d
	H3	83.6± 4.21ab	9.68± 0.16c	85.55± 4.17ab	13.848± 0.85ab	36.795± 3.29c	5.899± 0.313c	6.0231± 1.09d	430.18± 9.94c
CK	CK	67.0± 3.05e	8.12± 0.11e	67.98± 4.07e	11.927± 0.85d	29.112± 2.18e	4.547± 0.404e	5.8979± 1.07e	420.11± 8.55e

N, farm fertilizer; T, biochar; J, biological bacterial fertilizer; S, commercial organic fertilizer; H, mineral source potassium fulvic acid. 1:50% recommended amount, 2:100% recommended amount, 3:150% recommended amount.
Different lowercase letters indicate significant differences at the 0.05 probability level ($P < 0.05$), determined by one-way analysis of variance (ANOVA) and Duncan's post hoc test for significance.

10.3389/fpls.2024.1520272

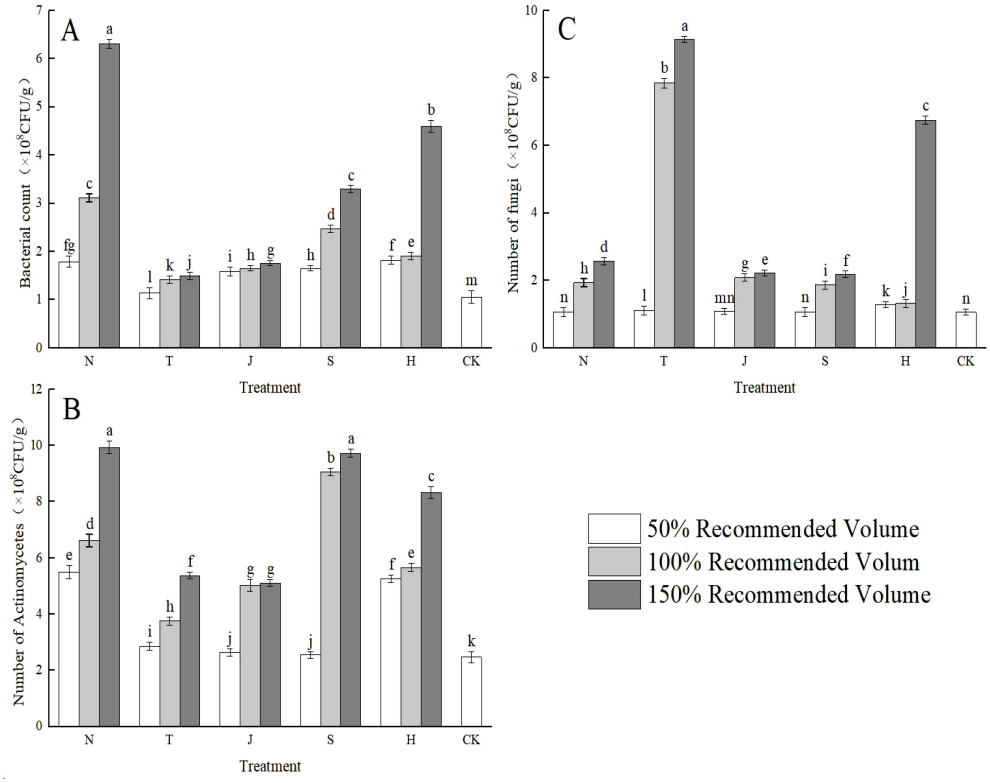

FIGURE 3
Effects of different organic materials on soil microbial population. Different lowercase letters indicate significant differences at the 0.05 probability level ($P < 0.05$), determined by one-way analysis of variance (ANOVA) and Duncan's *post hoc* test for significance. The vertical bar chart represents the mean ± standard deviation (SD) calculated from three repetitions. N: farm fertilizer, T: biochar, J: biological bacterial fertilizer, S: commercial organic fertilizer, H: mineral source potassium fulvic acid. **(A)** number of bacteria, **(B)** number of fungi, **(C)** number of actinomycetes

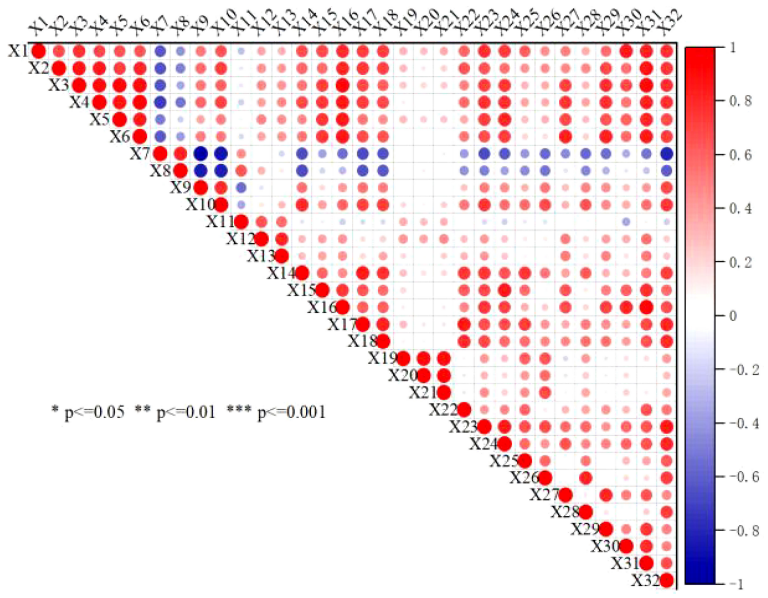

FIGURE 4
Correlation analysis between soil index and plant index.

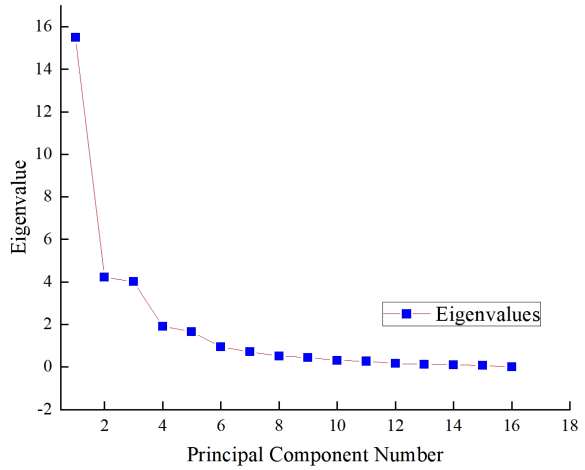

FIGURE 5
Rubble maps.

components was 76.619%, with specific contributions of 50.046% for the first component (PC1), 13.626% for the second (PC2), and 12.948% for the third (PC3). All eigenvalues were greater than 1, aligning with selection criteria, thus these three components were chosen as the main evaluation factors for soil improvement.

The analysis of eigenvectors revealed that PC1 primarily included indicators such as plant height, stem diameter, fresh weight of aerial parts, and fresh weight of underground parts, with significant contributions from the eigenvectors: 0.22179 (plant height), 0.22266 (stem diameter), 0.23039 (fresh weight of aerial parts), and 0.23498 (fresh weight of underground parts). PC2 was mainly associated with pH, soluble salts, and electrical conductivity at the 20-40 cm depth, while PC3 primarily involved soil bulk density and microbial counts.

3.2.1 Correlation analysis between soil index and plant index

The correlation analysis (Figure 4) further revealed significant relationships between organic matter content and various soil indicators. Specifically, it was significantly negatively correlated with bulk density at 20-40 cm ($p < 0.05$) and extremely negatively correlated with bulk density at 0-20 cm ($p < 0.001$). Additionally, it showed significant positive correlations with available phosphorus at 0-20 cm and hydrolyzable nitrogen at 20-40 cm ($p < 0.05$). There were also significant positive correlations with dry weights of both aerial and underground parts, as well as with soil porosity at 0-20 cm and microbial counts ($p < 0.01$). These results suggest that the application of organic materials can improve soil structure, reduce bulk density, promote microbial proliferation, and enhance nutrient utilization efficiency.

3.2.2 Cluster analysis between soil index and plant index

Cluster analysis (Figure 7) categorized the indicators from various treatments into five groups, with representative indicators including plant height, fresh weight of aerial parts, bulk density at 20-40 cm, soluble salts at 0-20 cm, and total nitrogen at 20-40 cm.

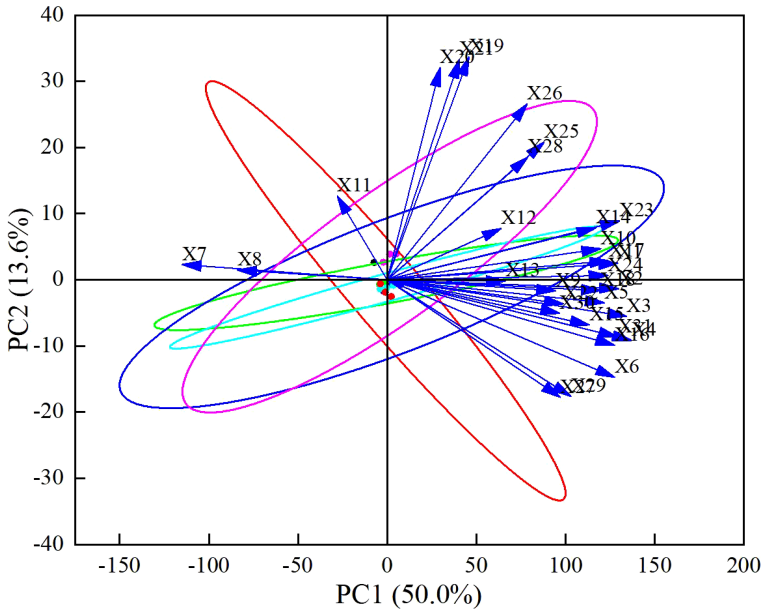

FIGURE 6
Principal component analysis.X1: Plant height, X2: Stem diameter, X3: Aboveground fresh weight, X4: Belowground fresh weight, X5: Aboveground dry weight, X6: Belowground dry weight, X7: Bulk density 0-20cm, X8: Bulk density 20-40cm, X9: Porosity 0-20cm, X10: Porosity 20-40cm, X11: pH 0-20cm, X12: Soluble salts 0-20cm, X13: Electrical conductivity 0-20cm, X14: Hydrolyzable nitrogen 0-20cm, X15: Available phosphorus 0-20cm, X16: Quick-acting potassium 0-20cm, X17: Organic matter 0-20cm, X18: Total nitrogen 0-20cm, X19: pH 20-40cm, X20: Soluble salts 20-40cm, X21: Electrical conductivity 20-40cm, X22: Hydrolyzable nitrogen 20-40cm, X23: Available phosphorus 20-40cm, X24: Quick-acting potassium 20-40cm, X25: Organic matter 20-40cm, X26: Total nitrogen 20-40cm, X27: Bacteria 0-40cm, X28: Fungi 0-40cm, X29: Actinomycetes 0-40cm, X30: Single ring weight, X31: Yield, X32: Organic matter content in organic materials.

10.3389/fpls.2024.1520272

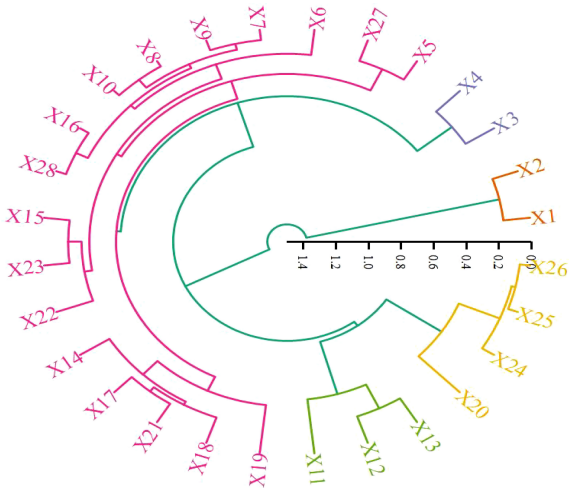

FIGURE 7
Cluster analysis between soil index and plant index.X1: Plant height, X2: Stem diameter, X3: Aboveground fresh weight, X4: Belowground fresh weight, X5: Aboveground dry weight, X6: Belowground dry weight, X7: Bulk density 0-20cm, X8: Bulk density 20-40cm, X9: Porosity 0-20cm, X10: Porosity 20-40cm, X11: pH 0-20cm, X12: Soluble salts 0-20cm, X13: Electrical conductivity 0-20cm, X14: Hydrolyzable nitrogen 0-20cm, X15: Available phosphorus 0-20cm, X16: Quick-acting potassium 0-20cm, X17: Organic matter 0-20cm, X18: Total nitrogen 0-20cm, X19: pH 20-40cm, X20: Soluble salts 20-40cm, X21: Electrical conductivity 20-40cm, X22: Hydrolyzable nitrogen 20-40cm, X23: Available phosphorus 20-40cm, X24: Quick-acting potassium 20-40cm, X25: Organic matter 20-40cm, X26: Total nitrogen 20-40cm, X27: Bacteria 0-40cm, X28: Fungi 0-40cm, X29: Actinomycetes 0-40cm, X30: Single ring weight, X31: Yield, X32: Organic matter content in organic materials.

This indicates that the application of organic materials not only promotes cotton growth but also effectively alleviates soil compaction.

3.2.2.1 The first principal component

F1 = 0.22X1 + 0.22X2 + 0.23X3 + 0.23X4 + 0.21X5 + 0.22X6 +-0.20X7-0.14X8 + 0.16X9 + 0.21X10-0.05X11 + 0.11X12 + 0.11X13 + 0.20X14 + 0.20X15 + 0.22X16 + 0.21X17 + 0.21X18 + 0.08X19 + 0.05X20 + 0.07X21 + 0.17X22 + 0.22X23 + 0.22X24 + 0.15X25 + 0.13X26 + 0.17X27 + 0.14X28 + 0.18X29 + 0.17X30 + 0.22X31.

3.2.2.2 The second principal component

F2 = 0.03X1-0.02X2-0.07X3-0.11X4-0.04X5-0.19X6 + 0.03X7 + 0.02X8-0.02X9 + 0.06X10 + 0.16X11 + 0.10X12-0.01X13 + 0.10X14-0.09X15-0.12X16 + 0.04X17-0.02X18 + 0.42X19 + 0.40X20 + 0.42X21-0.05X22 + 0.11X23 + 0.01X24 + 0.26X25 + 0.33X26-0.22X27 + 0.23X28-0.22X29-0.06X30-0.11X31.

3.2.2.3 The third principal component

F3 = 0.02X1 + 0.02X2 + 0.11X3 + 0.02X4 + 0.16X5 + 0.08X6 + 0.24X7 + 0.39X8-0.29X9-0.21X10 + 0.36X11 + 0.38X12 + 0.29X13-0.13X14 + 0.13X15 + 0.11X16-0.11X17-0.10X18 + 0.14X19 + 0.14X20 + 0.14X21-0.04X22-0.01X23 + 0.02X24-0.11X25-0.16X26 + 0.18X27-0.15X28 + 0.11X29 + 0.12X30 + 0.15X31.

Based on the variance contribution analysis, the first three principal components explain 50.05%, 13.63%, and 12.95% (Table 4) of the variance, respectively. Combining the principal component coefficients and their variance contributions, the comprehensive evaluation formula is: F=50.05F1 + 13.63F2 + 12.95F3 (Table 5). Using this formula, the comprehensive scores for the five types of organic materials and their different application rates on alleviating soil compaction, cotton seedling growth, and yield were calculated (Table 6). The results indicate that the effectiveness in alleviating soil compaction is ranked as follows:N3>T3>S3>J3>N2>T2>H3>J2>S2>T1>N1>H2>CK. Specifically, the 150% and 100% recommended rates of farmyard manure, biochar, microbial fertilizer, commercial organic fertilizer, and potassium humate from mineral sources, as well as the 50% recommended rates of farmyard manure and biochar, showed significant effects in alleviating soil compaction, while the other treatments did not demonstrate significant effects.

3.3 Structural equation model

We used structural equation model (SEM) to investigate the effects of organic matter input on soil microbial quantity, soil physicochemical properties and cotton yield (P value=0.138,Chi-square =0.99, CFI=1.000,RMSEA=0.000)(Figure 8). The results showed that the number of microorganisms was strongly responsive to the input of organic matter, and the effect of organic matter on soil chemical properties was the largest. Soil physical properties and soil chemical properties have a strong response to the number of microorganisms, and the effect value of the number of microorganisms on the interaction path of soil chemical properties is the largest. Soil physical properties and soil chemical properties have a strong response to the yield, and soil bulk density in soil physical properties has a negative response to

TABLE 4 Principal component analysis eigenvalue and contribution rate.

Ingredients	Initial eigenvalue			Extract the sum of squares of loads		
	Total	Percentage of variance	Cumulative (%)	Total	Percentage of variance	Cumulative (%)
1	15.51	50.05	50.05	15.51	50.05	50.05
2	4.22	13.63	63.67	4.22	13.63	63.67
3	4.01	12.94	76.61	4.01	12.95	76.62

10.3389/fpls.2024.1520272

TABLE 5 Principal component index load matrix and eigenvector.

Variable	Eigenvectors and eigenvalues			Load matrix		
	Principal component 1	Principal component 2	Principal component 3	Principal component 1	Principal component 2	Principal component 3
X1	0.22	0.03	0.02	0.87	0.06	0.03
X2	0.22	-0.02	0.02	0.87	-0.03	0.04
X3	0.23	-0.07	0.11	0.90	-0.14	0.22
X4	0.23	-0.11	0.02	0.92	-0.23	0.04
X5	0.21	-0.04	0.16	0.82	-0.09	0.31
X6	0.22	-0.18	0.08	0.86	-0.37	0.15
X7	-0.20	0.03	0.24	-0.77	0.05	0.47
X8	-0.14	0.02	0.39	-0.56	0.03	0.78
X9	0.16	-0.02	-0.29	0.63	-0.04	-0.57
X10	0.21	0.06	-0.21	0.80	0.12	-0.41
X11	-0.05	0.16	0.36	-0.18	0.32	0.71
X12	0.11	0.10	0.38	0.43	0.19	0.76
X13	0.11	-0.01	0.29	0.44	-0.01	0.57
X14	0.20	0.10	-0.13	0.79	0.20	-0.26
X15	0.19	-0.09	0.13	0.76	-0.17	0.25
X16	0.22	-0.12	0.11	0.86	-0.25	0.22
X17	0.21	0.04	-0.11	0.84	0.07	-0.22
X18	0.21	-0.02	-0.11	0.80	-0.04	-0.21
X19	0.08	0.42	0.14	0.30	0.86	0.27
X20	0.05	0.40	0.14	0.20	0.82	0.27
X21	0.07	0.42	0.14	0.27	0.85	0.27
X22	0.17	-0.05	-0.04	0.66	-0.09	-0.07
X23	0.22	0.11	-0.01	0.88	0.23	-0.00
X24	0.21	0.01	0.02	0.83	0.02	0.04
X25	0.15	0.26	-0.11	0.59	0.53	-0.22
X26	0.13	0.33	-0.16	0.53	0.68	-0.31
X27	0.17	-0.22	0.18	0.65	-0.45	0.35
X28	0.14	0.23	-0.15	0.53	0.47	-0.29
X29	0.18	-0.22	0.11	0.69	-0.45	0.21
X30	0.17	-0.06	0.11	0.65	-0.13	0.23
X31	0.22	-0.11	0.15	0.87	-0.22	0.29

the yield, which also indicates that the smaller the soil bulk density, the higher the cotton yield, which is consistent with the experimental results of this study. The mechanism further confirmed by this model is as follows: the input of organic matter mainly regulates the number of microorganisms and the richness of microbial species, and then improves the physicochemical properties of soil, thereby increasing the cotton yield.

4 Discussion

4.1 Effects of different organic materials on soil physical properties

In this study, the application of organic materials significantly increased the sand content in cotton fields while reducing the

TABLE 6 Principal component score table.

Treatment	F1	F2	F3	F synthesis	Rank
CK	-1.87	1.26	2.65	-42.22	13
N1	-0.49	-0.83	0.25	-32.74	11
N2	0.61	-0.35	0.44	31.71	5
N3	1.88	-0.38	1.89	113.67	1
T1	-0.53	1.29	-0.79	-19.36	10
T2	0.37	1.90	-1.19	28.68	6
T3	1.28	1.90	-0.46	83.69	2
J1	-1.06	-0.34	-0.58	-65.22	14
J2	-0.28	-0.18	-0.04	-17.19	8
J3	0.95	-0.14	-0.18	43.18	4
S1	-1.00	-0.68	-0.59	-67.13	16
S2	-0.09	-0.61	-0.35	-17.45	9
S3	0.89	-0.41	0.50	45.35	3
H1	-0.96	-0.30	-0.51	-58.54	15
H2	-0.29	-0.91	-0.53	-33.57	12
H3	0.61	-1.23	-0.50	7.18	7

N, farm fertilizer; T, biochar; J, biological bacterial fertilizer; S, commercial organic fertilizer; H, mineral source potassium fulvic acid. 1:50% recommended amount, 2:100% recommended amount, 3:150% recommended amount.

content of clay and silt particles. Soil bulk density and porosity are important indicators for assessing soil structure. High bulk density indicates increased soil density and reduced aggregate structure, while low bulk density reflects higher porosity and better soil structure (Yao et al., 2019). demonstrated that the application of organic materials can reduce soil bulk density, increase the content of organic matter, nitrogen, phosphorus, and potassium, and enhance the number of beneficial microorganisms, ultimately improving soil enzyme activity and promoting crop yield. Zhang et al. further supported this finding, stating that organic fertilizers positively impact crop growth and soil improvement (Zhao et al., 2025). In our experiment, all five organic materials significantly reduced soil bulk density to varying degrees, with biochar showing the most pronounced effect. The advantages of biochar in improving soil structure and water retention capacity have been well established. Its unique porous structure interacts with soil aggregates, increasing overall porosity and altering pore size distribution (Oguntunde et al., 2008; Abel et al., 2013; Petersen et al., 2016; Werdin et al., 2020). Studies have shown that compared to the control group, the application of biochar significantly improved soil overall porosity and saturated hydraulic conductivity while reducing soil bulk density. Additionally, as the application rate increased, both the bulk density and specific gravity of the 0-40 cm soil layer significantly decreased (Oguntunde et al., 2008). In this experiment, the T2 treatment (biochar application) significantly reduced soil bulk density, while the other four organic materials also contributed to this reduction to varying extents. Among them, T2 and T3 treatments showed the most significant improvement in soil porosity at depths of 0-20 cm and 20-40 cm. This may be attributed to the role of humic substances in organic materials as key binding agents that promote the formation of good soil structure. This process enhances the soil's thermal absorption capacity, improves fertility, reduces soil compaction, and consequently increases porosity. These changes facilitate the rapid exchange of water, soil, and air, ultimately leading to a decrease in soil bulk density (Zheng et al., 2012; Seiji and Nobuhisa, 2013; Mi et al., 2018; Ju et al., 2022).

4.2 Effects of different organic materials on soil chemical properties and salinity

The application of organic materials significantly impacts soil properties and structure, altering nutrient transformation processes, reducing nutrient loss, and enhancing crop nutrient absorption and utilization, thereby promoting plant growth (Study on the effect of

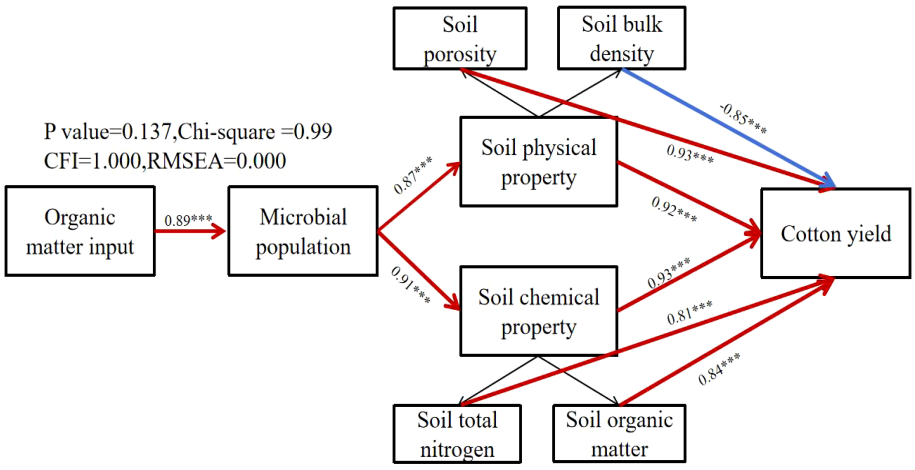

FIGURE 8
Structural equation model diagram. ***p < 0.001.

biomass modifier on sandy soil, 2023). Organic materials are rich in organic matter, nitrogen, phosphorus, potassium, and other mineral elements, which not only replenish nutrients lost due to mineralization and decomposition but also improve the availability of minerals like potassium and phosphorus (Liu et al., 2023).Jiang et al. indicated that the application of amendments could increase organic matter, total nitrogen, and available nutrients in the soil (Jiang et al., 2011). Furthermore, Song et al. found that applying cattle manure significantly increased the levels of available phosphorus, available potassium, total nitrogen, and alkaline nitrogen in the soil (Song et al., 2017). Our study results show that the application of organic fertilizers led to significant increases in total nitrogen, available phosphorus, available potassium, and organic matter content in the soil. These increases in available nutrients have a positive effect on crop biological absorption and utilization. Moreover, the overall performance of the N treatment group was superior to that of other treatment groups, possibly due to the higher microbial and enzyme content in cattle manure, which facilitated the mineralization of available nutrients and accelerated their accumulation in the soil. The potassium humic acid from mineral sources contains humic acid, fulvic acid, and other organic macromolecules, which react with alkaline substances in the soil upon application, leading to a decrease in soil pH. However, the impact of farm manure and biochar on soil pH was minimal, likely due to their strong acid-base buffering capacity. It is noteworthy that as the application of biochar increased, the soil pH exhibited an upward trend, which may be related to the inherent alkalinity of biochar. The functional groups in biochar (such as ester and ether bonds) and the cations released (such as potassium, calcium, and magnesium) collectively contributed to the increase in soil pH (Mi et al., 2018).

4.3 Effects of different organic materials on agronomic traits, yield and microorganisms of cotton

The damage to clay soil structure can lead to soil hardening and decreased oxygen availability, severely hindering the growth of crop roots. Reduced root vitality and diminished cellular respiration lead to insufficient energy levels, consequently affecting the roots' ability to absorb nutrients from the soil. This nutrient deficiency negatively impacts the growth of the above-ground plant parts, ultimately resulting in decreased yield and quality (Wang, 2018).Research indicates that the application of organic materials can significantly enhance the yield and quality of various crops, including tobacco, ginger, cassava, and cucumber (Bending et al., 2002; Zhang et al., 2018; Yao et al., 2019; Bai et al., 2020). By improving nutrient utilization efficiency, organic materials promote the growth of cotton seedlings, reflected in increased plant height and stem diameter (Sun et al., 2019). The application of five different organic fertilizers at varying doses significantly improved the cotton's plant height, stem diameter, dry weight, fresh weight, boll weight, and overall yield. Among them, the N3 treatment had the most pronounced impact on cotton agronomic traits, attributed to several factors: 1. Rich microbial content: Farm manure is abundant in beneficial microorganisms that can fix nitrogen and enhance the availability of phosphorus and potassium in the soil; 2. Symbiotic relationships: These beneficial microorganisms form symbiotic relationships with plant roots, optimizing the rhizosphere environment and stimulating plant growth (Zhang et al., 2010); 3. Plant growth hormones: Microorganisms can produce plant growth hormones and engage in biological control, thereby reducing the impact of pathogenic infections (Rouzi et al., 2011; Zhao et al., 2012).The application of organic materials introduces rich organic matter into the soil, establishing new biological systems and providing microorganisms with abundant nutrients and energy. This significantly enhances microbial activity and reproductive capacity (Ortega et al., 2016). The physiological activities of microorganisms not only decompose organic matter into nutrients that can be absorbed by crops but also synthesize new organic compounds that promote the continuous accumulation of soil nutrients. Additionally, microorganisms can release nutrients fixed in the soil and absorb those that are prone to loss, thereby enhancing the nutrient supply and storage capacity of the soil (Liu et al., 2022). The application of organic and biological fertilizers helps to enrich soil nutrients, increase microbial biomass, and optimize microbial community structure (Tan et al., 2007; Wang et al., 2018).In this study, the application of different types and amounts of organic materials significantly affected the microbial population in the soil. The application of organic materials provided rich carbon and nitrogen sources for the soil, leading to a significant increase in the number of bacteria, fungi, and actinomycetes (Gryta et al., 2020). Li et al (Li et al., 2019). found that both the individual application of organic fertilizers and their combined application with inorganic fertilizers significantly increased the populations of bacteria, fungi, and nitrogen-fixing bacteria in the soil compared to the control group. Among the treatments, the N group exhibited the most pronounced microbial population. This effect may be attributed to the high nutrient demand of crops during their growth stages, accelerating the decomposition of soil organic matter. Furthermore, the nutrients released during microbial decomposition support the growth and reproduction of these organisms, further enhancing their reproductive and metabolic activities. This process improves soil enzyme activity and enhances the soil's ability to retain water and nutrients. The competitive dynamics among microbial populations may also facilitate the dominance of beneficial microorganisms in farm manure. Previous studies have shown that the application of organic materials significantly increases the number of bacteria in the rhizosphere soil of crops, while the number of fungi decreases. This change indicates an enhancement in the richness and functional diversity of microbial communities, accompanied by an increase in enzyme activities (such as sucrase and urease) (Bending et al., 2002; Zhang et al., 2013). Therefore, farm fertilizers demonstrate superior effects on improving soil physical and chemical properties compared to general organic materials. Particularly, the microbial fermentation of cattle manure (bio-organic fertilizer) provides specific benefits for soil protection and yield enhancement, aligning closely with the goals of sustainable agricultural development and thus warranting further promotion. The aim of this study is to screen organic materials with different functions for soil improvement and to provide data support for subsequent experiments. We will continue to focus on the impact of applying organic materials on crop yield and growth under saline-alkali soil conditions, and explore the optimal application strategies for different organic materials.

5 Conclusions

This study showed that among the five organic materials, farm manure was an effective way to alleviate soil compaction and promote cotton growth. By adding farm manure to clay, soil bulk density and salinity were significantly reduced, and soil organic matter, total nitrogen and available nutrients were increased, thus promoting the growth of cotton under clay stress. The optimal addition amount is 36,000 Kg HM-2, which provides a new idea for the effective use of farm fertilizer and the improvement of bonding clay. At the same time, the application of farm manure is in line with sustainable development requirements, contributes to soil health and crop productivity, and is worth promoting in broader agricultural practices. In addition, future research could explore the effects of farm manure in different regions and soil types to further validate its important role in sustainable agriculture.

Data availability statement

The raw data supporting the conclusions of this article will be made available by the authors, without undue reservation.

Author contributions

YZ: Writing – original draft, Writing – review & editing. QB: Conceptualization, Writing – review & editing. ZD: Methodology, Writing – review & editing. XR: Formal Analysis, Writing – review & editing. ZW: Investigation, Writing – review & editing. YF: Investigation, Writing – review & editing. BC: Investigation, Writing – review & editing.

Funding

The author(s) declare financial support was received for the research, authorship, and/or publication of this article. This study was supported by the major science and Technology Project (sub-project) of Xinjiang Uygur Autonomous Region (2022A02007-2-3), the agricultural science and technology innovation and stability support project, and the key technology and product development of degraded farmland restoration (XJNKYWDZC-2023002-2).

Conflict of interest

The authors declare that the research was conducted in the absence of any commercial or financial relationships that could be construed as a potential conflict of interest.

Generative AI statement

The author(s) declare that no Generative AI was used in the creation of this manuscript.

Publisher's note

All claims expressed in this article are solely those of the authors and do not necessarily represent those of their affiliated organizations, or those of the publisher, the editors and the reviewers. Any product that may be evaluated in this article, or claim that may be made by its manufacturer, is not guaranteed or endorsed by the publisher.

References

(2023). *Study on the effect of biomass modifier on sandy soil* (Inner Mongolia Agricultural University). doi: 10.27229/d.cnki.gnmnu.2023.000985

Abel, S., Peters, A., Trinks, S., Schonsky, H., Facklam, M., and Wessolek, G. (2013). Impact of biochar and hydrochar addition on water retention and water repellency of sandy soil. *Geoderma* 202-203, 183–191. doi: 10.1016/j.geoderma.2013.03.003

Bai, Y., Tan, J. L., and Wang, X. N. (2020). Effects of bio-organic fertilizer on growth, yield and quality of Muskmelon in sand pressed soil. *Northern Horticulture* 22, 48–52. doi: 10.11937/bfyy.2020062

Bao, S. D. (2000). *Soil Agrochemical analysis* (Beijing: China Agriculture Press), 263–268.

Bending, D. G., Turner, K. M., and Jones, E. J. (2002). Interactions between crop residue and soil organic matter quality and the functional diversity of soil microbial communities. *Soil Biol. Biochem.* 34, 1073–1082. doi: 10.1016/S0038-0717(02)00040-8

Cheng, S., Zhang, S. M., YUAN, J. C., Liu, J. Z., Liu, S. T., Ren, J., et al. (2021). Effect of chemical fertilizer combined with organic fertilizer on black soil fertility and spring maize yield. *J. North China Agric.* 36, 124–131. doi: 10.7668/hbnxb.20192160

Conlin, T. (2000). Response of soil CO2 and 02 concentrations to forest soil compaction at the long-term soil productivity sites in central British Columbia. *Can. J. Soil Sci.* 80, 625–632. doi: 10.4141/S99-085

Cui, H., Luo, Y., and Chen, J. (2022). Straw return strategies to improve soil properties and crop productivity in a winter wheat-summer maize cropping system. *Eur. J. Agron.* 133, 126436. doi: 10.1016/j.eja.2021.126436

De Neve, S., and Hofman, G. (2000). Influence of soil compaction on carbon and nitrogen mineralization of soil organic matter and crop residues. *Biol. Fertility Soils* 30, 544–549. doi: 10.1007/s003740050034

Du, W. T., Ra, X., and Lu, H. Y. (2022). Effect of reduced application of nitrogen fertilizer on the yield of three major grain crops in our country. *Chin. Agric. Sci.* 55, 4863–4878. doi: 10.3864/j.issn.issn.0578-1752.2022.24.007

Figueiredo, P. G., Bicudo, S. J., and Chen, S. (2017). Effects of tillage options on soil physical properties and cas sava-dry-matter partitioning. *Field Crops Res.* 204, 191–198. doi: 10.1016/j.fcr.2016.11.012

Głąb, T. (2014). Effect of soil compaction and N fertilization on soil pore characteristics and physical quality of sandy loam soil under red clover/grass sward. *Soil Tillage Res.* 144, 8–19. doi: 10.1016/j.still.2014.05.010

Gryta, A., Frc, M., and Oszust, K. (2020). Genetic and metabolic diversity of soil micr robiome in response to exog enous organic matter amendments. *Agronomy* 4, 32–42. doi: 10.3390/agronomy10040546

Hamza, M. A., and Anderson, W. K. (2005). Soil compaction in cropping systems: A review of the nature, causes and possible solutions. *Soil Tillage Res.* 82, 121–145. doi: 10.1016/j.still.2004.08.009

Han, J.-p. (2015). *Study on the coupling mechanism of soil acidification and salinization under protected cultivation* (Hangzhou: Zhejiang University).

Haynes, R., and Naidu, R. (1998). Influence of lime, fertilizer and manurea pications on soil organic matter content and soi aphysical conditions:areview. *Nut rient Cycling Agroecos ystems* 51, 123–137. doi: 10.1023/a:1009738307837

Jiang, K. Y., Guo, J. B., Zhang, B., Cao, X. X., and Li, W. B. (2011). Study on the introduction of environmental-friendly land improvement agent and its improvement effect on sandy soil. *Hunan Agric. Sciences: First Half* 6, 76–78. doi: 10.16498/j.cnki.hnnykx.2011.11.002

Ju, J., Gu, Q., Zhou, H., Mao, W., Yang, H. J., Mi, W. H., et al. (2022). Effects of organic fertilizer combined with chemical fertilizer on nutrients, enzyme activities, and rice yield in reclaimed soil. *Commun. Soil Sci. Plant Anal.* 53, 3060–3071. doi: 10.1080/00103624.2022.2101661

Li, K. Y., Wang, Z. M., Xu, X. ,. Y., and Yang, H. F. (2019). Effects of different fertilization treatments on soil microbial quantity and enzyme activity in solar greenhouse. *J. Northwest Forestry Coll.* 34, 56–61. doi: 10.3969/j.issn.1001-7461.2019.02.09

Li, X. Q., Lu, Q. J., Li Ding, Y., Wang, D. Z., Ren, X. X., Yan, J. L., et al. (2022). Effects of two kinds of commercial organic fertilizers on growth and rhizosphere soil properties of corn on new reclamation land. *Plants* 11, 2553. doi: 10.3390/plants11192553

Liu, G. H., Mai, W., Xuan, Y. C., and Tian, C. Y. (2023). Effect of applying organic fertilizer on improving saline-alkali soil: Meta-analysis. *J. Agric. Resour. Environ.* 40, 86–96. doi: 10.13254/j.jare.2021.0892

Liu, X. Y. (1982). *Research Method of Soil Physics and soil Improvement* (Shanghai: Shanghai Science and Technology Press), 1–2.

Liu, Z., Zhou, H., and Xie, W. (2022). Effects of returning different organic materials in combination with inorganic fertilizers on the diversity ofeukaryotic microorganisms in semi-arid northern China. *Agronomy-Basel* 12, 3116. doi: 10.3390/agronomy12123116

Mi, W., Sun, Y., and Xia, S. (2018). Effect of inorganic fertilizers with organic amendments on soil chemical properties and rice yield in a low-productivity paddy soil. *Geoderma* 320, 23–29. doi: 10.1016/j.geoderma.2018.01.016

Ortega, R., Miralles, I., Meca, D. E., Gázquez, J. C., and Domene, M. Á. (2016). Effect of organic and synthetic fertilizers on the crop yield and macronutrients contents in soil and pepper. *Commun. Soil Sci. Plant Anal.* 47 (10), 1216–1226. doi: 10.1080/00103624.2016.1166246

Oguntunde, P. G., Abiodun, B. J., Ajayi, A. E., and van de Giesen, N. (2008). Effects of charcoal production on soil physical properties in Ghana. *J. Plant Nutr. Soil Sci.* 171, 591–596. doi: 10.1002/jpln.200625185

Petersen, C. T., Hansen, E., Larsen, H. H., Hansen, L. V., Ahrenfeldt, J., and Hauggaard-Nielsen, H. (2016). Pore-size distribution and compressibility of coarse sandy subsoil with added biochar. *Eur. J. Soil Sci.* 67, 726–736. doi: 10.1111/ejss.12383

Qiu, Y. S., Wang, X. N., Li, P. F., Hou, X. Q., Wang, Y. L., Wu, P. N., et al. (2019). Effects of different kinds of organic fertilizers and their application rates on soil fertility and maize yield in dry land in the current season. *Chin. Soil fertilizer* 6, 182–189. doi: 10.11838/sfsc.1673-6257.18498

Qu, Z. Y., Sun, H. H., and Yang, B. (2021). Effects of different amendments on soil microorganisms and tomato yield in saline-alkali soil. *Trans. Chin. Soc. Agric. Machinery* 52, 311–318+350. doi: 10.6041/j.issn.1000-1298.2021.04.033

Rouzi, M. T., Tayifu, S., and Juan, L (2011). Effects of substrate additive on rhizosphere environment and yield of cucumber. *Chin. Vegetables* Z1, 51–56. doi: 10.19928/j.cnki.1000-6346.2011.z1.010

Seiji, S., and Nobuhisa, K. (2013). Rapid change in soil C storage associated with vegetation recovery after cessation of cultivation. *Soil Sci.Plant Nutr.* 59, 27–34. doi: 10.1080/00380768.2012.736342

Song, Y. L., Yu, J., Xiao, C. Z., Chen, S. G., Li, Y. H., Su, X. R., et al. (2017). Effects of decomposed cow manure on soil physical and chemical properties and tomato yield. *Anhui Agric. Sci.* 45, 122–125. doi: 10.13989/j.cnki.0517-6611.2017.26.037

Stemmer, M., Gerzabek, M. H., and Kandeler, E. (1998). Organic matter and enzyme activity in particle-siz fractions of soils obtained after low-energy sonication LJ. *Soil Biol. iochemistry* 30, 9–1745. doi: 10.1016/s0038-0717(97)00093-x

Sun, G. L., Feng, K. Y., and Zhao, X. X. (2019). Effects of organic fertilizer replacement on cotton growth, development and yield. *Xinjiang Agric. Sci.* 57, 762–769. doi: 10.6048/j.issn.1001-4330.2020.04.023

Sun, H. J., Yao, Q. Q., He, Z. S., Wang, D. L., and Zhang, Y. (2021). Effects of nutrient expert system recommended fertilization on cotton yield and fertilizer efficiency. *Xinjiang Agric. Sci.* 58, 1406–1417. doi: 10.6048/j.issn.1001-4330.2021.08.005

Tan, Z. J., Zhou, W. J., Zhang, Y. Z., Zeng, X. B., Xiao, N. Q., and Liu, Q. (2007). Effects of different fertilization regimes on soil microorganisms in paddy field. *J. Plant Nutr. Fertilizer* 13, 430–4435.

Unger, P. (1978). Straw-mulch rate effect on soil water storage and sorghum yield. *Soil Sci. Soc. America J.* 42, 486–491. doi: 10.2136/sssaj1978.03615995004200030023x

Wang, W. H., Yi, L., Tang, H. M., Sun, Z. L., Li, B. Z., Ge, T. D., et al. (2018). Effects of long-term fertilization on soil microbial biomass, community structure and activity in paddy field. *Environ. Sci.* 39, 430–437. doi: 10.13227/j.hjkx.201706039

Wang, X. Y. (2018). The harm of soil compaction and its control measures. *Henan Agric.* 05, 19+21. doi: 10.15904/j.cnki.hnny.2018.05.012

Wei, H., Xihe, W., and Hongtao, J. (2024). Effects of organic replacement of phosphate fertilizer and straw returning to field on soil chemical properties and cotton yield and composition. *China Soil Fertilizer* 04, 64–75. doi: 10.11838/sfsc.1673-6257.23309

Wen, Y. C., Li, Y. Q., Yuan, L., Li, J., Li, W., Ling, Z. A., et al. (2015). Comprehensive Evaluation Method of soil fertility characteristics under different long-term fertilization systems. *Agric. Eng.* 31, 91–99. doi: 10.3969/j.issn.1002-6819.2015.07.014

Werdin, J., Fletcher, T. D., Rayner, J. P., Williams, N. S. G., and Farrell, C. (2020). Biochar made from low density wood has greater plant available water than biochar made from high density wood. *Sci. Total Environ.* 705, 135856. doi: 10.1016/j.scitotenv.2019.135856

Yao, X. Z., Hou, H. J., and Han, Z. D. (2019). Changes of soil nitrogen in paddy field under combined control of bio-organic fertilizer and water. *J. Water Resour. Water Eng.* 35, 217–224. doi: 10.11705/j.issn.1672-643X.2024.01.25

Zhang, F., Yang, Y., Wang, H., and Zhang, X. B. (2018). Effects of biological fertilizer and organic fertilizer on the improvement of physical and chemical properties and bacterial community of peach soil. *Chin. J. Horticulture* 51, 2089–2104. doi: 10.16420/j.issn.0513-353x.2023-0604

Zhang, P., Wei, Z., and Zhu, Z. (2013). Effects of bioorganic fertilizer on rhizosphere soil microflora and Rella solanicum in continuous cropping tomato and capsicum. *J. Nanjing Agric. Univ.* 36, 77–82. doi: 10.7685/j.issn.1000-2030.2013.04.013

Zhang, Y. M., Zhou, H. J., and Zhang, J. Y. (2010). Research progress of bio-organic fertilizer. *Jilin Agric. Sci.* 35, 37–40. doi: 10.16423/j.cnki.1003-8701.2010.03.003

Zhao, Y. P., Wang, Z. G., Fu, Y. B., Bian, Q. Y., and Chen, B. L. (2025). Effects of different organic materials on chemical properties and microbial population of clay soil in southern Xinjiang [J/OL. *J. Northwest A F Univ. (Natural Sci. Edition)* 03, 1–9. doi: 10.13207/j.cnki.jnwafu.2025.03.009

Zhao, Z., Yang, Y. J., and Lin, D. (2012). Effects of microbial fertilizer on growth, yield and quality of cucumber in solar greenhouse. *Chin. Vegetables* 18, 149–153. doi: 10.19928/j.cnki.1000-6346.2012.18.022

Zheng, P. H., Hao, B. P., Feng, Y. C., Ding, Y. C., Li, Y. F., Xuez, Q., et al. (2012). Effects of different saline-alkali amendments on soil physicochemical properties, growth and yield of alfalfa. *Chin. J. Eco-Agriculture* 20, 1216–1221. doi: 10.3724/SP.J.1011.2012.01216

frontiers | Frontiers in Plant Science

TYPE Original Research
PUBLISHED 24 January 2025
DOI 10.3389/fpls.2024.1469434

Check for updates

OPEN ACCESS

EDITED BY
Maruthi Sridhar Balaji Bhaskar,
Florida International University, United States

REVIEWED BY
Md Asaduzzaman,
Kyoto University of Advanced Science (KUAS), Japan
Qi Wu,
Shenyang Agricultural University, China

*CORRESPONDENCE
Rhuanito Soranz Ferrarezi
ferrarezi@uga.edu

RECEIVED 23 July 2024
ACCEPTED 17 December 2024
PUBLISHED 24 January 2025

CITATION
Hutchinson GK, Nguyen LX, Rubio Ames Z, Nemali K and Ferrarezi RS (2025) Sensor-controlled fertigation management for higher yield and quality in greenhouse hydroponic strawberries.
Front. Plant Sci. 15:1469434.
doi: 10.3389/fpls.2024.1469434

COPYRIGHT
© 2025 Hutchinson, Nguyen, Rubio Ames, Nemali and Ferrarezi. This is an open-access article distributed under the terms of the Creative Commons Attribution License (CC BY). The use, distribution or reproduction in other forums is permitted, provided the original author(s) and the copyright owner(s) are credited and that the original publication in this journal is cited, in accordance with accepted academic practice. No use, distribution or reproduction is permitted which does not comply with these terms.

Sensor-controlled fertigation management for higher yield and quality in greenhouse hydroponic strawberries

George Kerrigan Hutchinson[1], Lan Xuan Nguyen[1], Zilfina Rubio Ames[2], Krishna Nemali[3] and Rhuanito Soranz Ferrarezi[1]*

[1]Controlled Environment Agriculture Crop Physiology and Production Laboratory, Department of Horticulture, University of Georgia, Athens, GA, United States, [2]Small Fruit Laboratory, Department of Horticulture, University of Georgia, Tifton, GA, United States, [3]Controlled Environment Agriculture Laboratory, Department of Horticulture & Landscape Architecture, Purdue University, West Lafayette, IN, United States

Controlled environment agriculture (CEA) for strawberry (*Fragaria x ananassa*) production has experienced a growth in popularity in recent years, particularly in North America. One of the most common growing systems in CEA strawberry production is the soilless hydroponic system, which uses an inert substrate and nutrient solution to grow the plants. There are several strategies for water management in substrates, and most are based on a rigid schedule rather than variable plant water requirements over time. Comprehensive comparisons among the different strategies are lacking because they are often associated with complicated evapotranspiration models. The use of soil moisture sensors coupled with automated controllers that apply water when the substrate moisture drops below a set threshold has been proven efficient for select ornamental crops and citrus nursery crops but not for strawberries yet. This study aimed to compare various fertigation management strategies and, considering both yield and resource use, determine the optimal strategy for two newly released strawberry cultivars. 'Florida Brilliance' and 'Florida Beauty' were grown in a greenhouse hydroponic system under six different fertigation management strategies: one timer-based, one leaching fraction-based, and four sensor-based strategies that automatically applied fertilizer solution to maintain a constant volumetric water content threshold (0.36, 0.30, 0.225, or 0.15 $m^3 \cdot m^{-3}$). Yield and resource use were quantified during the 129-day experiment, and plants were harvested at the end of the experiment to measure biomass and foliar nutrients. The yield was used to calculate the water and energy use efficiencies for each strategy. Considering yield and resource use efficiencies, the two drier constant volumetric water content thresholds (0.225 and 0.15 $m^3 \cdot m^{-3}$) and the leaching fraction-based strategy had optimal performance. The results of this experiment can aid growers in employing more efficient fertigation management strategies to increase crop quality and reduce resource use for CEA strawberry production.

KEYWORDS

***Fragaria* × *ananassa*, volumetric water content, energy use efficiency, water use efficiency, substrate, frequency domain reflectometry, capacitance sensor**

1 Introduction

Strawberries (*Fragaria x ananassa*) are a widely cultivated and popular fruit crop, with active commercial production in nearly a third of countries globally (Hytönen et al., 2018). While most domestic strawberries are grown using the annual hill plasticulture system, there is a growing interest in the United States and worldwide in using controlled environment agriculture (CEA) for strawberry production (Samtani et al., 2019). Greenhouse and vertical farming technologies (known as CEA facilities) can insulate crops from extreme weather, lengthen the growing season, and decrease the need for pesticides compared to field production, being a viable option to produce strawberries (Gómez et al., 2019).

CEA strawberries have been produced outside of the United States on a commercial scale for many years using tunnels and greenhouses in South Korea, Japan, the Netherlands, Belgium, France, the United Kingdom, and Italy (Ahn et al., 2021; Neri et al., 2012; Yoshida, 2013). The CEA strawberry industry is making its way into North America as well. A Dutch company recently completed a 29-hectare greenhouse facility for commercial strawberry production in Ontario, Canada, the largest such facility on the continent (Hemmes, 2021). Furthermore, in 2022, a large CEA company announced a partnership with a global leader in the strawberry market to build what will purportedly be the largest CEA complex in the world in Virginia that will produce millions of pounds of strawberries annually using hydroponic growing systems (Green, 2023; Oller, 2022).

The most common type of hydroponic system used to produce strawberries using CEA is a substrate culture system, also known as an aggregate or soilless culture system (Gómez et al., 2019). Substrate culture systems provide a soilless material, usually peat, coco coir, perlite, or some mix thereof, into which the crop's roots can grow. The substrate can be irrigated using a nutrient solution containing fertilizers, which is called fertigation (a portmanteau of irrigation and fertilization), using drip emitters. There are several strategies to determine when and how much fertigation should be applied to the crops, most of them based on weather and soil parameters. The simplest and least expensive approach is to use a timer to regularly fertigate at a set amount at a set interval (Raviv et al., 2019). The most common and recommended strategy is regularly applying the fertigation solution until 20-30% of the applied volume leaches through the substrate (Kubota, 2019). An emerging approach is to use soil moisture sensors that can automatically activate irrigation based on real-time water uptake by the plants.

There are two common types of soil moisture sensors: tensiometers and dielectric capacitance sensors. Tube-shaped tensiometers contain a ceramic tip on one end and a pressure gauge on the other. They calculate matric potential by determining the tension experienced by moisture inside the tube, which is proportional to the wetness of the substrate (Raviv et al., 2019). The more popular type of soil moisture sensor for CEA is the dielectric capacitance sensor, also known as a capacitance sensor or a frequency domain reflectometry (FDR) sensor (Rhie and Kim, 2017). FDR sensors measure the dielectric permittivity of substrates by using parallel metal rods to analyze changes to the frequency domain of an electromagnetic pulse as it passes through the substrate (Raviv et al., 2019). FDR sensor-based fertigation has been successfully employed previously to increase crop quality while reducing water use and leachate waste in several ornamental and food crops in CEA production (Burnett and van Iersel, 2008; Ferrarezi et al., 2015; Nemali and van Iersel, 2006; Palumbo et al., 2021; van Iersel et al., 2009). Previous studies in CEA strawberry production have explored soil moisture sensor-based fertigation. These studies have mainly focused on comparing different soil moisture thresholds or comparing sensor-based fertigation management strategies to the simple but outdated timer-based fertigation (Bonelli et al., 2024; Choi et al., 2016, 2021; Cormier et al., 2020; Hoppula and Salo, 2007). However, few studies have compared sensor-based fertigation to timer-based fertigation and the commonly employed leachate fraction fertigation, especially in strawberries.

This experiment aimed to compare several soil moisture-based fertigation strategies to a timer-based and a leachate fraction fertigation in hydroponically grown strawberries and measure the differences in strawberry fruit yield and quality. Additionally, we quantified the resource inputs (i.e., water and energy) over the growth cycle and calculated the resource use efficiencies concerning the output, i.e., yield, to determine the optimal fertigation management strategy for CEA strawberry production.

2 Materials and methods

2.1 Location and environmental conditions

This experiment was conducted at the University of Georgia (College of Agricultural and Environmental Sciences, Department of Horticulture, Controlled Environment Agriculture Crop Physiology and Production laboratory) in Athens, Georgia, United States (latitude 33°55'55.10" N, longitude 83°21'50.51" W, altitude 198 m) from December 2022 to April 2023 in a polycarbonate greenhouse with controlled conditions.

Greenhouse air temperature and relative humidity were monitored using a digital sensor (HMP60; Vaisala, Helsinki, Finland) connected to a datalogger (CR1000X; Campbell Scientific, Logan, UT, United States) for automatic data collection. Average ± standard error day and night temperatures were 23.3 ± 0.04 and 18.2 ± 0.02°C, respectively. Day and night relative humidities were 40.5 ± 0.25 and 53.4 ± 0.24%, respectively. Vapor pressure deficit (VPD) was calculated using this temperature and relative humidity data and were 1.8 ± 0.01 and 0.96 ± 0.004 kPa for day and night, respectively. Ambient sunlight was augmented with light-emitting diode (LED) fixtures (SPYDRx; Fluence Bioengineering, Austin, TX, United States), which were controlled by a digital timer (Model 26898; Jasco Products LLC, Oklahoma City, OK, United States) to be activated from 4:00 PM to 7:30 PM daily. Canopy-level light was measured by a quantum sensor (SQ-610; Logan, UT, United States) connected to a separate datalogger (CR1000; Campbell Scientific, Logan, UT, United States) and resulted in a mean daily light integral (DLI) of 17.5 ± 0.67 $mol \cdot m^{-2} \cdot day^{-1}$.

2.2 Plant material

Live plugs of strawberry cultivars 'Florida Brilliance' and 'Florida Beauty' propagated in a commercial nursery (Production Lareault, Lavaltrie, QC, Canada) arrived at the greenhouse in October 2022. Plants were watered and fertilized regularly, sorted, and transplanted in November 2022. Plants were also watered and fertilized uniformly until treatments began in December 2022.

2.3 Hydroponic system

The recirculating hydroponic system consisted of 24 18-L troughs measuring 99.5 × 19.5 × 12.5 cm (L × W × H) (Article #7418; Beekenkamp Verpakkingen, Maasdijk, Netherlands), resting on 218 × 17.5 × 7 cm (L × W × H) metal drainage gutters (B200 profile; Haygrove Limited, Ledbury, United Kingdom) with two troughs per gutter. The gutters drained into 121 L plastic reservoirs (H-3687; Uline, Pleasant Prairie, WI, United States) for recirculation. Four plants of each cultivar were placed in every trough in two contiguous lines of four (eight total plants). The substrate was a 1:1 (volume:volume) mixture of super coarse perlite (Horticultural Perlite; Whittemore Co., Lawrence, MA, United States) and a bark-based media mix (Metro-Mix 830; Sun Gro Horticulture, Agawam, MA, United States). The solution was delivered per trough via drip irrigation with four emitters (Catalog no. 22000; Netafim, Tel Aviv, Israel).

2.4 Fertilization

A modified Yamazaki fertilizer solution was used for fertigation in all systems (Kroggel and Kubota, 2017). The solution contained (all values in $mg{\cdot}L^{-1}$): 77 total nitrogen (N) with 74 nitrate-nitrogen (NO_3-N) and 3 ammoniacal-nitrogen (NH_4-N), 15 phosphorous (P), 120 potassium (K), 52 calcium (Ca), 12 magnesium (Mg), 17 sulfur (S), 0.34 boron (B), 0.5 copper (Cu), 2 iron (Fe), 0.55 manganese (Mg), 0.05 molybdenum (Mo), and 0.33 zinc (Zn).

2.5 Treatments

We tested six different fertigation management strategies: one timer-based, one leaching fraction-based, and four sensor-based strategies that automatically applied nutrient solution to maintain a constant volumetric water content (θ) threshold (0.36, 0.30, 0.225, or 0.15 $m^3{\cdot}m^{-3}$), with four replications. Each treatment was randomly assigned to one group of four troughs, for a total of 24 troughs, and each group of four troughs was fertigated by a separate reservoir (H-3687; Uline, Pleasant Prairie, WI, United States) and pump (PE-1; Little Giant, Oklahoma City, OK, United States).

The timer-based treatment ("Timer") used the datalogger and relay to activate the pump for three minutes every three hours throughout the experiment. The leaching-fraction-based treatment ("Leach") was manually controlled and had a target of 20-30% leachate per fertigation event. The four thresholds for the θ treatments were selected based on fractions of the substrate container capacity (θ 0.42 $m^3{\cdot}m^{-3}$) to represent a broad range of substrate moisture contents. The four θ thresholds were (from high to low) 0.36, 0.30, 0.225, and 0.15 $m^3{\cdot}m^{-3}$, chosen based on previous experiments performed in our lab. These four treatments were monitored by a soil moisture sensor (GS3; METER Group, Pullman, WA, United States) positioned in the center of each trough. The soil moisture sensors (n = 24) were connected to a datalogger (CR1000X; Campbell Scientific, Logan, UT, United States) for automatic data collection and irrigation control. A relay (SDM-CD16AC; Campbell Scientific, Logan, UT, United States) connected to the datalogger was used for pump activation in all treatments.

2.6 Reservoir pH and electrical conductivity (EC) measurements

Leachate volume, pH, and EC were recorded after each fertigation event. The solution pH and EC were regularly measured with a digital probe (#HI98131; Hanna Instruments, Smithfield, RI, United States) and adjusted to maintain a range between 5.5 and 6.5 pH and 0.75 and 1.25 $dS{\cdot}m^{-1}$, respectively. A commercial product derived from phosphoric acid was used to reduce the solution pH (pH-Down; Advanced Nutrients, West Hollywood, CA, United States), while an 8M solution of potassium hydroxide was used to raise the solution pH. EC was lowered by diluting the solution with tap water.

2.7 Substrate θ and number of irrigations

The datalogger also automatically recorded θ measurements for all troughs every 15 minutes. The average of the four soil moisture sensor measurements in each treatment group was used to determine the number of irrigations or pump activations. If the average of the four θ measurements were below the treatment threshold, the pump would activate to fertigate all four troughs in the group for three minutes. The datalogger recorded the automatic pump activation time every 3 minutes throughout the experiment.

2.8 Fruit harvest measurements

Fruit harvests were conducted every other week between December 2022 and January 2023, then changed to every week for February through April 2023, with 15 harvests in total. This change was instituted to accommodate the larger fruit production as the season progressed and to minimize fruit losses due to fungal pathogens. Fruit that were 70% or more ripe were harvested from each measurement plant. Fruit from each plant were counted and collectively weighed using a digital scale (Item #30430061; Ohaus Corporation, Parsippany, NJ, United States) to measure the fresh fruit yield. Marketable fruit were also counted and collectively weighed to obtain the marketable yield. A fruit was considered marketable if it weighed at least 8 g and was nicely shaped (a sign was evenly pollinated). The largest marketable fruit (or simply the

largest fruit if none were marketable) was cut longitudinally in half. One of the halves was weighed and crushed using cheesecloth and a garlic press to measure total soluble solids (TSS) using a digital refractometer (#HI96801; Hanna Instruments, Smithfield, RI, United States). The other half and the remaining fruit from the plant were placed in an 80°C oven for several days until completely dehydrated. The dehydrated fruit were weighed again to obtain the dry fruit biomass. By weighing the half-fruit used for TSS analysis, the total fruit biomass before and after dehydration was known, and thus, fruit water content could be calculated.

2.9 Plant harvest measurements

The strawberry plants were terminated on April 27, 2023 (129 days after transplanting). Before harvesting, the plant height was measured using a meter stick. Plants were harvested by cutting the crown at the soil line. Plants were weighed using a digital scale (Model #PB3002; Mettler Toledo, Griefensee, Switzerland) to determine fresh shoot biomass. The number of flowers, fruit, runners, and leaves was counted for each plant. Plant mortality was also assessed at this stage by direct counting.

The harvest index was calculated using the total fruit yield and the fresh shoot biomass: total fruit fresh weight ÷ (total fruit fresh weight + plant fresh weight). Next, all healthy trifoliate leaves for each plant were scanned using a leaf area meter (LI-3100; LI-COR, Lincoln, NE, United States) to obtain the total leaf area (LA). Each plant was placed into a paper bag and dried at an 80°C drying oven for several days. Dry shoot biomass was measured using the same digital scale.

Dried trifoliate leaves were placed in sample bags and sent to a commercial lab (Waters Agricultural Laboratories, Camilla, GA, United States) for tissue nutrient concentration analysis. Leaf N was determined by a high-temperature combustion process (Nelson and Sommers, 1973). Leaf P, K, Mg, Ca, S, B, Fe, Cu, Mn, and Zn concentrations were determined by inductively coupled plasma atomic emission spectrophotometer after wet acid digestion using nitric acid and hydrogen peroxide (Twyman, 2005).

2.10 System measurements and resource use quantification

All reservoir volumes were tracked throughout the experiment. Reservoirs were filled to a known volume at the start of the experiment and filled again to that known volume after draining and refilling. Residual reservoir volume was measured during drain and refill events, triggered when reservoir volume was low and/or when the reservoir pH and EC were out of the ideal range. By knowing reservoir volume before and after refills, total system losses due to evapotranspiration (ET) were calculated by simple subtraction.

To calculate plant water use efficiency (WUE), ET per plant was calculated by dividing reservoir ET by the number of plants supplied by that reservoir. Yield per plant was then divided by this ET per plant (based on from which reservoir the plant was fertigated) to obtain plant WUE in grams per liter.

Total system energy use was calculated by tracking the total pump activation time in hours for each fertigation management strategy. As previously mentioned, the datalogger recorded the automatic fertigation activations for each of the four θ threshold treatments throughout the experiment. The Timer treatment was activated at a regular interval of 3 minutes every 3 hours, and the Leach treatment fertigation events were manually timed. All treatments used the same pump model, which has a power consumption of 36 W per manufacturer specifications. The total pump run times and power consumption rate were multiplied to obtain total energy use in kilowatt hours (kWh) for each fertigation management strategy.

To calculate plant energy use efficiency (EUE), energy use per plant was first calculated by dividing the total treatment energy use by the total number of plants (32). Yield per plant was then divided by this energy use per plant to obtain plant EUE in grams per kWh.

2.11 Experimental design and statistical analysis

The study was arranged on a randomized block design, with six treatments and four replications. Statistical analysis was performed by one-way analysis of variance (ANOVA) with Tukey's *post-hoc* test using statistical software (SigmaPlot Version 15; Systat Software, San Jose, CA, United States) to determine significant differences among treatments. When a data set did not meet the ANOVA's normality or equal variance conditions, a Kruskal-Wallis test with Dunn's *post-hoc* was conducted using the same statistical software. A probability (P) level of 0.05 was used in all tests. Results from each cultivar were analyzed separately.

3 Results

3.1 Reservoir pH and EC

Reservoir pH was controlled successfully in all treatments during the experiment (Figure 1A). Notably, the θ 0.36 $m^3 \cdot m^{-3}$ treatment induced the greatest pH variation and deviated from the other five treatments. There is one extreme deviation in the θ 0.225 $m^3 \cdot m^{-3}$ treatment at 65 DATS. The average ± standard error measured reservoir pH was 6.2 ± 0.09, 5.6 ± 0.12, 6.2 ± 0.09, 6.2 ± 0.12, 6.1 ± 0.11, and 6.2 ± 0.10 for the Leach, θ 0.36, 0.30, 0.225, 0.15 $m^3 \cdot m^{-3}$, and Timer treatments, respectively. Reservoir EC was more uniform except in the θ 0.36 $m^3 \cdot m^{-3}$ treatment (Figure 1B). The extreme deviation at 65 DATS for the θ 0.225 $m^3 \cdot m^{-3}$ treatment previously mentioned can also be seen in this graph. Average ± standard error measured reservoir EC was 0.86 ± 0.017, 1.30 ± 0.063, 0.85 ± 0.014, 0.88 ± 0.046, 0.84 ± 0.011, and 0.94 ± 0.023 $dS \cdot m^{-1}$, respectively.

10.3389/fpls.2024.1469434

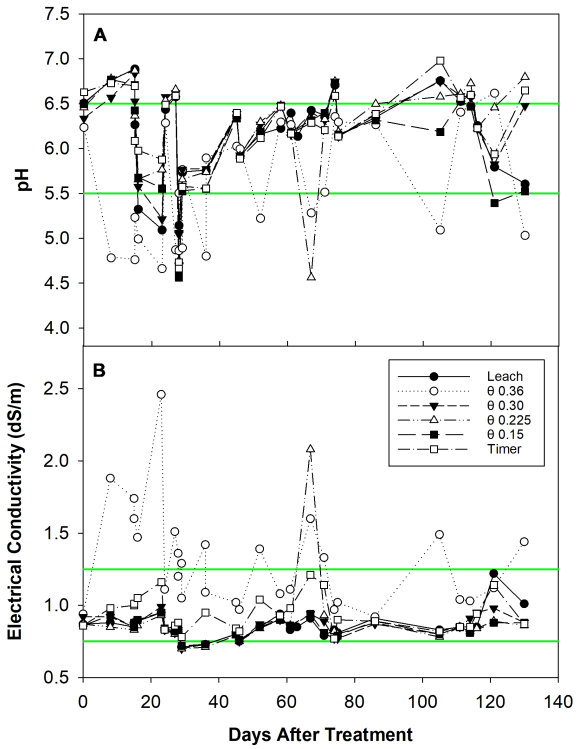

FIGURE 1
Reservoir pH **(A)** and electrical conductivity (EC) **(B)** for different fertigation management strategies from zero to 130 days after treatment. Individual data points represent pH or EC measurements. Green lines represent the bounds of the ideal range (5.5-6.5 for pH and 0.75-1.25 dS·m^{-1} for EC); data points between the green lines are considered within the range.

3.2 Pump activation and θ control

The treatments began at 10:00 AM on December 19, 2022, and ended at 10:00 AM on April 27, 2023. During this period, the θ 0.36 m^3·m^{-3} treatment pump was active for 35.4% of the time, which was by far the highest activation rate of all the treatments. This was followed by the θ 0.30 and 0.225 m^3·m^{-3} treatment pumps at 5.21% and 3.52% activation, respectively. The Timer treatment pump was active for 1.62% of the time, the Leach treatment pump was active for 1.44%, and the θ 0.15 m^3·m^{-3} treatment pump had the lowest activation rate at 1.25%. These pump activation rates correspond to a total applied solution volume of 1,065 L for the Leach treatment, 26,212, 3,859, 2,605, and 972 L for the θ 0.36, 0.30, 0.225, and 0.15 m^3·m^{-3} treatments, and 1,203 L for the Timer treatment. On average, each plant received a daily solution volume of 0.26 L in the Leach treatment, 6.35, 0.93, 0.63, and 0.22 L in the θ 0.36, 0.30, 0.225, and 0.15 m^3·m^{-3} treatments, and 0.29 L in the Timer treatment. The sensor-activated pump control system consistently maintained the target θ thresholds throughout the experiment (Figure 2). Minor deviations can be seen for the θ treatments due to control component failures that were quickly repaired. These occurred from 0-25 DATS for the θ 0.36 m^3·m^{-3} treatment, between 60 and 70 DATS for the θ 0.225 m^3·m^{-3} treatment, and at 110 DATS for the θ 0.30 and 0.15 m^3·m^{-3} treatments. The Leach treatment showed high variability during the first 70 days of the experiment, with this reducing during the second half. The Timer treatment resulted in a consistent and high θ level throughout the experiment.

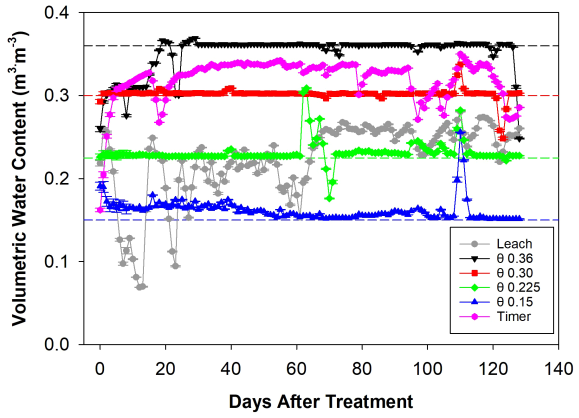

FIGURE 2
Daily volumetric water content (θ) data for different fertigation management strategies measured by the soil moisture sensors from zero to 130 days after treatment. Data points represent average ± standard error θ values for four troughs in 24 hours. Dashed lines represent θ target thresholds.

3.3 Total and marketable yield

The Leach, θ 0.36, 0.225, and 0.15 m^3·m^{-3} treatments resulted in at least 291% higher total yield than the Timer treatment for the 'Florida Brilliance' cultivar (P = 0.002) (Figure 3A). For 'Florida Beauty', the θ 0.225 m^3·m^{-3} treatment resulted in a 227% higher total yield than the Timer treatment (P = 0.021) (Figure 3B). There were no significant differences among any of the treatments in marketable yield for either 'Florida Brilliance' (P = 0.122) (Figure 3C) or 'Florida Beauty' (P = 0.206) (Figure 3D).

'Florida Brilliance' had at least 92% more fruit harvested from the θ 0.225 m^3·m^{-3} treatment than from the Timer and θ 0.30 m^3·m^{-3} treatments (Figure 4A). The Leach, θ 0.36, 0.225, and 0.15 m^3·m^{-3} treatments also resulted in at least 153% more fruit harvested than the Timer treatment for the same cultivar (P < 0.001). The θ 0.225 m^3·m^{-3} treatment resulted in 232% more fruit harvested than the Timer treatment in 'Florida Beauty', and this was the only significant difference among the treatments for this cultivar (P = 0.006) (Figure 4B). Similarly, there were no significant differences in the number of marketable fruit harvested among any treatments for 'Florida Brilliance' (P = 0.086) (Figure 4C) or 'Florida Beauty' (P = 0.099) (Figure 4D).

3.4 Fruit TSS, dry biomass, and water content

The Timer and the θ 0.30 m^3·m^{-3} treatments produced fruit with 44% higher TSS than the other treatments for 'Florida Brilliance' (P < 0.001) (Figure 5A). The Timer treatment also produced fruit with

10.3389/fpls.2024.1469434

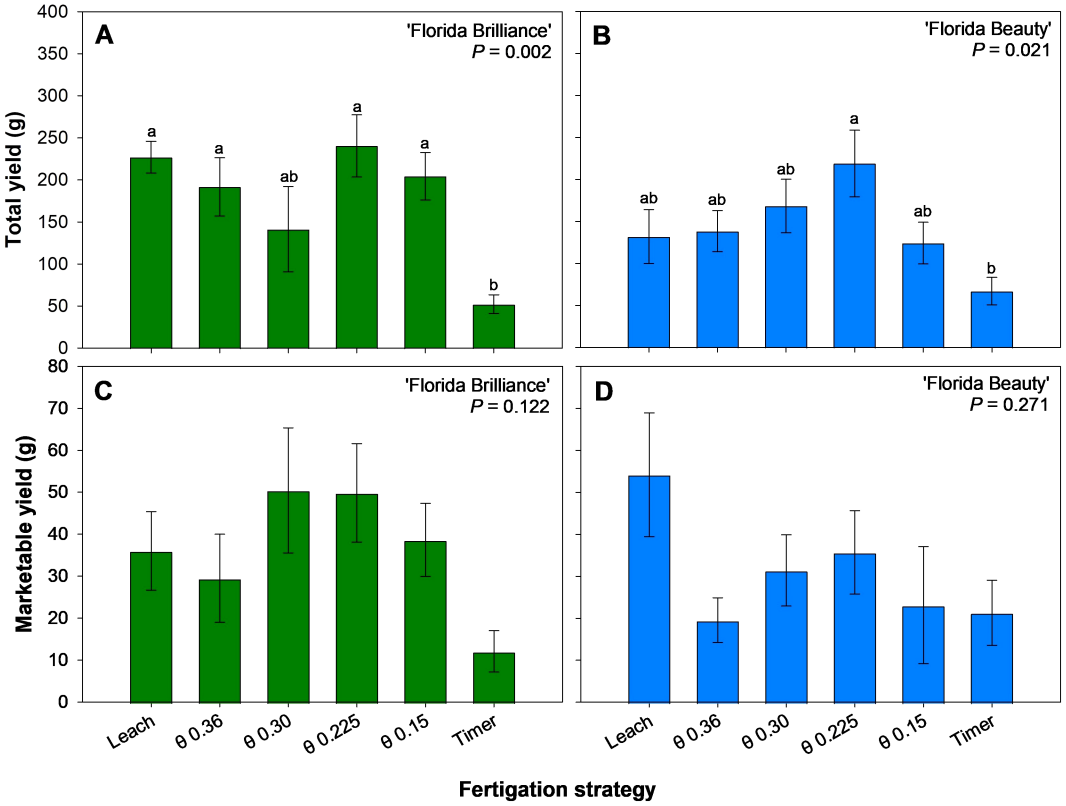

FIGURE 3
Total yield per plant for 'Florida Brilliance' **(A)** and 'Florida Beauty' **(B)**, and marketable yield per plant for 'Florida Brilliance' **(C)** and 'Florida Beauty' **(D)**. Each bar represents the average ± standard error of four replications with two measurement plants. Bars with the same letter show no significant difference; bars with different letters are statistically different at a 5% significance level ($P < 0.05$).

40% higher TSS than the θ 0.36 and 0.225 $m^3 \cdot m^{-3}$ treatments in 'Florida Beauty' ($P < 0.001$) (Figure 5B). The θ 0.225 $m^3 \cdot m^{-3}$ treatment for 'Florida Brilliance' resulted in 152% higher fruit dry biomass than the Timer treatment ($P = 0.025$) (Figure 5C). There were no significant differences among the treatments for 'Florida Beauty' fruit dry biomass ($P = 0.156$) (Figure 5D). Similarly to the 'Florida Brilliance' results for fruit dry biomass, the Leach treatment, along with the θ 0.36 and 0.225 $m^3 \cdot m^{-3}$ treatments, resulted in at least a 26% increase in fruit water content compared to the Timer treatment for the same cultivar ($P < 0.001$) (Figure 5E). For 'Florida Beauty', the θ 0.225 $m^3 \cdot m^{-3}$ treatment showed at least a 23% increase in fruit water content compared to the Timer treatment ($P < 0.001$) (Figure 5F). Furthermore, the θ 0.225 $m^3 \cdot m^{-3}$ treatment showed at least a 3.6% increase in fruit water content compared to the θ 0.30 $m^3 \cdot m^{-3}$ treatment ($P < 0.001$).

3.5 Plant height, fresh shoot biomass, and dry shoot biomass

'Florida Brilliance' plants grew at least 58% taller under the θ 0.36 $m^3 \cdot m^{-3}$ and Leach treatments compared to plants under the Timer treatment ($P < 0.001$) (Figure 6A). 'Florida Beauty' plants grew at least 37% taller with the θ 0.36 and 0.30 $m^3 \cdot m^{-3}$ treatments compared to the Timer treatment ($P = 0.005$) (Figure 6B). Fresh shoot biomass for 'Florida Brilliance' was at least 115% higher in the Leach and θ 0.36 $m^3 \cdot m^{-3}$ treatment than in the Timer treatment ($P = 0.002$) (Figure 6C). 'Florida Beauty' fresh shoot biomass was not significantly affected by the fertigation treatments ($P = 0.103$) (Figure 6D). The results for dry shoot biomass were extremely similar to the fresh shoot biomass results for both cultivars. 'Florida Brilliance' had at least 110% higher dry shoot biomass in the Leach and θ 0.36 $m^3 \cdot m^{-3}$ treatments compared to the Timer treatment ($P = 0.004$) (Figure 6E). The treatments did not significantly affect the 'Florida Beauty' dry shoot biomass ($P = 0.450$) (Figure 6F).

3.6 Harvest index and leaf area

'Florida Brilliance' harvest indices from the θ 0.225 and 0.15 $m^3 \cdot m^{-3}$ treatments showed at least a 57% increase from the Timer treatment harvest index ($P = 0.002$) (Figure 7A). The treatments did not significantly affect the 'Florida Beauty' harvest index ($P = 0.068$) (Figure 7B). The θ 0.36 $m^3 \cdot m^{-3}$ treatment for 'Florida Brilliance' resulted in at least 78% higher leaf area than the Timer treatment as well as the θ 0.30 and 0.225 $m^3 \cdot m^{-3}$ treatments (Figure 7C). The Leach treatment also resulted in a 133% higher leaf area than the Timer treatment for this cultivar ($P < 0.001$). The θ 0.36 $m^3 \cdot m^{-3}$

10.3389/fpls.2024.1469434

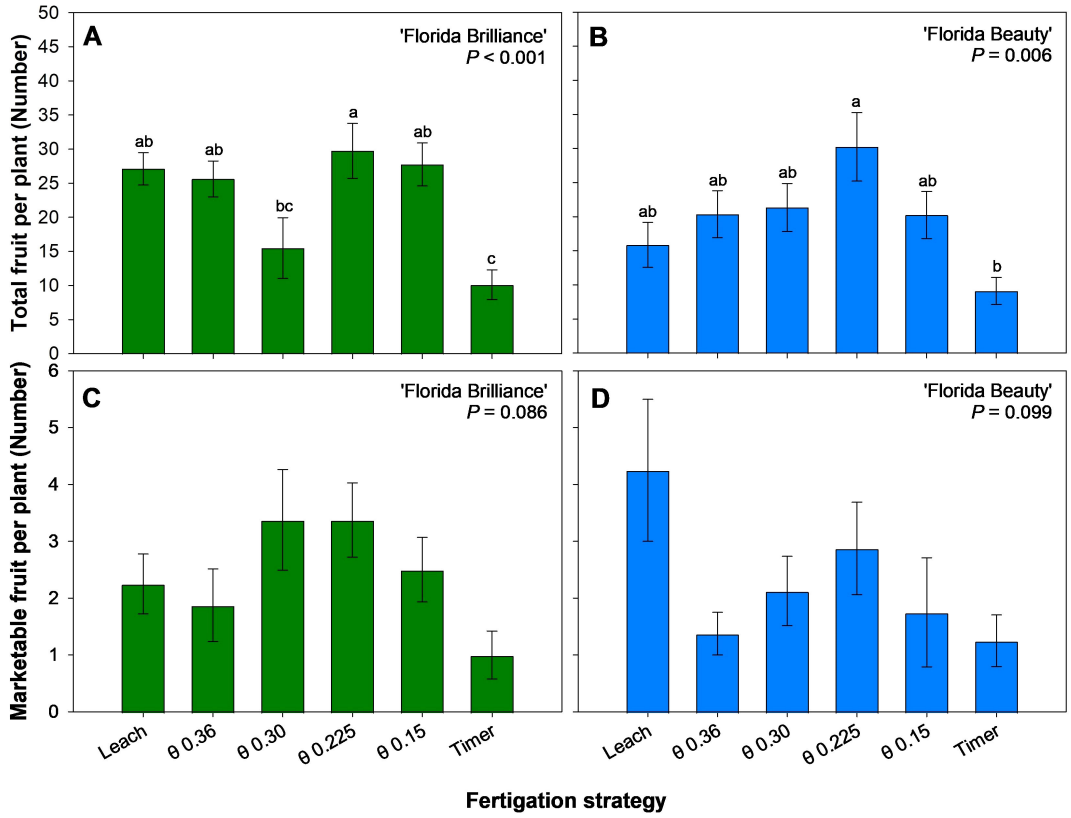

FIGURE 4
Total number of fruit per plant for 'Florida Brilliance' **(A)** and 'Florida Beauty' **(B)**, and number of marketable fruit per plant for 'Florida Brilliance' **(C)** and 'Florida Beauty' **(D)**. Each bar represents the average ± standard error of four replications with two measurement plants. Bars with the same letter show no significant difference; bars with different letters are statistically different at a 5% significance level ($P < 0.05$).

treatment resulted in 156% higher leaf area than the Timer treatment for 'Florida Beauty' ($P = 0.184$) (Figure 7D).

3.7 Leaf tissue macronutrient concentration

The fertigation management strategy treatments did not affect the 'Florida Brilliance' leaf N ($P = 0.145$) (Table 1). 'Florida Brilliance' leaf P was at least 47% higher in the θ 0.30 $m^3 \cdot m^{-3}$ and Timer treatments than the four other treatments ($P < 0.001$). Leaf K for 'Florida Brilliance' was 22% higher for the θ 0.30 $m^3 \cdot m^{-3}$ treatment than the Leach treatment ($P = 0.020$). The treatments did not affect the 'Florida Brilliance' leaf Mg ($P = 0.060$). 'Florida Brilliance' leaf Ca was 42% higher for the Timer treatment than for the θ 0.36 $m^3 \cdot m^{-3}$ treatment ($P = 0.019$). Finally, the treatments did not affect leaf S for 'Florida Brilliance' ($P = 0.134$). 'Florida Beauty' leaf N was 15% higher in the θ 0.30 $m^3 \cdot m^{-3}$ treatment than in the θ 0.15 $m^3 \cdot m^{-3}$ treatment ($P = 0.016$) (Table 1). Leaf P for 'Florida Beauty was significantly affected by the treatments ($P = 0.019$), however, the *post-hoc* test could not distinguish between treatments. The treatments did not affect 'Florida Beauty' leaf K ($P = 0.743$). Leaf Mg for 'Florida Beauty' was 37% higher for the Leach treatment than for the θ 0.36 $m^3 \cdot m^{-3}$ treatment ($P = 0.014$). Leaf Ca for 'Florida Beauty' was 52% higher in the Timer treatment than in the θ 0.36 $m^3 \cdot m^{-3}$ treatment ($P = 0.024$). Finally, the treatments did not affect 'Florida Beauty' leaf S.

3.8 Leaf tissue micronutrient concentration

'Florida Brilliance' leaf Zn was at least 38% higher in both the Timer and the θ 0.30 $m^3 \cdot m^{-3}$ treatments than in the other four treatments ($P < 0.001$) (Table 1). For 'Florida Brilliance' leaf Mn, the θ 0.225 $m^3 \cdot m^{-3}$ treatment was at least 135% higher than both the θ 0.36 $m^3 \cdot m^{-3}$ and Leach treatments. Furthermore, the θ 0.30 $m^3 \cdot m^{-3}$, θ 0.15 $m^3 \cdot m^{-3}$, and Timer treatments resulted in at least 179% higher leaf Mn than the θ 0.36 $m^3 \cdot m^{-3}$ treatment ($P < 0.001$). 'Florida Brilliance' leaf Fe was at least 121% higher in both the Leach and θ 0.225 $m^3 \cdot m^{-3}$ treatments than in the four other treatments ($P < 0.001$). Leaf B ($P = 0.224$) and leaf Cu ($P = 0.354$) were not affected by the treatments for this cultivar. 'Florida Beauty' leaf B was 44% higher in the Timer treatment than in the Leach treatment ($P = 0.022$) (Table 1). Leaf Mn for 'Florida Beauty' was 262% higher in the θ 0.225 $m^3 \cdot m^{-3}$ treatment than in the θ 0.36 $m^3 \cdot m^{-3}$ treatment ($P = 0.006$). 'Florida Beauty' leaf Fe was at least 447% higher in both the Leach and θ 0.225 $m^3 \cdot m^{-3}$ treatments than in the θ 0.30 $m^3 \cdot m^{-3}$ treatment ($P = 0.002$). Leaf Zn ($P = 0.237$) and leaf Cu ($P = 0.311$) were not affected by the treatments for this cultivar.

10.3389/fpls.2024.1469434

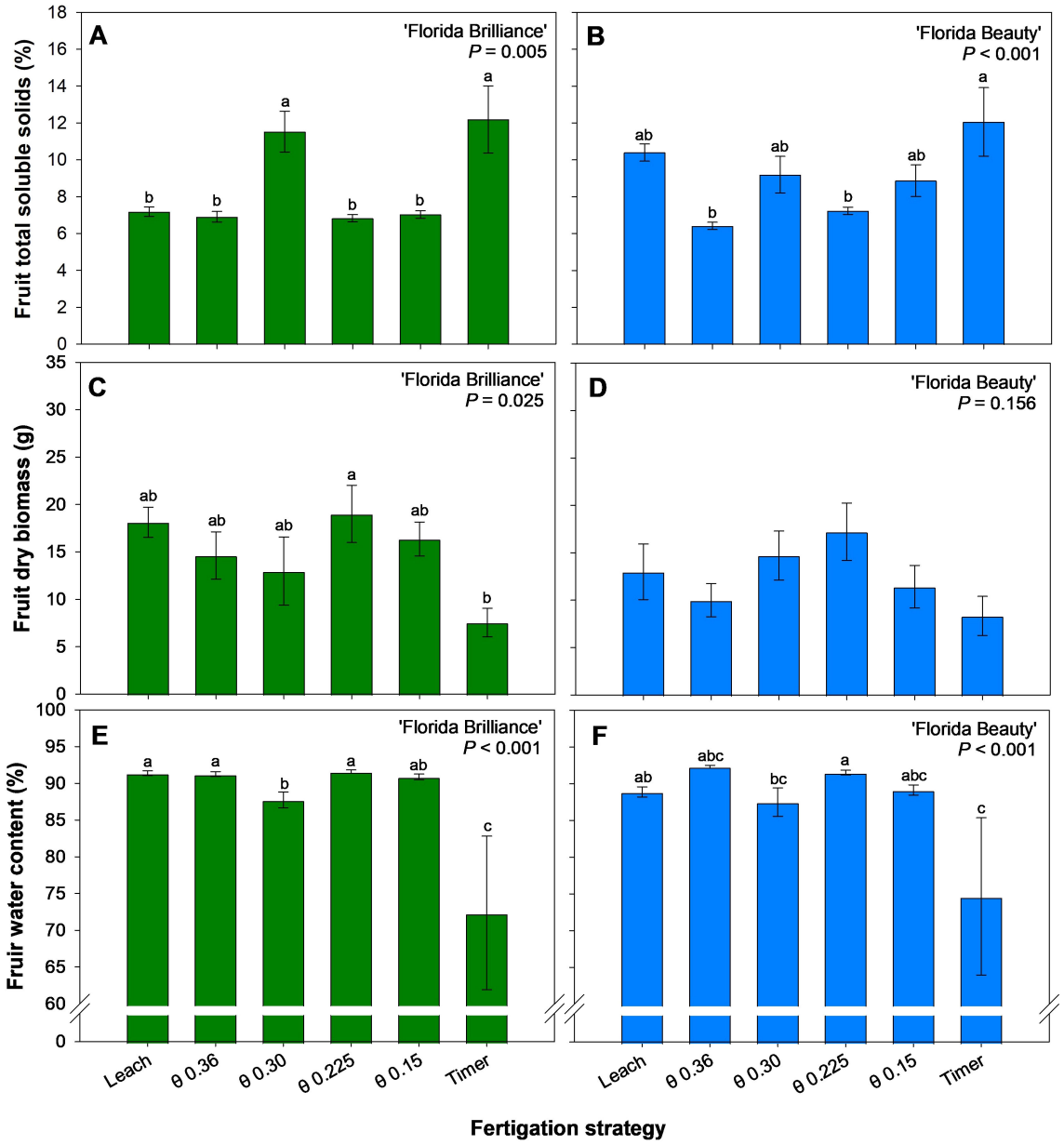

FIGURE 5
Fruit total soluble solids for 'Florida Brilliance' **(A)** and 'Florida Beauty' **(B)**, fruit dry biomass per plant for 'Florida Brilliance' **(C)** and 'Florida Beauty' **(D)**, and fruit water content for 'Florida Brilliance' **(E)** and 'Florida Beauty' **(F)**. Each bar represents the average ± standard error of four replications with two measurement plants. Bars with the same letter show no significant difference; bars with different letters are statistically different at a 5% significance level ($P < 0.05$).

3.9 Resource use efficiency

WUE was at least 331% higher for 'Florida Brilliance' in the Leach, θ 0.225 and 0.15 $m^3 \cdot m^{-3}$ treatments than in the Timer treatment ($P < 0.001$) (Figure 8A). For 'Florida Beauty', the θ 0.225 $m^3 \cdot m^{-3}$ treatment resulted in 214% higher WUE than the Timer treatment ($P = 0.023$) (Figure 8B). 'Florida Brilliance' EUE was at least 389% higher in the Leach and θ 0.15 $m^3 \cdot m^{-3}$ treatments than in the other treatments ($P < 0.001$) (Figure 8C). 'Florida Beauty' EUE was at least 1,496% higher in the Leach and θ θ 0.15 $m^3 \cdot m^{-3}$ treatments than in the θ 0.36 $m^3 \cdot m^{-3}$ treatment ($P < 0.001$) (Figure 8D).

4 Discussion

4.1 Fruit yield and plant biomass

The Timer treatment resulted in reduced yields (Figure 3), reduced number of fruit per plant (Figure 4) as well as reduced vegetative biomass, including height, fresh shoot biomass, dry shoot biomass (Figure 6), and leaf area (Figures 7C, D) for both cultivars. This trend, especially regarding vegetative biomass, was more pronounced in 'Florida Brilliance' than in 'Florida Beauty'. The Timer treatment also resulted in the highest fruit TSS in both cultivars (Figures 5A, B). This

10.3389/fpls.2024.1469434

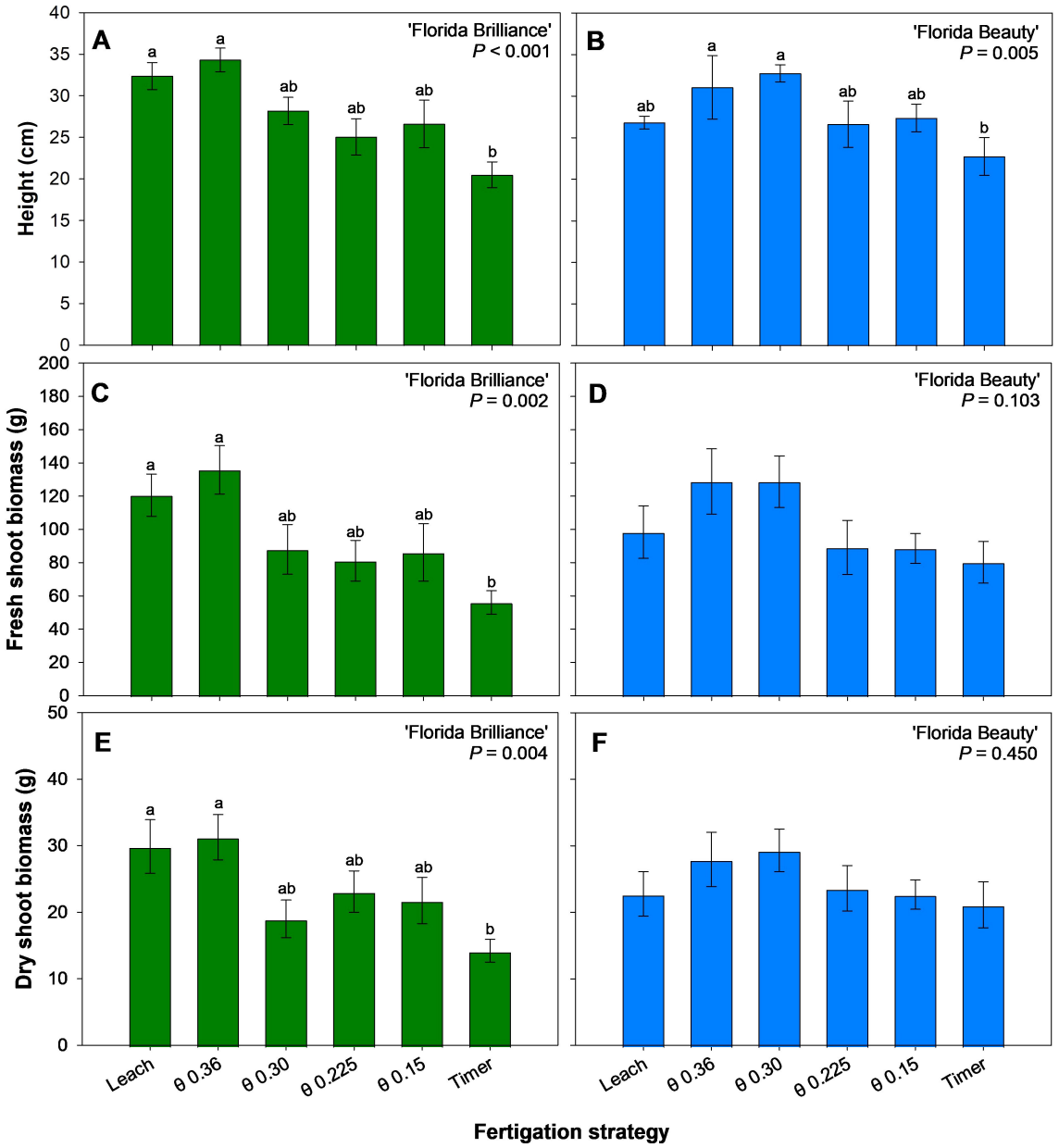

FIGURE 6
Plant height for 'Florida Brilliance' **(A)** and 'Florida Beauty' **(B)**, plant fresh shoot biomass for 'Florida Brilliance' **(C)** and 'Florida Beauty' **(D)**, and plant dry shoot biomass for 'Florida Brilliance' **(E)** and 'Florida Beauty' **(F)**. Each bar represents the average ± standard error of four replications with two measurement plants. Bars with the same letter show no significant difference; bars with different letters are statistically different at a 5% significance level ($P < 0.05$).

higher TSS is likely a result of the lower fruit water content in the Timer treatment (Figures 5E, F); as the water content decreases, solutes in the fruit become more concentrated, leading to a higher TSS. The Timer treatment being outperformed by sensor-based fertigation is not surprising, as previous studies have found similar results. One study reported a decrease in total and marketable yield for strawberries grown using timer-based fertigation compared to an FDR sensor-based fertigation (Bonelli et al., 2024). Another study observed a decrease in yield and plant fresh and dry biomass for strawberries grown using timer-based fertigation compared to one that used both solar irradiance sensors and soil moisture sensors to control fertigation automatically (Choi et al., 2021). Both of these previous experiments were conducted in greenhouses using soilless hydroponic substrate systems, and our study saw similar reductions from the Timer treatment compared to the sensor-based treatments.

In both cultivars, the θ 0.225 $m^3 \cdot m^{-3}$ treatment resulted in the highest total yield (Figures 3A, B), number of fruit (Figures 4A, B), and dry fruit biomass (Figures 5C, D). This treatment also resulted in the highest Mn and Fe foliar concentrations for both cultivars (Table 2). Mn is essential in the activation of several enzymes during the citric acid cycle, and it also aids in chlorophyll synthesis, nitrate assimilation, and the evolution of oxygen during photosynthesis. Fe

10.3389/fpls.2024.1469434

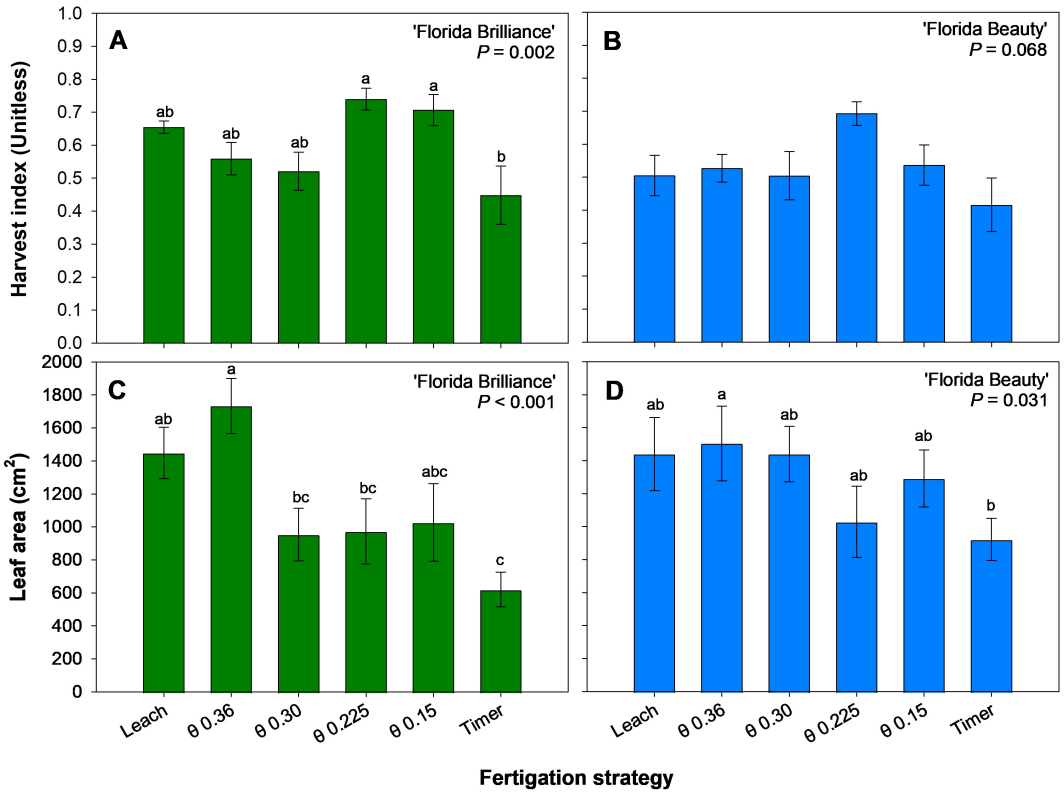

FIGURE 7
Harvest index for 'Florida Brilliance' **(A)** and 'Florida Beauty' **(B)**, and leaf area per plant for 'Florida Brilliance' **(C)** and 'Florida Beauty' **(D)**. Each bar represents the average ± standard error of four replications with two measurement plants. Bars with the same letter show no significant difference; bars with different letters are statistically different at a 5% significance level ($P < 0.05$).

TABLE 1 'Leaf macronutrient concentrations of 'Florida Brilliance' and 'Florida Beauty' strawberries (*Fragaria* × *ananassa*) in response to the six fertigation management strategies.

Cultivar	Fertigation Management Strategy	N (%)	P (%)	K (%)	Mg (%)	Ca (%)	S (%)
'Florida Brilliance'	Leach	2.38 ± 0.066	0.43 ± 0.025 b	2.31 ± 0.060 b	0.35 ± 0.020 ab	1.44 ± 0.057 ab	0.16 ± 0.005
	θ 0.36	2.48 ± 0.047	0.45 ± 0.018 b	2.38 ± 0.055 ab	0.30 ± 0.003 b	1.32 ± 0.066 b	0.16 ± 0.005
	θ 0.30	2.63 ± 0.135	0.66 ± 0.043 a	2.82 ± 0.111 a	0.37 ± 0.008 ab	1.70 ± 0.120 ab	0.18 ± 0.003
	θ 0.225	2.25 ± 0.077	0.42 ± 0.003 b	2.42 ± 0.077 ab	0.39 ± 0.010 a	1.72 ± 0.087 ab	0.17 ± 0.007
	θ 0.15	2.41 ± 0.036	0.43 ± 0.012 b	2.41 ± 0.152 ab	0.37 ± 0.008 ab	1.60 ± 0.081 ab	0.18 ± 0.010
	Timer	2.44 ± 0.139	0.67 ± 0.030 a	2.63 ± 0.114 ab	0.36 ± 0.023 ab	1.87 ± 0.176 a	0.17 ± 0.003
P		0.145	<0.001	0.020	0.060	0.019	0.134
Test		A	A	A	KW	A	KW
'Florida Beauty'	Leach	2.55 ± 0.084 ab	0.66 ± 0.019 a	2.59 ± 0.088	0.41 ± 0.006 a	1.60 ± 0.126 ab	0.18 ± 0.005
	θ 0.36	2.52 ± 0.057 ab	0.45 0.019 a	2.43 ± 0.043	0.30 ± 0.013 b	1.32 ± 0.050 b	0.16 ± 0.003
	θ 0.30	2.60 ± 0.047 a	0.58 ± 0.059 a	2.55 ± 0.060	0.35 ± 0.017 ab	1.50 ± 0.099 ab	0.18 ± 0.008
	θ 0.225	2.37 ± 0.048 ab	0.45 ± 0.005 a	2.61 ± 0.073	0.37 ± 0.012 ab	1.60 ± 0.044 ab	0.18 ± 0.006
	θ 0.15	2.27 ± 0.082 b	0.55 ± 0.090 a	2.60 ± 0.239	0.39 ± 0.019 ab	1.66 ± 0.084 ab	0.17 ± 0.005
	Timer	2.31 ± 0.087 ab	0.73 ± 0.051 a	2.52 ± 0.055	0.37 ± 0.017 ab	2.00 ± 0.223 a	0.16 ± 0.000
P		0.016	0.019	0.743	0.014	0.024	0.055
Test		A	KW	KW	KW	A	KW

Leaf nitrogen (N) was determined by the high-temperature phosphorous (P), potassium (K), magnesium (Mg), calcium (Ca), and sulfur (S) were determined by inductively coupled plasma atomic emission spectrophotometer (ICP-AES) after wet acid digestion using nitric acid and hydrogen peroxide. Statistical analysis for leaf N, P, K, and Ca was conducted using one-way ANOVA and Tukey's HSD (A), while the Kruskal-Wallis test with Dunn's post-hoc (KW) was used for leaf Mg and S due to invalid ANOVA assumptions. Each value represents the average ± standard error of four replications with two measurement plants. Means with the same letter show no significant difference; means with different letters are statistically different at a significance level of 5% ($P < 0.05$).

10.3389/fpls.2024.1469434

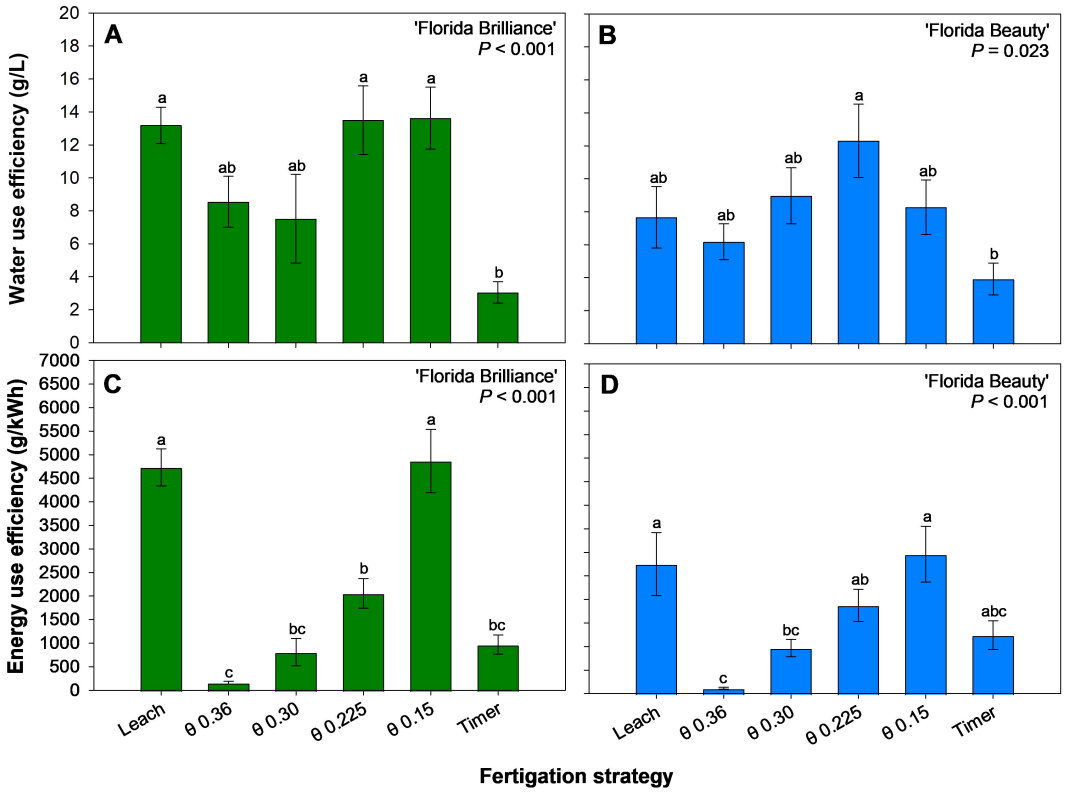

FIGURE 8
Water use efficiency for 'Florida Brilliance' **(A)** and 'Florida Beauty' **(B)**, and energy use efficiency for 'Florida Brilliance' **(C)** and 'Florida Beauty' **(D)**. Each bar represents the average ± standard error of four replications with two measurement plants. Bars with the same letter show no significant difference; bars with different letters are statistically different at a 5% significance level ($P < 0.05$).

is vital to the electron transport process during photosynthesis due to its inclusion in photosystem II, cytochrome *b6f*, photosystem I, and ferredoxin (Briat et al., 2015; Malone, 2014; Taiz and Zeiger, 2010). An increased foliar concentration of both essential micronutrients could have led to an increased availability of photosynthates, enhancing fruit growth and development. The increase in the concentrations of these two cations could be attributed to an improved cation exchange capacity due to the fertigation management strategy. Another possible explanation for the rise in yield, Mn, and Fe in the θ 0.225 $m^3 \cdot m^{-3}$ treatment is that this moisture level in the substrate could have been optimal for efficient and effective osmoregulation on a cellular level.

Marketable yield was not affected by the treatments for either cultivar (Figures 3C, D). This is likely a result of poor pollination causing low marketable yields for all treatments. Thorough pollination of strawberry flowers is essential for fruit to develop a symmetric, marketable shape. Strawberry flowers can self-pollinate, but biotic pollinators have been shown to improve pollination and produce larger, more evenly shaped fruit (Gudowska et al., 2024). We could not add biotic pollinators inside the greenhouse for this study and thus relied on active (deliberate with hands and blowers) and passive (from ambient air circulation) mechanical pollination, which might have reduced marketable yields.

The wettest θ treatment (0.36 $m^3 \cdot m^{-3}$) resulted in either the highest or second highest plant height, fresh shoot biomass, dry shoot biomass (Figure 6), and leaf area (Figures 7C, D) for both cultivars. This is an expected result because several other studies have reported a positive relationship between θ and plant biomass accumulation in ornamental plants. Gaura (*Gaura lindheimeri*) has previously exhibited positive correlations between θ and both shoot dry weight and leaf area when grown at several different θ thresholds (Burnett and van Iersel, 2008). Hibiscus (*Hibiscus acetosella*) has also demonstrated positive correlations between θ and both shoot height and shoot dry weight under several different θ thresholds (Ferrarezi et al., 2015). We saw similar strawberry vegetative biomass accumulation increased under elevated substrate θ thresholds.

The treatment θ 0.225 $m^3 \cdot m^{-3}$ resulted in the most efficient biomass allocation, with approximately 70% of fresh biomass produced going to fruit rather than vegetative tissue in both cultivars (Figures 7A, B). This is a byproduct of this treatment resulting in slightly reduced fresh shoot biomass, with 'Florida Brilliance' having the second lowest and 'Florida Beauty' having the third lowest of the six treatments (Figures 6C, D) and the highest yields as previously described (Figures 3A, B).

4.2 Resource use efficiencies

The treatment θ 0.225 $m^3 \cdot m^{-3}$ also resulted in the highest WUE for 'Florida Brilliance' (Figure 8A) and 'Florida Beauty' (Figure 8B).

10.3389/fpls.2024.1469434

TABLE 2 Leaf micronutrient concentrations of 'Florida Brilliance' and 'Florida Beauty' strawberries (*Fragaria* × *ananassa*) in response to the six fertigation management strategies.

Cultivar	Fertigation Management Strategy	B (mg/kg)	Zn (mg/kg)	Mn (mg/kg)	Fe (mg/kg)	Cu (mg/kg)
'Florida Brilliance'	Leach	151.50 ± 3.663	18.00 ± 0.816 b	187.75 ± 22.287 bc	514.00 ± 58.242 a	4.25 ± 0.250
	θ 0.36	139.00 ± 9.583	20.25 ± 0.854 b	102.50 ± 8.451 c	233.00 ± 12.994 b	3.75 ± 0.250
	θ 0.30	145.00 ± 9.600	30.75 ± 1.436 a	357.00 ± 65.029 ab	108.75 ± 15.024 b	4.25 ± 0.250
	θ 0.225	188.50 ± 11.064	22.25 ± 1.109 b	441.75 ± 24.095 a	559.50 ± 40.642 a	4.25 ± 0.629
	θ 0.15	170.25 ± 22.728	18.00 ± 1.472 b	285.50 ± 43.133 ab	230.50 ± 74.515 b	3.50 ± 0.289
	Timer	167.00 ± 21.973	32.00 ± 0.408 a	304.75 ± 50.954 ab	204.25 ± 67.288 b	4.25 ± 0.250
P		0.224	<0.001	<0.001	<0.001	0.354
Test		A	A	A	A	KW
'Florida Beauty'	Leach	129.00 ± 11.881 b	23.00 ± 1.683	203.25 ± 9.801 ab	517.00 ± 86.374 a	4.00 ± 0.408
	θ 0.36	134.75 ± 10.641 ab	22.75 ± 1.250	115.75 ± 21.800 b	286.50 ± 48.550 ab	6.25 ± 1.931
	θ 0.30	158.00 ± 11.402 ab	22.25 ± 1.652	238.00 ± 63.005 ab	94.50 ± 9.242 b	4.25 ± 0.250
	θ 0.225	180.50 ± 12.301 ab	23.75 ± 1.887	419.50 ± 25.366 a	546.50 ± 59.389 a	3.75 ± 0.250
	θ 0.15	148.75 ± 16.540 ab	18.50 ± 2.327	228.50 ± 14.773 ab	247.50 ± 40.292 ab	3.75 ± 0.250
	Timer	185.50 ± 11.139 a	27.00 ± 1.780	284.50 ± 33.952 ab	163.25 ± 18.531 ab	3.75 ± 0.250
P		0.022	0.237	0.006	0.002	0.311
Test		A	KW	KW	KW	KW

Leaf boron (B), iron (Fe), copper (Cu), manganese (Mn), and zinc (Zn) concentrations were determined by inductively coupled plasma atomic emission spectrophotometer (ICP-AES) after wet acid digestion using nitric acid and hydrogen peroxide. Statistical analysis for leaf B, Zn, Mn, and Fe were conducted using one-way ANOVA and Tukey's HSD (A), while the Kruskal-Wallis test with Dunn's post-hoc (KW) was used for leaf Cu due to invalid ANOVA assumptions. Each value represents the average ± standard error of four replications with two measurement plants. Means with the same letter show no significant difference; means with different letters are statistically different at a significance level of 5% ($P < 0.05$).

The differences in WUE among treatments were driven primarily by yield since the magnitude of the difference in average water use among treatments is not excessive. The θ 0.15 $m^3 \cdot m^{-3}$ treatment had an average water use of 15 L per plant, the Timer 17.08 L per plant, the Leach 17.21 L per plant, the θ 0.225 $m^3 \cdot m^{-3}$ 17.8 L per plant, the θ 0.30 $m^3 \cdot m^{-3}$ 18.79 L per plant, and the θ 0.36 $m^3 \cdot m^{-3}$ 22.4 L per plant. Despite the θ 0.225 $m^3 \cdot m^{-3}$ treatment having the third highest average water use, the high yields from the treatment resulted in high WUE. Overall, the WUE results match very closely with the yield results for both cultivars. 'Florida Brilliance' yield and WUE were the highest in the Leach treatment and the two drier θ treatments: 0.225 and 0.15 $m^3 \cdot m^{-3}$, all of which had close outcomes for both variables. 'Florida Beauty' yield and WUE were the highest in the θ 0.225 $m^3 \cdot m^{-3}$ treatment, the only treatment significantly different from the Timer treatment for either variable. A previous study also reported higher WUE in an FDR sensor-controlled fertigation compared to a timer-based fertigation for 'Seolhyang' strawberries grown in coco coir (Choi et al., 2016). This indicates that, generally, a θ level of 0.225 $m^3 \cdot m^{-3}$ could produce high yields in hydroponic strawberry production and utilize water efficiently to produce those yields.

EUE for both cultivars (Figures 8C, D) was driven almost exclusively by the differences in average energy consumption among treatments. The θ 0.36 $m^3 \cdot m^{-3}$ treatment had the highest average energy consumption per plant of all treatments by an order of magnitude with 1.181 kWh. The θ 0.30 $m^3 \cdot m^{-3}$ treatment had the second highest with 0.174 kWh, the θ 0.225 $m^3 \cdot m^{-3}$ treatment had the third highest at 0.117 kWh, the Timer treatment had the third lowest at 0.054 kWh, the Leach treatment had the second lowest at 0.048 kWh, and the θ 0.15 $m^3 \cdot m^{-3}$ treatment had the lowest average energy consumption per plant at 0.042 kWh. The EUE results closely followed this pattern in both cultivars, except for the Timer treatment, which had reduced EUE due to lower yield.

5 Conclusion

These findings underscore the significant advantages of sensor-based irrigation strategies in optimizing yield and resource use efficiency, particularly when employing drier thresholds (θ 0.225 and 0.15 $m^3 \cdot m^{-3}$) that align with leaching fraction approaches. By demonstrating superior performance over traditional timer-based methods, this study highlights the potential of precision irrigation to enhance sustainable agricultural practices, paving the way for future advancements in dynamic sensor-based systems. Future research should explore dual- instead of single-threshold sensor-based strategies that emulate the wetting and drying cycle in the leaching-fraction strategy more closely.

Data availability statement

The raw data supporting the conclusions of this article will be made available by the authors upon reasonable requests.

Author contributions

GH: Conceptualization, Data curation, Formal analysis, Investigation, Methodology, Validation, Visualization, Writing – original draft, Writing – review & editing. LN: Investigation, Writing – original draft, Writing – review & editing. ZA: Investigation, Writing – original draft, Writing – review & editing. KN: Investigation, Writing – original draft, Writing – review & editing. RF: Conceptualization, Funding acquisition, Investigation, Methodology, Project administration, Resources, Supervision, Validation, Visualization, Writing – original draft, Writing – review & editing.

Funding

The author(s) declare financial support was received for the research, authorship, and/or publication of this article. This research was funded by the United States Department of Agriculture (USDA) National Institute of Food and Agriculture (NIFA) Specialty Crop Research Initiative (SCRI) (grant 2018-51181-28365, Project 'LAMP: Lighting Approaches to Maximize Profits'), the University of Georgia the Department of Horticulture, the University of Georgia College of Agricultural and Environmental Sciences, and the University of Georgia Office of the Senior Vice President for Academic Affairs and Provost.

Acknowledgments

Thanks to all members of the CEA Crop Physiology and Production and Horticultural Physiology labs at the University of Georgia for assisting with this experiment. We also thank Lukaś Spichal and Pavel Klimeś for helping with the final plant harvest data collection. Finally, we thank Pete Stefanos and Haygrove, Frerick Laforge and Lareault Nursery, Brianne Reichenbach and Kenneth Parker, and the Florida Strawberry Growers Association for supporting this project.

Conflict of interest

The authors declare that the research was conducted in the absence of any commercial or financial relationships that could be construed as a potential conflict of interest.

Publisher's note

All claims expressed in this article are solely those of the authors and do not necessarily represent those of their affiliated organizations, or those of the publisher, the editors and the reviewers. Any product that may be evaluated in this article, or claim that may be made by its manufacturer, is not guaranteed or endorsed by the publisher.

References

Ahn, M. G., Kim, D. S., Ahn, S. R., Sim, H. S., Kim, S., and Kim, S. K. (2021). Characteristics and trends of strawberry cultivars throughout the cultivation season in a greenhouse. *Horticulturae* 7, 30. doi: 10.3390/horticulturae7020030

Bonelli, L., Montesano, F. F., D'Imperio, M., Gonnella, M., Boari, A., Leoni, B., et al. (2024). Sensor-based fertigation management enhances resource utilization and crop performance in soilless strawberry cultivation. *Agronomy* 14, 465. doi: 10.3390/agronomy14030465

Briat, J.-F., Dubos, C., and Gaymard, F. (2015). Iron nutrition, biomass production, and plant product quality. *Trends Plant Sci.* 20, 33–40. doi: 10.1016/j.tplants.2014.07.005

Burnett, S. E., and van Iersel, M. W. (2008). Morphology and irrigation efficiency of *Gaura lindheimeri* grown with capacitance sensor-controlled irrigation. *HortScience* 43, 1555–1560. doi: 10.21273/HORTSCI.43.5.1555

Choi, K.-Y., Choi, E.-Y., Kim, I. S., and Lee, Y.-B. (2016). Improving water and fertilizer use efficiency during the production of strawberry in coir substrate hydroponics using a FDR sensor-automated irrigation system. *Hortic. Environ. Biotechnol.* 57, 431–439. doi: 10.1007/s13580-016-0072-2

Choi, S. H., Kim, S. H., Choi, G. L., Jeong, H. J., Lim, M. Y., Kim, D. Y., et al. (2021). Growth and quality of the strawberry (*Fragaria annanassa* Dutch. cvs. 'Sulhyang') as affected by complex nutrient solution supplying control system using integrated solar irradiance and substrate moisture contents in hydroponics. *J. Bio Environ.* 30, 367–376. doi: 10.12791/KSBEC.2021.30.4.367

Cormier, J., Depardieu, C., Letourneau, G., Boily, C., Gallichand, J., and Caron, J. (2020). Tensiometer-based irrigation scheduling and water use efficiency of field-grown strawberries. *Agron. J.* 112, 2581–2597. doi: 10.1002/agj2.20205

Ferrarezi, R. S., van Iersel, M. W., and Testezlaf, R. (2015). Monitoring and controlling ebb-and-flow subirrigation with soil moisture sensors. *HortScience* 50, 447–453. doi: 10.21273/HORTSCI.50.3.447

Gómez, C., Currey, C. J., Dickson, R. W., Kim, H.-J., Hernández, R., Sabeh, N. C., et al. (2019). Controlled environment food production for urban agriculture. *HortScience* 54, 1448–1458. doi: 10.21273/HORTSCI14073-19

Green, T. (2023). *Plenty Unlimited is bringing Driscoll's strawberries and 300 jobs to Chesterfield with vertical farm* (Richmond, Virginia: Richmond Times-Dispatch).

Gudowska, A., Cwajna, A., Marjańska, E., and Moroń, D. (2024). Pollinators enhance the production of a superior strawberry – A global review and meta-analysis. *Agriculture Ecosyst. Environ.* 362, 108815. doi: 10.1016/j.agee.2023.108815

Hemmes, M. (2021). From zero to 72 acres of greenhouse-grown strawberries in five years. Available online at: https://www.hortidaily.com/article/9343487/from-zero-to-72-acres-of-greenhouse-grown-strawberries-in-five-years/ (Accessed 3.11.24).

Hoppula, K. I., and Salo, T. J. (2007). Tensiometer-based irrigation scheduling in perennial strawberry cultivation. *Irrig Sci.* 25, 401–409. doi: 10.1007/s00271-006-0055-7

Hytönen, T., Graham, J., and Harrison, R. (Eds.) (2018). *The Genomes of rosaceous berries and their wild relatives, Compendium of Plant Genomes* (Cham: Springer International Publishing). doi: 10.1007/978-3-319-76020-9

Kroggel, M., and Kubota, C. (2017). Controlled environment strategies for tipburn management in greenhouse strawberry production. *Acta Hortic.* 1156, 529–536. doi: 10.17660/ActaHortic.2017.1156.78

Kubota, C. (2019). Fertigation (Controlled Environment Berry Production Information). Available online at: https://u.osu.edu/indoorberry/fertigation/ (Accessed 2.25.24).

N. Malone (Ed.) (2014). *Strawberries: cultivation, antioxidant properties and health benefits, Nutrition and diet research progress* (New York: Nova Publishers).

Nelson, D. W., and Sommers, L. E. (1973). Determination of total nitrogen in plant material. *Agron. J.* 65, 109–112. doi: 10.2134/agronj1973.00021962006500010033x

Nemali, K. S., and van Iersel, M. W. (2006). An automated system for controlling drought stress and irrigation in potted plants. *Scientia Hortic.* 110, 292–297. doi: 10.1016/j.scienta.2006.07.009

Neri, D., Baruzzi, G., Massetani, F., and Faedi, W. (2012). Strawberry production in forced and protected culture in Europe as a response to climate change. *Can. J. Plant Sci.* 92, 1021–1036. doi: 10.4141/cjps2011-276

Oller, S. (2022). Plenty to invest $300M in indoor vertical farm campus (Food Dive). Available online at: https://www.fooddive.com/news/plenty-worlds-largest-vertical-farm-driscolls-strawberries/631686/ (Accessed 3.11.24).

Palumbo, M., D'Imperio, M., Tucci, V., Cefola, M., Pace, B., Santamaria, P., et al. (2021). Sensor-based irrigation reduces water consumption without compromising the yield and postharvest quality of the soilless green beans. *Agronomy* 11, 2485. doi: 10.3390/agronomy11122485

Raviv, M., Lieth, J. H., and Bar-Tal, A. (2019). *Soilless culture: theory and practice. 2nd edition* (London: Academic Press).

Rhie, Y. H., and Kim, J. (2017). Changes in physical properties of various coir dust and perlite mixes and their capacitance sensor volumetric water content calibrations. *HortScience* 52, 162–166. doi: 10.21273/HORTSCI11362-16

Samtani, J. B., Rom, C. R., Friedrich, H., Fennimore, S. A., Finn, C. E., Petran, A., et al. (2019). The status and future of the strawberry industry in the United States. *hortte* 29, 11–24. doi: 10.21273/HORTTECH04135-18

Taiz, L., and Zeiger, E. (2010). *Plant physiology. 5th ed* (Sunderland, MA: Sinauer Associates).

Twyman, R. M. (2005). *Sample dissolution for elemental analysis | Wet digestion, in Encyclopedia of Analytical Science*, 2nd Edition. Editors-in-Chief: Paul Worsfold, Alan Townshend and Colin Poole. (Amsterdam, Netherlands: Elsevier), 146–153. doi: 10.1016/B0-12-369397-7/00539-2

van Iersel, M. W., Seymour, R. M., Chappell, M., Watson, F., and Dove, S. (2009). "Soil moisture sensor-based irrigation reduces water use and nutrient leaching in a commercial nursery," in *SNA Research Conference*. 54, 17–21.

Yoshida, Y. (2013). Strawberry production in Japan: History and progress in production technology and cultivar development. *Int. J. Fruit Sci.* 13, 103–113. doi: 10.1080/15538362.2012.697027

frontiers | Frontiers in Plant Science

TYPE Original Research
PUBLISHED 06 February 2025
DOI 10.3389/fpls.2025.1522662

Check for updates

OPEN ACCESS

EDITED BY
Esameil Falalhi,
University of Idaho, United States

REVIEWED BY
Devinder Sandhu,
United States Department of Agriculture, United States
Siamak Shirani Bidabadi,
Arizona State University, United States

*CORRESPONDENCE
Amir Ali Khoddamzadeh
akhoddam@fiu.edu

RECEIVED 04 November 2024
ACCEPTED 21 January 2025
PUBLISHED 06 February 2025

CITATION
Nogueira Souza Costa B and Khoddamzadeh AA (2025) Data-driven nitrogen application for satinleaf: leveraging optical sensors in urban landscape management. *Front. Plant Sci.* 16:1522662. doi: 10.3389/fpls.2025.1522662

COPYRIGHT
© 2025 Nogueira Souza Costa and Khoddamzadeh. This is an open-access article distributed under the terms of the Creative Commons Attribution License (CC BY). The use, distribution or reproduction in other forums is permitted, provided the original author(s) and the copyright owner(s) are credited and that the original publication in this journal is cited, in accordance with accepted academic practice. No use, distribution or reproduction is permitted which does not comply with these terms.

Data-driven nitrogen application for satinleaf: leveraging optical sensors in urban landscape management

Bárbara Nogueira Souza Costa and Amir Ali Khoddamzadeh*

Department of Earth and Environment, Institute of Environment, Florida International University, Miami, FL, United States

The use of sensor technology is essential in managing fertilization, especially in urban landscape where excessive fertilization is a common issue that can lead to environmental damage and increased costs. This study focused on optimizing nitrogen fertilizer application for Satinleaf (*Chrysophyllum oliviforme*), a native Florida plant commonly used in South Florida landscaping. Fertilizer with an 8N-3P-9K formulation was applied in six different treatments: 15 g (control), 15 g (15 g twice; T1), 15 g (15 g once; T2), 30 g (15 g twice; T3), 30 g (15 g once; T4), and 45 g (15 g twice; T5). Evaluations of plant growth and nutrient status were conducted at several intervals: baseline (0), and 30, 60, 90, 120, 150, and 180 days post-fertilizer application. Three types of optical sensors-GreenSeeker™, SPAD meter, and atLEAF chlorophyll sensor - were used to monitor chlorophyll levels as an indicator of nitrogen content. The study found that the 30 g (15 g twice; T3) treatment was most effective in promoting plant growth and increasing nitrogen content in leaves and soil, while the 45 g (15 g twice; T5) treatment resulted in higher nutrient runoff, indicating potential environmental risks. These findings emphasize the value of using optical sensors for precise nitrogen management in plant nurseries to enhance growth, lower costs, and minimize environmental impact.

KEYWORDS

***Chrysophyllum oliviforme*, SPAD, AtLEAF, NDVI, runoff pollution, nitrogen fertilization**

1 Introduction

Satinleaf (*Chrysophyllum oliviforme*), a medium-sized tree in the Sapotaceae family, can reach heights of up to 45 feet and has a spread of approximately 25 feet. It is renowned for its unique and attractive foliage. Native to Florida, satinleaf is a prized choice in South Florida landscaping, often featured as a standout lawn specimen or integrated into shrub borders and naturalized settings (Gilman et al., 2019). Its popularity in urban landscaping is due to its aesthetic appeal and versatility in various environments (Meerow et al., 2020). In urban landscapes, satinleaf plays a crucial role by providing shade, enhancing air quality, and adding significant visual appeal to cityscapes.

Achieving optimal nitrogen (N) fertilization involves balancing nutrient supply with plant demand, a task complicated by the difficulty of accurately predicting both factors (Colaço and Bramley, 2018; Khoddamzadeh and Dunn, 2016; Fallahi et al., 2000). Satinleaf trees have moderate to high nitrogen needs and perform best in soils enriched with organic matter (Koeser et al., 2017). Therefore, tools like optical sensors are essential for managing nitrogen levels effectively.

Typically, only a small fraction of applied nitrogen is absorbed by crops, with the excess prone to environmental loss, leading to various ecological issues. Unused nitrogen can leach below the root zone or be lost through runoff (Randall and Goss, 2008; Cameron et al., 2013; Freidenreich et al., 2019), resulting in nitrate (NO_3^-) accumulation in natural water bodies (Pulido-Bosch et al., 2000; Ju et al., 2006). Elevated nitrate levels in water bodies are linked to human health risks (Addiscott, 1996) and eutrophication (Cameron et al., 2013). Furthermore, excess nitrogen contributes to environmental degradation through nitrous oxide (N_2O) emissions, which exacerbate global warming, and ammonia (NH_3) volatilization, which enriches natural ecosystems with nitrogen (Hartz, 2006; Meisinger et al., 2015; Galloway et al., 2008; Tilman et al., 2001).

Environmental protection and water pollution, especially in South Florida with its high precipitation rates and the prevalence of harmful algal blooms, have become critical issues. The restoration of the Everglades, a unique and vital ecosystem, has taken on added importance. This region faces significant challenges due to nutrient runoff, which contributes to ecological degradation and water quality concerns. Sustainable nitrogen management practices are therefore essential to safeguard the Everglades and surrounding water bodies.

Optical sensor technology has emerged as a key tool for optimizing nitrogen fertilization and mitigating its environmental impact. These sensors enable non-destructive, efficient assessments of crop nitrogen status, supporting informed fertilizer management decisions. Among the most widely used tools are the GreenSeeker™ handheld sensor (Trimble Navigation Ltd., CA), the SPAD meter (SPAD-502, Konica Minolta, Japan), and the atLEAF chlorophyll sensor (FT Green LLC, DE) (Basyouni et al., 2015; Khoddamzadeh et al., 2023).

The GreenSeeker™ sensor calculates the normalized difference vegetation index (NDVI) using active red and near-infrared light, providing insights into plant health and nitrogen levels. The SPAD meter evaluates chlorophyll content by analyzing light transmittance through leaves, offering a reliable indicator of nitrogen concentration. Similarly, the atLEAF chlorophyll sensor provides chlorophyll readings with the added benefit of digital integration for enhanced data analysis. These tools are not only adaptable across various growth stages but also require minimal labor, making them practical for large-scale implementation (Fox and Walthall, 2015; Tremblay et al., 2012).

This study aimed to determine the optimal nitrogen fertilizer dose for satinleaf by monitoring chlorophyll content using optical sensor technology. Additionally, it sought to evaluate the correlation between sensor readings and nitrogen content in satinleaf plants, identifying the fertilizer rate that minimizes nutrient runoff and supports sustainable agriculture in South Florida.

2 Materials and methods

2.1 Plant material and growing conditions

Satinleaf *(Chrysophyllum oliviforme)* plants were sourced from Santa Barbara Nursery in Miami, Florida. The potted plants were repotted and kept under shade house conditions at the Organic Garden of Florida International University (FIU). A slow-release fertilizer with an NPK 8-3-9 formulation (Harrell's®) was first applied in October, followed by various supplementary treatments.

2.2 Fertilizer treatments

Six different fertilizer treatments were employed: control (15-0-0), Treatment 1 (15-15-15), Treatment 2 (15-15-0), Treatment 3 (30-15-15), Treatment 4 (30-15-0), and Treatment 5 (45-15-15). Treatments were designed to evaluate the effects of varying nitrogen application rates on both plant growth and environmental impact (Table 1).

Assessments were conducted at seven timepoints: the baseline (day 0), and monthly intervals thereafter, up to 180 days post-fertilizer application (days 30, 60, 90, 120, 150, and 180). Parameters evaluated included plant growth, chlorophyll content (non-destructive), nitrogen and carbon concentration in leaf and substrate samples, as well as electrical conductivity and total nitrogen in leachate samples.

2.3 Growth assessment

Growth was monitored monthly by measuring the leaf count and the height of the plants. Five plants were selected from each treatment group for these measurements. Plant height was calculated by averaging the measurements from one larger and one smaller branch per plant, which were marked at the beginning of the experiment for consistency.

2.4 Chlorophyll content measurement

Chlorophyll content was determined using three types of devices: GreenSeeker™ NDVI sensor (Trimble Agriculture,

TABLE 1 Summary of fertilizer treatments, combinations and supplementary applications (SA) with corresponding dosages.

Treatments	Dosages	SA	Number and month of Application (SFT)
Control	15g	----	----
T1	15g	15g	2 - November and March
T2	15g	15g	1 - November
T3	30g	15g	2 - November and March
T4	30g	15g	1 - November
T5	45g	15g	2 - November and March

Sunnyvale, CA, USA), SPAD-502 chlorophyll meter (Konica Minolta, Japan), and atLEAF chlorophyll meter (Wilmington, DE, USA), and. Measurements for SPAD and atLEAF were taken from four mature leaves located in the middle section of each plant. The GreenSeeker™ sensor was placed 45 cm above the plant canopy to ensure uniform readings. Five plants were used from each treatment for these measurements.

2.5 Analysis of nitrogen/carbon content in soil and leaves

Leaf samples were collected every month from each treatment, while soil samples were obtained at the beginning and end of the experiment. Both leaf and soil samples were dried at 70°C for 48 hours, ground to a fine consistency, and then analyzed for total nitrogen and carbon content using standard protocols at FIU's Center for Aquatic Chemistry and Ecotoxicology (CAChE) Nutrient Analysis Core Facility (SOP-012). The analysis was conducted following the Carlo Erba NA1500 Series 1 Operating Manual, the Standard Operating Procedure for Instrumental Analysis for Total Organic Carbon and Total Nitrogen in Sediments (USGS Reston, Virginia Environmental Organic Geochemistry Laboratory, 13pp), and EPA Method 440.0 (Determination of Carbon and Nitrogen in Sediments and Particulates of Estuarine/Coastal Waters Using Elemental Analysis, U.S. Environmental Protection Agency, Washington, DC, EPA/600/R-15/009, 1997). Five plants were used to collect these samples.

2.6 Runoff collection and nutrient analysis

Runoff was collected using individual containers placed under each 3 gallons pot (Dimensions: 11" wide x 9.5" tall) during irrigation. Five plants from each treatment were used to collected leachate samples from each treatment, the plants were watered to saturation, and a further 350 ml of water was added to each pot to generate leachate. The total leachate collected was used to measure electric conductivity and salt content in situ. A 50 ml aliquot of the leachate was immediately refrigerated at 4°C and later analyzed for total nitrogen at the CAChE Nutrient Analysis Core Facility.

2.7 Statistical analysis

The experiment was conducted as a completely randomized design (CRD) consist of six treatments, each replicated five times, for a total of 30 plants (one per pot). Data were analyzed using ANOVA, and differences between treatment means were evaluated using Tukey's test at a 5% significance level through the SISVAR statistical program (Ferreira, 2011). Correlation analyses were conducted between sensor readings, leaf number, and nitrogen and carbon content in the leaves using GraphPad Prism software (v. 9.4.1, GraphPad, San Diego, CA, USA).

3 Results

3.1 Growth and chlorophyll content analysis

The data analysis revealed no significant ($p > 0.05$) association between fertilization rates and evaluation periods regarding the leaf number and Normalized Difference Vegetation Index (NDVI) values. Therefore, these factors were examined independently. The various fertilizer treatments did not significantly impact the number of leaves or NDVI values ($p > 0.05$). However, notable differences were observed in chlorophyll content as measured by the SPAD and atLEAF sensors ($p \leq 0.05$). The T5, T3, and control showed increased SPAD values (77.08, 76.91, and 77.39, respectively), compared to the T1, which had lower values (73.80). Similarly, the atLEAF readings were higher for the T2 (75.91) compared to the T1 (72.67) and T3 (73.73). The T5 also showed elevated atLEAF readings (75.33) in comparison to the T1 (72.67) (Table 2).

3.2 Effect of days post-fertilizer application on chlorophyll content

The number of leaves remained unaffected by days post-fertilizer application (DPFA) ($p > 0.05$). However, the chlorophyll content, as measured by SPAD and atLEAF, and NDVI values varied significantly over time ($p \leq 0.05$). The highest SPAD values were recorded at 90 (78.89), 150 (77.04), and 180 days post-fertilizer application (DPFA) (78.94) compared to 0 DPFA (72.77). The highest atLEAF readings occurred at 60 (76.36) and 180 DPFA (76.27), surpassing readings at 30 (73.38), 90 (73.00), and 120 DPFA (72.88). The lowest NDVI value was observed at 180 DPFA (0.73), which was significantly lower than the values recorded at 0 (0.84), 30 (0.84), 60 (0.86), 90 (0.85), 120 (0.86), and 150 DPFA (0.82) (Table 3).

TABLE 2 Number of leaves, chlorophyll Levels (SPAD and atLEAF Measurements), and NDVI values of satinleaf plants under different fertilizer treatments (FT).

Treatments	Number of Leaves (unit)	SPAD	atLEAF	NDVI
Control	96.26 a	77.39 a	74.71 abc	0.83 a
T1	112.77 a	73.80 b	72.67 c	0.83 a
T2	94.51 a	75.26 ab	75.91 a	0.82 a
T3	118.31 a	76.91 a	73.73 bc	0.84 a
T4	109.14 a	76.17 ab	74.66 abc	0.82 a
T5	90.37 a	77.08 a	75.33 ab	0.83 a

Means followed by the same letter lower case in the columns (Treatments) and upper case in the rows (DPFA) are not significantly different by Tukey's test ($p \leq 0.05$). Control (15-0-0), Treatment 1 (15-15-15), Treatment 2 (15-15-0), Treatment 3 (30-15-15), Treatment 4 (30-15-0), and Treatment 5 (45-15-15).

TABLE 3 Changes in number of leaves (NL), chlorophyll content (SPAD and atLEAF), and NDVI across days post-fertilizer application (DPFA) in satinleaf plants.

DPFA	NL (unit)	SPAD	atLEAF	NDVI
0	90.40 a	72.77 b	74.04 ab	0.84 a
30	91.60 a	74.95 ab	73.38 b	0.84 a
60	180.80 a	75.17 ab	76.36 a	0.86 a
90	96.47 a	78.89 a	73.00 b	0.85 a
120	105.73 a	74.95 ab	72.88 b	0.86 a
150	104.97 a	77.04 a	75.58 ab	0.82 a
180	104.97 a	78.94 a	76.27 a	0.73 b

Means followed by the same letter within columns are not significantly different by Tukey's test ($p \leq 0.05$).

3.3 Impact of fertilizer treatments on plant height and nutrient content

A significant ($p \leq 0.05$) association was found between fertilization rate and DPFA for plant height in Satinleaf plants. The highest increases in plant height were observed in the T3 and T4, reaching 129.40 cm and 119.40 cm, respectively, at 180 DPFA (Figure 1). Furthermore, there was significant ($p \leq 0.05$) association between fertilization rate and DPFA for total nitrogen (TN) and total carbon (TC) in leaf samples. The T4 achieved the highest total nitrogen concentration (2.95%) at 60 DPFA, while the highest total carbon content (49.33%) was recorded in the T1 at 150 DPFA (Table 4).

3.4 Soil nutrient content and runoff analysis

Significant ($p \leq 0.05$) association were also found between fertilizer rate and DPFA for nitrogen and carbon levels in soil samples. For instance, the T3 resulted in the highest total nitrogen (1.43%) and carbon content (33.91%) in the soil at 180 DPFA (Table 5). Runoff analysis indicated a significant ($p \leq 0.05$) correlation between fertilization rate and DPFA for salt content, electrical conductivity (EC), and total nitrogen (TN) in leachate samples. The T5 showed the highest levels of salt (2952 ppm), EC (5502 µs), and TN (192 ppm) at 30 DPFA, indicating substantial nutrient loss through runoff (Table 6).

3.5 Correlation analysis

Correlation analysis demonstrated strong negative correlations between SPAD readings and total carbon at 60 DPFA (-0.858) and between total nitrogen and total carbon at both 120 DPFA (-0.905) and 180 DPFA (-0.819). Additionally, a strong negative correlation was observed between SPAD and NDVI at 120 DPFA (-0.986). These correlations highlight the complex interplay between different parameters under varying fertilizer treatments (Table 7).

4 Discussion

Nitrogen is a vital nutrient that significantly influences plant growth and development, primarily as a core component of chlorophyll in leaves. Chlorophyll levels directly affect leaf area, biomass, plant height, and water usage. Inadequate nitrogen can cause deficiency symptoms that negatively impact plant health, productivity, and commercial value. On the other hand, excessive nitrogen application can lead to toxicity, resulting in stunted growth and poor plant quality. Over-application also raises production costs and poses environmental risks due to nutrient leaching and runoff, leading to contamination of water bodies and ecosystems (Khoddamzadeh and Dunn, 2016; Basyouni and Dunn, 2013). This study utilized optical sensors as a non-destructive method to estimate chlorophyll content and assess nitrogen status, aiming to

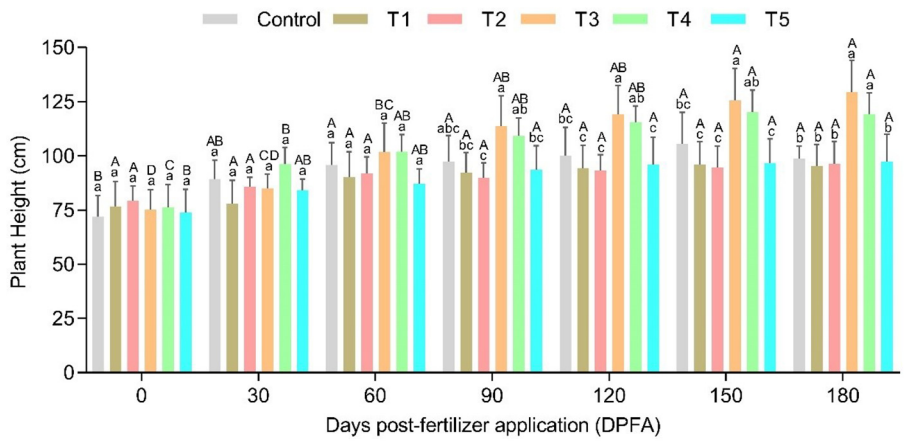

FIGURE 1
Plant height of satinleaf plants grown at Different Fertilization Levels and Days Post-Fertilizer Application (DPFA). Control (15-0-0), Treatment 1 (15-15-15), Treatment 2 (15-15-0), Treatment 3 (30-15-15), Treatment 4 (30-15-0), and Treatment 5 (45-15-15). Means followed by the same letter lower case (Treatments) and upper case (DPFA) are not significantly different by Tukey's test ($p \leq 0.05$).

TABLE 4 Total nitrogen, and total carbon in satinleaf plants across various fertilizer treatments and days post-fertilizer application (DPFA).

Treatments	DPFA						
	0	30	60	90	120	150	180
	Total Nitrogen (% dry leaf mass)						
Control	1.46 aA	1.46 fA	0.91 fF	1.16 fD	1.18 fC	1.14 fE	1.24 fB
T1	1.46 aG	1.82 cA	1.79 dB	1.68 eE	1.62 dF	1.73 eD	1.78 dC
T2	1.46 aF	1.80 dC	1.85 cB	1.96 cA	1.79 cD	1.79 dD	1.58 eE
T3	1.46 aG	1.62 eE	1.67 eD	1.72 dC	1.61 eF	1.95 cA	1.80 cB
T4	1.46 aF	2.72 aC	2.95 aA	2.75 aB	2.20 bE	2.72 aC	2.24 aD
T5	1.46 aF	2.00 bE	2.27 bB	2.03 bD	2.30 aA	2.30 bA	2.06 bC
	0	30	60	90	120	150	180
	Total Carbon (% dry leaf mass)						
Control	46.97 aC	46.97 cC	39.37 fF	47.41 cA	47.36 aB	46.43 fD	46.27 bE
T1	46.97 aD	46.89 dF	46.94 aE	47.53 bB	47.23 bC	49.33 aA	46.02 cG
T2	46.97 aB	48.18 aA	43.77 cG	46.93 dC	46.71 dE	46.72 eD	45.36 dF
T3	46.97 aE	47.35 bC	42.54 eG	48.74 aA	47.08 cD	48.52 bB	44.62 eF
T4	46.97 aC	46.05 fF	44.97 bG	46.42 eE	46.63 fD	48.43 cA	47.53 aB
T5	46.97 aB	46.78 eC	43.26 dG	45.44 fE	46.67 eD	47.98 dA	43.61 fF

Means followed by the same letter lower case in the columns (Treatments) and upper case in the rows (DPFA) are not significantly different by Tukey's test ($p \leq 0.05$). Control (15-0-0), Treatment 1 (15-15-15), Treatment 2 (15-15-0), Treatment 3 (30-15-15), Treatment 4 (30-15-0), and Treatment 5 (45-15-15).

TABLE 5 Total nitrogen, and total carbon in satinleaf cultivation at different fertilization levels measured at baseline and 180 days post-fertilizer application (DPFA).

Treatments	DPFA	
	0	180
	Total Nitrogen (% dry soil mass)	
Control	1.07 aB	1.19 dA
T1	1.07 aB	1.20 cA
T2	1.07 aA	1.05 f B
T3	1.07 aB	1.43 aA
T4	1.07 aB	1.18 eA
T5	1.07 aB	1.33 bA
	0	180
	Total Carbon (% dry soil mass)	
Control	28.60 aA	27.40 eB
T1	28.60 aA	26.62 fB
T2	28.60 aB	30.11 bA
T3	28.60 aB	33.91 aA
T4	28.60 aA	28.07 dB
T5	28.60 aB	29.47 cA

Means followed by the same letter lower case in the columns (Treatments) and upper case in the rows (DPFA) are not significantly different by Tukey's test ($p \leq 0.05$). 15g (control), 15g (15g applied twice in November and March; T1), 15g (15g November; T2), 30g (15g applied twice in November and March; T3), 30g (15g November; T4) and 45g (15g applied twice in November and March; T5).

identify the optimal fertilizer dosage for Satinleaf that balances growth and environmental sustainability.

The results indicated that the T3 effectively promoted Satinleaf growth, as evidenced by an increase in plant height and higher chlorophyll content measured by SPAD. This treatment also enhanced total nitrogen levels in both the leaves and soil substrate. These findings are consistent with those reported by Costa et al. (2023) for Cocoplum plants, where treatment 3 (30-15-15) treatment was also found to be the optimal nitrogen dose for promoting growth without excessive nutrient loss. These outcomes suggest that moderate nitrogen doses can provide sufficient nutrients for optimal plant growth while minimizing nutrient loss through runoff.

The results also show that the Control treatment provided higher values for SPAD, compared with the with higher doses. This may have happened due to high doses of nitrogen can generate severe vegetative growth, which can lead to the dilution effect where the concentration of chlorophyll per leaf unit decreases due to the increase in leaf area. This can also explain the why T4 has higher N concentrations in the leaf dry mass compared to T5.

The T4 achieved the highest total nitrogen concentration at 60 DPFA, while the highest total carbon content was recorded in the T1 at 150 DPFA. Furthermore, T1 also provided lower chlorophyll values (SPAD and atLEAF) compared to the other treatments, which shows that this plant was efficient in absorbing carbon, but was not efficient in converting it into chlorophyll through photosynthesis.

As observed in this study, chlorophyll content measured by SPAD and atLEAF sensors increased over time following fertilizer application, while NDVI values showed a decline towards the end of

TABLE 6 Leachate analysis of salt content, electrical conductivity, and total nitrogen in satinleaf plants under days post-fertilizer application (DPFA).

Treatments	DPFA						
	0	30	60	90	120	150	180
	Salt (ppm)						
Control	289.00 aB	1232.60 dA	541.60 dB	669.20 bAB	395.40 aB	463.20 bB	453.20 bcB
T1	289.00 aB	1974.00 bcA	1108.80 bcdB	1165.80 abB	636.00 AbcBC	1766.00 Aa	984.40 abB
T2	289.00 aB	1596.00 cdA	757.80 cdB	802.40 Bb	529.00 aB	441.40 bB	408.20 cB
T3	289.00 aC	2192.00 bA	1140.80 bcB	736.20 bBC	469.60 aC	1296.00 aB	765.40 abcBC
T4	289.00 aD	2142.00 bcA	1410.60 abB	1149.60 abBC	594.00 aCD	544.60 bD	434.80 bcD
T5	289.00 aE	2952.00 aA	1743.60 aB	1396.20 aBC	621.00 aDE	1664.00 aB	1046.20 aCD
	0	30	60	90	120	150	180
	Electrical Conductivity (µs/cm)						
Control	603.80 aA	2403.20 dB	1091.00 dB	1357.40 bAB	816.60 aB	949.60 bB	931.00 bB
T1	603.80 aC	3762.00 bcA	2214.20 bcB	2265.00 abB	1294.00 aBC	3364.00 aA	2059.40 aB
T2	603.80 aB	3110.00 cdA	1514.80 cdB	1607.60 bB	1063.40 aB	710.40 bB	842.60 bB
T3	603.80 aC	4172.00 bA	2199.80 bBc	1467.00 bBC	963.40 aC	2518.00 aB	1544.40 abBC
T4	603.80 aD	3988.00 bcA	2725.00 abB	2245.00 abBC	1210.40 aCD	1118.40 bD	899.00 bD
T5	603.80 aE	5502.00 aA	3354.40 aB	2734.00 aBC	1253.20 aDE	3170.00 aB	2053.80 aCD
	0	30	60	90	120	150	180
	Total Nitrogen (ppm)						
Control	3.03 aG	45.83 fA	8.73 fC	6.17 dE	5.73 fF	8.20 eD	13.55 eB
T1	3.03 aG	91.50 eA	40.50 cC	10.50 aE	6.23 eF	12.63 dD	44.90 cB
T2	3.03 aG	99.50 dA	12.75 eD	10.20 bE	47.67 aB	6.25 fF	20.66 dC
T3	3.03 aG	101.00 cA	38.50 dD	9.13 cF	9.45 dE	78.83 aB	45.41 bC
T4	3.03 aG	134.00 bA	77.75 bB	3.77 fF	13.00 cD	14.62 bC	8.30 fE
T5	3.03 aG	192.00 aA	108.25 aB	3.97 eF	16.77 bD	12.67 cE	58.40 aC

Means followed by the same letter lower case in the columns (Treatments) and upper case in the rows (DPFA) are not significantly different by Tukey's test ($p \leq 0.05$). Control (15-0-0), Treatment 1 (15-15-15), Treatment 2 (15-15-0), Treatment 3 (30-15-15), Treatment 4 (30-15-0), and Treatment 5 (45-15-15).

TABLE 7 Pearson's correlation coefficients (*r*) between sensor parameters, total nitrogen (TN), and total carbon (TC) in satinleaf plants measured across days post-fertilizer application (DPFA).

DPFA	Variables	Correlation Value	Significance
60	SPAD vs. TC (%)	-0.858	p≤ 0.05
120	SPAD vs. NDVI	-0.986	p ≤ 0.001
120	TN (%) vs. TC (%)	-0.905	p≤ 0.01
180	TN (%) vs. TC (%)	-0.819	p≤ 0.05

the experiment. The highest fertilizer dose T5, resulted in elevated salt concentration, electrical conductivity (EC), and total nitrogen levels in the runoff samples. This indicates substantial nitrogen loss due to runoff, which can harm the environment. A more sustainable approach to nitrogen management involves using moderate doses, such as the T3, which supports effective plant growth while reducing the risk of environmental contamination. Similar patterns were observed in studies on other native and non-native plants in South Florida, including Cocoplum (Costa et al., 2023) and Cacao (Khoddamzadeh and Souza Costa, 2023).

In general, all plants were watered manually, which may have resulted in different amount for each plant. However, for the nutrient runoff analysis, a methodology was followed in which the size of the pots was considered and the same amount was added to all the plants, in addition the saturation point was the same for all treatments and the water was observed the flowing through the pots. Therefore, the large amount of nutrient runoff may have been primarily due to the amount of fertilizers applied, thus showing the difference between the high fertilizer treatments and the control.

Correlation analysis revealed significant negative correlations between SPAD readings and total carbon at 60 days post-fertilizer application (DPFA) and between total nitrogen and total carbon at 120 and 180 DPFA. A strong negative correlation was also found between SPAD and NDVI. These negative correlations suggest that

as one parameter increases, the other decreases, reflecting the complex correlation between these variables. Khoddamzadeh and Souza Costa (2023) also noted similar negative correlations between total nitrogen and total carbon in Cacao plants grown under different fertilization rates, further emphasizing the need to balance these nutrients for optimal plant health and growth.

5 Conclusions

This study demonstrates that Satinleaf (Chrysophyllum oliviforme) plants can thrive with lower nitrogen fertilizer doses, which also help mitigate nutrient runoff pollution. The treatment with 30 g (15 g applied twice in November and March; T3) proved to be the most effective, enhancing plant growth and nitrogen levels in both soil and plant tissues. In contrast, the 45 g (15 g applied twice; T5) treatment resulted in substantial nutrient loss through runoff, making it less ideal for sustainable urban landscape management.

The findings underscore the importance of integrating sensor technologies, such as GreenSeeker™, SPAD meter, and atLEAF chlorophyll sensors, into fertilization management strategies. These tools enable precise monitoring of nitrogen levels, optimizing fertilization to reduce environmental impacts, minimize costs, and prevent over-fertilization.

Future research should focus on improving the sensitivity and accessibility of sensor technology to better serve landscape professionals. Additionally, further investigations into how sensor-based fertilization management can be adapted to diverse urban environments and plant species will enhance its practical application. These advancements can contribute significantly to more sustainable urban landscape practices and environmental resilience.

Data availability statement

The raw data supporting the conclusions of this article will be made available by the authors, without undue reservation.

Author contributions

BN: Data curation, Investigation, Software, Validation, Writing – original draft, Writing – review & editing. AK: Conceptualization, Funding acquisition, Investigation, Methodology, Project administration, Resources, Supervision, Validation, Visualization, Writing – review & editing.

Funding

The author(s) declare financial support was received for the research, authorship, and/or publication of this article. This study was supported by the Agricultural Marketing Service of the U.S. Department of Agriculture (USDA) under grant number AM200100XXXXG037. The content herein is the sole responsibility of the authors and does not necessarily represent the official views of the USDA.

Acknowledgments

We extend our gratitude to the students who participated in this project, including Daniel Tucker, Alejandra Carrillo, Milagros Munoz Salas, Regina Gonzalez, and Amir Sabir, as well as the staff at FIU's Conservation and Sustainable Horticulture Lab, for their invaluable support and assistance throughout this research. This is publication #1812 from the Institute of Environment at Florida International University.

Conflict of interest

The authors declare that the research was conducted in the absence of any commercial or financial relationships that could be construed as a potential conflict of interest.

Generative AI statement

The author(s) declare that no Generative AI was used in the creation of this manuscript.

Publisher's note

All claims expressed in this article are solely those of the authors and do not necessarily represent those of their affiliated organizations, or those of the publisher, the editors and the reviewers. Any product that may be evaluated in this article, or claim that may be made by its manufacturer, is not guaranteed or endorsed by the publisher.

References

Addiscott, T. M. (1996). "Fertilizers and nitrate leaching," in *Agricultural Chemicals and the Environment*. Eds. R. E. Hester and R. M. Harrison (The Royal Society of Chemistry, 1–26). doi: 10.1039/9781847550088-00001

Basyouni, R., and Dunn, B. (2013). Use of optical sensors to monitor plant nitrogen status in horticultural plants (HLA-6719-4). Stillwater.

Basyouni, R., Dunn, B. L., and Goad, C. (2015). Use of nondestructive sensors to assess nitrogen status in potted poinsettia (*Euphorbia pulcherrima* L. (Willd. ex Klotzsch)) production. *Sci. Hortic.* 192, 47–53. doi: 10.1016/j.scienta.2015.05.011

Cameron, K. C., Di, H. J., and Moir, J. L. (2013). Nitrogen losses from the soil/plant system: a review. *Ann. Appl. Biol.* 162, 145–173. doi: 10.1111/aab.12014

Colaço, A. F., and Bramley, R. G. V. (2018). Do crop sensors promote improved nitrogen management in grain crops? *Field Crops Res.* 218, 126–140. doi: 10.1016/j.fcr.2018.01.007

Costa, B. N. S., Tucker, D. A., and Khoddamzadeh, A. A. (2023). Precision horticulture: application of optical sensor technology for nitrogen monitoring status in cocoplum, a native landscaping plant. *Plants* 12, 760. doi: 10.3390/plants12040760

Fallahi, E., Michael Colt, W., Fallahi, B., and Chun, I. J. (2000). "Influence of different rates of nitrogen on fruit quality, yield and photosynthesis of'Fuji'apple," in *IV International Symposium on Mineral Nutrition of Deciduous Fruit Crops*, Vol. 564. 261–268. doi: 10.17660/ActaHortic.2001.564.30

Ferreira, D. F. (2011). Sisvar: a computer statistical analysis system. *Ciec. e Agrotecnol.* 35, 1039–1042. doi: 10.1590/S1413-70542011000600001

Fox, R. H., and Walthall, C. L. (2015). Crop monitoring technologies to assess nitrogen status. *Nitrogen Agricultural Systems* 49, 647–674. doi: 10.2134/agronmonogr49.c16

Freidenreich, A., Barraza, G., Jayachandran, K., and Khoddamzadeh, A. A. (2019). Precision agriculture application for sustainable nitrogen management of *Justicia brandegeana* using optical sensor technology. *Agriculture* 9, 98. doi: 10.3390/agriculture9050098

Galloway, J. N., Townsend, A. R., Erisman, J. W., Bekunda, M., Cai, Z., Freney, J. R., et al. (2008). Transformation of the nitrogen cycle: recent trends, questions, and potential solutions. *Sci. (1979)* 320, 889–892. doi: 10.1126/science.1136674

Gilman, E. F., Watson, D. G., Klein, R. W., Koeser, A. K., Hilbert, D. R., and McLean, D. C. (2019). *Chrysophyllum oliviforme: Satinleaf, ENH325.* (Gainesville: University of Florida Institute of Food and Agricultural).

Hartz, T. K. (2006). Vegetable production best management practices to minimize nutrient loss. *Horttechnology* 16, 398–403. doi: 10.21273/HORTTECH.16.3.0398

Ju, X. T., Kou, C. L., Zhang, F. S., and Christie, P. (2006). Nitrogen balance and groundwater nitrate contamination: Comparison among three intensive cropping systems on the North China Plain. *Environ. pollut.* 143, 117–125. doi: 10.1016/j.envpol.2005.11.005

Khoddamzadeh, A. A., and Dunn, B. L. (2016). Application of optical sensors for nitrogen management in Chrysanthemum. *HortScience* 51, 915–920. doi: 10.21273/HORTSCI.51.7.915

Khoddamzadeh, A. A., Flores, J., Griffith, M. P., and Souza Costa, B. N. (2023). Saltwater intrusion ecophysiological effects on Pseudophoenix sargentii, Roystonea regia, Sabal palmetto "Lisa," and Thrinax radiata in South Florida. *Front. Ecol. Evol.* 11. doi: 10.3389/fevo.2023.1127679

Khoddamzadeh, A. A., and Souza Costa, B. N. (2023). Best nitrogen management practices using sensor-based smart agriculture in nursery production of cacao. *Horticulturae* 9, 454. doi: 10.3390/horticulturae9040454

Koeser, A. K., Friedman, M. H., Hasing, G., Franck, A. R., Finley, H., and Schelb, J. (2017). *Trees: South Florida and the Keys*. (Gainesville: University of Florida, Institute of Food and Agricultural Sciences).

Meerow, A. W., Broschat, T. K., and Donselman, H. M. (2020). Native trees for South Florida.

Meisinger, J. J., Schepers, J. S., and Raun, W. R. (2015). Crop nitrogen requirement and fertilization. *Nitrogen Agricultural Systems* 49, 563–612. doi: 10.2134/agronmonogr49.c14

Pulido-Bosch, A., Bensi, S., Molina, L., Vallejos, A., Calaforra, J. M., and Pulido-Leboeuf, P. (2000). Nitrates as indicators of aquifer interconnection. Application to the Campo de Dalías (SE - Spain). *Environ. Geol.* 39, 791–799. doi: 10.1007/s002540050495

Randall, G. W., and Goss, M. J. (2008). "Nitrate Losses to Surface Water Through Subsurface, Tile Drainage," in *Nitrogen in the Environment* (Elsevier), 145–175. doi: 10.1016/B978-0-12-374347-3.00006-8

Tilman, D., Fargione, J., Wolff, B., D'antonio, C., Dobson, A., Howarth, R., et al. (2001). Forecasting agriculturally driven global environmental change. *Science* 292, 281–284. doi: 10.1126/science.1057544

Tremblay, N., Wang, Z., and Cerovic, Z. G. (2012). Sensing crop nitrogen status with fluorescence indicators. A review. *Agron. Sustain Dev.* 32, 451–464. doi: 10.1007/s13593-011-0041-1

frontiers | Frontiers in Plant Science

TYPE Original Research
PUBLISHED 26 February 2025
DOI 10.3389/fpls.2025.1536177

Check for updates

OPEN ACCESS

EDITED BY
Amir Ali Khoddamzadeh,
Florida International University, United States

REVIEWED BY
Jinhua Sun,
Henan Agricultural University, China
Dan Li,
Guangzhou Institute of Geography, China
Wahyu Nurkholis Hadi Syahputra,
University of Jember, Indonesia
Tao Zhang,
Inner Mongolia Agricultural University, China

*CORRESPONDENCE
Weiping Kong
kongwp@aircas.ac.cn
Huichun Ye
yehc@aircas.ac.cn

RECEIVED 28 November 2024
ACCEPTED 20 January 2025
PUBLISHED 26 February 2025

CITATION
Kong W, Ma L, Ye H, Wang J, Nie C, Chen B, Zhou X, Huang W and Fan Z (2025) Nondestructive estimation of leaf chlorophyll content in banana based on unmanned aerial vehicle hyperspectral images using image feature combination methods.
Front. Plant Sci. 16:1536177.
doi: 10.3389/fpls.2025.1536177

COPYRIGHT
© 2025 Kong, Ma, Ye, Wang, Nie, Chen, Zhou, Huang and Fan. This is an open-access article distributed under the terms of the Creative Commons Attribution License (CC BY). The use, distribution or reproduction in other forums is permitted, provided the original author(s) and the copyright owner(s) are credited and that the original publication in this journal is cited, in accordance with accepted academic practice. No use, distribution or reproduction is permitted which does not comply with these terms.

Nondestructive estimation of leaf chlorophyll content in banana based on unmanned aerial vehicle hyperspectral images using image feature combination methods

Weiping Kong[1,2]*, Lingling Ma[1], Huichun Ye[2,3]*, Jingjing Wang[4], Chaojia Nie[3], Binbin Chen[1], Xianfeng Zhou[5], Wenjiang Huang[6] and Zikun Fan[1]

[1]National Engineering Research Center for Satellite Remote Sensing Applications, Aerospace Information Research Institute, Chinese Academy of Sciences, Beijing, China, [2]Key Laboratory of Earth Observation of Hainan Province, Hainan Research Institute, Aerospace Information Research Institute, Chinese Academy of Sciences, Sanya, China, [3]Key Laboratory of Digital Earth Science, Aerospace Information Research Institute, Chinese Academy of Sciences, Beijing, China, [4]School of Forestry, Hainan University, Haikou, China, [5]College of Life Information Science and Instrument Engineering, Hangzhou Dianzi University, Hangzhou, China, [6]State Key Laboratory of Remote Sensing Science, Aerospace Information Research Institute, Chinese Academy of Sciences, Beijing, China

Introduction: Nondestructive quantification of leaf chlorophyll content (LCC) of banana and its spatial distribution across growth stages from remotely sensed data provide an effective avenue to diagnose nutritional deficiency and guide management practices. Unmanned aerial vehicle (UAV) hyperspectral imagery can document abundant texture features (TFs) and spectral information in a field experiment due to the high spatial and spectral resolutions. However, the benefits of using the fine spatial resolution accessible from UAV data for estimating LCC for banana have not been adequately quantified.

Methods: In this study, two types of image features including vegetation indices (VIs) and TFs extracted from the first-three-principal-component-analyzed images (TFs-PC1, TFs-PC2, and TFs-PC3) were employed. We proposed two methods of image feature combination for banana LCC inversion, which are a two-pair feature combination and a multivariable feature combination based on four machine learning algorithms (MLRAs).

Results: The results indicated that compared to conventionally used VIs alone, the banana LCC estimations with both proposed VI and TF combination methods were all significantly improved. Comprehensive analyses of the linear relationships between all constructed two-pair feature combinations and LCC indicated that the ratio of mean to modified red-edge sample ratio index (MEA/MSR_{re}) stood out (R^2 = 0.745, RMSE = 2.17). For multivariable feature combinations, four MLRAs using original or two selected VIs and TFs-PC1 combination groups resulted in better LCC estimation than the other input variables. We concluded that the nonlinear Gaussian process regression model with the VIs and TFs-PC1 combination selected by maximal information

coefficient as input achieved the highest accuracy in LCC prediction for banana, with the highest R^2 of 0.776 and lowest RMSE of 2.04. This study highlights the potential of the proposed image feature combination method for deriving high-resolution maps of banana LCC fundamental for precise nutritional diagnosing and operational agriculture management.

KEYWORDS

leaf chlorophyll content, banana, image feature combinations, machine learning, unmanned aerial vehicle hyperspectral imagery

1 Introduction

Banana is one of the important tropical fruits in China; it has been widely cultivated in many regions of China, such as Hainan Province, where banana planting has become one of the pillar industries and a major source of incomes for local farmers. In recent years, the banana cultivation industry shows a relatively stable increasing trend, with a planting area of 3.3×10^4 ha and an annual production of fresh fruits of 1.125×10^6 t in 2023. With the increasing competition in the fruit market, the consumer demand for fruit quantity and quality is also improving, which undoubtedly puts forward higher requirements for the local fruit industry in their production management capacity. However, for decades, the inappropriate application of chemical fertilizer in pursuit of high yields has resulted in serious soil and groundwater pollution, soil quality degradation, nutrient imbalance in the banana plants, and a decline in fruit quality (Guo et al., 2010; Huang et al., 2022). Therefore, to benefit the government and land managers in making informed decisions on agricultural practices, it is critical to improve the monitoring ability and accurately diagnose the nutritional status of banana plants.

The phenotype of banana leaves is broad and big; they are the most direct organ for identifying nutrient deficiencies and guiding fertilizer application because they are the main site of photosynthesis, which determines the primary processes occurring within the plant. Leaf chlorophyll, as the key photosynthetic pigment, can absorb light energy and transfer it into the photosynthetic apparatus, providing essential energy for the growth and development of plants (Curran et al., 1992). In addition, nitrogen is an important component of chlorophyll, so monitoring leaf chlorophyll content (LCC) can indirectly indicate nitrogen and nutritional status (Haboudane et al., 2008). LCC can also be related to plant stress and senescence since it tends to decrease when a plant suffers from external stress (e.g., fertilizer shortage or pest and disease) (Chappelle et al., 1992). Quantifying LCC, overall, has aroused great attention from both land managers and ecophysiologists.

Compared to traditional chemical analysis measured in the laboratory, remote sensing technology has been proven to be an effective way to assess vegetation LCC due to its advantages of rapid data acquisition and nondestructive and accurate monitoring at a large scale (Sims and Gamon, 2002; Wu et al., 2008). Optical sensors embedded on satellites and airborne platforms can acquire spectral information over large areas, which have long been used for vegetation monitoring. Although an increasing number of optical satellite images are freely available, the use of satellite imagery for LCC quantification is still limited by the fact that the image quality is usually susceptible to atmospheric conditions (e.g., clouds and suspended particles), and the spatial resolutions and revisit frequencies are seemingly not enough for supporting crop management activities at the field level and over short critical growth stages (Inoue et al., 2016; Jay et al., 2019; Pimmasarn et al., 2020). During the recent decades, unmanned aerial vehicle (UAV) equipped with RGB, multispectral and/or hyperspectral sensor has been attracting more and more attention particularly in agriculture. RGB and multispectral data are widely used by researchers to estimate LCC for various crops (Caruso et al., 2017; Xu et al., 2022; Barata et al., 2023). However, the broadband spectral information provided by RGB and the multispectral sensors that offer average spectral information over a wide range may result in loss of critical and subtle spectral features which are available in specific hyperspectral bands (Tao et al., 2020). Unlike RGB and multispectral observations, hyperspectral data containing full- and narrow-band spectral radiation information could describe various characteristics associated with the biochemical and physiological traits of targets (Sims and Gamon, 2002; Kong et al., 2022). Consequently, a hyperspectral sensor mounted on UAV will hold a promising potential in the accurate assessment of LCC. Earlier studies have made lots of attempts to extract the spectral response characteristic of LCC at visible light and near-infrared and analyze their ability in characterizing the growth and nutritional state of crops (Haboudane et al., 2002; Inoue et al., 2016). They established LCC estimation models and achieved acceptable accuracy and performance under specific conditions for wheat, maize, peanut, and other field crops (Qi et al., 2021; Zhang et al., 2021; Qiao et al., 2022). It has been accepted that UAV mounted with hyperspectral sensor is very flexible to adjust its flight heights and efficient to collect data at a higher spatial resolution (can reach up to the centimeter level) in a short time, enabling it to capture images of various vegetations with abundant spectral and textural information during each key growth period. These properties make it more suitable for monitoring vegetation

nutritional status especially in cloudy and rainy regions, such as Hainan Province. In comparison to the abovementioned field crops with relatively homogeneous canopies, fruit trees have more complex canopy structure and leaf morphology. At present, studies on the nutritional diagnosis of fruit trees from remote sensing data mainly focused on apple, pear, citrus, etc (Osco et al., 2019; Azadnia et al., 2023; Huang et al., 2024). However, for a tropical fruit tree such as banana, adoption of UAV hyperspectral remote sensing in LCC estimation remains largely unexplored.

Vegetation index (VI), calculated by the spectral reflectance of two or more bands according to linear or nonlinear mathematical formula, is widely applied for leaf biochemical parameters estimation owing to its simplicity and computational efficiency. A number of VIs were proposed based on knowledge of the reflectance properties of LCC and have been proven to have the ability of reducing the noise in hyperspectral reflectance caused by soil background, atmospheric absorption, and other leaf components, consequently maximizing the corresponding information on leaf variables of target (Rondeaux et al., 1996; Sims and Gamon, 2002; Wu et al., 2008). Lots of studies have been devoted to developing the linear relationship between VI and LCC (Gitelson et al., 2006; Wu et al., 2008; Kong et al., 2017a, Kong et al., 2017b). However, some studies showed that nonlinear models have more obvious advantages than linear models in quantitative prediction (Kira et al., 2015; Zhang et al., 2021). Lately, machine learning regression algorithms (MLRAs), e.g., Gaussian process regression (GPR), support vector regression (SVR), and adaptive regression splines (ARS), become powerful candidates for the estimation of LCC from spectral reflectance of multi-related bands or VIs because of their ability to perform adaptive, nonlinear data fitting (Verrelst et al., 2013a; Upreti et al., 2019; Guo et al., 2022). However, the VIs utilize only a limited amount of information available in spectral data and are susceptible to saturation at high canopy coverage (Kong et al., 2017a). Texture features (TFs) describe the grayscale properties and spatial arrangement of image pixels, can make up for the insensitivity of spectral information in the regional size and direction, and have a strong resistance to image noise (Khosravi and Alavipanah, 2019). To maximize the advantages of VIs and TFs, previous studies tried to combine both image features to track the variations in nutritional parameters. Some researchers extracted the VIs and TFs from remote sensing images and developed new combined image features, which were proven to provide better result for estimating LCC and nitrogen (Chen et al., 2019; Zheng et al., 2020; Guo et al., 2022). Inspired by the approved LCC modeling presented above, MLRAs seem also to be a useful tool for coupling the spectral and textural information to monitor crops (Khosravi and Alavipanah, 2019; Li et al., 2023; Biswal et al., 2024; Zhang et al., 2024). The high spatial resolution of UAV makes it possible to document abundant texture feature information in field experiments. However, the benefits of using the fine spatial resolution accessible from UAV imagery as well as the potential ability of the combined use of VIs and TFs for retrieving the LCC in banana plants, and what degree the image feature combinations can contribute to improve banana LCC compared to individual spectral features which are rarely reported and kept unknown and need to be investigated.

The aim of this study was to propose the approaches of spectral and texture feature combination based on UAV hyperspectral data then benefit the nondestructive estimation of banana LCC. The specific objectives were to (i) investigate the correlation between banana LCC and individual VI and TF and identify the optimal image features, (ii) develop two-pair feature combinations of VI and TF and establish the linear relationship with LCC, (iii) estimate the LCC using multiple MLRAs with the VIs, original VIs and TFs combination as well as selected VIs and TFs combination as input, and (iv) evaluate the potential ability of the best linear two-pair VI and TF combination and nonlinear MLRA models in banana LCC prediction and map its spatial distribution using UAV hyperspectral images.

2 Materials and methods

2.1 Study site

The experiment was conducted at the Banana Cultivation Research and Development Base in Danzhou Municipality (19° 23′ N, 109°58′ E), Hainan Province, during April 2024. A cultivar of banana (*Musa acuminate*, AA) was selected, and two plots were investigated in this study, referred to as plot 1 and plot 2, respectively (Figure 1). Because the banana plants of the two plots were planted at different times, they have different growth stages during the field campaign, i.e., leaf development stage (BBCH 18) and fruit development stage (BBCH 72). The banana plants in plot 1 had eight completely open leaves, with a homogenous yellowish green color, and the blades were relatively small and narrow, while the plants in plot 2 had 11 or 12 leaves, and the fruits were already formed, the leaves were all healthy and dark green, with the area approximately twice bigger than those at the leaf development stage. The soil is laterite, with nutrient content of about 10.78 g/kg of organic matter, 60.1 mg/kg available nitrogen, 25.41 mg/kg of available phosphorus, and 120.79 mg/kg of available potassium and pH of 5.28. All plots were managed in the same way, including the fertilization and irrigation treatments.

2.2 Data collection

2.2.1 UAV hyperspectral image acquisition and processing

The DJ M300RTK UAV platform equipped with the X20P hyperspectral imaging sensor (Cubert GmbH, Ulm, Baden-Württemberg, Germany) was used to acquire remote sensing data of the banana fields. The quality of the X20P hyperspectral imaging sensor is 630 g, and the size is 6 cm*10.7 cm*9.5 cm. Its spectral resolution is approximately 3.96 nm, with spinning wavelength of 350 to 1,000 nm with 164 bands. Radiometric calibration was taken before each flight. The flight height was approximately 80 m, and the spatial resolution of collected hyperspectral images was 2.87 cm. Its flying

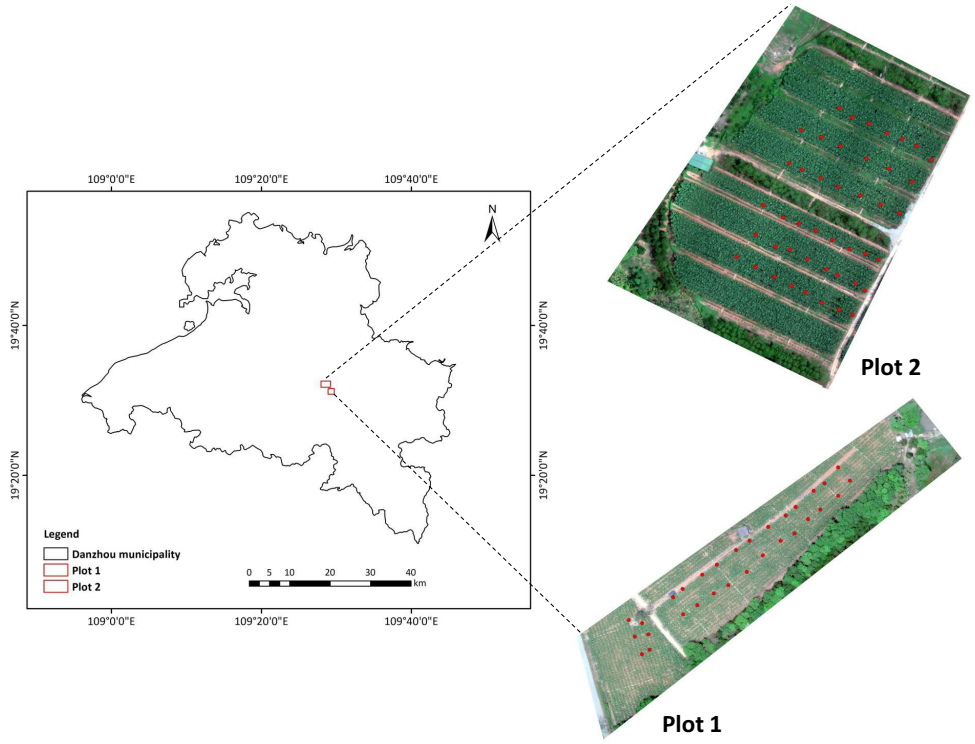

FIGURE 1
Location of study site. The red spots are the ground measurement locations for leaf chlorophyll content.

speed was 6 m/s, the forward overlap was about 90%, and the lateral overlap was about 90%. The flight was conducted under clear sky conditions between 11:00 a.m. and 13:00 p.m. (Beijing local time) to minimize shadowing in the images. The Cubert Utils Touch software was used for image radiometric calibration and fusion of the hyperspectral data and the corresponding panchromatic image. Agisoft PhotoScan (Agisoft, St. Petersburg, Russia) was employed to image mosaicking.

2.2.2 Leaf chlorophyll content measurement

The SPAD-502 meter (Konica-Minolta, Tokyo, Japan) measures the transmission of red (approximately 650 nm) and near-infrared (approximately 940 nm) radiation through plant leaves (Minolta, 1989). The increase of LCC could increase the absorption of red radiation, and the transmission of near-infrared radiation is used as a reference, so the calculated SPAD value was applied to represent the amount of LCC present in the sample leaf in many studies (Parry et al., 2014; Zhou et al., 2020; Zhang et al., 2022). In this study, LCC of banana was measured by the SPAD-502 meter. The central position of each measurement point was geo-located with GPS, and a total of 74 ground measurement points (30 points in plot 1 and 44 points in plot 2) were marked in Figure 1. The SPAD value of each point was generated from the mean SPAD of a total of five banana plants, i.e., the middle and four corner plants in each measurement point. Specifically, for a given measurement point, three leaves from the top of the canopies were selected from each of the five plants, and 20 SPAD measurements were conducted per leaf, with 60 measurements in total per plant. All measurements of the five plants were averaged to obtain the SPAD value for the corresponding ground measurement point. We performed the verification of the SPAD meter by quantifying the relationship between LCC determined in the laboratory and the SPAD value, but because of the limited experiment condition and operators, the LCC sampled from only 18 points were measured by chemical analysis (Figure 2). Several 1-cm circles were cut from each leaf sample. After weighing the fresh leaf weight, the samples were ground in 10 mL of 95% ethanol extract solution. After storing the solution in darkness for more than 24 h, the absorbance was measured with a UV-VIS spectrophotometer (Perkin-Elmer, Lambda 5, Waltham, MA, USA) at 649- and 665-nm wavelengths. The LCC were calculated using equations in Lichtenthaler (1987). From Figure 2, the SPAD value exhibited a strong exponential function relationship with LCC measured in the laboratory, which was in accordance with many published studies (Uddling et al., 2007; Parry et al., 2014), further indicating that it was reliable to use the SPAD meter for banana LCC measurement.

2.3 Extraction and screening of image features

2.3.1 Extraction of vegetation index and textural feature

A series of image features including VIs and TFs were extracted from the hyperspectral images. A total of 20 VIs that were

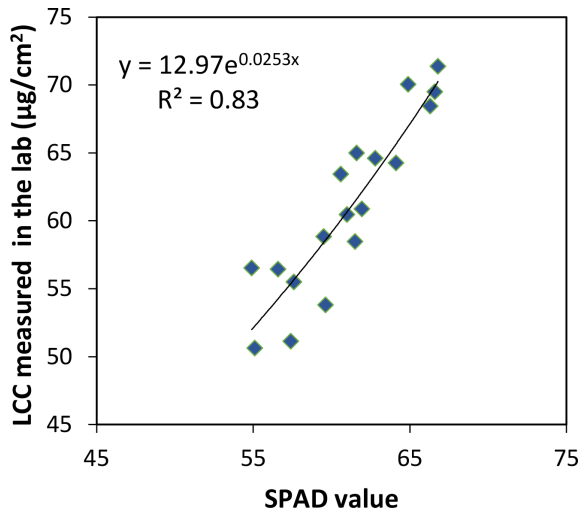

FIGURE 2
Verification of SPAD values using leaf chlorophyll content measured by chemical analysis in the laboratory.

previously used for LCC estimation in the published literatures were selected in this study (Table 1). They were classified into original vegetation index (VI_{org}) and red-edge vegetation index (VI_{re}). Previously developed VI_{re} that has analogous form with corresponding VI_{org} was chosen to compare the performance for LCC estimation. Before the extraction, the hyperspectral images were firstly separated into banana plants and soil background by the statistic-based segment method. The process of this method was as follows: The NDVI was selected as a standardized way to assess whether a pixel observed was vegetation or not (Devadas et al., 2009). In general, NDVI ranging from 0.3 to 1.0 was considered as vegetation (Zhang et al., 2019). To find out the banana plants and soil in the two plots more accurately, the pixels only containing banana plants and the pixels only containing soil were selected and counted from the corresponding hyperspectral images, respectively. The result showed that the optimal thresholds of NDVI for separating banana plants and soil was set as 0.48 for plot 1 and 0.5 for plot 2, which were used as the mask files to extract the plants. The pixels with NDVI larger than 0.48 in plot 1 and larger than 0.5 in plot 2 were regarded as banana plants; the rest of the pixels were regarded as soil. It should be noted that the pixels only containing banana plants were used for the subsequent calculation of VIs and TFs. For the ground measurement points, the VIs and TFs were extracted as follows: 50*50 pixels region of interest (ROI) centered around the measurement point was manually selected, and then the mean value of VI or TF within the ROI was deemed to represent the corresponding measurement point.

For the TFs extraction, the hyperspectral images were first transformed by principal component analysis (PCA) with the aim of reducing the dimensionality, redundancy, and collinearity of data. In this study, we analyzed the TFs generated from the first three principal component (PC) images, i.e., the first PC image (PC1), the second PC image (PC2), and the third PC image (PC3), which contained more than 96% of the cumulative variance, hereinafter referred to as TFs-PC1, TFs-PC2, and TFs-PC3, respectively. Eight TFs were extracted to evaluate their correlation with LCC (Table 2). They were based on the gray-level co-occurrence matrix defined by Haralick et al. (1973). A 3 × 3 calculation window was chosen when calculating the TFs, which could capture more local details and facilitate to detect subtle changes of image texture (Yue et al., 2019).

2.3.2 Screening of image features

Pearson correlation coefficient (r) and maximum information coefficient (MIC) were used to evaluate the correlation between VIs or TFs and LCC. Pearson correlation coefficient is a widely used index which can measure the linear correlation between two variables, with the r value ranging from -1 to 1, while MIC was explored to evaluate the linear and nonlinear between variables; the range is 0 to 1. The higher the absolute value of r ($|r|$) or MIC, the better correlation of the VI or TF with respect to LCC. In this study, the VI or TF who has $|r|$ or MIC higher than 0.8 was selected as one of the potential predictors for banana LCC using MLRAs method.

2.4 LCC estimation modeling and validation

In this section, we propose two types of methods for assessing banana LCC, i.e., two-pair image feature combination method and multivariable image feature combination using MLRAs. Model validation was also included.

2.4.1 LCC estimation based on two-pair image feature combination

The SR, NDVI, and DVI are three types of earlier proposed and the most classic and the most widely used formulas in leaf biochemical and physiological parameters estimation, which are composed of two spectral reflectance or features. Inspired by this, we calculated all possible VI and TF combinations in types of SR, NDVI, and DVI (referred to as two-pair image feature combination) for banana LCC assessment. Linear regression was adopted to model the relationship between LCC and each image feature combination, and their performances were tested to determine the best two-pair image feature combination for LCC estimation. They were defined as Equations 1–3). We consequently obtained a total of 160 image feature combinations for each type. All of the calculations were implemented using MATLAB R2021b (The MathWorks, Inc., Natick, MA, USA).

$$SR - type = \frac{TF}{VI} \quad (1)$$

$$NDVI - type = \frac{VI - TF}{VI + TF} \quad (2)$$

$$DVI - type = VI - TF \quad (3)$$

TABLE 1 Vegetation indices used in this study.

Vegetation index abbreviation	Vegetation index	Formula	Reference	Bands used
Original vegetation index (VI_{org})				
SR	Simple ratio	R_{nir}/R_{red}	(Jordan, 1969)	802 nm, 682 nm
NDVI	Normalized difference vegetation index	$(R_{nir} - R_{red})/(R_{nir} + R_{red})$	(Sims and Gamon, 2002)	802 nm, 682 nm
GDVI	Green difference vegetation index	$R_{green} - R_{red}$	(Sripada, 2005)	550 nm, 682 nm
RDVI	Red difference vegetation index	$R_{nir} - R_{red}$	(Huete et al., 1994)	802 nm, 682 nm
MDVI	Modified difference vegetation index	$(R_{nir} - R_{red})/\sqrt{R_{nir} + R_{red}}$	(Roujean and Breon, 1995)	802 nm, 682 nm
MSR	Modified SR	$(R_{nir}/R_{red} - 1)/\sqrt{R_{nir}/R_{red} + 1}$	(Chen, 1996)	802 nm, 682 nm
mNDVI	Modified NDVI	$(R_{nir} - R_{red})/(R_{nir} + R_{red} - 2R_{blue})$	(Sims and Gamon, 2002)	802 nm, 682 nm, 446 nm
CI_{green}	Green chlorophyll index	$R_{nir}/R_{green} - 1$	(Gitelson et al., 2006)	770 nm, 510 nm
OSAVI	Optimized soil-adjusted vegetation index	$(1 + 0.6)(R_{nir} - R_{red})(R_{nir} + R_{red} + 0.16)$	(Rondeaux et al., 1996)	802 nm, 682 nm
$OSAVI_{green}$	Optimized soil-adjusted vegetation index with green	$(1 + 0.6)(R_{nir} - R_{green})(R_{nir} + R_{green} + 0.16)$	(Qiao et al., 2022)	802 nm, 550 nm
SIPI	Structure insensitive pigment index	$(R_{nir} - R_{blue})/(R_{nir} - R_{red})$	(Penuelas et al., 1995)	802 nm, 446 nm, 682 nm
Corresponding red-edge vegetation index (VI_{re})				
SR_{re}	Red-edge simple ratio	$R_{nir}/R_{red-edge}$	(Sims and Gamon, 2002)	802 nm, 706 nm
$NDVI_{re}$	Red-edge normalized difference vegetation index	$(R_{nir} - R_{red-edge})/(R_{nir} + R_{red-edge})$	(Sims and Gamon, 2002)	802 nm, 706 nm
REDVI	Red-edge difference vegetation index	$R_{red-edge} - R_{red}$	(Sun et al., 2010)	710 nm, 682 nm
$MDVI_{re}$	Modified difference vegetation index with red-edge	$(R_{nir} - R_{red-edge})\Big/\sqrt{R_{nir} + R_{red-edge}}$	(Qiao et al., 2022)	802 nm, 710 nm
MSR_{re}	Modified red-edge SR	$(R_{nir}/R_{red-edge} - 1)\Big/\sqrt{R_{nir}/R_{red-edge} + 1}$	(Wu et al., 2008)	802 nm, 710 nm
$mNDVI_{re}$	Modified red-edge NDVI	$(R_{nir} - R_{red-edge})/(R_{nir} + R_{red-edge} - 2R_{blue})$	(Sims and Gamon, 2002)	802 nm, 710 nm, 446 nm
CI_{re}	Red-edge chlorophyll index	$R_{nir}/R_{red-edge} - 1$	(Gitelson et al., 2006)	770 nm, 710 nm
$OSAVI_{red\text{-}edge}$	Optimized soil-adjusted vegetation index with red-edge	$(1 + 0.6)(R_{nir} - R_{red-edge})(R_{nir} + R_{red-edge} + 0.16)$	(Wu et al., 2008)	802 nm, 706 nm
MTCI	MERIS terrestrial chlorophyll index	$(R_{nir} - R_{red-edge})/(R_{red-edge} - R_{red})$	(Dash and Curran, 2004)	802 nm, 710 nm, 682 nm

2.4.2 LCC estimation using multivariable image feature combination based on MLRAs

Four MLRAs, including PLSR, ARS, SVR, and GPR, were employed to combine more than two image features for LCC estimation. The VIs, original Vis, and TFs combinations, as well as the selected VIs and TFs combinations optimized by Pearson correlation and MIC, were respectively used as input variables in these MLRAs. The ARS, SVR, and GPR models were conducted to build nonlinear relationships between input variable and LCC, while the PLSR model was carried out to build their linear relationship.

PLSR is a bilinear calibration method for retrieving vegetation biochemical parameters. It integrates multiple linear regression, least square regression, and principal component analysis, which compresses the independent variables (e.g., multiply image features) into several latent variables with the strongest explanation to the model system and finally reduces the multi-collinearity problem of input variables and influence of data noise on the regression model (Hansen and Schjoerring, 2003).

ASR is a basic function-based nonparametric regression, which was firstly developed by Friedman and Roosen (1995). ASR has the ability of automatically identifying the most relevant variables available from remote sensing data and of handling variable interactions, which is crucial for integrating multi-type data (e.g., VIs and TFs). It also provides an explicit expression for prediction model, making it easier to interpret the relationships between input features and vegetation parameters.

10.3389/fpls.2025.1536177

TABLE 2 Texture features used in this study.

Texture feature abbreviation	Texture feature	Formula
MEA	Mean	$MEA = \sum_{i,j=1}^{G} ip(i,j)$
VAR	Variance	$VAR = \sum_{i=1}^{G}\sum_{j=1}^{G}(i-u)^2 p(i,j)$
HOM	Homogeneity	$HOM = \sum_{i=1}^{G}\sum_{j=1}^{G}\frac{p(i,j)}{1+(i-j)^2}$
CON	Contrast	$CON = \sum_{i=1}^{G}\sum_{j=1}^{G}(i-j)^2 p(i,j)$
DIS	Dissimilarity	$DIS = \sum_{i=1}^{G}\sum_{j=1}^{G}p(i,j)\lvert i-j\rvert$
ENT	Entropy	$ENT = -\sum_{i=1}^{G}\sum_{j=1}^{G}p(i,j)\log p(i,j)$
SEC	Second moment	$SEC = \sum_{i=1}^{G}\sum_{j=1}^{G}p(i,j)^2$
COR	Correlation	$COR = \sum_{i=1}^{G}\sum_{j=1}^{G}\frac{(i-j)(j-i)p(i,j)}{\sqrt{VAR_i \times VAR_j}}$

In the formulas, i and j represent the row number and column number of the image, respectively, and $p(i,j)$ represents the relative frequency of two neighboring pixels.

SVR was derived from the statistical learning theory proposed by Cortes and Vapnek (1995). It can effectively capture the complex nonlinear relationships between remote sensing data and vegetation parameters by employing kernel functions to map input variables into a high-dimensional feature space. Additionally, SVR relies primarily on support vectors for training, making it useful when the number of samples was limited in biochemical parameters estimation (Guo et al., 2022).

GPR is a probabilistic approximation to nonparametric kernel-based regression. It has been proven to have significant advantages in vegetation parameter retrieval due to its powerful nonlinear modeling capability, small sample adaptability, and ability to quantify prediction uncertainty (Campos-Taberner et al., 2016; Upreti et al., 2019). It offers an explicit form of the predictive model, which establishes a nonlinear relation between the input (e.g., VIs and TFs) and the output variable (i.e., LCC). Moreover, GPR is particularly suitable for scenarios with limited ground-measured data and supports the integration of multi-source and high-dimensional input features.

2.4.3 Model validation

The validity of LCC estimation models was assessed based on a k-fold (k = 10) cross-validation procedure, which splits the dataset into 10 equal-sized subsets. In each iteration, nine subsets were used as the training set, and the remaining one was used as the validation set to evaluate the models. The coefficient of determination (R^2) and the root mean square error (RMSE) of the measured and predicted LCC values were used to evaluate the prediction ability of the models based on two-pair image feature combination method and multivariable image feature combination using MLRAs.

3 Results

3.1 Correlation analysis between image feature and LCC

The correlations between LCC and all VIs in Table 1 and all TFs extracted from three PC images in Table 2 were calculated and analyzed. Figure 3 shows the $|r|$ and MIC values for different types of VIs and TFs. The values of $|r|$ or MIC larger than 0.8 were selected and presented in Table 3. From the correlations of different VIs with respect to LCC, as expected, a majority of VI_{re} were superior to the corresponding VI_{org} with similar forms. For instance, the GDVI showed weakness in correlating LCC with $|r|$ of 0.38 and MIC of 0.33, while the REDVI dramatically increased by 88% and 98% respectively, compared to the GDVI. The values of MIC of the $MDVI_{re}$ and $OSAVI_{re}$ were also improved greater than 14% in comparison of the MDVI and OSAVI. This result highlighted a strong potential for use in banana LCC estimation with red-edge spectral band. The best VI was MSR_{re}, which generated the correlation of 0.836 with LCC. For the TFs, the TFs-PC1 were generally correlated better with LCC than the TFs-PC2 and TFs-PC3, owing to the larger values of both $|r|$ and MIC. From Table 3, we found that all eight TFs obtained in PC1 image were selected using Pearson correlation, while none of the TF extracted in PC3 image reached the threshold of MIC. The MEA was selected not only in all PC images by Pearson correlation method but also in PC1 image by MIC.

3.2 Banana LCC estimation using two-pair feature combination of VI and TF

Figure 4 shows all coefficient of determination (R^2) values based on the linear regression analyses of LCC against all possible two-pair combinations of the VI and TF used in types of SR, NDVI, and DVI. The closer to yellow and the higher the size of the scatter, the larger R^2 value and better accuracy of the model derived from the image feature combination. The results indicated that for all the three types, image feature combinations calculated from the TFs-PC1 paired with VIs exhibited the strongest relationship with LCC (Figures 4A–C) and then those calculated from the TFs-PC2 (Figures 4D–F) followed by the TFs-PC3 (Figures 4G–I). This means that textural information on the PC1 image contributed more in LCC determination compared to that on the PC2 and PC3 images. Furthermore, it should be noteworthy that in comparison to other TFs, the MEA combined with almost all VIs preserved higher sensitivity to LCC variability, which was coincident with the results in Figure 3 where the MEA is showing better correlation and also being selected from the PC1 and PC2 as well as PC3 images. This phenomenon was more obvious when extracting the MEA from PC2 and PC3 images, with the size and color of scatters revealing relatively high R^2 values (Figures 4D–I).

From Figures 4A–C, almost all image feature combinations showed similar patterns among the SR, NDVI, and DVI types. A high degree of image feature combinations constructed by the TFs-PC1 and VIs behaved well against LCC. The MSR_{re} together with

10.3389/fpls.2025.1536177

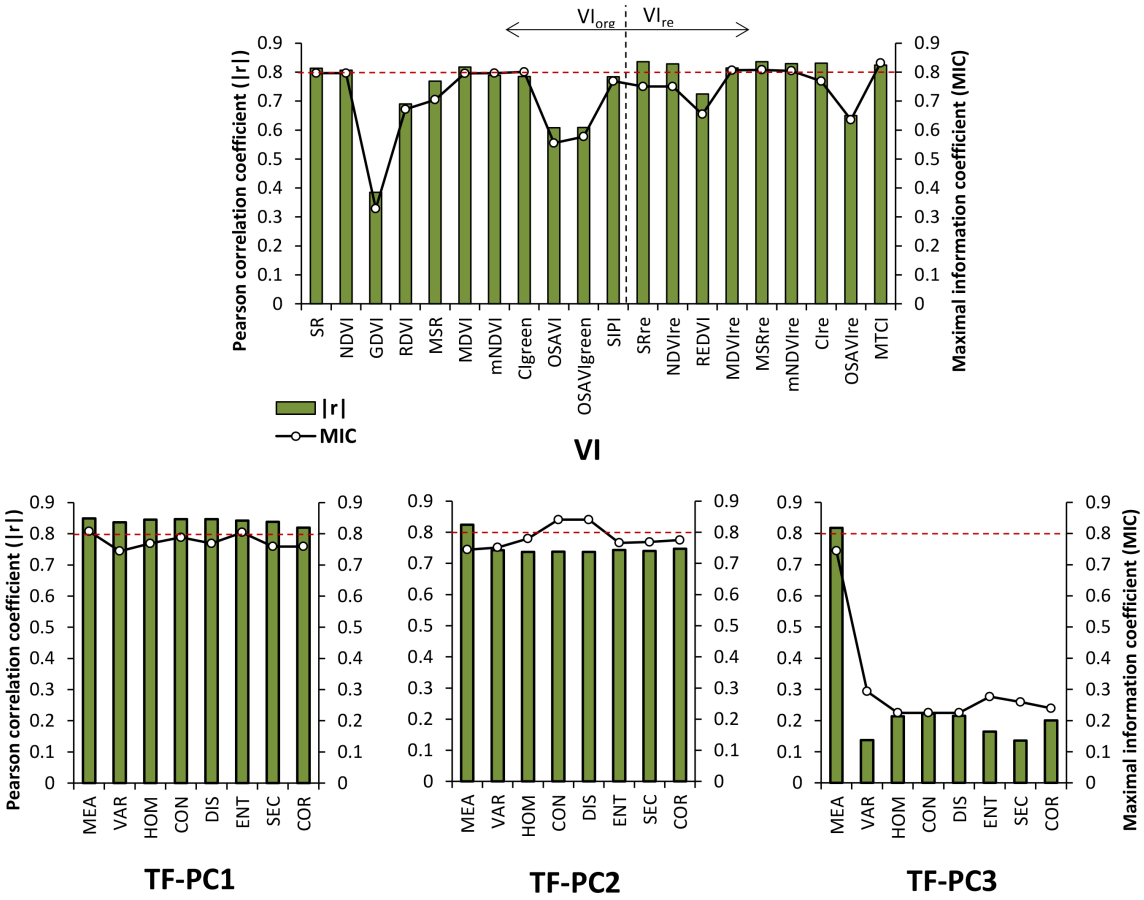

FIGURE 3
Pearson correlation coefficient (|*r*|) and maximal information coefficient (MIC) between different types of VIs and TFs vs. LCC. The green histogram indicates the value of |*r*|, the black broken line indicates the value of MIC, and the red dashed line indicates |*r*| = 0.8 or MIC = 0.8.

MEA were thereinto selected from every 160 feature combinations in each type due to their outstanding performances in capturing variations in CCC with higher R^2 than 0.75. The result is shown in Table 4. It can be seen that the most effective feature combination was provided by the ratio of MEA to MSR_{re} (referred to as MEA/MSR_{re}), which explained 78.9% of the variation in LCC, implying that the ratio clearly combines the abilities of the given VI and TF responding to LCC. Whereas feature combinations that showed weakness in characterizing LCC were different among the tree types,

TABLE 3 Selected VIs and TFs using Pearson correlation coefficient (|*r*|) and maximal information coefficient (MIC).

Image feature	Selected by |r| value	Selected by MIC value
VI	SR, NDVI, MSR, SR_{re}, $NDVI_{re}$, $MDVI_{re}$, MSR_{re}, $mNDVI_{re}$, CI_{re}, MTCI	SR, NDVI, MSR, mNDVI, CI_{green}, $MDVI_{re}$, MSR_{re}, $mNDVI_{re}$, MTCI
TF-PC1	MEA, VAR, HOM, CON, DIS, ENT, SEC, COR	MEA, ENT
TF-PC2	MEA	CON, DIS
TF-PC3	MEA	–

the R^2 values obtained using the HOM/GDVI, SEM/GDVI, MEA −SR_{re}, and CON−MSR_{re} were less than 0.1.

3.3 Banana LCC estimation using multivariable image feature combinations

PLSR, ARS, SVR, and GPR methods were employed to combine more than two image features for LCC estimation. Three variable groups were included, i.e., VIs, original Vis, and TFs combinations, and selected VIs and TFs combinations from Pearson correlation as well as from MIC as shown in Table 3. To assess the predictive capabilities of the models, R^2 and RMSE were calculated for all of the modeling results (Table 5). Overall, the models using all VIs showed a relatively moderate performance, with R^2 values around 0.615 to 0.63 and RMSE values around 2.65 to 2.75. In comparison with all VIs, the models based on VI_{re} provided a more accurate estimation in terms of R^2 and RMSE values when using the four MLRAs, with R^2 increased to a range of 0.63 to 0.67 and RMSE decreased to a range of 2.492 to 2.643. More importantly, the image feature combinations, which not only included spectral information but also image textures, dramatically improved the estimation results for LCC across the three input groups compared to using

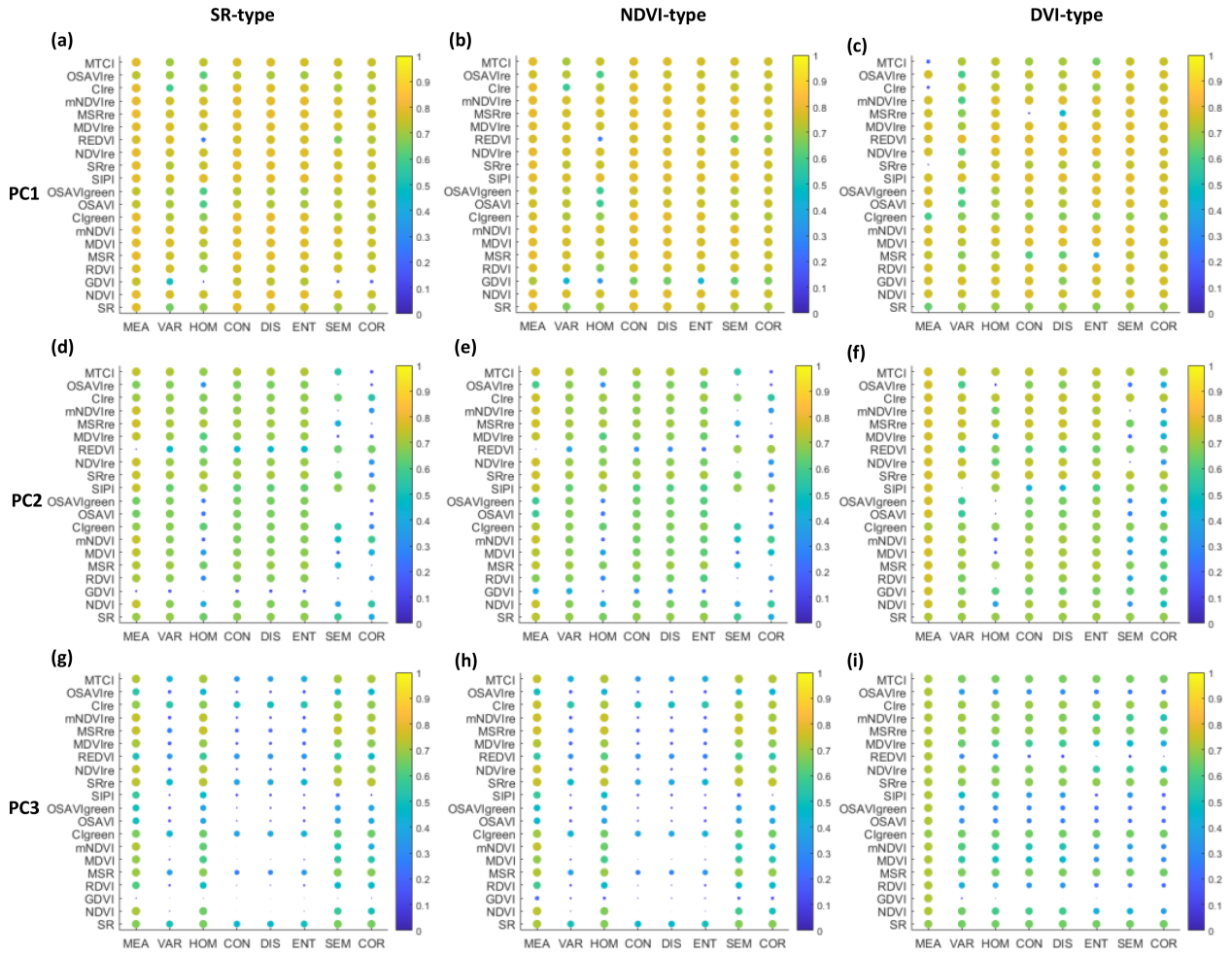

FIGURE 4
Coefficient of determination (R^2) based on the linear relationship between LCC and all possible two-pair feature combinations of VI and TF extracted from PC1 **(A–C)**, PC2 **(D–F)**, and PC3 **(G–I)** images in types of SR, NDVI, and DVI.

the VIs alone. However, MLRAs showed varying estimation performances for different feature combinations.

From the results of original feature combination and two selected feature combination groups, it could be observed that the examination of different feature combinations input showed that the combinations of TFs-PC1 and VIs resulted in better LCC estimates than the combinations of TFs-PC2 and VIs, with almost all R^2 values exceeding 0.75. Similar performances with models using TFs-PC2 can be found in the models using TFs-PC3. With respect to the MLRAs used, the GPR method acquired a slightly better accuracy when considering the VIs+TFs-PC1 as input variable in the three feature combination groups.

As expected, the VIs+TFs-PC1 combination selected using Pearson correlation method provided a robust improvement, especially for the ARS, SVR, and GPR models, with R^2 ranging from 0.765 to 0.768 and RMSEs close to 2.074. Meanwhile, the desirable result was also seen for models derived from the VIs+TFs-PC1 combination selected through MIC, especially the GPR model, which outperformed all other MLRAs, demonstrating that it was the best model for LCC estimation.

TABLE 4 Optimal two-pair feature combination selected in types of SR, NDVI, and DVI, linear relationship, and coefficient of determination (R^2) between optimal feature combination and LCC.

Type	PC image	Optimal two-pair feature combination	Model	R^2
SR-type	PC1	MEA/MSR_{re}	$y = 4.4405x + 52.45$	0.789
NDVI-type	PC1	$(MEA - MSR_{re})/(MEA + MSR_{re})$	$y = -1.7169x + 76.08$	0.77
DVI-type	PC1	$MEA - MSR_{re}$	$y = -197.89x + 243.61$	0.756

x and y in the "Model" column refer to the optimal two-pair feature combination and LCC, respectively.

TABLE 5 Predicted LCC results using PLSR, ARS, SVR, and GPR with different input variables.

Variable group	Input variable	Number of features	PLSR		ARS		SVR		GPR	
			R^2	RMSE	R^2	RMSE	R^2	RMSE	R^2	RMSE
Original features	All VIs	20	0.615	2.696	0.63	2.652	0.63	2.652	0.6	2.754
	All VI_{re}	9	0.63	2.643	0.67	2.492	0.65	2.542	0.66	2.538
	All VIs+TFs-PC1	28	**0.756**	2.082	**0.75**	2.064	**0.75**	2.169	**0.76**	2.09
	All VIs+TFs-PC2	28	0.725	2.262	0.735	2.326	0.698	2.369	0.71	2.307
	All VIs+TFs-PC3	28	0.726	2.261	0.71	2.34	0.71	2.248	0.669	2.499
Features selected by Pearson correlation ($\|r\| > 0.8$)	Selected VIs+TFs-PC1	18	**0.753**	2.041	**0.767**	2.078	**0.765**	2.09	**0.768**	2.074
	Selected VIs+TFs-PC2	11	0.718	2.176	0.704	2.345	0.737	2.209	0.735	2.218
	Selected VIs+TFs-PC3	11	0.735	2.22	0.736	2.214	0.732	2.231	0.725	2.258
Features selected by MIC (MIC > 0.8)	Selected VIs+TFs-PC1	11	0.749	2.162	0.748	2.168	**0.767**	2.124	**0.776**	2.04
	Selected VIs+TFs-PC2	11	0.711	2.318	0.699	2.368	0.729	2.245	0.672	2.467

R^2 values higher than 0.75 are in bold.
All VIs+TFs-PC1, image feature combination combined by all VIs and all TFs-PC1; Selected VIs+TFs-PC1, selected feature combination combined by selected VIs and selected TFs-PC1 from Pearson correlation coefficient ($|r| > 0.8$) or maximal information coefficient (MIC > 0.8); TFs-PC1, textural features extracted from the first principal component images; TFs-PC2, textural features extracted from the second principal component images; TFs-PC3, textural features extracted from the third principal component images.

3.4 Evaluation of LCC prediction using UAV hyperspectral images

We compared the performance of the best two-pair image feature combination and that obtained in a multivariable calibration based on GPR algorithm for LCC prediction, i.e., models derived from the MEA/MSR_{re} and the selected VIs+TFs-PC1 extracted through the MIC method. Figure 5 shows the scattering plot between LCC estimated from UAV hyperspectral reflectance data and LCC measured in the field campaign. We found that the predictive capability of the two models seems satisfactory, which had led to high coefficients of determination ($R^2 > 0.74$) and good RMSE values, and they all reached the 0.001 significance level. However, judging by the scattering point distribution, a slight dispersion of the MEA/MSR_{re} model occurred; prediction using the GPR model achieved the best result, with the highest R^2 of 0.776 and the lowest RMSE of 2.04.

Based on the results presented above, the GPR model was applied to UAV hyperspectral images to map chlorophyll status over the two large plots of banana, as shown in Figure 6. Because they corresponded to the LCC distribution at different growth stages of banana, various spatial variability in each plot was exhibited. A first observation across the different sites was that the banana LCC in plot 1 was overall homogeneous at the leaf development stage (Figure 6, left). Nevertheless, at the fruit development stage, a more obvious spatial heterogeneity of LCC appeared in plot 2 (Figure 6, right) due, in large part, to the different degrees of nutritional absorption and migration at the later stage of the banana. Moreover, the dynamic changes of LCC were revealed; they gradually increased as the progress of growth. The range of LCC at leaf development stage was concentrated from 54 to 60, while the LCC at fruit development stage dominated the range of 58 to 70.

4 Discussion

The assessment and monitoring of banana LCC status and spatial distribution are of importance for addressing crucial issues, such as growth monitoring, nutritional stress, and management practices. In this study, we estimated LCC by various feature combinations of spectral and textural information derived from UAV hyperspectral images for banana at different growth stages. The VI method is widely used in quantifying vegetation parameters. However, many literatures have indicated that soil background has a strong influence on canopy reflectance and the derived VIs relating to leaf parameters, especially at the early growth stages (Zha et al., 2020). A meaningful process we conducted to the original UAV hyperspectral images was to remove the soil background pixels by statistic threshold segment method. Then, a series of VIs and TFs were extracted based on pixels only containing vegetation, further ensuring the reliability of LCC estimation. However, relative experiments should be conducted to further verify the specific impact of soil background on banana LCC quantification in the future.

The red-edge spectral bands located between 700 and 740 nm with being not static but rather shifting during vegetation stress or in a good condition was proven to have the potential for improving LCC estimation for a variety of vegetation, such as maize, wheat, maple, sugar beet, etc (Gitelson et al., 2006; Wu et al., 2008; Jay et al., 2017; Kong et al., 2022), which inspired the inclusion of red-edge bands into not only airborne but also satellite sensors. The VI_{re} used in our study was likewise expected to perform better for banana. It is interesting to note that a desirable result was obtained when using UAV hyperspectral data. It is pronounced in banana LCC determination where the VI_{re} showed higher sensitivity as compared with the original VI with a similar form, which often

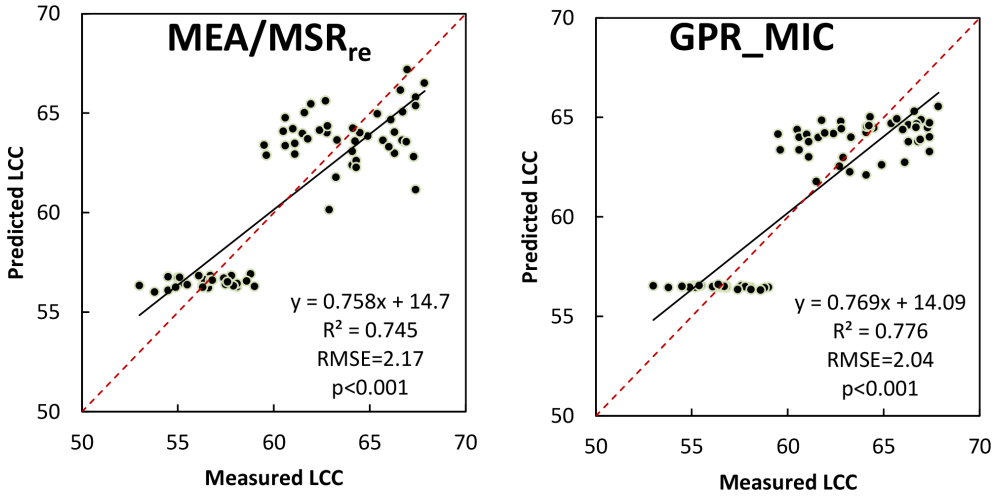

FIGURE 5
Comparison between predicted LCC from UAV hyperspectral reflectance data and ground-measured LCC using the best two-pair MEA/MSR_{re} combination (left) and GPR model derived from selected VIs+TFs-PC1 extracted through the MIC method (right).

suffers from saturation problems (Wu et al., 2008). To identify the specific band in the red-edge region from UAV hyperspectral image that can substantially make the VI_{re} achieve the best result for banana, we applied the spectral reflectance that ranged from 702 to 742 nm to replace the original red-edge band contained in the VI_{re} one by one and further compared their performances in LCC estimation. The R^2 values of linear relationships with LCC are presented in Figure 7. An important information revealed in the figure was that the trends of all VI_{re} curves, except for the REDVI and $OSAVI_{re}$, were generally similar, showing the best correlation with LCC when 730-nm red-edge band participated in the regression model. This implied that the red-edge band centered mostly at 730 nm could help in the design of an index or a sensor band that could better estimate the LCC for banana.

In addition to individual VI, the linear two-pair feature combination and nonlinear multivariable MLRAs were independently applied to combine the VI and TF features derived from hyperspectral images for LCC assessment. Based on Figure 4 and Table 5, the more accurate estimation results were generated when the TFs (especially the MEA) were involved in LCC models compared to models only using spectral information. Guo et al. (2022); Yue et al. (2019), and Reddersen et al. (2014) also reported that combing VIs and TFs can lead to better LCC and aboveground biomass estimates for crops and grassland. Our outcomes open the possibility to couple the potential of spectral and textural features for further improving the accuracy of LCC retrieval for tropical fruit tree (i.e., banana) at the field scale. In the present study, eight TFs were selected, and a total of 24 TFs were extracted from the first three images after principal component analysis. However, different performances of VI paired with TF extracted from different PC images were obtained; the combined uses of VI and TF-PC1 achieved better results than others combined by TF-PC2 and TF-PC3 whether in linear relationships or nonlinear MLRAs. One of the main reasons for such results is that the growing of banana

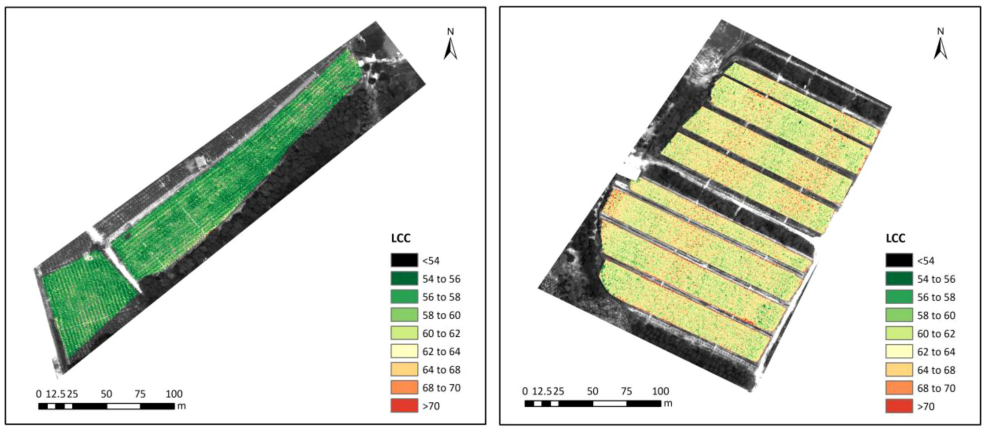

FIGURE 6
Spatial distributions of banana LCC in plot 1 (left) and plot 2 (right) mapped using the best GPR model.

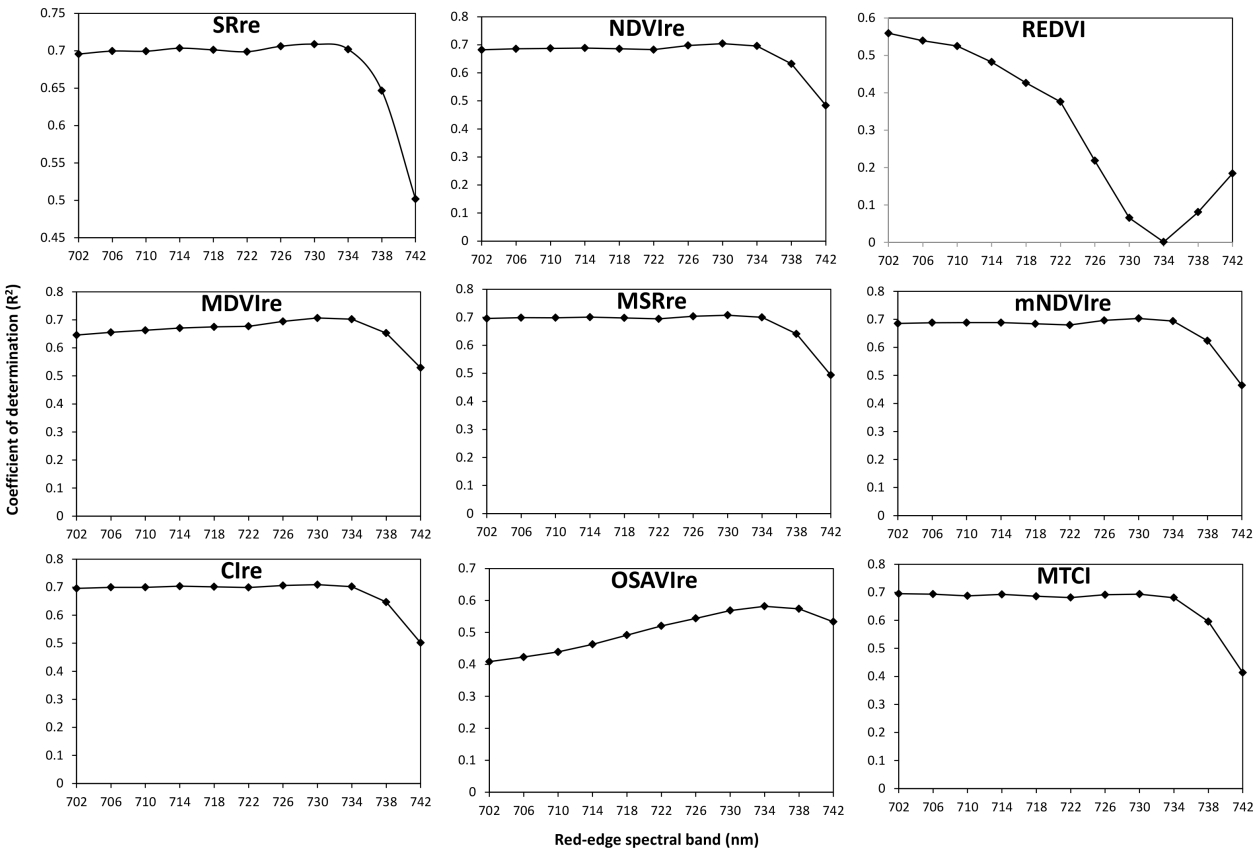

FIGURE 7
R^2 values of linear relationships between LCC and the VI_{re} derived from the red-edge spectral band from 702 to 742 nm.

plants could cause the changes in TFs of UAV image data. The TFs extracted from PC1 image captured more information related to the spatial resolution of the dark and bright areas of the image (Haralick et al., 1973), facilitating the accuracy of LCC prediction.

Compared to the two-pair image feature combination method, MLRAs using a combination of multiple VIs and TFs-PC1 as input had a slightly better ability for LCC prediction, especially the VIs +TFs-PC1 selected by Pearson correlation and MIC. This was expected since they utilized more features and nonlinear transforms. Among all MLRAs, the GPR model based on not only the original but also the selected feature combinations stood out as being the most accurate than the rest of the MLRAs (Table 5), suggesting that it is the optimum algorithm for banana LCC. This is in accordance with previous studies which reported that the GPR satisfied in varied leaf parameter retrieval using airborne or spaceborne satellite data (Verrelst et al., 2013a; Upreti et al., 2019; Zhou et al., 2020). The GPR with selected VIs+TFs-PC1 by MIC as input provided the best result in terms of both high accuracy and low error (Figure 5, right) for LCC ground validation test. In essence, GPR is based on non-parametric regression in a Bayesian framework. It builds models by taking fully into account the characteristics of the data itself, making it affordable to deal with complex, nonlinear, or irregular data (Campos-Taberner et al., 2016). Furthermore, the model was earlier evaluated as a potential predictor with a relatively small dataset (Verrelst et al., 2013a), which was another reason that ensuring it still had an outstanding performance when the number of banana ground-based samples was limited in our study. More importantly, along with pixelwise estimation maps for banana LCC at two growth stages, GPR can provide the accompanying confidence intervals, which was a significant advantage over other competitive MLRAs (e.g., PLSR, ASR, and SVR) because these confidences put forward some insight in the robustness and reliability of the LCC retrieval (Verrelst et al., 2013b). Furthermore, a total of 11 image features were screened by the MIC, including five original vegetation indices, four red-edge vegetation indices, and two texture features extracted from PC1 images. The selected VIs contained the narrow bands in red, red-edge, and near-infrared spectral regions which were proven to be sensitive and closely related to the LCC (Gitelson et al., 2006; Wu et al., 2008; Zhou et al., 2024). The introduced green band could suppress the saturation phenomenon of the relationship of absorptions *versus* LCC and is resistant to atmospheric effects (Gitelson et al., 1996, Gitelson et al., 2003). The selected two TFs, i.e., MEA and ENT, provided a more comprehensive analysis of texture features of UAV images, helping to understand the global brightness distribution and texture complexity (Haralick et al., 1973). This suggests that the inclusion of multiple effective image features in the regression model allowed for the incorporation of more valid spectral and textural information related to the LCC variable, resulting in improved estimation for banana. Even though

the GPR model based on VIs+TFs-PC1 selected using MIC achieved a relatively high accuracy with limited samples of LCC, it is still needed to collect more ground-measured samples throughout the whole growth periods of banana in future research.

5 Conclusion

The analyses of this study indicated the potential of UAV hyperspectral images in efficient LCC monitoring for tropical fruit trees, i.e. banana plants, across different growth stages. We first analyzed if using the red-edge bands in UAV hyperspectral data improved the estimation of banana LCC over conventionally used original red or green bands in VIs. The result demonstrated that the VI_{re} presented better correlation and achieved higher sensitivity in LCC estimation based on MLRAs compared to the VI_{org}, expanding the positive role of red-edge bands in assessing LCC for banana. In addition to VIs, several TFs, especially the MEA, also showed satisfactory correlations with LCC. To investigate the contribution of VIs integrated with TFs, on one hand, we proposed a comprehensive two-pair VI and TF combination method to explore the best two-pair feature combination for estimating LCC; on the other hand, MLRAs with multivariable groups containing VIs and TFs as input were also developed and applied. We found that the combination of VI and TF significantly improved the accuracy of LCC retrieval in comparison to using VI alone. The most robust two-pair feature combination was MEA/MSR{sb}{/sb}$_{re}$, and the GPR model using the selected VIs+TFs-PC1 extracted through MIC as input variable outperformed the other MLRAs (i.e., PLSR, ASR, and SVR). They improved the prediction accuracy with R^2 of 0.745 ($p < 0.001$) and 0.776 ($p < 0.001$), respectively, also implying that the latter model was the most suitable one for quantifying banana LCC. This study provides insights into the remote estimation of LCC for tropical fruit trees. Our proposed retrieval approaches by combing the spectral and image textural features could offer great possibilities for more accurate diagnosing of nutritional status and providing practical guidance for precision fertilization.

Data availability statement

The original contributions presented in the study are included in the article/supplementary material. Further inquiries can be directed to the corresponding authors.

Author contributions

WK: Data curation, Formal Analysis, Funding acquisition, Methodology, Writing – original draft, Writing – review & editing. LM: Data curation, Investigation, Methodology, Writing – review & editing. HY: Data curation, Investigation, Methodology, Writing – review & editing. JW: Data curation, Methodology, Resources, Writing – review & editing. CN: Data curation, Investigation, Validation, Writing – review & editing. BC: Methodology, Validation, Writing – review & editing. XZ: Data curation, Investigation, Methodology, Software, Writing – review & editing. WH: Conceptualization, Methodology, Supervision, Writing – review & editing. ZF: Data curation, Investigation, Methodology, Writing – review & editing.

Funding

The author(s) declare that financial support was received for the research, authorship, and/or publication of this article. This work was supported by the National Key Research and Development Program of China (Grant No. 2023YFB3905803, 2023YFB3905304), Hainan Provincial Natural Science Foundation of China (Grant No. 623QN325, 420QN293), the Hainan Province Science and Technology Special Fund (ZDYF2021GXJS038), and the National Natural Science Foundation of China (Grant No. 41871339, 41901369).

Acknowledgments

The authors are grateful to Dr. Donghua Wang and Mr. Yue Zhang for their assistance in data collection. The authors are grateful to the reviewers for their helpful comments. We also would like to acknowledge the contributions from the field campaign at the Banana Cultivation Research and Development Base, Hainan Province, China.

Conflict of interest

The authors declare that the research was conducted in the absence of any commercial or financial relationships that could be construed as a potential conflict of interest.

Generative AI statement

The author(s) declare that no Generative AI was used in the creation of this manuscript.

Publisher's note

All claims expressed in this article are solely those of the authors and do not necessarily represent those of their affiliated organizations, or those of the publisher, the editors and the reviewers. Any product that may be evaluated in this article, or claim that may be made by its manufacturer, is not guaranteed or endorsed by the publisher.

References

Azadnia, R., Rajabipour, A., Jamshidi, B., and Omid, M. (2023). New approach for rapid estimation of leaf nitrogen, phosphorus, and potassium contents in apple-trees using Vis/NIR spectroscopy based on wavelength selection coupled with machine learning. *Comput. And Electron. In Agric.* 207, 107746. doi: 10.1016/j.compag.2023.107746

Barata, R. A. P., Ferraz, G. A. E. S., Bento, N. L., Soares, D. V., Santana, L. S., Marin, D. B., et al. (2023). Evaluation of coffee plants transplanted to an area with surface and deep liming based on multispectral indices acquired using unmanned aerial vehicles. *Agronomy-Basel* 13, 2623. doi: 10.3390/agronomy13102623

Biswal, S., Pathak, N., Chatterjee, C., and Mailapalli, D. R. (2024). Estimation of aboveground biomass from spectral and textural characteristics of paddy crop using UAV-multispectral images and machine learning techniques. *Geocarto Int.* 39 (1), 2364725. doi: 10.1080/10106049.2024.2364725

Campos-Taberner, M., Garcia-Haro, F. J., Camps-Valls, G., Grau-Muedra, G., Nutini, F., Crema, A., et al. (2016). Multitemporal and multiresolution leaf area index retrieval for operational local rice crop monitoring. *Remote Sens. Of Environ.* 187, 102–118. doi: 10.1016/j.rse.2016.10.009

Caruso, G., Tozzini, L., Rallo, G., Primicerio, J., Moriondo, M., Palai, G., et al. (2017). Estimating biophysical and geometrical parameters of grapevine canopies ('Sangiovese') by an unmanned aerial vehicle (UAV) and VIS-NIR cameras. *Vitis* 56, 63–70. doi: 10.5073/vitis.2017.56.63-70

Chappelle, E. W., Kim, M. S., and McMurtrey, J. E. (1992). Ratio analysis of reflectance spectra (RARS) - an algorithm for the remote estimation of the concentrations of chlorophyll-a, chlorophyll-b, and carotenoids in soybean leaves. *Remote Sens. Of Environ.* 39, 239–247. doi: 10.1016/0034-4257(92)90089-3

Chen, J. M. (1996). Evaluation of vegetation indices and a modifiedsimple ratio for boreal applications. *Can. J. Remote Sens.* 22, 229–242.

Chen, P., Feng, H., Li, C., Yang, G., Yang, J., Yang, W., et al. (2019). Estimation of chlorophyll content in potato using fusion of texture and spectral features derived from UAV multispectral image. *Trans. Chin. Soc. Agric. Eng.* 35, 63–74.

Cortes, C., and Vapnek, V. (1995). Support vector networks. *Mach. Learn.* 20, 273–297. doi: 10.1007/BF00994018

Curran, P. J., Dungan, J. L., Macler, B. A., Plummer, S. E., and Peterson, D. L. (1992). Reflectance spectroscopy of fresh whole leaves for the estimation of chemical concentration. *Remote Sens. Of Environ.* 39, 153–166. doi: 10.1016/0034-4257(92)90133-5

Dash, J., and Curran, P. J. (2004). The MERIS terrestrial chlorophyll index. *Int. J. Of Remote Sens.* 25, 5403–5413. doi: 10.1080/0143116042000274015

Devadas, R., Lamb, D. W., Simpfendorfer, S., and Backhouse, D. (2009). Evaluating ten spectral vegetation indices for identifying rust infection in individual wheat leaves. *Precis. Agric.* 10, 459–470. doi: 10.1007/s11119-008-9100-2

Friedman, J. H., and Roosen, C. B. (1995). An introduction to multivariate adaptive regression splines. *Stat. Methods Med. Res.* 4, 197–217. doi: 10.1177/096228029500400303

Gitelson, A. A., Gritz, Y., and Merzlyak, M. N. (2003). Relationships between leaf chlorophyll content and spectral reflectance and algorithms for non-destructive chlorophyll assessment in higher plant leaves. *J. Of Plant Physiol.* 160, 271–282. doi: 10.1078/0176-1617-00887

Gitelson, A. A., Kaufman, Y. J., and Merzlyak, M. N. (1996). Use of a green channel in remote sensing of global vegetation from EOS-MODIS. *Remote Sens. Of Environ.* 58, 289–298. doi: 10.1016/S0034-4257(96)00072-7

Gitelson, A. A., Keydan, G. P., and Merzlyak, M. N. (2006). Three-band model for noninvasive estimation of chlorophyll, carotenoids, and anthocyanin contents in higher plant leaves. *Geophysical Res. Lett.* 33, L11402. doi: 10.1029/2006gl026457

Guo, Y., Chen, S., Li, X., Cunha, M., Jayavelu, S., Cammarano, D., et al. (2022). Machine learning-based approaches for predicting SPAD values of maize using multi-spectral images. *Remote Sens.* 14, 1337. doi: 10.3390/rs14061337

Guo, J. H., Liu, X. J., Zhang, Y., Shen, J. L., Han, W. X., Zhang, W. F., et al. (2010). Significant acidification in major chinese croplands. *Science* 327, 1008–1010. doi: 10.1126/science.1182570

Haboudane, D., Miller, J. R., Tremblay, N., Zarco-Tejada, P. J., and Dextraze, L. (2002). Integrated narrow-band vegetation indices for prediction of crop chlorophyll content for application to precision agriculture. *Remote Sens. Of Environ.* 81, 416–426. doi: 10.1016/s0034-4257(02)00018-4

Haboudane, D., Tremblay, N., Miller, J. R., and Vigneault, P. (2008). Remote estimation of crop chlorophyll content using spectral indices derived from hyperspectral data. *IEEE Trans. Geosci. And Remote Sens.* 46, 423–437. doi: 10.1109/tgrs.2007.904836

Hansen, P. M., and Schjoerring, J. K. (2003). Reflectance measurement of canopy biomass and nitrogen status in wheat crops using normalized difference vegetation indices and partial least squares regression. *Remote Sens. Environ.* 86, 542–553. doi: 10.1016/s0034-4257(03)00131-7

Haralick, R. M., Shanmugam, K., and Dinstein, I. (1973). Textural features for image classification. *IEEE Trans. systems man cybernetics* SMC-3, 187–191. doi: 10.1109/TSMC.1973.4309314

Huang, L., Cheng, S., Liu, H., Zhao, Z., Wei, S., and Sun, S. (2022). Effects of nitrogen reduction combined with organic fertilizer on growth and nitrogen fate in banana at seedling stage. *Environ. Res.* 214, 113826. doi: 10.1016/j.envres.2022.113826

Huang, Y., Li, D., Liu, X., and Ren, Z. (2024). Monitoring canopy SPAD based on UAV and multispectral imaging over fruit tree growth stages and species. *Front. In Plant Sci.* 15. doi: 10.3389/fpls.2024.1435613

Huete, A., Justice, C., and Liu, H. (1994). Development of vegetation and soil indices for MODIS-EOS. *Remote Sens. Environ.* 49, 224–234. doi: 10.1016/0034-4257(94)90018-3

Inoue, Y., Guerif, M., Baret, F., Skidmore, A., Gitelson, A., Schlerf, M., et al. (2016). Simple and robust methods for remote sensing of canopy chlorophyll content: a comparative analysis of hyperspectral data for different types of vegetation. *Plant Cell And Environ.* 39, 2609–2623. doi: 10.1111/pce.12815

Jay, S., Baret, F., Dutartre, D., Malatesta, G., Heno, S., Comar, A., et al. (2019). Exploiting the centimeter resolution of UAV multispectral imagery to improve remote-sensing estimates of canopy structure and biochemistry in sugar beet crops. *Remote Sens. Of Environ.* 231, 110898. doi: 10.1016/j.rse.2018.09.011

Jay, S., Maupas, F., Bendoula, R., and Gorretta, N. (2017). Retrieving LAI, chlorophyll and nitrogen contents in sugar beet crops from multi-angular optical remote sensing: Comparison of vegetation indices and PROSAIL inversion for field phenotyping. *Field Crops Res.* 210, 33–46. doi: 10.1016/j.fcr.2017.05.005

Jordan, C. F. (1969). Derivation of leaf-area index from quality of light on forest floor. *Ecology* 50, 663–666. doi: 10.2307/1936256

Khosravi, I., and Alavipanah, S. K. (2019). A random forest-based framework for crop mapping using temporal, spectral, textural and polarimetric observations. *Int. J. Of Remote Sens.* 40, 7221. doi: 10.1080/01431161.2019.1601285

Kira, O., Linker, R., and Gitelson, A. (2015). Non-destructive estimation of foliar chlorophyll and carotenoid contents: Focus on informative spectral bands. *Int. J. Of Appl. Earth Observation And Geoinformation* 38, 251–260. doi: 10.1016/j.jag.2015.01.003

Kong, W., Huang, W., Casa, R., Zhou, X., Ye, H., and Dong, Y. (2017a). Off-nadir hyperspectral sensing for estimation of vertical profile of leaf chlorophyll content within wheat canopies. *Sensors* 17, 2711. doi: 10.3390/s17122711

Kong, W. P., Huang, W. J., Liu, J. G., Chen, P. F., Qin, Q. M., Ye, H. C., et al. (2017b). Estimation of canopy carotenoid content of winter wheat using multi-angle hyperspectral data. *Adv. In Space Res.* 60, 1988–2000. doi: 10.1016/j.asr.2017.07.015

Kong, W. P., J., H. W., Ma, L. L., R., L. C., L., T. L., W., G. J., et al. (2022). Biangular-combined vegetation indices to improve the estimation of canopy chlorophyll content in wheat using multi-angle experimental and simulated spectral data. *Front. In Plant Sci.* 13. doi: 10.3389/fpls.2022.866301

Li, W., Wang, J., Zhang, Y., Yin, Q., Wang, W., Zhou, G., et al. (2023). Combining texture, color, and vegetation index from unmanned aerial vehicle multispectral images to estimate winter wheat leaf area index during the vegetative growth stage. *Remote Sens.* 15, 5715. doi: 10.3390/rs15245715

Lichtenthaler, H. K. (1987). Chlorophylls and carotenoids: Pigments of photosynthetic biomembranes. *Methods In Enzymology* 148, 350–382. doi: 10.1016/0076-6879(87)48036-1

Minolta (1989). "Chlorophyll meter SPAD-502," in *Instruction manual.* (Minolta Co., Ltd., Osaka, Japan).

Osco, L. P., Ramos, A. P. M., Pereira, D. R., Moriya, E. A. S., Imai, N. N., Matsubara, E. T., et al. (2019). Predicting canopy nitrogen content in citrus-trees using random forest algorithm associated to spectral vegetation indices from UAV-imagery. *Remote Sens.* 11, 2925. doi: 10.3390/rs11242925

Parry, C., Blonquist, J. M. Jr., and Bugbee, B. (2014). *In situ* measurement of leaf chlorophyll concentration: analysis of the optical/absolute relationship. *Plant Cell And Environ.* 37, 2508–2520. doi: 10.1111/pce.12324

Penuelas, J., Baret, F., and Filella, I. (1995). Semiempirical indices to assess carotenoids chlorophyll- a ratio from leaf spectral reflectance. *Photosynthetica* 31, 221–230.

Pimmasarn, S., Tripathi, N. K., Ninsawat, S., and Sasaki, N. (2020). Applying liDAR to quantify the plant area index along a successional gradient in a tropical forest of Thailand. *Forests* 11, 15. doi: 10.3390/f11050520

Qi, H. Z., Z., Zhang, L., Li, J., Zhou, J., Jun, Z., et al. (2021). Monitoring of peanut leaves chlorophyll content based on drone-based multispectral image feature extraction. *Comput. And Electron. In Agric.* 187, 106292. doi: 10.1016/j.compag.2021.106292

Qiao, L., Tang, W., Gao, D., Zhao, R., An, L., Li, M., et al. (2022). UAV-based chlorophyll content estimation by evaluating vegetation index responses under different crop coverages. *Comput. And Electron. In Agric.* 196, 106775. doi: 10.1016/j.compag.2022.106775

Reddersen, B., Fricke, T., and Wachendorf, M. (2014). A multi-sensor approach for predicting biomass of extensively managed grassland. *Comput. And Electron. In Agric.* 109, 247–260. doi: 10.1016/j.compag.2014.10.011

Rondeaux, G., Steven, M., and Baret, F. (1996). Optimization of soil-adjusted vegetation indices. *Remote Sens. Of Environ.* 55, 95–107. doi: 10.1016/0034-4257(95)00186-7

Roujean, J. L., and Breon, F. M. (1995). Estimating PAR absorbed by vegetation from bidirectional reflectance measurements. *Remote Sens. Environ.* 51, 375–384. doi: 10.1016/0034-4257(94)00114-3

Sims, D. A., and Gamon, J. A. (2002). Relationships between leaf pigment content and spectral reflectance across a wide range of species, leaf structures and developmental stages. *Remote Sens. Of Environ.* 81, 337–354. doi: 10.1016/s0034-4257(02)00010-x

Sripada, R. P. (2005). Determining in-season nitrogen requirements for corn using aerial color-infrared photography. (dissertation). North Carolina State University, North Carolina, United States.

Sun, H., Li, M., Zhang, Y., Zhao, Y., and Wang, H. (2010). Detection of corn chlorophyll content using canopy spectral reflectance. *Sensor Lett.* 8, 134–139. doi: 10.1166/sl.2010.1215

Tao, H. L., Feng, H. K., Xu, L. J., Miao, M. K., Long, H. L., Yue, J. B., et al. (2020). Estimation of crop growth parameters using UAV-based hyperspectral remote sensing data. *Sensors* 20, 1296. doi: 10.3390/s20051296

Uddling, J., Gelang-Alfredsson, J., Piikki, K., and Pleijel, H. (2007). Evaluating the relationship between leaf chlorophyll concentration and SPAD-502 chlorophyll meter readings. *Photosynthesis Res.* 91, 37–46. doi: 10.1007/s11120-006-9077-5

Upreti, D., Huang, W. J., Kong, W. P., Pascucci, S., Pignatti, S., Zhou, X. F., et al. (2019). A comparison of hybrid machine learning algorithms for the retrieval of wheat biophysical variables from sentinel-2. *Remote Sens.* 11, 481. doi: 10.3390/rs11050481

Verrelst, J., Alonso, L., Caicedo, J. P. R., Moreno, J., and Camps-Valls, G. (2013a). Gaussian process retrieval of chlorophyll content from imaging spectroscopy data. *IEEE J. Of Selected Topics In Appl. Earth Observations And Remote Sens.* 6, 867–874. doi: 10.1109/jstars.2012.2222356

Verrelst, J., Rivera, J. P., Moreno, J., and Camps-Valls, G. (2013b). Gaussian processes uncertainty estimates in experimental Sentinel-2 LAI and leaf chlorophyll content retrieval. *Isprs J. Of Photogrammetry And Remote Sens.* 86, 157–167. doi: 10.1016/j.isprsjprs.2013.09.012

Wu, C., Niu, Z., Tang, Q., and Huang, W. (2008). Estimating chlorophyll content from hyperspectral vegetation indices: Modeling and validation. *Agric. And For. Meteorology* 148, 1230–1241. doi: 10.1016/j.agrformet.2008.03.005

Xu, H., Wang, J., Qu, Y., Hu, L., Tang, Y., Zhou, Z., et al. (2022). Estimating leaf chlorophyll content of moso bamboo based on unmanned aerial vehicle visible images. *Remote Sens.* 14, 2864. doi: 10.3390/rs14122864

Yue, J., Yang, G., Tian, Q., Feng, H., Xu, K., and Zhou, C. (2019). Estimate of winter-wheat above-ground biomass based on UAV ultrahigh-ground-resolution image textures and vegetation indices. *Isprs J. Of Photogrammetry And Remote Sens.* 150, 226–244. doi: 10.1016/j.isprsjprs.2019.02.022

Zha, H., Miao, Y., Wang, T., Li, Y., Zhang, J., Sun, W., et al. (2020). Improving unmanned aerial vehicle remote sensing-based rice nitrogen nutrition index prediction with machine learning. *Remote Sens.* 12, 2864. doi: 10.3390/rs12020215

Zhang, X., Han, L., Dong, Y., Shi, Y., Huang, W., Han, L., et al. (2019). A deep learning-based approach for automated yellow rust disease detection from high-resolution hyperspectral UAV images. *Remote Sens.* 11. doi: 10.3390/rs11131554

Zhang, Y., Hui, J., Qin, Q., Sun, Y., Zhang, T., Sun, H., et al. (2021). Transfer-learning-based approach for leaf chlorophyll content estimation of winter wheat from hyperspectral data. *Remote Sens. Of Environ.* 267, 112724. doi: 10.1016/j.rse.2021.112724

Zhang, Y. Y., Li, X., Wang, M. Q., Xu, T., Huang, K., Sun, Y. H., et al. (2024). Early detection and lesion visualization of pear leaf anthracnose based on multi-source feature fusion of hyperspectral imaging. *Front. In Plant Sci.* 15, 1461855. doi: 10.3389/fpls.2024.1461855

Zhang, R., Yang, P., Liu, S., Wang, C., and Liu, J. (2022). Evaluation of the methods for estimating leaf chlorophyll content with SPAD chlorophyll meters. *Remote Sens.* 14, 5144. doi: 10.3390/rs14205144

Zheng, H., Ma, J., Zhou, M., Li, D., Yao, X., Cao, W., et al. (2020). Enhancing the Nitrogen Signals of Rice Canopies across Critical Growth Stages through the Integration of Textural and Spectral Information from Unmanned Aerial Vehicle (UAV) Multispectral Imagery. *Remote Sens.* 12, 957. doi: 10.3390/rs12060957

Zhou, X. F., Zhang, J. C., Chen, D. M., Huang, Y. B., Kong, W. P., Yuan, L., et al. (2020). Assessment of leaf chlorophyll content models for winter wheat using landsat-8 multispectral remote sensing data. *Remote Sens.* 12, 2574. doi: 10.3390/rs12162574

Zhou, X. F., Zhang, J. C., Wu, K. H., Chen, D. M., Ma, H. Q., Huang, W. J., et al. (2024). A digital sensor with non-imaging multi-spectral and image modules for continuous monitoring of plant growth conditions: Development and validation. *Comput. And Electron. In Agric.* 225, 109299. doi: 10.1016/j.compag.2024.109299

frontiers | Frontiers in Plant Science

TYPE Original Research
PUBLISHED 10 March 2025
DOI 10.3389/fpls.2025.1512598

Check for updates

OPEN ACCESS

EDITED BY
Amir Ali Khoddamzadeh,
Florida International University, United States

REVIEWED BY
El-Sayed Ewis Omran,
Suez Canal University, Egypt
Abu Selim,
International Centre for Integrated Mountain Development, Nepal

*CORRESPONDENCE
Elia Scudiero
elia.scudiero@ucr.edu
Michael P. Schmidt
Mike.Schmidt@usda.gov

RECEIVED 17 October 2024
ACCEPTED 19 February 2025
PUBLISHED 10 March 2025

CITATION
Scudiero E, Schmidt MP, Skaggs TH, Ferreira JFS, Zaccaria D, Pourreza A and Corwin DL (2025) Apparent soil electrical conductivity and gamma-ray spectrometry to map particle size fraction in micro-irrigated citrus orchards in California.
Front. Plant Sci. 16:1512598.
doi: 10.3389/fpls.2025.1512598

COPYRIGHT
© 2025 Scudiero, Schmidt, Skaggs, Ferreira, Zaccaria, Pourreza and Corwin. This is an open-access article distributed under the terms of the Creative Commons Attribution License (CC BY). The use, distribution or reproduction in other forums is permitted, provided the original author(s) and the copyright owner(s) are credited and that the original publication in this journal is cited, in accordance with accepted academic practice. No use, distribution or reproduction is permitted which does not comply with these terms.

Apparent soil electrical conductivity and gamma-ray spectrometry to map particle size fraction in micro-irrigated citrus orchards in California

Elia Scudiero[1,2*], Michael P. Schmidt[2*], Todd H. Skaggs[2], Jorge F. S. Ferreira[2], Daniele Zaccaria[3], Alireza Pourreza[4] and Dennis L. Corwin[2]

[1]Environmental Sciences Department, University of California, Riverside, Riverside, CA, United States, [2]U.S. Salinity Laboratory, United States Department of Agriculture (USDA) – Agriculture Research Service, Riverside, CA, United States, [3]Department of Land, Air and Water Resources, University of California, Davis, Davis, CA, United States, [4]Biological and Agricultural Engineering Department, University of California, Davis, Davis, CA, United States

In specialty crops, water and nutrient management may be optimized using accurate, high-resolution soil maps, especially in resource-constrained farmland, such as California. We evaluated the use of soil apparent electrical conductivity (EC_a) and gamma-ray spectrometry (GRS) to map particle size fraction across three micro-irrigated non-saline citrus orchards in California. Our research showed that EC_a was a reliable predictor of soil texture, particularly sand and silt contents, with Pearson correlation coefficients (r) as high as -0.92 and 0.94, respectively, at the field level. Locally-adjusted analysis of covariance (ANOCOVA) regressions using EC_a data returned accurate sand, silt, and clay content estimations with mean absolute errors (MAE) below 0.06, even when calibrated with a limited dataset (n=5 per field). On the other hand, we observed mixed results with GRS. We observed negative correlations between GRS total counts and sand content over the entire dataset (r = -0.55). However, one site (Strathmore) showed a field-scale positive correlation (r = 0.88). Clay content significantly correlated with gamma-ray total counts (TC) over the entire dataset (r = 0.37) but not at the field scale. Additional soil data analyses using GRS radionuclide ratios and soil laboratory analyses using diffuse reflectance infrared Fourier transform spectroscopy and acid ammonium oxalate extractable elements indicated unique geochemical and mineralogical characteristics in Strathmore, suggesting that factors such as soil mineralogy influenced the GRS measurements. This inconsistency prevented the development of a multi-field GRS-based soil texture ANOCOVA model. These findings confirm that EC_a is highly effective for soil texture mapping in non-saline soils using linear modeling, while GRS may require field-specific calibration due to variations in local mineralogy. Integrating multi-sensor data is a viable means for reducing ground-truthing requirements and related costs, and improving the quality and accuracy of soil maps in agriculture.

KEYWORDS

particle size fraction, precision agriculture, apparent electrical conductivity, gamma-ray spectrometry, near-ground sensing

1 Introduction

Accurate soil maps are critical for efficient and sustainable nitrogen and water management in specialty crops like citrus. Variations in soil properties, such as texture and moisture content, remarkably influence the availability and uptake of nutrients and water. Soil texture, determined by the proportion of sand, silt, and clay particles, affects key soil processes such as water retention, drainage, and nutrient-holding capacity. These processes, in turn, influence the movement and availability of water-soluble nitrogen and other macro and micro elements applied as fertilizers and diffused within the soil profile. Nitrogen-deficient citrus plants are stunted, whereas excessive nitrogen promotes vegetative growth and increases susceptibility to diseases that damage fruit, kill spurs, and may reduce yields in following years (Muhammad et al., 2018). Timing of nitrogen fertilization is crucial in citrus. Peak nitrogen uptake in citrus trees happens during blooming and early fruit growth (Muhammad et al., 2018). In areas with coarse-textured soils (e.g., sandy soils), the high permeability and low water-retention capacity may lead to nitrogen leaching, particularly in the form of nitrate (NO_3^-), beyond the root zone and into groundwater. Nutrient leaching reduces the fertilizer use efficiency by crops and increases the risk of groundwater contamination, contributing to issues such as eutrophication of water bodies and pollution of drinking water sources. Conversely, in fine-textured soils (e.g., clay-rich soils), higher water retention and slower drainage may lead to waterlogged conditions, especially in low-lying areas. Under such anaerobic conditions, denitrification processes may dominate, converting nitrate into gaseous forms of nitrogen such as nitrous oxide (N_2O), a potent greenhouse gas. Fields characterized by wide variability of soil texture and terrain attributes may have contrasting propensities for nitrogen loss through leaching or denitrification (Luo et al., 2023). Without accurate mapping and management of these variations, uniform application prescriptions of nitrogen and other nutrients can result in over-application in some areas and under-application in others. Over-application can intensify nitrogen losses and environmental impacts, especially in coarser soil (Syvertsen and Smith, 1996; Muhammad et al., 2018; Luo et al., 2023).

In the United States of America, soil survey maps developed by the government (e.g., USDA-NRCS soil survey maps) provide valuable broad-scale information on soil types and properties (Beaudette and O'geen, 2009; Chaney et al., 2016). Still, they are generally inadequate for guiding detailed field-scale water and nutrient management (Scudiero et al., 2024b). These maps, typically created at scales of 1:12,000 to 1:24,000, offer an overview of soil variability across landscapes but often fail to capture the fine-scale heterogeneity within individual fields, which is critical for precision agriculture (Reyes et al., 2018).

On-the-go soil sensing technologies provide an efficient means to generate high-resolution soil maps across agricultural fields. Among these technologies, apparent soil electrical conductivity (EC_a), gamma-ray spectrometry (GRS), and other on-the-go near-ground sensing technologies have been widely studied for their potential to map soil texture (Sudduth et al., 2005; Pätzold et al., 2020).

Apparent soil electrical conductivity (EC_a) is a measure of how easily electrical current passes through the soil, influenced by factors such as soil texture, moisture content, salinity, and temperature (Rhoades et al., 1976; Corwin and Lesch, 2003). EC_a is commonly used in precision agriculture to map soil variability, as it provides indirect information about soil properties that affect crop growth, such as clay content and water-holding capacity (Corwin and Lesch, 2003). This non-invasive, on-the-go sensing method is valuable for identifying zones within a field that require different management practices (Córdoba et al., 2016). Geospatial EC_a is arguably the most used sensor measurement for field-scale soil mapping by practitioners and scientists due to its relative ease of use, cost-effectiveness, and ability to capture spatial variability in soil properties influenced by factors such as moisture content, salinity, and clay content (Corwin and Lesch, 2003; Doolittle and Brevik, 2014). However, in environments where soil salinity is expected, such as in California and other mediterranean, arid, and semi-arid irrigated farmland worldwide, EC_a may not be the ideal tool for soil texture mapping because of salinity becoming a primary factor influencing the EC_a measurement (Corwin and Scudiero, 2016). Notably, EC_a measurements should be carried out over moist soils (i.e., around field capacity or slightly drier) to ensure reliable correlations with target soil properties (Corwin and Lesch, 2005b). To this regard, micro-irrigated orchards in water-scarce environments present unique challenges for EC_a sensing due to the very-short scale spatial heterogeneity of wetting soil conditions, which influences the sensor measurements. Soil moisture levels are generally ideal for reliable EC_a surveys in the hardly accessible areas under dense canopies, where micro irrigation is applied. Conversely, easily accessible alleyways have generally much drier soils (Pedrera-Parrilla et al., 2016; Corwin et al., 2022; Scudiero et al., 2024a). Soil compaction may also be remarkably different between below-canopy areas and the alleyways due to field equipment passages and other traffic. Even after precipitation events, EC_a surveys in the alleyways of micro-irrigated orchards may potentially lead to biased representation of field-scale soil spatial variability. Corwin and Lesch (2013) recommend surveying EC_a both in alleyways and along the tree lines distinctively in orchards and vineyards.

Gamma-ray spectrometry (GRS) measures, non-invasively, the natural gamma radiation emitted by isotopes of potassium (K), uranium (U), and thorium (Th) present in the soil. The entire energy spectrum of the gamma radiation, typically around the 0.1 to 3 MeV range, is also measured as Total Counts (TC) of gamma emission. Gamma-ray emitting nuclides are naturally present in soils and rocks. At the field scale, these gamma emissions correlate with specific soil properties, such as texture and mineral composition. Some factors influence gamma-ray emissions, e.g., increasing water content and bulk density decrease the measured gamma-ray volume (Grasty, 1979; Cook et al., 1996; Reinhardt and Herrmann, 2019). Mahmood et al. (2013) and Reinhardt and Herrmann (2019) provided detailed descriptions of GRS and its use for soil mapping and precision agriculture. Unlike EC_a, which primarily reflects soil moisture and salinity, GRS provides information on the mineralogical composition of the soil, offering

a different perspective on soil heterogeneity. Moreover, it is recommended that EC_a measurements are carried out in moist soils (Corwin and Lesch, 2005b), whereas GRS is attenuated by high soil moisture (Reinhardt and Herrmann, 2019). In water-scarce and dry micro-irrigated orchards, where spatial variability in soil moisture is extremely short-scaled due to localized irrigation application under the tree canopies, GRS can complement EC_a taken along the driplines by providing additional data on particle size distribution and mineral content with measurements done in the drier alleyways (Scudiero et al., 2024a). This dual-sensor approach, developed and described by Scudiero et al. (2024a), can enhance the accuracy of soil maps, enabling more precise water and nutrient management in these complex environments.

Developing field-scale models from sensor data typically requires extensive ground-truthing (Reyes et al., 2018), involving the collection of numerous soil samples to calibrate and validate the sensor measurements (Corwin and Lesch, 2005b), as otherwise sensor maps only serve as a qualitative indication of soil spatial variability (Corwin and Scudiero, 2016). For regional-scale models, two primary approaches can be utilized: universal models, which apply broadly across regions (Lobell et al., 2010; Pätzold et al., 2020), and locally adjusted models, such as analysis of covariance (ANOCOVA) regression models (Corwin and Lesch, 2014), which tailor the sensor data to specific local conditions. The choice between these approaches depends on the degree of variability within the region, the desired accuracy of the soil maps, and the available resources that can be used for the ground truthing campaign. The reliability of soil property models, whether universal or locally adjusted, is highly dependent on the rigor and consistency of sensor and soil data collection protocols (Corwin and Lesch, 2005b). Standardized calibration, maintenance, and handling of sensors are essential to ensure accurate and comparable measurements across different locations and times. Proper spatial sampling design and timing are critical to capturing the full range of soil variability (Lesch, 2005), while standardized soil sampling and laboratory procedures ensure the accuracy of ground-truthing data (Corwin and Yemoto, 2017). Consistent adherence to these protocols minimizes measurement-induced variability, leading to more reliable and generalizable soil property models (Corwin and Scudiero, 2016). Protocols for field to regional scale soil mapping with EC_a and for EC_a-directed soil sampling have been developed and updated by Dennis Corwin and colleagues at the USDA-ARS US Salinity Lab (Corwin and Lesch, 2005b; Corwin and Scudiero, 2016). However, no equivalent protocols or recommendations for GRS are available (Reinhardt and Herrmann, 2019).

Universal models, also referred as "site-independent models" (Pätzold et al., 2020) should predict soil properties at novel agricultural fields without the need for additional ground truthing. For these models to be reliable in predicting soil properties across a broad region, several conditions must be met. There should be a quantifiable mechanistic relationship between the sensor measurements and the target soil properties across the entire region. This requires that the physical processes being measured, such as electrical conductivity or gamma-ray emissions, correlate strongly and predictably with soil attributes like texture, moisture content, or mineral composition, regardless of local variations in soil type or environmental conditions. The data used to develop the model should be representative of the full range of conditions within the region, ensuring that the model is not biased toward specific soil types or microclimates. Modeling approaches like support vector machines were shown as good candidates for predicting soil properties from on-the-go sensor measurements over datasets with diverse pedogenesis (Heggemann et al., 2017). Additionally, the secondary factors influencing the sensor measurements, e.g., soil-forming processes, land use history, tillage, and other factors (Corwin and Lesch, 2005b; Reinhardt and Herrmann, 2019), are similar enough across the region that a single model can adequately describe the soil property-sensor relationships everywhere. Finally, to confirm its accuracy and generalizability, a universal model should be validated against independent data sets from different locations within the region (Ramcharan et al., 2018) and with robust cross-validation techniques (Roberts et al., 2017).

Locally adjusted models, such as the ANOCOVA method operate under the assumptions that sensors consistently measure physical processes related to the target soil property across a given geographical regions and that any secondary influencing factors can be accounted for by adding local ground-truth data any time a new site is surveyed. If this assumption holds true, in ANOCOVA models, a constant slope can be applied to the model, allowing for the estimation of a local random effect (i.e., a field-specific intercept coefficient) with limited soil sampling (Harvey and Morgan, 2009; Corwin and Lesch, 2014, 2017; Scudiero et al., 2017). This approach potentially reduces the need for extensive ground-truthing while still providing accurate soil property estimates at the regional scale (Scudiero et al., 2017). In the context of calibrating on-the-go sensor measurements to map soil texture, ANOCOVA regression relies on several assumptions to ensure accurate results. First, ANOCOVA assumes a linear relationship between the sensor measurements (covariate) and the soil texture properties (dependent variable) across the region of interest, with the slope of this relationship being consistent across different conditions. Any interaction between sensor data and geographical or management differences should not significantly alter the slope of the relationship for the ANOCOVA model to be reliable. Second, ANOCOVA assumes that the residuals, or errors, of the regression model are normally distributed and exhibit homoscedasticity, meaning that the variability of these errors is consistent across all levels of the covariate. Moreover, the model assumes that the covariate is measured without error, which is critical for the reliability of the calibration process. For this, it is recommended that the sensor data collection procedure is methodologically consistent across the entire dataset (Corwin and Lesch, 2014).

The objective of this study was to evaluate the use of GRS for mapping particle size fraction in micro-irrigated citrus orchards in California and to compare its performance to that of EC_a, which served as the benchmark. Additionally, the study aimed to test whether the ANOCOVA approach could be effectively applied to GRS data to develop accurate soil maps with reduced ground-truthing requirements.

2 Materials and methods

2.1 Research sites

Soils at three micro-irrigated citrus orchards in California, USA, were investigated in this research (Figure 1). The sites are named in this manuscript after their location. A 4.2-ha commercial 'Navel' orange (*Citrus sinensis* L.) orchard site was in Lemon Cove, Tulare County (Figure 1b). A 0.4-ha 'Navel' orange orchard was located at the University of California, Riverside Agricultural Experimental Station, Riverside, Riverside County (Figure 1c). A 3.7-ha commercial 'Page' mandarin (*Citrus reticulata* B.) orchard located in Strathmore, Tulare County (Figure 1d). Trees at the 'Navel' orange sites were planted on flat terrain, while trees at the 'Page' mandarin site were planted on 0.3-m raised berms made with local soils.

The primary soil types (USDA soil series) were retrieved from Soil-Web (Beaudette and O'geen, 2009): in Lemon Cove they were Havala loam and Yettem sandy loam; in Riverside they were Monserate sandy loam; and in Strathmore they were Porterville clay, San Joaquin loam, and a portion of the field was classified as "Riverwash".

2.2 Sensor-directed spatial sampling scheme delineation and soil sampling

At each site, sensor-directed spatial sampling selected 20 sampling locations using Response Surface Sampling Design (RSSD) with the ESAP software (Lesch et al., 2000). The RSSD was used with the assumption that geospatial sensors utilized to direct the sampling would correlate with target soil and plant properties of horticultural interest for on-farm experiments. The RSSD identifies a set of candidate principal component coordinates that are representative for the entire sensor survey (i.e., average and standard deviation of the sample equivalent to the one of the population), then selects samples proximal to these principal-component coordinates that are also geographically sparse (i.e., samples are as far as possible from each other, to reduce the risk

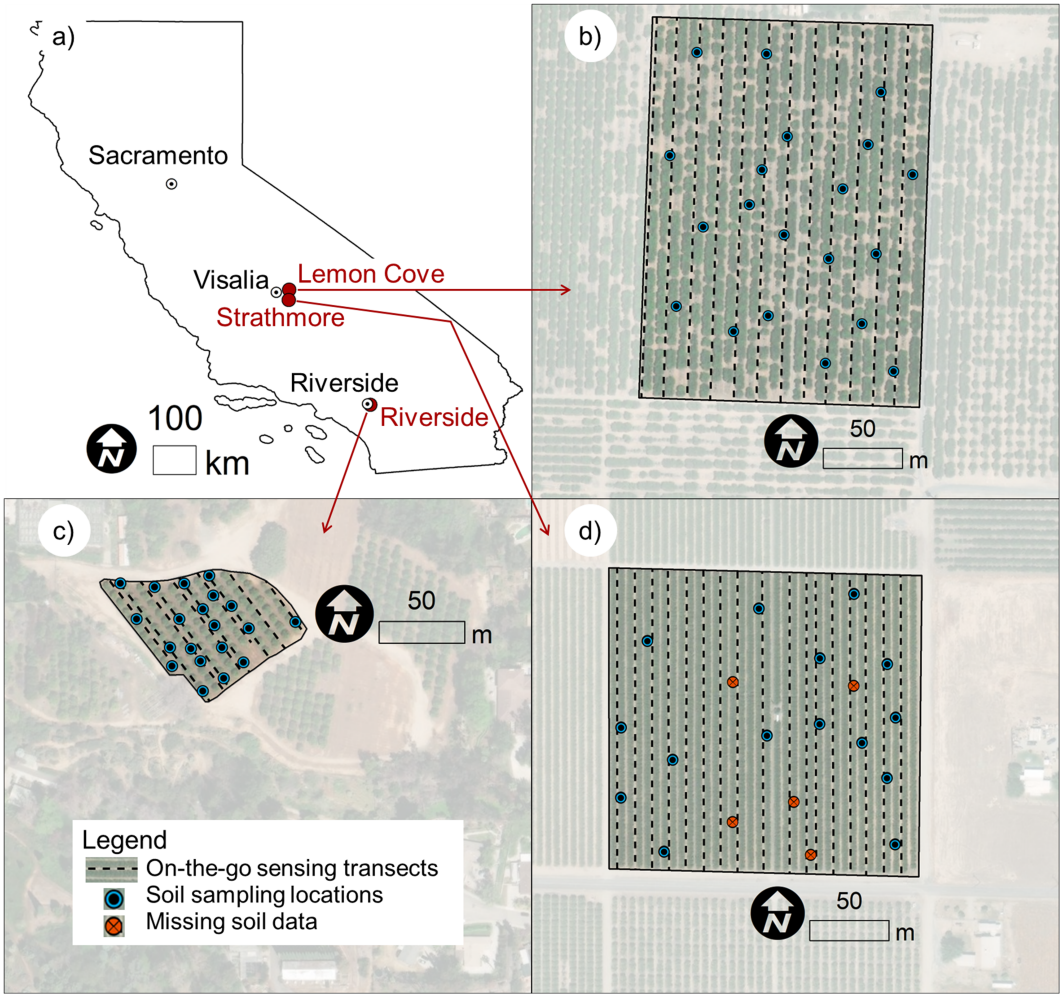

FIGURE 1
(a) the three research sites located in California, USA; **(b)** the 4.2-ha 'Navel' orange orchard located in Lemon Cove; **(c)** the 0.4-ha 'Navel' orange orchard located in Riverside; and **(d)** the 3.7-ha 'Page' mandarin. The location of the on-the-go soil sensing transects, the soil sampling locations, and the missing soil data locations (at the Strathmore site only) are depicted in the figure.

ofautocorrelated residuals when using ordinary least square linear modeling) (Lesch et al., 1995; Lesch, 2005; Fitzgerald et al., 2006). Figure 2 shows the candidate RSSD sites and selected sites for the three study orchards.

The data from the Lemon Cove and Strathmore orchards were collected as part of an on-farm experiments to map soil with GRS and EC_a and to deepen the understanding of soil physical and chemical properties with citrus leaf nutrient contents and fruit yield and quality. At these study sites, spatial sampling was directed using high-resolution multispectral imagery collected with an unmanned aerial vehicle (UAV). Scudiero et al. (2019) detailed the use of ESAP to direct spatial sampling at the Strathmore site. The same methodology was used in Lemon Cove and is briefly described below.

Data at the Riverside site was collected to evaluate on-the-go soil sensing when EC_a is measured under the canopy of the trees (i.e., closer to the micro irrigation emitters) with the apparatus discussed by Scudiero et al. (2024a). At this site, EC_a and GRS were used to direct the soil sampling scheme delineation as detailed by Scudiero et al. (2024a) and briefly described below.

2.2.1 Lemon cove

Five-band multispectral (Blue, Green, Red, NIR, and Red Edge) imagery was collected with RedEdge Multispectral Camera from MicaSense Inc. (Seattle, WA, USA) flown at an altitude of 100 m above ground level in February 2019. Based on the methodologies described by Zhang et al. (2021), a polygon system was created to uniquely identify each citrus tree in the orchard. The multispectral imagery underwent radiometric calibration, and the allocated area for each tree was segmented using the generated polygons. Subsequently, each tree was segmented from its background (soil) by applying empirical thresholds on the excess green index (EGI) and normalized difference vegetation index (NDVI), where a binary mask was created by multiplying the binary masks of EGI and NDVI, effectively isolating the canopy pixels from non-canopy areas (Moghimi et al., 2020). Average reflectance was calculated for each tree at each band separately and a feature vector consisting of sample trees (rows) and 5 spectral features (columns) was created. This dataset was transformed into two uncorrelated principal components (collectively representing 94.3% of the dataset variance) using STATISTICA (version 12, StatSoft Inc., Tulsa, OK, USA). The two principal components were used to direct the sampling scheme. The Kolmogorov-Smirnov Two-Sample Test was used to confirm that the multispectral reflectance values from the selected trees (i.e., the sample) were not significantly different from those of the entire orchard (i.e., the population). Additionally, the Average Nearest Neighbor tool in ArcMap (v.10.5.1, ESRI, Redlands, CA) was used to confirm that the selected sampling scheme was geographically sparse. Soil was sampled in December 2019, at 40 cm increments, down to 1.2 m. Only the data for the 0-40 cm soil profile will be discussed in this manuscript, as GRS is primarily sensing topsoil properties.

2.2.2 Riverside

In August 2019, GRS and EC_a were measured at the Riverside orchard. The EC_a (0-1.5m) survey was carried out using the EM38-DD (Geonics Ltd., Mississauga, Ontario, Canada) paired to a cm-scale Trimble R2 GNSS receiver (Trimble, Inc.; Sunnyvale, CA, USA) at 244 locations. GRS was carried out with an RSX-1 detector and the RS-701 gamma-ray spectrometer (Radiation Solutions Inc.; Mississauga, ON, Canada) using the sensor's internal GPS at 1563 locations. The GRS total counts (TC) data were interpolated using simple kriging with the Geostatistical Analyst toolbox in ArcMap. The kriging model's leave-one-out cross-validation had $R^2 = 0.75$. The kriged TC values at the EC_a locations were extracted. The EC_a and TC data were then used in ESAP to identify 20 sampling locations. The representativeness and geographic spread of the sampling scheme were tested analogously to the Lemon Cove site. Soil cores from 0-40 cm were collected in August 2019.

2.2.3 Strathmore

The Strathmore sampling scheme was determined using ESAP and multispectral UAV imagery collected in 2019 as described by Scudiero et al. (2019) and analogously to the procedure described in Section 2.2.1. At Strathmore, the two principal components collectively represented 96.5% of the multispectral reflectance dataset variance. Soil was sampled in December 2019, at 40 cm increments, down to 1.2 m. The data for the 0-40 cm soil profile will be discussed in this manuscript. Soil sampling was interrupted because of rainfall. The soil sampling crew could not return to the site to complete the soil sampling due to the COVID-19 pandemic that started in early 2020. Because of this, soil was collected only at 15 out of 20 locations (see Figure 1d).

2.3 On-the-go soil sensing

The on-the-go soil sensing surveys at the three sites were carried out using the same sensors and according to the field protocols described by Corwin and Lesch (2005b). The GRS sensor was mounted on an all-terrain utility vehicle and the EC_a sensor was on a non-metallic sled towed by the same vehicle. All surveys were carried out at speeds slower than 8 km per hour, typically around 6 km per hour.

The CMD Mini Explorer 6L or ME6L (GF Instruments, S.R.O.; Brno, Czech Republic) was used to measure EC_a at all sites. The sensor was placed on a sled and connected via cable to the GF Instruments data logging unit (CMD/C), which was in the drivers cabin during operation. The ME6L, in the Hi mode, measures EC_a at the nominal depth of 0.3, 0.5, 0.8, 1.1, 1.6, and 2.3 m. At the three sites the upper five EC_a measurements showed high positive correlations. The fourth layer, the EC_a for the 0-1.1 m soil profile, was used in this research. The Trimble R2 GNSS receiver was paired to the CMD/C. The EC_a was estimated at the soil sampling locations using simple kriging. Kriging interpolations were carried out on Normal-Score transformed data, with a first-order trend removal. Kriging details for each orchard are reported in Table 1.

The GRS was carried out with the RS-701 spectrometer, which detects total counts (TC) in the 0.4 to 2.81 MeV range, and emissions of potassium (K, %), uranium (U, ppm), and thorium (Th, ppm). On-the-go GRS measurements are usually characterized by a high signal-to-noise ratio (Minty, 1997; Viscarra-Rossel et al., 2007). Simple kriging in ArcMap was used to reduce the noise of the TC data, which showed autocorrelated spatial data at the three sites.

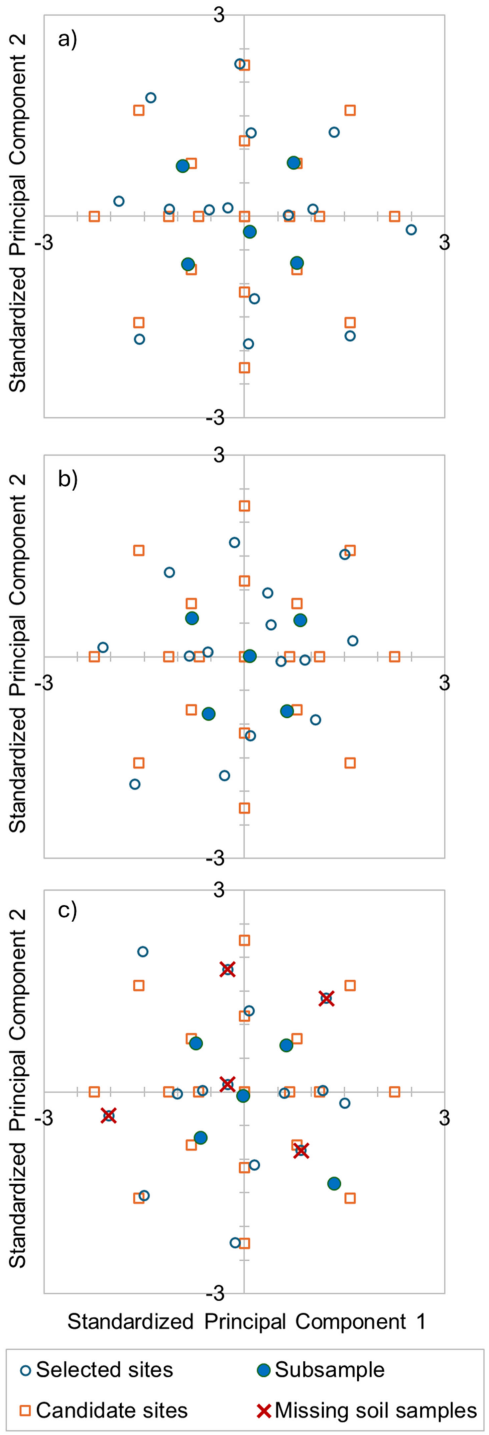

FIGURE 2
Plots of standardized principal component target response surface sampling design levels (empty squares) and the optimal sites having good spatial uniformity (i.e., selected sites, empty circles) at the three sites: **(a)** Lemon Cove, **(b)** Riverside, and **(c)** Strathmore. The selected subsamples for the Limited Data regression models and soil mineralogy lab analyses are depicted with full circles. At Strathmore, the missing soil samples are depicted with cross symbols.

Kriging interpolations were carried out on Normal Score transformed data, with a first-order trend removal. Kriging details for each orchard are reported in Table 2. The kriged TC values were then extracted at the soil sampling locations for further analyses. The K, U, and Th did not consistently show autocorrelated spatial structures and were not, therefore, interpolated with kriging.

2.4 Soil laboratory analyses

Gravimetric water content (GWC) at time of sampling was measured for all samples. Soil was dried and sieved discarding particles larger than 2 mm. The soil samples were analyzed in the laboratory to measure saturation percentage (SP) and the saturated paste electrical conductivity (EC_e) (Corwin and Yemoto, 2017). SP is used as a proxy of particle size fraction, with reported very strong positive correlations with clay content and very strong and negative correlations with sand content. The hydrometer method (Gee and Bauder, 1986) was used to determine particle size fraction.

For each field, five soil samples were selected for diffuse reflectance infrared Fourier-transform spectroscopy (DRIFTS) and acid ammonium oxalate extractable element analyses. These five samples were selected to be a balanced subsample of the RSSD design at each field: one sample was at the average point for the two principal components for the sensors that directed the soil samples, and the other four samples were at symmetrical target standard deviation coordinates; e.g., RSSD level coordinates for PC1 and PC2, respectively: (1) -0.79, -0.79; (2) -0.79, 0.79; (3) 0, 0; (4) 0.79, -0.79; and (5) 0.79, 0.79) (see Figure 2).

To analyze the mineralogy of soils across sites, DRIFTS and selective chemical extraction were used to probe aluminiosilicate and active, poorly crystalline mineral components, respectively. The DRIFTS spectra were collected from selected soils that were ball milled and diluted to 10% mass concentration with spectroscopic grade KBr prior to analysis. Spectra were collected on an Invenio -R spectrometer (Bruker Optics Inc., Billerica, MA) using an EasiDiff sampling accessory (Pike Technologies, Madison, WI). Spectra were collected from 4000-400 cm^{-1} with 4 cm^{-1} resolution and represented an average of 256 scans. All spectra were collected against a ground KBr background. After collection, spectra were post-processed by atmospheric compensation, smoothing (Savitzky-Golay, 17 points), baseline correction and min-max normalization. Selective extractions of Fe, Al, Mn, Si, U and Th associated with poorly-crystalline, active oxide components from soils was conducted by previously established methods (Mckeague and Day, 1966). Briefly, these components were selectively extracted through addition of 10 mL of 0.2 M acid ammonium oxalate solution to 0.25 g of ball milled soil in a 35 mL polypropylene centrifuge tube and shaken for 4 h in the dark. Extracts were subsequently purified through centrifugation at 10000 x g for 10 min and gravity filtered through Whatman 42 filter paper prior to inductively coupled plasma optical emission spectrophotometric (ICP-OES) quantification of elements (Optima 8000, Perkin Elmer).

2.5 Data analysis

The Pierson correlation coefficients (r) were calculated to investigate the relationships between soil properties and EC_a or TC for each orchard and for the entire dataset.

TABLE 1 Semivariogram and Kriging cross-validation specification for the soil apparent electrical conductivity at the three research sites.

Site	Date	Raw measurements	Semivariogram				Kriging Cross-Validation
		n	Model	Nugget (%)	Partial sill (%)	Range (m)	R^2
Lemon Cove	Dec-2019	481	Spherical	12.9	87.1	145.0	0.90
Riverside	Oct-2021	534	Stable	8.8	91.2	7.8	0.84
Strathmore	Dec-2019	633	Stable	5.9	94.1	96.1	0.90

The date of acquisition and the number (n) of sensor measurements are reported. The interpolation cross-validation coefficient of determination (R^2) is reported.

The use of analysis of covariance (ANOCOVA) regression (Corwin and Lesch, 2014) to build regional sensor to soil property calibrations was tested. ANOCOVA models feature a site-independent (regional) slope coefficient and orchard-specific intercept coefficients. Gamma-ray TC and EC_a were used as predictors to map SP and sand, silt, and clay contents. For these regression data a square root transformation was employed to ensure unbiased residuals. The models were evaluated using the coefficient of determination (R^2), the root mean square error (RMSE), and the mean absolute error (MAE). Models with MAE > 5% were considered not acceptable (Pätzold et al., 2020). The ANOCOVA models were calibrated on all available data (All Data model) and using five soil samples per field (Limited Data model), using the same subsample used for DRIFTS and acid oxalate extractable element analyses. The Limited Data models were evaluated at the left-out locations. Following the methodology of Corwin and Lesch (2014), the regression models were developed using STATISTICA (version 12, StatSoft Inc., Tulsa, OK, USA).

The raw GRS data was investigated to identify any differences in the ratios between TC, K, U, and Th. Differences in these ratios, such as in the Th/K ratio, are often interpreted as differences in parent material clay mineralogy and soil type (Herrmann et al., 2010; Wibowo et al., 2020; Al-Jafar and Al-Jaberi, 2022). At the orchard level, the slope and *r* of the TC linear relations with K, U, and Th, as well as these from K with U and Th, and of U with Th were compared.

Differences in soil concentrations of extractable Fe, Al, Mn, Si, U and Th across study sites were tested with a one-way analysis of variance and the Fisher's Least Significant Difference *post-hoc* test in STATISTICA. The Th data was left-censored, as three samples had concentrations below limits of detection (0.0004 mg g^{-1}). The missing values were estimated dividing the limit of detection by two (Hornung and Reed, 1990).

3 Results

3.1 Field specific and regional linear relationships between EC_a, TC, and soil properties

Table 3 shows the average, median, minimum, maximum, and standard deviation values for the measured soil properties, EC_a, and TC across the entire dataset, and within the three orchard sites. Lemon Cove was the site with the coarsest soil, 5 locations were classified as Sand, 5 were Loamy Sand, and 10 were Sandy Loam. Riverside had the most homogeneous soil texture, with 19 locations classified as Sandy Loam and 1 as Loam. Strathmore had the most heterogeneous texture: 4 locations were Sandy Loam, 6 were Sandy Clay Loam, 1 was Loam, and 4 were Silt Loam. Most of the soil locations had non-salt affected (EC_e < 2 dS/m) soils, 5 locations were slightly saline (2 < EC_e < 4 dS/m), of which 3 were in Lemon Cove and 2 were in Riverside.

Table 4 shows the Pearson *r* coefficients for EC_a and TC with the measured soil properties over the entire dataset and for each field. The correlation of EC_a with sand was negative and significant ($p < 0.05$) for all sites and within each orchard. The correlations of TC with sand were significantly negative for the whole dataset, but were non-significant at Lemon Cove, significant and negative at Riverside, and significant and positive at Strathmore. Correlations between silt and EC_a and TC were similar to those of sand but with the reverse sign. Clay correlations with EC_a were non-significant over the entire dataset and at the Riverside site, they were significant and positive at Lemon Cove and significant and negative at Strathmore. Clay content correlated positively over the entire dataset with TC, but no significant correlations emerged at the single sites. Notably, clay content showed a weak significant

TABLE 2 Semivariogram and Kriging cross-validation specification for the gamma-ray Total Counts at the three research sites.

Site	Date	Raw measurements	Semivariogram				Kriging Cross-Validation
		n	Model	Nugget (%)	Partial sill (%)	Range (m)	R^2
Lemon Cove	Dec-2019	4992	Exponential	37.6	62.4	34.1	0.84
Riverside	Aug-2019	1563	Exponential	36.0	64.0	39.2	0.75
Strathmore	Dec-2019	4483	Exponential	0.5	99.5	49.2	0.71

The date of acquisition and the number (n) of sensor measurements are reported. The interpolation cross-validation coefficient of determination (R^2) is reported.

10.3389/fpls.2025.1512598

TABLE 3 Basic statistics for sand, silt, and clay contents; saturated soil extract conductivity (EC_e); gravimetric water content (GWC) at the time of sampling; saturation percentage (SP), soil apparent electrical conductivity (EC_a) at the soil sampling locations; and gamma-ray spectrometry (GRS) total counts at the soil sampling locations for the entire dataset and for the three research sites.

	Mean	Median	Minimum	Maximum	Standard Deviation
All sites (n = 55)					
Sand	0.64	0.62	0.30	0.94	0.15
Silt	0.25	0.23	0.04	0.64	0.14
Clay	0.11	0.10	0.02	0.33	0.07
EC_e (dS m^{-1})	1.08	0.79	0.30	3.41	0.74
GWC	0.14	0.13	0.04	0.38	0.06
SP	0.32	0.33	0.19	0.52	0.08
EC_a (mS m^{-1})	26.97	23.12	14.46	56.66	10.56
GRS Total Counts (cps)	2653.31	2758.54	1584.51	3623.98	744.95
Lemon Cove (n = 20)					
Sand	0.79	0.77	0.64	0.94	0.09
Silt	0.15	0.16	0.04	0.23	0.06
Clay	0.07	0.07	0.02	0.13	0.04
EC_e (dS m^{-1})	1.11	0.78	0.39	3.41	0.87
GWC	0.14	0.14	0.11	0.17	0.02
SP	0.24	0.25	0.19	0.29	0.02
EC_a (mS m^{-1})	21.31	21.07	18.63	26.73	1.93
GRS Total Counts (cps)	1775.30	1761.19	1584.51	2054.51	117.57
Riverside (n = 20)					
Sand	0.58	0.59	0.45	0.71	0.06
Silt	0.30	0.31	0.20	0.37	0.04
Clay	0.12	0.12	0.07	0.18	0.03
EC_e (dS m^{-1})	1.39	1.36	0.58	2.85	0.69
GWC	0.09	0.09	0.04	0.15	0.03
SP	0.35	0.35	0.33	0.39	0.02
EC_a (mS m^{-1})	21.87	23.12	14.46	25.96	3.54
GRS Total Counts (cps)	3477.27	3488.88	3302.50	3623.98	93.49
Strathmore (n = 15)					
Sand	0.52	0.53	0.30	0.77	0.15
Silt	0.31	0.20	0.06	0.64	0.20
Clay	0.16	0.17	0.02	0.33	0.09
EC_e (dS m^{-1})	0.62	0.51	0.30	1.18	0.28
GWC	0.21	0.19	0.13	0.38	0.07
SP	0.39	0.33	0.27	0.52	0.09
EC_a (mS m^{-1})	41.31	35.10	30.47	56.66	10.26
GRS Total Counts (cps)	2725.37	2758.54	2471.73	2992.12	182.13

The number of soil sampling locations (n) is reported.

TABLE 4 Pearson correlation coefficients for soil apparent electrical conductivity and gamma-ray total counts with sand, silt, and clay contents; saturated soil extract conductivity (EC_e); gravimetric water content (GWC) at the time of sampling; and saturation percentage (SP).

	All sites	Lemon Cove	Riverside	Strathmore
Apparent Electrical Conductivity				
Sand	**-0.70**	**-0.73**	**-0.55**	**-0.92**
Silt	**0.65**	**0.67**	**0.59**	**0.94**
Clay	0.24	**0.72**	0.32	**-0.56**
EC_e	**-0.35**	0.22	-0.34	-0.12
GWC	**0.81**	0.10	0.41	**0.80**
SP	**0.72**	0.08	-0.03	**0.94**
Gamma-Ray Total Counts				
Sand	**-0.55**	0.11	**-0.58**	**0.88**
Silt	**0.43**	-0.13	**0.63**	**-0.83**
Clay	**0.37**	-0.05	0.32	0.40
EC_e	0.14	0.17	-0.27	0.02
GWC	**-0.32**	0.22	-0.07	**-0.68**
SP	**0.54**	**-0.47**	-0.23	**-0.91**

Bold and red coefficients were significant at the $p<0.05$ level.

correlation with sand content (r = -0.43) over the entire dataset, but no other significant correlation with other soil properties. The clay-sand correlations were strongly negative at Lemon Cove (r = -0.91) and Riverside (r = -0.80), but non-significant at Strathmore. The clay-silt correlations were positive at Lemon Cove (r = 0.77) and Riverside (r = 0.51), but negative at Strathmore (r = -0.72). Over the entire dataset, the relationships between SP and sand were strong and negative (r =-0.86), but non-significant with clay. Over the entire dataset, TC had a non-significant correlation with EC_a. The only significant relationship was observed between TC and EC_a at the Strathmore site with r = -0.89.

Table 5 reports the ANOCOVA regressions for sand, silt, and clay content, and SP with EC_a as the predictor. The ANOCOVA regression models were developed on square root transformed data. ANOCOVA regression assumptions were met. The goodness-of-fit metrics (R^2, RMSE, and MAE) were calculated for the back-transformed data. For all models, except the one predicting clay content, the ANOCOVA slopes in the All Data models and Limited Data models had slope values with overlapping standard errors. The calibration of the All Data and Limited Data models were significant at the $p<0.05$ level. The model calibration errors were low, all calibration MAEs were acceptably low (i.e., MAE < 0.05). The independent evaluations of the Limited Data models had MAE <0.06. The calibration RMSE values were under 0.06 in the All Data and Limited Data calibrations. The RMSE for the independent evaluations of the Limited Data models were 0.07 for sand, silt, and SP and 0.073 for clay content.

The ANOCOVA approach could not be employed to estimate any of the texture-related soil properties using TC. The relationships between the sensor and each soil property could not be represented with a single slope across the entire dataset.

3.2 Differences in soil characteristics across the three sites

Figure 3 reports the slope and the Pearson r for the linear relationships for all combinations between TC, K, U, and Th from the raw (i.e., non-kriged) sensor datasets. The sample sizes for the three datasets were large (see Table 1). The r values were all significant at the $p<0.05$ level. For all considered linear relationships, the r values were visibly higher at Strathmore than at the other two sites. Similarly, the slope coefficient values for all relationships were remarkably higher at Strathmore than at the other two sites. In Figure 3, the error bars represent the 5th to 95th confidence interval for the regression slopes. Notably, the slope intervals at Lemon Cove and Riverside overlapped (i.e., not significantly different) for the TC (dependent) and U (independent) relationship (Figure 3b), for the K (dependent) and U (independent) relationship (Figure 3d), and for the U (dependent) and Th (independent) relationship (Figure 3f).

Across all sites, DRIFTS spectra showed prominent aluminosilicate clay mineral vibrations which informed the nature of clay minerals present (Figure 4). This includes features generally related to structural -OH (≈3697 and 3623 cm^{-1}), Si-O (≈1100, 1035-1015, 790-430 cm^{-1}), octahedral Al-Al-OH (≈915 cm^{-1}), Al-O-Si (≈535 cm^{-1}) and clay-associated water (≈3400 and 1638 cm^{-1}) vibrations present across all sites (Madejová and Komadel, 2001; Madejová, 2003; Petit, 2006). The -OH stretching mode at 3697 cm^{-1} was indicative of kaolinite clay present in soils, while peaks around 3620 and 3400 cm^{-1} have been identified previously as being characteristic of montmorillonite, suggesting the presence of these two clay minerals across sites (Khang et al., 2016). There were subtle differences between sites that suggested some differences in mineralogy between sites. This was primarily observed for the Strathmore soils, which showed some vibrational features either distinct or more pronounced when compared to the Lemon Cove and Riverside soils. This includes a pronounced peak at 798 cm^{-1}, a more pronounced shoulder at 878 cm^{-1}, a reduction of the 750 cm^{-1} feature, and a primary Si-O peak at 1035 cm^{-1} in Strathmore compared with 1019 cm^{-1} in Lemon Cove and Riverside soils. These differences could have potentially resulted from changes in clay octahedral sheet substitution for a given clay mineral type, which could have enhanced absorbance near 878 cm^{-1} as well as impacted the position of the primary Si-O stretching peak near ≈1030-1015 cm^{-1} (Madejová and Komadel, 2001; Madejová, 2003). Differences in mineral composition between Strathmore and the Lemon Cove and Riverside sites, including aluminosilicate and oxide species, could also have resulted in different absorbances across sites as several different minerals have DRIFTS features in this range (e.g., goethite, silicon oxide minerals) (Madejová, 2003; Parikh et al., 2014). All of these potential influences indicated a Strathmore soil mineralogy distinct from Lemon Cove and Riverside.

Poorly crystalline forms of Fe, Al, Mn and Si (i.e., organically bound and amorphous mineral species) varied between sites (Table 6). Lemon Cove soils had the highest average concentration of acid ammonium oxalate extractable Fe and was significantly higher than Strathmore, with Riverside being statistically similar to both. Strathmore soils had significantly

TABLE 5 The analysis of covariance regression statistics for soil apparent electrical conductivity (independent variable) and sand, silt, and clay content, and saturation percentage (SP) (dependent variables).

Dependent variable	Slope (standard error)*		R^2			RMSE			MAE		
	A.D.	L.D.	A.D.	L.D.	Ind. Eval.	A.D.	L.D.	Ind. Eval.	A.D.	L.D.	Ind. Eval.
Sand	-0.112(0.011)	-0.12(0.014)	0.84	0.94	0.80	0.060	0.040	0.066	0.049	0.030	0.055
Silt	0.183(0.019)	0.21(0.022)	0.81	0.97	0.73	0.059	0.030	0.069	0.048	0.024	0.055
Clay	-0.05(0.023)	-0.13(0.031)	0.38	0.65	0.10	0.052	0.037	0.073	0.039	0.027	0.054
SP	0.061(0.008)	0.067(0.01)	0.84	0.93	0.81	0.031	0.020	0.035	0.025	0.016	0.028

*Regression slopes and standard errors are for the square-root-transformed data.
The regression slope (standard error in parenthesis) for the All Data (A.D.) and Limited Data (L.D.) models are reported. The goodness of fit for the A.D. and L.D. models and the independent evaluation of the L.D. models are reported: the coefficient of determination (R^2), the root mean square error (RMSE), and the mean absolute error (MAE).

higher average extractable concentrations of Al and Mn than Lemon Cove, with Riverside comparable to both sites. Extractable Si was highest for Riverside, with Lemon Cove significantly lower. U associated with these forms was highest in Lemon Cove, followed by Riverside and then Strathmore, with Strathmore being significantly lower than Lemon Cove. Th was significantly higher in Lemon Cove compared to Strathmore, which had detectable Th in only 2 of the 5 soils analyzed, with Riverside not significantly different from either. Across all sites, U and Th associated with extractable elements showed a positive correlation with extractable Fe phases, while extractable Al, Mn and Si had a negative relationship with associated U and Th (Table 7).

4 Discussion

Arguably, on-the-go soil sensors should reliably correlate with the target soil properties that they developed to justify their broad and consistent use in high-resolution soil mapping. On-the-go sensors measuring EC_a capture a complex process which is influenced by many soil properties such as water content, salinity, and soil texture. These complex interactions contributing to EC_a have been studied in agricultural soils for many decades (Rhoades et al., 1976, 1989; Corwin and Lesch, 2003; 2005a), and are fairly well understood: e.g., higher clay content, water content, and salinity contribute to higher EC_a. Moreover, it is often the case that the spatial patterns of the soil properties influencing EC_a are locally correlated at the field scale, e.g., the soil physical properties and terrain drive the spatial variability of soil moisture and salinity, making statistical EC_a-to-soil-property calibrations at the field-scale fairly straightforward (Corwin and Scudiero, 2016). Because of the complex interactions between soil properties influencing EC_a, unexpected soil relationships are sometimes reported. For example, Scudiero et al. (2016) reported a negative relationship between EC_a and clay content from fields in shallow soils on hilly landscape in Colorado, USA. The GRS as reviewed by Mahmood et al. (2013) measures a more straightforward process: the emissions of gamma radiation from radionucleotides naturally occurring in soils and rocks (mainly from ^{40}K, ^{238}U, and ^{232}Th) and from anthropogenic ^{137}Cs. The overall TC are expected to be lower in sandy soils than in finer soils (Mahmood et al., 2013; Reinhardt and Herrmann, 2019); and others, and as supported by the global Pearson correlation coefficients observed in this study (Table 4). Unfortunately, at the field-scale, TC relationships with soil texture can be erratic as shown by Pätzold et al. (2020) in Germany, by Maxton and Lund (2020) in the US Midwest, and as observed in this California citrus study (Table 4).

Despite the potential of observing unexpected correlations between EC_a and GRS with texture-related field properties, we observed significant relationships between most target soil properties and sites using either of the sensors (Table 4). Moreover, as discussed by Scudiero et al. (2024a), data fusion (e.g., principal component analysis, multiple regression) between the two sensors can be a means to obtain very accurate soil texture maps. Unfortunately, even when leveraging the spatial information from on-the-go sensing in spatial models (Reyes et al., 2018) and/or directing the soil sampling to calibrate ordinary least square models (Lesch, 2005), the amount of ground-truth data needed to develop accurate field-scale maps is too high (e.g., dozens of soil samples per field). The burden and the cost associated with the collection of ground-truth data from numerous locations within each field is a major bottleneck for the widespread application of on-the-go sensing for quantitative and accurate soil texture mapping.

Beyond the field-scale, the potential for developing regional site-independent models that would allow predicting soil properties at new sites without the need for collecting local ground-truth data has been investigated by many scientist in the past decades. Sudduth et al. (2005) investigated the use of EC_a from different sensors to map texture and cation exchange capacity across six US Midwest states. Their study sites from six states included soils of differing parent material, weathering, levels of organic matter content, and agricultural management. They observed R^2 values ≥ 0.55 for the two soil properties across their entire dataset. Although encouraging, their models were not sufficiently accurate to predict field-scale texture for precision agriculture. For GRS, Heggemann et al. (2017) developed a site-independent model to predict soil texture using data collected from ten agricultural fields in Germany across sites with diverse mineralogy and parent material. They developed site-independent support vector machines models that yielded R^2 of 0.96 (sand), 0.93 (silt), and 0.78 (clay), and with MAE values < 0.04. However, Pätzold et al. (2020) evaluated the model by Heggemann et al. (2017) at independent fields in Germany. They observed that the "model was not generally capable of predicting soil

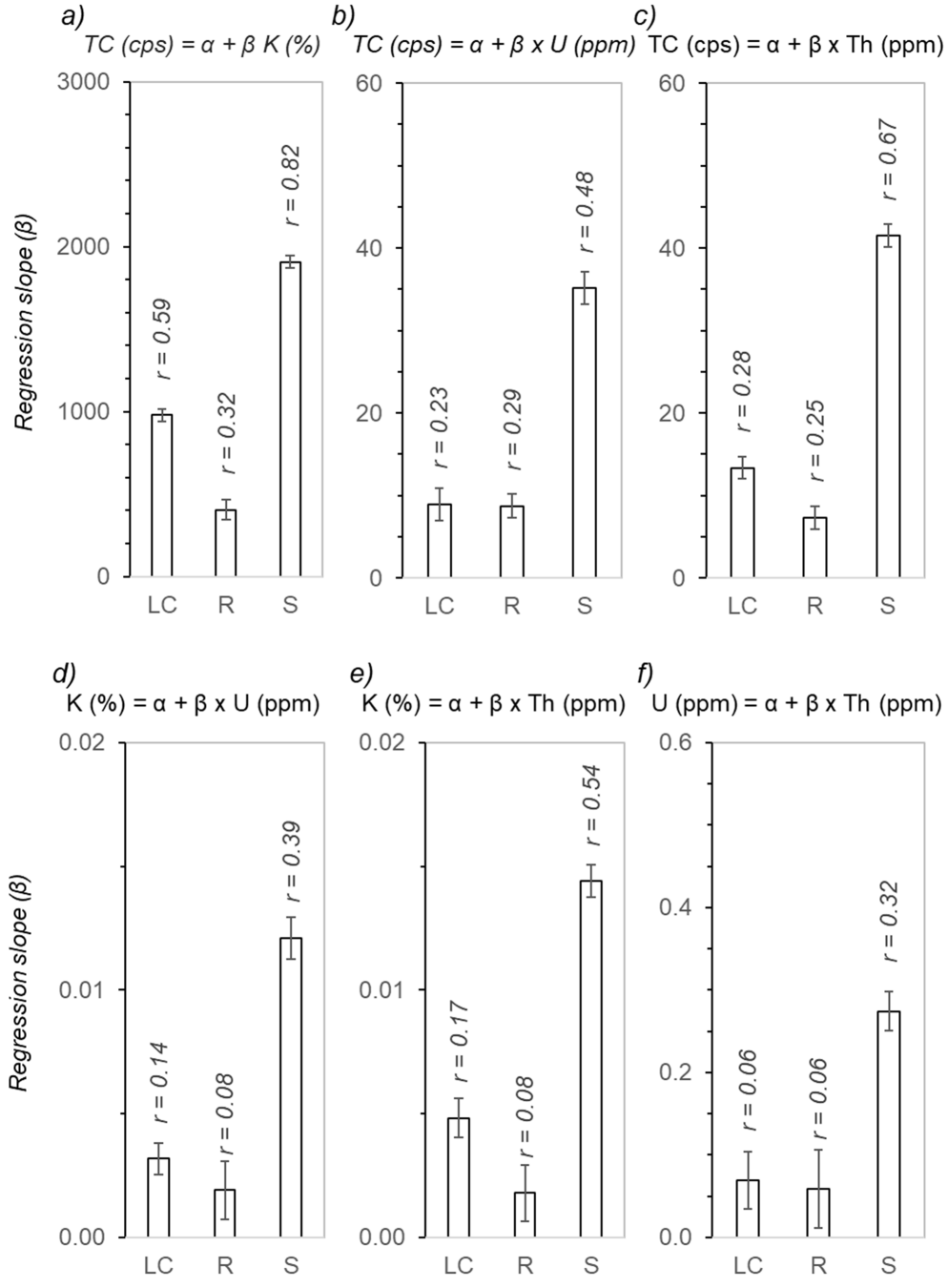

FIGURE 3
Regression slope coefficients (bars are the 5_{th} to 95_{th} confidence interval for the coefficients) and Pearson correlation coefficients (*r*) for relationships between gamma-ray spectrometry total counts (TC), potassium (K), uranium (U), and thorium (Th). Each quadrant compares regression slopes at the three research sites, Lemon Cove (LC), Riverside (R), and Strathmore (S), for the simple linear regression model (α is the regression intercept) specified at the top of each quadrant: TC as a function of **(a)** K, **(b)** U, and **(c)** Th; K as a function of **(d)** U, and **(e)** Th; and **(f)** U as a function of Th.

texture at sites that were not adequately represented in the calibration set".

ANOCOVA regression as an alternative approach to universal models has been widely discussed for EC_a-to-salinity calibrations (Corwin and Lesch, 2014, 2017; Scudiero et al., 2017). Harvey and Morgan (2009) discussed the potential of ANOCOVA for texture mapping on three fields in Texas, USA, and observed prediction errors below 4% for clay. In this study, we report calibration MAE values < 0.05 for ANOCOVA EC_a-texture predictions (Table 5). Previous research concluded that ANOCOVA may be a means to reducing field-scale soil samples (Corwin and Lesch, 2014; Scudiero et al., 2017). In particular, the regression slope common for all fields is calibrated over the entire available dataset, whereas only three or more samples per field may be needed to estimate the field-specific intercept. For the first time, this research shows that minimal data (n=5 per field) can be used to calibrate accurate ANOCOVA EC_a-texture regression with

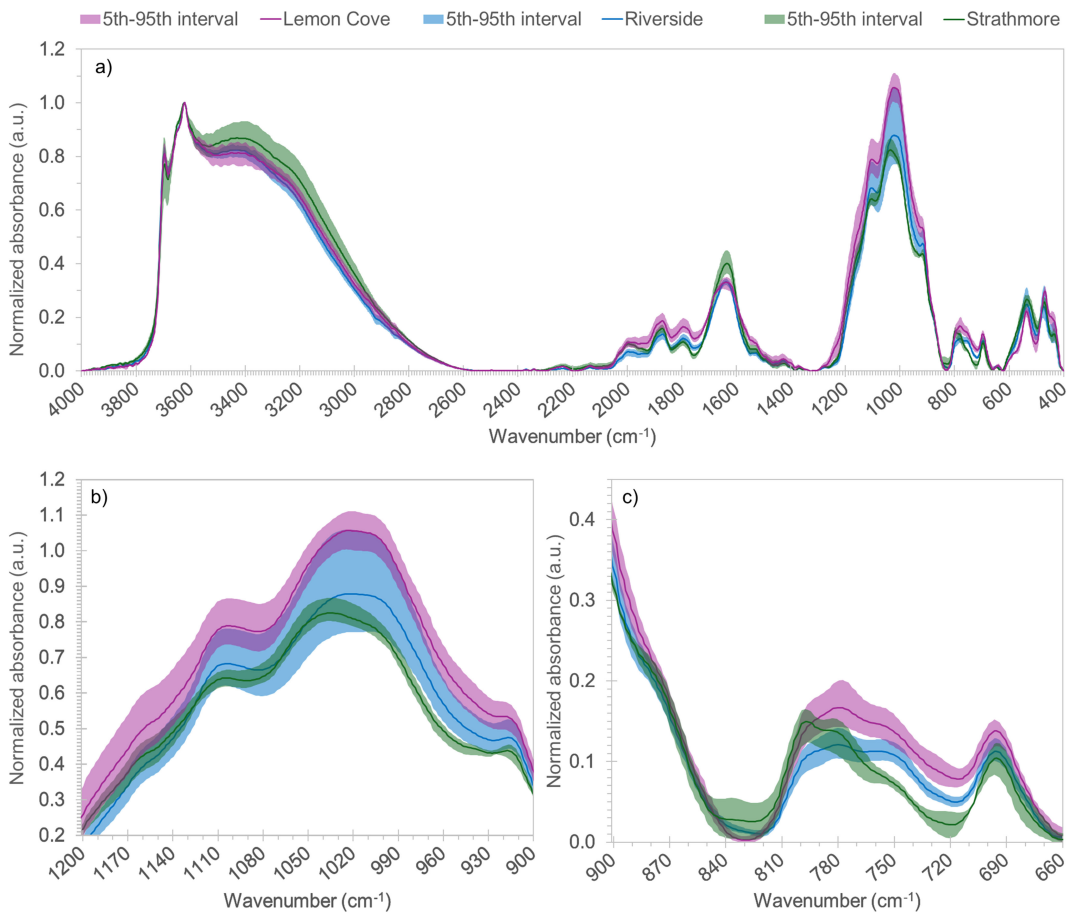

FIGURE 4
Diffuse reflectance infrared Fourier transform spectra for soil samples from the three sites. The average spectral signature for each site (solid lines) and the 5th to 95th interval (shaded areas) are depicted. The 4000-400 cm-1 spectra are shown in quadrant **(a)**. Quadrant **(b)** shows the specra between 1200 and 900 cm-1. Quadrant **(c)** shows the specra between 900 and 660 cm-1.

very low calibration and independent evaluation errors (Table 5). Generating high-resolution, accurate soil maps using as few as five ground-truth sites per agricultural field may benefit practitioners seeking to decrease the costs related to soil sampling and laboratory analyses.

ANOCOVA regression was shown in this research to be a very powerful tool to map texture with limited data, but it relies on postulating the slope between the sensor and the target soil property to be stable over multiple fields. This was not the case for GRS-TC making ANOCOVA regression modeling not feasible. Over the three fields, the TC showed expected (e.g., positive *r* with clay) and unexpected (e.g., negative *r* with clay) with the target soil texture properties. These inconsistencies make GRS unsuitable for texture mapping in California citrus orchards using ANOCOVA. Field-specific modeling may be needed instead. Mahmood et al. (2013) and Pätzold et al. (2020) indicated that differences in parent material and clay mineralogy may be responsible for contrasting GRS and texture relationships over multiple fields. If fields with unexpected GRS-texture relationships could be identified from raw GRS data or using available landscape-scale soil maps, then soil scientists may decide whether to include such fields in ANOCOVA models or to calibrate field-specific models (which require larger ground-truthing). Moreover, reliable classification of the expected nature of the GRS-texture relationship may enable the calibration of

TABLE 6 Fe, Mn, Al and Si in acid oxalate extractable solid phases along with Th and U associated with these phases.

Site	Fe_{ao}	Mn_{ao}	Al_{ao}	Si_{ao}	Th_{ao}	U_{ao}
	(mg g^{-1} soil)					
Lemon Cove	2.57 a	0.13 c	0.45 b	0.29 b	0.011 a	0.027 a
Riverside	1.01 b	0.27 b	0.59 b	0.51 a	0.0061 ab	0.015 b
Strathmore	0.76 b	0.44 a	0.84 a	0.41 a	0.0016 b	0.011 b

Denoted statistical significance ($p<0.05$ level) was determined through one way Analysis of Variance and the Fisher's Least Significant Difference as a *post-hoc* test.

TABLE 7 Pearson correlation coefficients for soil concentrations of extractable Th and U with the extractable Fe, Mn, Al, and Si.

	Fe	Mn	Al	Si
Th	**0.60**	**-0.69**	**-0.62**	-0.48
U	**0.98**	**-0.81**	**-0.62**	**-0.57**

Bold and red coefficients were significant at the $p<0.05$ level.

reliable site-independent models (Pätzold et al., 2020). For this reason, soils from the three citrus sites were analyzed using DRIFTS, extraction of active mineral phases, and available USDA soil maps (Beaudette and O'geen, 2009) in relationship to the raw GRS TC, K, Th, and U observed at the three sites.

Mineralogical analysis through DRIFTS and extraction of active Fe, Al, and Mn oxides highlighted notable differences in soil clay fraction mineralogy between sites. The aluminosilicate and active oxide phases probed here both represent prevalent, reactive and high surface area minerals in soil clay size fractions that are known to retetain several elements in soils, including K, Th, and U (Mcbride, 1994; Duff et al., 2002; Bachmaf and Merkel, 2011; Hongxia et al., 2016; Dublet et al., 2017; Wang et al., 2021). As such, variation in this mineralogy between sites may translate to different affinities of these isotopes for the clay fraction of these soils. In the case of the soil minerals probed by DRIFTS, there were apparent differences in clay substitution, clay composition and/or oxide chemistry between the Strathmore site and Lemon Cove and Riverside soils. These factors could have impacted surface hydroxyl group availability (e.g., 1:1 vs. 2:1 clay), cation exchange capacity and exchange selectivity, which may greatly impact mineral retention of ions, including Th and U (Duff et al., 2002; Bachmaf and Merkel, 2011; Hongxia et al., 2016; Wang et al., 2017). In addition to the distinct aluminosilicate mineralogy at the Strathmore site, differences in extractable Fe, Al, Mn, and Si provide further insight into the deviation in GRS-texture relationship at the Strathmore site. An observation apparent in our data is the role of poorly-crystalline and amorphous Fe species in U and Th retention across sites, in alignment with previous studies showing the strong association of these Fe species for U and Th through adsorption and co-precipitation (Duff et al., 2002; Dublet et al., 2017; Li et al., 2019; Wang et al., 2021). Interestingly, poorly-crystalline Al, Mn, and Si forms showed a weak inverse relationship with extracted U and Th, indicating they did not associate to the same extent as with Fe. Provided the relatively lower proportion of Fe in total extracted poorly-crystalline mineral phases at the Strathmore site compared to Lemon Cove and Riverside, it is conceivable that this reduced the affinity of Th and U for fine-grained active oxides in Strathmore. This could, in turn, weaken or alter the relationship between soil clay content and GRS through lower radionuclide retention. While these results overall indicate that mineralogy may have played a role in observed inconsistencies in assessment of soil texture across sites with GRS, more detailed mineralogical analyses (e.g., X-ray diffraction "XRD"), extended X-ray absorption fine structure "EXAFS" spectroscopy) and isotope retention studies of isolated textural fractions across sites would further explore this relationship.

The mineralogical results align with the previous suggestion that differences in clay fraction mineralogy may result in contrasting trends of GRS and clay determination between field sites (Mahmood et al., 2013; Pätzold et al., 2020). This suggests that fundamental knowledge of site mineralogy may inform the applicability of GRS for soil textural determination between sites. This could relate further to variable environmental factors that may impact mineralogy of soil clay fractions, such as parent material, drainage and climate (Mcbride, 1994). For example, formation and dissolution of poorly crystalline Fe species related to Th and U retention across the Lemon Cove, Riverside and Strathmore sites are notably sensitive to soil redox fluctuations that may in turn impact radionuclide retention (Duff et al., 2002; Winkler et al., 2018). Knowing in advance the pedological properties of a soil may therefore provide some indication of what type of GRS defined textural relationships could be expected for a given site. Defining these relationships with respect to widely available soil survey data may also represent a future area for exploration with substantial implications for GRS application at regional scales.

5 Conclusions

As smart fertilizer and water management practices become increasingly important for California's specialty crops, driven by factors such as resource scarcity, rising costs, and regulations, the need for accurate, high-resolution soil maps will grow. Geospatial sensors, such as soil apparent electrical conductivity (EC_a) and gamma-ray spectrometry (GRS), were confirmed in this study as reliable tools for field-scale soil mapping of particle size fraction, based on data from three citrus orchards in California. Model-based sampling schemes, such as the response surface sampling design used here, enable the creation of accurate soil maps using a relatively small set of ground-truth soil samples. Multi-field modeling using universal, site-independent models may not be feasible due to unknown secondary influences on sensor measurements at the individual field level. For EC_a, locally adjusted analysis of covariance (ANOCOVA) regressions modeled particle size fractions with high accuracy. Notably, the ANOCOVA regressions can be calibrated using limited (n=5 per field) data. This novel insight marks a step forward in making high-resolution mapping affordable for practitioners and their clientele. More research is needed to understand how ANOCOVA models that use minimal soil data can be developed, calibrated, evaluated, and improved over time (e.g., when any new field is added to a preexisting dataset).

In one of the orchards (the Strathmore orchard), GRS exhibited an unexpected negative correlation with clay content, making the use of ANOCOVA for GRS-texture regressions not possible. Although such relationships have been reported previously, the causes behind them remain poorly understood. To investigate this further, GRS ratios, diffuse reflectance infrared Fourier-transform spectroscopy (DRIFTS), and acid ammonium oxalate extractable elements were analyzed at all three sites. The Strathmore orchard displayed unique GRS ratios, DRIFTS, and acid ammonium oxalate extractable element profiles compared to the other sites. These novel insights may guide future research and help predict whether positive (expected) or unexpected GRS-clay content relationships are likely to occur at a given field, based either on raw GRS data or geochemical information. Such a-priori knowledge could inform soil scientists' decisions about ground-truthing efforts (e.g., allocating additional resources to increase the number of soil samples for an accurate map) or be used as an additional predictor in regional models, such as support vector machines or random forest regression models. Here, the odd GRS-texture relationships were observed in one site only, which had fewer sampling locations than the other two sites. Further research is needed to identify other sites showing unexpected GSR-

texture relationships to understand commonalities amongst these and contrasting features compared to sites where GSR performs as expected.

Data availability statement

The raw data supporting the conclusions of this article will be made available by the authors, without undue reservation.

Author contributions

ES: Conceptualization, Data curation, Formal analysis, Funding acquisition, Investigation, Methodology, Project administration, Resources, Supervision, Visualization, Writing – original draft, Writing – review & editing. MS: Data curation, Formal analysis, Investigation, Methodology, Supervision, Visualization, Writing – original draft, Writing – review & editing. TS: Funding acquisition, Investigation, Methodology, Project administration, Resources, Supervision, Writing – original draft, Writing – review & editing. JF: Funding acquisition, Investigation, Methodology, Resources, Supervision, Writing – original draft, Writing – review & editing. DZ: Formal analysis, Funding acquisition, Investigation, Methodology, Writing – original draft, Writing – review & editing. AP: Data curation, Formal analysis, Funding acquisition, Investigation, Methodology, Project administration, Supervision, Writing – original draft, Writing – review & editing. DC: Data curation, Formal analysis, Funding acquisition, Investigation, Methodology, Resources, Supervision, Writing – original draft, Writing – review & editing.

Funding

The author(s) declare financial support was received for the research, authorship, and/or publication of this article. The authors are grateful for the financial support from the California Department of Food and Agriculture's Specialty Crop Block Grant Program projects titled "Decision Support Tools for Spatiotemporal Integration of Citrus Virtual Orchard and Soil Sensing" (Award number #18-0001-030-SC) and "Updating Information on Citrus Water Use for Resource-Efficient Citrus Irrigation Management in the San Joaquin Valley" (Award number #17-0275-037-SC).

Acknowledgments

We gratefully acknowledge the valuable contributions of the following individuals to this research, both in the field and in the laboratory: Theodor Bughici, Nydia Celis, Layton Chhour, Renata Minhoni, Paul Markley, Kayluh Menefee, Tait Rounsaville, and German Zuniga. Their dedication and hard work were integral to the success of this study.

Conflict of interest

The authors declare that the research was conducted in the absence of any commercial or financial relationships that could be construed as a potential conflict of interest.

Generative AI statement

The author(s) declare that no Generative AI was used in the creation of this manuscript.

Publisher's note

All claims expressed in this article are solely those of the authors and do not necessarily represent those of their affiliated organizations, or those of the publisher, the editors and the reviewers. Any product that may be evaluated in this article, or claim that may be made by its manufacturer, is not guaranteed or endorsed by the publisher.

References

Al-Jafar, M. K., and Al-Jaberi, M. H. (2022). Determination of clay minerals using gamma ray spectroscopy for the Zubair Formation in Southern Iraq. *J. Petroleum Explor. Production Technol.* 12, 299–306. doi: 10.1007/s13202-021-01371-3

Bachmaf, S., and Merkel, B. J. (2011). Sorption of uranium(VI) at the clay mineral–water interface. *Environ. Earth Sci.* 63, 925–934. doi: 10.1007/s12665-010-0761-6

Beaudette, D. E., and O'geen, A. T. (2009). Soil-Web: An online soil survey for California, Arizona, and Nevada. *Comput. Geosciences* 35, 2119–2128. doi: 10.1016/j.cageo.2008.10.016

Chaney, N. W., Wood, E. F., Mcbratney, A. B., Hempel, J. W., Nauman, T. W., Brungard, C. W., et al. (2016). POLARIS: A 30-meter probabilistic soil series map of the contiguous United States. *Geoderma* 274, 54–67. doi: 10.1016/j.geoderma.2016.03.025

Cook, S., Corner, R., Groves, P., and Grealish, G. (1996). Use of airborne gamma radiometric data for soil mapping. *Soil Res.* 34, 183–194. doi: 10.1071/SR9960183

Córdoba, M. A., Bruno, C. I., Costa, J. L., Peralta, N. R., and Balzarini, M. G. (2016). Protocol for multivariate homogeneous zone delineation in precision agriculture. *Biosyst. Eng.* 143, 95–107. doi: 10.1016/j.biosystemseng.2015.12.008

Corwin, D. L., and Lesch, S. M. (2003). Application of soil electrical conductivity to precision agriculture: Theory, principles, and guidelines. *Agron. J.* 95, 455–471. doi: 10.2134/agronj2003.4550

Corwin, D. L., and Lesch, S. M. (2005a). Apparent soil electrical conductivity measurements in agriculture. *Comput. Electron. Agric.* 46, 11–43. doi: 10.1016/j.compag.2004.10.005

Corwin, D. L., and Lesch, S. M. (2005b). Characterizing soil spatial variability with apparent soil electrical conductivity I. Survey protocols. *Comput. Electron. Agric.* 46, 103–133. doi: 10.1016/j.compag.2004.11.002

Corwin, D. L., and Lesch, S. M. (2013). Protocols and guidelines for field-scale measurement of soil salinity distribution with ECa-directed soil sampling. *J. Environ. Eng. Geophysics* 18, 1–25. doi: 10.2113/JEEG18.1.1

Corwin, D. L., and Lesch, S. M. (2014). A simplified regional-scale electromagnetic induction - Salinity calibration model using ANOCOVA modeling techniques. *Geoderma* 230, 288–295. doi: 10.1016/j.geoderma.2014.03.019

Corwin, D. L., and Lesch, S. M. (2017). Validation of the ANOCOVA model for regional-scale ECa to ECe calibration. *Soil Use Manage.* 33, 178–190. doi: 10.1111/sum.2017.33.issue-2

Corwin, D. L., and Scudiero, E. (2016). "Field-Scale Apparent Soil Electrical Conductivity," in *Methods of Soil Analysis*. Ed. S. Logsdon (Soil Science Society of America, Madison, WI, USA).

Corwin, D. L., Scudiero, E., and Zaccaria, D. (2022). Modified ECa – ECe protocols for mapping soil salinity under micro-irrigation. *Agric. Water Manage.* 269, 107640. doi: 10.1016/j.agwat.2022.107640

Corwin, D. L., and Yemoto, K. (2017). Salinity: electrical conductivity and total dissolved solids. *Methods Soil Anal.* 2. doi: 10.1002/saj2.20154

Doolittle, J. A., and Brevik, E. C. (2014). The use of electromagnetic induction techniques in soils studies. *Geoderma* 223, 33–45. doi: 10.1016/j.geoderma.2014.01.027

Dublet, G., Lezama Pacheco, J., Bargar, J. R., Fendorf, S., Kumar, N., Lowry, G. V., et al. (2017). Partitioning of uranyl between ferrihydrite and humic substances at acidic and circum-neutral pH. *Geochimica Cosmochimica Acta* 215, 122–140. doi: 10.1016/j.gca.2017.07.013

Duff, M. C., Coughlin, J. U., and Hunter, D. B. (2002). Uranium co-precipitation with iron oxide minerals. *Geochimica Cosmochimica Acta* 66, 3533–3547. doi: 10.1016/S0016-7037(02)00953-5

Fitzgerald, G. J., Lesch, S. M., Barnes, E. M., and Luckett, W. E. (2006). Directed sampling using remote sensing with a response surface sampling design for site-specific agriculture. *Comput. Electron. Agric.* 53, 98–112. doi: 10.1016/j.compag.2006.04.003

Gee, G. W., and Bauder, J. W. (1986). "Particle-size Analysis," in *Methods of Soil Analysis: Part 1—Physical and Mineralogical Methods*. Ed. A. Klute (Soil Science Society of America, American Society of Agronomy, Madison, WI), 383–411.

Grasty, R. (1979). Gamma ray spectrometric methods in uranium exploration. *Economic Geology Report Geological Survey Canada* 31, 147–161.

Harvey, O. R., and Morgan, C. L. S. (2009). Predicting regional-scale soil variability using a single calibrated apparent soil electrical conductivity model. *Soil Sci. Soc. America J.* 73, 164–169. doi: 10.2136/sssaj2008.0074

Heggemann, T., Welp, G., Amelung, W., Angst, G., Franz, S. O., Koszinski, S., et al. (2017). Proximal gamma-ray spectrometry for site-independent in *situ* prediction of soil texture on ten heterogeneous fields in Germany using support vector machines. *Soil Tillage Res.* 168, 99–109. doi: 10.1016/j.still.2016.10.008

Herrmann, L., Schuler, U., Rangubpit, W., Erbe, P., Surinkum, A., Zarei, M., et al. The potential of gamma-ray spectrometry for soil mapping. *Proc. 19th World Congress Soil Sci.* (2010) Brisbane, Australia 1–6.

Hongxia, Z., Xiaoyun, W., Honghong, L., Tianshe, T., and Wangsuo, W. (2016). Adsorption behavior of Th(IV) onto illite: Effect of contact time, pH value, ionic strength, humic acid and temperature. *Appl. Clay Sci.* 127-128, 35–43. doi: 10.1016/j.clay.2016.03.038

Hornung, R. W., and Reed, L. D. (1990). Estimation of average concentration in the presence of nondetectable values. *Appl. Occup. Environ. Hygiene* 5, 46–51. doi: 10.1080/1047322X.1990.10389587

Khang, V. C., Korovkin, M. V., and Ananyeva, L. G. (2016). Identification of clay minerals in reservoir rocks by FTIR spectroscopy. *IOP Conf. Series: Earth Environ. Sci.* 43, 012004. doi: 10.1088/1755-1315/43/1/012004

Lesch, S. M. (2005). Sensor-directed response surface sampling designs for characterizing spatial variation in soil properties. *Comput. Electron. Agric.* 46, 153–179. doi: 10.1016/j.compag.2004.11.004

Lesch, S. M., Rhoades, J. D., and Corwin, D. L. (2000). *ESAP-95 Version 2.10R: User Manual and Tutorial Guide* (Riverside, CA, USA: USDA-ARS, U.S. Salinity Laboratory).

Lesch, S. M., Strauss, D. J., and Rhoades, J. D. (1995). Spatial prediction of soil-salinity using electromagnetic induction techniques.2. An efficient spatial sampling algorithm suitable for multiple linear-regression model identification and estimation. *Water Resour. Res.* 31, 387–398. doi: 10.1029/94WR02180

Li, Y., Taggart, M. A., Mckenzie, C., Zhang, Z., Lu, Y., Pap, S., et al. (2019). Utilizing low-cost natural waste for the removal of pharmaceuticals from water: Mechanisms, isotherms and kinetics at low concentrations. *J. Cleaner Production* 227, 88–97. doi: 10.1016/j.jclepro.2019.04.081

Lobell, D. B., Lesch, S. M., Corwin, D. L., Ulmer, M. G., Anderson, K. A., Potts, D. J., et al. (2010). Regional-scale assessment of soil salinity in the red river valley using multi-year MODIS EVI and NDVI. *J. Environ. Qual.* 39, 35–41. doi: 10.2134/jeq2009.0140

Luo, Y., Wu, X., Xiao, H., Toan, N.-S., Liao, B., Wu, X., et al. (2023). Leaching is the main pathway of nitrogen loss from a citrus orchard in Central China. *Agriculture Ecosyst. Environ.* 356, 108559. doi: 10.1016/j.agee.2023.108559

Madejová, J. (2003). FTIR techniques in clay mineral studies. *Vibrational Spectrosc.* 31, 1–10. doi: 10.1016/S0924-2031(02)00065-6

Madejová, J., and Komadel, P. (2001). Baseline studies of the clay minerals society source clays: Infrared methods. *Clays Clay Minerals* 49, 410–432. doi: 10.1346/CCMN.2001.0490508

Mahmood, H. S., Hoogmoed, W. B., and Van Henten, E. J. (2013). Proximal gamma-ray spectroscopy to predict soil properties using windows and full-spectrum analysis methods. *Sensors* 13, 16263–16280. doi: 10.3390/s131216263

Maxton, C., and Lund, E. D. (2020). "Evaluating Proximal Soil Sensors for measurement of soil physical and chemical properties," in *15th International Conference on Precision Agriculture* (International Society of Precision Agriculture, Minneapolis, MN, USA).

Mcbride, M. B. (1994). *Environmental chemistry of soils* (New York, NY, USA: Oxford University Press, Inc).

Mckeague, J. A., and Day, J. H. (1966). Dithionite- and oxalate-extractable fe and al as aids in differentiating various classes of soils. *Can. J. Soil Sci.* 46, 13–22. doi: 10.4141/cjss66-003

Minty, B. R. S. (1997). Fundamentals of airborne gamma-ray spectrometry. *AGSO J. Aust. Geology Geophysics* 17, 39–50.

Moghimi, A., Pourreza, A., Zuniga-Ramirez, G., Williams, L. E., and Fidelibus, M. W. (2020). A novel machine learning approach to estimate grapevine leaf nitrogen concentration using aerial multispectral imagery. *Remote Sens.* 12, 3515. doi: 10.3390/rs12213515

Muhammad, S., Khalsa, S., and Brown, P. H. (2018). "Nitrogen Management in Citrus and Avocado," in *Nitrogen Management Advice for Fruit, Nuts, and Other Crops* (University of California, Division of Agriculture and Natural Resources, Davis, CA, USA).

Parikh, S. J., Goyne, K. W., Margenot, A. J., Mukome, F. N. D., and Calderón, F. J. (2014). "Chapter One - Soil Chemical Insights Provided through Vibrational Spectroscopy," in *Advances in Agronomy*. Ed. D. L. Sparks (Academic Press), 1–148.

Pätzold, S., Leenen, M., and Heggemann, T. W. (2020). Proximal mobile gamma spectrometry as tool for precision farming and field experimentation. *Soil Syst.* 4, 31. doi: 10.3390/soilsystems4020031

Pedrera-Parrilla, A., Van De Vijver, E., Van Meirvenne, M., Espejo-Perez, A. J., Giraldez, J. V., and Vanderlinden, K. (2016). Apparent electrical conductivity measurements in an olive orchard under wet and dry soil conditions: significance for clay and soil water content mapping. *Precis. Agric.* 17, 531–545. doi: 10.1007/s11119-016-9435-z

Petit, S. (2006). "Chapter 12.6 Fourier Transform Infrared Spectroscopy," in *Developments in Clay Science*. Eds. F. Bergaya, B. K. G. Theng and G. Lagaly (Elsevier), 909–918.

Ramcharan, A., Hengl, T., Nauman, T., Brungard, C., Waltman, S., Wills, S., et al. (2018). Soil property and class maps of the conterminous United States at 100-meter spatial resolution. *Soil Sci. Soc. America J.* 82, 186–201. doi: 10.2136/sssaj2017.04.0122

Reinhardt, N., and Herrmann, L. (2019). Gamma-ray spectrometry as versatile tool in soil science: A critical review. *J. Plant Nutr. Soil Sci.* 182, 9–27. doi: 10.1002/jpln.201700447

Reyes, J., Wendroth, O., Matocha, C., Zhu, J., Ren, W., and Karathanasis, A. D. (2018). Reliably mapping clay content coregionalized with electrical conductivity. *Soil Sci. Soc. America J.* 82, 578–592. doi: 10.2136/sssaj2017.09.0327

Rhoades, J. D., Manteghi, N. A., Shouse, P. J., and Alves, W. J. (1989). Soil electrical conductivity and soil salinity: New formulations and calibrations. *Soil Sci. Soc. America J.* 53, 433–439. doi: 10.2136/sssaj1989.03615995005300020020x

Rhoades, J. D., Raats, P. A. C., and Prather, R. J. (1976). Effects of liquid-phase electrical conductivity, water content, and surface conductivity on bulk soil electrical conductivity. *Soil Sci. Soc. America J.* 40, 651–655. doi: 10.2136/sssaj1976.03615995004000050017x

Roberts, D. R., Bahn, V., Ciuti, S., Boyce, M. S., Elith, J., Guillera-Arroita, G., et al. (2017). Cross-validation strategies for data with temporal, spatial, hierarchical, or phylogenetic structure. *Ecography* 40, 913–929. doi: 10.1111/ecog.2017.v40.i8

Scudiero, E., Corwin, D. L., Markley, P. T., Pourreza, A., Rounsaville, T., Bughici, T., et al. (2024a). A system for concurrent on-the-go soil apparent electrical conductivity and gamma-ray sensing in micro-irrigated orchards. *Soil Tillage Res.* 235, 105899. doi: 10.1016/j.still.2023.105899

Scudiero, E., Corwin, D. L., and Skaggs, T. H. (2024b). Useful soil maps in microirrigated orchards. *Progressive Crop Consultants* 9, 14–17.

Scudiero, E., Corwin, D. L., Wienhold, B. J., Bosley, B., Shanahan, J. F., and Johnson, C. K. (2016). Downscaling Landsat 7 canopy reflectance employing a multi-soil sensor platform. *Precis. Agric.* 17, 53–73. doi: 10.1007/s11119-015-9406-9

Scudiero, E., Skaggs, T. H., and Corwin, D. L. (2017). Simplifying field-scale assessment of spatiotemporal changes of soil salinity. *Sci. Total Environ.* 587, 273–281. doi: 10.1016/j.scitotenv.2017.02.136

Scudiero, E., Zuniga, G., and Pourreza, A. (2019). Using the ESAP-RSSD software to direct citrus tree sampling with aerial multispectral data. *FastTIMES* 24, 130–133.

Sudduth, K. A., Kitchen, N. R., Wiebold, W. J., Batchelor, W. D., Bollero, G. A., Bullock, D. G., et al. (2005). Relating apparent electrical conductivity to soil properties across the north-central USA. *Comput. Electron. Agric.* 46, 263–283. doi: 10.1016/j.compag.2004.11.010

Syvertsen, J., and Smith, M. (1996). Nitrogen uptake efficiency and leaching losses from lysimeter-grown Citrus trees fertilized at three nitrogen rates. *J. Am. Soc. Hortic. Sci.* 121, 57–62. doi: 10.21273/JASHS.121.1.57

Viscarra-Rossel, R. A., Taylor, H. J., and Mcbratney, A. B. (2007). Multivariate calibration of hyperspectral γ-ray energy spectra for proximal soil sensing. *Eur. J. Soil Sci.* 58, 343–353. doi: 10.1111/j.1365-2389.2006.00859.x

Wang, Y., Wang, J., Li, P., Qin, H., Liang, J., and Fan, Q. (2021). The adsorption of U (VI) on magnetite, ferrihydrite and goethite. *Environ. Technol. Innovation* 23, 101615. doi: 10.1016/j.eti.2021.101615

Wang, Q., Zhu, C., Yun, J., and Yang, G. (2017). Isomorphic substitutions in clay materials and adsorption of metal ions onto external surfaces: A DFT investigation. *J. Phys. Chem. C* 121, 26722–26732. doi: 10.1021/acs.jpcc.7b03488

Wibowo, R. C., Pertiwi, A. P., and Kurniati, S. (2020). Identification of clay mineral content using spectral gamma ray on Y1 well in karawang area, west java, Indonesia. *J. Geoscience Engineering Environment Technol.* 5, 136–142. doi: 10.25299/jgeet.2020.5.3.4504

Winkler, P., Kaiser, K., Thompson, A., Kalbitz, K., Fiedler, S., and Jahn, R. (2018). Contrasting evolution of iron phase composition in soils exposed to redox fluctuations. *Geochimica Cosmochimica Acta* 235, 89–102. doi: 10.1016/j.gca.2018.05.019

Zhang, X., Pourreza, A., Cheung, K. H., Zuniga-Ramirez, G., Lampinen, B. D., and Shackel, K. A. (2021). Estimation of fractional photosynthetically active radiation from a canopy 3D model; case study: almond yield prediction. *Front. Plant Sci.* 12. doi: 10.3389/fpls.2021.715361

frontiers | Frontiers in Plant Science

TYPE Original Research
PUBLISHED 17 March 2025
DOI 10.3389/fpls.2025.1550946

Check for updates

OPEN ACCESS

EDITED BY
Amir Ali Khoddamzadeh,
Florida International University, United States

REVIEWED BY
Qian Zhang,
Chinese Academy of Forestry, China
Jiangwen Nie,
Yangtze University, China

*CORRESPONDENCE
Huijing Ni
hjni0529@163.com

RECEIVED 24 December 2024
ACCEPTED 24 February 2025
PUBLISHED 17 March 2025

CITATION
Yang Z, Zhao J and Ni H (2025) Silkworm excrement organic fertilizer substitution compound fertilizer improves bamboo shoot yield by altering soil properties and bacterial communities of Moso bamboo *(Phyllostachys edulis)* forests in subtropical China. *Front. Plant Sci.* 16:1550946. doi: 10.3389/fpls.2025.1550946

COPYRIGHT
© 2025 Yang, Zhao and Ni. This is an open-access article distributed under the terms of the Creative Commons Attribution License (CC BY). The use, distribution or reproduction in other forums is permitted, provided the original author(s) and the copyright owner(s) are credited and that the original publication in this journal is cited, in accordance with accepted academic practice. No use, distribution or reproduction is permitted which does not comply with these terms.

Silkworm excrement organic fertilizer substitution compound fertilizer improves bamboo shoot yield by altering soil properties and bacterial communities of Moso bamboo *(Phyllostachys edulis)* forests in subtropical China

Zhenya Yang[1,2], Jiancheng Zhao[1,2] and Huijing Ni[1,2]*

[1]Zhejiang Academy of Forestry, Hangzhou, China, [2]Northwest Zhejiang Bamboo Forest Ecosystem Positioning Observation and Research Station, Hangzhou, China

To achieve high economic benefits, reapplying fertilizers has been a common business measure taken for harvesting Moso bamboo shoots and timber in the past decades in subtropical China. Applying compound and organic fertilizers is an effective measure to enhance soil fertility and promote plant production. To demonstrate how compound fertilizer (CF) decrement and application of silkworm excrement organic fertilizer (SEOF) effect on soil quality, bamboo shoot yield and quality of Moso bamboo plantations, six CF decrement treatments (0 %, 25 %, 50 %, 75 %, and 100 % SEOF substitution, and no fertilization) were examined in our study. Soil nutrients, enzyme activities, bacterial community structures, bamboo shoot yield and quality were determined, and their relationships were analyzed. The results showed that adding SEOF improved soil quality and bamboo shoot yield. Compared with CF, the combined CF-SEOF treatments increased soil pH, soil organic carbon, N and P availability, and the activities of enzymes related to C, N, and P cycling. SEOF substitution significantly changed the soil bacterial community structure and increased the relative abundance of Proteobacteria and Actinobacteria. Higher proportions of organic fertilizer substitution (OF75, OF) enhanced the bamboo shoot yield (by 20.23 % and 16.55 %, respectively) and their total flavonoid and vitamin C content, compared to CF ($p< 0.05$). Moreover, the soil quality index of OF75 and OF50 was significantly higher than that of OF and OF25 in the 0–40 cm soil layer ($p< 0.05$). Pearson's correlation tests showed that bamboo shoot yield was positively related with soil nutrients ($p< 0.05$). In addition, SEM revealed that fertilization affected soil enzyme activities through soil microorganisms, thereby affecting soil nutrient availability and promoting SQI

and bamboo shoot yield. In conclusion, our study revealed that SEOF production is advisable for improving soil quality and bamboo shoot yield, providing evidence that soil nutrients and bacteria contribute to shoot yield and promote the sustainable management of soil and Moso bamboo forests.

KEYWORDS

Moso bamboo, silkworm excrement organic fertilizer, compound fertilizer decrement, bacterial community, soil quality, yield

Introduction

Moso bamboo (*Phyllostachys edulis*) is a fast-growing species that is excellent for harvesting bamboo shoots and timber. This forest resource is distributed extensively and covers approximately 73 % of the bamboo acreage in China, significantly influencing the country's bamboo industry and economic development (Ni and Su, 2024; Song et al., 2011). Moreover, bamboo shoots are widely known for their edible value, great taste, and high nutritional content. It is rich in proteins, vitamins, amino acids, dietary fiber, and flavonoids, making it a staple traditional vegetable in Chinese dishes (Ni et al., 2024a). Intensive management practices, such as cutting and applying large amounts of compound fertilizer (CF) and cutting, have been the main ways to obtain high economic yields of bamboo (Ni et al., 2021). However, the long-term application of chemical fertilizers has resulted in the deterioration of overall soil quality and various problems, such as soil acidification and compaction, increased soil respiration, nutrient depletion, loss of biodiversity, the decline in stand productivity, and ecological environmental damage (Yang et al., 2019; Yao et al., 2022).

In contrast to chemical fertilizers, organic fertilizers are rich in organic matter, nutrients and beneficial microorganisms (Li et al., 2018; Liu et al., 2021; Shao et al., 2024), and they have shown positive effects on soil quality which is typically evaluated using the soil quality index (SQI) (Yang and Zhang, 2023; Ying et al., 2023; Wang et al., 2024). Applying organic fertilizers like manure generally increases the soil organic carbon (SOC) content, nutrient availability and enzymatic activities. It also changes the microbial diversity and composition (Li et al., 2018; Shao et al., 2024). A previous study reported that organic fertilizers can promote nutrient conversion and stimulate plant growth, benefitting crop yields (Oladele et al., 2019). Notably, applying organic fertilizers also affects the nutritional composition of vegetables and fruits (Shankar et al., 2013). A study by Ni et al. (2024b) showed that, compared with CF, humic acid fertilizer increased the SOC and AP content, sucrase (SC) and acid phosphatase (ACP) activities, and bamboo shoot yield in *Phyllostachys violascens* 'Prevernalis' plantations. Applying organic fertilizers is an effective means of decreasing chemical fertilizer input and improving crop yield and soil quality (Ge et al., 2021; He et al., 2022; Ying et al., 2023). Numerous studies have shown that combining CF and organic fertilizers produces the same significant effects. Compared with chemical fertilizers alone (N, P and K), the combined application of inorganic and organic fertilizers can promote the productivity of forestry plants (Liu et al., 2021) and crops like rice, wheat, and corn (Oladele et al., 2019; Shahid et al., 2017; Tang et al., 2018). Combined application can also increase the aboveground biomass of rice (Moe et al., 2019).

Silkworm excrement organic fertilizer (SEOF) is produced by the aerobic and high-temperature composting of silkworm excrement and leftover mulberry leaves, which are fermented by beneficial microorganisms. It is rich in organic matter, N, P, K, and trace elements such as Ca and Mg. It also contains small amounts of alkaloids, various vitamins, and niacin (Chen et al., 2011; Ni et al., 2024c). Its heavy metal and NaCl contents are low, and long-term application cannot easily cause secondary salinization. It has a pH of 8 to 9 and can slow down the progression of soil acidification (Li et al., 2015). It is easily absorbed and utilized by plants, and it can promote plant absorption of N, P, and K, increase their aboveground biomass, and improve crop quality (Luo et al., 2011; Yang et al., 2022). Currently, SEOFs are widely used in the agricultural production of various crops, such as leafy vegetables, peanuts, and corn, increasing soil fertility and crop yield. Its fertilizer efficiency is greater than that of other organic fertilizers like animal manure (chicken, pig, and sheep). For example, compared with chicken manure, SEOF produces higher mass fractions of soil organic matter, total nitrogen (TN), total phosphorus (TP), AN, and AP (Li et al., 2015). SEOF also enhances soil bacterial diversity, promotes the growth of functional and beneficial bacteria, and alleviates obstacles to ensure the continuous cultivation of chrysanthemum (Peng et al., 2015). Moreover, applying SEOF allows the reuse of agricultural and forestry waste, thus reducing environmental pollution and decreasing plant dependence on chemical fertilizers.

The soil is an active site for material cycling and energy exchange in forest ecosystems, providing water and nutrients for plant growth (Li et al., 2023a). Soil quality directly determines plant productivity. Fertilization can alter plant root exudates, microbial growth and reproduction, and soil nutrient retention and mineralization, thereby affecting plant growth (Li et al., 2023b; Yang et al., 2023; Zhou et al., 2015). Soil physical (e.g., bulk density and porosity), chemical (e.g., pH, nutrient content) and biological (e.g., enzyme activities) properties are important components of soil

quality (Ning et al., 2020; Wang et al., 2024). Changes in these properties with different fertilization treatments can reflect the sustainability of the soil resource, affecting the yield and quality of bamboo shoots. Previous studies have reported the effects of chemical fertilizers on soil quality and bamboo shoot yield in Moso bamboo forests. Nevertheless, the effects of CF decrement and SEOF application on soil properties and bamboo shoots remain unclear. Thus, we aimed to (1) explore how different percentages of CF combined with SEOF affect soil physicochemical and biological properties; (2) assess the bamboo shoot yield and quality, soil quality index (SQI) in response to fertilization treatments; (3) elucidate the internal links among soil properties, microbial communities, and bamboo shoot yield and quality. The research aimed to provide a theoretical basis for using SEOF to improve soil quality and bamboo yield in Moso bamboo forest sustainable development.

Materials and methods

Field site

The research site is located in Maowu Village, Daixi Town (120° 0' 47.3" E, 30° 39' 33.7" N), Huzhou City, Zhejiang Province, China, and has an altitude of 65 m. Its climate is categorized under the northern subtropical monsoon climate zone, with an average annual temperature of 12.2–17.3 °C and an average annual precipitation of 1277.6 mm. The Moso bamboo forests were cultivated to enable experimentation, and NPK CF has been applied at a rate of 1500 kg/(ha y) since 2001 to manage the benefits of bamboo shoot production. The forests had a standing bamboo density of 2325–2625 stems/ha and an average diameter at breast height of 10.22–11.59 cm. The soils in the region are classified as red soil. The soil bulk density and pH were 1.24–1.39 g/cm^3 and 4.36–4.52, respectively.

Experimental design

In May 2022, six sites were selected for investigation based on their similarities in altitude, slope, and aspect. Thirty 20 m × 20 m plots were divided into six different fertilization treatments, with five replicate plots for each treatment, separated by an interval of 3 m between each plot. In June 2022, sprinkled CF or SEOF was applied to the soil surface, followed by tillage (to a depth of 20–25 cm), and understory vegetation was removed. In August 2023, we dug a ditch 25 cm deep and 15 cm wide, sprinkled CF or SEOF into the ditch, and covered it with soil. The CF had a total nutrient content of ≥ 45 % (N:P_2O_5:K_2O = 20:4:8). The SEOF had a pH of 8.85 and mass fractions of 40 %, 2 %, 1 %, and 2 % for organic matter, N, P, and K, respectively. Based on the proportion of SEOF in the TN input, the treatments were as follows: (1) CF: 100 % CF; (2) OF25: 25 % SEOF and 75 % CF; (3) OF50: 50 % SEOF and 50 % CF; (4) OF75: 75 % SEOF and 25 % CF; (5) OF: 100 % SEOF; and (6) CK: no fertilization. Table 1 presents the annual fertilization amounts of the experimental Moso bamboo forests.

Soil sampling and analysis

In May 2024, soil samples (0–20 cm and 20–40 cm) were collected using a soil drill to collect three soil cores from each plot. The cores were mixed to form one composite sample per plot for a total of 30 composite samples. The fresh soil samples were passed through a 2 mm sieve. A part of the soil was stored at −80°C to extract and determine microbial DNA, and another was collected in a plastic self-sealing bag and air-dried to measure chemical properties and enzyme activities.

Soil pH was determined from a 1:2.5 (V/V) soil-water extract using an electrode pH meter. SOC was measured using a TOC analyzer (Multi N/C 3100; Analytik, Jena, Germany). TN, TP, AN, and AP content were measured using Kjeldahl nitrogen determination method, concentrated H_2SO_4 and $HClO_4$ digestion method, alkali hydrolyzed diffusion method, and molybdenum antimony colorimetric method, respectively (Ni et al., 2021). Soil urease (UE), SC, and ACP activities were determined with test kits using the 3,5-dinitrosalicylic acid colorimetric method, phenol sodium hypochlorite colorimetric method, and sodium phenylphosphate colorimetric method, respectively (Ni et al., 2024c).

DNA extraction and high-throughput sequencing

Soil DNA was extracted from a 0.5 g soil sample using a soil DNA Kit (Magen, Guangzhou, China) according to the manufacturer's protocols. The V3–V4 region was amplified using the following primers: 5′-CCTACGGGNGGCWGCAG-3′ (338F) and 5′-GACTACHVGGGTATCTAATCC-3′ (806R). The 16S rDNA target region of the ribosomal RNA gene were amplified by PCR (95°C for 5 min, followed by 30 cycles at 95°C for 1 min, 60°C for 1 min, and 72°C for 1 min and a final extension at 72°C for 7 min). 50 μL mixture containing 10 μL of 5 × Q5@ Reaction Buffer, 10 μL of 5 × Q5@ High GC Enhancer, 1.5 μL of 2.5 mM dNTPs, 1.5 μL of each primer (10 μM), 0.2 μL of Q5@ High-Fidelity DNA Polymerase, and 50 ng of template DNA. Related PCR reagents were from New England Biolabs, USA. The PCR-purified products from each locus were mixed and subsequently sequenced using Illumina on a NovaSeq 6000 platform at Gene Denovo, Guangzhou, China.

The Amplicon Sequence Variants (ASVs) feature list was generated using the DADA2 (Divisive Amplicon Denoising

TABLE 1 Annual fertilization amount used in the experimental forests.

Fertilizer treatments	Annual fertilization amount
CF (100% CF)	1500 kg/ha CF
OF25 (75% CF+25% SEOF)	1125 kg/ha CF+3750 kg/ha SEOF
OF50 (50% CF+50% SEOF)	750 kg/ha CF+7500 kg/ha SEOF
OF75 (25% CF+75% SEOF)	375 kg/ha CF+11250 kg/ha SEOF
OF (100% SEOF)	15000 kg/ha SEOF
CK	No fertilization

Algorithm 2) pipeline (Callahan et al., 2016). Subsequently, taxonomic annotations were assigned to the ASVs using the SILVA taxonomy database (Pruesse et al., 2007). Further analyses were conducted using the ASV abundance table after normalization to account for variations in sequencing depth across samples.

Bamboo shoot yield determination

From March to May 2024, the fresh weight of the bamboo shoots at each sampling site was recorded daily, from the excavation of bamboo shoots to the end of the shoot period. In April 2024, during the peak period of bamboo shoot growth, approximately 5 cm of intact bamboo shoots were randomly excavated from each plot. The shoots were peeled, and 2 kg of the peeled shoots was placed in an icebox and brought back to the laboratory. The samples were crushed and mixed, then used for the determination of total flavonoids and vitamin C content. Total flavonoids content was measured using spectrophotometry and sulfosalicylic acid iron complex colorimetric method. Vitamin C content was determined using test kits.

Soil quality evaluation

To evaluate the influence of different fertilization treatments on soil quality, the total dataset method (consisting of 12 soil indicators: pH, SOC, TN, TP, AN, AP, SC, UE, ACP, Shannon, Chao1, and ACE) was employed to establish a soil quality index (SQI) for each treatment. The procedure for the calculation is as follows:

All data were standardized and transformed into dimensionless values between 0 and 1 to achieve dimensional normalization of the indicators using the following equations (He et al., 2022):

$$F(Xi)' = \frac{x_i - x_{min}}{x_{max} - x_{min}}$$

$$F(Xi)'' = \frac{x_{max} - x_i}{x_{max} - x_{min}}$$

where (Xi), $F(Xi)'$, and $F(Xi)''$ is the score of the i_{th} indicator, and x_i, x_{max}, and x_{min} are the measured, maximum, and minimum values of the i_{th} indicator, respectively.

Principal component analysis was performed on standard deviation data using SPSS 20.0 (SPSS Inc., Chicago, IL, USA); the common factor variance of soil quality indicators was calculated, and the proportion of the common factor variance of each indicator to the total common factor variance was used as the weight of each indicator.

The SQI was calculated with the equation:

$$SQI = \sum Wi \times F(Xi)$$

where Wi the weight of the i_{th} indicator, and $F(Xi)$ the membership value of the i_{th} indicator.

Statistical analysis

All statistical analyses were performed using SPSS and Excel 2016. One-way analysis of variance followed by Duncan's multiple range test was used to detect significant differences ($p< 0.05$) between the treatment means. Pearson's correlation and redundancy analyses were conducted to examine the links between soil chemical properties, bacterial communities, and bamboo shoot yield. Structural equation modeling (SEM) was conducted to examine the relationships among soil properties, enzymatic activities, bacterial diversity, SQI, and bamboo shoot yield. Data from the CF, OF25, OF50, OF75, and OF treatments were used to construct the SEM. All figures were created using Origin 2024 software and R package.

Results

Soil chemical properties and enzyme activities

Table 2 presents the chemical properties of the soil from bamboo forests treated with different fertilizers. The pH, SOC, TN, TP, AN, and AP content from the six treatments showed various trends. Compared with CK, soil pH was significantly higher in OF25, OF50, OF75, and OF by 1.86 %, 3.94 %, 4.87 %, and 4.41 % in the 0–20 cm soil layer, respectively, and by 2.63 %, 9.79 %, 10.26 %, and 14.08 % in the 20–40 cm soil layer, respectively. The SOC contents of OF25, OF50, OF75, and OF were significantly higher than those of CK and CF in the 0–40 cm soil layer. The order of SOC content in the six treatments was OF > OF75 > OF50 > OF25 > CK > CF. The TN, TP, and AN content were significantly higher in OF50, OF75, and OF than in CK and CF. The AP content was significantly higher in OF25, OF50, OF75, and OF than in CF. Compared with CF, OF50, OF75, OF significantly increased the C/N in the 0–40 cm soil layer.

Different fertilizer treatments had significant effects ($p< 0.05$) on the soil enzyme activity in each soil layer (Figure 1). Compared with CF, the following were observed: OF25, OF75, and OF had increased SC activity in the 0–40 cm soil layer; OF25, OF50, and OF75 had increased UE activity in the 0–20 cm soil layer; and OF25, OF50, and OF had increased ACP activity in the 0–40 cm soil layer. The SC and ACP activities of OF75 were highest in the 0–20 cm soil layer, and those of OF were highest in the 20–40 cm soil layer.

Soil bacterial community structure

Statistical analysis of high-throughput sequencing results revealed a total of 81 930 ASVs (ranging from 5795–9091 per sample) assigned with a similarity level of ≥ 97 % found across the 60 soil samples (Table 3). The alpha diversity indices for community richness (ACE and Chao1) and community diversity (Shannon) in the soil varied among treatments. In the 0–20 cm soil layer, the Shannon index of CF was significantly higher than that of CK but did not differ significantly from those of the other four fertilizer treatments (OF25, OF50, OF75,

10.3389/fpls.2025.1550946

TABLE 2 Soil chemical properties in Moso bamboo forests treated with different fertilizers.

Treatments	pH	SOC	TN	TP	AN	AP	C/N
		g/kg	g/kg	g/kg	mg/kg	mg/kg	
0–20 cm							
CF	4.04 ± 0.03e	10.42 ± 0.30e	1.04 ± 0.02c	0.41 ± 0.02d	104.42 ± 0.60b	76.54 ± 0.10d	10.02 ± 0.21d
OF25	4.30 ± 0.03c	11.73 ± 0.33d	1.06 ± 0.01c	0.66 ± 0.02c	100.15 ± 1.07b	147.32 ± 1.88b	11.07 ± 0.14c
OF50	4.60 ± 0.04b	13.02 ± 0.14c	1.13 ± 0.01b	0.77 ± 0.05a	143.82 ± 0.92a	151.94 ± 3.10b	11.52 ± 0.23c
OF75	4.62 ± 0.04b	20.14 ± 0.30b	1.59 ± 0.00a	0.79 ± 0.03b	148.37 ± 0.88a	173.54 ± 0.35a	12.67 ± 0.15b
OF	4.78 ± 0.02a	21.90 ± 0.59a	1.57 ± 0.03a	0.75 ± 0.04b	122.58 ± 0.54c	129.61 ± 0.29c	13.95 ± 0.26a
CK	4.19 ± 0.03d	10.79 ± 0.53e	0.90 ± 0.04d	0.40 ± 0.04d	85.94 ± 1.62c	73.46 ± 1.02d	11.99 ± 0.32c
20–40 cm							
CF	4.32 ± 0.03d	9.03 ± 0.31e	0.73 ± 0.01c	0.27 ± 0.02c	82.10 ± 0.93b	10.16 ± 0.29c	12.37 ± 0.18c
OF25	4.39 ± 0.02c	10.62 ± 0.18d	0.87 ± 0.01b	0.46 ± 0.03a	95.93 ± 1.95a	57.86 ± 2.21a	12.21 ± 0.27c
OF50	4.48 ± 0.02b	13.79 ± 0.33c	1.01 ± 0.01a	0.43 ± 0.04a	92.59 ± 0.71a	54.32 ± 1.66a	13.65 ± 0.25b
OF75	4.52 ± 0.02a	15.02 ± 0.48b	0.98 ± 0.01a	0.44 ± 0.03a	93.34 ± 0.62a	55.71 ± 1.11a	15.33 ± 0.34a
OF	4.50 ± 0.04a	15.27 ± 0.43a	1.02 ± 0.04a	0.38 ± 0.01b	81.09 ± 0.46b	43.04 ± 1.75b	14.97 ± 0.28a
CK	4.31 ± 0.01d	9.08 ± 0.09e	0.72 ± 0.01c	0.27 ± 0.01c	72.61 ± 1.57c	17.11 ± 1.45c	12.61 ± 0.15c

Different lowercase letters indicate significant differences ($p < 0.05$) between treatments.

and OF). In the 20–40 cm soil layer, the Shannon index of OF50 was significantly higher than those of the other treatments. The ACE and Chao1 indices of OF50 were significantly higher than those OF and CK in the 0–20 cm soil layer and significantly higher than those of all other treatments in the 20–40 cm soil layer.

Figure 2 shows the most abundant bacterial phylum in all samples. During the entire incubation period, Acidobacteria, Proteobacteria, Chloroflexi, and Actinobacteria were the most dominant phyla across all treatments, accounting for 28.74 %, 10.43 %, 8.02 %, and 5.36 % of the population in the 0–20 cm soil layer, respectively, and 39.04 %, 16.45 %, 12.86 %, and 8.01 % in the 20–40 cm soil layer, respectively. The relative abundance of Proteobacteria in the 0–40 cm soil layer was significantly higher in OF50, OF75, and OF than in CF. The relative abundance of Acidobacteria was lower in OF50, OF75, and OF than in CF and OF25. Based on the Bray–Curtis distance, non-metric multidimensional scaling analysis revealed significant differences in the bacterial community composition at the ASV level (Figure 3).

Bamboo shoot yield and quality

After two years of fertilization, the bamboo yields of OF75 and OF were 35 745 and 34 650 kg/ha, respectively (Figure 4). Compared with CF and CK, OF75 increased the yield by 20.23 % and 59.72 %, respectively, and OF increased the yield by 16.55 % and 54.83 %, respectively ($p< 0.05$). Compared with CF and CK, OF75 significantly increased the total flavonoid content by 122.1 % and 101.3 %, respectively, whereas OF increased it by 41.2 % and 28.0 %, respectively (Figure 5). OF50 and OF75 significantly

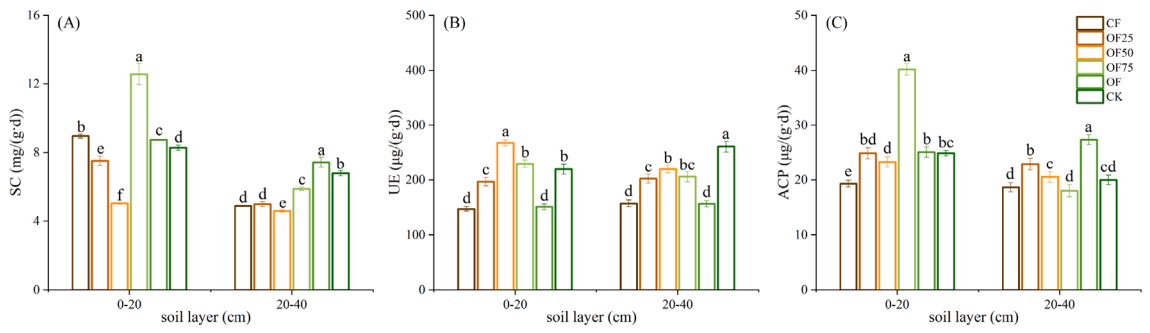

FIGURE 1
Impact of different fertilization treatments on soil **(A)** sucrase (SC), **(B)** urease (UE), and **(C)** acid phosphatase activities (ACP) in 0–20 cm and 20–40 cm soil layers. Different lowercase letters indicate significant differences ($p< 0.05$) between fertilizer treatments.

10.3389/fpls.2025.1550946

TABLE 3 Sequence statistics and alpha diversity indices of soil bacteria in Moso bamboo forests treated with different fertilizers.

Treatments	ASVs	Shannon	Chao1	ACE	Good Coverage
0–20 cm					
CF	7447 ± 685ab	11.84 ± 0.12a	7447 ± 685ab	7447 ± 685ab	1.00 ± 0.00
OF25	7085 ± 1226ab	11.49 ± 0.20ab	7085 ± 1226ab	7085 ± 1226ab	1.00 ± 0.00
OF50	8112 ± 1187a	11.77 ± 0.30ab	8112 ± 1187a	8112 ± 1187a	1.00 ± 0.00
OF75	7242 ± 780ab	11.54 ± 0.24ab	7242 ± 780ab	7242 ± 780ab	1.00 ± 0.00
OF	6436 ± 296b	11.47 ± 0.07ab	6436 ± 296b	6436 ± 296b	1.00 ± 0.00
CK	6241 ± 963b	11.41 ± 0.25b	6241 ± 963b	6241 ± 963b	1.00 ± 0.00
20–40 cm					
CF	6532 ± 1404b	11.44 ± 0.33b	6532 ± 1404b	6532 ± 1404b	1.00 ± 0.00
OF25	5851 ± 684b	11.17 ± 0.12b	5851 ± 684b	5851 ± 684b	1.00 ± 0.00
OF50	9091 ± 723a	11.96 ± 0.08a	9091 ± 723a	8091 ± 723a	1.00 ± 0.00
OF75	6377 ± 1713b	11.37 ± 0.39b	6377 ± 1713b	6377 ± 1713b	1.00 ± 0.00
OF	6721 ± 1316b	11.55 ± 0.30b	6721 ± 1316b	6721 ± 1316b	1.00 ± 0.00
CK	5795 ± 1056b	11.13 ± 0.29b	5795 ± 1056b	5795 ± 1056b	1.00 ± 0.00

increased the vitamin C content by 5.8 % and 15.0 %, respectively, compared with CF.

Relationships among soil properties, enzyme activities, bacterial community structure, and bamboo shoot yield and quality

The correlation heatmap (Figure 6) shows the relationships between soil bacterial community composition (phylum level) and the main soil characteristics. SOC, TN, and ACP were positively correlated with Firmicutes and Actinobacteria. In the 0–20 cm soil layer, AN, TP, AP, and UE were positively correlated with Bacteroidetes, whereas SOC, TN, AN, TP, AP, UE, and ACP were negatively correlated with Chloroflexi. In the redundancy analysis, the first two axes explained 47.04 % and 27.66 %, 47.82 % and 23.35 % of the variation observed in the microbial communities in the 0–20 cm and 20–40 cm soil layer, respectively (Figure 7). In the 0–40 cm soil layer, SOC, TP, AP, and UE had significant effects on the soil bacterial communities (Table 4).

Pearson's correlation tests were performed to examine whether variations in the bamboo shoots were influenced by soil properties (Figure 8). Total flavonoid and vitamin C content were positively correlated with pH, SOC, TN and TP. Shoot yield was positively correlated with pH, SOC, TN, TP, AN and AP.

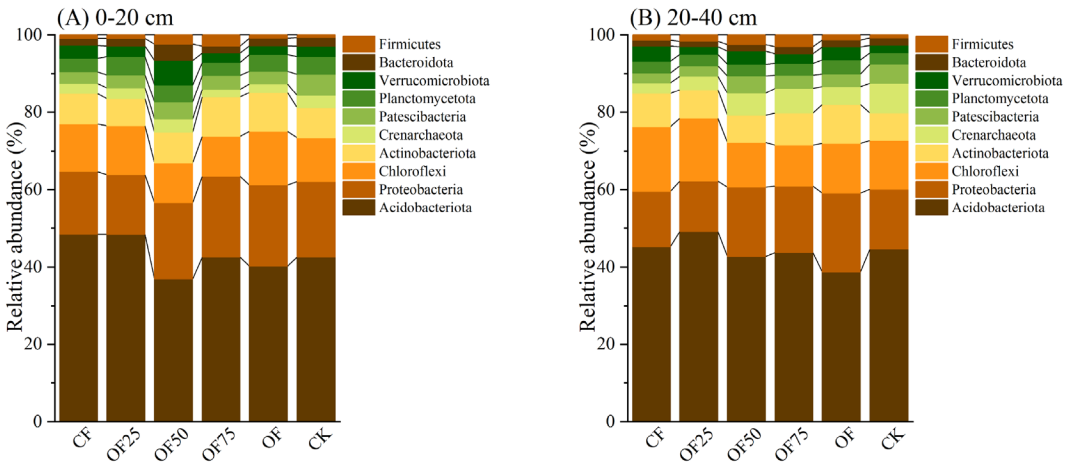

FIGURE 2
Species composition of soil bacteria at the phylum level in **(A)** 0-20 cm and **(B)** 20-40 cm soil layers in Moso bamboo forests treated with different fertilizers.

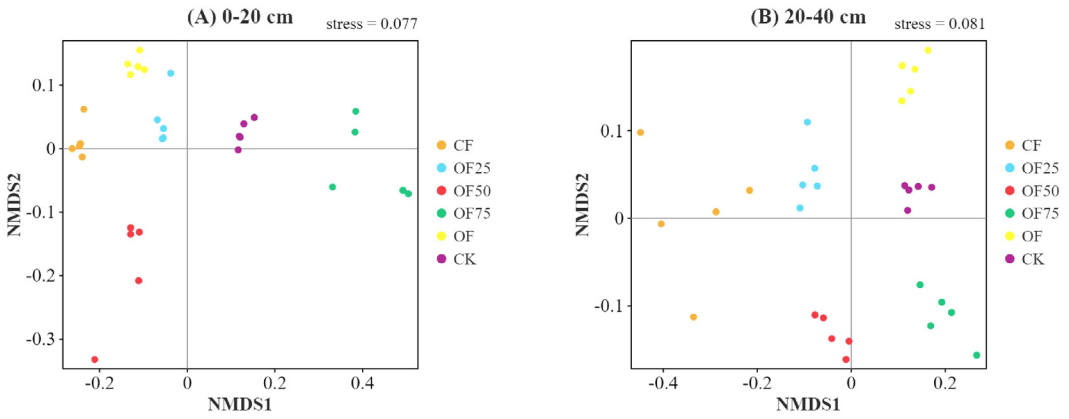

FIGURE 3
Changes in soil bacterial beta diversity in **(A)** 0-20 cm and **(B)** 20-40 cm soil layers in based on the Bray-Curtis distance Moso bamboo forests treated with different fertilizers at the ASV level.

Soil quality evaluation and its correlation with bamboo shoot yield

The SQI of the six treatments followed the order OF75 > OF50 > OF > OF25 > CF > CK in the 0–20 cm soil layer and OF50 > OF > OF75 > OF25 > CK > CF in the 20–40 cm soil layer (Figures 9A, B). Moreover, in the 0–40 cm soil layer, SQI was significantly higher in OF50 and OF75 than that in CF and CK (Figure 9C). Correlation analysis showed a significant positive correlation between SQI and bamboo yield ($p< 0.05$, Figure 9D).

SEM analysis showed that the fertilization treatments had direct and indirect effects on soil properties, SQI, and bamboo shoot yield (GFI = 0.855, df =28, Figure 10). The fertilization treatments had positive and indirect effects on SQI by positively affecting SOC and negatively affecting AN and AP. Additionally, the fertilization treatments had negative effects on AN, AP, and bacterial diversity. Bacterial diversity had a positive effect on enzymatic activities (SC, UE, and ACP), which had direct significant positive effects on SOC ($p< 0.001$), AN ($p< 0.001$), and AP ($p< 0.001$). Finally, SQI had a significant positive effect on bamboo shoot yield ($p< 0.01$).

Discussion

Impacts of different fertilization treatments on soil chemical properties

Our results indicated that after adding different SEOF treatments (OF25, OF50, OF75, and OF) to the soil for two years, the soil pH increased compared with that of CK (Table 2) because SEOF is alkaline and can reduce soil acidification. Zhang et al. (2019) reported that soil acidification is more effectively alleviated by applying high proportions of organic fertilizer than by applying lower proportions. The SOC content of OF50, OF75, and OF were significantly higher than those of CK and CF in the 0–20 cm and 20–40 cm soil layers, respectively. Possible reasons for the increase in soil C stocks are as follows: first, the C content of the SEOF used in this experiment was 40 %; and second, the input of organic carbon and organic matter from the SEOF increased microbial activity and metabolites which is beneficial for the conversion of exogenous carbon into SOC, further promoting the accumulation of SOC (Wang et al., 2015). The combination of chemical and organic fertilizers can increase crop biomass and the input of fresh organic matter into the soil and crop root exudates, further improving the accumulation and fixation of SOC (Yu et al., 2012).

Decreasing the application of CF and applying organic fertilizer as an alternative increased the soil nutrient availability, which is consistent with the results of previous studies (Chen et al., 2020; He et al., 2022; Luo et al., 2018; Ying et al., 2023; Lu et al., 2024). In this study, SEOF effectively improved soil nutrient availability, as shown by the increased levels of soil nutrients (e.g., TN, TP, AN, and AP) compared with CK and CF (Table 2). Similarly, previous studies have reported that a combination of chemical and organic fertilizers improves soil fertility (Li et al., 2023b; Liu et al., 2021). The increased availability of N and P in the soil is partly due to the slow release of nutrients from organic fertilizers. Organic acids generated during organic material decomposition can promote nutrient release, thereby improving the effectiveness of soil nutrients (Cheng et al., 2024). In addition, the large amount of organic matter input from organic fertilizers increases the availability of substrates for microorganisms, which enhances microbial activity, accelerates the decomposition of animal and plant residues, converts soil organic N into inorganic N, and releases effective nutrients for plant utilization (Ning et al., 2017). Applying organic fertilizers also promotes the activation of inorganic P in the soil and increases the AP content (Ying et al., 2023).

Impacts of different fertilization treatments on soil enzyme activities

Soil enzymes are indicators of soil quality and are mainly derived from soil microorganisms, animal and plant residues, and organic fertilizers (Ni et al., 2021). Soil enzyme activities are closely related to SOC decomposition, nutrient mineralization, and plant

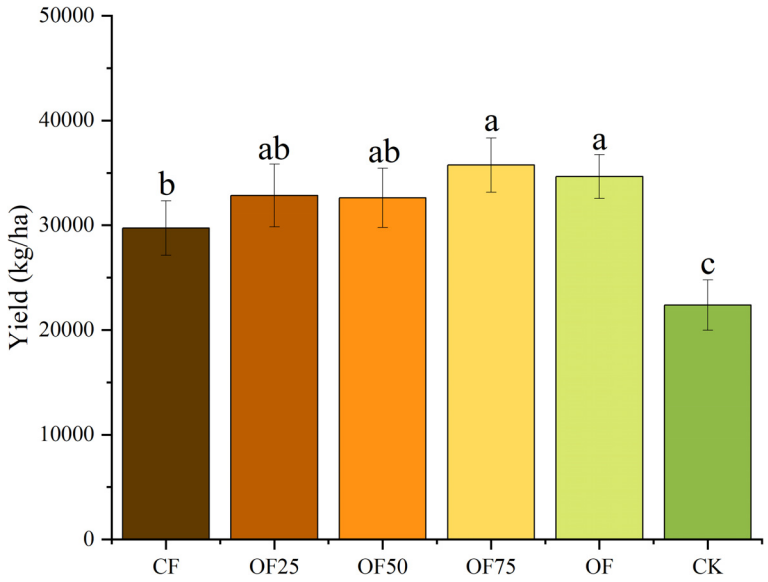

FIGURE 4
Changes in bamboo shoot yield under different fertilization treatments. Different lowercase letters indicate significant differences ($p < 0.05$) between treatments.

nutrient absorption and utilization, and they are highly sensitive to external environmental changes (Ni and Su, 2024). Applying SEOF increased soil SC activity, which catalyzes the hydrolysis of sucrose into fructose and glucose for plant absorption and utilization. SC also participates in the mineralization of organic carbon, and its activity is closely related to SOC content (Ni et al., 2024b). The SC and ACP activities of OF75 were highest in the 0–20 cm soil layer, which indicates that applying a combined fertilizer with a high proportion of organic fertilizer improved soil enzyme activities. Phosphatases are important, because they provide P for plant uptake by releasing phosphate ion from immobile organic P (Liu et al., 2010). Urease catalyzes the hydrolysis of urea to CO_2 and NH_3. UE activity was significantly higher in OF25, OF50, and OF75 than in CF in the 0–40 cm soil layer (Figure 1), indicating that applying a certain amount of SEOF promoted the hydrolysis of urea, which in turn improves soil N availability and N supply capacity. Similar results have also been reported by other researches, who found organic fertilizer had strongly effect on the urease activity (Saha et al., 2008; Liu et al., 2010).

The increase in soil enzyme activity after organic fertilizer treatment may be because of the increased concentrations of organic matter. In addition, the increase in nutrient availability can also stimulate microbial growth (Zhang et al., 2019). On the other hand, the decrease in soil enzyme activity after CF treatment may be because of the changes in the microbial community structure caused by the acidification induced by chemical fertilizers (Zhang et al., 2019). Another study also reported that adding chemical fertilizer negatively influenced both acid and alkaline phosphatase activities (Saha et al., 2008), which is consistent with our findings.

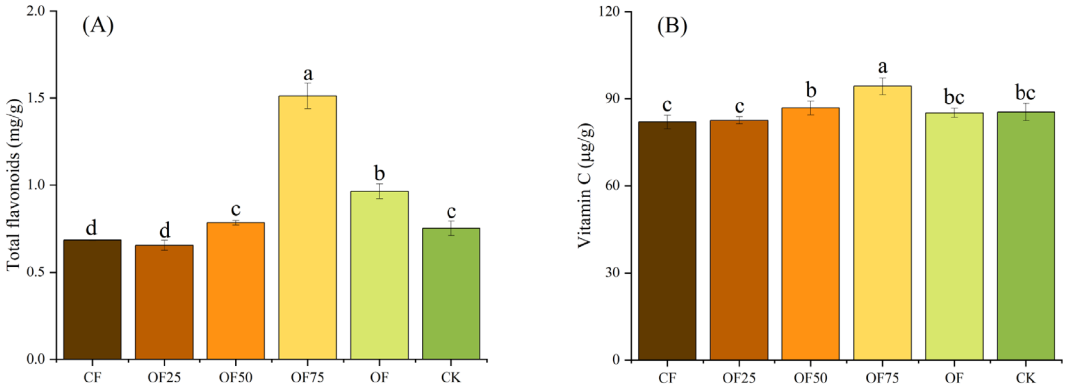

FIGURE 5
The effects of different fertilization treatments on the nutritional qualities [**(A)** Total flavonoids, **(B)** Vitamin C] of bamboo shoots. Different lowercase letters indicate significant differences ($p < 0.05$) between treatments.

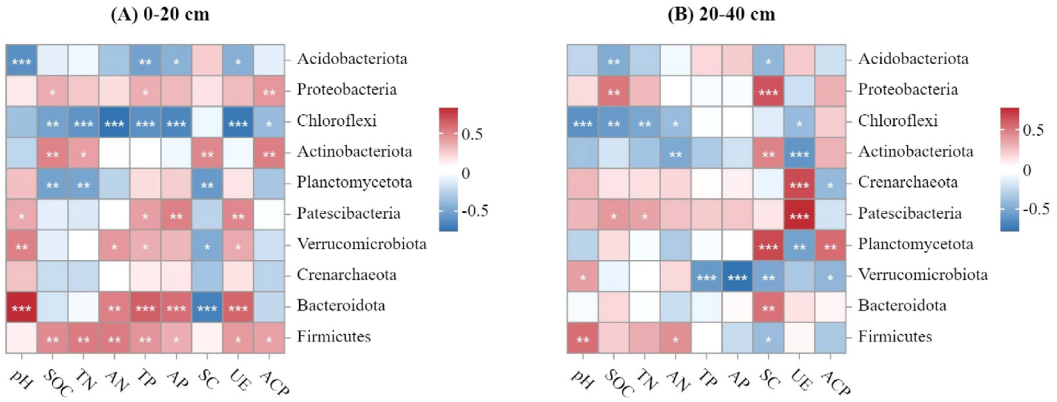

FIGURE 6
Correlation heatmap of soil bacterial community compositions (phylum level) and soil properties in **(A)** 0-20 cm and **(B)** 20-40 cm soil layers in Moso bamboo forests. (*p<0.05, **p<0.01, ***p<0.001).

Impacts of different fertilization treatments on soil bacterial community structures

Microbial community structures respond to different fertilization treatments. Our study showed that adding fertilizer significantly changed the α–diversity of the soil bacterial community based on the community indices. In the 0–40 cm soil layer, the ACE and Chao1 indices of OF50 were significantly higher than those OF and CK, indicating that apply 50% organic substitution improved the bacterial community richness. The enhanced richness of bacterial under organic and compound fertilization was consistent with other papers (Hartmann et al., 2015), and confirmed that variation of community mainly attributed to quality of the organic fertilizers. These results are similar to the studies, which showed that fertilization can directly enrich specific microbial communities or indirectly affect bacterial composition by altering soil characteristics (Guo et al., 2018).

The main bacterial phyla in all treatments were Acidobacteria, Proteobacteria, Chloroflexi, and Actinobacteria (Figure 2), which is similar to the results of a previous study (Ni et al., 2024c). This is mainly because a large amount of nutrient input can stimulate the growth of microorganisms in the soil (Ying et al., 2023). However, in our study, the relative abundance of Acidobacteria decreased, and that of Proteobacteria increased after treatment with a higher proportion of organic fertilizer. Some studies have demonstrated that adding organic fertilizer primarily decreases oligotrophic taxa, such as Chloroflexi and Acidobacteria, and increases copiotrophic taxa, such as Bacteroidetes and Proteobacteria (Li et al., 2021a; Zeng et al., 2016). These changes are consistent with the copiotrophic hypothesis, which states that under nutrient-rich conditions, faster-growing copiotrophic taxa increase whereas slower-growing oligotrophic taxa decline (Fierer et al., 2012; Ying et al., 2023). In addition, Actinobacteria enriched the soil after organic fertilizer treatment because they rapidly decompose organic matter and convert it into available nutrients (N, P, and K) that plants can use, thereby providing nutrients for plant growth (Ni et al., 2024c; Yang et al., 2023). Therefore, we speculate that applying organic fertilizers may affect the bacterial community structure through various soil factors, such as soil pH, enzyme activity, and nutrient bioavailability.

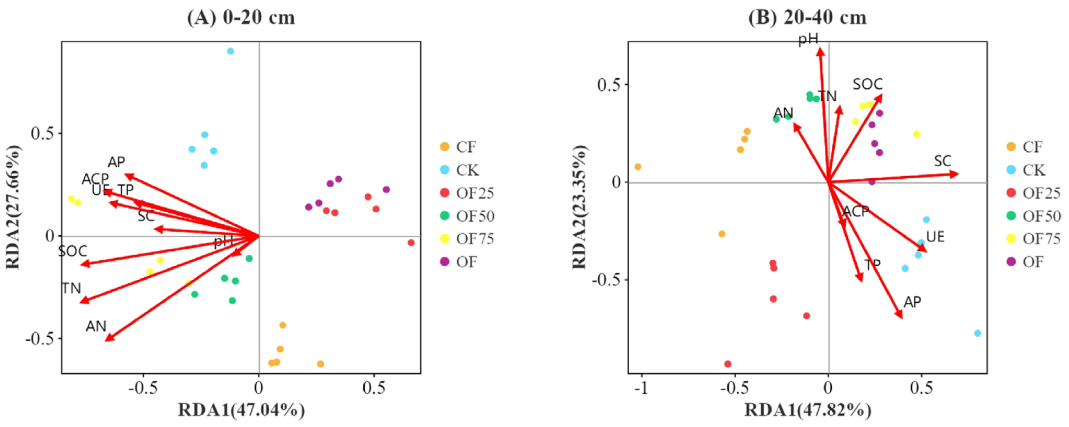

FIGURE 7
Redundancy analysis (RDA) of soil bacterial community (ASV level) and soil properties for individual samples in **(A)** 0-20 cm and **(B)** 20-40 cm soil layers.

10.3389/fpls.2025.1550946

TABLE 4 Environmental factors affecting soil bacterial communities in Moso bamboo forests.

Envfit	R^2	*p*–value	R^2	*p*–value
	0–20 cm		20–40 cm	
pH	0.0168	0.8	0.4041	0.003
SOC	0.5302	0.001	0.2409	0.018
TN	0.622	0.001	0.1287	0.165
AN	0.6293	0.001	0.1009	0.248
TP	0.2612	0.015	0.2428	0.029
AP	0.348	0.005	0.5475	0.002
SC	0.1682	0.074	0.4188	0.002
UE	0.3692	0.005	0.3401	0.003
ACP	0.4137	0.001	0.0474	0.506

Bamboo shoot yield and quality and their relationship with soil quality

In our study, OF75 and OF increased the bamboo shoot yield by 20.23 % and 16.55 %, respectively, compared with CF (Figure 4). This indicates that adding a certain amount of SEOF increased the yield of bamboo shoots. This is consistent with previous studies, which demonstrated that adding organic fertilizer can increase crop yield (He et al., 2022; Liu et al., 2021; Ni et al., 2024b). Organic fertilizer improved soil structure, capacity to preserve moisture and fertility, and microbial activity, thereby providing better growth conditions for crops (Liu et al., 2010; Liu et al., 2022b). In addition, the process of slow decomposition and nutrient release of organic materials provides more continuous nutrient supply for crop growth (Gai et al., 2018; Li et al., 2021b). Fertilization enhances plant growth and development and improves plant quality by increasing nutrients like vitamin C and total flavonoids (He et al., 2022). In our study, applying organic fertilizer (OF75, OF) significantly increased the total flavonoid and vitamin C content of bamboo shoots and improved their nutritional value compared with applying CF alone.

Several workers had shown that environmental factors significantly impact the abundance, diversity, and function of soil microorganisms (Ge et al., 2021; Yang et al., 2023). In this study, redundancy analysis showed that SOC, TP, AP, and UE were strongly correlated with soil bacterial communities (Figure 7, Table 4). In the 20–40 cm soil layer, the correlation heatmap showed a significant positive correlation between Acidobacteria, Proteobacteria, and SOC (Figure 6). Acidobacteria and Proteobacteria are primarily involved in organic matter decomposition and biological N fixation. Chloroflexi is a bacterial phylum that generates energy through photosynthesis and can break down polysaccharides in soil into organic acids and hydrogen, thereby promoting the degradation of organic matter and cellulose (Ni et al., 2024c). The positive links among SOC, TN, AN, UE, and Chloroflexi demonstrate that Chloroflexi is closely related to C cycling and bamboo forest productivity.

The SQI constructed from multiple soil properties can reflect the effect of fertilization on soil quality (Li et al., 2020; Chen et al., 2021; He et al., 2022). Our study showed that the SQI of OF75 was highest, and followed by OF50 in the 0–40 cm soil layer. All treatments involving the organic fertilizers showed an increased SQI, indicating that any combination of reduced compound fertilizer containing organic fertilizer was superior to a single compound fertilizer. This agrees with the works that in D'Hose et al. (2014). We found that bamboo shoot yield was positively correlated with soil pH, SOC, N, P and SQI (Figures 9, 10), indicating that soil pH and fertility levels affected shoot yield and that yield changes with soil quality. This may be because applying organic fertilizers alleviated soil acidification by providing the nutrients required for bamboo shoot growth and development. Similarly, some studies have reported increased yields of wheat and rice (He et al., 2022; Liu et al., 2022a). Additionally, organic fertilizers have a long-term effect on maintaining soil fertility and the sustainable management of bamboo forests (Li et al., 2023b). Fertilization can be expected to increased plant growth either directly or indirectly via influence the soil nutrients, activities and microbial communities. Our SEM analysis showed that fertilization treatments had a positive and indirect effect on SQI by positively affecting SOC and that SQI had a positive effect on bamboo yield (Figure 10). These results demonstrate that decreasing CF and

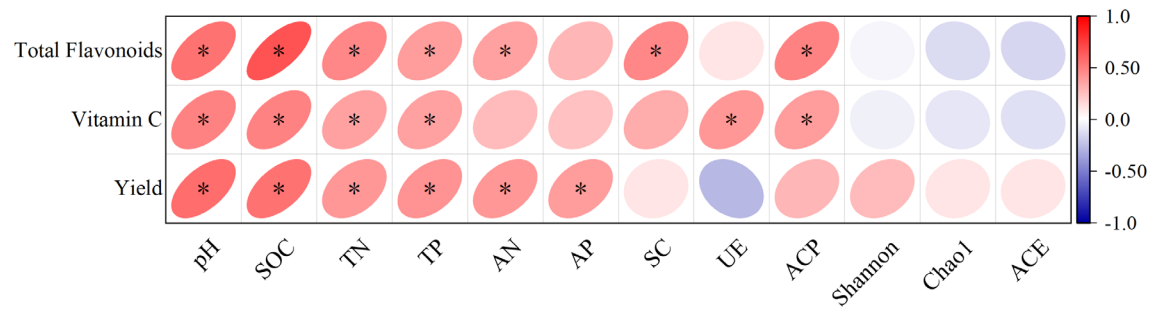

FIGURE 8
Pearson's correlation for testing the association among bamboo shoot qualities, yield and soil properties in Moso bamboo forests treated with different fertilizers. (*p<0.05).

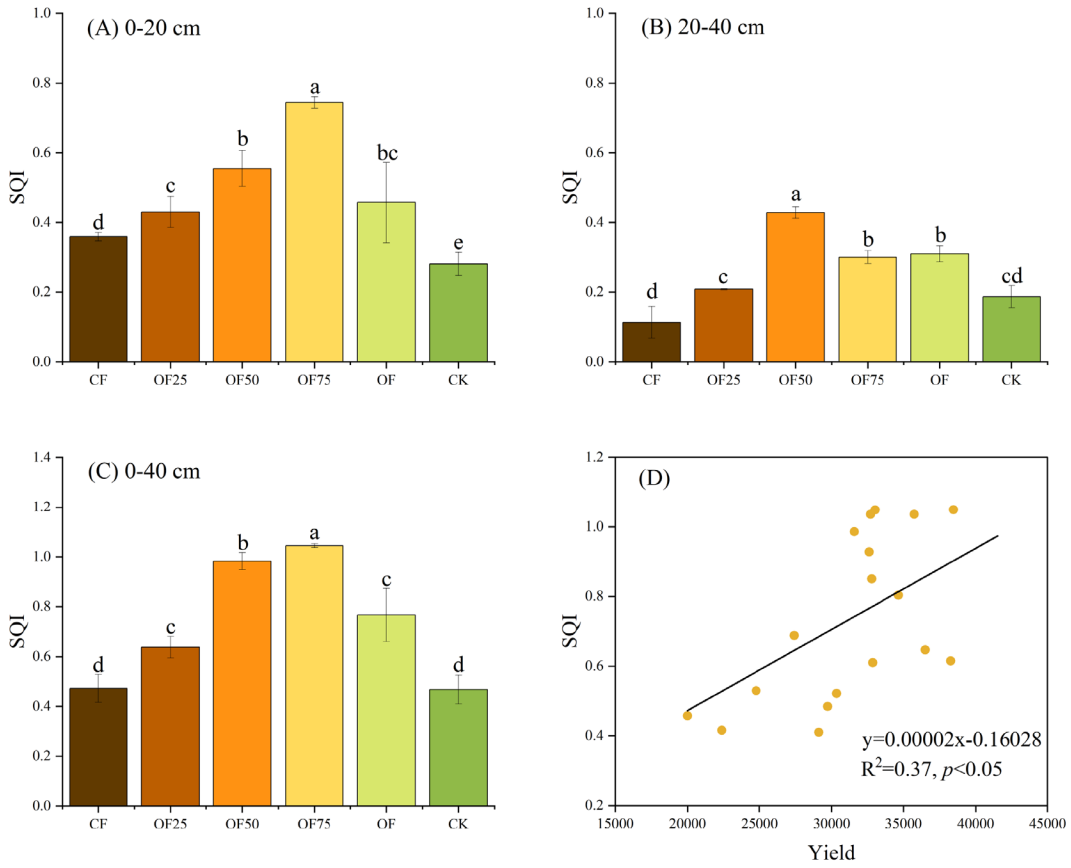

FIGURE 9
Effects of different fertilizer treatments on soil quality index (SQI, **(A)** 0–20 cm, **(B)** 20–40 cm, **(C)** 0–40 cm) and its correlation with bamboo shoot yield **(D)**. Different lowercase letters indicate significant differences ($p < 0.05$) between treatments.

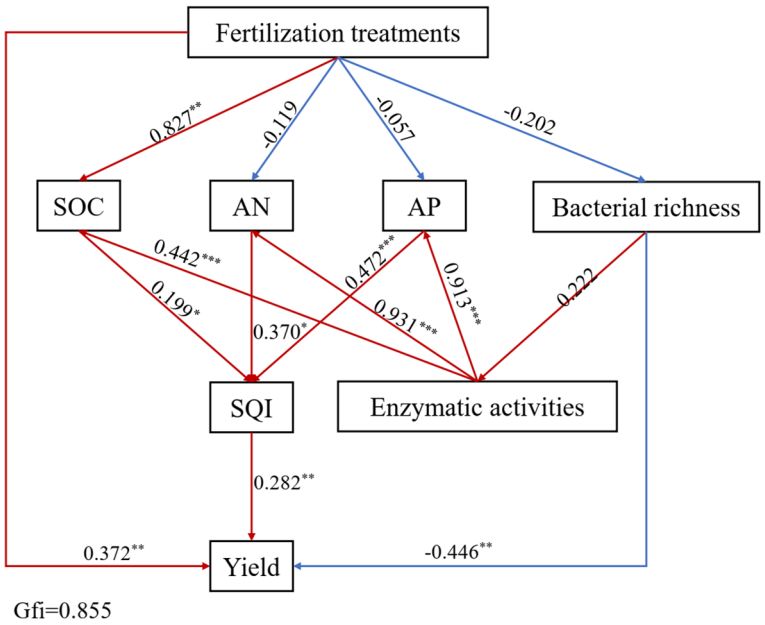

FIGURE 10
Structural equation modeling (SEM) analysis performed to evaluate pathways of fertilizer treatments influence on the bamboo yield, soil properties, enzymatic activities, bacterial diversity and SQI in the 0–40 cm soil layer. Red and blue arrows indicate significantly ($p<0.05$) positive and negative relationships, respectively. Numbers on arrows represent standardized path coefficients. (*$p<0.05$, **$p<0.01$, ***$p<0.001$).

applying organic fertilizer as an alternative increased bamboo shoot yield by improving soil quality. This agrees with previous studies reporting that improving soil quality is beneficial for increasing crop yields (wheat and maize) (Li et al., 2020; Pan et al., 2020). Li et al. (2021b) reported that organic fertilizer addition increased yield and soil quality compared with adding chemical fertilizers alone in a double cropping system in China, which is consistent with our findings. Moreover, fertilization promoted enzyme activity by affecting bacterial diversity, thereby enhancing soil quality and bamboo shoot yield (Figure 10). These results indicate that the changes in soil nutrient status and microbial community caused by organic fertilizers are closely related and may work together to improve yield (Liu et al., 2021).

The impact of organic fertilizer application on soil improvement and bamboo shoot yield is a long-term and slow process. This experiment was only conducted for 2 years, and long-term monitoring experiments should be conducted in the future to more comprehensively evaluate the effect of applying organic fertilizer on soil quality, shoot yield, and shoot quality in Moso bamboo forests.

Conclusions

Our study highlighted that adding organic fertilizers improved the quality of the soil and the yield of the bamboo shoots. Compared with CF addition alone, the combined application of CF and organic fertilizer increased soil pH, SOC, N, and P availability, and the activities of enzymes related to C, N, and P cycling. Organic fertilizer substitution also significantly changed the soil bacterial community structure and increased the relative abundance of beneficial bacteria, such as Proteobacteria and Actinobacteria. Higher proportions of organic fertilizer substitution (OF75, OF) enhanced the bamboo shoot yield (by 20.23 % and 16.55 %, respectively) and their total flavonoid and vitamin C content, compared to CF. In addition, SEM revealed that fertilization affected soil enzyme activities through soil microorganisms, thereby affecting soil nutrient availability and promoting SQI and bamboo shoot yield. Moreover, the SQI of OF75 and OF50 was significantly higher than that of OF and OF25 in the 0–40 cm soil layer. In conclusion, our study revealed that SEOF production is advisable for improving soil quality and bamboo shoot yield.

Data availability statement

The raw data supporting the conclusions of this article will be made available by the authors, without undue reservation.

Author contributions

ZY: Conceptualization, Writing – original draft. JZ: Writing – original draft, Investigation. HN: Funding acquisition, Writing – review & editing.

Funding

The author(s) declare that financial support was received for the research and/or publication of this article. This work was supported by the Special Project of Zhejiang Provincial Scientific Research Institutes (2023F1068-1) and Forestry Science and Technology Project of Zhejiang Province (2023SY12).

Conflict of interest

The authors declare that the research was conducted in the absence of any commercial or financial relationships that could be construed as a potential conflict of interest.

Generative AI statement

The author(s) declare that no Generative AI was used in the creation of this manuscript.

Publisher's note

All claims expressed in this article are solely those of the authors and do not necessarily represent those of their affiliated organizations, or those of the publisher, the editors and the reviewers. Any product that may be evaluated in this article, or claim that may be made by its manufacturer, is not guaranteed or endorsed by the publisher.

References

Callahan, B. J., Mcmurdie, P. J., Rosen, M. J., Han, A. W., Johnson, A. J. A., and Holmes, S. P. (2016). DADA2: High-resolution sample inference from Illumina amplicon data. *Nat. Methods.* 13 (7), 581–583. doi: 10.1038/nmeth.3869

Chen, Q. L., Ding, J., Zhu, D., Hu, H. W., Delgado-Baquerizo, M., Ma, Y.-B., et al. (2020). Rare microbial taxa as the major drivers of ecosystem multifunctionality in long-term fertilized soils. *Soil Biol. Biochem.* 141, 107686. doi: 10.1016/j.soilbio.2019.107686

Chen, Q. Y., Liu, Z. J., Zhou, J. B., Xu, X. P., and Zhu, Y. J. (2021). Long-term straw mulching with nitrogen fertilization increases nutrient and microbial determinants of soil quality in a maize-wheat rotation on China's Loess Plateau. *Sci. Total Environ.* 775, 145930. doi: 10.1016/j.scitotenv.2021.145930

Chen, X. P., Xie, Y. J., Luo., G. E., and Shi, W. G. (2011). Silkworm excrement organic fertilizer: Its nutrient properties and application effect. *Chin. J. Appl. Ecol.* 22, 1803–1809. doi: 10.13287/j.1001-9332.2011.0253

Cheng, Q., Mao, X. L., Sun, T., Wang, X. J., Ma, Q. X., and Wu, L. H. (2024). Effects of long-term combined application of chemical fertilizers with different organic materials on soil microbial ecological stoichiometry and community structure. *J. Plant Nutr. Fertil.* 30, 209–220. doi: 10.11674/zwyf.2023398

D'Hose, T., Cougnon, M., De Vliegher, A., Vandecasteele, B., Viaene, N., Cornelis, W., et al. (2014). The positive relationship between soil quality and crop production: A case study on the effect of farm compost application. *Appl. Soil Ecol.* 75, 189–198. doi: 10.1016/j.apsoil.2013.11.013

Fierer, N., Lauber, C. L., Ramirez, K. S., Zaneveld, J., Bradford, M. A., and Knight, R. (2012). Comparative metagenomic, phylogenetic and physiological analyses of soil microbial communities across nitrogen gradients. *ISME J.* 6, 1007–1017. doi: 10.1038/ismej.2011.159

Gai, X. P., Liu, H. B., Liu, J., Zhai, L. M., Yang, B., Wu, S. X., et al. (2018). Long-term benefits of combining chemical fertilizer and manure applications on crop yields and soil carbon and nitrogen stocks in North China Plain. *Agric. Water Manage.* 208, 384–392. doi: 10.1016/j.agwat.2018.07.002

Ge, Z., Li, S. Y., Bol, R., Zhu, P., Peng, C., An, T. T., et al. (2021). Differential long-term fertilization alters residue-derived labile organic carbon fractions and microbial community during straw residue decomposition. *Soil Tillage Res.* 213, 105120. doi: 10.1016/j.still.2021.105120

Guo, J., Liu, W., Zhu, C., Luo, G., Kong, Y., Ling, N., et al. (2018). Bacterial rather than fungal community composition is associated with microbial activities and nutrient-use efficiencies in a paddy soil with short-term organic amendments. *Plant Soil* 424, 335–349. doi: 10.1007/s11104-017-3547-8

Hartmann, M., Frey, B., Mayer, J., Mäder, P., and Widmer, F. (2015). Distinct soil microbial diversity under long-term organic and conventional farming. *ISME J.* 9, 1177–1194. doi: 10.1038/ismej.2014.210

He, H., Peng, M. W., Lu, W. D., Hou, Z. N., and Li, J. H. (2022). Commercial organic fertilizer substitution increases wheat yield by improving soil quality. *Sci. Total Environ.* 851, 158132. doi: 10.1016/j.scitotenv.2022.158132

Li, P., Fu, H. T., Zhang, F. B., Pang, Y. W., Huang, Q. Y., and Tang, S. H. (2015). Effects of silkworm excrement-derived organic fertilizer on yield and quality of crops and soil property. *J. South. Agric.* 46, 1195–1199. doi: 10.3969/j:issn.2095-119.2015.7.1195

Li, P., Kong, D., Zhang, H., Xu, L., Li, C., Wu, M., et al. (2021a). Different regulation of soil structure and resource chemistry under animal and plant-derived organic fertilizers changed soil bacterial communities. *Appl. Soil Ecol.* 165, 104020. doi: 10.1016/j.apsoil.2021.104020

Li, P., Li, Y. B., Xu, L. Y., Zhang, H. J., Shen, X. S., Xu, H. F., et al. (2021b). Crop yield soil quality balance in double cropping in China's upland by organic amendments: a meta-analysis. *Geoderma* 403, 115197. doi: 10.1016/j.geoderma.2021.115197

Li, X., Qiao, L., Huang, Y. P., Li, D. C., Xu, M. G., Ge, T. D., et al. (2023a). Manuring improves soil health by sustaining multifunction at relatively high levels in subtropical area. *Agr. Ecosyst. Environ.* 353, 108539. doi: 10.1016/j.agee.2023.108539

Li, J., Wu, X. P., Gebremikael, M. T., Wu, H. J., Cai, D. X., Wang, B. S., et al. (2018). Response of soil organic carbon fractions, microbial community composition and carbon mineralization to high-input fertilizer practices under an intensive agricultural system. *PloS One* 13, 1–156. doi: 10.1371/journal.pone.0195144

Li, P., Wu, M. C., Kang, G. D., Zhu, B. J., Li, H. X., Hu, F., et al. (2020). Soil quality response to organic amendments on dryland red soil in subtropical China. *Geoderma* 373, 114416. doi: 10.1016/j.geoderma.2020.114416

Li, Y. L., Wu, L., Tang, L. Y., Ren, F. L., Wang, X. H., Zhu, P., et al. (2023b). Manure application decreases soil organic carbon priming by increasing mineral protection and nitrogen availability. *Geoderma* 439, 116676. doi: 10.1016/j.geoderma.2023.116676

Liu, H. W., Du, X. F., Li, Y. B., Han, X., Li, B., Zhang, X. K., et al. (2022b). Organic substitutions improve soil quality and maize yield through increasing soil microbial diversity. *J. Clean. Prod.* 347, 131323. doi: 10.1016/j.jclepro.2022.131323

Liu, M., Linna, C., Ma, S. M., Ma, Q., Song, W. F., Shen, M. Z., et al. (2022a). Biochar combined with organic and inorganic fertilizers promoted the rapeseed nutrient uptake and improved the purple soil quality. *Front. Nutri.* 9. doi: 10.3389/fnut.2022.997151

Liu, J. A., Shu, A. P., Song, W. F., Shi, W. C., Li, M. C., Zhang, W. X., et al. (2021). Long-term organic fertilizer substitution increases rice yield by improving soil properties and regulating soil bacteria. *Geoderma* 404, 115287. doi: 10.1016/j.geoderma.2021.115287

Liu, E. K., Yan, C. R., Mei, X. R., He, W. Q., Bing, S. H., Ding, L. P., et al. (2010). Long-term effect of chemical fertilizer, straw, and manure on soil chemical and biological properties in northwest China. *Geoderma* 158, 173–180. doi: 10.1016/j.geoderma.2010.04.029

Lu, W. D., Hao, Z. Q., Ma, X. L., Gao, J. L., Fan, X. Q., Guo, J. F., et al. (2024). Effects of different proportions of organic fertilizer replacing chemical fertilizer on soil nutrients and fertilizer utilization in gray desert soil. *Agronomy* 14, 228. doi: 10.3390/agronomy14010228

Luo, G., Rensing, C., Chen, H., Liu, M., Wang, M., Guo, S., et al. (2018). Deciphering the associations between soil microbial diversity and ecosystem multifunctionality driven by long-term fertilization management. *Funct. Ecol.* 32, 1103–1116. doi: 10.1111/1365-2435.13039

Luo, Z., Zhang, Y. T., Shen, H., and Guo, T. (2011). Effect of organic fertilizer from fermented silkworm excrement on the growth and quality of Tobacco. *Sci. Sericult.* 37, 775–779. doi: 10.13441/j.cnki.cykx.2011.04.012

Moe, K., Htwe, A. Z., Thu, T. T. P., Kajihara, Y., and Yamakawa, T. J. A. (2019). Effects on NPK status, growth, dry matter and yield of rice (*Oryza sativa*) by organic fertilizers applied in field condition. *Agr* 9, 109. doi: 10.3390/agriculture9050109

Ni, H. J., and Su, W. H. (2024). Spatial distribution of fine root traits in relation to soil properties and aggregate stability of intensively managed Moso bamboo (*Phyllostachys edulis*) plantations in subtropical China. *Plant Soil* 2024, 498(1-2):487–503. doi: 10.1007/s11104-023-06449-x

Ni, H. J., Su, W. H., Fan, S. H., and Chu, H. Y. (2021). Effects of intensive management practices on rhizosphere soil properties, root growth, and nutrient uptake in Moso bamboo plantations in subtropical China. *For. Ecol. Manage.* 493, 119083. doi: 10.1016/j.foreco.2021.119083

Ni, H. J., Zhao, J. C., and Yang, Z. Y. (2024c). Effects of compound fertilizer decrement and water-soluble humic acid fertilizer application on soil properties, bacterial community structure, and shoot yield in Lei bamboo (*Phyllostachys praecox*) plantations in subtropical China. *Forests* 15, 400. doi: 10.3390/f15030400

Ni, H. J., Zhao, J. C., Yang, Z. Y., Shi, J., Chen, Y. J., Wu, Y. F., et al. (2024b). The effects of organic fertilizer derived from silkworm excrement on the soil physicochemical properties and enzyme activity of *Phyllostachys Violascens* 'Prevernalis' Forests. *J. Northeast forestry Univ.* 52, 109114. doi: 10.13759/j.cnki.dlxb.2024.09.002

Ni, H. J., Zhao, J. C., and Zhong, J. P. (2024a). The effect of silkworm sand organic fertilizer on the yield and quality of Lei bamboo (*Phyllostachys praecox*) shoots. *J. Zhejiang For Sci. Technol.* 2024, 44(05):8085. doi: 10.3969/j.issn.1001-3776.2024.05.010

Ning, Q., Chen, L., Jia, Z., Zhang, C., Ma, D., Li, F., et al. (2020). Multiple long-term observations reveal a strategy for soil pH-dependent fertilization and fungal communities in support of agricultural production. *Agric. Ecosyst. Environ.* 293, 106837. doi: 10.1016/j.agee.2020.106837

Ning, C. C., Gao, P. D., Wang, B. Q., Lin, W. P., Jiang, N. H., and Cai, K. Z. (2017). Impacts of chemical fertilizer reduction and organic amendments supplementation on soil nutrient, enzyme activity and heavy metal content. *J. Integr. Agric.* 16, 1819–1831. doi: 10.1016/S2095-3119(16)61476-4

Oladele, S. O., Adeyemo, A. J., and Awodun, M. A. (2019). Influence of rice husk biochar and inorganic fertilizer on soil nutrients availability and rain-fed rice yield in two contrasting soils. *Geoderma* 336, 1–11. doi: 10.1016/j.geoderma.2018.08.025

Pan, J. X., Shang, Y. W., Zhang, W. J., Chen, X. P., and Cui, Z. L. (2020). Improving soil quality for higher grain yields in Chinese wheat and maize production. *Land Degrad. Dev.* 31, 1125–1137. doi: 10.1002/ldr.3515

Peng, S. M., Wang, B. L., Xu, J. Z., Ding, Z. S., and Yuan, X. F. (2015). Effects of organic fertilizer from fermented Silkworm excrement Application on Soil Microorganisms of Chrysanthemum Morifolium under continuous Cropping. *Zhejiang Instit. Tradit. Chin. Med.* 2), 77–83. doi: 10.16466/j.issn1005-5509.2015.02.001

Pruesse, E., Quast, C., Knittel, K., Fuchs, B. M., Ludwig, W., Peplies, J., et al. (2007). SILVA: a comprehensive online resource for quality checked and aligned ribosomal RNA sequence data compatible with ARB. *Nucleic Acids Res.* 35, 7188–7196. doi: 10.1093/nar/gkm864

Saha, S., Prakash, V., Kundu, S., and Kumar, N. (2008). Soil enzymatic activity as affected by long term application of farm yard manure and mineral fertilizer under a rainfed soybean-wheat system in N-W Himalaya. *Eur. J. Soil Biol.* 44, 309–315. doi: 10.1016/j.ejsobi.2008.02.004

Shahid, M., Nayak, A. K., Puree, C., Tripathi, R., Lal, B., Gautam, P., et al. (2017). Carbon and nitrogen fractions and stocks under 41 years of chemical and organic fertilization in a sub-humid tropical rice soil. *Soil Tillage Res.* 170, 136–146. doi: 10.1016/j.still.2017.03.008

Shankar, K. S., Sumathi, S., Shankar, M., Rani, K. U., and Reddy, N. N. (2013). Effect of organic farming on nutritional profile, quality characteristics and toxic parameters of amaranthus. *Indian J. Hortic.* 70, 378–382. doi: 10.1016/j.scienta.2013.07.023

Shao, G. D., Xu, Y., Zhou, J., Tian, P., Ai, J. J., Yang, Y. D., et al. (2024). Enhanced soil organic carbon stability in rhizosphere through manure application. *Soil Tillage Res.* 244, 106223. doi: 10.1016/j.still.2024.106223

Song, X. Z., Zhou, G. M., Jiang, H., Yu, S., Fu, J., Li, W., et al. (2011). Carbon sequestration by Chinese bamboo forests and their ecological benefits: Assessment of potential, problems, and future challenges. *Environ. Rev.* 19, 418–428. doi: 10.1139/a11-015

Tang, H., Xiao, X., Tang, W., Li, C., Wang, K., Li, W., et al. (2018). Long–term effects of NPK fertilizers and organic manures on soil organic carbon and carbon management index under a double-cropping rice system in Southern China. *Commun. Soil Sci. Plant Anal.* 49, 1976–1989. doi: 10.1080/00103624.2018.1492600

Wang, C. L., Ma, Y. Q., He, W. H., Kuzyakov, Y., Bol, R., Chen, H. Q., et al. (2024). Soil quality and ecosystem multifunctionality after 13–year of organic and nitrogen fertilization. *Sci. Total Environ.* 931, 172789. doi: 10.1016/j.scitotenv.2024.172789

Wang, J. H., Wang, X. J., Xu, M. G., Feng, G., Zhang, W. J., and Lu, C. A. (2015). Crop yield and soil organic matter after long-term straw return to soil in China. *Nutr. Cycl. Agroecosyst.* 102, 371–381. doi: 10.1007/s11027-014-9564-5

Yang, C. B., Ni, H. J., Zhong, Z. K., Zhang, X. P., and Bian, F. Y. (2019). Changes in soil carbon pools and components induced by replacing secondary evergreen broadleaf forest with Moso bamboo plantations in subtropical China. *Catena* 180, 309–319. doi: 10.1016/j.catena.2019.02.024

Yang, L. H., Sun, R. H., Li, J. G., Zhai, L. M., Cui, H. L., Fan, B. Q., et al. (2023). Combined organic-inorganic fertilization builds higher stability of soil and root microbial networks than exclusive mineral or organic fertilization. *Soil Ecol. Lett.* 5, 220142. doi: 10.1007/s42832-022-0142-6

Yang, Q. S., Xu, L. F., Guo, D. Q., Qi, J. S., Zhao, J. J., and Zhou, N. (2022). Effect of fermented silkworm excrement fertilizer on yield and quality of Corydalis yanhusuo W.T. wang under continuous cropping. *Sci. Sericult.* 48, 77–82. doi: 10.13441/j.cnki.cykx.2022.01.011

Yang, Q. Y., and Zhang, M. K. (2023). Effect of bio-organic fertilizers partially substituting chemical fertilizers on labile organic carbon and bacterial community of citrus orchard soils. *Plant Soil* 483, 255–272. doi: 10.1007/s11104-022-05735-4

Yao, Y., Cao, S., Gong, X., Singh, B. P., Fang, Y., Ge, T., et al. (2022). Intensive management of a bamboo forest significantly enhanced soil nutrient concentrations but decreased soil microbial biomass and enzyme activity: a long-term chronosequence study. *J. Soils Sedim.* 22, 2640–2653. doi: 10.1007/s11368-022-03253-5

Ying, D., Chen, X. L., Hou, J. F., Zhao, F. C., and Li, P. (2023). Soil properties and microbial functional attributes drive the response of soil multifunctionality to long-term fertilization management. *Appl. Soil Ecol.* 192, 105095. doi: 10.1016/j.apsoil.2023.105095

Yu, H., Ding, W., Luo, J., Geng, R., Ghani, A., and Cai, Z. (2012). Effects of long-term compost and fertilizer application on stability of aggregate-associated organic carbon in an intensively cultivated sandy loam soil. *Bio. Fert. Soils.* 48, 325–336. doi: 10.1007/s00374-011-0629-2

Zeng, J., Liu, X., Song, L., Lin, X., Zhang, H., Shen, C., et al. (2016). Nitrogen fertilization directly affects soil bacterial diversity and indirectly affects bacterial community composition. *Soil Biol. Biochem.* 92, 41–49. doi: 10.1016/j.soilbio.2015.09.018

Zhang, Y. L., Sun, C. X., Chen, Z. H., Zhang, G. N., Cheng, L. J., and Wu, Z. J. (2019). Stoichiometric analyses of soil nutrients and enzymes in a Cambisol soil treated with inorganic fertilizers or manures for 26 years. *Geoderma* 353, 382–390. doi: 10.1016/j.geoderma.2019.06.026

Zhou, J., Guan, D. W., Zhou, B. K., Zhao, B. S., Ma, M. C., Qin, J., et al. (2015). Influence of 34–years of fertilization on bacterial communities in an intensively cultivated black soil in northeast China. *Soil Biol. Biochem.* 90, 42–51. doi: 10.1016/j.soilbio.2015.07.005

frontiers | Frontiers in Plant Science

TYPE Original Research
PUBLISHED 05 June 2025
DOI 10.3389/fpls.2025.1584608

Check for updates

OPEN ACCESS

EDITED BY
Amir Ali Khoddamzadeh,
Florida International University, United States

REVIEWED BY
Qianwen Zhang,
Mississippi State University, United States
Boris Pisinov,
Institute for Plant Protection and Environment (IZBIS), Serbia

*CORRESPONDENCE
Huang Fenglan
329341679@qq.com
Zhao Yong
zhao_yong90@126.com

†These authors contributed equally to the work

RECEIVED 27 February 2025
ACCEPTED 07 May 2025
PUBLISHED 05 June 2025

CITATION
Mingjing L, Xuemei H, Rui L, Chunhua Z, Ruimei H, Guibin X, Guorui L, Jianjun D, Cheng W, Xiaohui G, Zhimin S, Ruxin L, Yong Z and Fenglan H (2025) By promoting growth and development, castor bean meal biofertilizer improves the yield and quality of Tartary buckwheat and indirectly improves the growth and development of Tartary buckwheat sprouts. *Front. Plant Sci.* 16:1584608. doi: 10.3389/fpls.2025.1584608

COPYRIGHT
© 2025 Mingjing, Xuemei, Rui, Chunhua, Ruimei, Guibin, Guorui, Jianjun, Cheng, Xiaohui, Zhimin, Ruxin, Yong and Fenglan. This is an open-access article distributed under the terms of the Creative Commons Attribution License (CC BY). The use, distribution or reproduction in other forums is permitted, provided the original author(s) and the copyright owner(s) are credited and that the original publication in this journal is cited, in accordance with accepted academic practice. No use, distribution or reproduction is permitted which does not comply with these terms.

By promoting growth and development, castor bean meal biofertilizer improves the yield and quality of Tartary buckwheat and indirectly improves the growth and development of Tartary buckwheat sprouts

Li Mingjing[1†], Hu Xuemei[1†], Luo Rui[1], Zhang Chunhua[2], Hu Ruimei[2], Xue Guibin[3], Li Guorui[1], Di Jianjun[1], Wang Cheng[1], Gu Xiaohui[1], Su Zhimin[1], Li Ruxin[1], Zhao Yong[4*] and Huang Fenglan[1,5,6,7,8*]

[1]College of Life Science and Food, Inner Mongolia Minzu University, Tongliao, China, [2]Tongliao Scientific Research Institute of Agriculture and Animal Husbandry, Tongliao, China, [3]Beijing Zhongmin Sunshine Biotechnology Co, Beijing, China, [4]College of Life Science, Baicheng Normal University, Baicheng, China, [5]Key Laboratory of Castor Breeding of State Ethnic Affairs Commission, Tongliao, China, [6]Inner Mongolia Key Laboratory of Castor Breeding and Comprehensive Utilization, Tongliao, China, [7]Inner Mongolia Engineering Research Center of Industrial Technology Innovation of Castor, Tongliao, China, [8]Inner Mongolia Industrial Engineering Research Center of Universities for Castor, Tongliao, China

Introduction: Fertilizer selection and application is closely related to crop yield and quality. Tartary buckwheat is a medicinal and food crops, has a broad space for development. However, the effect of castor bean meal biofertilizer on the growth and development, yield and quality of Tartary buckwheat and Tartary buckwheat buds is not clear. The aim of this study was to elucidate the effect of castor bean meal biofertilizer on Tartary buckwheat yield and quality, and then to elucidate the effect of castor bean meal biofertilizer indirectly on Tartary buckwheat bud yield and quality.

Methods: Tong buckwheat 3 as the test material, in 2 years of field trials, no fertilizer, chemical fertilizer and cow manure as a control, a total of 10 types of fertilizer treatment, respectively, CK (0 kg·ha^{-1}), F1, F2, F3 (fertilizer, 225, 300, 375kg·ha^{-1}); N1, N2, N3 (cow manure, 7500, 15000, 22500kg·ha^{-1}); B1, B2, B3 (Castor bean meal biofertilizer, 7500, 15000, 22500kg·ha^{-1}).

Results: (1) under different fertilizer treatments, Tartary buckwheat plant height, stem thickness, the number of main stem nodes, the number of main stem branches, leaf area and chlorophyll content; single plant grain weight, thousand grain weight and yield of castor bean meal biofertilizer treatment is good, and in the B2 treatment to reach the maximum value. (2) under different fertilizer treatments, Tartary buckwheat protein, starch, cellulose, fat, flavonoid fractions and bioflavonoids are B2 treatment when the highest content. (3) Different

fertilization treatments of Tartary buckwheat cultivated Tartary buckwheat buds bud length, fresh weight and dry weight there are significant differences. Tartary buckwheat buds in the 0-16d free amino acids, soluble sugars, total phenols, vitamin C and bioflavonoids content of Tartary buckwheat seeds in the B2 treatment of Tartary buckwheat cultivated Tartary buckwheat buds of the best indicators.

Discussion: In short, this study provides a new fertilization option to improve Tartary buckwheat yield and quality.

KEYWORDS

castor bean meal biofertilizer, Tartary buckwheat, Tartary buckwheat sprouts, yield, quality

1 Introduction

Buckwheat(*Fagopyrum esculentumMoench.*) is an annual dicotyledonous herbaceous plant in the family Polygonaceae and genus *Fagopyrum* (Fan et al., 2021). Buckwheat is widely planted in Asia, Europe, and the Americas and is mainly distributed in China, Russia, France, and Ukraine (Jha et al., 2024). There are three main cultivars of buckwheat in China: common buckwheat, Tartary buckwheat, and sweet buckwheat. Buckwheat planting is distributed mainly in the southwest and northern regions of China. Hure Banner in Tongliao city, Inner Mongolia Autonomous Region, known as the "Hometown of Buckwheat in China", is mainly planted with the Tartary buckwheat(*Fagopyrum tataricum (L.) Gaertn.*) variety (He et al., 2024). Tartary buckwheat is rich in protein, starch, fat, dietary fiber, minerals, vitamins, and a variety of bioactive components (flavonoids, phenolic acids, and alkaloids) (Sonawane et al., 2024). Tartary buckwheat has hypoglycemic, hypolipidemic, antioxidant, anticancer, and antitumor effects and prevents coronary heart disease (Zhang et al., 2012; Gimenez-Bastida and Zielinski, 2015). Therefore, Tartary buckwheat is considered a medicinal and edible crop and has great development and economic value.

Studies have shown that fertilization is the most effective method for improving crop yield and quality (Wang et al., 2020). The application of an appropriate amount of chemical fertilizer can increase the nutrient content in the soil so that crops can quickly obtain sufficient nutrients for crop growth and development (Wang et al., 2024; Ahmed et al., 2021). However, overfertilization not only leads to soil compaction and acidification, a microbial proportion imbalance, and a decrease in fertilizer use efficiency but also causes imbalances in crop nutrition, hinders internal synthesis and transformation mechanisms, and ultimately affects the yield and quality of crops (Miao et al., 2010; Sparks, 2020). Therefore, coordinating the relationship between the fertilizer application rate and crop yield and quality is important for achieving high and stable crop yields, improving crop quality, and achieving safe production.

At present, the most common fertilizers on the market are divided into three types: chemical fertilizers, organic fertilizers, and bioorganic fertilizers (Bhunia et al., 2021). The extensive use of chemical fertilizers has led to serious incidental problems, such as environmental pollution, chemical resistance of pests, and reduced food safety (Khatri et al., 2023). Owing to the need for sustainable agricultural development, increasing research has been devoted to the study of bioorganic fertilizers that are less harmful to the environment, crops, and food. Castor bean meal (CBM) biofertilizer is a kind of bio-organic fertilizer formed by the fermentation of beneficial bacteria and soil enzymes, Compared with other fertilizers, CBM biofertilizer is not only rich in organic matter but also contains many beneficial microorganisms. These beneficial microorganisms can form symbiotic relationships with soil microorganisms to inhibit the development of harmful bacteria and promote healthy crop growth. In recent years, many scholars have conducted systematic studies on the effects of bioorganic fertilizers on crops. Lin et al. (2024) reported that the application of an appropriate amount of bioorganic fertilizer effectively improved soil fertility and significantly increased yield indicators such as fresh weight, dry weight, and the content of bioactive components in lettuce. Liu et al. (2023) reported that the addition of bioorganic fertilizers such as *Bacillus megaterium*, *Bacillus mucilaginosus*, and *Bacillus subtilis* resulted in the most significant improvement in tea yield and quality, and compared with conventional chemical fertilizers, the qualities of tea polyphenols, amino acids, and caffeine in tea treated with the three bioorganic fertilizers were significantly higher. Some scholars have conducted relevant research on buckwheat. Wan et al. (2023) reported that bioorganic fertilizers improved agronomic traits such as plant height and yield, promoted plant growth and dry matter accumulation, and increased the contents of protein, starch, and bioflavonoids in buckwheat. Tao et al. (2023) reported that the starch content of Tartary buckwheat first

increased but then decreased with increasing bioorganic fertilizer application rate. Preliminary studies have shown that castor cake fertilizer significantly improves the root length, plant height, stem diameter, fresh weight, and dry weight of rapeseed. Li et al. (2024) used three types of fertilizers, inorganic fertilizer, organic fertilizer, and castor cake fertilizer, separately during peanut cultivation and reported that, compared with the other two types of fertilizers, castor cake fertilizer not only improved the soil physicochemical environment but also substantially improved peanut agronomic traits and yields, promoted the synthesis of peanut nutrients, and further enhanced the high quality and high yield of peanuts. Suzuki et al. (2021) reported that, unlike the differences in the quality of buckwheat grains harvested under different fertilization treatments, the differences in the growth and development and nutrients of buckwheat sprouts bred from buckwheat treated with different fertilizers were even greater. To date, there are fewer studies on CBM biofertilizer, so it is important to understand the effect of CBM biofertilizer on buckwheat yield and quality for the development and utilization of CBM biofertilizer.

Based on the above studies, the hypotheses of this study are as follows: (i) CBM biofertilizer may improve the yield and quality of buckwheat by regulating the plant height, stem diameter, number of main stem nodes, number of main stem branches, leaf blade area, and chlorophyll content of Tartary buckwheat; (ii) the length, sprout diameter, tap root length, fresh weight, dry weight, and contents of free amino acids, soluble sugars, vitamin C, bioflavonoids, and total phenols of buckwheat sprouts grown from grains harvested under different fertilization treatments may be different. However, relevant studies are lacking. Therefore, a Tartary buckwheat variety named Tongqiao No. 3 was used as the experimental material in this study, and different application rates of chemical fertilizer, cow manure, and CBM biofertilizer were employed to evaluate the effects of CBM biofertilizer on the agronomic traits, yield, and quality of Tartary buckwheat and Tartary buckwheat sprouts. The main purpose of this study was to reveal the effects of CBM biofertilizer on the growth, development, yield, and quality of Tartary buckwheat. The results of this study provide a theoretical basis and technical reference for the high-quality and high-yield cultivation of Tartary buckwheat.

2 Materials and methods

2.1 Test material and growth

The Tartary buckwheat variety used in the experiments was "Tongqiao No. 3", which was provided by the Key Laboratory of Castor Breeding of the State Ethnic Affairs Commission. Buckwheat sprouts were cultivated from the Tartary buckwheat seeds grown in this study. The experiment was conducted during the buckwheat growing season (July-October) in 2021–2022 at the experimental field of the Institute of Agricultural and Animal Husbandry Sciences, Tongliao City, Inner Mongolia Autonomous Region (altitude 178 m, 122°32′E, 43°44′N). The soil type was sandy loam soil. The nutrient contents of the plow layer (0–20 cm) were as follows: available nitrogen content, 70.76 $mg{\cdot}kg^{-1}$; available phosphorus content, 83.10 $mg{\cdot}kg^{-1}$; available potassium content, 255.91 $mg{\cdot}kg^{-1}$; organic matter content, 14.76 $g{\cdot}kg^{-1}$. The soil nutrient content was measured by Nanjing Cavens Testing Technology Co., Ltd.

The experiments used a randomized block design (RBD) with one factor, and each treatment was repeated three times. The seeds were sown on July 1, 2022, and July 5, 2023. Row sowing was used. The plot area was 6 m^2 (5 m long, 1.2 m wide, three rows with 30 cm row spacing), and the planting density was 50 plants/m^2. Observation lanes and isolation rows were established between each plot. The width of the observation lanes was 2 m, and the width of the isolation rows was 1 m to prevent the mixing of fertilizers. According to previous studies, 10 fertilization treatments were implemented: no fertilization (CK, 0 $kg{\cdot}ha^{-1}$), low concentration of chemical fertilizer (F1, 225 $kg{\cdot}ha^{-1}$), medium concentration of chemical fertilizer (F2, 300 $kg{\cdot}ha^{-1}$), high concentration of chemical fertilizer (F3, 375

TABLE 1 Test treatment and fertilizer dosage.

Treatment	Rate of fertilizer application (kg ha^{-1})	N (kg ha^{-1})	P_2O_5 (kg ha^{-1})	K_2O (kg ha^{-1})
CK	0	0	0	0
F1	225	33.75	16.88	40.50
F2	300	45.00	21.10	50.63
F3	375	56.25	26.50	63.29
N1	7500	22.5	11.25	27.00
N2	15000	45.00	22.50	54.00
N3	22500	67.50	33.75	81.00
B1	7500	22.50	10.50	24.83
B2	15000	45.00	21.00	49.65
B3	22500	67.50	31.50	74.48

CK: control without fertilization; F1: 225 kg ha^{-1}; F2: 300 kg ha^{-1}; F3: 375 kg ha^{-1}; N1: 7–500 kg ha^{-1}; N2: 15–000 kg ha^{-1}; N3: 22–500 kg ha^{-1}; B1: 7–500 kg ha^{-1}; B2: 15–000 kg ha^{-1}; B3: 22–500 kg ha^{-1}.

kg·ha^{-1}), low concentration of cow manure (N1, 7500 kg·ha^{-1}), medium concentration of cow manure (N2, 15,000 kg·ha^{-1}), high concentration of cow manure (N3, 22,500 kg·ha^{-1}), low concentration of CBM biofertilizer (B1, 7500 kg·ha^{-1}), medium concentration of CBM biofertilizer (B2, 15,000 kg·ha^{-1}), and high concentration of CBM biofertilizer (B3, 22,500 kg·ha^{-1}). The specific fertilization conditions are shown in Table 1. In each treatment, the fertilizer was applied to the plot as the base fertilizer once before planting, and no fertilizer was applied during the entire growth period. Thinning or filling of the seedlings was performed at the seedling stage to maintain the planting density at 50 plants/m^2. The buckwheat grains in each plot were harvested when 70% of the buckwheat grains were mature (October 26, 2022, and October 28, 2023). During the flowering and grain-filling periods, artificial irrigation was performed according to the principle of no less than 80% of the field capacity, and natural precipitation was used in the other periods. The other field management and pest control methods used were the same as those used for local high-yield cultivation. The Tartary buckwheat growth status under the different fertilization treatments is shown in Figure 1. The average temperature, sunshine duration, and precipitation from July to October 2022 were 20.3°C, 269.4 h, and 34.5 mm, respectively, and those in 2023 were 22.7°C, 232.1 h, and 42.3 mm, respectively.

2.2 Test fertilizer

Castor bean meal (CBM) biofertilizer (provided by the Key Laboratory of Castor Breeding State People's Committee) had a pH value of 6.20, an organic carbon content of 69.00 g/kg, a total nitrogen content of 3.00 g/kg, a total phosphorus content of 1.40 g/kg, a total potassium content of 3.31 g/kg, an alkaline dissolved nitrogen content of 0.25 mg/kg, an alkaline phosphorus content of 2.70 mg/kg, and a fast-acting potassium content of 9.40 mg/kg. Castor bean meal (CBM) biofertilizer contained strains and enzyme activities are shown in Table 2. chemical fertilizer (purchased from Stanley Agricultural Group Co., Ltd.) total nutrient content ≥45%, N-P_2O_5-K_2O:15-15-15. cow manure (provided by Tongliao Agricultural and Animal Husbandry Scientific Research Institute, Inner Mongolia) pH 6.50-8.50, organic matter content 14.50%, total nitrogen content 0.20%-0.45%, total phosphorus content 0.15%-0.25%, alkaline phosphorus content 0.15%-0.25%. 0.15%~0.25%, total potassium content was 0.10%~0.15%.

2.3 Sample preparation

During the seedling stage, flowering stage, grain-filling stage, and maturity stage, 30 Tartary buckwheat plants with stable growth and an intact root system were randomly excavated from each treatment plot. After rinsing with tap water, 20 Tartary buckwheat plants were selected for each treatment to measure the plant height, stem diameter, number of main stem nodes, and number of main stem branches. The leaves of the remaining 10 Tartary buckwheat plants (located at nodes 4–6 at the top of the main stem) were selected, One part was treated with liquid nitrogen for 30 s and then stored in a refrigerator at -80°C for the determination of chlorophyll content, and the other part was cleaned and stored in a refrigerator at 4°C for the determination of leaf blade area.

The specific mechanism of buckwheat sprout cultivation was as follows: 300 buckwheat grains were selected from each fertilization treatment, the seeds were washed three times with deionized water and then soaked for 5 min, the soaked seeds were placed into a disinfection tray and soaked in 1% NaClO solution for 15 min for

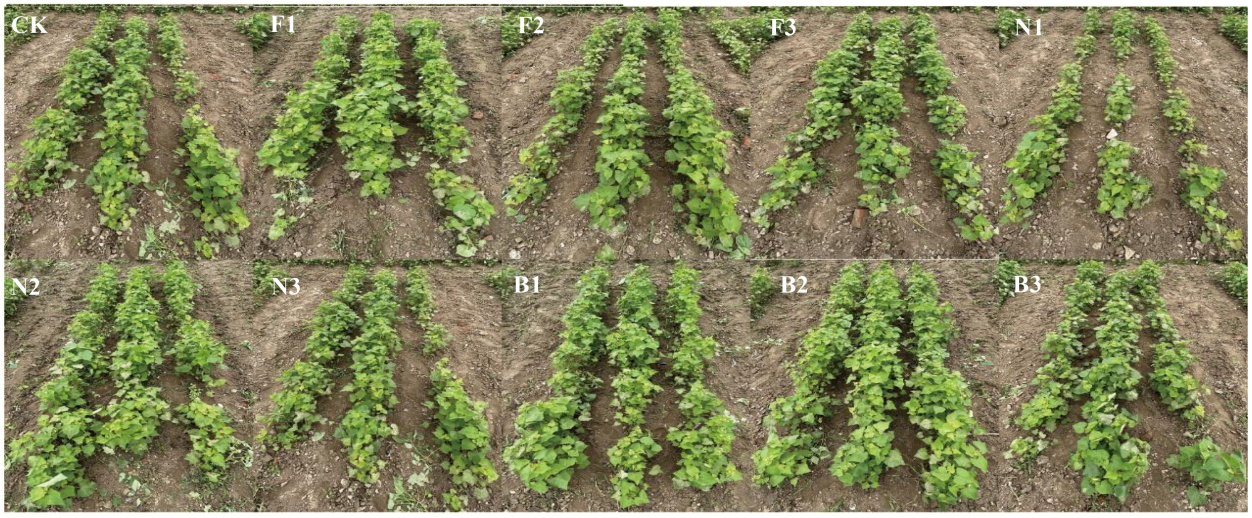

FIGURE 1
Field growth of buckwheat at seedling periods with different fertilization treatments CK: Fertilizer application rate of 0 kg·ha^{-1}; F1: chemical fertilizer application rate of 225 kg·ha^{-1}; F2: chemical fertilizer application rate of 300 kg·ha^{-1}; F3: chemical fertilizer application rate of 375 kg·ha^{-1}; N1: cow manure application rate of 7,500 kg·ha^{-1}; N2: cow manure application rate of 15,000 kg·ha^{-1}; N3: cow manure application rate of 22,500 kg·ha^{-1}; B1: CBM fertilizer application rate of 7,500 kg·ha^{-1}; B2: CBM fertilizer application rate of 15,000 kg·ha^{-1}; and B3: CBM fertilizer application rate of 22,500 kg·ha^{-1}.

TABLE 2 Beneficial bacteria and enzyme activity of castor bean meal biofertilizer.

Index	Castor bean meal biofertilizer							
Strains	*Bacillus subtilis*	*Saccharomyces cerevisiae*	*Arthrospira platensis*	*Acetobacter aceti*	*Lactobacillus acidophilus*	*Streptomyces coelicolor*	*Aspergillus oryzae*	
Enzyme activity	Urease	Phosphatase	Sucrase	Catalase	Acid converting enzyme	Olyphenol oxidase	Protease	Cellulase

disinfection, and the disinfected seeds were then washed three times and placed at room temperature (25°C). Tartary buckwheat seeds subjected to the different treatments were then soaked in sterile water for 24 h prior to germination. Incubation was performed for 16 d with 24 h as the base. At 0 d, 4 d, 8 d, 12 d, and 16 d of buckwheat sprout growth, 30 sprouts with consistent growth were selected, treated with liquid nitrogen for 30 s, and then stored in a -80°C freezer for the subsequent measurement of amino acid, soluble sugar, vitamin C, bioflavonoid, and total phenolic contents.

2.4 Measurements

In accordance with the methods of Yang et al. (2024), the plant height, stem diameter, number of main stem nodes, number of main stem branches, the grain weight per plant, and 1,000-grain weight were measured for each treatment during each growth period. An area of 1 m^2 was randomly selected in the center of each plot (no sampling was performed, and the border plants were not included) for the collection of grains from all plants, and the grains were air-dried to measure the yield. The leaf blade area during each period was measured via a Handheld Laser leaf blade area Meter (CI-203, CID, USA) (Yuan et al., 2024a). The chlorophyll content was determined via a chlorophyll content kit (BC0995), which was purchased from Beijing Solarbio Science and Technology Co., Ltd.

The length, diameter, tap root length, fresh weight, and dry weight of the buckwheat sprouts obtained from each fertilization treatment were measured according to the methods of Starič et al. (2023). Three days after germination, the germination rates of Tartary buckwheat harvested under different fertilization treatments were measured with the sprout length of 2 mm as the base.

The buckwheat protein content was determined using the Protein Content Assay Kit (A045-2-2; Nanjing Jiancheng Bioengineering Institute, which utilizes the Coomassie brilliant blue G-250 method to determine protein content. The content of free amino acids in the buckwheat sprouts was determined using a free amino acid content detection kit (BC1575; Beijing Solarbio Science and Technology Co., Ltd. The anthrone method was used to determine the starch content. Briefly, 0.1 g of sample was weighed, 50 mL of 80% ethanol solution was added, and the solution was heated in a constant-temperature water bath at 45°C for 10 min. After suction filtration, 1 mL of the filtrate was added to a colorimetric tube, followed by the addition of 0.5 mL of anthrone solution and 4.5 mL of concentrated sulfuric acid. After shaking, the tube was covered and placed in a boiling water bath for 10 min. After cooling to room temperature, the optical density (OD) was measured at 620 nm use Tecan Spark multifunctional enzyme marker assay (Yang et al., 2019). The cellulose content was determined using a cellulose analyzer (SQ-XW06, Hebei Yunpu Analytical Instrument Co., Ltd.). A plant flavonoid content detection kit (BC1330; Beijing Solarbio Science and Technology Co., Ltd. was used to determine the plant flavonoid content in Tartary buckwheat and buckwheat sprouts; this kit uses the spectrophotometric method to determine the plant flavonoid content. The soluble sugar content in the sprouts was determined using a soluble sugar content detection kit (BC0030; Beijing Solarbio Science and Technology Co., Ltd. this kit uses the anthrone method. The total phenolic content in buckwheat sprouts was determined using a total plant phenolic content detection kit (BC1340; Beijing Solarbio Science and Technology Co., Ltd. and this kit uses the spectrophotometric method. The vitamin C content in the sprouts was determined using a vitamin C content detection kit (BC1234; Beijing Solarbio Science and Technology Co., Ltd. The bioflavonoid components were measured at ProNet Biotech Co., Ltd. using high-performance liquid chromatography-mass spectrometry(Tsushima LCMS-2050 High Performance Liquid Chromatography Mass Spectrometer). The fat content of Tartary buckwheat was determined by Soxhlet extraction method according to Lo Presti et al. (2023) Briefly, 2–5 g of dried and ground sample was accurately weighed, mixed with sea sand, and transferred to a filter paper tube. Then, the filter paper tube was placed into a Soxhlet extractor, anhydrous ether was added at the upper end of condenser, and the extractor was heated on a water bath to continuously reflux the ether for 6–12 h of extraction. After suction filtration, the receiving bottle was removed. When the bottle contained 1–2 cm of ether, the extractor was placed on a water bath to evaporate the ether and then dried at 100-105°C for 2 h. The extract was then removed and placed in a desiccator to cool for 30 min and weighed, and the process was repeated until a constant weight was obtained. The fat content was calculated according to the following formula:

$$\text{Fat content} = (M2 - M1)/M \times 100\,\%$$

where M_2 is the sum of the masses of the receiving bottle and the fat, M1 is the mass of the receiving bottle, and M is the mass of the sample.

2.5 Statistical analysis

Microsoft Excel 2016 and SPSS 25.0 were used for data processing. All the data were analyzed via one-way analysis of variance (ANOVA) and multiple comparison test (Tukey). The differences among the treatments were compared ($P<0.05$). The

growth rate under each fertilizer treatment was calculated using the formula (actual value - control value)/control value * 100%, and the rate of decrease was determined using the formula (control value - actual value)/control value * 100%. The results in 2022 and 2023 were similar. Therefore, the two-year averages are presented, and the data from each of these two years are presented as supplementary data. GraphPad Prism 10 was used to plot the data results and Photoshop 2020 was used for image processing.

3 Results

3.1 Effects of CBM biofertilizer on the agronomic traits of Tartary buckwheat

During the growth period, the plant height, stem diameter, number of main stem nodes, and number of main stem branches of Tartary buckwheat in the different fertilization treatments increased.

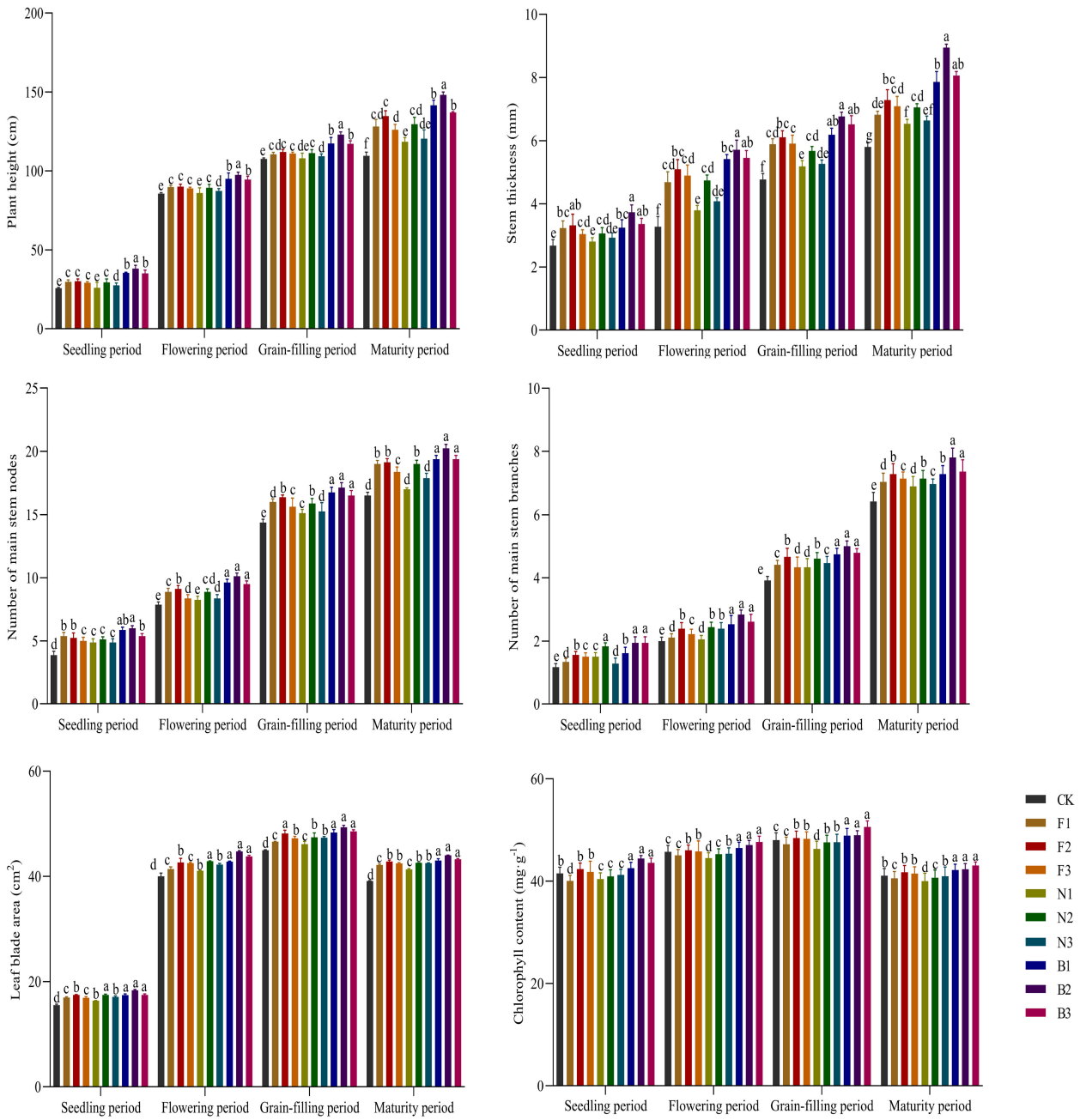

FIGURE 2
Effects of CBM biofertilizer on the agronomic traits of Tartary buckwheat Small letter in the same column means significant difference at $p< 0.05$. CK: Fertilizer application rate of 0 kg·ha^{-1}; F1: chemical fertilizer application rate of 225 kg·ha^{-1}; F2: chemical fertilizer application rate of 300 kg·ha^{-1}; F3: chemical fertilizer application rate of 375 kg·ha^{-1}; N1: cow manure application rate of 7,500 kg·ha^{-1}; N2: cow manure application rate of 15,000 kg·ha^{-1}; N3: cow manure application rate of 22,500 kg·ha^{-1}; B1: CBM fertilizer application rate of 7,500 kg·ha^{-1}; B2: CBM fertilizer application rate of 15,000 kg·ha^{-1}; and B3: CBM fertilizer application rate of 22,500 kg·ha^{-1}.

The plant height, stem diameter, number of main stem nodes, and number of main stem branches under the CBM biofertilizer treatments (B1, B2, and B3) were greater than those under the no fertilizer, chemical fertilizer, and cow manure treatments, and there were significant differences between the B2 treatment and the other fertilization treatments (Figure 2). The leaf area and chlorophyll content of Tartary buckwheat first increased but then decreased as growth progressed, reaching a maximum at the grain-filling stage, and those in the B2 treatment were significantly greater than those in the other fertilization treatments. The plant height, stem diameter, number of main stem nodes, number of main stem branches, leaf blade area, and chlorophyll content increased first but then decreased with increasing fertilizer application rate, with the highest values under the B2 treatment and the lowest under the CK treatment. Compared with those in the CK, F1, F2, F3, N1, N2, N3, B1, and B3 treatments, the plant height in the B2 treatment on average was 23.81%, 13.52%, 10.85%, 14.50%, 20.19%, 13.11%, 18.02%, 4.42%, and 5.96% greater, respectively; the average stem diameter in the B2 treatment was 52.25%, 21.98%, 15.38%, 20.21%, 37.26%, 22.55%, 32.98%, 10.81%, and 7.54% greater, respectively; the average number of main stem nodes under the B2 treatment was 25.51%, 8.63%, 7.27%, 12.93%, 18.23%, 9.46%, 15.36%, 3.63%, and 5.42% greater, respectively; the number of main stem branches under the B2 treatment was on average 30.25%, 18.05%, 10.67%, 15.72%, 18.94%, 9.74%, 16.40%, 8.80%, and 5.21% greater, respectively; and the leaf blade area in the B2 treatment was on average 12.01%, 6.34%, 3.52%, 4.90%, 7.94%, 4.04%, 4.83%, 3.22%, and 2.19% greater, respectively.

3.2 Effects of the CBM biofertilizer on the yield of Tartary buckwheat

The different fertilization treatments significantly affected the grain weight per plant and the 1000-grain weight. Figure 3 shows that the buckwheat grains harvested in the B2 treatment were relatively large and had a high fullness. With increasing fertilizer application rate, the grain weight per plant, the 1,000-grain weight, and the yield of Tartary buckwheat first increased but then decreased, with those of the B2 treatment being significantly greater than those of the other fertilization treatments. Compared with those in the CK, F1, F2, F3, N1, N2, N3, B1, and B3 treatments, the grain weight per plant in the B2 treatment was 43.12%, 29.40%, 26.79%, 36.31%, 32.66%, 25.33%, 27.98%, 23.81%, and 20.78% greater, respectively; the 1000-grain weight in the B2 treatment was 8.61%, 5.94%, 2.91%, 5.52%, 6.60%, 5.15%, 8.82%, 6.11%, and 6.29% greater, respectively; and the yield in the B2 treatment was 43.0%, 29.39%, 26.78%, 36.34%, 32.70%, 25.37%, 28.89%, 23.87%, and 20.74% greater, respectively (Figure 4).

3.3 Effects of CBM biofertilizer on the flavonoid components of Tartary buckwheat

The bioflavonoid components of the Tartary buckwheat grains harvested from the different fertilization treatments were determined, and 33 components were found, including quercetin,

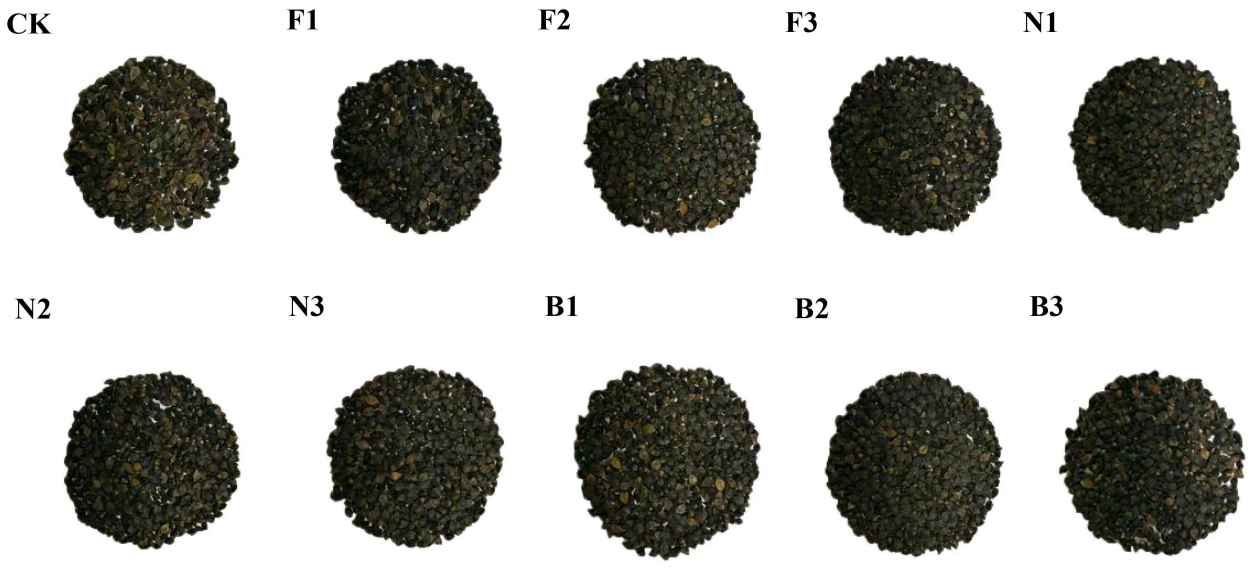

FIGURE 3
Buckwheat kernels harvested from different fertilization treatments CK: Fertilizer application rate of 0 kg·ha^{-1}; F1: chemical fertilizer application rate of 225 kg·ha^{-1}; F2: chemical fertilizer application rate of 300 kg·ha^{-1}; F3: chemical fertilizer application rate of 375 kg·ha^{-1}; N1: cow manure application rate of 7,500 kg·ha^{-1}; N2: cow manure application rate of 15,000 kg·ha^{-1}; N3: cow manure application rate of 22,500 kg·ha^{-1}; B1: CBM fertilizer application rate of 7,500 kg·ha^{-1}; B2: CBM fertilizer application rate of 15,000 kg·ha^{-1}; and B3: CBM fertilizer application rate of 22,500 kg·ha^{-1}.

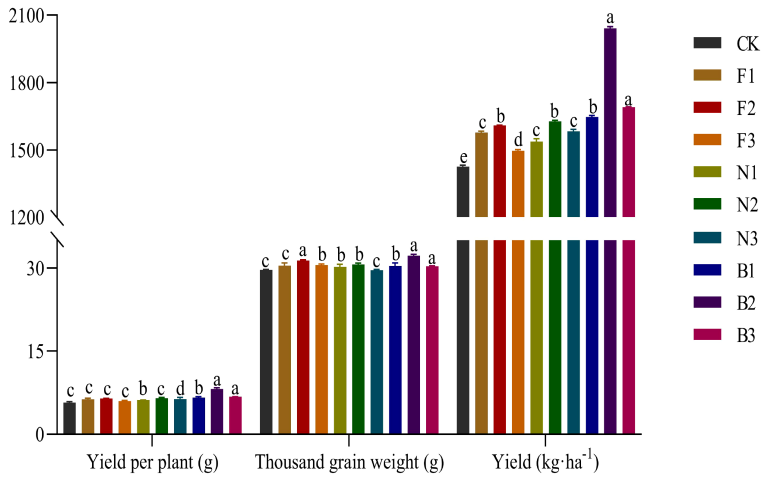

FIGURE 4
Effects of the CBM biofertilizer on the yield of Tartary buckwheat. Small letter in the same column means significant difference at $p< 0.05$. CK: Fertilizer application rate of 0 kg·ha^{-1}; F1: chemical fertilizer application rate of 225 kg·ha^{-1}; F2: chemical fertilizer application rate of 300 kg·ha^{-1}; F3: chemical fertilizer application rate of 375 kg·ha^{-1}; N1: cow manure application rate of 7,500 kg·ha^{-1}; N2: cow manure application rate of 15,000 kg·ha^{-1}; N3: cow manure application rate of 22,500 kg·ha^{-1}; B1: CBM fertilizer application rate of 7,500 kg·ha^{-1}; B2: CBM fertilizer application rate of 15,000 kg·ha^{-1}; and B3: CBM fertilizer application rate of 22,500 kg·ha^{-1}.

rutin, hyperoside, kaempferol, kaempferol 3-0-rutinoside, psoralen, bergamot lint, hydroxychalcone, dragon's blood, alfalfa, boreletin, isomangiferin, genistein, baicalin, *Ginkgo biloba* diflavonoids, ruthenium naringenin, protocatechindehyde, protocatechuic acid, umbellifera, gallic acid, caffeic acid, resveratrol, apigenin, emodin, naringenin, rhododendron, high psyllium, orange cassia, chlorogenic acid, vitexin, isocarin, ursolic acid, and naringin. Different fertilization treatments had significant effects on these 33 flavonoids. Among them, the most abundant components were quercetin, rutin, hyperoside, kaempferol, and kaempferol 3-0-rutinoside, which have decisive effects on bioflavonoid synthesis (Figure 5). In terms of the effects of the different fertilization treatments on the contents of bioflavonoids, the contents of nine bioflavonoid components, namely, quercetin, protocatechuic acid, hyperoside, kaempferol, kaempferol 3-0-rutinoside, hydroxychalcone, boreletin, protocatechindehyde, and umbellifera, were greater under the B2 treatment than under the other treatments. For Tartary buckwheat in the CK treatment, the levels of five bioflavonoids, namely, rutin, isomangiferin, Ginkgo biloba diflavonoids, ruthenium naringenin, and naringin, were relatively high. In the N1 treatment, the levels of four bioflavonoids, including alfalfa, protocatechuic acid, vitexin, and isocarin, were relatively high. In the N2 treatment, the levels of four bioflavonoids, namely, emodin, bergamot lint, apigenin, and chlorogenic acid, were relatively high. In the B3 treatment, the levels of three bioflavonoids, namely, psoralen, baicalin, and chlorogenic acid, were relatively high. In the F1 treatment, the levels of three bioflavonoids, namely, gallic acid, caffeic acid, and resveratrol, were relatively high. In the B1 treatment, the levels of two bioflavonoids, namely, dragon's blood and genistein, were relatively high. Compared with the other fertilization treatments, the B2 treatment had the greatest effect on the bioflavonoid components of Tartary buckwheat.

3.4 Effects of CBM biofertilizer on the quality of Tartary buckwheat

With increasing fertilization application rate, the Tartary buckwheat protein, starch, cellulose, fat, and bioflavonoid contents first increased but then decreased, with the protein, starch, cellulose, and bioflavonoid contents in the B2 treatment being significantly greater than those in the other treatments. Among the fertilization treatments, the fat content in the F2 treatment was greater than that in the other fertilization treatments, but the differences among the treatments were relatively small (Figure 6). Compared with the CK, F1, F2, F3, N1, N2, N3, B1, and B3 treatments, the buckwheat protein content under the B2 treatment was 53.31%, 68.52%, 25.52%, 39.23%, 24.54%, 23.93%, 34.25%, 19.74%, and 12.94% greater, respectively; the starch contents in the B2 treatment were 38.74%, 46.34%, 25.80%, 48.60%, 119.12%, 30.65%, 71.27%, 40.64%, and 30.97% greater, respectively; the cellulose content under the B2 treatment was 65.32%, 51.12%, 38.65%, 62.42%, 30.80%, 12.14%, 21.35%, 33.15%, and 10.79% greater, respectively; and the bioflavonoid content in the B2 treatment was 45.0%, 48.85%, 29.98%, 39.47%, 47.29%, 27.62%, 38.10%, 51.53%, and 26.09% greater, respectively.

3.5 Effects of CBM biofertilizer on the yield of Tartary buckwheat sprouts

There were significant differences in the sprout length, fresh weight, and dry weight of the Tartary buckwheat sprouts harvested from the different fertilization treatments (Figure 7). With increasing fertilizer application rate, the sprout length, sprout diameter, tap root length, fresh weight, and dry weight of the sprouts from each treatment first increased but then decreased.

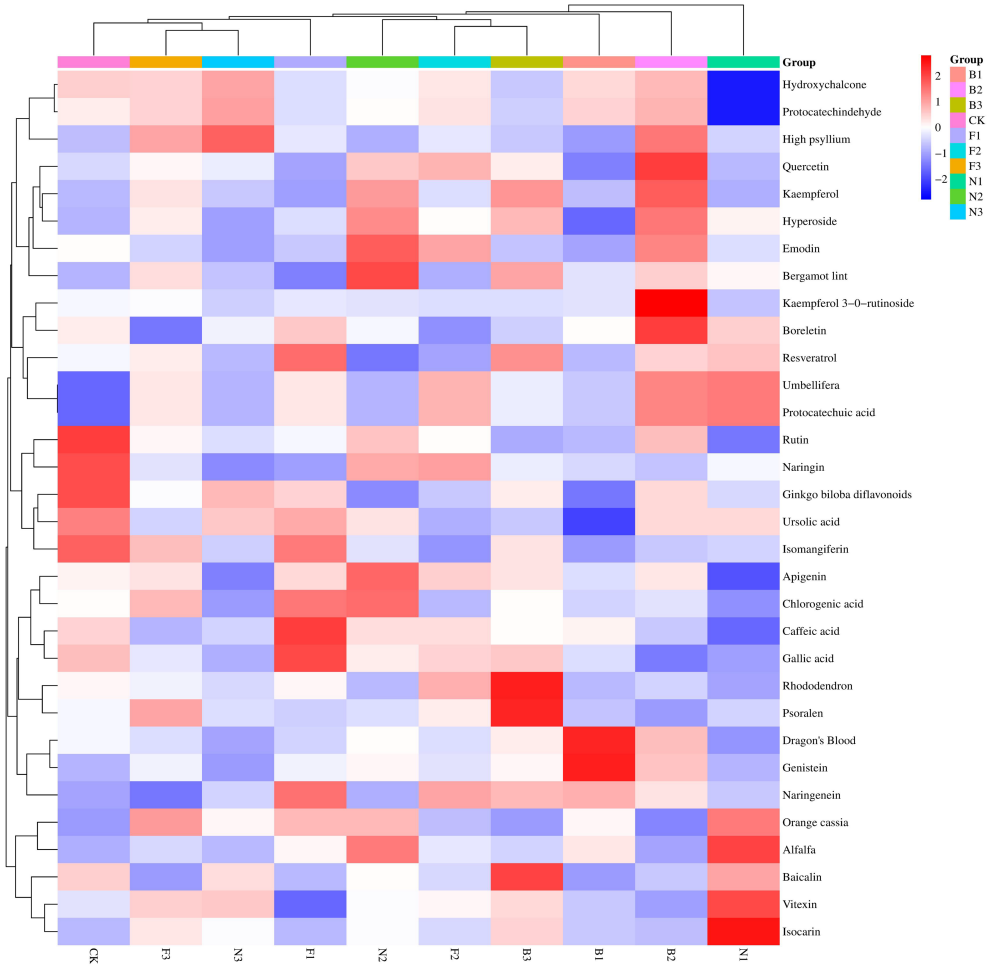

FIGURE 5
Buckwheat bioflavonoid fraction content clustering heat map Small letter in the same column means significant difference at $p< 0.05$. The abscissa is different fertilization treatments, and the vertical axis is the content of each component of flavonoids. Red represents high content and blue represents low content. CK: Fertilizer application rate of 0 kg·ha^{-1}; F1: chemical fertilizer application rate of 225 kg·ha^{-1}; F2: chemical fertilizer application rate of 300 kg·ha^{-1}; F3: chemical fertilizer application rate of 375 kg·ha^{-1}; N1: cow manure application rate of 7,500 kg·ha^{-1}; N2: cow manure application rate of 15,000 kg·ha^{-1}; N3: cow manure application rate of 22,500 kg·ha^{-1}; B1: CBM fertilizer application rate of 7,500 kg·ha^{-1}; B2: CBM fertilizer application rate of 15,000 kg·ha^{-1}; and B3: CBM fertilizer application rate of 22,500 kg·ha^{-1}.

The sprout length, fresh weight, and dry weight of the sprouts were significantly greater under the B2 treatment than under the other fertilization treatments. Compared with the CK, F1, F2, F3, N1, N2, N3, B1, and B3 treatments, the length of the sprouts cultured from buckwheat harvested in the B2 treatment was 24.17%, 13.84%, 12.59%, 13.55%, 13.84%, 5.51%, 2.92%, 10.83%, and 5.01% greater, respectively; the fresh weight was 34.13%, 22.38%, 11.61%, 17.39%, 3.93%, 2.16%, 0.21%, and 4.91% greater, respectively; and the dry weights were 40.07%, 18.54%, 7.98%, 62.62%, 13.46%, 8.81%, 4.26%, 7.02%, and 4.78% higher, respectively. The sprout diameters and tap root lengths of the sprouts bred from buckwheat harvested under the different fertilization treatments were similar, with small differences among the treatments (Figure 8).

3.6 Effects of CBM biofertilizer on the quality of Tartary buckwheat sprouts

With increasing duration of cultivation, the contents of free amino acids, soluble sugars, and total phenolics in the Tartary buckwheat sprouts under the different fertilization treatments first increased but then decreased, with the highest contents occurring at 12 d of cultivation(Figure 9); for the buckwheat harvested under the B2 treatment, the contents of free amino acids, soluble sugars, and total phenolics of the cultured sprouts were significantly greater than those under the other fertilization treatments. With increasing cultivation period, the vitamin C and bioflavonoid contents of the sprouts under the different fertilization treatments continuously increased, with the vitamin C and bioflavonoid contents of the

sprouts cultivated from buckwheat harvested under the B2 treatment being significantly greater than those under the other fertilization treatments. The contents of free amino acids, soluble sugars, vitamin C, bioflavonoids, and total phenolics in the sprouts bred from grains harvested under the different fertilization treatments were significantly different and initially increased and then decreased with increasing fertilizer application rate, with the highest values under the B2 treatment and the lowest under the CK treatment. Compared with the CK, F1, F2, F3, N1, N2, N3, B1, and B3 treatments, the free amino acid content of the sprouts cultured from buckwheat harvested in the B2 treatment was on average 8.27%, 8.21%, 5.59%, 7.20%, 6.56%, 5.76%, 6.84%, 2.57%, and 2.14% greater, respectively, the soluble sugar content was on average 13.13%, 7.78%, 5.13%, 15.60%, 22.77%, 10.67%, 16.42%, 9.14%, and 4.22% greater, respectively, the vitamin C content was on average 12.13%, 12.43%, 3.23%, 8.33%, 13.04%, 5.05%, 7.77%, 10.93%, and 8.62% greater, respectively, the bioflavonoid contents were on average 27.70%, 29.14%, 15.15%, 25.02%, 29.04%, 21.49%, 25.59%, 32.93%, and 24.08% greater, respectively, and the total phenolic content was on average 11.38%, 7.30%, 1.84%, 10.03%, 10.49%, 5.88%, 8.44%, 7.34%, and 3.31% greater, respectively.

4 Discussion

4.1 Effect of different fertilization treatments on the agronomic traits of Tartary buckwheat

The agronomic traits of Tartary buckwheat during the growth process are closely associated with the grain weight and final yield. Plant height is an important agronomic trait in Tartary buckwheat. Buckwheat plants that are too tall are potentially prone to lodging, and plants that are too short may exhibit poor nutrition; therefore, plant height may affect buckwheat yield to some extent (Jha et al., 2024). Many studies have shown that the plant height of Tartary buckwheat under different fertilization treatments varies during different periods (Fang et al., 2018). Zhou et al. (2023b) reported that, compared with CK, different organic fertilizer application rates increased the plant height and improved agronomic traits. Tang Z. et al. (2024) reported that appropriate organic fertilizer treatment increased the plant height. In this study, compared with no fertilization, chemical fertilizer, or cow manure, CBM biofertilizer significantly increased the plant height of Tartary buckwheat, with the B2 treatment resulting in the maximum plant height, consistent with previous results. This result may be due to the rich nitrogen, phosphorus, and potassium contained in the CBM fertilizer, thus meeting the plant's needs for nitrogen, phosphorus, and potassium during different growth periods. A sufficient nutrient supply can significantly promote the growth of Tartary buckwheat plants, thus increasing their height (Tang L. et al., 2024). Zhang et al. (2021) applied organic fertilizer to corn and reported significant improvement in plant traits, increased stalk diameter, and significant promotion of plant growth. The results of this study were consistent with these results, possibly because the CBM biofertilizer contains not only the basic nutrients needed for Tartary buckwheat growth but also trace elements and organic nutrients, which provide a rich material base for growth and contribute to stem growth and development, thereby increasing stem diameter (Xiang et al., 2019). Yang et al. (2024) reported that biological fertilizer can significantly affect the number of main stem nodes and the number of main stem branches and is beneficial for the

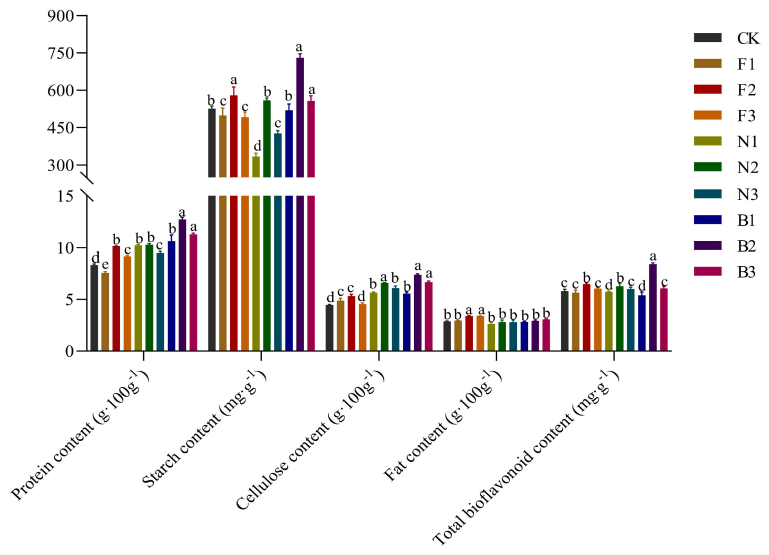

FIGURE 6
Effects of CBM biofertilizer on the quality of Tartary buckwheat. Small letter in the same column means significant difference at $p< 0.05$. CK: Fertilizer application rate of 0 kg·ha^{-1}; F1: chemical fertilizer application rate of 225 kg·ha^{-1}; F2: chemical fertilizer application rate of 300 kg·ha^{-1}; F3: chemical fertilizer application rate of 375 kg·ha^{-1}; N1: cow manure application rate of 7,500 kg·ha^{-1}; N2: cow manure application rate of 15,000 kg·ha^{-1}; N3: cow manure application rate of 22,500 kg·ha^{-1}; B1: CBM fertilizer application rate of 7,500 kg·ha^{-1}; B2: CBM fertilizer application rate of 15,000 kg·ha^{-1}; and B3: CBM fertilizer application rate of 22,500 kg·ha^{-1}.

FIGURE 7
Growth of buckwheat buds in different fertilization treatments CK: Fertilizer application rate of 0 kg·ha^{-1}; F1: chemical fertilizer application rate of 225 kg·ha^{-1}; F2: chemical fertilizer application rate of 300 kg·ha^{-1}; F3: chemical fertilizer application rate of 375 kg·ha^{-1}; N1: cow manure application rate of 7,500 kg·ha^{-1}; N2: cow manure application rate of 15,000 kg·ha^{-1}; N3: cow manure application rate of 22,500 kg·ha^{-1}; B1: CBM fertilizer application rate of 7,500 kg·ha^{-1}; B2: CBM fertilizer application rate of 15,000 kg·ha^{-1}; and B3: CBM fertilizer application rate of 22,500 kg·ha^{-1}.

environmental adaptability of buckwheat, thus improving the yield. In this study, compared with no fertilization, chemical fertilizer, or cow manure, the application of CBM biofertilizer increased the number of main stem nodes, and consistent with previous results, the B2 treatment had the greatest effect among the treatments, possibly because the beneficial microorganisms in the CBM biofertilizer can produce growth-promoting substances, such as auxin, which can increase the number of main stem nodes and the number of main stem branches in Tartary buckwheat (Zheng et al., 2023). Rotili et al. (2023) revealed that the leaf blade area decreased during the maturity stage in buckwheat because the accumulated dry matter in the plant transferred to the grains, consistent with the leaf growth pattern during each growth period in this study. Chlorophyll participates in photosynthesis in plant leaves. Zhou et al. (2023a) reported that the application of nitrogen fertilizer and increasing the planting density increased the chlorophyll content in Tartary

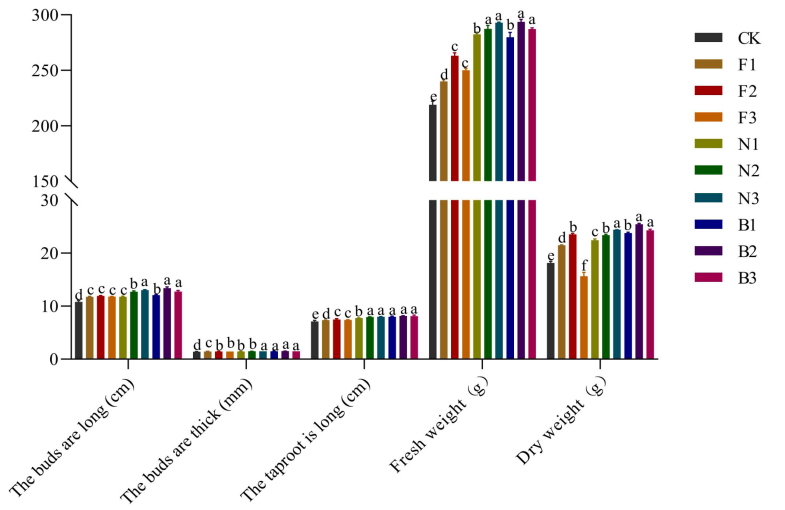

FIGURE 8
Effects of CBM biofertilizer on the yield of Tartary buckwheat sprouts. Small letter in the same column means significant difference at $p< 0.05$. CK: Fertilizer application rate of 0 kg·ha^{-1}; F1: chemical fertilizer application rate of 225 kg·ha^{-1}; F2: chemical fertilizer application rate of 300 kg·ha^{-1}; F3: chemical fertilizer application rate of 375 kg·ha^{-1}; N1: cow manure application rate of 7,500 kg·ha^{-1}; N2: cow manure application rate of 15,000 kg·ha^{-1}; N3: cow manure application rate of 22,500 kg·ha^{-1}; B1: CBM fertilizer application rate of 7,500 kg·ha^{-1}; B2: CBM fertilizer application rate of 15,000 kg·ha^{-1}; and B3: CBM fertilizer application rate of 22,500 kg·ha^{-1}.

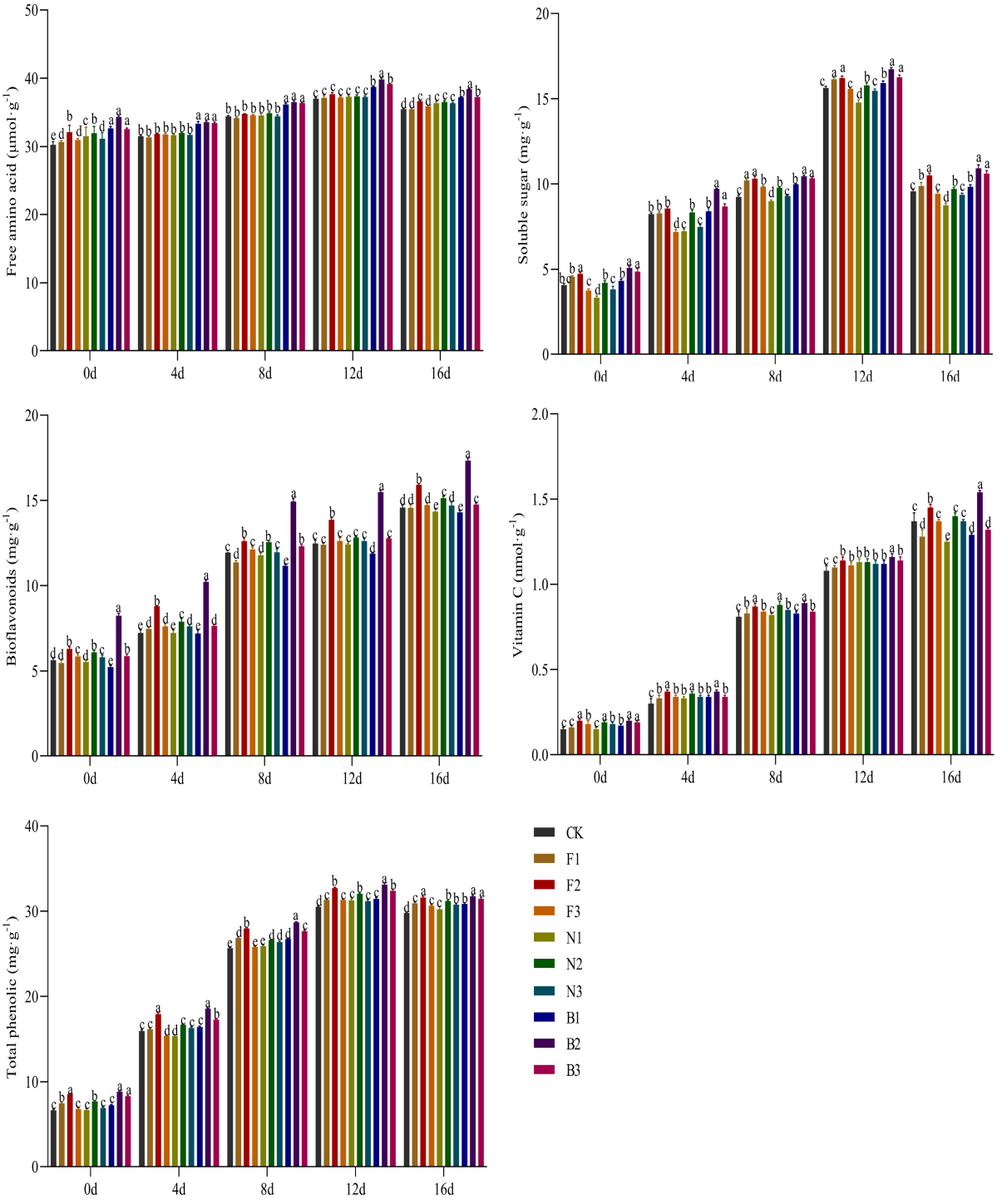

FIGURE 9
Effects of CBM biofertilizer on the quality of Tartary buckwheat sprouts. Small letter in the same column means significant difference at $p< 0.05$. CK: Fertilizer application rate of 0 kg·ha^{-1}; F1: chemical fertilizer application rate of 225 kg·ha^{-1}; F2: chemical fertilizer application rate of 300 kg·ha^{-1}; F3: chemical fertilizer application rate of 375 kg·ha^{-1}; N1: cow manure application rate of 7,500 kg·ha^{-1}; N2: cow manure application rate of 15,000 kg·ha^{-1}; N3: cow manure application rate of 22,500 kg·ha^{-1}; B1: CBM fertilizer application rate of 7,500 kg·ha^{-1}; B2: CBM fertilizer application rate of 15,000 kg·ha^{-1}; and B3: CBM fertilizer application rate of 22,500 kg·ha^{-1}.

buckwheat leaves. In this study, compared with no fertilization, chemical fertilizer, or cow manure, CBM biofertilizer significantly increased the chlorophyll content of the leaves, and consistent with previous results, the B2 treatment had the highest chlorophyll content, possibly because the CBM biofertilizer can significantly increase the photosynthetic intensity, promote chlorophyll synthesis, increase the leaf blade area, and increase the accumulation of photosynthetic products (Hornyák et al., 2022).

4.2 Effect of different fertilization treatments on the yield of Tartary buckwheat

The grain weight per plant and the 1,000-grain weight are important factors in determining the Tartary buckwheat yield. The higher the grain weight per plant is, the greater the yield, whereas the 1,000-grain weight indirectly affects yield by affecting the grain weight per plant and grain quality (Sobhani et al., 2014). Popović et al. (2013) showed that compared with that under conventional planting, the grain weight per plant and 1,000-grain weight of buckwheat plants grown with organic fertilizer were significantly greater, 7.28% and 9% respectively, indicating that organic fertilizer can increase buckwheat yield. Radchenko et al. (2018) reported that the application of organic fertilizer in the planting of buckwheat significantly increased the grain weight per plant, the 1000-grain weight, and the yield in southern Ukraine. Guo et al. (2022) combined organic straw and inorganic fertilizer and reported that, compared with CK, the combined application of organic manure and organic fertilizer significantly increased the grain weight per plant, the 1000-grain weight, and the final yield of buckwheat through increases in the soil nutrient content and improvements in the soil physicochemical environment. In this study, the application of CBM biofertilizer significantly increased the grain weight per plant, the 1,000-grain weight, and the yield of Tartary buckwheat, with the B2 treatment resulting in the highest grain weight per plant, 1,000-grain weight, and yield, 1.43, 1.08, and 1.43 times those of CK, respectively, indicating that CBM biofertilizer significantly increased the yield. This finding is consistent with the results of previous studies, possibly because CBM biofertilizer contains a variety of bacteria and soil enzymes that not only improve the soil environment and promote growth and development buckwheat but also improve plant immunity and increase disease resistance, which ultimately manifests as a significant increase in yield. The appropriate application of CBM biofertilizer may be beneficial for the absorption of soil nutrients by Tartary buckwheat plants, can promote the growth and development of Tartary buckwheat plants, increase the plant height, stem diameter, number of main stem nodes, and number of main stem branches, improve the leaf photosynthetic rate, increase the leaf blade area and chlorophyll content, and thus increase the aboveground biomass and yield (Yuan et al., 2024b).

4.3 Effect of different fertilization treatments on the quality of Tartary buckwheat

The quality of crops directly affects their nutritional value and economic benefits. Some studies have shown that fertilization is conducive to the absorption of nutrients by crops and plays an important role in improving the nutritional quality of grains (El-Saadony et al., 2021). Gao et al. (2024) reported that, compared with no fertilization, the application of an appropriate amount of organic fertilizer significantly increased the starch, cellulose, and fat contents of buckwheat. Gao et al. (2023) reported that appropriate applications of nitrogen fertilizer and organic fertilizer can promote endosperm development and starch synthesis in buckwheat, thereby increasing the contents of starch, cellulose, fat, and bioflavonoids in buckwheat grains. Wan et al. (2021) reported that fertilization can promote buckwheat starch anabolism and amino acid biosynthesis and increase the starch and protein contents of buckwheat grains. In this study, compared with no fertilization, chemical fertilizer, or cow manure, CBM biofertilizer significantly increased the protein, starch, cellulose, fat, and bioflavonoid contents of Tartary buckwheat grains, with the B2 treatment having the highest contents. This finding was consistent with the results of previous studies, possibly because, on the one hand, CBM biofertilizer contains a variety of microorganisms, and application of CBM to soil can promote soil microbe activity, increase soil biodiversity, and promote buckwheat growth and development, thereby improving yield and quality (Martinez et al., 2022); on the other hand, CBM biofertilizer contains high amounts of nitrogen, phosphorus, potassium, and trace elements, and nitrogen, phosphorus, and potassium can be used to develop a buckwheat root system and improve plant photosynthesis, organic synthesis, and transport ability, thus improving yield and quality (Çürük et al., 2020). Habtemariam (2019) reported that the application of green manure can promote the synthesis of rutin, quercetin, kaempferol, and resveratrol in buckwheat, thereby improving the bioflavonoid content and antioxidant activity. Jiang et al. (2007) found that fertilization may significantly increase the contents of rutin, procyanidin, gallic acid, and naringenin in buckwheat grains. Lee et al. (2016) observed that fertilization can regulate the synthesis and metabolism of flavonoid components (such as rutin, quercetin, and catechin), thereby increasing the total flavonoid content. The results of this study revealed that the B2 treatment significantly increased the contents of nine flavonoid components, all of which are key substances for bioflavonoid synthesis; these results are consistent with previous results, suggesting that CBM biofertilizer promotes bioflavonoid synthesis, possibly because some components of CBM biofertilizer may directly or indirectly participate in physiological metabolic processes in buckwheat, affecting flavonoid component synthetic pathways and regulatory mechanisms and thereby increasing flavonoid content (Li et al., 2019).

4.4 Effect of different fertilization treatments on buckwheat sprouts

Buckwheat sprouts are buckwheat seeds germinated under the right conditions to form young shoots, rich in a variety of bioactive ingredients (Kim et al., 2004). Rauf et al. (2019) observed significant differences in the sprout length, sprout diameter, fresh weight, and dry weight of buckwheat sprouts obtained from buckwheat harvested under different fertilization treatments. In this study, compared with buckwheat sprouts obtained from buckwheat harvested under no fertilizer, chemical fertilizer, and cow manure

treatments, the sprout length, sprout diameter, tap root length, fresh weight, and dry weight of sprouts harvested in the B2 treatment were the greatest, consistent with previous results. These findings indicate that CBM biofertilizer can indirectly affect the growth status of buckwheat sprouts by affecting the nutrient contents of buckwheat grains. Studies have shown that after breeding of buckwheat sprouts, the contents of free amino acids, soluble sugars, vitamins, flavonoids, and phenolic substances increase significantly (Sytar et al., 2018). Dong et al. (2023) reported that during cultivation, the contents of free amino acids, flavonoids, and phenolic substances constantly changed, presenting a greater nutritional value than that of buckwheat grains. Zhang et al. (2015) reported that germination has significant effects on the nutritional components and various bioactive components of buckwheat, and the differences between grains subjected to different treatments could be visually observed through buckwheat sprouts. The results of this study showed that, compared with the use of buckwheat sprouts obtained from plants under no fertilizer, chemical fertilizer, or cow manure treatment, the application of CBM biofertilizer improved the quality of Tartary buckwheat, thereby indirectly increasing the contents of free amino acids, soluble sugars, vitamin C, bioflavonoids, and total phenolics, and the effect of the B2 treatment was the most significant. This finding is consistent with the results of previous studies and may be due to the greater quality of Tartary buckwheat plants grown with CBM biofertilizer, which can provide sufficient nutrients for sprout growth and development. During germination, macromolecular proteins, polysaccharides, and other substances in buckwheat undergo moderate decomposition by a variety of enzymes and are converted into free amino acids and soluble sugars and other substances that are easily absorbed by the human body, thereby affecting the quality of buckwheat sprouts (Borgonovi et al., 2023).

Notably, with a further increase in the CBM biofertilizer application rate, the yield and quality of Tartary buckwheat decreased, possibly due to an excess of nutrients in the soil, such as nitrogen, phosphorus, and potassium, caused by the excessive application of CBM biofertilizer. These surplus nutrients may not be effectively used by buckwheat but may instead inhibit the uptake of other nutrients, affecting normal crop growth and development and resulting in reduced yield and quality (Lu and Tian, 2017). In addition, excessive CBM biofertilizer may generate acidic substances or harmful gases during decomposition, which may damage the crop root system and affect normal crop growth and development, eventually affecting yield and quality (Li et al., 2018). In general, CBM biofertilizer has a positive effect on the growth and development of Tartary buckwheat and Tartary buckwheat sprouts, but farmers should reasonably control the amount of fertilizer applied. These findings indicate that high Tartary buckwheat yield and quality can be achieved through CBM biofertilizer application and that CBM fertilizer should be used in the planting of Tartary buckwheat. However, this study has some limitations, in this study, different fertilization treatments in buckwheat bioflavonoid fractions have significant differences, but did not further explore the reasons for the differences in bioflavonoid fractions, therefore, in the future, different fertilization treatments can be carried out on the buckwheat genomics and metabolomics of the joint analysis of gene expression of individual genes in the synthesis of bioflavonoids, to verify whether the gene up-regulation or down-regulation whether it led to differences in bioflavonoid fractions between different fertilization treatments.

5 Conclusion

An appropriate amount of CBM biofertilizer (15,000 kg·ha^{-1}) increased the plant height, stem diameter, number of main stem nodes, and number of main stem branches, increased the leaf blade area and chlorophyll content, and increased the grain weight per plant and the 1,000-grain weight, thereby increasing the yield of Tartary buckwheat. This amount of CBM biofertilizer increased the contents of protein, starch, cellulose, and fat in Tartary buckwheat grains and increased the bioflavonoid content by promoting the synthesis of flavonoids. For buckwheat plants grown under this amount of CBM biofertilizer, after the harvested Tartary buckwheat grains were bred into Tartary buckwheat sprouts, the sprout length, sprout diameter, tap root length, and fresh weight of the sprouts were improved, and the contents of free amino acids, soluble sugars, vitamin C, total phenols, and bioflavonoids were greater than those in the other treatments. In order to achieve high-yield and high-quality cultivation of buckwheat, it is recommended that the CBM biofertilizer as a new type of bio-organic fertilizers used to reduce the amount of fertilizers and increase the efficiency of the promotion of green and organic agriculture to provide theoretical guidance for sustainable development.

Data availability statement

The original contributions presented in the study are included in the article/supplementary material. Further inquiries can be directed to the corresponding authors.

Author contributions

LM: Conceptualization, Data curation, Investigation, Software, Validation, Writing – original draft, Writing – review & editing. HX: Formal Analysis, Investigation, Project administration, Validation, Writing – review & editing. LuR: Conceptualization, Data curation, Methodology, Supervision, Writing – review & editing. ZC: Data curation, Resources, Writing – review & editing. HR: Data curation, Writing – review & editing. XG: Conceptualization, Data curation, Writing – review & editing. LG: Resources, Supervision, Writing – review & editing. DJ: Conceptualization, Investigation, Supervision, Writing – review & editing. WC: Conceptualization, Methodology, Writing – review & editing. GX: Data curation, Formal Analysis, Software, Visualization, Writing – review & editing. SZ: Investigation, Methodology, Writing – review & editing. LiR: Conceptualization,

Validation, Writing – review & editing. ZY: Data curation, Funding acquisition, Methodology, Project administration, Resources, Supervision, Validation, Visualization, Writing – review & editing. HF: Conceptualization, Data curation, Formal Analysis, Funding acquisition, Investigation, Methodology, Project administration, Resources, Software, Supervision, Validation, Visualization, Writing – review & editing.

Funding

The author(s) declare that financial support was received for the research and/or publication of this article. The authors would like to thank all of the staff who helped manage the field experiment and our colleagues who helped us collect and analyze the data. This study was supported by the Open Fund Project of the Key Laboratory of Castor Breeding State People's Committee (MDK2023001 and MDK2022011), the Rolling Support Program for Grassland Talent Chuangxin Team-Castor Molecular Breeding Research Innovative Talent Team of Inner Mongolia Autonomous Region (2022), and the Open Fund Project of the Collaborative Innovation Center of Castor Industry of Inner Mongolia Autonomous Region (MDK2022014, MDK2021011, MDK2022016), 2023, 2024, 2025 Inner Mongolia Autonomous Region Castor Breeding and Comprehensive Utilization Key Laboratory Construction Project (2023KYPT0024, 2024KYPT0093, 2025KYPT0089), Inner Mongolia University for Nationalities, 2022 annual basic scientific research operational expenses of colleges and universities directly under the Autonomous Region (237), castor-oilseed hemp industry technological innovation in the Inner Mongolia Autonomous Region Engineering Research Center Open Fund Project (MDK2022006) was funded.

Conflict of interest

Author XG was employed by the company Beijing Zhongmin Sunshine Biotechnology Co.

The remaining authors declare that the research was conducted in the absence of any commercial or financial relationships that could be construed as a potential conflict of interest.

Generative AI statement

The author(s) declare that no Generative AI was used in the creation of this manuscript.

Publisher's note

All claims expressed in this article are solely those of the authors and do not necessarily represent those of their affiliated organizations, or those of the publisher, the editors and the reviewers. Any product that may be evaluated in this article, or claim that may be made by its manufacturer, is not guaranteed or endorsed by the publisher.

References

Ahmed, U., Lin, J. C. W., Srivastava, G., and Djenouri, Y. (2021). A nutrient recommendation system for soil fertilization based on evolutionary computation. *Comput. Electron Agr.* 189, 106407. doi: 10.1016/j.compag.2021.106407

Bhunia, S., Bhowmik, A., Mallick, R., and Mukherjee, J. (2021). Agronomic efficiency of animal-derived organic fertilizers and their effects on biology and fertility of soil: A review. *Agronomy.* 11, 823. doi: 10.3390/agronomy11050823

Borgonovi, S. M., Chiarello, E., Pasini, F., Picone, G., Marzocchi, S., Capozzi, F., et al. (2023). Effect of sprouting on biomolecular and antioxidant features of common buckwheat (Fagopyrum esculentum). *Foods.* 12, 2047. doi: 10.3390/foods12102047

Çürük, U., Işık, M., Ferahoğlu, E., Kırıcı, S., and Ortaş, İ. (2020). Effect of organic and inorganic fertilizer applications on buckwheat yield and micro element nutrition. *Turkish JAF Sci.Tech.* 8, 145–149. doi: 10.24925/turjaf.v8isp1.145-149.4063

Dong, Y., Wang, N., Wang, S., Wang, J., and Peng, W. (2023). A review: The nutrition components, active substances and flavonoid accumulation of Tartary buckwheat sprouts and innovative physical technology for seeds germinating. *Front. Nutr.* 10. doi: 10.3389/fnut.2023.1168361

El-Saadony, M. T., ALmoshadak, A. S., Shafi, M. E., Albaqami, N. M., Saad, A. M., El-Tahan, A. M., et al. (2021). Vital roles of sustainable nano-fertilizers in improving plant quality and quantity-an updated review. *Saudi J. Biol. Sci.* 28, 7349–7359. doi: 10.1016/j.sjbs.2021.08.032

Fan, Y., Jin, Y. N., Ding, M., Tang, Y., Cheng, J., Zhang, K., et al. (2021). The complete chloroplast genome sequences of eight Fagopyrum species: Insights into genome evolution and phylogenetic relationships. *Front. Plant Sci.* 12. doi: 10.3389/fpls.2021.799904

Fang, X., Li, Y., Nie, J., Wang, C., Huang, K., Zhang, Y., et al. (2018). Effects of nitrogen fertilizer and planting density on the leaf photosynthetic characteristics, agronomic traits and grain yield in common buckwheat (Fagopyrum esculentum M.). *Field Crop Res.* 219, 160–168. doi: 10.1016/j.fcr.2018.02.001

Gao, L., Haesaert, G., Van Bockstaele, F., Vermeir, P., Skirtach, A., and Eeckhout, M. (2024). Combined effects of nitrogen and sulfur fertilizers on chemical composition, structure and physicochemical properties of buckwheat starch. *Food Chem.* 459, 140351. doi: 10.1016/j.foodchem.2024.140351

Gao, L., Wang, H., Wan, C., Wang, P., Eeckhout, M., and Gao, J. (2023). Suitable nitrogen fertilizer application drives the endosperm development and starch synthesis to improve the physicochemical properties of common buckwheat grain. *Int. J. Biol. Macromol.* 235, 123837. doi: 10.1016/j.ijbiomac.2023.123837

Gimenez-Bastida, J. A., and Zielinski, H. (2015). Buckwheat as a functional food and its effects on health. *J. Agr. Food Chem.* 63, 7896–7913. doi: 10.1021/acs.jafc.5b02498

Guo, R., Zhang, X., Tang, Z., Zhang, Y., and Huang, K. (2022). Effects of rice straw combined with inorganic fertilizer on grain filling and yield of common buckwheat. *Agronomy.* 12, 1287. doi: 10.3390/agronomy12061287

Habtemariam, S. (2019). Antioxidant and rutin content analysis of leaves of the common buckwheat (Fagopyrum esculentum Moench) grown in the United Kingdom: a case study. *Antioxidants.* 8, 160. doi: 10.3390/antiox8060160

He, Y., Zhang, K., Shi, Y., Lin, H., Huang, X., Lu, X., et al. (2024). Genomic insight into the origin, domestication, dispersal, diversification and human selection of Tartary buckwheat. *Genome Biol.* 25, 61. doi: 10.1186/s13059-024-03203-z

Hornyák, M., Dziurka, M., Kula-Maximenko, M., Pastuszak, J., Szczerba, A., Szklarczyk, M., et al. (2022). Photosynthetic efficiency, growth and secondary metabolism of common buckwheat (Fagopyrum esculentum Moench) in different controlled-environment production systems. *Sci. Rep.* 12, 257. doi: 10.1038/s41598-021-04134-6

Jha, R., Zhang, K., He, Y., Mendler-Drienyovszki, N., Magyar-Tábori, K., Quinet, M., et al. (2024). Global nutritional challenges and opportunities: Buckwheat, a potential bridge between nutrient deficiency and food security. *Trends Food Sci. Technol.* 104365. doi: 10.1016/j.tifs.2024.104365

Jiang, P., Burczynski, F., Campbell, C., Pierce, G., Austria, J. A., Briggs, C. J., et al. (2007). Rutin and flavonoid contents in three buckwheat species Fagopyrum esculentum, F. tataricum and F. homotropicum and their protective effects against lipid peroxidation. *Food Res. Int.* 40, 356–364. doi: 10.1016/j.foodres.2006.10.009

Khatri, P., Kumar, P., Shakya, K. S., Kirlas, M. C., and Tiwari, K. K. (2023). Understanding the intertwined nature of rising multiple risks in modern agriculture and food system. *Environ. Dev. Sustain.* 26, 24107–24150. doi: 10.1007/s10668-023-03638-7

Kim, S. L., Kim, S. K., and Park, C. H. (2004). Introduction and nutritional evaluation of buckwheat sprouts as a new vegetable. *Food Res. Int.* 37, 319–327. doi: 10.1016/j.foodres.2003.12.008

Lee, L. S., Choi, E. J., Kim, C. H., Sung, J. M., Kim, Y. B., Seo, D. H., et al. (2016). Contribution of flavonoids to the antioxidant properties of common and tartary buckwheat. *J. Cereal Sci.* 68, 181–186. doi: 10.1016/j.jcs.2015.07.005

Li, M., Luo, R., Yin, M., Wang, Z., Su, Z., Gu, X., et al. (2024). Castor bean meal fertilizer improves peanut yield and quality by regulating the soil physicochemical environment and soil enzyme activities. *J. Soil Sci. Plant Nutt.* 24, 4681–4701. doi: 10.1007/s42729-024-01863-1

Li, H., Lv, Q., Ma, C., Qu, J., Cai, F., Deng, J., et al. (2019). Metabolite profiling and transcriptome analyses provide insights into the flavonoid biosynthesis in the developing seed of tartary buckwheat (Fagopyrum tataricum). *J. Agric. Food Chem.* 67, 11262–11276. doi: 10.1021/acs.jafc.9b03135

Li, C., Xiong, Y., Qu, Z., Xu, X., Huang, Q., and Huang, G. (2018). Impact of biochar addition on soil properties and water-fertilizer productivity of tomato in semi-arid region of Inner Mongolia, China. *Geoderma*. 331, 100–108. doi: 10.1016/j.geoderma.2018.06.014

Lin, S., Wang, Q., Wei, K., Sun, Y., Shao, F., Lei, Q., et al. (2024). Enhancing pakchoi (Brassica chinensis L.) agriculture with magnetized-ionized brackish water and organic fertilizers: A sustainable approach to soil quality and crop yield optimization. *J. Clean Prod.* 450, 141935. doi: 10.1016/j.jclepro.2024.141935

Liu, W., Cui, S., Wu, L., Qi, W., Chen, J., Ye, Z., et al. (2023). Effects of bio-organic fertilizer on soil fertility, yield, and quality of tea. *J. Soil Sci. Plant Nutt.* 23, 5109–5121. doi: 10.1007/s42729-023-01195-6

Lo Presti, V., Tudisco, R., Di Rosa, A. R., Musco, N., Iommelli, P., Infascelli, F., et al. (2023). Influence of season on milk fatty acid profile and sensory characteristics of grazing goats in a Mediterranean environment: a sustainable agro-food system. *Anim. Prod. Sci.* 63, 689–703. doi: 10.1071/an21538

Lu, C., and Tian, H. (2017). Global nitrogen and phosphorus fertilizer use for agriculture production in the past half century: shifted hot spots and nutrient imbalance. *Earth Syst. Sci. Data.* 9, 181–192. doi: 10.5194/essd-9-181-2017

Martinez, S., Gabriel, J. L., Allende-Montalbán, R., San-Juan-Heras, R., and Delgado, M. D. M. (2022). The application of a bio-stabilized municipal solid waste-based fertilizer for buckwheat production. *Agriculture.* 12, 776. doi: 10.3390/agriculture12060776

Miao, Y., Stewart, B. A., and Zhang, F. (2010). Long-term experiments for sustainable nutrient management in China. A review. *Agrono Sustain Dev.* 31, 397–414. doi: 10.1051/agro/2010034

Popović, V., Sikora, V., Glamočlija, Đ., Ikanović, J., Filipović, V., Tabaković, M., et al. (2013). Influence of agro-ecological conditions and foliar fertilization on yield and yield components of buckwheat in conventional and organic cropping system. *Biotechnol.* 29, 537–546. doi: 10.2298/BAH1303537P

Radchenko, M. V., Butenko, A. O., and Hlupak, Z. I. (2018). The influence of fertilizer system and efficacy of growth regulator on buckwheat productivity under the conditions of north-east forest steppe of Ukraine. *Ukr. J. Ecol.* 8, 89–94. doi: 10.15421/2018_314

Rauf, M., Yoon, H., Lee, S., Lee, M. C., Oh, S., and Choi, Y. M. (2019). Evaluation of sprout growth traits and flavonoid content in common and tartary buckwheat germplasms. *Plant Breed Biotechnol.* 7, 375–385. doi: 10.9787/pbb.2019.7.4.375

Rotili, D. H., Guglielmini, A., Caccavo, M., Antequera, S., Rocca, C. M., and Miralles, D. J. (2023). Grain yield, yield components and nitrogen economy of irrigated second-crop common Buckwheat (Fagopyrum esculentum Moench) in a cold-temperate region. *Eur. J. Agron.* 144, 126750. doi: 10.1016/j.eja.2023.126750

Sobhani, M. R., Rahmikhdoev, G., Mazaheri, D., and Majidian, M. (2014). Influence of different sowing date and planting pattern and N rate on buckwheat yield and its quality. *Aust. J. Crop Sci.* 8, 1402–1414. doi: 10.3316/informit.752483727431353

Sonawane, S., Shams, R., Dash, K. K., Patil, V., Pandey, V. K., and Dar, A. H. (2024). Nutritional profile, bioactive properties and potential health benefits of buckwheat: A review. *EFood.* 5, e171. doi: 10.1002/efd2.171

Sparks, D. L. (2020). A golden period for environmental soil chemistry. *Geochem T.* 21, 1–5. doi: 10.1186/s12932-020-00068-6

Starič, P., Remic, L., Vogel-Mikuš, K., Junkar, I., Vavpetič, P., Kelemen, M., et al. (2023). Exploring the potential of cold plasma treatment followed by zinc-priming for biofortification of buckwheat sprouts. *Front. Nutr.* 10. doi: 10.3389/fnut.2023.1151101

Suzuki, T., Hara, T., and Katsu, K. (2021). Breeding of buckwheat for usage of sprout and pre-harvest sprouting resistance. *Plants.* 10, 997. doi: 10.3390/plants10050997

Sytar, O., CHRENKOVá, M., Ferencová, J., POLAčIKOVá, M., Rajský, M., and Ferencová, J. (2018). Nutrient capacity of amino acids from buckwheat seeds and sprouts. *J. Food Nutr. Res.* 57, 38–47. Available online at: https://webofscience.clarivate.cn/wos/alldb/full-record/WOS:000430630000004.

Tang, Z., Guo, R., Yang, X., Min, J., He, P., Huang, X., et al. (2024). Appropriate concentration of rice straw decomposition liquid prompted germination and seedling growth of common buckwheat. *J. Soil Sci. Plant Nutt.* 24, 3861–3872. doi: 10.1007/s42729-024-01805-x

Tang, L., Tang, J., Huang, K., and Huang, X. (2024). Potassium fertilizer promotes the thin-shelled Tartary buckwheat yield by delaying senescence and promoting grain filling. *Front. Plant Sci.* 15. doi: 10.3389/fpls.2024.1385548

Tao, J., Wan, C., Leng, J., Dai, S., Wu, Y., Lei, X., et al. (2023). Effects of biochar coupled with chemical and organic fertilizer application on physicochemical properties and *in vitro* digestibility of common buckwheat (Fagopyrum esculentum Moench) starch. *Int. J. Biol. Macromol.* 246, 125591. doi: 10.1016/j.ijbiomac.2023.125591

Wan, C., Gao, S., Wang, J., Lei, X., Ge, J., Tao, J., et al. (2023). Optimal planting density combined with phosphorus input promotes common buckwheat resource use efficiency and productivity to increase grain yield. *Agric. Water Manage.* 287, 108468. doi: 10.1016/j.agwat.2023.108468

Wan, C., Gao, L., Wang, J., Lei, X., Wu, Y., and Gao, J. (2021). Proteomics characterization nitrogen fertilizer promotes the starch synthesis and metabolism and amino acid biosynthesis in common buckwheat. *Int. J. Biol. Macromol.* 192, 342–349. doi: 10.1016/j.ijbiomac.2021.09.170

Wang, Z., Hassan, M. U., Nadeem, F., Wu, L., Zhang, F., and Li, X. (2020). Magnesium fertilization improves crop yield in most production systems: a meta-analysis. *Front. Plant Sci.* 10. doi: 10.3389/fpls.2019.01727

Wang, T., Xu, J., Chen, J., Liu, P., Hou, X., Yang, L., et al. (2024). Progress in microbial fertilizer regulation of crop growth and soil remediation research. *Plants.* 13, 346. doi: 10.3390/plants13030346

Xiang, D., Song, Y., Wu, Q., Ma, C., Zhao, J., Wan, Y., et al. (2019). Relationship between stem characteristics and lodging resistance of Tartary buckwheat (Fagopyrum tataricum). *Plant Prod. Sci.* 22, 202–210. doi: 10.1080/1343943x.2019.1577143

Yang, J., Gu, Z., Zhu, L., Cheng, L., Li, Z., Li, C., et al. (2019). Buckwheat digestibility affected by the chemical and structural features of its main components. *Food Hydrocolloids.* 96, 596–603. doi: 10.1016/j.foodhyd.2019.06.001

Yang, Q., Tang, J., Huang, X., and Huang, K. (2024). The effect of exogenous gibberellin and its synthesis inhibitor treatments for morphological and physiological characteristics of Tartary buckwheat. *Sci. Rep.* 14, 20117. doi: 10.1038/s41598-024-71142-7

Yuan, H., Wang, Q., Qi, A., Li, S., Hu, Y., Hu, Z., et al. (2024a). Morphological, physiological, and photosynthetic differences of tartary buckwheat induced by post-anthesis drought. *Plants.* 13, 2161. doi: 10.3390/plants13152161

Yuan, H., Wang, Q., Tan, J., Wu, J., Liang, C., Wang, Y., et al. (2024b). Ionic titanium is expected to improve the nutritional quality of Tartary buckwheat sprouts through flavonoids and amino acid metabolism. *Food Chem.* 461, 140907. doi: 10.1016/j.foodchem.2024.140907

Zhang, Z., Wu, Y., Truong, V. K., and Zhang, D. (2021). Earthworm (Eisenia fetida) mucus inspired bionic fertilizer to stimulate maize (Zea mays L.) growth. *Sustainability.* 13, 4299. doi: 10.3390/su13084299

Zhang, G., Xu, Z., Gao, Y., Huang, X., Zou, Y., and Yang, T. (2015). Effects of germination on the nutritional properties, phenolic profiles, and antioxidant activities of buckwheat. *J. Food Sci.* 80, H1111–H1119. doi: 10.1111/1750-3841.12830

Zhang, Z. L., Zhou, M. L., Tang, Y., Li, F. L., Tang, Y. X., Shao, J. R., et al. (2012). Bioactive compounds in functional buckwheat food. *Food Res. Int.* 49, 389–395. doi: 10.1016/j.foodres.2012.07.035

Zheng, M., Zhong, S., Wang, W., Tang, Z., Bu, T., and Li, Q. (2023). Serendipita indica promotes the growth of tartary buckwheat by stimulating hormone synthesis, metabolite production, and increasing systemic resistance. *J. Fungi.* 9, 1114. doi: 10.3390/jof9111114

Zhou, Q., He, P., Tang, J., Huang, K., and Huang, X. (2023a). Increasing planting density can improve the yield of Tartary buckwheat. *Front. Plant Sci.* 14, 1313181. doi: 10.3389/fpls.2023.1313181

Zhou, Q., Tang, J., Liu, C., Huang, K., and Huang, X. (2023b). Effects of phosphate fertilizer application on the growth and yield of Tartary buckwheat under low-nitrogen condition. *Agronomy.* 13, 1886. doi: 10.3390/agronomy13071886

frontiers | Frontiers in Plant Science

TYPE Original Research
PUBLISHED 13 June 2025
DOI 10.3389/fpls.2025.1604427

Check for updates

OPEN ACCESS

EDITED BY
Ioannis Roussis,
Agricultural University of Athens, Greece

REVIEWED BY
Sharif Ahmed,
International Rice Research Institute (IRRI), Philippines
Meng Xu,
Chinese Academy of Agricultural Sciences, China
Paola Leija-Martínez,
Universidad Autónoma Agraria Antonio Narro, Mexico
Zhipeng Sha,
Kunming University of Science and Technology, China

*CORRESPONDENCE
Chunjie Li
chunjie@lzu.edu.cn

†These authors have contributed equally to this work

RECEIVED 02 April 2025
ACCEPTED 29 May 2025
PUBLISHED 13 June 2025

CITATION
Zhang R, Wang Y, Malik K, Wang J, Zhao G and Li C (2025) Optimal fertilizer rate and sowing density can improve oat quality, yield and N and P comprehensive efficiency in the Loess Plateau of China. *Front. Plant Sci.* 16:1604427. doi: 10.3389/fpls.2025.1604427

COPYRIGHT
© 2025 Zhang, Wang, Malik, Wang, Zhao and Li. This is an open-access article distributed under the terms of the Creative Commons Attribution License (CC BY). The use, distribution or reproduction in other forums is permitted, provided the original author(s) and the copyright owner(s) are credited and that the original publication in this journal is cited, in accordance with accepted academic practice. No use, distribution or reproduction is permitted which does not comply with these terms.

Optimal fertilizer rate and sowing density can improve oat quality, yield and N and P comprehensive efficiency in the Loess Plateau of China

Ruochen Zhang[1,2,3,4,5†], Yue Wang[1,2,3,4,5†], Kamran Malik[1,2,3,4,5], Jianjun Wang[1,2,3,4,5], Guiqin Zhao[6] and Chunjie Li[1,2,3,4,5*]

[1]State Key Laboratory of Herbage Improvement and Grassland Agro-ecosystems, Lanzhou University, Lanzhou, China, [2]Key Laboratory of Grassland Livestock Industry Innovation, Ministry of Agriculture and Rural Affairs, Beijing, China, [3]Engineering Research Center of Grassland Industry, Ministry of Education, Beijing, China, [4]Gansu Tech Innovation Center of Western China Grassland Industry, Lanzhou, China, [5]College of Pastoral Agriculture Science and Technology, Lanzhou University, Lanzhou, China, [6]Pratacultural College, Gansu Agricultural University, Lanzhou, China

Introduction: Oat is a nutritious native species in Loess Plateau for forage and animal husbandry. By focusing on the sowing density and fertilizer rate, oats can achieve better productivity performance while maximizing nutrients use efficiency. However, the information on the responses of oats yield, quality and nutrients use efficiency to fertilization and sowing density is limited.

Methods: In this study, from 2022 to 2023, a two-factor randomized block design field trial was conducted in Loess Plateau. The three sowing densities (SD, L: 75 kg/ha; M: 150 kg/ha; H: 225 kg/ha) were coupled with six fertilizer rates (FR, N0P0: no fertilization; N2: 100 N kg/ha; P2: 90 P kg/ha; N1P2: 50 N kg/ha, 90 P kg/ha; N2P1: 100 N kg/ha, 45 P kg/ha; N2P2: 100 N kg/ha, 90 P kg/ha). The effects of FR and SD on oat forage yield, quality, agronomic efficiency (AE), N/P content, uptake and its uptake efficiency and recover efficiency were investigated. In order to compare N/P efficiency more intuitively, we combined N/P content, N/P uptake, N/P uptake efficiency and N/P recover efficiency to calculate N/P comprehensive efficiency.

Results: Overall, the M-N1P2 treatment promoted the oat growth and achieved the maximum oat forage yield and quality. In the M treatment, the average crude protein (CP) content, relative feed value (RFV), forage yield, CP yield, N content, P content, N uptake and P uptake increased by 20.2%, 4.9%, 73.2%, 100%, 30.4%, 26.3%, 128.5% and 118.4%, respectively, compared with those under the no fertilization treatment; while the average neutral detergent fiber (NDF) decreased by 2.6% in the N1P2 treatment compared to no fertilization treatment. The optimum agronomic efficiency (AE), N uptake efficiency and N recover efficiency were also observed under M-N1P2 during both years. The comprehensive analysis revealed M-N1P2 also had the highest N comprehensive efficiency and P comprehensive efficiency among all treatments. The results of correlation analysis revealed significant positive correlations ($P< 0.05$) of forage yield and CP with nutrients efficiency of oat, but negative correlations with fiber content.

Discussion: This study determined the appropriate sowing density and fertilization rate (M-N1P2) for cultivating oat in Loess Plateau and provided a foundation for promoting productivity of oats.

KEYWORDS

oat, sowing density, fertilizer rate, yield, quality, nutrients use efficiency

1 Introduction

Oat has high yield and nutritional quality, and is suitable for cultivation over a wide range of soil types and climatic conditions (Jakubus and Graczyk, 2022). It is the most widely grown annual forage cereal in the world (Andrzejewska et al., 2019). Due to oat forage's rich composition of nutrients, including proteins, antioxidants, and various amino acids, it possesses a high nutritional value. There is growing interest in the oat cultivation as a result of an increasing appreciation of the feeding benefits of oat forage. Among oat consumption all over the world, feeding is the main, supplemented by food, and feeding consumption accounts for almost 60% (Marshall et al., 2013).

Historically, the Loess Plateau has been one of the key primary livestock production hubs, contributing significantly to the national livestock population with 12,311,000 cattle and 56,525,000 sheep, representing 11% and 19% of China's total livestock, respectively (Zhang et al., 2017b). Thus, demand of forages in the Loess Plateau is on the rise due to market demand fueled by the animal industry. However, recent studies on forage crops in the region mainly focus corn and alfalfa (Jia et al., 2018; Zhang et al., 2017b; Kamran et al., 2022; Liu et al., 2021), and often neglects oats, a high-quality forage that is resistant to drought and infertility. Therefore, it is necessary to conduct further research on oats to fill this gap. Oat is grown by smallholder farmers focus on forage for livestock in this region. However, the agroecosystems of Loess Plateau in semi-arid regions are highly vulnerable due to limited available soil nutrient (Li et al., 2022; Wang et al., 2018), the growth of oat forages is usually negatively impacted by poor soil fertility. Maximizing the potential of oat cultivation, and improving oat nutrient efficiency crude protein (CP) yield in this region is a crucial strategy for addressing forage issues and fostering regional economic development.

Fertilization and planting density are two critical agronomic practices in cropping system for high productivity (Fu et al., 2021). Nitrogen is a limiting nutrient for plant growth and development (Gaudinier et al., 2018), while phosphorus is significant for plant development and reproduction (Zou et al., 2022). Both are essential macronutrients for improving agricultural productivity and maintaining ecosystem stability, and their combined application can lead to significant improvements in quality and yield of crop. Understanding the complex interactions between N and P use is critical for maximizing their nutrient efficiency in crops. Research indicates that their bilateral interaction promotes each other in the uptake and utilization of nutrition (Wang et al., 2020), and their combined application can enhance crop's capacity to absorb nutrients (Zhang et al., 2021a). But the nutrient use efficiency varies with N and P supply levels, rapid nutrients loss occurs if the fertilizer rate is beyond the uptake capacity of crops. On the other hand, achieving high-yield and improved nutrients use efficiency under increasing planting density has been the priority goal of oat production. However, the higher planting densities may lead to increased competition among plants for nutrients, which may decrease the uptake of nitrogen and P, ultimately reduce protein and dry matter in the harvested crop. Hence, optimum fertilizer rate and planting density varies depending on field fertility condition as well as uptake capacity of crop, it is necessary to understand the mechanisms of nutrition use efficiency improvement of oats, which will in turn facilitate progress in management for field fertilizer.

The optimal fertilization rate coupled improving sowing density are the effective ways to improve crop productivity and maintain sustainable crop production (Yousaf et al., 2016). By focusing on the interplay between planting density and nutrient utilization can achieve better crop performance while minimizing negative environmental impacts (Hawkesford and Griffiths, 2019). Several studies have confirmed that improving planting density compatible with fertilizers application might benefit crop production for high yield with high fertilizer use efficiency. While, the improving planting density may compensate for the yield loss from fertilizer input reduction (Zhu et al., 2016; Huang et al., 2018). Notably, improving sole fertilizer application does not maximize the yield potential of crop population, while coupled appropriate planting density can significantly enhance the productivity of crop populations, resulting in increased yield of target crops (Wu et al., 2024). Moreover, enhancing nutrient efficiency through appropriate planting density coupled fertilizers not only contributes to greater nutrient accumulation but also supports sustainable agricultural practices by reducing the need for excessive fertilization. This is particularly important regarding the environmental concerns associated with fertilizers loss and soil degradation (Xu et al., 2012; Chen and Liao, 2017). In summary, the strategic management of sowing density, when coordinated with effective nutrients uptake and utilization practices, can lead to significant improvements in crop productivity and sustainability.

Moreover, yield and resource utilize efficiency of oat are affected by soil moisture, nutrients, light, and many other factors. The soil water and fertility conditions and agriculture systems are highly diverse in time and space, and the strategy of optimal sowing

density and fertilization rate for another region may not be suitable for Loess Plateau (Kamran et al., 2023). Farmers in Loess Plateau of China are experiencing a lack of scientific recommendations of fertilizer application and reasonable sowing density for oats. They generally use intensive agronomic practices to increase the yield due to limited precipitation and soil degradation (Si et al., 2020; Tang et al., 2018). However, the negative impact on resource efficiency and the ecological environment is often ignored. Excess fertilizer amount and sowing density produce severe soil-ecological disruption and addition of cultivation cost, these intensive agronomic practices are untenable, both from economic and ecological benefit perspectives. To the best of our knowledge, there are very few reports from quality characteristics of oat in Loess Plateau, and even less about the response of nutrient efficiency to fertilizer and sowing density, thereby, little is known if forage yield, nutritive quality and resource efficiency of oat can simultaneously be improved with optimized fertilization and density in the Loess Plateau.

We hypothesized that the current fertilizers amount and plant density management for oat in the Loess Plateau is unreasonable and not conducive to cultivation of oat. Instead, optimizing fertilizer rate and sowing density would be valuable in improving yield, nutritional quality and nutrients use efficiency. Therefore, the present study was aimed to investigate the effects of different fertilizer rate and sowing density on forage yield, quality, nutrients indices and nutrients use efficiency for oat, and to determine a suitable management practice for maximize oat productivity in the Loess Plateau of northwest China. The results of this study would ensure the demands of taking full advantage of nutrient, while sustaining forage production and could provide new insights into the sustainable cultivation of oat on nutrient-limited land of Loess Plateau.

2 Materials and method

2.1 Experimental site details

Field experiments were conducted during 2022–2023 in Huan County, Gansu Province (36°16' N, 107°31' E; elevation, 1150 m), located in the Loess Plateau, Northwest China. The average annual precipitation in this region is 430 mm and 70% occurs during oat growing season (May to September). The annual precipitation is 414.5 and 364.6 mm in 2022 and 2023, the average temperature over oat growing season is 19.6 °C. The soil at the experimental site is classified as "loessial soil". Basic soil properties were as follows: organic matter, available nitrogen, available phosphorus, available potassium and pH in the 0-20 cm soil layer was determined as 4.7 g kg^{-1}, 54.1 mg kg^{-1}, 11.3 mg kg^{-1}, 166.4 mg kg^{-1} and 8.5, respectively.

2.2 Experimental design details

Field experiments were conducted to evaluate six fertilizer rates: N0P0, no fertilization; N2, 100 N kg/ha; P2, 90 P kg/ha; N1P2, 50 N kg/ha + 90 P kg/ha; N2P1, 100 N kg/ha + 45 P kg/ha; N2P2, 100 N kg/ha + 90 P kg/ha. Three sowing densities: L, 75 kg/ha; M, 150 kg/ha; H, 225 kg/ha. The combination of fertilizer rates and sowing densities were a total of eighteen treatments. In detail, the fertilizer rates and sowing densities were determined by considering both the soil base nutrition status and the farmers' practices (namely, N2P2 treatment and H treatment; Zhang et al., 2025a). Fertilizer rates were divided into two gradients, increasing N fertilizer amount at the same P fertilizer level (N0P2, N1P2, N2P2); increasing P fertilizer amount at the same N fertilizer level (N2P0, N2P1, N2P2).

The experiment was conducted in a randomized complete block design with four replicates. Each plot covered an area of 24 m^2 (4 × 6 m) and with a row spacing of 1 m, ridges were established between each adjacent plot to minimize runoff and fertilizer movement. Ridge cultivation of each plot was performed before sowing, fertilizer was applied in equal parts at the sowing (50%) and jointing (50%) stages. On 28th May 2022 and 18th May 2023, oat seeds (Baiyan No.7, provided by the Baicheng Academy of Agricultural Sciences) were manually sown at a soil depth of 4–5 cm with a 20 cm row spacing. Irrigation was not applied during the oat growing seasons, and weed and pest control were conducted manually. The harvesting of plants took place on 10th October 2022 and 5th October 2023, depending on the prevailing weather conditions.

2.3 Data collection and measurement

2.3.1 Measurement of forage yield and quality

At heading and maturity stages of oat, three separate areas (each 1 m^2) were randomly chosen from each plot, harvested aboveground oat plants and subjected to a drying process at 85°C until reaching a constant weight. The measured result of above dry matter accumulation was considered as forage yield.

Oven-dried oat samples were crushed into fine powder, passed through a 1-mm mesh screen, and prepared for the determination of forage quality and content of N and P. The concentration of crude protein (CP, %) was estimated by determining N content, and the N content was determined via Elementar Vario MAX CNS/CN (Elementar Trading Co., Ltd, Frankfurt, Germany).

The calculation equation (Equation 1) used for CP content were as follows (Zhang et al., 2018):

$$CP\ \ content = N\ \ content \times 6.25 \quad (1)$$

The concentrations of acid detergent fiber (ADF, %) and neutral detergent fiber (NDF, %) were determined following the methods of Vansoest et al. (1991).

2.3.2 Calculation of forage feeding values

The relative feed value (RFV) of oat was calculated in maturity stage. The CP yield (kg ha^{-1}) was calculated in heading and maturity stages. The equations (Equations 2, 3) used for calculation were as follows (Lithourgidis et al., 2006):

$$RFV = (88.9 - 0.779 \times ADF) \times (120/NDF)/1.29 \quad (2)$$

$$CP\ \ yield = aboveground\ \ dry\ \ matter\ \ yield \times CP\ \ content \quad (3)$$

2.3.3 Measurement of forage N and P content and uptake

N content (g kg^{-1}) of oat in heading and maturity stages were determined via Elementar Vario MAX CNS/CN (producer information provided in section 2.3.1). Oat samples were digested with H_2SO_4-H_2O_2, and the P content (g kg^{-1}) of oat at heading and maturity stages were determined with molybdate blue colorimetry as described by (Cao et al., 2021).

Total N and P uptake (kg ha^{-1}) of heading and maturity stages were calculated according to aboveground dry weight (t ha^{-1}) and N/P content (Equations 4, 5):

$$N\ \ uptake = N\ \ content \times aboveground\ \ dry\ \ matter\ \ yield \quad (4)$$

$$P\ \ uptake = P\ \ content \times aboveground\ \ dry\ \ matter\ \ yield \quad (5)$$

2.3.4 Calculation of forage N and P efficiency

The fertilizer agronomic efficiency (AE), N uptake efficiency (NupE), P uptake efficiency (PupE), N recovery efficiency (NRE) and P recovery efficiency (PRE) of oat was calculated in maturity stage and according to forage yield and N/P uptake of maturity stage.

The calculation formula (Equations 6–10) as follows (Yang et al., 2024):

$$AE = \frac{forage\ \ yield - forage\ \ yield\ \ of\ \ no\ \ fertilizer}{Total\ \ fertilizer\ \ input} \quad (6)$$

$$NupE = N\ \ uptake / \ input\ \ of\ \ N \quad (7)$$

$$PupE = P\ \ uptake / \ input\ \ of\ \ P \quad (8)$$

$$NRE = (N\ \ uptake - N\ \ uptake\ \ of\ \ no\ \ fertilizer) / \ input\ \ of\ \ N \quad (9)$$

$$PRE = (P\ \ uptake - P\ \ uptake\ \ of\ \ no\ \ fertilizer) / \ input\ \ of\ \ P \quad (10)$$

2.3.5 Comprehensive evaluation of N and P

Membership function analysis was implemented for comprehensive evaluation of N and P. The N evaluation indicator include N content of heading stage, N content of maturity stages, N uptake of heading stage, N uptake of maturity stages, NupE and NRE; the P evaluation indicator include P content of heading stage, P content of maturity stages, P uptake of heading stage, P uptake of maturity stages, PupE and PRE. The comprehensive analysis score of each indicator of nitrogen was defined as "NCS (nitrogen comprehensive score)", and the comprehensive analysis score of each indicator of phosphorus was defined as "PCS (phosphorus comprehensive score)". The optimal fertilization and density treatment was evaluated by result of analysis.

The calculation method Equations 11, 12 of the comprehensive evaluation indicator was as follows (Li et al., 2023):

$$NCS = \sum\ \ MN_1 W_1 + MN_2 W_2 + \ldots + MN_n W_n \quad (11)$$

$$PCS = \sum\ \ MP_1 W_1 + MP_2 W_2 + \ldots + MP_n W_n \quad (12)$$

where *MN* is the N indicator's membership value, *MP* is the P indicator's membership value, and *W* is the weighting factor. The weightings of each indicator were the same at one in six in this study.

The membership values were counted as follows (Equation 13):

$$M(X_i) = (X_i - X_{min})/(X_{max} - X_{min}) \quad (13)$$

where *M(Xi)* is the membership value, and *M(Xi)* ∈[0,1]; *Xi* is each index's measured value; *Xmin* and *Xmax* are each index's minimum and maximum values.

2.4 Statistical analysis

Statistical data analysis was performed using analysis of variance (ANOVA) in SPSS statistics software 27.0 (IBM Corporation, USA). Multiple comparisons between different treatments were conducted using the Tukey's significant test that significance level of $P< 0.05$. The relationship and interactions of measured variables assessed by Pearson's correlation and principal component analysis (PCA). Figures were used via Origin 2019 (Origin Lab Corporation, USA).

3 Result

3.1 Nutritive quality of oat

The statistical results revealed that the sowing density (SD) had no significant impact on oat crude protein (CP) content except heading stage of 2022. However, the effect of fertilizer rate (FR) on CP was significant ($P< 0.05$) in all stages of two years. The interaction effect of the SD and FR had no significant impact on the CP content (Supplementary Table S1). The CP content was increased with fertilizer application in the two growth seasons, and the highest average CP content of three sowing densities (15.47 and 14.12%) were obtained under the N1P2 treatment, markedly increased by 23.1 and 17.2% in 2022 and 2023, respectively, compare with that in the no fertilization treatment (Figures 1a, b).

The SD had significant ($P< 0.05$) effect on acid detergent fiber (ADF) of oat, the FR had significant ($P< 0.05$) impact on oat ADF except heading stage of 2023, and the interaction effect of the SD and FR had no significant imapct on the ADF during two years (Supplementary Table S1). A lower ADF was observed under the M treatment than that under the L and H treatments in heading stage of 2022 and maturity stage of 2023 (Figures 2a, b). The FR more

10.3389/fpls.2025.1604427

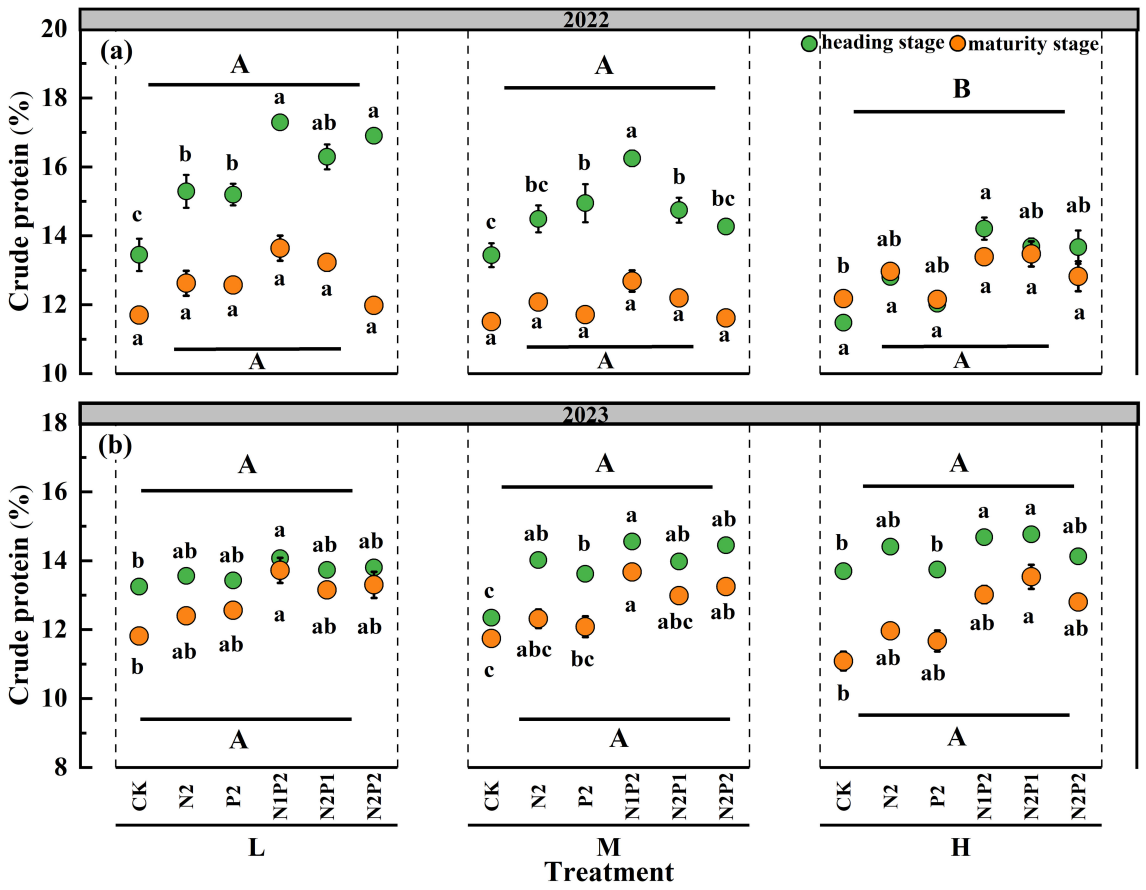

FIGURE 1
Variations in oat crude protein under different sowing densities (SD) and fertilizer rates (FR) at heading and maturity stages in 2022 **(a)** and 2023 **(b)**. L, low sowing density; M, moderate sowing density; H, high sowing density. Vertical bars represent SE values ($P< 0.05$). Different lower-case letters above or under the circles denote significant differences for different fertilizer rates under the same sowing density ($P< 0.05$). Different upper-case letters in top or bottom of figure indicate significant differences between sowing densities ($P< 0.05$).

markedly affected the ADF at the maturity stage compare with that at the heading stage (Figures 2a, b).

The effects of the SD and FR on the neutral detergent fiber (NDF) of oats were significant ($P< 0.05$) in both years, but the interaction effect of the SD and FR had no significant impact on the NDF (Supplementary Table S1). The M treatment significantly decreased the NDF except maturity stage of 2023. At the M treatment, compared with that in the no fertilization treatment, the NDF under the N1P2 was significantly decreased by 1.7 and 3.5% in 2022 and 2023, respectively (Figures 3a, b).

The CP, ADF and NDF significantly differed between the heading and maturity stages. Compared with those in the heading stage, the average CP in the two years were decreased 13.0% in the maturity stage, while the average ADF and NDF in the two years were increased 8.0% and 7.2% in the maturity stage (Figures 1-3).

Different SD and FR treatments significantly ($P< 0.05$) affected the relative feed value (RFV) but their interaction was not. At the M treatment, compare with that in the no fertilization treatment, the RFV values peaking at N1P2 and increasing by 3.2 and 6.6% in 2022 and 2023, respectively (Figures 4a, b).

3.2 Forage yield, crude protein yield and agronomic efficiency

The SD, FR and their interaction effect significantly ($P< 0.05$) affected the forage yield and CP yield of oats (Table 1). Compared with that in the M treatment, the forage yield under L and H treatments were decreased by 18% and 23.9% in 2022 and 34.3% and 46.1% in 2023, respectively. CP yield also reached a maximum at M treatment, and reduced or increase sowing density treatments showed detrimental effects on CP yield. Compare with no fertilizer treatment, the average forage yield of two stages was markedly increased 54.5 and 91.8% under the N1P2 treatment in 2022 and 2023, respectively. The average CP yield showed the same trend with the change of forage yield, peaked at the N1P2 treatment and increasing by 81.2 and 118.8% in 2022 and 2023, respectively, compare with that under the no fertilization treatment. The heading stage had a higher CP content than maturity stage, but maturity stage obtained more forage yield and CP yield, these trends remained steady throughout the experimental duration (Table 1).

10.3389/fpls.2025.1604427

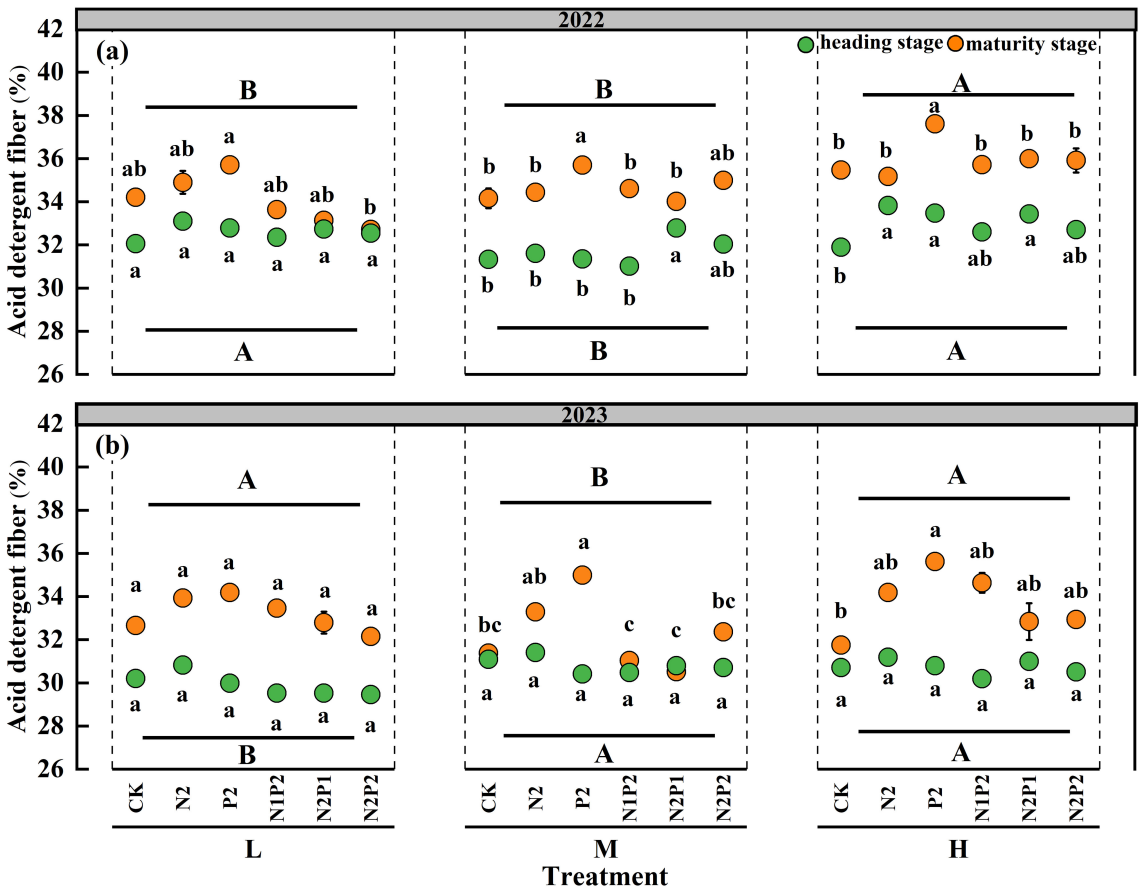

FIGURE 2
Variations in acid detergent fiber under different sowing densities (SD) and fertilizer rates (FR) at heading and maturity stages in 2022 **(a)** and 2023 **(b)**. L, low sowing density; M, moderate sowing density; H, high sowing density. Vertical bars represent SE values ($P< 0.05$). Different lower-case letters above or under the circles denote significant differences for different fertilizer rates under the same sowing density ($P< 0.05$). Different upper-case letters in top or bottom of figure indicate significant differences between sowing densities ($P< 0.05$).

Agronomic efficiency (AE) of oats was significantly ($P< 0.05$) affected by SD and FR but not their interaction effect (Table 1). The average AE under M treatment was greater than with other density treatments of two years. At the M density, compare with that in the other fertilization treatments, the N1P2 treatment significantly increased the AE by 66.0–109.6% and 27.6–390.8% in 2022 and 2023, respectively (Table 1).

3.3 Content, uptake, efficiency and comprehensive score of nitrogen

In both oat growing seasons, there were significant ($P< 0.05$) differences in N content among the FR treatments, the SD had significant ($P< 0.05$) effect on the N content only in 2023, the interaction effect of the SD and FR had no significant impact on the N content (Supplementary Table S2). The N content of oats markedly increased with the fertilization, and the maximum values were achieved under the N1P2 treatment in all seasons of two years. Under the N1P2 treatments, the average N content of two stages was significantly increased by 23.4% in 2022 and 37.3% in 2023 than that in the no fertilization treatment, respectively. Compared with FR treatment, the effect of SD treatment on N content was less. The SD treatments had no significant effects on the N content in 2022. Compared with that in the M and H treatments, the N content increased under the L treatment in 2023. During oat growing seasons, the N content decreased in the maturity stage compare with heading stage (Figures 5a, b).

Statistically, FR, SD and their interaction effect had a significant ($P< 0.05$) impact on N uptake of oats. The M treatment significantly increased the N uptake in maturity stage of two years, as showed in the Table 2. The N uptake markedly increased with the fertilization and peaked at N1P2 treatment in all stages of both years. At the M treatment, the average N uptake of two stages in the N1P2 treatment increased by 94.0 and 162.9% in 2022 and 2023, respectively, compared with that in the no fertilizer treatment (Table 2). Although the heading stage had greater N content of oat, the maturity stage obtained greater N uptake because of more forage yield (Figure 5; Table 2).

The FR and SD treatments had significant effects on nitrogen uptake efficiency (NupE) and nitrogen recovery efficiency (NRE). The highest NupE and NRE were obtained in the M-N1P2

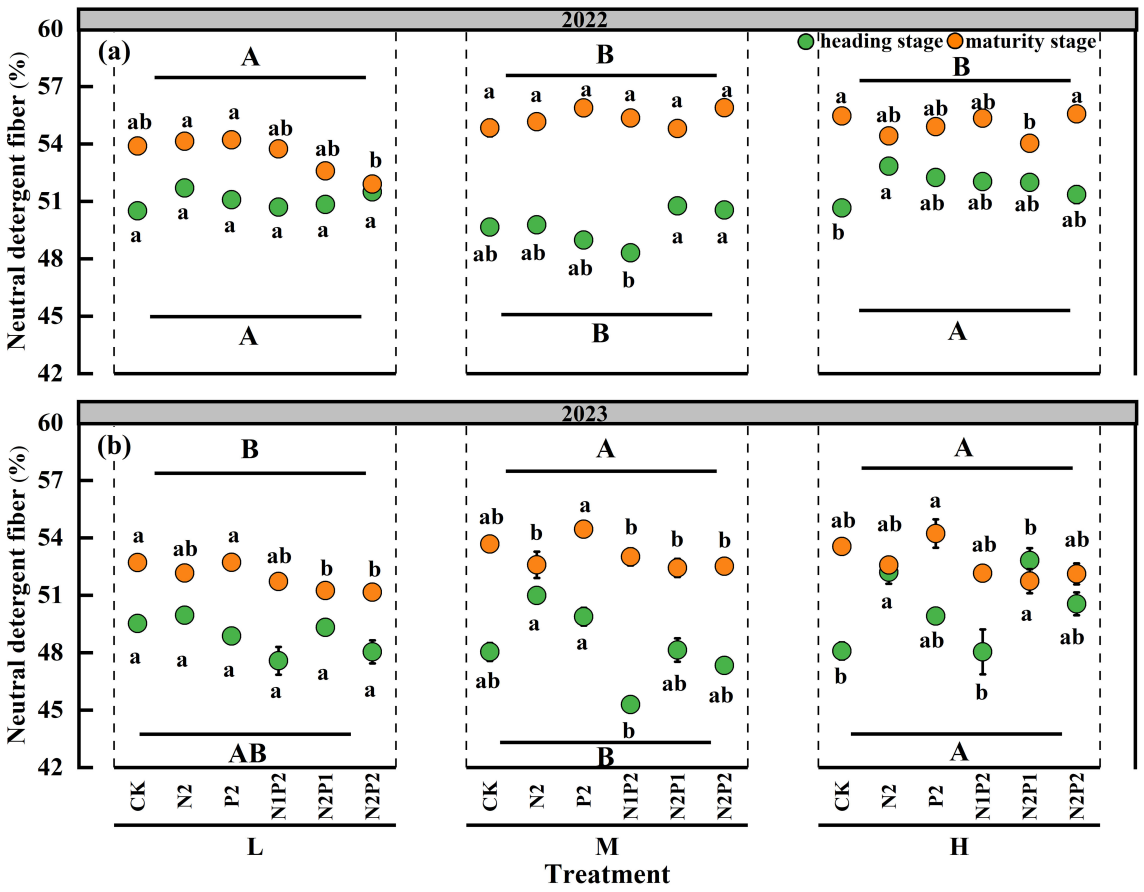

FIGURE 3
Variations in neutral detergent fiber under different sowing densities (SD) and fertilizer rates (FR) at heading and maturity stages in 2022 **(a)** and 2023 **(b)**. L, low sowing density; M, moderate sowing density; H, high sowing density. Vertical bars represent SE values ($P< 0.05$). Different lower-case letters above or under the circles denote significant differences for different fertilizer rates under the same sowing density ($P< 0.05$). Different upper-case letters in top or bottom of figure indicate significant differences between sowing densities ($P< 0.05$).

treatment. At the M treatments, N1P2 increased NupE and NRE by 155.5–212.5% and 275–768.4% in 2022 and 158.3–283.5% and 213.3–710.3% in 2023, respectively, compared with those in the other treatments (Table 2).

In the evaluation system of N, a single indicator might produce a random error for evaluation result, so it was important to combine multiple indicators for their comprehensive evaluation to obtain more objective and accurate evaluation results. The indicators of N comprehensive evaluation include N content and N uptake of heading and maturity stages, NupE and NRE. The result of N comprehensive evaluation showed that N1P2 has the highest N comprehensive score (NCS) among all treatments (Figure 6).

3.4 Content, uptake, efficiency and comprehensive score of phosphorus

The results revealed that the FR had significant ($P< 0.05$) effect on the P content in both years, the SD had significant ($P< 0.05$) effect on the P content only in 2023, and their interaction had no significant effect on the P content (Supplementary Table S2). The P content of oats exhibited a similar trend in both years and markedly increased with the fertilization. P2 and N1P2 treatment were significantly increased the P content compared with that in the other fertilization. Under the M treatment, the N1P2 slightly increased P content by 41.9% and 10.7% in 2022 and 2023, respectively, compared with that in the no fertilization treatment. The differences between SD treatments were not statistically significant for P content in 2022, however, the H treatment decreased the P content in 2023 (Figures 7a, b).

The Table 3 showed that the FR, SD and their interaction had significant affect ($P< 0.05$) on P uptake and efficiency. The P uptake increased with the fertilization and peaked at the M-N1P2 treatment in both two years. At the M treatment, the average P uptake of two stages in the N1P2 treatment increased by 128.1% and 108.6% compared with that in the no fertilizer treatment in 2022 and 2023, respectively (Table 3). Although the heading stage had higher P content of oat, the increase of forage yield led to more P uptake in maturity stage (Figure 7; Table 3).

The FR and SD treatments had significant effects on phosphorus uptake efficiency (PupE) and phosphorus recovery efficiency (PRE), the N2P1 treatment has the highest PupE and PRE, however,

10.3389/fpls.2025.1604427

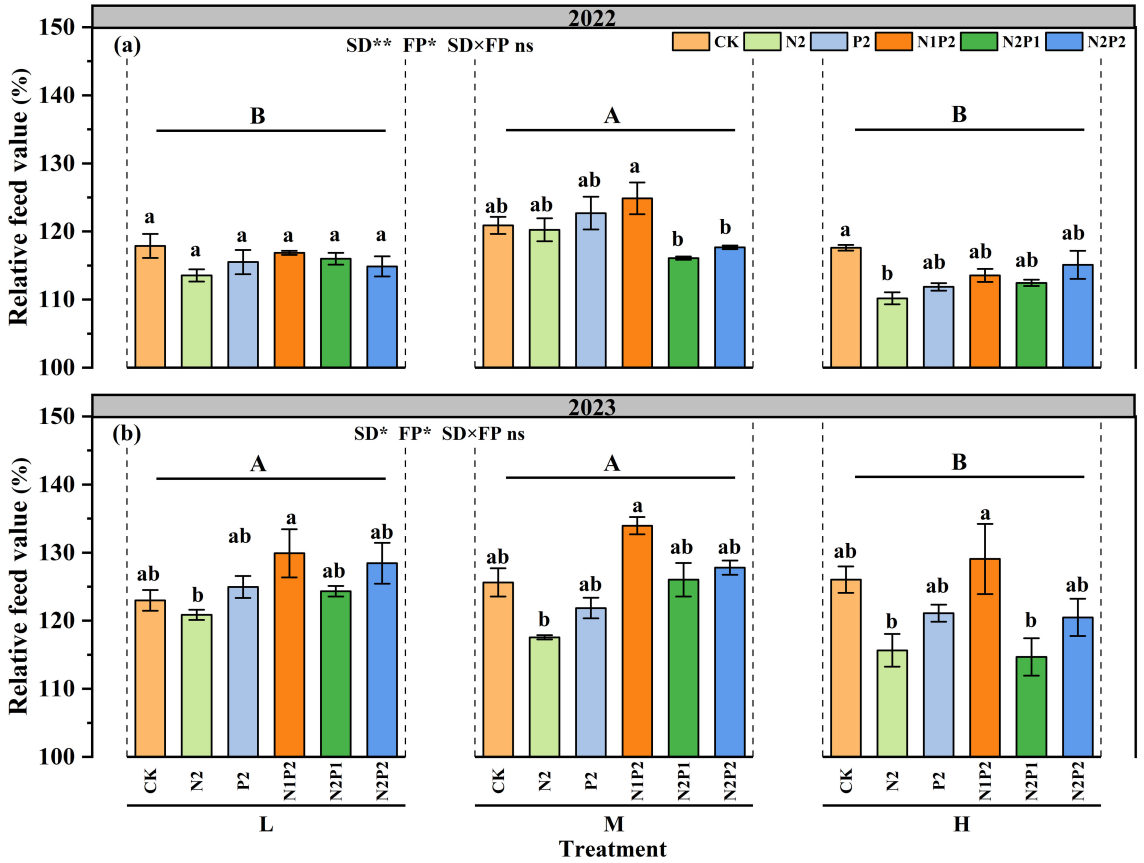

FIGURE 4
Variations in relative feed value under different sowing density (SD) and fertilizer rates (FR) during 2022 **(a)** and 2023 **(b)**. L, low sowing density; M, moderate sowing density; H, high sowing density. Vertical bars represent SE values ($P< 0.05$). Different lower-case letters above the bars denote significant differences for different fertilizer rates under the same sowing density ($P< 0.05$). Different upper-case letters indicate significant differences between sowing density ($P< 0.05$).

membership function analysis revealed that the highest P comprehensive score (PCS) under the N1P2 treatment (Figure 8).

Overall, the optimum combination of SD and FR (M-N1P2) for maximizing oat N/P content, uptake and comprehensive efficiency was the same in both years. Integrated nutrient management comprising N/P fertilizers in combined was better than solely applying fertilizer (Figures 5-8; Tables 2, 3).

3.5 Comprehensive evaluation analysis

The correlation analysis revealed significant positive correlations of forage yield, CP yield, nitrogen content and RFV with nutrient uptake and use efficiency (AE, NupE, NRE, NCS, PupE, PRE and PCS) of oat, but negative relations with ADF and NDF content. The CP content and phosphorus content followed a strong positive relationship with other variables except NDF. In addition, the correlation analysis indicated a significant positive relationship between ADF and NDF (Figure 9).

The principal component analysis (PCA) was prepared to present the concerted information on the forage yield and quality traits, nutrient content, uptake and use efficiency in relation to FR and SD treatments. For fertilizer rate (Figure 10a), the first two principal components explained 72.6% of the total variance (being 53.1% in PC1 and 19.5% in PC2). The result revealed the clear segregation of the variables and fertilizer treatments into different quadrants. The upper left quadrant of the negative side of PC1 included the CK, solely applying fertilizer (N2 and P2) and N2P2 treatment that delivered high ADF and NDF contents (Figure 10a). The upper right quadrant and lower right quadrant included N1P2 and N2P1 treatment representing higher forage yield, nutrient content, feed value, nutrient uptake and nutrient efficiency along with premium forage quality of oats. Finally, CK, N2, P2 and N2P2 treatments in left quadrant had the lower yield, quality, and nutrient content and efficiency, but higher ADF and NDF (Figure 10a). For sowing density (Figure 10b), the first two principal components explained 65.1% of the total variance (being 44.7% in PC1 and 20.4% in PC2). The L and H treatments clustered on the upper left and lower left quadrants that depicted the lower yield, quality, nutritional indictors and higher fiber content. The M treatment in right quadrants had the higher yield, quality, feed value and nutritional indictors (Figure 10b).

10.3389/fpls.2025.1604427

TABLE 1 Forage yield, crude protein (CP) yield and agronomic efficiency (AE) of oat at 2022 and 2023.

Years	Sowing densities	Fertilizer rates	Forage yield (t ha^{-1})		CP yield (kg ha^{-1})		AE (kg kg^{-1})
			Heading stage	Maturity stage	Heading stage	Maturity stage	
2022	L	CK	2.97b	4.58b	405.11b	522.96b	
		N2	3.15ab	5.18ab	485.55b	652.44ab	5.96b
		P2	3.15ab	4.91ab	477.12b	623.45ab	3.59b
		N1P2	4.07a	6.43a	706.82a	890.99a	13.2a
		N2P1	3.38ab	5.81ab	550.95ab	765.72ab	8.45ab
		N2P2	3.07ab	5.42ab	519.31ab	621.79ab	4.40b
		Mean	**3.30B**	**5.39B**	**524.14B**	**679.56B**	**7.12B**
	M	CK	3.77b	5.60c	503.39b	633.44b	
		N2	4.37ab	6.69b	641.83b	774.87b	10.9b
		P2	3.80b	6.49c	570.80b	642.11b	9.92b
		N1P2	6.35a	8.13a	1021.07a	1037.56a	18.09a
		N2P1	4.96ab	6.85b	764.01ab	871.04ab	8.63b
		N2P2	4.27ab	7.34ab	604.89b	849.87ab	9.2b
		Mean	**4.59A**	**6.68A**	**684.33A**	**801.48A**	**10.41A**
	H	CK	3.25b	4.53b	364.72b	539.34b	
		N2	4.52a	6.00ab	601.91ab	767.86ab	14.62a
		P2	4.10a	5.04ab	484.13b	611.23ab	5.58b
		N1P2	4.74a	6.79a	656.92a	906.97a	16.14a
		N2P1	4.54a	5.93ab	623.67a	827.51ab	9.65ab
		N2P2	4.21a	5.66ab	584.60ab	710.49ab	5.93b
		Mean	**4.23A**	**5.66B**	**552.66B**	**727.23AB**	**10.38A**
	ANOVA	SD	**	**	*	*	*
		FR	**	**	**	**	**
		SD*FR	*	*	*	*	ns
2023	L	CK	2.29b	3.35c	306.83b	396.07c	
		N2	3.07ab	5.31ab	414.54bc	649.08bc	19.61a
		P2	2.56b	4.59bc	344.16b	572.07bc	13.75b
		N1P2	3.95a	6.06a	556.35a	876.18a	19.36a
		N2P1	3.32ab	5.32ab	453.90ab	696.06ab	13.57b
		N2P2	3.29ab	5.36ab	453.76ab	700.72ab	10.55b
		Mean	**3.08B**	**5.00B**	**421.59B**	**648.36B**	**15.4AB**
	M	CK	2.58c	5.34bc	319.65c	634.63b	
		N2	3.38bc	5.85bc	477.92bc	690.29b	5.11c
		P2	2.78c	5.87c	380.95c	540.76b	5.64c
		N1P2	4.91a	10.28a	710.90a	1376.17a	35.31a
		N2P1	4.67ab	9.35ab	651.81ab	1215.36a	27.68ab
		N2P2	4.17abc	8.43abc	604.07ab	1108.48a	16.24b

(Continued)

10.3389/fpls.2025.1604427

TABLE 1 Continued

Years	Sowing densities	Fertilizer rates	Forage yield (t ha^{-1})		CP yield (kg ha^{-1})		AE (kg kg^{-1})
			Heading stage	Maturity stage	Heading stage	Maturity stage	
		Mean	**3.75A**	**7.29A**	**524.22A**	**927.61A**	**17.2A**
	H	CK	3.18b	4.20ab	439.47b	493.24b	
		N2	3.31b	4.95ab	476.14b	586.23b	7.53b
		P2	3.41b	4.69b	470.56b	441.79b	5.44b
		N1P2	4.61a	7.75a	674.75a	1044.79a	25.40a
		N2P1	4.37a	7.46ab	644.13a	1026.84a	22.47a
		N2P2	3.24b	4.53ab	448.76b	584.79b	1.74c
		Mean	**3.69A**	**5.43B**	**525.64A**	**696.28B**	**11.76B**
	ANOVA	SD	*	**	*	**	*
		FR	**	**	**	**	*
		SD*FR	*	*	*	*	ns

Data represent the mean. Different lower-case letters denote significant differences within same sowing density (SD) for different fertilizer rates (FR; $P< 0.05$). Different upper-case letters denote significant differences for different sowing densities ($P< 0.05$).
L means low sowing density; M means moderate sowing density; H means high sowing density.
ANOVA indicates analysis of variance; ** indicates $P< 0.01$; *indicates $P< 0.05$; ns indicates no significance.

4 Discussion

4.1 Oat nutrient quality, N/P content and feed value response to fertilization and density

For forage producers, achieving greater biomass is a primary objective; however, high nutritional quality is equally important as it enhances the profitability of both forage production and the livestock enterprises it supports (Zhang et al., 2018). Crude protein is a key indicator of the nutrient availability in the forage, which is vital for feed efficiency and development of livestock. Fiber content is important for maintaining proper digestive health in ruminants. It aids in the fermentation process within the rumen, promoting a healthy microbial population and nutrient absorption (Gonzalez et al., 2020). RFV combines both ADF and NDF to provide a comprehensive measure of forage digestibility. CP content, fiber content, and RFV are the essential quality metrics used for assessing forage nutritive values (Agnew et al., 2022). These metrics not only guide the selection of appropriate fertilizer but also enhance the overall efficiency of livestock production systems, contributing to sustainable agricultural practices (Sharma et al., 2018).

The above indicators showed a marked difference between heading and maturity stages in our study, the CP and fiber content in the heading stage was greater than that in maturity stage. This observed trends in crop might be related to plant canopy characteristics and the reduction in leaf area associated with the of leaf senescence (Liu et al., 2021). Photosynthesis is the physiological base of crop growth and crop nutrient formation, while more than 90% of crop biomass is derived from photosynthetic products (Zhang et al., 2025b), and the reduction of photosynthesis in the maturity stage greatly decrease the oat nutritional quality. Moreover, the increase of stem rigidity in maturity stage led to the enhanced accumulation of fiber content (Zhang et al., 2018). These changes collectively contributed to a decline of nutritive quality in the maturity stage.

In general, increasing N/P levels and sowing density are believed to increase crop quality (Li et al., 2023; Shao et al., 2024). However, the increased N/P levels or sowing density couldn't increase oat quality indefinitely in our study, and excess fertilization and density (N2P2 treatment and H treatment) show a detrimental effect on nutrient quality of oat. These results partly support our hypothesis that the farmers' practiced N/P application and sowing density in the Loess Plateau of northwest China are excessive, and would limit the water and nutrient demands required for optimal growth and productivity of oat. In our study, M-N1P2 markedly improved the nutritive quality both in heading and maturity stages, evidenced by greater CP and RFV and lower NDF content compared to that of other treatment. Consistently, previous studies have also reported high forage quality of crops with optimized fertilization and sowing density (Li et al., 2021). The response of forage quality to increasing fertilization amounts and planting density follows a parabolic curvilinear relationship. Excessive fertilization and planting density frequently lead to a reduction in forage quality. This is attributed to their impact on enhancing cell wall components and fiber content (Kamran et al., 2023). These findings were corroborated by the elevated levels of NDF and ADF observed in our study. In addition, overapplication of fertilizers has been shown to reduce the protein content in grains and forages, as well as the bioavailability of essential nutrients. This suggests that there is an optimal N and phosphorus application that maximizes nutritional quality without compromising yield (Zhang

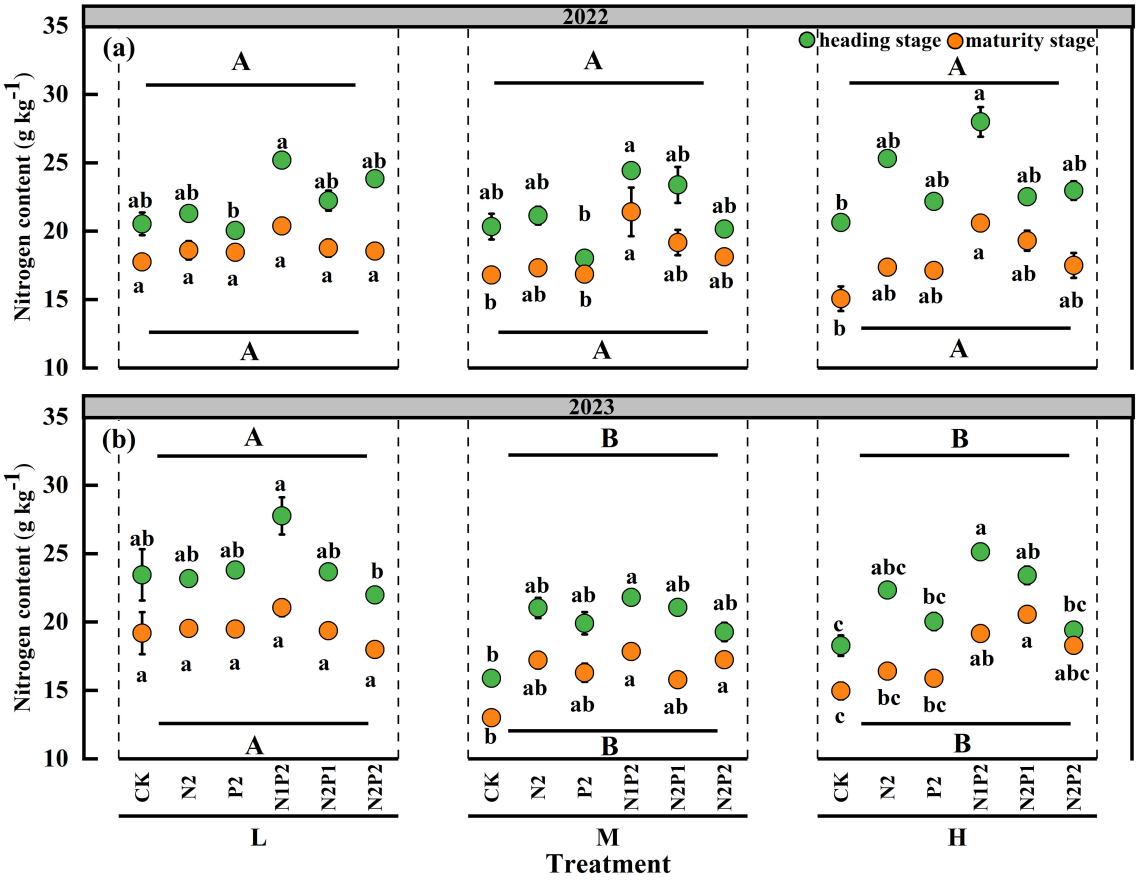

FIGURE 5
Variations in oat N content under different sowing density (SD) and fertilizer rates (FR) at heading and maturity stages in 2022 **(a)** and 2023 **(b)**. L, low sowing density; M, moderate sowing density; H, high sowing density. Vertical bars represent SE values ($P< 0.05$). Different lower-case letters above or under the circles denote significant differences for different fertilizer rates under the same sowing density ($P< 0.05$). Different upper-case letters in top or bottom of figure indicate significant differences between sowing densities ($P< 0.05$).

et al., 2017a). Optimal N and P treatment increase crops N and P uptake and use, thereby enhancing the synthesis of amino acid and protein contents (Kaplan et al., 2019).

Moreover, our study highlights the interaction between optimizing sowing density and fertilizer rate is crucial. The combination of the optimal agronomic practices directly influences the crop's ability to use fertilizers effectively, particularly in fertility-poor soils (Gregoire et al., 2022). The moderate sowing density of forage crops can enhance the uptake efficiency of fertilizers which significantly improve nutritive efficiency of oat forage. It is also essential for meeting the growing forage demands sustainably.

4.2 Oat forage yield, CP yield and N/P uptake response to fertilization and density

The forage yield response is an important variable for evaluating nutrient efficiency in agroecosystems, because it reflects the condition of nutrients in agroecosystems (Mueller et al., 2012). CP yield and N/P uptake are also important indicators directly act to reflect the overall plant nutrition and yield. The forage yield, CP yield and N/P uptake of oats exhibited a consistent trend in both years, peaked at the M-N1P2 treatment, and showed a strong correlation between CP yield, N/P accumulation and forage yield (Figure 9).

Some study showed that high N/P amounts are regarded as the main way to increase forage yield and productivity (Ahmad et al., 2023; Chen et al., 2024). However, excessive fertilization (N2P2) failure to produce positive outcomes for crop yield and nutrient in harvested oat forage in the present study. A study showed that under the high N and P supply, only 15% of fertilizers could transform into forage and grain and the remaining nutrients were lost as gaseous emissions or leached from the soil (Shi et al., 2016). Farmers of our experimental region apply excessive fertilizer lavishly to try to maximize crop yields, this leads to the decline of fertilizer efficiency, and crops cannot take up excess fertilizer after saturation of fertilizer uptake, which ultimately leads to the increase of planting costs and environmental pollution. Previous study showed that optimal fertilizer application could increase the crop yield by increasing the nutrient uptake and nutrient efficiency (Wang et al., 2023). This study confirmed this viewpoint that the forage yield, CP yield and N/P uptake increased under same sowing density with application of fertilizers. Thus, precisely formulating an

10.3389/fpls.2025.1604427

TABLE 2 Total N uptake (kg ha^{-1}), N uptake efficiency (NupE, kg ha^{-1}) and N recovery efficiency (NRE, kg ha^{-1}) of oat.

SD	FR	2022				2023			
		N uptake		NupE	NRE	N uptake		NupE	NRE
		Heading stage	Maturity stage			Heading stage	Maturity stage		
L	CK	58.65b	79.33b			57.18b	65.13c		
	N2	66.95b	96.58b	0.97b	0.17b	71.05b	101.75ab	1.02b	0.37b
	P2	62.81b	91.40b			61.17b	89.27bc		
	N1P2	103.00a	127.00a	2.54a	0.95a	111.84a	128.86a	2.58a	1.27a
	N2P1	77.46b	107.23ab	1.07b	0.28b	77.50b	106.81ab	1.07b	0.42b
	N2P2	73.27b	95.13b	0.95b	0.16b	71.87b	95.32bc	0.95b	0.30b
	Mean	**73.69B**	**99.44B**	**0.92B**	**0.26B**	**75.10B**	**97.86B**	**0.94B**	**0.39B**
M	CK	73.72c	92.52c			40.37c	68.07d		
	N2	91.67bc	111.70bc	1.12b	0.19b	69.10bc	96.91bc	0.97b	0.29c
	P2	68.07c	92.49c			63.47bc	73.43cd		
	N1P2	153.38a	174.99a	3.50a	1.65a	99.30a	185.79a	3.72a	2.35a
	N2P1	117.11b	136.84ab	1.37b	0.44b	100.35a	143.52ab	1.44b	0.75b
	N2P2	86.50bc	134.99ab	1.35b	0.42b	76.83ab	143.49ab	1.43b	0.75b
	Mean	**98.41A**	**123.92A**	**1.22A**	**0.45A**	**74.90B**	**118.53A**	**1.26A**	**0.69A**
H	CK	65.84c	65.14c			59.01c	61.50b		
	N2	115.09bc	101.90bc	1.02b	0.37b	78.00bc	80.71b	0.81b	0.19b
	P2	89.25bc	87.07bc			74.08bc	60.96b		
	N1P2	133.38a	136.83a	2.74a	1.43a	117.69a	153.49a	3.07a	1.84a
	N2P1	101.47b	113.12ab	1.13b	0.48b	100.65ab	153.86a	1.54b	0.92b
	N2P2	97.34bc	97.23bc	0.97b	0.32b	73.38bc	85.56b	0.86b	0.24b
	Mean	**100.39A**	**100.21B**	**0.98B**	**0.43A**	**83.80A**	**99.35B**	**1.05B**	**0.53AB**
ANOVA	SD	*	*	*	*	*	*	*	*
	FR	**	**	**	**	*	**	**	**
	SD*FR	*	*	ns	ns	*	*	ns	ns

Data represent the mean. Different lower-case letters denote significant differences within same sowing density (SD) for different fertilizer rates (FR; $P< 0.05$). Different upper-case letters denote significant differences for different sowing densities ($P< 0.05$).
L means low sowing density; M means moderate sowing density; H means high sowing density.
ANOVA indicates analysis of variance; ** indicates $P< 0.01$; * indicates $P< 0.05$; ns indicates no significance.

optimal fertilizer rate should refer to the maximal fertilizer uptake for a certain crop.

In our two consecutive years of field experiments, sowing density of 150 kg ha^{-1} simultaneously have resulted in maximum forage yield, CP yield and N/P uptake, and decreasing or increasing the sowing density had negative effects on these indicators. A study indicated that the low density of oat in the fields might produce high forage yield per plant, but achieving high forage yield per hectare is difficult (Chen et al., 2024). Increase of sowing density can improve forage yield per hectare by increasing the number of plants. The increasing sowing density can also minimize the waste of applied fertilizers by increasing total tillering number and expanding root-canopy structure, thus increasing use efficiency of nutrients and improving N/P uptake and CP yield (Shao et al., 2024). However, the increased sowing density couldn't increase oat yield indefinitely and excess population density will reduce the field yield of oat. The reason could be that too dense plant density exacerbated the competition for resources, led to excessive population density, poor ventilation, light transmission, and the breeding of diseases and pests (Zhang et al., 2021b; Hou et al., 2019), thus resulting in yield per plant loss, made difficult to achieve a high yield per hectare. Another possible reason is that the climatic and soil conditions are highly diverse in time and space (Kamran et al., 2023), and the sowing density for other regions may not be suitable for Loess Plateau, the poor soil moisture and nutrient conditions in this region do not support a larger population density of oats.

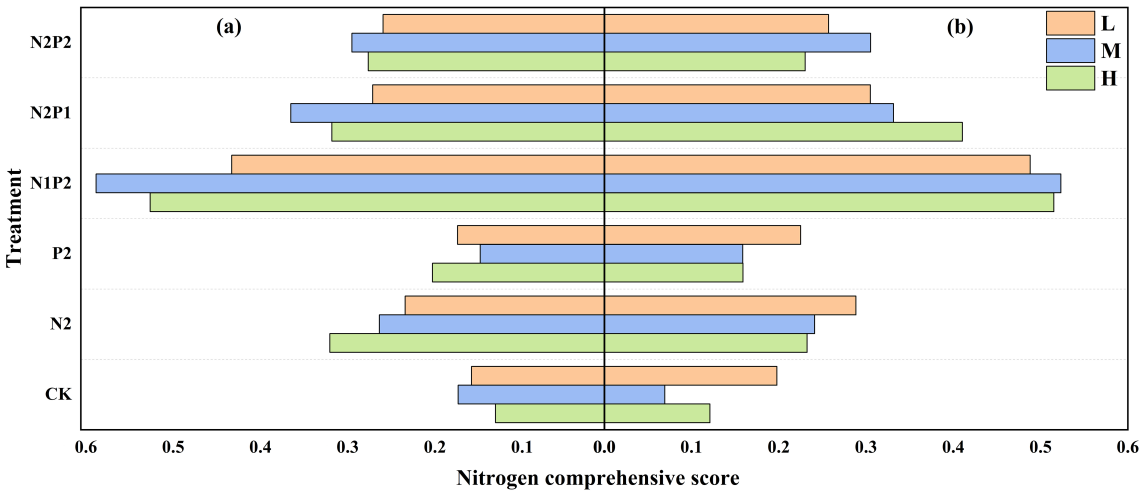

FIGURE 6
Variations in oat N comprehensive score under different sowing density (SD) and fertilizer rates (FR) in 2022 **(a)** and 2023 **(b)**. L, low sowing density; M, moderate sowing density; H, high sowing density.

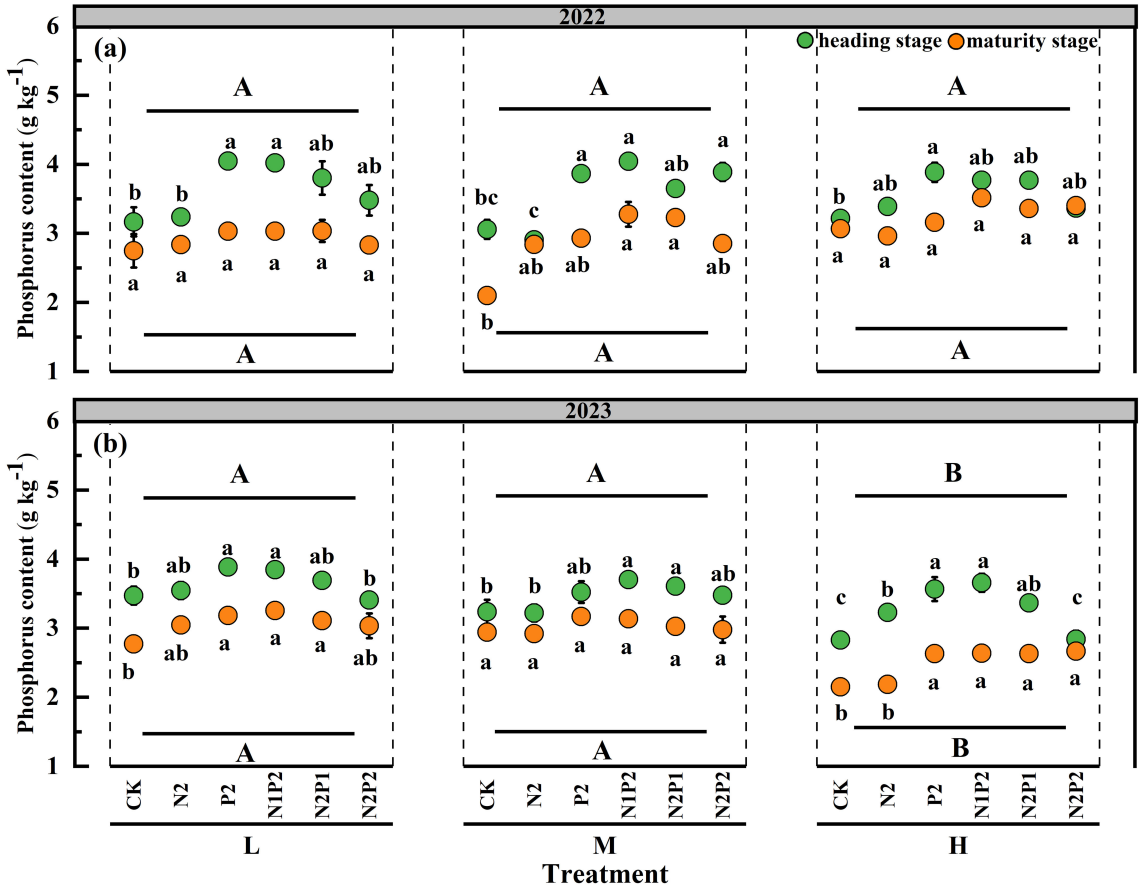

FIGURE 7
Variations in oat P content under different sowing density (SD) and fertilizer rates (FR) at heading and maturity stages in 2022 **(a)** and 2023 **(b)**. L, low sowing density; M, moderate sowing density; H, high sowing density. Vertical bars represent SE values ($P< 0.05$). Different lower-case letters above or under the circles denote significant differences for different fertilizer rates under the same sowing density ($P< 0.05$). Different upper-case letters in top or bottom of figure indicate significant differences between sowing densities ($P< 0.05$).

10.3389/fpls.2025.1604427

TABLE 3 Total P uptake (kg ha^{-1}), P uptake efficiency (PupE, kg ha^{-1}) and P recovery efficiency (PRE, kg ha^{-1}) of oat.

SD	FR	2022				2023			
		P uptake		PupE	PRE	P uptake		PupE	PRE
		Heading stage	Maturity stage			Heading stage	Maturity stage		
L	CK	8.97c	12.52c			7.49b	9.30b		
	N2	10.25bc	14.73bc			10.92ab	15.84ab		
	P2	12.73b	15.00b	0.17b	0.03b	10.00ab	14.52ab	0.16b	0.06c
	N1P2	16.42a	19.32a	0.21b	0.08ab	14.94a	20.32a	0.23b	0.12b
	N2P1	13.08ab	17.40ab	0.39a	0.11a	12.24ab	17.15ab	0.38a	0.17a
	N2P2	10.61bc	14.38bc	0.16b	0.02b	11.17ab	16.23ab	0.18b	0.08c
	Mean	**12.01B**	**15.56B**	**0.15B**	**0.04B**	**11.13B**	**15.56B**	**0.16B**	**0.07A**
M	CK	11.23c	11.64c			8.80c	15.45c		
	N2	12.82bc	18.24bc			10.85bc	16.35c		
	P2	14.71bc	16.08bc	0.18c	0.05c	11.07bc	13.45c	0.15c	-0.02c
	N1P2	25.30a	26.86a	0.30b	0.17ab	17.72a	32.86a	0.37b	0.19b
	N2P1	18.83ab	23.06ab	0.51a	0.25a	17.26a	28.33ab	0.63a	0.29a
	N2P2	16.34bc	20.97b	0.23bc	0.10bc	14.44ab	24.63bc	0.27c	0.10c
	Mean	**16.54A**	**19.47A**	**0.20A**	**0.10A**	**13.36A**	**21.85A**	**0.24A**	**0.09A**
H	CK	10.26b	13.34c			9.51c	8.96c		
	N2	15.40ab	17.89abc			11.30bc	11.30b		
	P2	15.69ab	15.67bc	0.17b	0.03c	12.91bc	9.77c	0.11b	0.01c
	N1P2	17.64a	24.09a	0.27b	0.12b	17.05a	20.41a	0.23b	0.13b
	N2P1	17.15a	20.77ab	0.46a	0.17a	14.72ab	19.61a	0.44a	0.24a
	N2P2	14.23ab	18.61abc	0.21b	0.06c	10.33c	12.50b	0.14b	0.04c
	Mean	**15.06A**	**18.40AB**	**0.19A**	**0.06AB**	**12.64AB**	**13.76B**	**0.15B**	**0.07A**
ANOVA	SD	**	*	*	*	*	**	**	ns
	FR	**	**	**	**	*	**	**	**
	SD*FR	*	*	ns	ns	*	*	ns	ns

Data represent the mean. Different lower-case letters denote significant differences within same sowing density (SD) for different fertilizer rates (FR; $P< 0.05$). Different upper-case letters denote significant differences for different sowing densities ($P< 0.05$).
L means low sowing density; M means moderate sowing density; H means high sowing density.
ANOVA indicates analysis of variance; ** indicates $P< 0.01$; * indicates $P< 0.05$; ns indicates no significance.

Hence, a site-specific implementation strategy is needed to identify appropriate sowing density of oat in the Loess Plateau.

Notably, the oat yield was significantly influenced by the interaction between fertilization and density (Table 1). The positive impact of N1P2 treatment on yield was more pronounced under the M treatment compared with that under the L and H. This revealed that only an optimal sowing density can maximize the effectiveness of fertilizers, thereby significantly improving productivity and sustainability. Results underscored the importance of coupled fertilizer rate and sowing density.

4.3 Oat nutrient efficiency response to fertilization and density

Nutrient efficiency is an important index to evaluate forage, particularly in the context of increasing global forage demand and environmental concerns associated with nitrogen and P fertilizer use. Improving N/P efficiency can lead to enhanced forage quality and yield, which are vital for increasing productivity of livestock and agriculture. Our study showed that the N1P2 treatment significantly increased the agronomic efficiency, N fertilizer

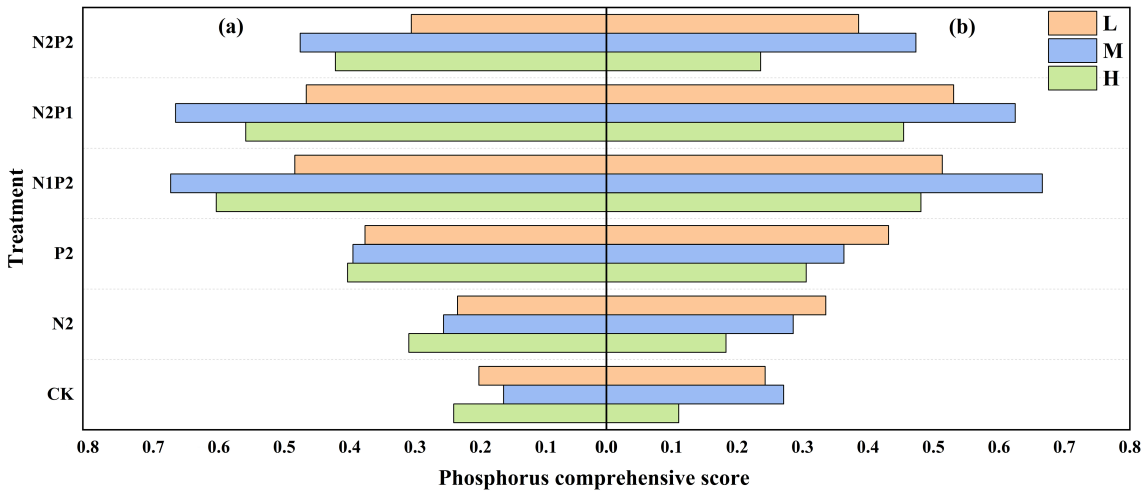

FIGURE 8
Variations in oat P comprehensive score under different sowing density (SD) and fertilizer rates (FR) in 2022 **(a)** and 2023 **(b)**. L, low sowing density; M, moderate sowing density; H, high sowing density.

recovery efficiency and N uptake, however, the P recovery and uptake efficiency peaked at the N2P1 treatment. Thus, we used the comprehensive evaluation to calculated the comprehensive scores of N and P, and the results of evaluation showed that the N1P2 treatment still had the highest NCS and PCS. Previous study reported that the combination of N and P application not only increased grain yield but also enhanced nutrient use efficiency and agronomic efficiency in agricultural systems (Li et al., 2023). Plant N and P content and LAI increased with optimal levels of N/P application, resulting in higher nutrients use efficiency by enhancing photosynthetic rate (Nasar et al., 2022). Moreover, optimal fertilization promotes the growth of crop roots, and a

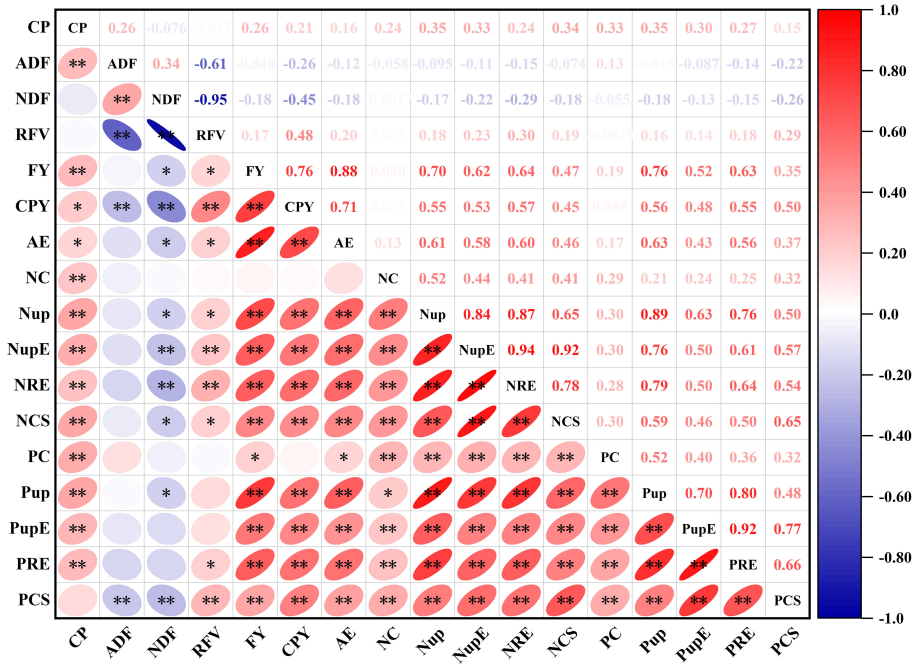

FIGURE 9
Correlation analysis for the correlations between quality, yield, nutrient efficiency and comprehensive score of oat forage. The variables included CP, crude protein; ADF, acid detergent fiber; NDF, neutral detergent fiber; RFV, relative feed value; FY, forage yield; CPY, crude protein yield; AE, agronomic efficiency; NC, nitrogen content; Nup, nitrogen uptake; NupE, nitrogen uptake efficiency; NRE, nitrogen recovery efficiency; NCS, nitrogen comprehensive score; PC, phosphorus content; Pup, phosphorus uptake; PupE, phosphorus uptake efficiency; PRE, phosphorus recovery efficiency; PCS, phosphorus comprehensive score. The color gradient denotes correlation coefficient. * and **represent the significant differences at $P< 0.05$ and $P< 0.01$, respectively.

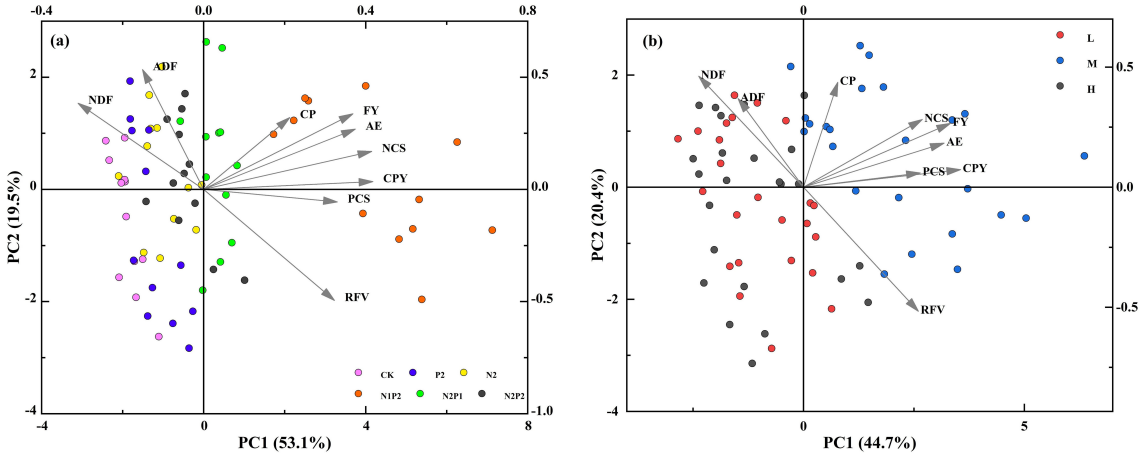

FIGURE 10
The principal component analysis (PCA) shows the relationship between variables and represents the separation of fertilizer rate treatments **(a)** and sowing density treatments **(b)** among the first two principal components. Abbreviations for indicator names are similar to Figure 9.

vigorous root system enable crops to absorb more nutrients of soil, contributing to the higher nutrient efficiency and productivity.

Optimizing sowing density can significantly influence the root distribution, nutrient uptake efficiency and overall yield of crops. For instance, a study on winter wheat indicated that improved sowing density led to enhanced root length density and nitrogen uptake efficiency, which ultimately resulted in higher yields (Wang et al., 2012). Similarly, another investigation of maize production demonstrated that adjusting planting density not only improved the leaf area index and radiation use efficiency but also optimized N use efficiency, thereby stabilized the yield in loess plateau (Jia et al., 2018). It was consistent with our results that optimizing sowing density (M treatment) significantly increased agronomic efficiency of fertilizers and efficiency of N and P.

Moreover, a study highlighted that the application of fertilizers in conjunction with optimized planting density resulted in increased nitrogen accumulation and translocation during the critical post-anthesis phase, leading to improved yield and nitrogen use efficiency (Yuan et al., 2024). In our study, the interaction between fertilization and sowing density played a vital role in maximizing nutrients use efficiency. This synergistic approach underscores the importance of integrating agronomic practices to enhance both resource use efficiency and crop productivity, the combination of optimal sowing density and fertilization could be an excellent strategy to optimize resource use. This integrated approach not only supports sustainable agriculture but also laying the foundation for achieving high oat yield in Loess Plateau.

4.4 Implications for fertilizer rate and sowing density

Yield and quality indicators are important for forages, but the nutrients use efficiency is equally important, especially to avoid the waste of fertilizers. Thus, when formulating an agronomic practice, these two points should be fully balanced. Previous studies have reported a trade-off between maximizing forage productivity and nutrients use efficiency (Kamran et al., 2022; Kaplan et al., 2019). This trade-off requires both consideration of maximizing the economic benefits and minimizing environmental pollution, while formulating density and fertilization management practices.

Low nutrient use efficiency is mainly caused by unreasonable fertilizer application, mass nutrient loss, and an imbalance between crop nutrient supply and demand (Yang et al., 2016). This is evident in agricultural systems where overuse of fertilizers without considering the specific needs of the crops, particularly nitrogen and phosphorus, can result in nutrient leaching, soil acidification, and a decline in soil biodiversity. In addition to these ecological concerns, the financial implications of excessive fertilizer use and improper sowing density cannot be overlooked, the costs associated with purchasing fertilizers and seeds can escalate quickly, particularly when they lead to diminished soil health and reduced crop yields over time. This indicates that finding the optimal sowing density and fertilizer rate is essential for maintaining soil health and ecological balance.

A study has shown that optimizing sowing density and fertilization can enhance soil fertility and crop productivity while reducing the reliance on fertilizers inputs. In the semi-arid areas, reducing fertilizers application while optimizing planting density has been proved to improve yield and nitrogen use efficiency, thereby minimizing the negative impacts associated with excess fertilizers use (Wu et al., 2024). Similarly, our study indicated that the yield, quality, N use efficiency and agronomic efficiency of oats under the M-N1P2 treatment were higher than other treatments. These results revealed that the optimal density and fertilization could ensure oat yield while improving nutrients use efficiency, it showed a reduced need for fertilizers, thus reducing the negative impact of excess fertilizers input on the environment. The current study has the potential for improving productivity and promoting ecological conservation, and could be a promising strategy for the efficient production of oats in Loess Plateau.

5 Conclusion

The findings of the two-year field study revealed that the optimal sowing density and fertilizer rate (M-N1P2) greatly increased the CP content, relative feed value, forage yield, CP yield, agronomic efficiency, N/P content, N/P uptake, N uptake efficiency and N recover efficiency, while decreased the NDF of oat. The results of correlation analysis showed significant positive correlations of forage CP content and yield with agronomic efficiency, N/P uptake efficiency and N/P recover efficiency, but negative correlations with ADF and NDF. The results of comprehensive evaluation exhibited that M-N1P2 had the highest N comprehensive score and P comprehensive score among all treatments. Hence, the M-N1P2 treatment was able to maintain yield and quality while maximizing agronomic efficiency and N efficiency without much reduction in the P efficiency across the two growing seasons. Therefore, a sowing density of 150 kg ha^{-1} coupled with 50 kg ha^{-1} N and 90 kg ha^{-1} P is recommended as the optimal tillage practice for oats in the Loess Plateau.

Present findings illustrated significant prospects for optimizing the fertilizer rate and sowing density for oat in the Loess Plateau of northwest China. Nevertheless, the precipitation levels and soil characteristics, may vary between different semi-arid regions, and the optimal fertilizer rate and sowing density identified in this study may not be applicable for achieving maximum productivity in other semi-arid areas. Therefore, future multi-locational studies are suggested to clarify how climatic variations in different semi-arid regions would influence the potential effects of fertilization and sowing density on oat production, forage nutritive quality, and resource use efficiency. More precise guidelines will aid farmers in minimizing fertilizer and seed inputs while maximizing economic profitability within agricultural production systems.

Data availability statement

The raw data supporting the conclusions of this article will be made available by the authors, without undue reservation.

Author contributions

RZ: Data curation, Formal Analysis, Investigation, Software, Writing – original draft, Writing – review & editing. YW: Data curation, Investigation, Writing – review & editing. KM: Writing – review & editing. JW: Investigation, Writing – review & editing. GZ: Writing – review & editing. CL: Conceptualization, Funding acquisition, Supervision, Visualization, Writing – review & editing.

Funding

The author(s) declare that financial support was received for the research and/or publication of this article. This study was supported by Gansu Provincial Science and Technology Major Projects (23ZDKA013) and China Agriculture Research System (CARS-07-C, Oat).

Acknowledgments

The authors would like to thank the reviewers for their helpful and constructive comments on an earlier version of this manuscript.

Conflict of interest

The authors declare that the research was conducted in the absence of any commercial or financial relationships that could be construed as a potential conflict of interest.

Generative AI statement

The author(s) declare that no Generative AI was used in the creation of this manuscript.

Publisher's note

All claims expressed in this article are solely those of the authors and do not necessarily represent those of their affiliated organizations, or those of the publisher, the editors and the reviewers. Any product that may be evaluated in this article, or claim that may be made by its manufacturer, is not guaranteed or endorsed by the publisher.

Supplementary material

The Supplementary Material for this article can be found online at: https://www.frontiersin.org/articles/10.3389/fpls.2025.1604427/full#supplementary-material

References

Agnew, J., Sprenger, C., Kendel, Z., Jefferson, P. G., Hnatowich, G., Weber-Enns, J., et al. (2022). The effect of nitrogen fertility rate and seeding rate on yield, nutritive value and economics of forage corn in a low corn heat unit region of Western Canada. *Field Crops Res.* 283, 108520. doi: 10.1016/j.fcr.2022.108520

Ahmad, I., Batyrbek, M., Ikram, K., Ahmad, S., Kamran, M., Misbah,, et al. (2023). Nitrogen management improves lodging resistance and production in maize (*Zea mays* L.) at a high plant density. *J. Integr. Agric.* 22, 417–433. doi: 10.1016/j.jia.2022.08.074

Andrzejewska, J., Contreras-Govea, F. E., Pastuszka, A., Kotwica, K., and Albrecht, K. A. (2019). Performance of oat (*Avena sativa* L.) sown in late summer for autumn forage production in Central Europe. *Grass Forage Sci.* 74, 97–103. doi: 10.1111/gfs.12400

Cao, D., Lan, Y., Chen, W., Yang, X., Wang, D., Ge, S., et al. (2021). Successive applications of fertilizers blended with biochar in the soil improve the availability of phosphorus and productivity of maize (*Zea mays* L.). *Eur. J. Agron.* 130, 126344. doi: 10.1016/j.eja.2021.126344

Chen, L., and Liao, H. (2017). Engineering crop nutrient efficiency for sustainable agriculture. *J. Integr. Plant Biol.* 59, 710–735. doi: 10.1111/jipb.12559

Chen, L., Ma, P., Li, J., Liu, J., Guo, F., Wang, Y., et al. (2024). *Lespedeza potaninii* Vass seed yield response to plant density and phosphate fertilization in Northwest China. *Eur. J. Agron.* 156, 127173. doi: 10.1016/j.eja.2024.127173

Fu, Y.-Q., Zhong, X.-H., Zeng, J.-H., Liang, K.-M., Pan, J.-F., Xin, Y.-F., et al. (2021). Improving grain yield, nitrogen use efficiency and radiation use efficiency by dense planting, with delayed and reduced nitrogen application, in double cropping rice in South China. *J. Integr. Agric.* 20, 565–580. doi: 10.1016/s2095-3119(20)63380-9

Gaudinier, A., Rodriguez-Medina, J., Zhang, L., Olson, A., Liseron-Monfils, C., Bagman, A.-M., et al. (2018). Transcriptional regulation of nitrogen-associated metabolism and growth. *Nature* 563, 259–25+. doi: 10.1038/s41586-018-0656-3

Gonzalez, J., Diaz-Royon, F., Vanegas, J. L., Arroyo, J. M., and Carro, M. D. (2020). Ruminal use of undegraded-feed soluble protein and accuracy of the estimations of the nutrient content in ruminal bacteria. *J. Sci. Food Agric.* 100, 1608–1615. doi: 10.1002/jsfa.10169

Gregoire, G., Benjannet, R., and Desjardins, Y. (2022). Contribution of grass clippings to turfgrass fertilization and soil water content under four nitrogen levels. *Sci. Total Environ.* 837, 155765. doi: 10.1016/j.scitotenv.2022.155765

Hawkesford, M. J., and Griffiths, S. (2019). Exploiting genetic variation in nitrogen use efficiency for cereal crop improvement. *Curr. Opin. Plant Biol.* 49, 35–42. doi: 10.1016/j.pbi.2019.05.003

Hou, W., Khan, M. R., Zhang, J., Lu, J., Ren, T., Cong, R., et al. (2019). Nitrogen rate and plant density interaction enhances radiation interception, yield and nitrogen use efficiency of mechanically transplanted rice. *Agric. Ecosyst. Environ.* 269, 183–192. doi: 10.1016/j.agee.2018.10.001

Huang, M., Chen, J., Cao, F., and Zou, Y. (2018). Increased hill density can compensate for yield loss from reduced nitrogen input in machine-transplanted double-cropped rice. *Field Crops Res.* 221, 333–338. doi: 10.1016/j.fcr.2017.06.028

Jakubus, M., and Graczyk, M. (2022). Quantitative changes in various nutrient ratios in fodder plants as an effect of compost and fly ash application. *Int. J. Environ. Res. Public Health* 19, 8136. doi: 10.3390/ijerph19138136

Jia, Q., Sun, L., Ali, S., Zhang, Y., and Ren, X. (2018). Effect of planting density and pattern on maize yield and rainwater use efficiency in the Loess Plateau in China. *Agric. Water Manage.* 202, 19–32. doi: 10.1016/j.agwat.2018.02.011

Kamran, M., Yan, Z., Chang, S., Ning, J., Lou, S., Ahmad, I., et al. (2023). Interactive effects of reduced irrigation and nitrogen fertilization on resource use efficiency, forage nutritive quality, yield, and economic benefits of spring wheat in the arid region of Northwest China. *Agric. Water Manage.* 275, 108000. doi: 10.1016/j.agwat.2022.108000

Kamran, M., Yan, Z., Jia, Q., Chang, S., Ahmad, I., Ghani, M. U., et al. (2022). Irrigation and nitrogen fertilization influence on alfalfa yield, nutritive value, and resource use efficiency in an arid environment. *Field Crops Res.* 284, 108587. doi: 10.1016/j.fcr.2022.108587

Kaplan, M., Kara, K., Unlukara, A., Kale, H., Beyzi, S. B., Varol, I. S., et al. (2019). Water deficit and nitrogen affects yield and feed value Sudangrass silage. *Agric. Water Manage.* 218, 30–36. doi: 10.1016/j.agwat.2019.03.021

Li, C., Feng, H., Luo, X., Li, Y., Wang, N., Wu, W., et al. (2022). Limited irrigation and fertilization in sand-layered soil increases nitrogen use efficiency and economic benefits under film mulched ridge-furrow irrigation in arid areas. *Agric. Water Manage.* 262, 107406. doi: 10.1016/j.agwat.2021.107406

Li, G.-H., Cheng, Q., Li, L., Lu, D.-L., and Lu, W.-P. (2021). N, P and K use efficiency and maize yield responses to fertilization modes and densities. *J. Integr. Agric.* 20, 78–86. doi: 10.1016/s2095-3119(20)63214-2

Li, T., Feng, R., Zhang, Z., Zhao, Y., Lan, Y., Malik, K., et al. (2023). Balancing quality and productivity of *Apocynum venetum* with N and P fertilizer management under drip irrigation in arid conditions of Northwest China. *Ind. Crops Prod.* 201, 116884. doi: 10.1016/j.indcrop.2023.116884

Lithourgidis, A. S., Vasilakoglou, I. B., Dhima, K. V., Dordas, C. A., and Yiakoulaki, M. D. (2006). Forage yield and quality of common vetch mixtures with oat and triticale in two seeding ratios. *Field Crops Res.* 99, 106–113. doi: 10.1016/j.fcr.2006.03.008

Liu, M., Wang, Z., Mu, L., Xu, R., and Yang, H. (2021). Effect of regulated deficit irrigation on alfalfa performance under two irrigation systems in the inland arid area of midwestern China. *Agric. Water Manage.* 248, 106764. doi: 10.1016/j.agwat.2021.106764

Marshall, A., Cowan, S., Edwards, S., Griffiths, I., Howarth, C., Langdon, T., et al. (2013). Crops that feed the world 9. Oats- a cereal crop for human and livestock feed with industrial applications. *Food Secur* 5, 13–33. doi: 10.1007/s12571-012-0232-x

Mueller, N. D., Gerber, J. S., Johnston, M., Ray, D. K., Ramankutty, N., and Foley, J. A. (2012). Closing yield gaps through nutrient and water management. *Nature* 490, 254–257. doi: 10.1038/nature11420

Nasar, J., Wang, G.-Y., Ahmad, S., Muhammad, I., Zeeshan, M., Gitari, H., et al. (2022). Nitrogen fertilization coupled with iron foliar application improves the photosynthetic characteristics, photosynthetic nitrogen use efficiency, and the related enzymes of maize crops under different planting patterns. *Front. Plant Sci.* 13. doi: 10.3389/fpls.2022.988055

Shao, H., Chi, H., Zhu, F., Liu, J., Duan, J., Shi, W., et al. (2024). How does increasing planting density affect nitrogen use efficiency of maize: A global meta-analysis. *Field Crops Res.* 311, 109369. doi: 10.1016/j.fcr.2024.109369

Sharma, N. K., Choct, M., Toghyani, M., Laurenson, Y. C. S. M., Girish, C. K., and Swick, R. A. (2018). Dietary energy, digestible lysine, and available phosphorus levels affect growth performance, carcass traits, and amino acid digestibility of broilers. *Poult Sci.* 97, 1189–1198. doi: 10.3382/ps/pex405

Shi, D.-Y., Li, Y.-H., Zhang, J.-W., Liu, P., Zhao, B., and Dong, S.-T. (2016). Increased plant density and reduced N rate lead to more grain yield and higher resource utilization in summer maize. *J. Integr. Agric.* 15, 2515–2528. doi: 10.1016/s2095-3119(16)61355-2

Si, Z., Zain, M., Mehmood, F., Wang, G., Gao, Y., and Duan, A. (2020). Effects of nitrogen application rate and irrigation regime on growth, yield, and water-nitrogen use efficiency of drip-irrigated winter wheat in the North China Plain. *Agric. Water Manage.* 231, 106002. doi: 10.1016/j.agwat.2020.106002

Tang, C., Yang, X., Chen, X., Ameen, A., and Xie, G. (2018). Sorghum biomass and quality and soil nitrogen balance response to nitrogen rate on semiarid marginal land. *Field Crops Res.* 215, 12–22. doi: 10.1016/j.fcr.2017.09.031

Vansoest, P. J., Robertson, J. B., and Lewis, B. A. (1991). Methods for dietary fiber, neutral detergent fiber, and nonstarch polysaccharides in relation to animal nutrition. *J. Dairy Sci.* 74, 3583–3597. doi: 10.3168/jds.S0022-0302(91)78551-2

Wang, S.-L., He, M.-R., Dai, X.-L., and Zhou, X.-H. (2012). Effects of planting density on root spatiotemporal distribution and plant nitrogen use efficiency of winter wheat. *Yingyong Shengtai Xuebao* 23, 1839–1845. doi: 10.13287/j.1001-9332.2012.0211

Wang, D., Li, G., Mo, Y., Cai, M., and Bian, X. (2018). Evaluation of optimal nitrogen rate for corn production under mulched drip fertigation and economic benefits. *Field Crops Res.* 216, 225–233. doi: 10.1016/j.fcr.2017.10.002

Wang, Y., Peng, Y., Lin, J., Wang, L., Jia, Z., and Zhang, R. (2023). Optimal nitrogen management to achieve high wheat grain yield, grain protein content, and water productivity: A meta-analysis. *Agric. Water Manage.* 290, 108587. doi: 10.1016/j.agwat.2023.108587

Wang, X., Wang, H.-F., Chen, Y., Sun, M.-M., Wang, Y., and Chen, Y.-F. (2020). The transcription factor NIGT1.2 modulates both phosphate uptake and nitrate influx during phosphate starvation in arabidopsis and maize. *Plant Cell* 32, 3519–3534. doi: 10.1105/tpc.20.00361

Wu, X., Li, Z., Li, W., Xue, X., Yang, L., Xu, J., et al. (2024). Reducing fertilization with high planting density increases maize yield stability and nitrogen use efficiency in semi-arid areas. *Eur. J. Agron.* 159, 127223. doi: 10.1016/j.eja.2024.127223

Xu, G., Fan, X., and Miller, A. J. (2012). Plant nitrogen assimilation and use efficiency. *Annu. Rev. Plant Biol.* 63, 153–182. doi: 10.1146/annurev-arplant-042811-105532

Yang, X., Geng, J., Li, C., Zhang, M., Chen, B., Tian, X., et al. (2016). Combined application of polymer coated potassium chloride and urea improved fertilizer use efficiencies, yield and leaf photosynthesis of cotton on saline soil. *Field Crops Res.* 197, 63–73. doi: 10.1016/j.fcr.2016.08.009

Yang, G., Xiang, H., Fu, Y., Zhou, C., Wang, X., Yuan, S., et al. (2024). Optimal nitrogen management increases nitrogen use efficiency of direct-seeded double-season rice using ultrashort-duration cultivars. *Field Crops Res.* 316, 109495. doi: 10.1016/j.fcr.2024.109495

Yousaf, M., Li, X., Zhang, Z., Ren, T., Cong, R., Ata-Ul-Karim, S. T., et al. (2016). Nitrogen fertilizer management for enhancing crop productivity and nitrogen use efficiency in a rice-oilseed rape rotation system in China. *Front. Plant Sci.* 7. doi: 10.3389/fpls.2016.01496

Yuan, M., Wu, G., Wang, J., Liu, C., Hu, Y., Hu, R., et al. (2024). Blended controlled-release nitrogen fertilizer increases rice post-anthesis nitrogen accumulation, translocation and nitrogen-use efficiency. *Front. Plant Sci.* 15. doi: 10.3389/fpls.2024.1354384

Zhang, Q., Bell, L. W., Shen, Y., and Whish, J. P. M. (2018). Indices of forage nutritional yield and water use efficiency amongst spring-sown annual forage crops in north-west China. *Eur. J. Agron.* 93, 1–10. doi: 10.1016/j.eja.2017.11.003

Zhang, Q., Du, Y., Cui, B., Sun, J., Wang, J., Wu, M., et al. (2021a). Aerated irrigation offsets the negative effects of nitrogen reduction on crop growth and water-nitrogen utilization. *J. Cleaner Prod.* 313, 127917. doi: 10.1016/j.jclepro.2021.127917

Zhang, W., Liu, D., Liu, Y., Chen, X., and Zou, C. (2017a). Overuse of phosphorus fertilizer reduces the grain and flour protein contents and zinc bioavailability of winter wheat (*Triticum aestivum* L.). *J. Agric. Food. Chem.* 65, 1473–1482. doi: 10.1021/acs.jafc.6b04778

Zhang, R., Wang, Y., Kamran, M., Wang, J., Li, T., Zhao, G., et al. (2025a). Optimal sowing density and fertilizer rate can increase oat yield by improving root structure, water use efficiency and fertilizer productivity in semi-arid region. *Plant Soil*. doi: 10.1007/s11104-025-07435-1

Zhang, R., Wang, J., Xue, L., Kamran, M., Wang, Y., Wei, X., et al. (2025b). The impact of bacterial leaf blight disease (*Pantoea agglomerans*) on grain yield and nutritional quality of oat. *Microorganisms* 13, 141. doi: 10.3390/microorganisms13010141

Zhang, Z., Whish, J. P. M., Bell, L. W., and Nan, Z. (2017b). Forage production, quality and water-use-efficiency of four warm-season annual crops at three sowing times in the Loess Plateau region of China. *Eur. J. Agron.* 84, 84–94. doi: 10.1016/j.eja.2016.12.008

Zhang, Y., Xu, Z., Li, J., and Wang, R. (2021b). Optimum planting density improves resource use efficiency and yield stability of rainfed maize in semiarid climate. *Front. Plant Sci.* 12. doi: 10.3389/fpls.2021.752606

Zhu, X., Zhang, J., Zhang, Z., Deng, A., and Zhang, W. (2016). Dense planting with less basal nitrogen fertilization might benefit rice cropping for high yield with less environmental impacts. *Eur. J. Agron.* 75, 50–59. doi: 10.1016/j.eja.2016.01.003

Zou, T., Zhang, X., and Davidson, E. A. (2022). Global trends of cropland phosphorus use and sustainability challenges. *Nature* 611, 81–8+. doi: 10.1038/s41586-022-05220-z

frontiers | Frontiers in Plant Science

TYPE Original Research
PUBLISHED 13 June 2025
DOI 10.3389/fpls.2025.1590774

Check for updates

OPEN ACCESS

EDITED BY
Amir Ali Khoddamzadeh,
Florida International University, United States

REVIEWED BY
Raman Selvakumar,
Indian Agricultural Research Institute (ICAR), India
Milka Brdar-Jokanović,
Institute of Field and Vegetable Crops, Serbia

*CORRESPONDENCE
Yanling Chen
chenyanling21@163.com

†These authors have contributed equally to this work and share first authorship

RECEIVED 10 March 2025
ACCEPTED 27 May 2025
PUBLISHED 13 June 2025

CITATION
Zhao Y, Gong Y, Li Y, Xin H, Chi R and Chen Y (2025) High-quality carrots in relation to the superior phloem parenchyma cells and proportion of xylem vessel in coordinated water-fertilizer management.
Front. Plant Sci. 16:1590774.
doi: 10.3389/fpls.2025.1590774

COPYRIGHT
© 2025 Zhao, Gong, Li, Xin, Chi and Chen. This is an open-access article distributed under the terms of the Creative Commons Attribution License (CC BY). The use, distribution or reproduction in other forums is permitted, provided the original author(s) and the copyright owner(s) are credited and that the original publication in this journal is cited, in accordance with accepted academic practice. No use, distribution or reproduction is permitted which does not comply with these terms.

High-quality carrots in relation to the superior phloem parenchyma cells and proportion of xylem vessel in coordinated water-fertilizer management

Ying Zhao[1†], Yanchen Gong[1†], Yun Li[1], Hua Xin[1], Ruiping Chi[2] and Yanling Chen[1*]

[1]College of Resources and Environment Science, Qingdao Agricultural University, Qingdao, Shandong, China, [2]Agricultural Technology Extension Service Center, Laixi Agriculture and Rural Bureau, Qingdao, China

Background: The coordinated management of water and fertilizer is essential for improving vegetable yield and quality. However, its role in connecting quality with the anatomical structure of the phloem and xylem in carrots remains unclear.

Methods: This study involved a two-year field trial with four different water and fertilizer treatments: farmer practices (FP), an optimized water and fertilizer system (OPT), 30% organic substitution with compressed peanut shells (PS), and 30% organic substitution with Pleurotus ostreatus residue (M) combined with water and fertilizer optimization.

Results: Compared with the FP treatment, the OPT, PS, and M treatments increased both yield and quality. Flavor quality increased by 17.51%, 13.04%, and 15.05%, and nutritional quality increased by 11.04%, 8.12%, and 17.35% in the upper, middle, and lower segments, respectively, in the OPT treatment. In contrast, the organic substitution treatments (average of PS and M) resulted in even greater improvements, with flavor quality increasing by 32.50%, 18.21%, and 38.07%, and nutritional quality increasing by 10.28%, 4.69%, and 25.41%, respectively. In the phloem, flavor and nutritional quality increased by 9.59% and 13.50%, respectively, in the OPT treatment and by 12.35% and 17.69%, respectively, in the organic substitution treatment. In the xylem, flavor and nutritional quality increased by 1.64% and 19.09%, respectively, in the OPT treatment, whereas in the organic substitution treatments, flavor quality increased by 16.89%, and nutritional quality increased by 1.94%. Compared with those in the FP treatment, the phloem parenchyma cell area (Pca) and the proportion of xylem vessels to secondary xylem (Pxv) in the upper segment were 9.17% and 88.40% greater in the OPT treatment, respectively, and 18.44% and 116.22% greater in the organic substitution treatment, respectively. The parameters characterizing Pca and Pxv in the upper segment, along with Pca in the lower segment, were positively correlated with flavor and nutritional quality, whereas the xylem vessel area (Xva) and diameter (Xvd) were negatively correlated.

Conclusion: In conclusion, the coordinated management of water, organic, and inorganic fertilizers improves flavor and nutritional quality across the upper, middle, and lower segments, as well as in the phloem and xylem. The superior phloem parenchyma cell area and xylem vessel proportion in the upper segment may serve as physiological traits in breeding carrots for quality improvement.

KEYWORDS

carrot, flavor quality, nutritional quality, parenchyma cell, xylem vessel

1 Introduction

Carrots are well-known vegetable crops worldwide and are prized for their abundance of nutrients such as carotene, amino acids, and vitamins (Zhang et al., 2020). China accounts for almost 40% of the global carrot planting area (FAO, 2022). Nevertheless, in recent years, farmers have been using excessive water and fertilizers more frequently to increase yields, leading to issues related to crop quality and the environment (Rietra et al., 2017). The optimization of water and fertilizer management is crucial for decreasing input costs while improving both yield and quality (Gan et al., 2023).

Carotenoid levels in the aboveground and root sections are higher with fractional nitrogen (N) fertilizer treatments than with one-third N treatments (Colombari et al., 2018). Compared with conventional methods, organic management offers greater commerciality, reduced waste, and increased vitamin C content in carrots (Olle and Williams, 2021). The evaluation of high-quality carrots is based on their appearance, flavor, and nutritional quality (Carrillo-López and Yahia, 2019). The shape of carrot taproots is primarily determined by the balance of length, elongation, and thickness, leading to various root types ranging from circular to conical or cylindrical (Kjellenberg et al., 2016). Cylindrical roots are regarded as a standard for appearance quality (Thompson, 1969). Flavor quality is determined by the balance between sweetness and acidity (Kader, 2008).

Carrot quality and the distribution of the main primary and secondary metabolites vary significantly across genotypes and radially distributed tissues (Aubert et al., 2022). In two carrot genotypes, the malic acid content is greater in the xylem than in the phloem, whereas α-carotene, β-carotene, and carotenoids are more abundant in the phloem (Aubert et al., 2022; Perrin et al., 2017). The levels of metabolites, sucrose, and carotenoids decrease from the top to the bottom of the tissue. Among the three carrot varieties, carotenes are most concentrated in the secondary phloem (Kim et al., 2010). However, the understanding of carrot quality across vertical segments and radial distribution under optimal water-fertilizer management is limited, which is crucial for the cultivation of high-yield and high-quality carrots.

The formation and expansion of carrot roots involve structural changes, material accumulation, and gene regulation (Khadr et al., 2020). The vascular cambium divides the root into two parts: the secondary phloem (cortex) and the secondary xylem (core) (Perrin et al., 2017). The xylem transports water, whereas the phloem carries amino acids and sucrose (Zhao et al., 2005). The phloem expands significantly during growth, especially with increasing parenchyma cell number and volume (Suojala, 2000). Its metabolic function surpasses that of the xylem, resulting in the accumulation of more nutrients (Aubry et al., 2019). Sugars are mainly stored in parenchyma vacuoles (Nilsson, 1987), and carotenoids are synthesized in chloroplasts (Perrin et al., 2017). However, the relationships between the phloem and xylem structure and quality in carrots remain unclear.

Previous studies have shown that optimizing water and fertilizer management can greatly improve the overall quality of carrots in long-term experiments (Tang et al., 2024). This study delves deeper into the underlying physiological mechanisms by examining the following hypotheses: a) optimized water-fertilizer management enhances flavor and nutritional quality across different vertical segments of carrots, and b) a superior phloem and xylem structure in the horizontal radial distribution promotes the accumulation of soluble solids, sugars, and carotene, contributing to excellent flavor and nutritional quality under coordinated water–fertilizer management.

Abbreviations: Cd, Compaction degree; Ci, Color index; FAA, formaldehyde, acetic acid–alcohol; FP, farmers' practice; LSD, Least significant difference test; M, 30% *Pleurotus ostreatus* residue organic substitution; OPT, water and fertilizers system optimization; Pc, parenchyma cell; Pca, the phloem parenchyma cell area; Phr, Pulp heart rate; PL, Phloem in the lower segment; PM, Phloem in the middle segment; PS, 30% compressed peanut shell organic substitution; PU, Phloem in the upper segment; Pxv, the proportion of xylem vessel to secondary xylem; RDA, Redundancy analysis; Rtci, Root, tail convergence index; SG, starch granule; Ve, vessel; TSS, Total soluble solids; TSS, to, TA ratio, Total soluble solids, to, titratable acid ratio; XL, Xylem in the lower segment; XM, Xylem in the middle segment; XU, Xylem in the upper segment; Xva, xylem vessel area; Xvd, xylem vessel diameter.

2 Materials and methods

2.1 Field experiments

Field experiments were conducted in 2022 and 2023 as part of a long-term study on water and fertilizer management that was

initiated in 2020 at the Science and Technology Backyard of LaiXi in Houtun village, Qingdao city, Shandong Province (36°N; 120°E). The experimental site has a temperate continental monsoon climate, with annual average temperatures of 13°C in 2022 and 14°C in 2023. The total rainfall during the two growing seasons was 715.5 mm in 2022 and 445.8 mm in 2023. The soil used in the experiment was mortar black soil, with the following properties at a depth of -20 cm: alkali-hydrolysable N, 175.7 mg·kg^{-1}; Olsen P, 27.7 mg·kg^{-1}; available K, 117.6 mg·kg^{-1}; pH, 6.80; and organic matter, 12.3 g·kg^{-1}.

Pleurotus ostreatus is abundant in nutrients, including protein, amino acids, vitamins, and various other substances that can be converted into organic fertilizer (Huang et al., 2023). Peanut shells are high in fiber, vitamins, flavonoids, and mineral nutrients such as calcium (Camargo et al., 2017). They can also serve as seedling substrate material postfermentation (Sun et al., 2003). Since local farmers cultivate peanuts and *Pleurotus ostreatus*, there is an abundance of residue available for utilization. The water and fertilizer treatments included (1) farmer practices (FP), where water and fertilizers are applied following traditional methods in Laixi; (2) an optimized water and fertilizer system(OPT), which uses real-time soil water or nutrient data and field capacity, employing sensors to fulfill carrot nutrient needs; (3) 30% organic substitution with compressed peanut shells + OPT (PS); and (4) 30% organic substitution with *Pleurotus ostreatus* residue + OPT (M). In the PS and M treatments, 30% of the N fertilizer was substituted with compressed peanut shells or *Pleurotus ostreatus* residue, maintaining total water and fertilizer levels similar to those in the OPT treatment. In 2022 and 2023, FP application rates were established at 323 kg N ha^{-1}, 225 kg P_2O_5 ha^{-1}, and 285 kg K_2O ha^{-1} on the basis of local surveys (Table 1). The OPT rates were 252 and 236 kg N ha^{-1}, 54 and 59 kg P_2O_5 ha^{-1}, and 240 and 300 kg K_2O ha^{-1}, as determined by carrot growth stages, respectively. The PS rates were 252 and 236 kg N ha^{-1}, 63 and 74 kg P_2O_5 ha^{-1}, and 240 and 300 kg K_2O ha^{-1}, respectively. The application rates of the M treatment were 252 and 236 kg N ha^{-1}, 78 and 88 kg P_2O_5 ha^{-1}, and 240 and 300 kg K_2O ha^{-1}, respectively. Urea (N 46%) was used as the N fertilizer, diammonium phosphate (N 18%, P_2O_5 46%) was used as the P source, and potassium sulfate (K_2O 50%) was used for K. The organic fertilizer consisted of an agricultural microbial agent (N 4%). The agricultural microbial agents were applied in FP and OPT at a rate of 1200 kg ha^{-1}. In 2022 and 2023, the PS treatment was applied at rates of 4740 kg·ha^{-1} and 4440 kg·ha^{-1} peanut shell compressed particles, whereas the M treatment was applied at rates of 4995 kg·ha^{-1} and 4680 kg·ha^{-1} mushroom residue. The fertilizer is applied in liquid form by dissolving the powder in water. This experiment utilized elemental fertilizer to achieve the necessary N, P, and K content ratios for optimal carrot growth.

In terms of water management, the FP treatment utilized customary irrigation volumes, whereas the remaining treatments were modified according to the real-time soil moisture and field capacity data provided by sensors. The total irrigation volumes were 924 and 1835 m^3·ha^{-1} for the FP treatment, 862 and 1587 m^3·ha^{-1} for the OPT treatment, 894 and 1605 m^3·ha^{-1} for the PS treatment, and 875 and 1587 m^3·ha^{-1} for the M treatment, in 2022 and 2023. Details of the nutrient and water inputs at each stage can be found in Supplementary Table S1.

In this experiment, four large plots, each measuring 220.5 m^2, were established. Each large plot was divided into four repetitions. The carrot varieties Zhenjiuhong in 2022 and Hongta313 in 2023 were selected on the basis of their climate adaptability in spring and autumn. Planting was conducted on raised ridges, with each ridge supporting two rows, resulting in a total of 7 ridges and 14 rows. The ridges had a spacing of 67–70 cm, height of 15 cm, top width of 28 cm, and spacing of 5–6 cm. Carrot seeds were sown at a depth of 1.5–2 cm on August 24, 2022, and January 9, 2023, and were harvested on December 10, 2022, and May 20, 2023, respectively.

2.2 Plant sampling and measurement

2.2.1 Yield and plant sampling

At maturity, the central four rows (5 meters in length and 1.4 meters in width) in each plot were harvested. Carrots were extracted from the soil, counted, and weighed, and the yield per hectare was calculated on the basis of harvest density. Furthermore, fifteen uniform and representative carrot roots were collected and washed from each plot. One-third of these roots were utilized to assess appearance quality and then dried, after which the total N, total phosphorus (P), and total potassium (K) contents were measured. The total N content was determined using the Kjeldahl method. The total P content was analyzed using the molybdenum antimony colorimetric method. The total K content was measured via flame photometry (Bao, 2000). The remaining roots were divided as follows: five roots were segmented equally into upper, middle, and lower parts to analyze flavor and nutritional quality

TABLE 1 Total input of nutrient and water in each treatment in 2022 autumn and 2023 spring.

Year/ Treatments		2022 Autumn				Water and fertilizers reduction (%)	2023 Spring				Water and fertilizers reduction (%)
		FP	OPT	PS	M		FP	OPT	PS	M	
N	(kg ha^{-1})	323	252	252	252	-21.9	323	236	236	236	-26.8
P_2O_5	(kg ha^{-1})	225	54	63	78	-71.1	225	59	74	88	-67.4
K_2O	(kg ha^{-1})	285	240	240	240	-15.8	285	300	300	300	5.3
Water	(m^3 ha^{-1})	924	862	894	875	-5.1	1835	1587	1605	1587	-13.2

Water and fertilizers reduction = (the average of water and fertilizers input amount in the OPT, PS, M treatments – the water and fertilizers input amount in the FP treatment)/the water and fertilizers input amount in the FP treatment.

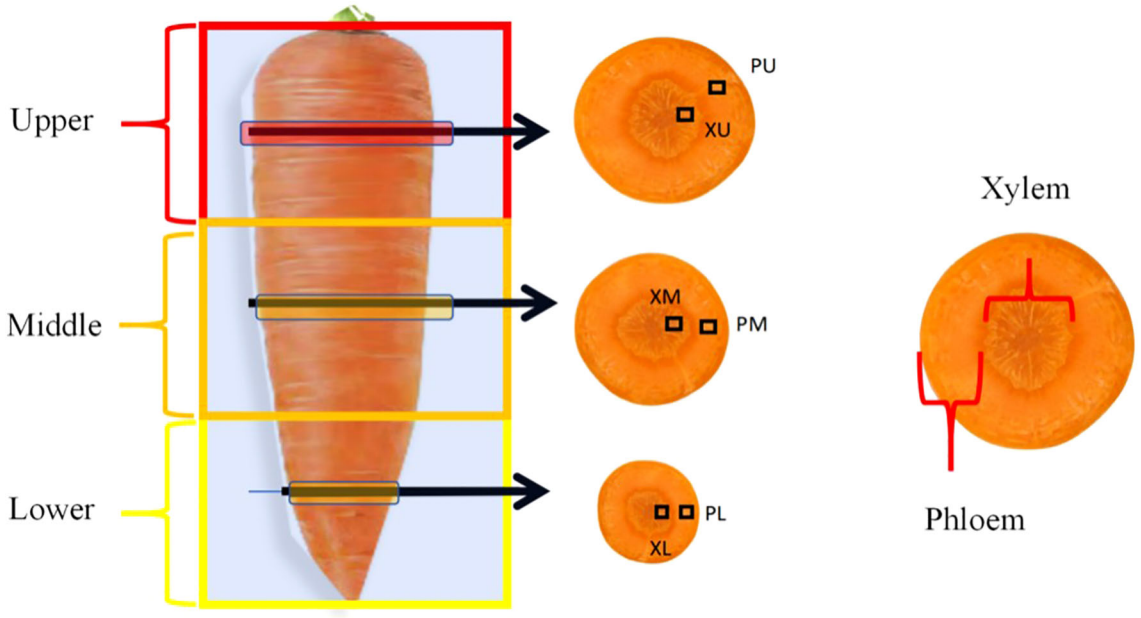

FIGURE 1
Sampling schematic diagram of phloem and xylem in the upper, middle and lower segments at equal proportion in carrot. PU, Phloem in the upper segment, XU, Xylem in the upper segment; PM, Phloem in the middle segment, XM, Xylem in the middle segment; PL, Phloem in the lower segment; XL, Xylem in the lower segment.

postjuicing with household appliances, while the remaining five roots were separated into phloem and xylem tissues using a peeler and knife (Figure 1). These tissues were preserved in formaldehyde-acetic acid–alcohol (FAA) fixative for observation of anatomical structure and evaluation of flavor and nutritional quality. Segmenting carrots into upper, middle, and lower parts for analysis aims to provide a more precise assessment of their nutrient composition and quality attributes, as well as to identify varietal differences. This process is crucial for carrot variety selection, food processing, and nutritional assessment.

2.2.2 Quality measurement

Appearance Quality: The color index (Ci) was determined using an SC-10 colorimeter (Guangdong Sanenshi Technology Limited Company, China). Red-to-green tones were denoted as +a to –a, yellow-to-blue tones were represented as +b to –b, and brightness was denoted as L. Ci was calculated with the formula Ci = 1000a*/(Lb) (Passafiume et al., 2023). The compaction degree (Cd) was calculated as the ratio of the weight of a single root to the product of the root length and middle diameter. The root–tail convergence index (Rtci) was determined by the ratio of the bottom 0.5 cm to the top 0.5 cm. The pulp heart rate (Phr) was calculated as the ratio of the xylem diameter to the entire pulp diameter using a Vernier caliper.

Flavor Quality: The assessment of flavor quality, particularly the influence of sugars on taste, included the evaluation of total soluble solids (TSS) and the total soluble solids-to-titratable acid (TA) ratio (Beckles, 2012; Stevens et al., 1979). The TSS was determined using a handheld TD-32 sugar meter (Shanghai Lichen Bangxi Instrument Technology Limited Company, China). TA was measured through titration with sodium hydroxide. The TSS-to-TA ratio was computed to evaluate the equilibrium between soluble solids and organic acids (Baldwin et al., 1998).

Nutritional quality: Vitamin C content was determined by 2% oxalic acid extraction and titration with 2,6-dichloroindophenol (Ranganna, 1977). The carotene content was quantified using the acetone extraction method (Costache et al., 2012). Soluble protein levels were assessed using the Coomassie Brilliant Blue method (Sedmak and Grossberg, 1977), whereas free amino acids were quantified through ninhydrin colorimetry (Moore, 1968).

2.2.3 Anatomical structure of the phloem and xylem

The carrot cross-sectional structure was analyzed using the paraffin sectioning method (Wang et al., 2016). Slices (5 mm thick) were taken from the longitudinal middle of the upper, middle, and lower segments of each sample and fixed. Half of the radial middle of the phloem and xylem in each slice was observed (Figure 1). The distribution, density, diameter, and area of phloem parenchyma cells (Pc) and xylem vessels (Ve) were quantified. The samples were dehydrated with a gradient of ethyl alcohol and xylene, embedded in paraffin, and sectioned to 8 μm using a Leica RM2126RT (Leica, Germany) (Yuan et al., 2023). The sections, which were stained with saffron O solid green, were visualized under an Olympus CX33 microscope (Olympus Corporation, Japan) and processed with MShot Image Analysis System software (Guangzhou Microshot Technology Limited Company, China), and cell measurements were conducted using ImageJ (National Institutes of Health). Nine visual fields per replicate were utilized to determine the Pc and vessel diameter, area, and secondary xylem proportion.

2.3 Statistical analysis

Data across water and fertilizer treatments and years were pooled and analyzed with a one-way ANOVA in the DPS data processing system. Differences were evaluated using the least significant difference test at a significance level of 0.05. Since the quality improvements were similar in the PS and M treatments, these improvements were averaged and considered organic alternatives in the analysis. Figures were generated in Origin 2024. Redundancy analysis (RDA) was performed in Canoco 5 (Ter Braak and Smilauer, 2002) to examine correlations between nutrient concentration, anatomical structure, flavor, and nutritional quality.

3 Results

3.1 Yield, nutrient concentration and quality of whole fleshy roots

Compared with that in the FP treatment, the yield significantly increased in the OPT, PS, and M treatments in 2022 but not in 2023. There was no significant difference in yield between OPT and PS or M over the two years (Figure 2A). The total nitrogen (N) and total potassium (K) concentrations significantly increased in the OPT, PS, and M treatments in both years (Figures 2B, D). The total phosphorus (P) concentration significantly increased in the PS and M treatments in 2022, and it also significantly increased in the OPT, PS, and M treatments in 2023 (Figure 2C). Compared with that in the FP treatment, the Ci significantly increased in the M treatment but remained unchanged in the OPT and PS treatments in 2023 (Figure 3A). The Cd concentration significantly increased in the OPT treatment but remained unchanged in the PS and M treatments in 2022 (Figure 3B). The Rtci increased in the PS and M treatments in 2022, increased only in the PS treatment in 2023, and remained unchanged in the OPT treatment over the two-year period (Figure 3C). The Phr significantly decreased in the OPT and PS treatments but not in the M treatment in 2022 (Figure 3D). There was no significant difference in Ci in 2022 or in Cd or Phr in 2023 among the OPT and PS or M treatments (Figures 3A-D).

In terms of nutritional quality, compared with that in the FP treatment, the vitamin C concentration significantly increased in the OPT, PS, and M treatments in both years (Figure 3E). The soluble protein content significantly increased in the OPT and PS treatments but decreased in the M treatment in 2022 (Figure 3F). The carotene content significantly increased in the PS treatment but remained unchanged in the OPT and M treatments in 2023 (Figure 3G). The Free amino acid content significantly increased

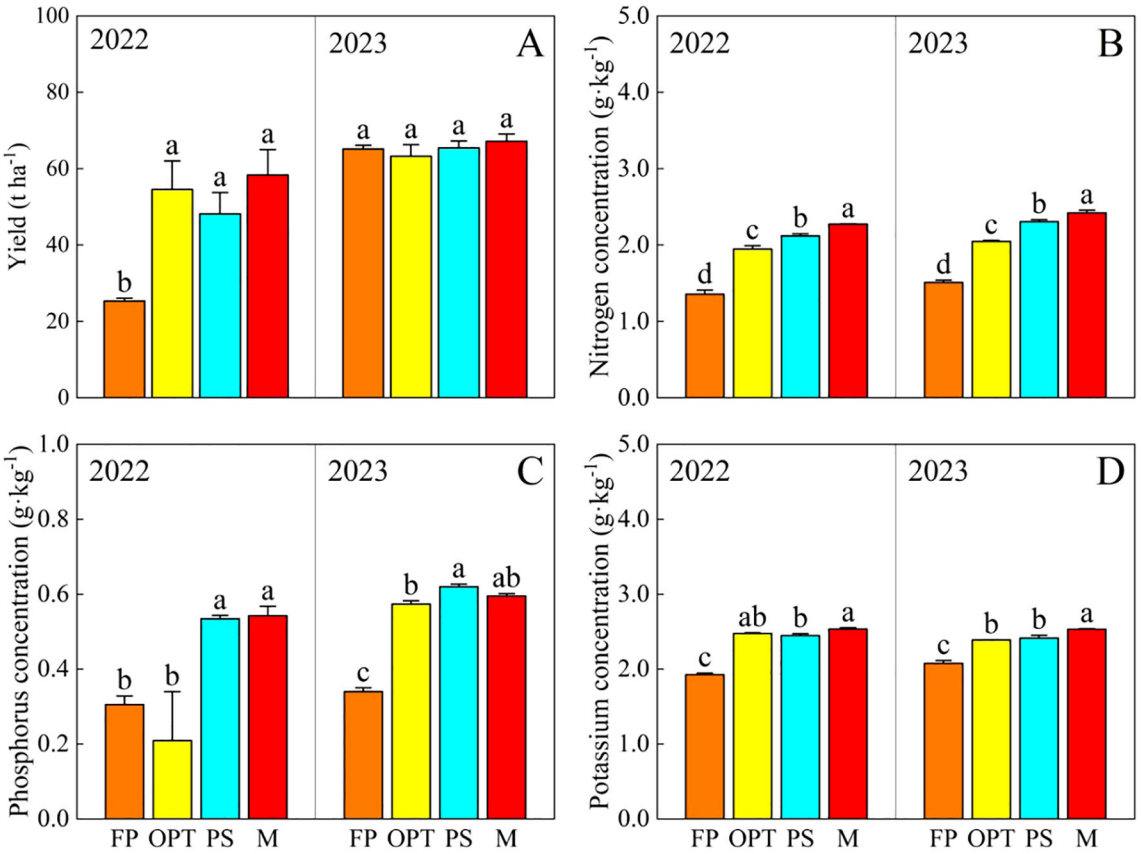

FIGURE 2
Effects of water and fertilizers management on yield and total nitrogen, total phosphorus, total potassium concentration in carrot. **(A–D)** represent yield, total nitrogen, total phosphorus, total potassium concentration in carrot, respectively. Different letters indicate significant differences among different water and fertilizers managements ($P < 0.05$). Values shown are means (n = 3 replicates).

10.3389/fpls.2025.1590774

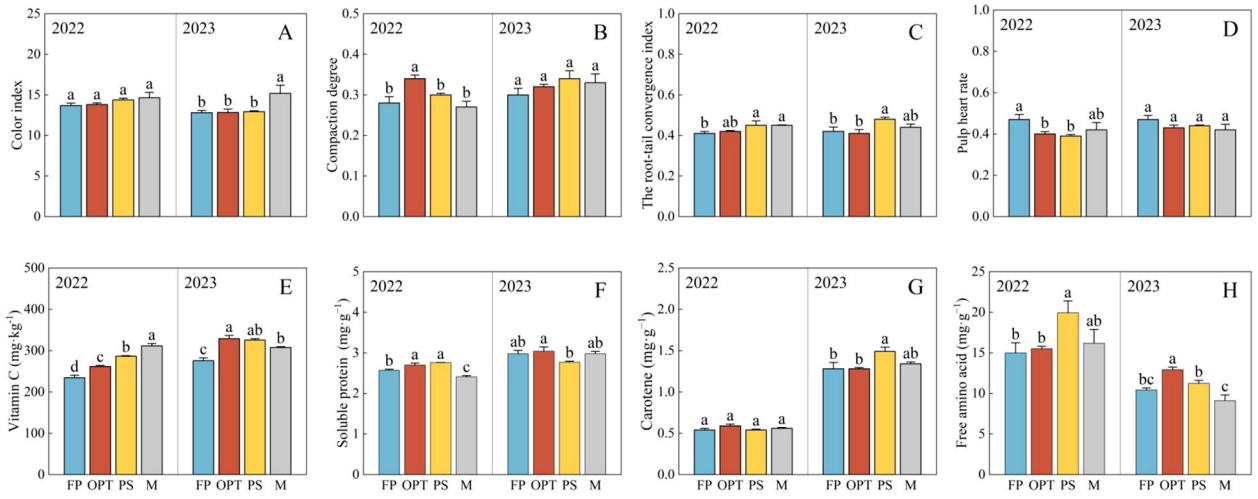

FIGURE 3
Effects of water and fertilizers management on appearance and nutritional quality in carrot. Different letters indicate significant differences among different water and fertilizers managements (P < 0.05). Values shown are means (n = 3 replicates). **(A–D)** represent color index, compaction degree, the root-tail convergence index, pulp heart rate of FP, OPT, PS and M treatments, respectively. **(E–H)** represent vitamin C, soluble protein, carotene, free amino acid of FP, OPT, PS and M treatments, respectively.

in the PS treatment but remained unchanged in the OPT and M treatments in 2022. In 2023, free amino acid content significantly increased in the OPT treatment but remained unchanged in the PS and M treatments (Figure 3H). No significant differences were found in the carotene content in 2022 or soluble protein content in 2023 between the OPT and PS or M treatments compared to FP treatment (Figures 3F, G).

In terms of flavor quality, compared with that in the FP treatment, the TSS content significantly increased in the PS treatment but remained unchanged in the OPT and M treatments in 2022. The TA significantly decreased in the OPT, PS, and M treatments in both years. The TSS-to-TA ratio significantly increased in the OPT, PS, and M treatments in both years. The soluble sugar content significantly increased in the PS and M treatments but remained unchanged in the OPT treatment in both years. Glucose levels significantly decreased in the OPT treatment group in 2023 but remained unchanged in the PS and M treatment groups. Sucrose levels significantly increased in the OPT and PS treatments but remained unchanged in the M treatment in 2022. In 2023, sucrose levels significantly increased in all the OPT, PS and M treatments. No significant differences were found in glucose levels in 2022 or in TSS levels in 2023 among the OPT and PS or M treatments (Table 2).

3.2 Flavor and nutritional quality in the upper, middle, and lower segments

Significant differences in flavor and nutritional quality were observed among the FP, OPT, PS, and M treatments (Table 3; Figure 4). In terms of flavor quality in the upper carrot segment, compared with that in the FP treatment, the TSS significantly increased in the PS treatment but remained unchanged in the OPT and M treatments in both years (Table 3). The TA

TABLE 2 Effects of water and fertilizers management on flavor quality in carrot.

Treatments/ index		Total soluble solid (%)	Titratable acid (%)	TSS-to-titratable acid ratio	Soluble sugar (mg g^{-1} DW)	Glucose (mg g^{-1} DW)	Sucrose (mg g^{-1} DW)
2022	FP	7.86 ± 0.10b	0.84 ± 0.06a	10.65 ± 0.31b	403.82 ± 19.73b	149.99 ± 33.49a	154.52 ± 24.51b
	OPT	7.81 ± 0.13b	0.72 ± 0.02b	13.13 ± 0.73a	450.60 ± 17.29ab	121.97 ± 34.57a	209.71 ± 43.63a
	PS	8.31 ± 0.22a	0.64 ± 0.02bc	15.02 ± 1.21a	505.24 ± 58.82a	123.96 ± 53.92a	220.71 ± 13.81a
	M	7.96 ± 0.08b	0.57 ± 0.07c	15.02 ± 2.13a	503.27 ± 16.44a	127.99 ± 22.96a	191.72 ± 20.64ab
2023	FP	11.22 ± 0.34ab	1.52 ± 0.03a	7.43 ± 0.36d	536.08 ± 32.32b	195.88 ± 33.25a	137.05 ± 17.97b
	OPT	11.22 ± 0.12ab	1.15 ± 0.04b	9.82 ± 0.41c	595.61 ± 17.71b	117.24 ± 16.32b	228.27 ± 28.88a
	PS	11.53 ± 0.09a	0.95 ± 0.04c	12.41 ± 0.48a	679.92 ± 38.84a	243.84 ± 29.32a	238.30 ± 11.21a
	M	11.18 ± 0.07b	0.98 ± 0.04c	11.55 ± 0.40b	683.19 ± 34.53a	249.28 ± 31.41a	205.83 ± 4.83a

Different letters indicate significant differences among different water and fertilizers managements (P < 0.05). Values shown are means (n = 3 replicates).

10.3389/fpls.2025.1590774

TABLE 3 Effects of water and fertilizers management on the flavor quality in the upper, middle, lower segments in carrot.

Treatments/index			Total soluble solid (%)	Titratable acid (%)	TSS-to-titratable acid ratio	Soluble sugar (mg g^{-1} DW)	Glucose (mg g^{-1} DW)	Sucrose (mg g^{-1} DW)
Upper	2022	FP	8.10 ± 0.17b	0.58 ± 0.01a	14.55 ± 1.27b	351.22 ± 11.58a	116.29 ± 24.75ab	118.49 ± 12.28b
		OPT	8.17 ± 0.15ab	0.42 ± 0.06b	20.13 ± 2.57a	416.01 ± 14.42a	85.00 ± 37.88ab	191.36 ± 46.92a
		PS	8.47 ± 0.25a	0.43 ± 0.06b	20.37 ± 2.15a	448.86 ± 106.23a	139.42 ± 49.87a	176.95 ± 12.43a
		M	8.00 ± 0.00b	0.45 ± 0.11b	18.43 ± 3.90ab	422.37 ± 27.77a	66.98 ± 28.37b	221.54 ± 25.78a
	2023	FP	11.73 ± 0.15b	1.53 ± 0.04a	7.71 ± 0.33d	489.11 ± 5.11c	139.50 ± 100.16ab	149.36 ± 31.00b
		OPT	11.93 ± 0.15ab	1.21 ± 0.06b	9.94 ± 0.58c	608.60 ± 12.95b	83.62 ± 20.38b	229.50 ± 66.64a
		PS	12.20 ± 0.17a	1.00 ± 0.06c	12.29 ± 0.47a	682.72 ± 75.65ab	210.40 ± 66.60ab	265.45 ± 13.03a
		M	11.63 ± 0.25b	1.05 ± 0.01c	11.15 ± 0.15b	697.26 ± 42.59a	234.49 ± 60.42a	218.56 ± 14.58ab
Middle	2022	FP	7.87 ± 0.15b	0.74 ± 0.10a	10.88 ± 1.37b	400.91 ± 22.42b	132.09 ± 68.13a	222.47 ± 59.12a
		OPT	7.70 ± 0.10b	0.64 ± 0.05ab	12.28 ± 0.87b	441.06 ± 20.80b	208.85 ± 31.04a	208.22 ± 35.92a
		PS	8.33 ± 0.25a	0.55 ± 0.05b	16.07 ± 1.95a	548.61 ± 50.98a	104.68 ± 73.26a	247.57 ± 30.81a
		M	7.93 ± 0.12b	0.51 ± 0.07b	15.86 ± 1.99a	511.61 ± 16.96a	117.22 ± 36.08a	207.79 ± 55.06a
	2023	FP	11.37 ± 0.78a	1.54 ± 0.07a	7.41 ± 0.83b	650.25 ± 61.30a	279.26 ± 25.02a	159.18 ± 7.72b
		OPT	11.27 ± 0.35a	1.20 ± 0.05b	9.46 ± 00.62a	621.95 ± 36.74a	85.26 ± 29.6b	309.66 ± 71.02a
		PS	11.53 ± 0.12a	1.07 ± 0.15b	11.04 ± 1.67a	687.39 ± 44.23a	245.27 ± 20.14a	243.99 ± 4.58a
		M	11.50 ± 0.46a	1.08 ± 0.10b	10.64 ± 0.56a	676.24 ± 61.10a	232.05 ± 41.17a	243.12 ± 6.76a
Lower	2022	FP	7.60 ± 0.10b	1.18 ± 0.10a	6.53 ± 0.51c	459.33 ± 33.45c	201.58 ± 52.65a	122.59 ± 33.04b
		OPT	7.57 ± 0.25b	1.11 ± 0.06a	6.98 ± 0.50c	494.72 ± 18.33bc	72.05 ± 49.19b	229.54 ± 58.69a
		PS	8.13 ± 0.15a	0.95 ± 0.06b	8.61 ± 0.56b	518.26 ± 38.46b	127.77 ± 70.29ab	237.62 ± 27.60a
		M	7.93 ± 0.12a	0.74 ± 0.07c	10.78 ± 0.92a	575.84 ± 14.15a	199.76 ± 15.85a	145.84 ± 22.80b
	2023	FP	10.57 ± 0.29ab	1.48 ± 0.03a	7.18 ± 0.18c	468.86 ± 30.59c	168.87 ± 58.84b	102.61 ± 15.33c
		OPT	10.47 ± 0.15b	1.05 ± 0.11b	10.06 ± 1.13b	556.28 ± 29.51b	182.82 ± 4.26b	145.66 ± 11.36b
		PS	10.87 ± 0.21a	0.78 ± 0.01c	13.91 ± 0.18a	669.66 ± 33.31a	275.85 ± 20.35a	205.46 ± 19.08a
		M	10.40 ± 0.00b	0.81 ± 0.04c	12.86 ± 0.54a	676.07 ± 31.38a	281.30 ± 56.38a	155.80 ± 6.83b

Different letters indicate significant differences among different water and fertilizers managements ($P < 0.05$). Values shown are means (n = 3 replicates).

significantly decreased in the OPT, PS, and M treatments in both years. The TSS-to-TA ratio significantly increased in the OPT and PS treatments but remained unchanged in the M treatment in 2022. However, in 2023, the TSS-to-TA ratio significantly increased in the OPT, PS, and M treatments. In 2023, there was a significant increase in soluble sugars in the OPT, PS and M treatments. In 2022, sucrose levels significantly increased in the OPT, PS, and M treatments. However, in 2023, sucrose levels significantly increased in the OPT and PS treatments but remained unchanged in the M treatment. There were no significant differences in soluble sugar or glucose levels in 2022 or in glucose levels in 2023 between the OPT and PS or M treatments and the FP treatment. In terms of nutritional quality, compared with those in the FP treatment, vitamin C levels significantly increased in the OPT, PS, and M treatment groups in 2022. Conversely, in 2023, vitamin C levels significantly increased in the PS treatment but remained unchanged in the OPT and M treatments (Figure 4A). In 2022, the soluble protein content significantly increased in the OPT and PS treatments but remained unchanged in the M treatment (Figure 4B). Carotene significantly decreased in the M treatment but did not change in the OPT and PS treatments in 2022. In 2023, carotene significantly increased in the PS treatment but remained unchanged in the OPT and M treatments (Figure 4C). Free amino acids significantly increased in the PS treatment but did not change in the OPT and M treatments in 2022. In 2023, free amino acids significantly increased in the OPT and PS treatments but remained unchanged in the M treatment (Figure 4D).

In terms of flavor quality in the middle carrot segment, the TSS content significantly increased in the PS treatment group compared with the FP treatment group but remained unchanged in the OPT and M treatment groups in 2022 (Table 3). Glucose levels significantly decreased in the OPT treatment, with no changes

10.3389/fpls.2025.1590774

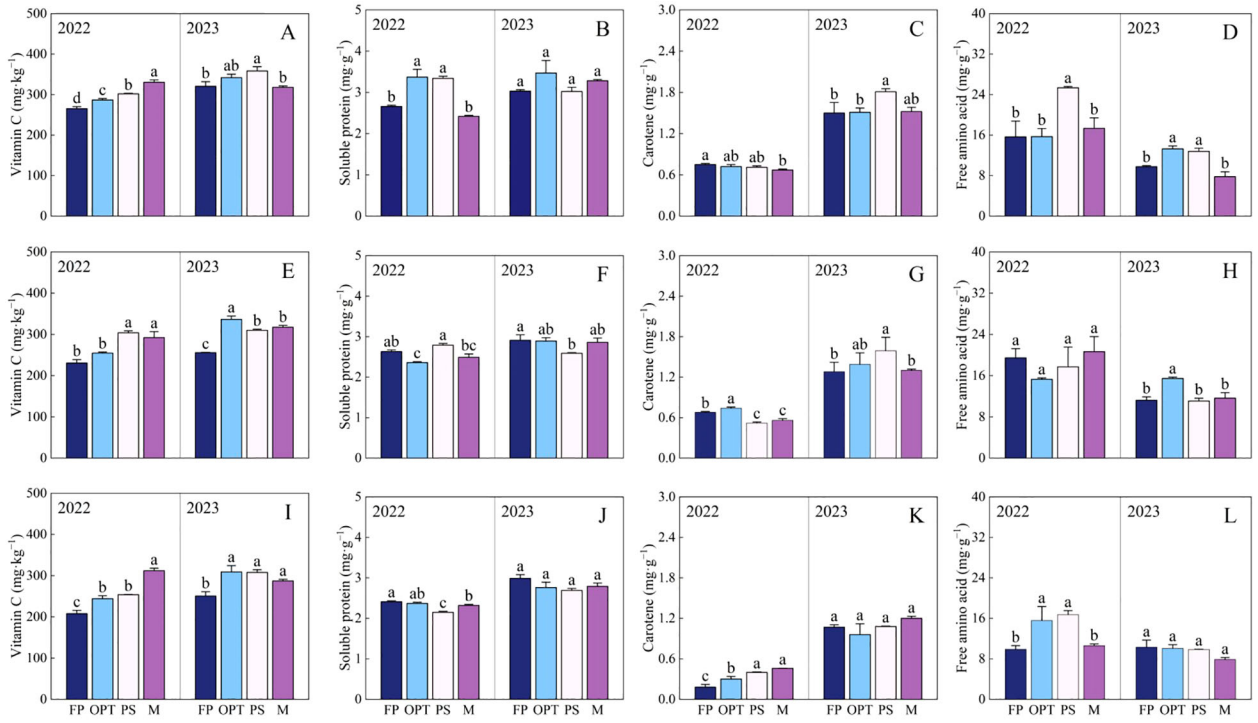

FIGURE 4
Effects of water and fertilizers management on nutritional quality in the upper, middle and lower segments in carrot. Different letters indicate significant differences among different water and fertilizers managements ($P < 0.05$). Values shown are means (n = 3 replicates). **(A–D)** represent nutritional quality in the upper of FP, OPT, PS, and M treatments, respectively. **(E–H)** represent nutritional quality in the middle of FP, OPT, PS, and M treatments of FP, OPT, PS, and M treatments, respectively. **(I–L)** represent nutritional quality in the lower of FP, OPT, PS, and M treatments.

observed in the PS and M treatments in 2023. Additionally, in 2022, the TA significantly decreased, whereas the TSS-to-TA ratio and soluble sugars significantly increased in the PS and M treatments, but those parameters did not change in the OPT treatment. Furthermore, in 2023, the TA significantly decreased, whereas the TSS-to-TA ratio and sucrose content significantly increased in the OPT, PS, and M treatments. There were no significant differences in glucose or sucrose content in 2022, TSS content, or soluble sugar content among the OPT and PS or M treatments in 2023. In terms of nutritional quality, vitamin C significantly increased in the PS and M treatments but remained unchanged in the OPT treatment in 2022. In 2023, the vitamin C levels significantly increased in the OPT, PS, and M treatments (Figure 4E). The soluble protein levels significantly decreased in the OPT treatment, with no change observed in the PS and M treatments in 2022. Conversely, in 2023, the soluble protein content significantly decreased in the PS treatment, whereas no change was detected in the OPT and M treatments (Figure 4F). Carotene levels significantly increased in the OPT treatment but significantly decreased in the PS and M treatments in 2022. However, in 2023, carotene levels significantly increased in the PS treatment, with no change in the OPT and M treatments (Figure 4G). Free amino acid levels significantly increased in the OPT treatment, whereas no change was detected in the PS and M treatments in 2023. There were no significant differences in free amino acid levels in 2022 (Figure 4H).

In terms of flavor quality in the lower segment of carrots, compared with that in the FP treatment, the TSS significantly increased in the PS and M treatments but remained unchanged in the OPT treatment in 2022 (Table 3). The TA significantly decreased in the PS and M treatments but remained unchanged in the OPT treatment in 2022. In 2023, the TA significantly decreased in the OPT, PS, and M treatments. Glucose significantly decreased in the OPT treatment but remained unchanged in the PS and M treatments in 2022. In 2023, glucose significantly increased in the PS and M treatments but remained unchanged in the OPT treatment. Sucrose significantly increased in the OPT and PS treatments but remained unchanged in the M treatment in 2022. In 2023, sucrose significantly increased in the OPT, PS, and M treatments. The TSS-to-TA ratio and soluble sugar content significantly increased in the PS and M treatments but remained unchanged in the OPT treatment in 2022. In 2023, the TSS-to-TA ratio and soluble sugar content significantly increased in the OPT, PS, and M treatments. There were no significant differences in the TSS content between the OPT, PS, and M treatments and the FP treatment in 2023. In terms of nutritional quality, vitamin C significantly increased in the OPT, PS, and M treatments in both years (Figure 4I). The soluble protein content significantly decreased in the PS and M treatments but did not change in the OPT treatment in 2022 (Figure 4J). Carotene significantly increased in the OPT, PS, and M treatments in 2022

10.3389/fpls.2025.1590774

(Figure 4K). Free amino acids significantly increased in the OPT and PS treatments but remained unchanged in the M treatment in 2022 (Figure 4L). No significant differences were found in soluble protein, carotene or free amino acids in 2023 (Figures 4J–L).

3.3 Flavor and nutritional quality in the phloem and xylem

Carrots were separated into phloem and xylem to assess flavor and nutritional quality on the basis of their radial distribution (Figure 1). The flavor and nutritional quality of the phloem and xylem are similar to the growth patterns of the whole fleshy roots (Table 4; Figure 5). Compared with that in the FP treatment with respect to flavor quality of the phloem in 2022, TSS significantly increased in the PS treatment but remained unchanged in the OPT and M treatments (Table 4). The TA and glucose contents significantly decreased in the M treatment, whereas no changes were detected in the OPT and PS treatments. The TSS-to-TA ratio significantly increased in the M treatment but did not change in the OPT and PS treatments. The soluble sugar content significantly increased in the OPT treatment but remained unchanged in the PS and M treatments. The sucrose content significantly increased in the PS and M treatments, whereas no changes were detected in the OPT treatment. In terms of flavor quality in the phloem in 2023, compared with those in the FP treatment, the contents of TSS and TA significantly decreased in the M treatment, with no changes in the OPT and PS treatments. The TSS-to-TA ratio significantly increased in the M treatment, with no changes in the OPT and PS treatments. Glucose levels significantly decreased in the PS and M treatments but remained unchanged in the OPT treatment. Sucrose levels significantly increased in the PS and M treatments but remained unchanged in the OPT treatment. There were no significant differences in soluble sugar content in 2023. In terms of flavor quality in the xylem in 2022, compared with those in the FP treatment, the contents of TSS, soluble sugars, and sucrose significantly increased in the PS and M treatments but remained unchanged in the OPT treatment (Table 4). Compared with that in the FP treatment, the flavor quality of the xylem in the OPT, PS, and M treatments significantly improved in terms of the TSS-to-TA ratio in 2023. Additionally, the TA significantly decreased in the OPT, PS, and M treatments in 2023. The soluble sugar levels significantly increased in the PS and M treatments but did not change in the OPT treatment. There were no significant differences observed in TA, TSS-to-TA, or glucose concentrations in 2022 or in TSS or glucose concentrations in 2023.

In terms of nutritional quality in the phloem, compared with that in the FP treatment, vitamin C significantly increased in the PS and M treatments but remained unchanged in the OPT treatment in both years (Figure 5A). The soluble protein content significantly increased in the PS and M treatments but remained unchanged in the OPT treatment in 2022. However, in 2023, the soluble protein content significantly increased in the OPT and PS treatments, but remained unchanged in the M treatment (Figure 5B). Carotene

TABLE 4 Effects of water and fertilizers management on the flavor quality of phloem and xylem in carrot.

Treatments/index			Total soluble solid (%)	Titratable acid (%)	TSS-to-titratable acid ratio	Soluble sugar (mg g^{-1} DW)	Glucose (mg g^{-1} DW)	Sucrose (mg g^{-1} DW)
2022	Phloem	FP	8.13 ± 0.06b	0.54 ± 0.14a	15.97 ± 4.44b	475.10 ± 28.73b	130.33 ± 14.10ab	184.96 ± 15.27b
		OPT	8.37 ± 0.15b	0.49 ± 0.00ab	17.92 ± 0.58ab	545.68 ± 30.39a	172.49 ± 49.68a	197.21 ± 35.96b
		PS	8.70 ± 0.26a	0.43 ± 0.06ab	20.94 ± 2.73ab	513.34 ± 9.48ab	68.88 ± 48.37bc	251.90 ± 25.94a
		M	8.20 ± 0.00b	0.36 ± 0.05b	24.77 ± 6.08a	507.99 ± 28.87ab	33.72 ± 27.74c	275.89 ± 14.88a
	Xylem	FP	7.63 ± 0.12b	1.27 ± 0.11a	6.02 ± 0.45a	365.47 ± 32.54c	96.84 ± 29.55a	162.85 ± 6.79c
		OPT	7.70 ± 0.10b	1.20 ± 0.06a	6.49 ± 0.43a	397.74 ± 32.90bc	70.50 ± 23.49a	162.41 ± 2.04c
		PS	8.13 ± 0.12a	1.21 ± 0.07a	6.72 ± 0.30a	445.23 ± 27.36b	53.03 ± 13.07a	224.78 ± 26.51b
		M	7.93 ± 0.12a	1.20 ± 0.06a	6.74 ± 0.40a	509.32 ± 27.64a	90.85 ± 38.72a	259.01 ± 8.91a
2023	Phloem	FP	12.43 ± 0.21a	1.14 ± 0.04a	10.97 ± 0.29b	696.18 ± 25.93a	303.72 ± 27.96a	143.12 ± 1.75b
		OPT	12.53 ± 0.21a	1.09 ± 0.06a	11.53 ± 0.58ab	745.63 ± 27.64a	342.86 ± 33.58a	152.38 ± 7.69b
		PS	12.67 ± 0.15a	1.08 ± 0.01a	11.81 ± 0.05ab	719.19 ± 31.68a	196.64 ± 29.85b	275.57 ± 10.95a
		M	11.87 ± 0.32b	0.97 ± 0.08b	12.32 ± 0.81a	753.26 ± 44.81a	163.53 ± 34.35b	332.07 ± 61.09a
	Xylem	FP	10.53 ± 0.31a	2.50 ± 0.16a	4.24 ± 0.39d	490.98 ± 34.63c	188.00 ± 22.59a	134.10 ± 19.19b
		OPT	10.53 ± 0.15a	1.91 ± 0.06b	5.51 ± 0.19c	526.93 ± 18.48bc	123.99 ± 54.74a	130.22 ± 9.22b
		PS	10.40 ± 0.10a	1.71 ± 0.02c	6.09 ± 0.01b	584.24 ± 35.73ab	120.65 ± 41.94a	215.04 ± 5.31a
		M	10.20 ± 0.00a	1.54 ± 0.02c	6.61 ± 0.10a	607.22 ± 34.12a	146.39 ± 16.42a	192.41 ± 13.25a

Different letters indicate significant differences among different water and fertilizers managements ($P < 0.05$). Values shown are means (n = 3 replicates).

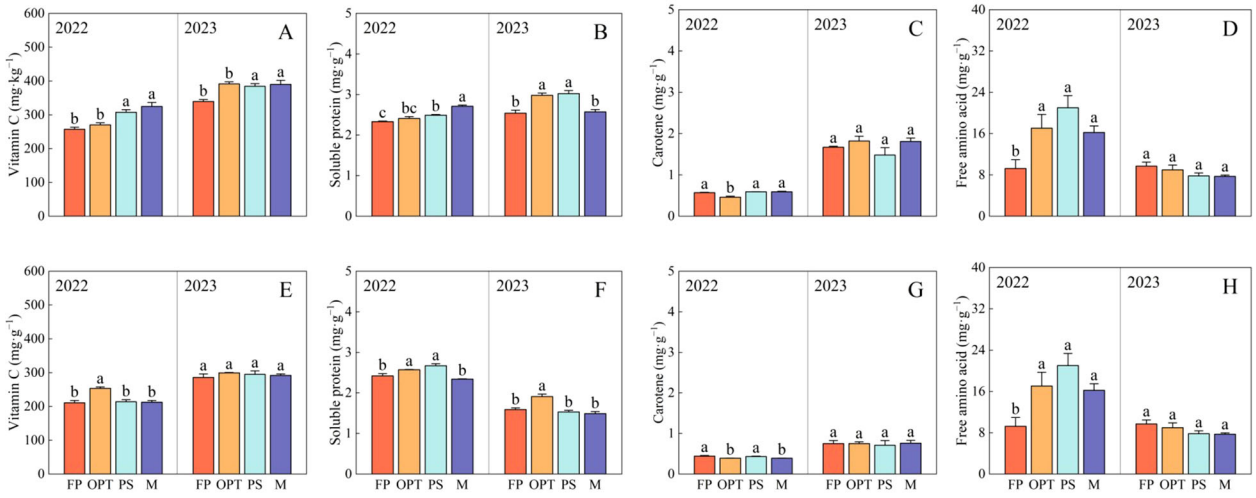

FIGURE 5
Effects of water and fertilizers management on the nutritional quality of phloem and xylem in carrot. Different letters indicate significant differences among different water and fertilizers managements ($P < 0.05$). Values shown are means (n = 3 replicates). Different letters indicate significant differences among different water and fertilizers managements ($P < 0.05$). Values shown are means (n = 3 replicates). **(A–D)** represent nutritional quality in the phloem of FP, OPT, PS, and M treatments, respectively. **(E–H)** represent nutritional quality in the xylem of FP, OPT, PS, and M treatments of FP, OPT, PS, and M treatments, respectively.

significantly decreased in the OPT treatment but remained unchanged in the PS and M treatments in 2022 (Figure 5C). Free amino acids significantly increased in the OPT, PS, and M treatments in 2022 (Figure 5D). There were no significant differences in carotene or free amino acids in 2023 (Figures 5C, D). In terms of nutritional quality in the xylem, compared with that in the FP treatment, vitamin C significantly increased in the OPT treatment but remained unchanged in the PS and M treatments in 2022 (Figure 5E). In 2022, the soluble protein content significantly increased in the OPT and PS treatments but remained unchanged in the M treatment. Conversely, in 2023, the soluble protein content significantly increased in the OPT treatment but remained unchanged in the PS and M treatments (Figure 5F). Carotene levels significantly decreased in the OPT and M treatments, with no significant change in the PS treatment in 2022 (Figure 5G). Free amino acid levels significantly increased in the OPT, PS, and M treatments in 2022 (Figure 5H). However, there were no significant differences in vitamin C, carotene or free amino acid contents in 2023 (Figures 5E–H).

Overall, compared with that in the FP treatment, the flavor quality increased by 17.51%, 13.04%, and 15.05% in the upper, middle, and lower segments, respectively, whereas the nutritional quality increased by 11.04%, 8.12%, and 17.35%, respectively, in the OPT treatment (Figure 6). In the organic substitution treatments (average of PS and M), the flavor quality increased by 32.50%, 18.21%, and 38.07%, and the nutritional quality increased by 10.28%, 4.69%, and 25.41%, respectively. Compared with those in the OPT treatment, the flavor and nutritional quality of all the segments in the PS and M treatments improved, with the most significant increase observed in the lower segment. Specifically, the flavor quality increased by 20.05%, 19.19%, and 28.81% in the upper, middle, and lower segments, respectively, while the nutritional quality increased by 0.77% and 5.46% in the upper and lower segments, respectively, under the organic substitution treatments. These findings indicate that the enhancements in flavor and nutritional quality of whole carrot roots are due mainly to improvements in the upper and lower segments under coordinated water and organic–inorganic fertilizer management. In the phloem, flavor and nutritional quality increased by 9.59% and 13.50%, respectively, in the OPT treatment compared with the FP treatment and by 12.35% and 17.69%, respectively, in the organic substitution treatment. In the xylem, flavor and nutritional quality increased by 1.64% and 19.09%, respectively, in the OPT treatment, whereas flavor quality increased by 16.89% and 1.94%, respectively, in the organic substitution treatment. Compared with the OPT treatment, the flavor and nutritional quality of the phloem increased by 5.23% and 3.88%, respectively, in the organic substitution treatment. These results suggest that enhancing the flavor and nutritional quality of both the phloem and xylem can improve the overall flavor and nutritional quality of the entire fleshy root in terms of radial distribution under coordinated water and organic–inorganic fertilizer management.

3.4 Anatomical structure of the phloem and xylem in the upper, middle, and lower segments

In the upper segment, Pca significantly increased in the PS and M treatments compared with the FP treatment but remained unchanged in the OPT treatment in 2022 (Figures 7, 8A). In 2023, Pca significantly increased in the OPT and PS treatments, whereas no change was detected in the M treatment. In 2023, the xylem vessel diameter (Xvd) significantly increased in the M

10.3389/fpls.2025.1590774

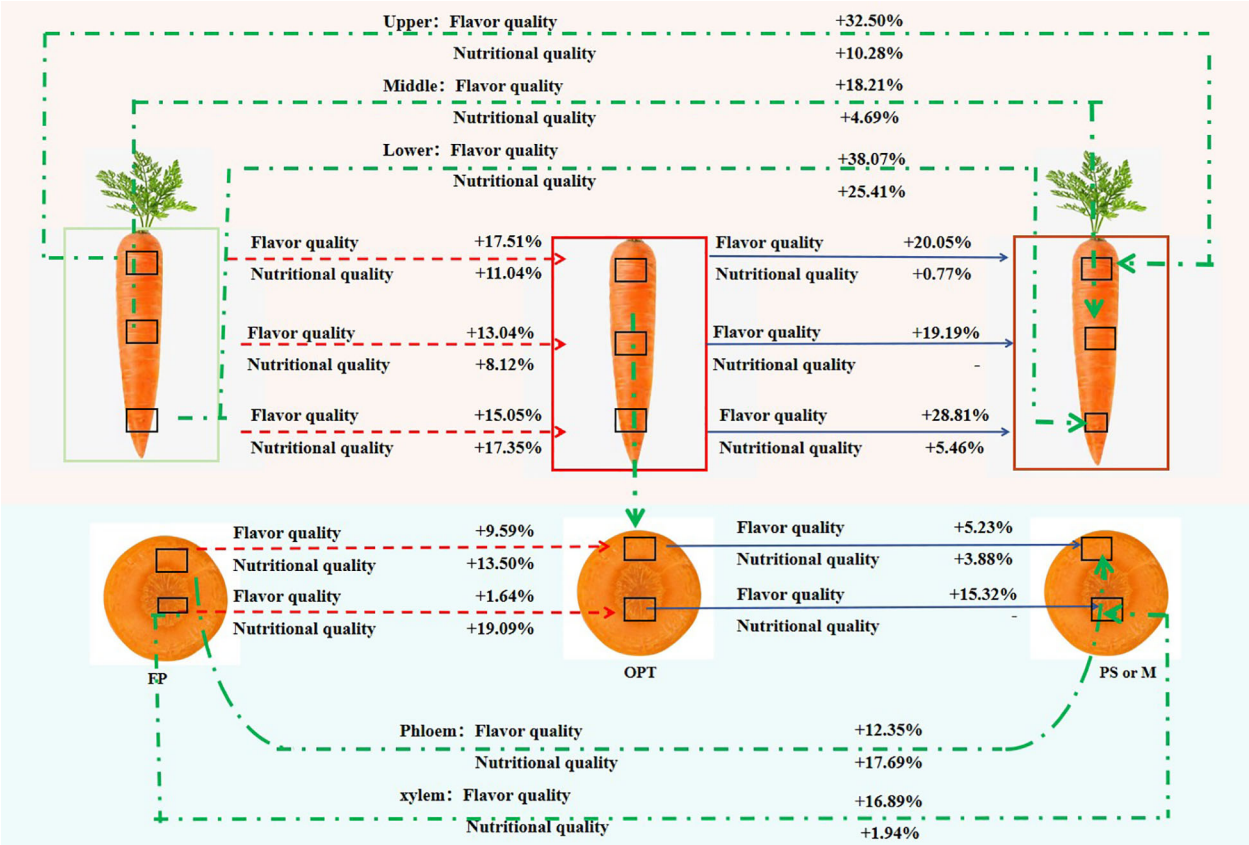

FIGURE 6
The changes of quality from farmers' habit (FP) to coordinated water-fertilizers management (OPT, PS, or M) in the upper, middle and lower segments and phloem and xylem in carrot. + indicates the percentage of quality improvement, and - indicates no difference. The red background indicates the changes of quality in the upper, middle and lower segments. The blue background indicates the changes of quality in phloem and xylem. The red line indicates the changes of quality the FP treatment to OPT treatment in the upper, middle and lower segments and phloem and xylem. The blue line indicates the changes of quality the OPT treatment to PS or M treatment in the upper, middle and lower segments and phloem and xylem. The green line indicates the changes of quality the FP treatment to PS or M treatment in the upper, middle and lower segments and phloem and xylem.

treatment (Figures 7, 8B). The Pxv significantly increased in the M treatment in 2022 (Figures 7, 8C). In 2023, the Pxv significantly increased in the OPT and M treatments but remained unchanged in the PS treatment (Figures 7, 8D). No significant differences were detected in Xvd or the xylem vessel area (Xva) in 2022 or in Xva in 2023 (Figures 7, 8B, C). In the middle segment, no significant differences were found in Pca, Xvd, Xva, or Pxv among the four treatments (Figures 7, 8E–H). Compared with that in the FP treatment, the Pca in the lower segment significantly increased in the PS treatment but remained unchanged in the OPT and M treatments in 2022 (Figure 8I). Xvd significantly increased in the PS and M treatments but remained unchanged in the OPT treatment in 2022 (Figure 8J). In 2022, Xva significantly increased in the PS treatment but remained unchanged in the OPT and M treatments (Figure 8K). No significant differences were found in Pxv in 2022 or in Pca, Xvd, Xva, or Pxv in 2023 (Figures 8E–H). These results suggest that the primary distinctions between the FP treatment and optimized water-fertilizer management lie in Pca and Pxv in the upper segment.

3.5 Correlations between quality and the anatomical structural characteristics of the upper, middle, and lower segments of the phloem and xylem

In the upper segment, Pca and Pxv were significantly correlated with flavor quality and nutritional quality ($P<0.05$), whereas Xva and Xvd were not correlated (Figure 9A). Specifically, Pca was positively correlated with soluble protein, sucrose, soluble sugars, vitamin C, the TSS-to-TA ratio, free amino acids, TSS, and carotene. Pxv was positively correlated with glucose, soluble protein, soluble sugar, sucrose, vitamin C, the TSS-to-TA ratio, free amino acids and TSS. However, no significant correlations were detected in the middle segment (Figure 9B). In the lower segment, Pca was significantly correlated with flavor quality and nutritional quality ($P<0.05$), whereas Pxv, Xva, and Xvd were not significantly correlated (Figure 9C). Pca was positively correlated with carotene, glucose, soluble sugars, the TSS-to-TA ratio, vitamin C, sucrose, TSS, and free amino acids. In the phloem, Pca was significantly

10.3389/fpls.2025.1590774

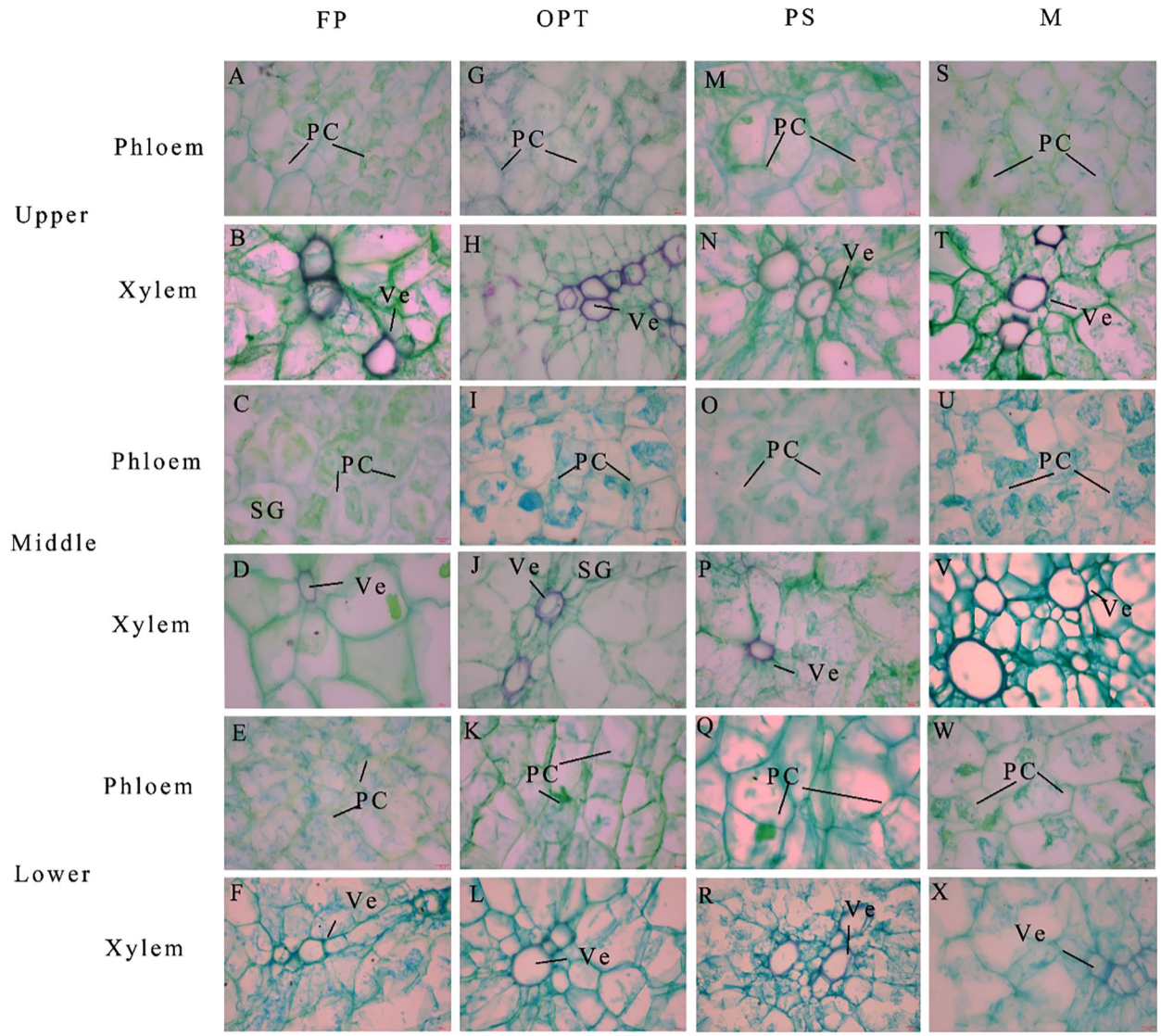

FIGURE 7
Effects of water and fertilizers management on the anatomical structure of phloem and xylem in carrot. **(A, C, E)** and **(G, I, K)** and **(M, O, Q)** and **(S, U, W)** represent the cross sections of phloem in the FP, OPT, PS, and M treatments in the upper, middle and lower segments, respectively. **(B, D, F)** and **(H, J, L)** and **(N, P, R)** and **(T, V, X)** represent the cross sections of xylem in the FP, OPT, PS, and M treatments in the upper, middle and lower segments, respectively. Parenchymal cell (PC), starch granule (SG) and vessel (Ve) are marked. Scale bars are 20 mm length in all the figures.

correlated with flavor quality and nutritional quality ($P<0.05$), whereas Pxv, Xvd, and Xva were not significantly correlated (Figure 9D). Pca was positively correlated with TSS, sucrose, vitamin C, soluble protein, the TSS-to-TA ratio, free amino acids, and soluble sugars. Within the xylem, Pca was significantly correlated with flavor quality and nutritional quality ($P<0.05$), whereas Pxv, Xvd, and Xva were not significantly correlated (Figure 9E). Pca was positively correlated with soluble protein, free amino acids, vitamin C, TSS, the TSS-to-TA ratio, soluble sugars, and sucrose. These findings indicate that the increase in quality in the upper segment was driven primarily by improvements in Pca and Pxv, whereas the increase in quality in the lower segment was associated predominantly with an increase in Pca (Figure 10). The improvement in the quality of the phloem and xylem was attributed mainly to the increase in Pca.

3.6 Correlations between the quality and nutrient concentration of whole fleshy roots

The concentrations of N and P were correlated with both flavor quality and nutritional quality ($P<0.05$) (Figure 9F). Specifically, the N concentration was positively correlated with soluble protein, free amino acids, sucrose, VC, the TSS-to-TA ratio, soluble sugars, TSS, carotene, and glucose. Similarly, the P concentration was positively

10.3389/fpls.2025.1590774

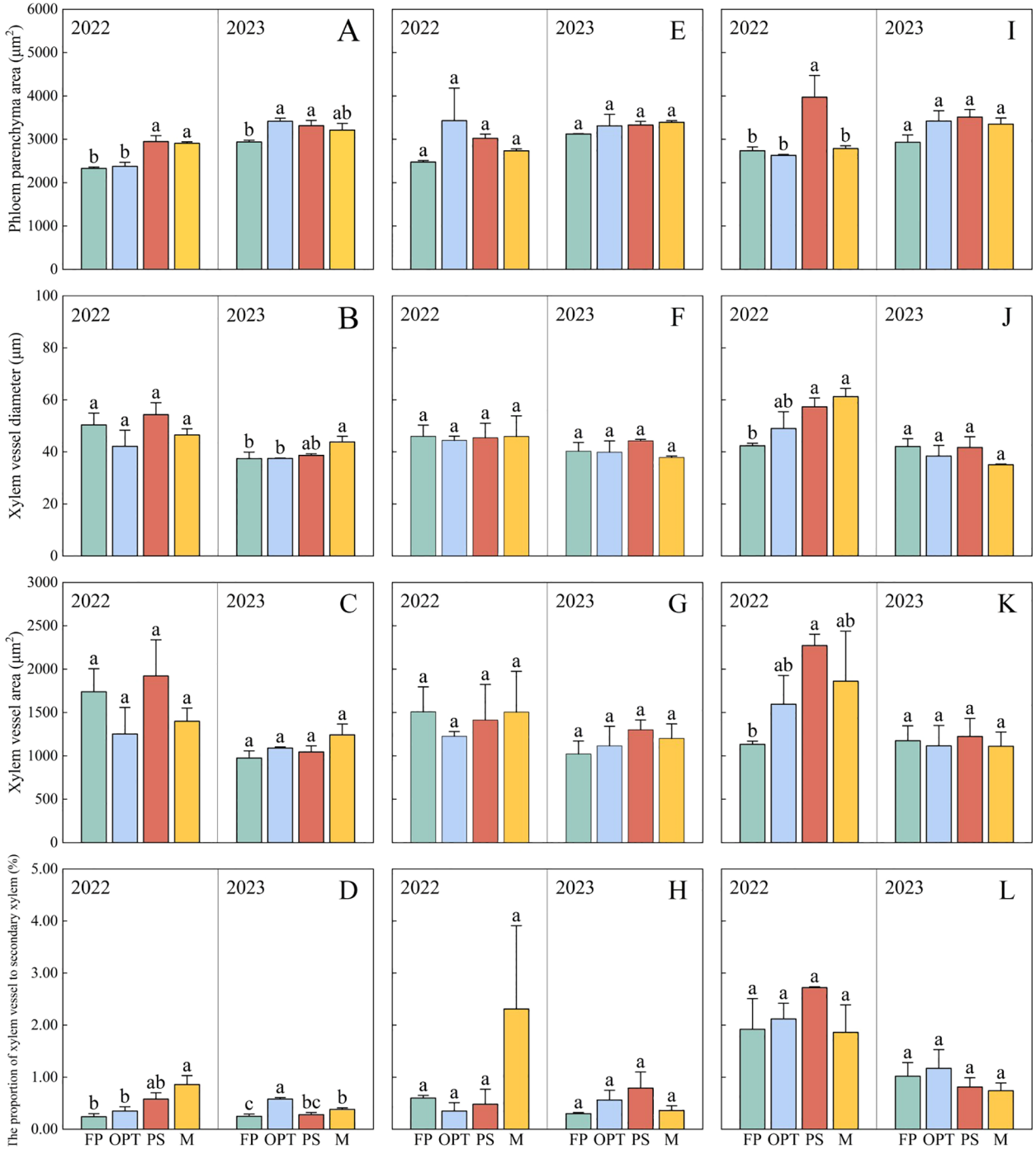

FIGURE 8
Effects of water and fertilizers management on the anatomical structure of phloem and xylem in carrot. **(A–D)** represent parenchyma cell area, xylem vessel diameter, xylem vessel area, the proportion of xylem vessel to secondary xylem of FP, OPT, PS, and M treatments, in the upper segment, respectively. **(E–H)** represent parenchyma cell area, xylem vessel diameter, xylem vessel area, the proportion of xylem vessel to secondary xylem of FP, OPT, PS, and M treatments, in the middle segment, respectively. **(I–L)** represent parenchyma cell area, xylem vessel diameter, xylem vessel area, the proportion of xylem vessel to secondary xylem of FP, OPT, PS, and M treatments, in the lower segment, respectively. Data are the means for the 2 years. Different letters indicate significant differences among different water and fertilizers managements ($P < 0.05$). Values shown are means (n = 3 replicates).

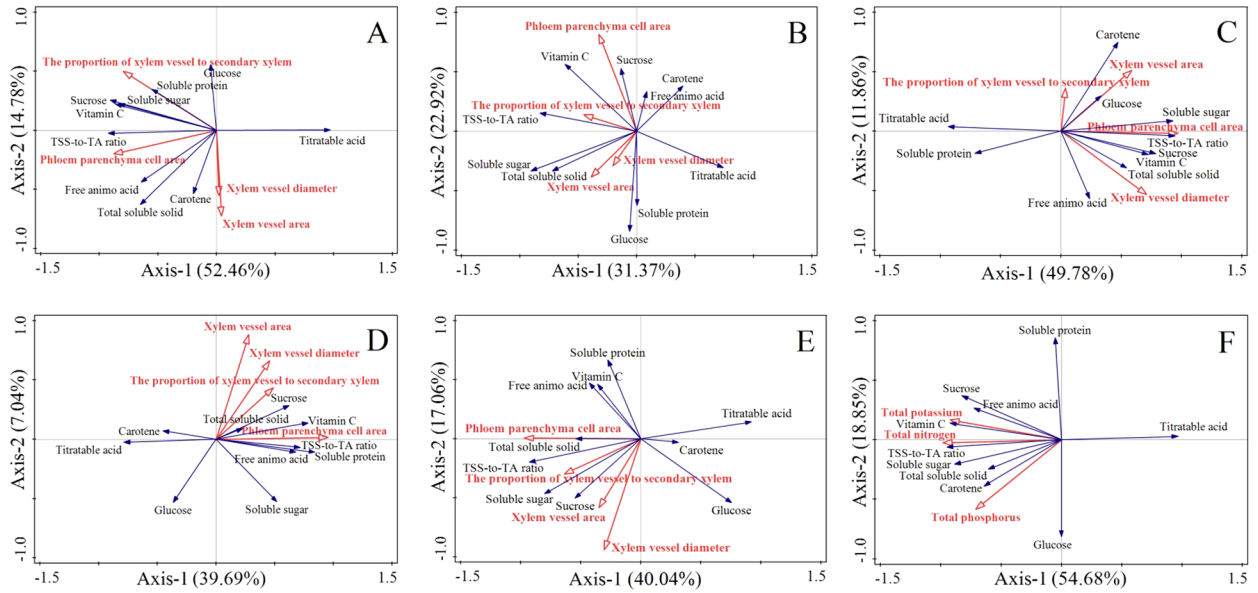

FIGURE 9
Independent and interactive actions of phloem parenchyma cell area, xylem vessel diameter, xylem vessel area, the proportion of xylem vessel to secondary xylem and total nitrogen, phosphorus, total potassium on various properties shown in ordination diagrams obtained from redundancy analysis (RDA). **(A-E)** represent RDA analysis in the upper, middle, lower segment, phloem and xylem of carrots in the FP, OPT, PS, or M treatment, respectively. The coordinate of the first and second ordination axes explained 52.46% and 14.78% of the variance in **(A)** 31.37% and 22.92% of the variance in **(B)** 49.78% and 11.86% of the variance in **(C)** 39.69% and 7.04% of the variance in **(D)** 40.04% and 17.06% of the variance in **(E)**. **(F)** represent RDA analysis of carrots in the FP, OPT, PS, or M treatment, respectively. The coordinate of the first and second ordination axes explained 54.68% and 18.85% of the variance in F.

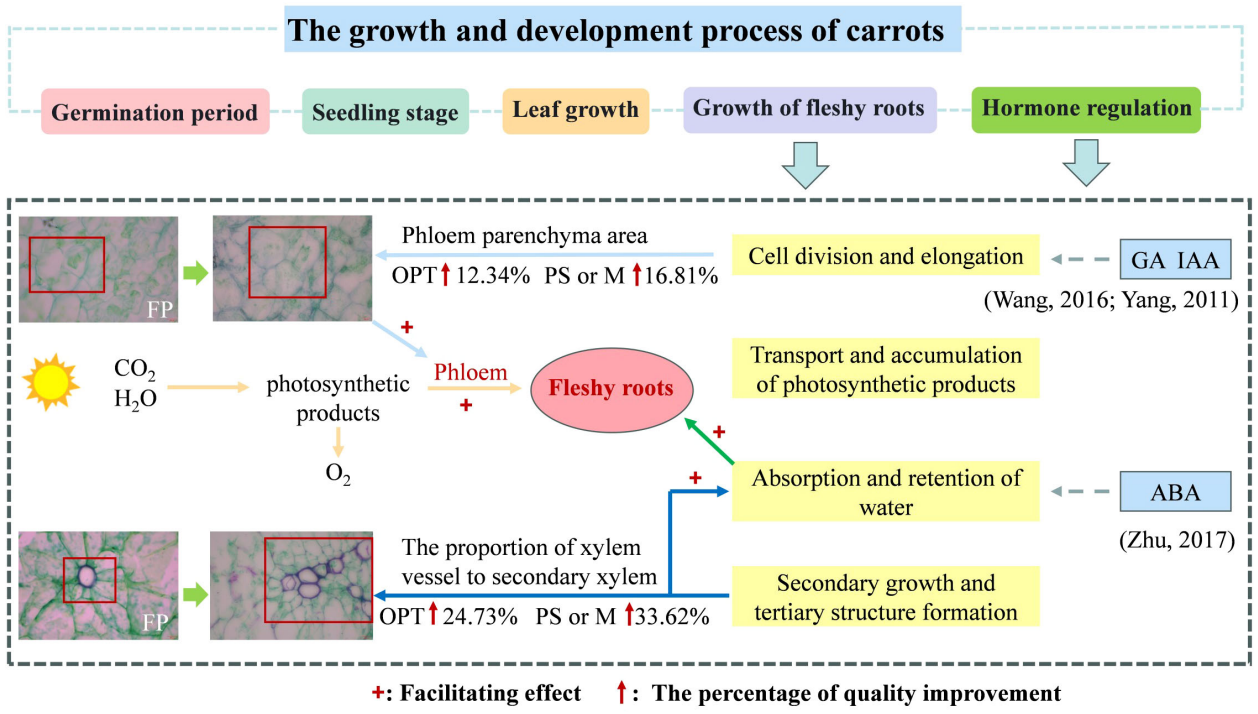

FIGURE 10
Physiological changes of carrot in optimizing water and fertilizer management compared to farmers practice. + indicates facilitation. ↑indicates the percentage of quality improvement compared to FP.

correlated with sucrose, free amino acids, VC, the TSS-to-TA ratio, soluble sugars, TSS, carotene, and glucose. These results suggest that the nutrient levels of N and P may influence carrot quality.

4 Discussion

4.1 Role of coordinated water and fertilizer management on yield and quality

Coordinated water-fertilizer management plays a key role in vegetable yield and quality (Lin et al., 2020). Efficient irrigation is essential for promoting crop growth, especially considering that the response of crops to moisture levels directly impacts their physiological and metabolic functions (He et al., 2021). The incorporation of water-fertilizer technology led to a 20% reduction in nitrogen (N), phosphorus (P), and potassium (K) fertilizers, resulting in increased yield, quality, and fertilizer utilization in tomato (Huang and Chen, 2020). Compared with those under the FP treatment, the yield and quality of whole fleshy roots significantly increased under coordinated water-fertilizer management, particularly when 30% of the chemical fertilizers were substituted with compressed organic fertilizers (Table 2; Figures 2, 3). This finding aligns with those of previous studies. Accurate management of integrated water and fertilizer is crucial for growth regulation, improving efficient water-fertilizer utilization, and achieving high yields (Liu et al., 2021). The combination of water and fertilizer can improve the ecological environment and the soil nutrient content (Liu et al., 2023). The appropriate regulation of water and fertilizer can increase leaf area and root growth, thereby increasing crop water and nutrient uptake through osmoregulation and antioxidant capacity (Zhao et al., 2022). Various irrigation and fertilization rates result in differences in root uptake efficiency, impacting root growth, the root–soil contact area, and ultimately, yield (Chen et al., 2001). In this study, the yields of the four treatments in 2022 varied significantly (Figure 2). This could be due to the increase in local precipitation after carrot sowing, which caused excessive soil moisture that hindered the complete germination of certain carrot seeds. Additionally, the use of different carrot varieties may have contributed to yield discrepancies between the two years, ultimately impacting the overall carrot yield.

This study confirmed that carrot quality can be enhanced with PS or M treatment (Table 2; Figure 3). A previous study revealed that replacing 25–50% of inorganic N, P, and K fertilizer with organic modifiers led to the highest nutritional quality of food crops (Ishfaq et al., 2023). The substitution of 25% N fertilizer with organic fertilizer significantly affects the levels of vitamin C, soluble sugar, soluble protein, and nitrate in cucumbers (Zhang, 2023). Organic fertilizers contain sufficient nutrients and release them slowly, thereby improving crop yield and quality to different extents (Jiang et al., 2021). Organic substitution can increase soil bacterial and fungal biomass, thereby improving soil physicochemical conditions and fertility (Zhao et al., 2023). Organic fertilizers not only provide essential nutrients for crops but also harbor microorganisms that improve the soil environment (Pang, 2023). Nevertheless, compared with OPT, organic substitution has limited efficacy in enhancing the appearance, flavor, and nutritional quality of carrots (Table 2; Figure 3). This is possibly due to the slow-release nature of fertilizers in organic substitution and the relatively short duration of the substitution, hindering the complete exploitation of the long-term benefits of organic amendments.

4.2 The contribution of the quality of different segments to the overall quality of the fleshy root

N, P, and K are crucial for biomass allocation and root elongation in tubers; thus, regulating assimilate allocation is also essential (Cakmak et al., 1994). This phenomenon may, in turn, affect the quality of the upper, middle, and lower segments of root crops. These findings were consistent with the results that the concentrations of N and P were correlated with both flavor quality and nutritional quality ($P<0.05$) (Figure 9F). Moreover, in root crops, the number of root tips determines the efficiency of water and nutrient absorption (Yuan et al., 2023). Previous studies have focused on the assimilation processes of both aboveground and underground plant parts (Cheng et al., 2023). In this study, the flavor quality and nutritional quality of carrots were improved under coordinated water-fertilizer management (OPT, PS, or M treatments), particularly in the upper and lower plant parts (Table 3; Figures 4, 6). The superior quality in the upper segment could be attributed to the shorter distance between the aboveground parts, leading to an increased ion concentration gradient between the soil and roots, facilitating diffusion, and thereby improving quality (Barber, 1995). The quality of the lower segment may improve due to an increase in the number of carrot root tip cells, likely because of the presence of more ultrastructures (such as the endoplasmic reticulum, mitochondria, Golgi apparatus, ribosomes, vacuoles, microsomes, and plasma membrane ATPases) in the root tip cells that are vital for root function (Yang et al., 2012). Plant root tip cells may undergo structural damage and organelle deformation in cases of nutrient deficiencies, such as phosphorus, zinc, and silicon deficiencies (Miras et al., 2022), resulting in hindered nutrient transport to the roots (Dinar and Rudich, 1985). Compared with N in surface soil, N in deep soil is prone to leaching (Tei et al., 2020). In this study, optimizing water-fertilizer management, especially in the PS or M treatments, provided nutrients and water at appropriate times to improve root morphological indices (root tips) and improve quality in the lower segment (Table 3; Figures 4, 6).

This study revealed a significant improvement in the nutritional quality of soluble sugars, sucrose, and vitamin C in the upper, middle, and lower segments (Table 3; Figures 4, 6). Within the framework of integrated water-fertilizer management, this mechanism facilitates the translocation of carbohydrates from vegetative tissues to storage organs, potentially increasing the enzymatic activity of Frk and starch synthase, along with sucrose levels (Hennion et al., 2019). Munch's hypothesis suggests that the flow of solution through the phloem is

driven by a hydrostatic pressure gradient (Winfried and Michael, 2022). Many plant growth regulators, including auxins, gibberellins, humic acids, and cytokinins derived from microorganisms, are rich in organic fertilizers, thereby increasing vitamin C (Zuo et al., 2018). As a result, the nutritional quality significantly improved in the upper, middle, and lower segments under coordinated water-fertilizer management.

4.3 The effects of the anatomical structure of the phloem and xylem on quality

The taproot of the root tubers comprises two primary regions: the outer ring of the phloem parenchyma and the inner core of the xylem parenchyma. These regions originate from a cambium formed between the xylem and phloem vessels in seedling roots (Liu et al., 2022). Vascular parenchyma cell activity in the root is crucial for metabolic and energy connections, supporting water and nutrient transport in the xylem and facilitating both short- and long-distance symbiotic transport (Spicer, 2014). Expanding the area of ducts, xylem, and phloem establishes a strong transport network that optimizes the water supply, guaranteeing regular growth and development (Wang et al., 2023). Various abiotic stresses, such as N deficiency and temperature, influence the size and density of parenchyma, thereby compromising water and nutrient transportation among organs and affecting quality (Ren et al., 2021). In this study, Pca and Pxv in the upper segment of the OPT, PS, or M treatments were 9.17%, 88.40%, and 18.44%, 116.22% greater, respectively, than those in the FP treatment (Figures 7, 8, 10). Zhao and Gu (1999) reported that an increased volume of parenchymatous cells improved the nutritional quality of carrots. Furthermore, RDA revealed a positive correlation between Pca and Pxv levels in the upper segment and flavor as well as nutritional quality (Figure 9). Under coordinated water-fertilizer management, isocompounds typically move faster from the active phloem outward (centrifugally) than inward (Korolev et al., 2000). The increased growth of phloem parenchyma tissue and carbon deposition may increase the competitiveness of growing organs for available photosynthates, possibly because of their unique transport characteristics within the carrot taproot (Wareing and Patrick, 1975). This structure supports sucrose accumulation with low glucose content in the taproot (Liu et al., 2018). Vacuoles in phloem parenchyma cells store nutrients, such as soluble sugars, thereby improving carrot quality. The optimized water-fertilizer management in this study resulted in an increased Pca and vessel proportions distributed across the xylem region, potentially promoting xylem tissue expansion (Figure 10). Studies indicate that cell size influences sucrose absorption in beets (Hoffmann, 2010). The radish taproot xylem vessels, which are radially distributed but not densely packed, facilitate parenchyma development (Feng et al., 2017). The improvement in flavor and nutritional quality of both the upper and lower segments is likely linked to elevated Pca and Pxv levels. Carrots with relatively high Pca and Pxv values presented improved flavor and nutritional quality. It has been demonstrated that gibberellic acid (GA) regulates root growth by promoting cell elongation and controlling cell number (Inada and Shimmen, 2000; Shani et al., 2013; Ubeda-Tomás et al., 2009). IAA stimulates the formation of lateral root primordia, and the occurrence and elongation of lateral roots depend on the direct or indirect regulatory effects of growth hormone (Kazan, 2013). ABA can help plants adapt to diverse environments by regulating the growth and development of primary and lateral roots, thereby indirectly aiding in anchoring plants and facilitating water and nutrient absorption (Zhu et al., 2017). However, this study did not delve deeply into the effects of phytohormones. Therefore, further investigation into the influence of phytohormones on the expansion of carrot fleshy roots is warranted in future research.

5 Conclusion

Compared with traditional farming practices, coordinated water-fertilizer management can increase both quality and yield, with 30% organic substitution resulting in superior results. This improvement in quality is attributed to improved flavor and nutritional characteristics in the upper and lower segments, as well as in the phloem and xylem tissues. High-quality carrots present increased phloem parenchyma cells and a greater proportion of xylem vessels. Therefore, improving the flavor and nutritional quality of the upper and lower segments could serve as an effective approach to improve the overall quality of high-yield carrot. The phloem parenchyma cell area and xylem vessel proportion are potentially valuable physiological traits for optimizing quality. Additionally, further research is needed to investigate the impact of phytohormones on the growth of carrot fleshy roots.

Data availability statement

The original contributions presented in the study are included in the article/Supplementary Material. Further inquiries can be directed to the corresponding author.

Author contributions

YZ: Data curation, Methodology, Resources, Writing – original draft. YG: Data curation, Resources, Writing – review & editing. YL: Writing – review & editing, Data curation, Resources. HX: Data curation, Resources, Writing – review & editing. RC: Data curation, Resources, Writing – review & editing. YC: Conceptualization, Funding acquisition, Writing – review & editing.

Funding

The author(s) declare that financial support was received for the research and/or publication of this article. This work was funded by the central government guides local special plans for science (grant number 22-1-3-7-zyyd-nsh) and technology development "Integration and demonstration of key technologies of carrots

continuous cropping system" and Regional Agricultural Green Development Integration of Industry and Education Graduate Joint Training Demonstration Base (grant number 015/1121001).

Acknowledgments

We gratefully acknowledge the financial support of the central government guides local special plans for science (grant number 22-1-3-7-zyyd-nsh); Technology development "Integration and demonstration of key technologies of carrots continuous cropping system" and Regional Agricultural Green Development Integration of Industry and Education Graduate Joint Training Demonstration Base (grant number 015/1121001).

Conflict of interest

The authors declare that the research was conducted in the absence of any commercial or financial relationships that could be construed as a potential conflict of interest.

Generative AI statement

The author(s) declare that no Generative AI was used in the creation of this manuscript.

Publisher's note

All claims expressed in this article are solely those of the authors and do not necessarily represent those of their affiliated organizations, or those of the publisher, the editors and the reviewers. Any product that may be evaluated in this article, or claim that may be made by its manufacturer, is not guaranteed or endorsed by the publisher.

Supplementary material

The Supplementary Material for this article can be found online at: https://www.frontiersin.org/articles/10.3389/fpls.2025.1590774/full#supplementary-material

References

Aubert, C., Bruaut, M., and Chalot, G. (2022). Spatial distribution of sugars, organic acids, vitamin C, carotenoids, tocopherols, 6-methoxymellein, polyacetylenic compounds, polyphenols and terpenes in two orange Nantes type carrots (Daucus carota L.). *J. Food Compos. Anal.* 108, 104421. doi: 10.1016/j.jfca.2022.104421

Aubry, E., Dinant, S., Vilaine, F., Bellini, C., and Le Hir, R. (2019). Lateral transport of organic and inorganic solutes. *Plants.* 8, 20. doi: 10.3390/plants8010020

Baldwin, E. A., Scott, J. W., Einstein, M. A., Malundo, T. M. M., Carr, B. T., Shewfelt, R. L., et al. (1998). Relationship between sensory and instrumental analysis for tomato flavor. *J. Am. Soc Hortic. Sci.* 123, 906–915. doi: 10.21273/JASHS.123.5.906

Bao, S. D. (2000). *Soil and Agricultural Chemistry Analysis* (China: Agricultural Press).

Barber, S. A. (1995). *Soil Nutrient Bioavailability: A Mechanistic Approach* (New York: Wiley).

Beckles, D. M. (2012). Factors affecting the postharvest soluble solids and sugar content of tomato (Solanum lycopersicum L.) fruit. *Postharvest Biol. Tec.* 63, 129–140. doi: 10.1016/j.postharvbio.2011.05.016

Cakmak, I., Hengeler, C., and Marschner, H. (1994). Partitioning of shoot and root dry matter and carbohydrates in bean plants suffering from phosphorus, potassium and magnesium deficiency. *J. Exp. Bot.* 45, 1245–1250. doi: 10.1093/jxb/45.9.1245

Camargo, A. C. D., Regitano-d'Arce, M. A. B., Rasera, G. B., Canniatti-Brazaca, S. G., Prado-Silva, L. D., Alvarenga, V. O., et al. (2017). Phenolic acids and flavonoids of peanut by-products:antioxidant capacity and antimicrobial effects. *Food Chem.* 237, 538–544. doi: 10.1016/j.foodchem.2017.05.046

Carrillo-López, A., and Yahia, E. M. (2019). Chapter 6-morphology and anatomy. *Postharvest Physiol. Biochem. Fruits Veg.*, 113–130. doi: 10.1016/B978-0-12-813278-4.00006-3

Chen, Y. M., Wang, Y., Liang, Y. R., Zhang, Y. P., Wang, Y., Li, J. Q., et al. (2001). Factors affecting carrot quality and preventive measures. *Inner Mongolia Agric. Sci. Technol.* 29, 15–16.

Cheng, S. B., Liu, Y. H., Su, L. H., Liu, X. X., Chu, Q. W., He, Z. Q., et al. (2023). Physiological, anatomical and quality indexes of root tuber formation and development in chayote (Sechium edule). *Bmc. Plant Biol.* 23, 413. doi: 10.1186/s12870-023-04427-0

Colombari, L. F., Lanna, N. B. L., Guimaraes, L. R. P., and Inacio Cardoso, A. I. (2018). Production and quality of carrot in function of split application of nitrogen doses in top dressing. *Hortic. Bras.* 36, 306–312. doi: 10.1590/S0102-053620180304

Costache, M. A., Campeanu, G., and Neata, G. (2012). Studies concerning the extraction of chlorophyll and total carotenoids from vegetables. *Rom. Biotech. Lett.* 17, 7702–7708.

Dinar, M., and Rudich, J. (1985). Effect of heat stress on assimilate partitioning in tomato. *Ann. Bot.* 56, 239–248. doi: 10.1093/oxfordjournals.aob.a0870

FAO (2022). Carrots-Area harvested (hectares). Available online at: https://www.fao.org/faostat/en/#data/QCL (Accessed June 4, 2025).

Feng, H., Xu, L., Wang, Y., Tang, M., Zhu, X., Zhang, W., et al. (2017). Identification of critical genes associated with lignin biosynthesis in radish (Raphanus sativus L.) by *de novo* transcriptome sequencing. *Mol. Genet. Genomics* 292, 1151–1163. doi: 10.1007/s00438-017-1338-9

Gan, X., Sun, S., Fan, H., Liu, H., Zhang, J., and Ding, Z. (2023). Research on soil nitrogen balance mechanism and optimal water and nitrogen management model for crop rotation of vegetables in facilities. *Water.* 15, 2878. doi: 10.3390/w15162878

He, Z. H., Li, M. N., Cai, Z. L., Zhao, R. S., Hong, T. T., Yang, Z., et al. (2021). Optimal irrigation and fertilizer amounts based on multi-level fuzzy comprehensive evaluation of yield, growth and fruit quality on cherry tomato. *Agric. Water Manage.* 243, 106360. doi: 10.1016/j.agwat.2020.106360

Hennion, N., Durand, M., Vriet, C., Doidy, J., Maurousset, L., Lemoine, R., et al. (2019). Sugars en route to the roots. Transport, metabolism and storage within plant roots and towards microorganisms of the rhizosphere. *Physiol. Plantarum.* 165, 44–57. doi: 10.1111/ppl.12751

Hoffmann, C. M. (2010). Sucrose accumulation in sugar beet under drought stress. *J. Agron. Crop Sci.* 196, 243–252. doi: 10.1111/j.1439-037X.2009.00415.x

Huang, Y. Q., and Chen, S. (2020). Effect of reducing fertilizer application on yield, quality and fertilizer utilization of greenhouse cultivation tomato under integration of water and fertilizer. *J. South. Agric.* 14, 187–188. doi: 10.19415/j.cnki.1673-890x.2020.05.095

Huang, M., Lu, Y. J., Shi, W. J., Shi, Z., and Han, E. Y. (2023). Research on fermentation process of organic fertilizer from *Pleurotus ostreatus* residue. *Agric. Eng. Technol.* 43, 76–77.

Inada, S., and Shimmen, T. (2000). Regulation of elongation growth by gibberellin in root segments of Lemna minor. *Plant Cell Physiol.* 41, 932–939. doi: 10.1093/pcp/pcd018

Ishfaq, M., Wang, Y. Q., Xu, J. L., Hassan, M. U., Yuan, H., Liu, L. L., et al. (2023). Improvement of nutritional quality of food crops with fertilizer: a global meta-analysis. *Agron. Sustain. Dev.* 43, 74. doi: 10.1007/s13593-023-00923-7

Jiang, B., Xue, Z. M., Wang, J., Xu, J. C., Chen, M. L., and Wu, J. (2021). Effects of substitution proportion of organic nitrogen on broccoli yield and quality. *Anhui Agric. Sci.* 61, 142–144. doi: 10.3969/j.issn.0517-6611.2021.11.039

Kader, A. A. (2008). Flavor quality of fruits and vegetables. *J. Sci. Food Agr.* 88, 1863–1868. doi: 10.1002/jsfa.3293

Kazan, K. (2013). Auxin and the integration of environmental signals into plant root development. *Ann. Bot.* 112, 1655–1665. doi: 10.1093/aob/mct229

Khadr, A., Wang, Y., Que, F., Li, T., Xu, Z., and Xiong, A. (2020). Exogenous abscisic acid suppresses the lignification and changes the growth, root anatomical structure and related gene profiles of carrot. *Acta Bioch. Bioph. Sin.* 52, 97–100. doi: 10.1093/abbs/gmz138

Kim, J. E., Rensing, K. H., Douglas, C. J., and Cheng, K. M. (2010). Chromoplasts ultrastructure and estimated carotene content in root secondary phloem of different carrot varieties. *Planta.* 231, 549–558. doi: 10.1007/s00425-009-1071-7

Kjellenberg, L., Johansson, E., Gustavsson, K. E., Granstedt, A., and Olsson, M. E. (2016). Influence of organic manures on carrot (Daucus carota L.) crops grown in a long-term field experiment in Sweden. *Renew. Agr. Food Syst.* 31, 258–268. doi: 10.1017/S1742170515000174

Korolev, A. V., Tomos, A. D., and Farrar, J. F. (2000). The trans-tissue pathway and chemical fate of 14C photoassimilate in carrot taproot. *New Phytol.* 147, 299–306. doi: 10.1046/j.1469-8137.2000.00699.x

Lin, N., Wang, X. P., Zhang, Y. H., Hu, X. P., and Ruan, J. H. (2020). Fertigation management for sustainable precision agriculture based on Internet of Things. *J. Clean. Prod.* 277, 124119. doi: 10.1016/j.jclepro.2020.124119

Liu, Q. Q., Li, J. Q., Han, R. L., Wang, H. W., and Liu, W. X. (2022). Comparative analysis of anatomical structure, assimilate accumulation and gene expression in lignin and carbohydrate metabolism pathway during taproot thickening of taicai and pak choi. *Sci. Hortic-Amsterdam.* 301, 111046. doi: 10.1016/j.scienta.2022.111046

Liu, X. N., Tuo, Y. F., Wang, Z. Y., Lai, J. Q., Xiang, P., He, X. H., et al. (2023). Response of soil nutrients, enzyme activities, yield and saponin content of Panax notoginseng to different water and fertilizer combinations. *J. Plant Nutr. Fert.* 29, 2332–2344. doi: 10.11674/zwyf.2023133

Liu, Y. J., Wang, G. L., Ma, J., Xu, Z. S., Wang, F., and Xiong, A. S. (2018). Transcript profiling of sucrose synthase genes involved in sucrose metabolism among four carrot (Daucus carota L.) cultivars reveals distinct patterns. *Bmc. Plant Biol.* 18, 1–12. doi: 10.1186/s12870-017-1221-1

Liu, J., Xu, A. Z., and Yan, G. L. (2021). Effect of drip irrigation fixed rate water and fertiliser integration treatment on yield and quality of spring wheat. *Seed Sci. Technol.* 39, 12–14. doi: 10.19904/j.cnki.cn14-1160/s.2021.23.005

Miras, M., Pottier, M., Schladt, T. M., Ejike, J. O., Redzich, L., Frommer, W. B, et al. (2022). Plasmodesmata and their role in assimilate translocation. *J. Plant Physiol.* 270, 153633. doi: 10.1016/j.jplph.2022.153633

Moore, S. (1968). Amino acid analysis: aqueous dimethyl sulfoxide as solvent for the ninhydrin reaction. *J. Biol. Chem.* 243, 6281–6283. doi: 10.1016/S0021-9258(18)94488-1

Nilsson, T. (1987). Growth and chemical composition of carrots as influenced by the time of sowing and harvest. *J. Agric. Sci.* 108, 459–468. doi: 10.1017/S0021859600079508

Olle, M., and Williams, I. H. (2021). Organic cultivation of vegetables. *Sustain. Agric. Rev.* 52, 1–19. doi: 10.1007/978-3-030-73245-5_1

Pang, X. (2023). Research progress on effects of bio-organic fertilizer on soil characteristics of farmland, crop yield and quality. *Hans J. Soil Sci.* 11, 100–106. doi: 10.12677/HJSS.2023.112013

Passafiume, R., Farina, V., and La Mantia, T. (2023). Portugal and Common Blond Oranges: are they the same Variety? Characteristics and Enhancement of the Oldest European Sweet Orange Variety. *Open Agric. J.* 17, e18743315273225. doi: 10.2174/0118743315273225231121042141

Perrin, F., Hartmann, L., Dubois-Laurent, C., Welsch, R., Huet, S., Hamama, L., et al. (2017). Carotenoid gene expression explains the difference of carotenoid accumulation in carrot root tissues. *Planta.* 245, 737–747. doi: 10.1007/s00425-016-2637-9

Ranganna, S. (1977). *Manual of Analysis of Fruit and Vegetable Products* (New York: Tata McGraw-Hill).

Ren, H., Jiang, Y., Zhao, M., Qi, H., and Li, C. F. (2021). Nitrogen supply regulates vascular bundle structure and matter transport characteristics of spring maize under high plant density. *Front. Plant Sci.* 11. doi: 10.3389/fpls.2020.602739

Rietra, R. P. J. J., Heinen, M., Dimkpa, C. O., and Bindraban, P. S. (2017). Effects of nutrient antagonism and synergism on yield and fertilizer use efficiency. *Commun. Soil Sci. Plant* 48, 1895–1920. doi: 10.1080/00103624.2017.1407429

Sedmak, J. J., and Grossberg, S. E. (1977). A rapid, sensitive, and versatile assay for protein using Coomassie brilliant blue G250. *Anal. Biochem.* 79, 544–552. doi: 10.1016/0003-2697(77)90428-6

Shani, E., Weinstain, R., Zhang, Y., Castillejo, C., Kaiserli, E., Chory, J., et al. (2013). Gibberellins accumulate in the elongating endodermal cells of Arabidopsis root. *Proc. Natl. Acad. Sci. U.S.A.* 110, 4834–4839. doi: 10.1073/pnas.1300436110

Spicer, R. (2014). Symplasmic networks in secondary vascular tissues: parenchyma distribution and activity supporting long-distance transport. *J. Exp. Bot.* 65, 1829–1848. doi: 10.1093/jxb/ert459

Stevens, M., Kader, A. A., and Albright, M. (1979). Potential for increasing tomato flavor via increased sugar and acid content1. *J. Am. Soc Hortic. Sci.* 104, 40–42. doi: 10.21273/JASHS.104.1.40

Sun, Z. Q., Zhao, Y. Y., and Ni, X. J. (2003). Effect of fermented peanut shells substrates on tomato seedling. *Acta Agric. Boreali-Sin.* 18, 86–90. doi: 10.3321/j.issn:1000-7091.2003.04.024

Suojala, T. (2000). Pre- and postharvest development of carrot yield and quality. Available online at: https://api.semanticscholar.org/CorpusID:14218519 (Accessed June 4, 2025).

Tang, W. H., Zhang, C. Y., Zhang, P. Q., Zhao, Y., Guo, M. Y., Li, Y., et al. (2024). Optimized fertilizer-water management improves carrot quality and soil nutrition and reduces greenhouse gas emissions on the North China plain. *Sci. Hortic.* 10, 151.

Tei, F., De Neve, S., de Haan, J., and Kristensen, H. L. (2020). Nitrogen management of vegetable crops. *Agr. Water Manage.* 240, 106316. doi: 10.1016/j.agwat.2020.106316

Ter Braak, C. J. F., and Smilauer, P. (2002). *CANOCO Reference Manual and User's Guide: Software for Ordination, version 5.0* (Ithaca USA: Microcomputer Power). Available at: https://edepot.wur.nl/405659.

Thompson, R. (1969). Some factors affecting carrot root shape and size. *Euphytica.* 18, 277–285. doi: 10.1007/BF00035699

Ubeda-Tomás, S., Federici, F., Casimiro, I., Beemster, G. T. S., Bhalerao, R., Swarup, R., et al. (2009). Gibberellin signaling in the endodermis controls arabidopsis root meristem size. *Curr. Biol.* 19, 1194–1199. doi: 10.1016/j.cub.2009.06.023

Wang, G. L., Huang, Y., Zhang, X. Y., Xu, Z. S., Wang, F., and Xiong, A. S. (2016). Transcriptome-based identification of genes revealed differential expression profiles and lignin accumulation during root development in cultivated and wild carrots. *Plant Cell Rep.* 35, 1743–1755. doi: 10.1007/s00299-016-1992-0

Wang, L. J., Yu, T. L., Gao, X. D., Li, G. X., Li, W. D., Li, B. H., et al. (2023). Effects of water and fertilizer management practices on watermelon yield quality and economic benefits in Changle County. *Mod. Agric. Sci. Technol.* 52, 56–61. doi: 10.3969/j.issn.1007-5739.2023.24.015

Wareing, P. F., and Patrick, J. (1975). "Source-sink relations in the partitioning of assimilates in the plant," in *Photosynthesis and Productivity in Different Environments*. Ed. J. P. Cooper (Cambridge University Press, The United Kingdom).

Winfried, S. P., and Michael, K. (2022). How Münch's adaptation of Pfeffer's circulating water flow became the pressure-flow theory, and the resulting problems — A historical perspective. *J. Plant Physiol.* 272, 153672. doi: 10.1016/j.jplph.2022.153672

Yang, J. C., Zhang, H., and Zhang, J. H. (2012). Root morphology and physiology in relation to the yield formation of rice. *J. Integr. Agr.* 11, 920–926. doi: 10.1016/S2095-3119(12)60082-3

Yuan, Y. C., Wang, Q. J., Tong, B. Q., Liu, D., Liu, H. Z., Yan, Q. K., et al. (2023). Morphological studies of developing glandular trichomes and a novel HD-ZIP gene LjROC3 increasing glandular trichome density on leaves in honeysuckle (Lonicera japonica). *Ind. Crop Prod.* 198, 116696. doi: 10.1016/j.indcrop.2023.116696

Zhang, X. H. (2023). Effect of organic fertilizer replacing nitrogen fertilizer on yield and quality of cucumber. *Spec. Econ. Plants Anim.* 26, 7–9.

Zhang, X., Wang, R., Ning, H., Li, W., Bai, Y., and Li, Y. (2020). Evaluation and management of fungal-infected carrot seeds. *Sci. Rep.* 10, 10808. doi: 10.1038/s41598-020-67907-5

Zhao, C., Craig, J. C., Petzold, H. E., Dickerman, A. W., and Beers, E. P. (2005). The xylem and phloem transcriptomes from secondary tissues of the Arabidopsis root-hypocotyl. *Plant Physiol.* 138, 803–818. doi: 10.1104/pp.105.060202

Zhao, L. H., and Gu, Y. (1999). Anatomcal Studies on Developmental Morphology of Fleshy Tap Root of Daucus carota L.var. sativa DC. *J. Jilin Agric. Univ.* 21, 4. doi: 10.3969/j.issn.1000-5684.1999.02.006

Zhao, W. J., Ma, F., Cao, W., Ma, F. F., and Han, L. (2022). Effects of water and fertilizer coupling on the yield and quality of tomatoes. *J. Agr. Eng.* 38, 95–101. doi: 10.11975/j.issn.1002-6819.2022.02.011

Zhao, C. L., Yu, J., Guo, X. S., Zhu, F. J., Liang, M. R., Chen, L. Q., et al. (2023). Effects of replacing chemical fertilizers with organic fertilizers on yield, quality and soil properties of facility tomato. *Shandong Agric. Sci.* 55, 116–120. doi: 10.3969/j.issn.1673-2871.2021.04.008

Zhu, X. C., Zhang, H. M., and Nan, W. B. (2017). Progress in the regulation of plant root growth and development by abscisic acid. *J. Plant Physiol.* 53, 1123–1130. doi: 10.1111/jipb.12899

Zuo, Y. N., Zhang, J. X., Zhao, R., Dai, H. Y., and Zhang, Z. H. (2018). Application of vermicompost improves strawberry growth and quality through increased photosynthesis rate, free radical scavenging and soil enzymatic activity. *Sci. Hortic-Amsterdam.* 233, 132–140. doi: 10.1016/j.scienta.2018.01.023

frontiers | Frontiers in Plant Science

TYPE Original Research
PUBLISHED 18 June 2025
DOI 10.3389/fpls.2025.1581120

Check for updates

OPEN ACCESS

EDITED BY
Amir Ali Khoddamzadeh,
Florida International University, United States

REVIEWED BY
Xin Li,
Chinese Academy of Agricultural Sciences, China
Xiaojuan Chen,
Guangxi University, China
Zhang Zhenggui,
Institute of Cotton Research (CAAS), China

*CORRESPONDENCE
Hong Liao
hliao@fafu.edu.cn

RECEIVED 21 February 2025
ACCEPTED 26 May 2025
PUBLISHED 18 June 2025

CITATION
Huang S, Yu Y, Cui J, Luo Z, Luo L, Song C and Liao H (2025) Organic fertilizer substitution optimizes aroma metabolites in Wuyi Rock tea.
Front. Plant Sci. 16:1581120.
doi: 10.3389/fpls.2025.1581120

COPYRIGHT
© 2025 Huang, Yu, Cui, Luo, Luo, Song and Liao. This is an open-access article distributed under the terms of the Creative Commons Attribution License (CC BY). The use, distribution or reproduction in other forums is permitted, provided the original author(s) and the copyright owner(s) are credited and that the original publication in this journal is cited, in accordance with accepted academic practice. No use, distribution or reproduction is permitted which does not comply with these terms.

Organic fertilizer substitution optimizes aroma metabolites in Wuyi Rock tea

Shuping Huang[1], Yongdong Yu[1], Jilai Cui[2,3], Zhengwei Luo[4], Lanxin Luo[4], Chuankui Song[4] and Hong Liao[1]*

[1]Root Biology Center, College of Resources and Environment, Fujian Agriculture and Forestry University, Fuzhou, China, [2]Dabie Mountain Laboratory, College of Tea and Food Science, Xinyang Normal University, Xinyang, Henan, China, [3]Henan Key Laboratory of Tea Plant Biology, College of Tea and Food Science, Xinyang Normal University, Xinyang, Henan, China, [4]State Key Laboratory of Tea Plant Biology and Utilization, Anhui Agricultural University, Hefei, Anhui, China

Pleasant aroma is a distinctive character of Wuyi Rock tea, but its optimization through agricultural practices remains largely unexplored. Here, we conducted a two-year field trials in the core-region of Wuyi Rock tea production area with organic or chemical fertilizer. The results indicated that organic fertilizer significantly improves soil fertility, as indicated by increased pH and organic matter. GC-MS analysis showed that organic fertilizer obviously affects the aroma metabolites in tea leaves, with the levels of 1-Hexanol ($C_6H_{14}O$), 2-Ethyl-1-hexanol ($C_8H_{18}O$), (E,E)-2,4-Heptadienal ($C_7H_{10}O$), E-Nerolidol ($C_{15}H_{26}O$) and 3-octen-2-one ($C_8H_{14}O$) increasing by 56.55%, 104.44%, 64.39%, 64.10% and 48.10%, respectively, compared to chemical fertilizer, thereby improving its aroma quality. The correlation analysis and PLS-PM model combined with the results from ionomics and metabolomics, further elucidated that soil fertility significantly impacted the mineral nutrients in tea leaves, thereby regulating the content of volatile metabolites. Altogether, the research findings provide practical fertilizer usage guidelines for tea farmers, helping to improve the aroma quality and overall market value of tea.

KEYWORDS

organic fertilizer, aroma, soil, Wuyi Rock tea, metabolites

Introduction

Oolong tea is renowned for its exquisite processing, time-honored history, health benefits, and unique taste (Wang et al., 2022a). Among the various types of oolong tea, Wuyi Rock tea, produced in Wuyi Mountain City of Fujian, is a paragon among Fujian oolong teas. Wuyi Rock tea is globally recognized for its unique rock rhyme, rich texture, and aroma, securing its niche in the tea industry (Ho et al., 2015). The characteristic flavor of Wuyi Rock tea primarily stems from its distinctive manufacturing process, which involves withering, tumbling and aeration, enzyme inactivation, shaping, and drying, bestowing the tea with its unique taste and floral aroma (Liu et al., 2022a). While many

studies have focused on identifying aromatic compounds in the production process and the final product (Zheng et al., 2022), the influence of fresh tea leaves on Wuyi Rock tea's aroma is still poorly understood.

Fertilization is a crucial management practice that ensures both tea yield and quality. Nutrient deficiency can notably reduce the content of amino acids and aromatic compounds, with the L-theanine content decreasing to 11.4% of the control level (Zhou et al., 2022), thereby degrading the quality of tea. While chemical fertilizers are widely used to ensure nutrient supply, their long-term excessive and improper use can reduce the biosynthesis of polyphenols and flavonoids, leading to a bitter taste in tea (Ye et al., 2022). This practice also threatens the sustainable production of tea (Arafat et al., 2019; Ni et al., 2019). High-phosphorus conditions decrease the accumulation of polyphenols in tea plants (Zhang et al., 2023), while elevated phosphorus and potassium reduce free amino acids such as theanine and glutamic acid, simultaneously increasing flavonoid-related metabolites (Wei et al., 2022). Moreover, overuse of chemical fertilizers leads to soil degradation, including decreased beneficial microorganisms, nutrient leaching, soil structure deterioration, and acidification (Li et al., 2016).

In contrast to chemical fertilizers, organic fertilizers offer several benefits for soil health and tea quality. Organic fertilizer can effectively alleviate soil acidification and increase soil organic matter (Wang et al., 2025). Studies indicate that the rational use of organic fertilizers can promote the synthesis of amino acids and flavonoids in tea (Ruan et al., 2019). However, relying solely on organic fertilizers can reduce tea yield by 10-20%, impacting economic profitability (Das et al., 2016; Piyasena and Hettiarachchi, 2023). Currently, many tea plantations adopt a fertilization strategy that integrates organic and chemical fertilizers. This approach ensures tea yield (Manzoor et al., 2024), promotes catechin and flavonoid synthesis in tea leaves (Raza et al., 2024) and increases the levels of aromatic compounds such as D-limonene, linalool, and cis-3-hexenyl hexanoate in green tea (Huang et al., 2022). Nevertheless, more research is needed to understand the effects of using organic fertilizers alone on tea plantation soils and tea quality.

It was reported that a high-nitrogen, low-phosphorus, and medium-potassium nutrient ratio is optimal for the growth of high-quality Wuyi Rock tea (Wang et al., 2022b). Based on this, we developed a tea plant-specific organic fertilizer. To explore the effects of organic fertilizer on the yield and quality of Wuyi Rock tea, we established a two-year field trial including organic fertilizer and chemical fertilizer. The impact of different fertilization treatments on the soil of tea plantations and the key metabolites of tea plants was analyzed using Inductively Coupled Plasma Mass Spectrometry (ICP-MS) and Gas Chromatography-Mass Spectrometry (GC-MS). Further, our study elucidated the effects of organic fertilizer on the yield and quality of Wuyi Rock tea, providing a theoretical reference for rational fertilization and the enhancement of tea quality in Wuyi tea plantations, while offering practical fertilizer usage guidelines for tea farmers to improve the aroma quality and overall market value of tea.

Materials and methods

Plant material and fertilizer treatment

The tea variety (*Camellia sinensis* L. cv. "Rougui") was used in this study. The trial field of tea plants was located in the core-region of Wuyi Rock tea production area, Wuyi Mountain city, Fujian province, China (27°32'36"-27°55'15"N; 117°24'12"-118°02'50"E). The basic soil chemical properties of the soil (0–20 cm) were as follows: pH 4.25; alkali-hydrolysable nitrogen (AN), 77.68 mg/kg; available phosphorus (AP), 145.68 mg/kg; rapid-acting potassium (AK), 143.75 mg/kg; and organic matter (OM), 19.55 mg/kg.

This experiment employed two fertilization treatments: chemical fertilizers and organic fertilizer. Each treatment was replicated three times, with plot sizes of 60 m^2 (6 m × 10 m), ensuring a consistent spacing of 1.5 m between rows of tea trees. The application rate for both fertilization treatments was uniformly set at 750 kg/ha. For the chemical fertilizer treatment, a compound fertilizer was selected, with a nutrient ratio of N:P_2O_5:K_2O = 15:15:15. In contrast, the organic fertilizer treatment utilized a tea-specific organic fertilizer, primarily composed of cow manure, spent mushroom substrate, and soybean meal, which underwent ultra-high temperature fermentation (exceeding 80°C), resulting in a nutrient ratio of N:P_2O_5:K_2O = 10:1:5, and an organic matter content of no less than 30%. The fertilization practices were conducted during the autumn seasons of 2022 and 2023, employing trench application methods, with the depth of fertilization controlled at 20 cm.

Collection of tea leaves and soil samples

Tea leaf samples (one-tip-three-leaf) were manually harvested in May 2023 and May 2024. Fresh leaf samples, amounting to 20 grams from each tea plant, were collected, with 10 plants chosen at random for biological replication. The samples were fixed at 105°C for 30 minutes, then dried at 75°C until reaching a constant weight, and subsequently ground for further analysis. Soil samples were gathered from 10 random sites within each plot in July 2023 and July 2024, after visible plant residues and stones were removed, using a stainless steel soil corer to collect samples from a depth of 0–20 cm. The soil samples were air-dried, pulverized, and sieved through 2 mm and 0.0149 mm screens for subsequent analysis.

Analysis of nutrient concentrations

The mineral elements in tea leaf were measured according to methods previously described (Peng et al., 2018). In brief, the concentration of macronutrients (N, P, K) was measured by a flow autoanalyzer (SKALAR SAN++, Skalar, Breda, Netherlands). The concentrations of calcium (Ca), Natrium (Na), magnesium (Mg), aluminum (Al), manganese (Mn), iron (Fe), zinc (Zn), copper (Cu), boron (B), nickel (Ni), molybdenum (Mo) and cobalt (Co)

were measured by inductively coupled plasma-mass spectrometry (ICP-MS 7900, Agilent Technologies, Santa Clara, California, US).

Analysis of physicochemical properties of soil samples

The soil samples were measured using the method as described by Liu et al. (2022b). In brief, the soil pH was determined using a pH meter (ORION3STAR, Thermo Fisher Scientific, USA) in a 1:25 (w/v) paste with deionized water. OM and AN were quantified using high-temperature potassium dichromate oxidation and the alkali-hydrolysable diffusion method, respectively. AP was extracted using the BrayI method, and readily AK was extracted from an ammonium acetate solution.

Analysis of volatiles via GC-MS

Gas chromatography-mass spectrometry (GC-MS) was performed according to the previous study (Cui et al., 2023). The volatile compounds were examined utilizing a TRACE 1300 gas chromatograph coupled with a DSQ II mass spectrometer (Thermo Fisher Scientific, Waltham, USA). A 1 µL aliquot of the previously prepared concentrated distillate was introduced into the GC in a splitless mode at an injection port temperature of 250°C. Separation of the volatiles was achieved on a DB-5 fused silica capillary column DB-5, 30 m × 0.25 mm, 0.25 µm film thickness, J&W Scientific, CA, USA). The GC column oven temperature was programmed to initially maintain at 50°C for 5 minutes, subsequently increase at a rate of 4°C per minute to 160°C (held for 3 minutes), and further ascend at 8°C per minute to 230°C (held for 2 minutes). Helium (purity > 99.999%) served as the carrier gas, flowing at a rate of 1 mL per minute. The ion source functioned in positive ion mode at an ionization energy of 70 eV and a temperature of 230°C. The volatiles were detected using full scan mode with a mass range of m/z 35-450.

A mixture of n-alkanes (C8–C25) was injected under the same GC-MS conditions as the samples to calculate the retention index (RI) of each volatile. The volatiles were identified by comparing the detected mass spectra to those in the National Institute of Standards and Technology (NIST17) database. Compounds with a mass spectra similarity higher than 800 and an RI difference of <20 were identified as volatiles in samples. When available, compounds were also identified based on the retention times, retention indices and mass spectra of the standards. The volatile compounds were quantified by comparing the peak area of each compound to that of the internal standard (ethyl caprate) using their respective characteristic ions (Supplementary Table 2).

Data analysis

All experimental data were organized using Microsoft Excel 2019 (Microsoft Corporation, USA). Data processing and figure creation were conducted with Graphpad Prism 9.5 software and R language packages. The obtained data were subjected to normality tests, two-way ANOVA, and Student's *t*-test using the SPSS sofaware (Version 19.0.0, International Business Machines Corporation, Chicago, America). OPLS-DA analysis (Orthogonal Partial Least Squares-Discriminant Analysis), Mantel test analysis and PLS-PM analysis were performed using the "ropls," "linkET," and "plspm" packages in R. *: $0.01 < P \leq 0.05$; **: $0.001 < P \leq 0.01$; ***: $P \leq 0.001$, ns: no significant difference.

Results

The effects of organic fertilizer substitution on soil fertility

To investigate the impact of organic fertilizer substitution on tea plantation soils, five soil fertility indexes were measured, including pH value, organic matter (OM), alkali-hydrolysable nitrogen (AN), available phosphorus (AP) and available potassium (AK) concentrations. Interestingly, the average soil pH values in the tea plantation treated with organic fertilizer for two years were 4.42 and 4.48, while treated with chemical fertilizer had average soil pH values of 4.19 and 4.17 (Figure 1A), showing that organic fertilizer treatment effectively mitigated soil acidification. The soil OM content was also significantly increased, with increases of 35.66% and 33.02% compared to the chemical fertilizer treatment (Figure 1B). In contrast, after two years of organic fertilizer application, the soil's AN, AP and AK in the tea plantation decreased by 7.07% and 18.22%, 18.28% and 44.93%, and 28.66% and 25.03% (Figures 1C-E), respectively, compared to the chemical fertilizer application. These results indicated that organic fertilizer significantly changes soil fertility in tea plantation.

The effects of organic fertilizer substitution on tea quality

A two-year field trials in the core-region of Wuyi Rock tea production area was conducted to study the effects of organic fertilizer on tea yield and quality. Results showed that organic fertilizer application did not decrease tea yield but increased the number of standard leaves per unit area compared to chemical fertilizer treatment (Supplementary Figure 1). Analysis of mineral nutrients revealed that organic fertilizer significantly reduced phosphorus (P), magnesium (Mg), iron (Fe), and zinc (Zn) concentrations but increased boron (B) concentration in tea leaves relative to chemical fertilizer (Table 1).

To investigate the impact of organic fertilizer on the volatile metabolites of tea leaves, an analysis of volatile metabolites was conducted. A total of 113 volatile metabolites in tea leaves were identified through GC-MS analysis (Supplementary Table 1). An OPLS-DA model (Figure 2A) with high reliability (R2x = 0.651, R2y = 0.966, Q2 = 0.557, Figure 2B) revealed 25 differential metabolites (6 alcohols, 5 aldehydes, 4 esters, 2 ketones) based on

10.3389/fpls.2025.1581120

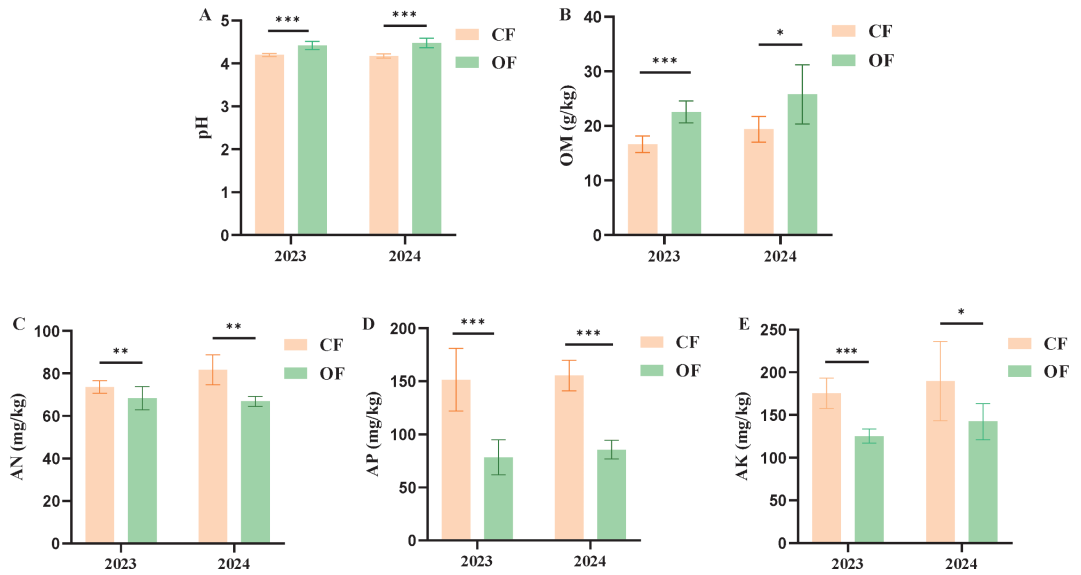

FIGURE 1
Soil fertility changes in tea plantation. **(A)** Soil pH; **(B)** Soil organic matter content; **(C)** Soil alkali-hydrolysable nitrogen content; **(D)** Soil available potassium content; **(E)** Soil available phosphorus content; n = 10. CF, chemical fertilizer; OF, organic fertilizer. The differences between groups were assessed using *t*-tests. *0.01 < $P \leq 0.05$; **0.001 < $P \leq 0.01$; ***$P \leq 0.001$, ns, no significant difference.

VIP > 1 and $P < 0.05$ (Figure 2C). The content of key aroma compounds—1-hexanol, 2-Ethyl-1-hexanol, (E,E)-2,4-Heptadienal, E-Nerolidol, and 3-Octen-2-one—increased by 56.55%, 104.44%, 64.39%, 64.10%, and 48.10%, respectively, under organic fertilizer treatment (Figure 2D). These findings indicate that organic fertilizer enhances tea aroma quality by increasing aldehyde, alcohol, and ester metabolites without compromising yield.

TABLE 1 Table of mineral element concentrations in fresh tea leaves under various fertilization treatments.

Mineral Nutrient	Treatments		*P*
	OF	CF	
N ($mg \cdot g^{-1}$)	28.01 ± 1.30	28.75 ± 1.46	0.255 ns
P ($mg \cdot g^{-1}$)	2.74 ± 0.17	2.94 ± 0.14	0.015*
K ($mg \cdot g^{-1}$)	12.38 ± 0.62	11.95 ± 0.47	0.094 ns
Ca ($mg \cdot g^{-1}$)	3.34 ± 0.46	3.45 ± 0.33	0.556 ns
Mg ($mg \cdot g^{-1}$)	1.58 ± 0.19	1.82 ± 0.18	0.011*
Al ($mg \cdot g^{-1}$)	0.64 ± 0.08	0.59 ± 0.06	0.201 ns
Mn ($\mu g \cdot g^{-1}$)	105.78 ± 25.97	112.01 ± 21.1	0.563 ns
B ($\mu g \cdot g^{-1}$)	26.44 ± 6.46	19.86 ± 4.40	0.016*
Na ($\mu g \cdot g^{-1}$)	30.61 ± 15.67	22.08 ± 6.84	0.132 ns
Fe ($\mu g \cdot g^{-1}$)	62.22 ± 4.85	80.11 ± 10.11	0.0002***
Co ($\mu g \cdot g^{-1}$)	0.07 ± 0.03	0.09 ± 0.03	0.689 ns
Ni ($\mu g \cdot g^{-1}$)	4.42 ± 0.96	4.87 ± 0.84	0.281 ns
Cu ($\mu g \cdot g^{-1}$)	6.62 ± 0.9	7.17 ± 1.02	0.221 ns
Zn ($\mu g \cdot g^{-1}$)	9.39 ± 2.83	12.31 ± 2.34	0.022*
Mo ($\mu g \cdot g^{-1}$)	0.06 ± 0.03	0.09 ± 0.25	0.265 ns

The differences between groups were assessed using t-tests. * 0.01<P≤0.05; ***P≤0.001, ns, no significant difference.

The relationship between mineral nutrients and aroma metabolites

To explore the impact of mineral nutrients on the volatile metabolites in fresh tea leaves, mantel test correlation analysis was conducted between 1-Hexanol, 2-Ethyl-1-hexanol, (E,E)-2,4-Heptadienal, E-Nerolidol, 3-Octen-2-one and various mineral nutrients (Figure 3). The result revealed that 1-Hexanol exhibited correlations with N and Fe. (E,E)-2,4-Heptadienal demonstrated correlations with Fe. Furthermore, 3-Octen-2-one exhibited correlations with P, K and Fe. Notably, 2-Ethyl-1-hexanol showed a significant correlation with K and Fe. Collectively, these results indicate that mineral nutrients were significantly associated with key tea aroma metabolites.

The relationship between soil fertility and aroma metabolites

To further elucidate the influence of soil fertility on the volatile metabolites of fresh tea leaves, 1-hexanol, 2-Ethyl-1-hexanol, (E,E)-2,4-Heptadienal, E-Nerolidol and 3-Octen-2-one were selected for linear regression analysis with soil nutrients. The results showed that 2-Ethyl-1-hexanol, (E,E)-2,4-Heptadienal and 3-Octen-2-one were significantly positively correlated with OM, and notably, all compounds also exhibited a significant negative correlation with AK (Figures 4A-F). In addition, the concentration of 1-Hexanol was also negatively correlated with AK (Figure 4G). 3-Octen-2-one

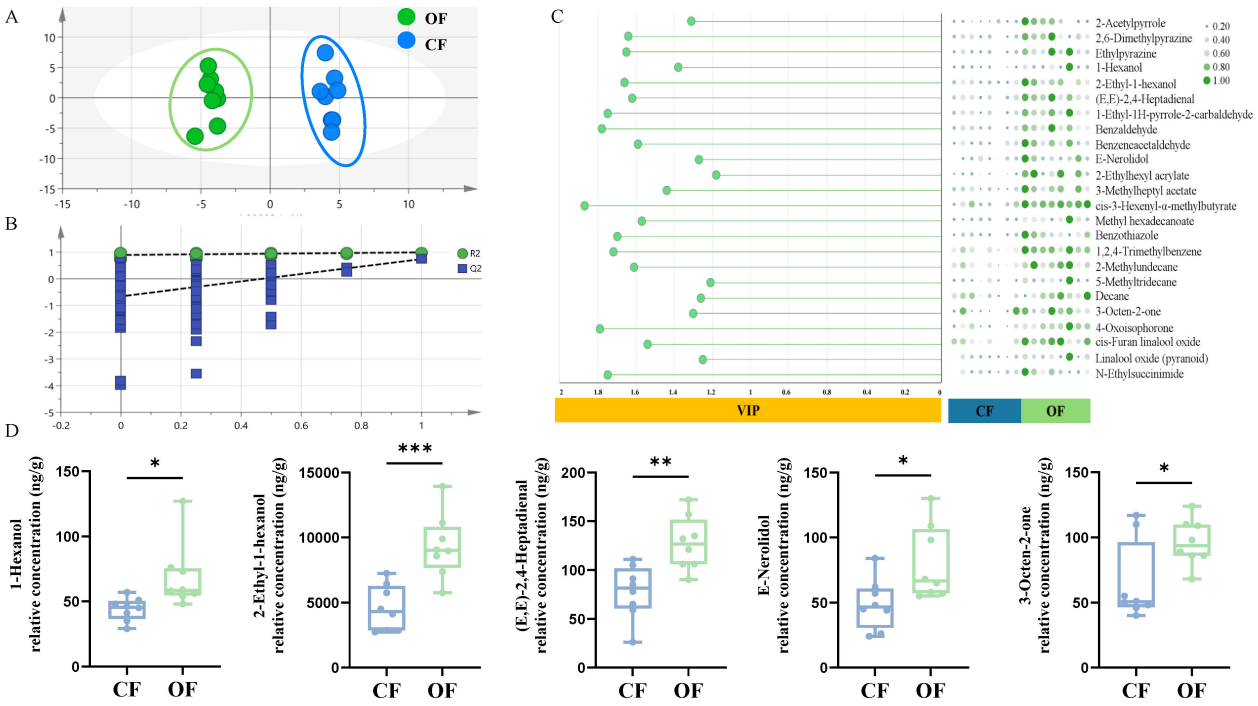

FIGURE 2
Differential metabolite processing analysis chart. **(A)** OPLS-DA model plot; **(B)** Cross-validation plot of the PLS-DA model; **(C)** VIP values and heatmap of differential metabolites **(D)**; Box plot of differential aroma metabolites. The differences between groups were assessed using *t*-tests. *0.01 < $P \leq 0.05$; **0.001 < $P \leq 0.01$; ***$P \leq 0.001$, ns, no significant difference.

concentrations was significantly negatively correlated with pH (Figure 4H). Furthermore, the concentration of 2-Ethyl-1-hexanol was significantly negatively correlated with AP (Figure 4I). These results indicated that OM significantly positively correlated with 2-Ethyl-1-hexanol, (E,E)-2,4-Heptadienal and 3-Octen-2-one in tea leaves, while AP and AK show negative correlations with the volatile metabolites.

Partial least squares path model analysis

To further clarify the effects of fertilization on tea yield and quality, PLS-PM model was used to reveal the relationships among soil fertility, soil pH, yield, tea nutrients, tea aroma and tea taste (Figure 5A). The model explained 55%, 69%, 66%, and 62% of the variation in mineral nutrients of tea, tea aroma, tea taste, and soil pH, respectively, within a goodness-of-fit index of 0.64. Soil fertility had positive direct effects on tea nutrients with a path coefficient (pc) of 0.97 and yield with a path coefficient (pc) of 1.09, whereas soil fertility exhibited a direct negative effect on tea aroma (pe = -1.13) and soil pH (pc = -0.79). Soil pH directly and significantly influenced tea yield (pc = 0.96) and tea taste (pc = 0.94), whereas contributed less to tea aroma (pc = -0.34) and tea nutrients (pc = 0.33). Additionally, the mineral nutrients of tea positively influenced tea taste (pc = 0.60) and aroma (pc = 0.10). Soil fertility exhibited the strongest total effects on tea amora, followed by soil pH and mineral nutrients of tea (Figure 5B). Taken together, fertilization may affect tea yield and the concentration of mineral nutrients by altering soil fertility and pH, thereby modulating the aroma of tea.

Discussion

The impact of organic fertilizers as a substitute for chemical fertilizers on tea yield

Harvesting annually depletes the mineral elements in tea plants, requiring the soil to be maintained rich in minerals. For tea cultivation, it is crucial to replenish the soil with sufficient mineral nutrients via fertilization (Ma et al., 2021). Effective nutrient management requires the rational use and selection of the most suitable nutrient sources (Johnston and Bruulsema, 2014). Fertilization can help restore and maintain soil nutrient levels, improving soil fertility and fostering conditions for stable, high tea yields (Ma et al., 2021). Nitrogen, phosphorus, and potassium are key macronutrients in tea plantations, but studies show that overuse of chemical fertilizers and nutrient imbalances are now urgent concerns (Mishima et al., 2010). In China, the average total nutrient input (N, P_2O_5, K_2O) in tea plantations is 796 kg·hm^{-2}, with about 36% receiving excessive inputs (≥ 750 kg·hm^{-2}) (Ni et al., 2019). Excess nitrogen, phosphorus, and potassium can negatively impact tea quality (Chen et al., 2021). Many tea plantations have recently switched from chemical to organic fertilizers to address

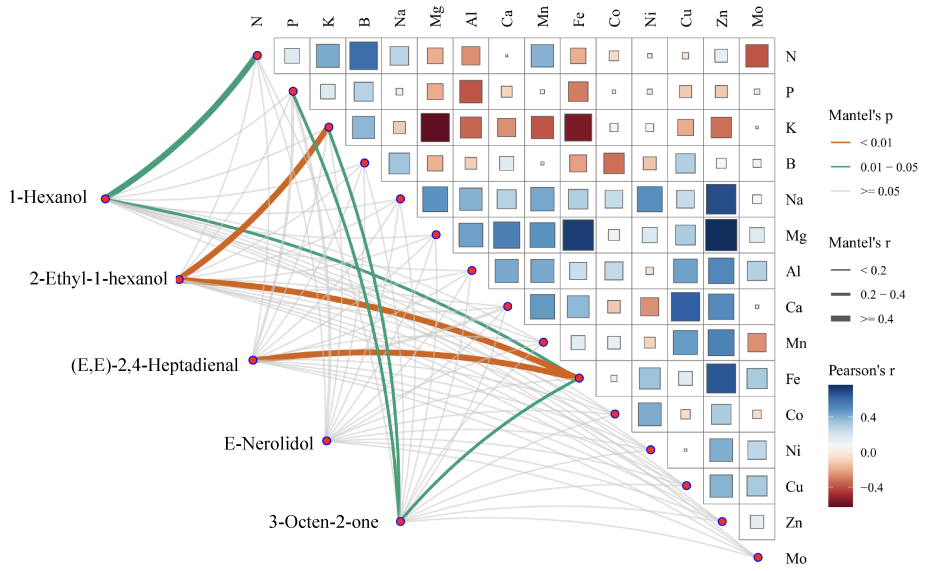

FIGURE 3
Correlation network between mineral nutrients and 1-hexanol, 2-Ethyl-1-hexanol, (E, E)-2,4-Heptadienal, E-Nerolidol and 3-Octen-2-one. The color scale represents Pearson's correlation coefficients: blue for positive correlations, red for negative correlations. Mantel's *P*-values are indicated by light (0.01 to 0.05) and green (> 0.05) shading, with line thickness corresponding to the strength of Mantel's correlation (r), where thicker lines denote stronger correlations.

these issues. However, it was reported that 10-20% decrease in tea yield after the application of organic fertilizers (Das et al., 2016; Piyasena and Hettiarachchi, 2023; Shi et al., 2024). In contrast, this study found that tea plants treated with organic fertilizer saw yield increases of 14.31% and 11.11% over two years, and a rise in standard leaf counts of 17.67% and 15.51% (Supplementary Figure 1). These results indicate that using specialized organic fertilizer in place of chemical fertilizer can ensure the maintenance of tea yield.

The influence of organic fertilizers substituting chemical fertilizers on tea quality

The complexity of tea flavor is largely determined by the balance of flavonoids, tea polyphenols, amino acids, and caffeine (Liu et al., 2022a). The concentration of these key compounds plays a critical role in the quality of tea (Li et al., 2022). Notably, metabolites synthesis is not only regulated by genetics, but also significantly affected by cultivation practices, fertilization strategies, and environmental factors such as temperature and light (Ahmed et al., 2019). Fertilization, as a common practice in tea plantation management, can enhance the synthesis of amino acids while reducing the ratio of tea polyphenols to total amino acids, thereby improving the overall flavor profile of tea (Qiu et al., 2024). However, different fertilizer types have varying effects on tea quality. For example, organic fertilizers typically promote amino acid and flavonoid synthesis (Ruan et al., 2019), whereas excessive chemical fertilizer use can impede polyphenol and flavonoid biosynthesis, resulting in a bitter and astringent taste (Ye et al., 2022; Piyasena and Hettiarachchi, 2023). In this study, treated with organic fertilizer, significantly increased flavonoid content in tea leaves (Supplementary Table 1). Additionally, the water-soluble substances in tea leaves increased significantly with organic fertilizer treatment, suggesting that specific organic fertilizers can boost the steeping durability of Wuyi Rock tea, highlighting organic fertilizers' positive impact on tea quality.

Approximately 700 volatile compounds have been successfully identified in tea leaves, with most forming during post-harvest processing (Ho et al., 2015). Studies show that excessive nitrogen fertilizer application increases fatty acid derivatives, raising the levels of fatty acid aromatic compounds (Chen et al., 2021), negatively impacting tea quality. Conversely, moderate nitrogen fertilizer application balances lipid metabolism and aroma precursor formation, enhancing tea aroma quality (Liu et al., 2017). Aldehydes, a key component of tea aroma, are especially prevalent in green, oolong, and black teas, comprising the largest share of total volatiles (Flaig et al., 2020). Most aldehydes in tea leaves provide a citrus and green flavor profile (Zhai et al., 2022). This study found that the levels of (E,E)-2,4-Heptadienal, and E-Nerolidol significantly increased after OF treatment, enhancing tea's fresh green aroma (Figure 2D). It was reported that 1-hexanol, linalool oxide, linalool, geraniol, (E)-β-ionone, isoamyl acetate, and 2-methylpropanal as contributors to a floral aroma, while 3-methyl-butanal, 2-Ethyl-1-hexanol, indole, and β-damascone were associated with a chestnut aroma (Liu et al., 2023). In this study, organic fertilizer treatment resulted in a significant increase in the levels of 1-Hexanol and 2-Ethyl-1-hexanol by 56.55% and 104.44%, respectively, thereby enhancing the aroma of tea. Furthermore, alcohol compounds are also significant volatile components in the formation of tea aroma (Zhu et al., 2021). In this study, we observed improvements in water-soluble substances, flavonoids (Supplementary Table 1), 1-Hexanol

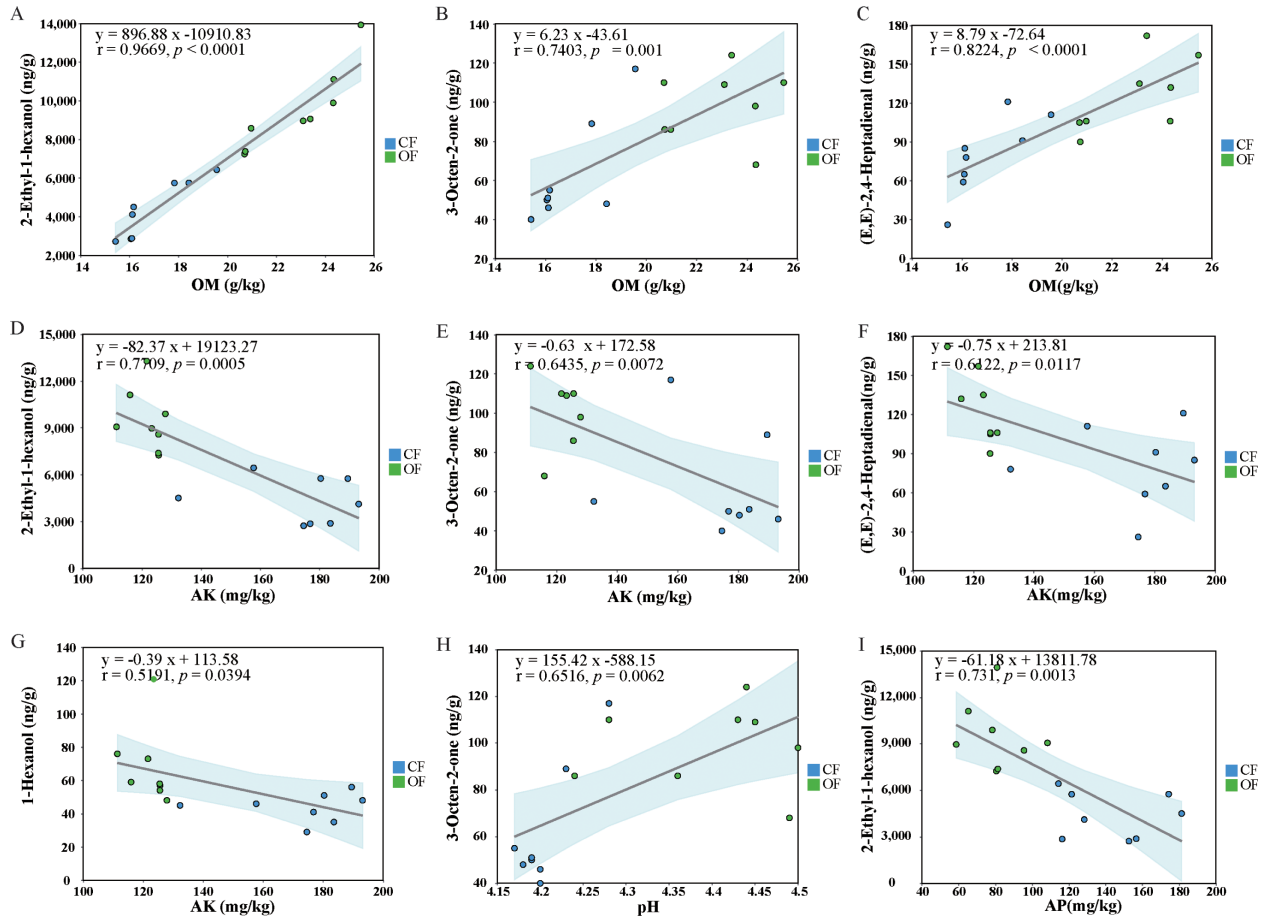

FIGURE 4
The correlation diagram of soil nutrients and differential aroma metabolites **(A)** Linear regression plot of 2-Ethyl-1-hexanol versus OM; **(B)** Linear regression plot of 3-Octen-2-one versus OM; **(C)** Linear regression plot of (E,E)-2,4-Heptadienal versus OM; **(D)** Linear regression plot of 2-Ethyl-1-hexanol versus AK; **(E)** Linear regression plot of 3-Octen-2-one versus AK; **(F)** Linear regression plot of (E,E)-2,4-Heptadienal versus OM; **(G)** Linear regression plot of 1-Hexanol versus AK; **(H)** Linear regression plot of 3-Octen-2-one versus available pH; **(I)** Linear regression plot of 2-Ethyl-1-hexanol versus AP. The shaded areas represent the 95% confidence intervals.

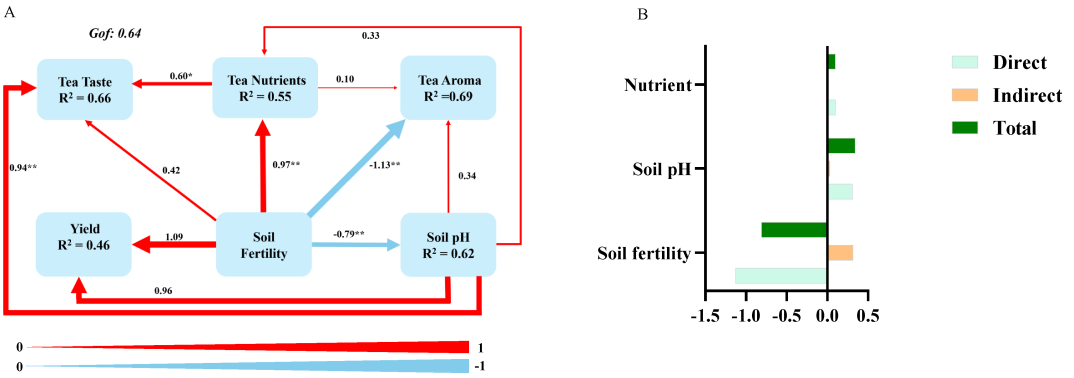

FIGURE 5
(A) The figures on the arrows represent standardized path coefficients, with the values of these coefficients denoted by the thickness of the arrows; red arrows signify positive impacts, while blue arrows denote negative impacts. The path coefficients and coefficients of determination (R^2) are calculated following 999 bootstrap replications. The R^2 values indicate the variance explained by the model; the model's evaluation is based on the Goodness of Fit statistic, a measure of overall predictive performance; pc: path coefficient, pe: path effect. **(B)** A diagram illustrating the degree of influence of tea nutrients, soil pH, and soil fertility on aroma.

and 2-Ethyl-1-hexanol and other aroma components in tea leaves after organic fertilizer treatment (Figure 2D), strongly supporting the use of organic fertilizers to enhance Wuyi Rock tea quality.

The effect of replacing chemical fertilizers with organic fertilizers on soil conditions

Soil, an indispensable natural resource, serves as a habitat for countless organisms and is crucial for ecological balance and human survival (Doran, 2002). The state of soil health, particularly its compositional diversity, profoundly influences crop productivity, climate stability, environmental health and human welfare (Manter et al., 2017). As a sophisticated life support system, soil contains numerous microbial communities essential to nutrient cycling (Morris and Blackwood, 2023). Nevertheless, soil health is influenced by various natural and human-induced factors (Withers et al., 2020; Yang et al., 2020) with fertilization practices having a notable effect on soil health in agricultural systems (Bai et al., 2018; Li et al., 2023). Therefore, understanding the connection between fertilization and soil health is critical for developing sustainable agricultural practices.

Tea plants are mainly grown in subtropical and tropical regions with high temperatures and heavy rainfall, leading to significant leaching of soil minerals. Numerous studies have highlighted that adding organic matter to soil greatly affects the availability of minerals and how efficiently plants absorb and use them (Sönmez et al., 2016; Turan, 2021). Nutrient use efficiency is crucial for tea growth and quality, but excess nutrients can harm tea tree growth and metabolism, potentially reducing tea quality (Chen et al., 2021). Moreover, excessive fertilization threatens the environment, potentially causing soil acidification, increased greenhouse gas emissions, and reduced biodiversity (Ma et al., 2021). Long-term reliance on inorganic fertilizers challenges sustainable land use, potentially leading to soil acidification and compaction, disrupting the nutrient balance in tea plantation soils (Yang et al., 2018). Therefore, replacing chemical fertilizers with organic fertilizers is seen as an effective way to decrease dependence on chemicals inputs. Organic fertilizers are value for their rich nutrient content, non-toxicity, environmental friendliness, long-lasting efficacy, and positive impact on soil health (Shaji et al., 2020). The average pH value of soils in Chinese tea plantations is 4.68, ranging from 3.96 to 5.48 across provinces (Yan et al., 2020). Tea trees prefer acidic soils, optimally between pH 4.0 and 5.5 (Yan et al., 2018). This study found that applying tea-specific organic fertilizer significantly raised the pH of tea plantation soil to a range of 4.28-4.54 (Figure 1A), benefiting tea tree growth and reducing soil acidification. This result is consistent with earlier studies (Saha et al., 2019; Zhang et al., 2019). After the organic fertilizer treatment, soil fertility in the tea plantation neared the high-quality standards for the Wuyi Tea Region (Zhou et al., 2019), providing optimal conditions for premium Wuyi Rock tea production.

The organic fertilizer enriches soil with exogenous organic matter, thus increasing organic content in the tea plantation soil (Figure 1B). This allows nutrients to be retained in the soil longer, in forms more accessible for plant uptake (Akinbode, 2011). It was reported that high-phosphorus conditions decrease the accumulation of polyphenols in tea plants (Zhang et al., 2023). In this study, OF treatment significantly reduced soil available phosphorus (AP) content (Figure 1D), which in turn decreased phosphorus levels in tea leaves (Table 1). Concurrently, the concentration of 2-Ethyl-1-hexanol in tea leaves increased (Figure 2D). The correlation analysis further revealed a significant correlation between phosphorus concentration in tea leaves and 2-Ethyl-1-hexanol content (Figure 4I). This suggests that organic fertilizer treatment can enhance tea aroma by reducing phosphorus levels in tea leaves, thereby increasing the concentration of aroma compounds like 2-Ethyl-1-hexanol. Consequently, the strategic use of organic fertilizer can strengthen soil quality and enhance the efficiency of nutrient uptake and use by tea plants (Birkhofer et al., 2008). In summary, this study offers theoretical and empirical evidence for combating soil acidification in tea plantations and boosting their sustainable development.

Sustainability outlook

This study demonstrates the pivotal role of organic fertilizers in enhancing soil fertility and improving the aromatic profile of Wuyi rock tea, demonstrating that organic fertilization effectively regulates volatile metabolites and reduces soil acidification. However, it is necessary to comprehensively evaluate the long-term efficacy of organic fertilizers, extended longitudinal studies are needed to continuously monitor soil health and tea quality variations, and accumulate multi-year datasets for a more precise assessment of their enduring impact on soil and tea. Additionally, replicating experiments across diverse soil types and climatic zones is essential to validate the generalizability of the findings. These efforts will improve our understanding of organic fertilizers' adaptability in different environmental settings and provide a strong scientific basis for broader tea cultivation practices.

Conclusion

Tea-specific organic fertilizers, as substitutes for conventional fertilizers, maintain tea yield while significantly enhancing the levels of water-soluble substances and flavonoids, thereby improving tea taste. Moreover, the application of tea-specific organic fertilizers notably elevated the levels of key aroma compounds, including 1-hexanol, 2-Ethyl-1-hexanol, (E,E)-2,4-Heptadienal, E-Nerolidol and 3-Octen-2-one intensifying the tea's aroma. Furthermore, the use of tea-specific organic fertilizers effectively reduced soil acidification and increased soil organic matter content in tea plantations. However, it must be noted that the present results are constrained by its regional scope, and different regions with diverse soil types and climatic conditions should be extended to enhance the generalizability of the results. In conclusion, this study provides a scientific rationale for optimized fertilization practices in Wuyi Mountain tea plantations, enhancing Wuyi Rock tea quality

and the sustainability of tea garden production, while offering practical fertilizer usage guidelines for tea farmers to improve the aroma quality and overall market value of tea.

Data availability statement

The original contributions presented in the study are included in the article/Supplementary Material. Further inquiries can be directed to the corresponding author.

Author contributions

SH: Writing – original draft. YY: Writing – review & editing. JC: Writing – review & editing. LL: Writing – review & editing. ZL: Writing – review & editing. CS: Writing – review & editing. HL: Writing – review & editing.

Funding

The author(s) declare that financial support was received for the research and/or publication of this article. This research was financially supported by the Wuyi Mountain Tea Industry Research Institute 105-KJG21001A, the University Innovation Fund and Root Biology Research Center Fund of Fujian Agriculture and Forestry University (105-118310040), the Natural Science Foundation of Fujian Province in China (2023J01484) and the Key R & D Special Project of Dabie Mountain Laboratory (DMLP002).

Acknowledgments

We would like to acknowledge the students of the Root Biology Center, Fujian Agriculture and Forestry University for tea and soil sample collection.

Conflict of interest

The authors declare that the research was conducted in the absence of any commercial or financial relationships that could be construed as a potential conflict of interest.

The author(s) declared that they were an editorial board member of Frontiers, at the time of submission. This had no impact on the peer review process and the final decision.

Generative AI statement

The author(s) declare that no Generative AI was used in the creation of this manuscript.

Publisher's note

All claims expressed in this article are solely those of the authors and do not necessarily represent those of their affiliated organizations, or those of the publisher, the editors and the reviewers. Any product that may be evaluated in this article, or claim that may be made by its manufacturer, is not guaranteed or endorsed by the publisher.

Supplementary material

The Supplementary Material for this article can be found online at: https://www.frontiersin.org/articles/10.3389/fpls.2025.1581120/full#supplementary-material

SUPPLEMENTARY FIGURE 1
Graph representing tea yield under various fertilization treatments. **(A)** Fresh tea leaf yield within an area of 0.1 m^2; **(B)** Number of standard leaves within an area of 0.1 m^2. CF, chemical fertilizer; OF, organic fertilizer. Inter-group differences were assessed using *t*-tests; *$0.01 < P \leq 0.05$; **$0.001 < P \leq 0.01$; ***$P \leq 0.001$; ns, no significant difference; n = 10.

SUPPLEMENTARY FIGURE 2
Correlation network between soil nutrients and 1-Hexanol, 2-Ethyl-1-hexanol, (E,E)-2,4-Heptadienal, E-Nerolidol and 3-Octen-2-one.The color scale represents Pearson's correlation coefficients: blue for positive correlations, red for negative correlations. Mantel's *P*-values are indicated by light (0.01 to 0.05) and green (> 0.05) shading, with line thickness corresponding to the strength of Mantel's correlation (r), where thicker lines denote stronger correlations.

SUPPLEMENTARY TABLE 1
Concentration of non-volatile metabolites in fresh tea leaves under various fertilization treatments.

SUPPLEMENTARY TABLE 2
Volatile compounds identified in fresh tea leaves.

References

Ahmed, S., Griffin, T. S., Kraner, D., Schaffner, M. K., Sharma, D., Hazel, M., et al. (2019). Environmental factors variably impact tea secondary metabolites in the context of climate change. *Front. Plant Sci.* 10. doi: 10.3389/fpls.2019.00939

Akinbode, O. A. O. (2011). Comparative study of different organic manures and NPK fertilizer for improvement of soil chemical properties and dry matter yield of maize in t-wo different soils. *J. Soil Sci. Environ. Manage.* 2, 9–13. doi: 10.5897/JSSEM.9000022

Arafat, Y., Tayyab, M., Khan, M. U., Chen, T., and Lin, S. (2019). Long-term monoculture negatively regulates fungal community composition and abundance of tea orchards. *Agronomy* 9, 466. doi: 10.3390/agronomy9080466

Bai, Z. G., Caspari, T., Gonzalez, M. R., Batjes, N. H., Mäder, P., Bünemann, E. K., et al. (2018). Effects of agricultural management practices on soil quality: A review of long-term experiments for Europe and China. *Agric. Ecosyst. Environ.* 265, 1–7. doi: 10.1016/j.agee.2018.05.028

Birkhofer, K., Bezemer, T. M., Bloem, J., Bonkowski, M., Christensen, S., Dubois, D., et al. (2008). Long-term organic farming fosters below and aboveground biota: Implications for soil quality, biological control and productivity. *Soil Biol. Biochem.* 40, 2297–2308. doi: 10.1016/j.soilbio.2008.05.007

Chen, Y. Z., Wang, F., Wu, Z. D., Jiang, F. Y., Yu, W. Q., Yang, J., et al. (2021). Effects of long-term nitrogen fertilization on the formation of metabolites related to tea quality in subtropical China. *Metabolites* 11, 146. doi: 10.3390/metabo11030146

Cui, J. L., Zhou, J., Du, W. K., Guo, D. Y., Tang, X. Y., Zhao, W., et al. (2023). Distribution of and temporal variation in volatiles in tea (*Camellia sinensis*) flowers during the opening stages. *J. Agric. Food Chem.* 71, 19682–19693. doi: 10.1021/acs.jafc.3c02690

Das, S., Borua, P. K., and Bhagat, R. M. (2016). Soil nitrogen and tea leaf properties in organic and conventional farming systems under humid sub-tropical conditions. *Organic Agric.* 6, 119–132. doi: 10.1007/s13165-015-0116-4

Doran, J. W. (2002). Soil health and global sustainability: translating science into practice. *Agr. Ecosyst. Environ.* 88, 119–127. doi: 10.1016/S0167-8809(01)00246-8

Flaig, M., Qi, S., Wei, G. D., Yang, X. G., and Schieberle, P. (2020). Characterisation of the key aroma compounds in a *Longjing* green tea infusion (*Camellia sinensis*) by the sensomics approach and their quantitative changes during processing of the tea leaves. *Eur. Food Res. Technol.* 246, 2411–2425. doi: 10.1007/s00217-020-03584-y

Ho, C. T., Zheng, X., and Li, S. (2015). Tea aroma formation. *Food Sci. Hum. Wellness* 4, 9–27. doi: 10.1016/j.fshw.2015.04.001

Huang, D. J., Wang, Y. P., Chen, X., Wu, J., Wang, H. J., Tan, R. R., et al. (2022). Application of tea-specific fertilizer combined with organic fertilizer improves aroma of green tea. *Horticulturae* 8, 950. doi: 10.3390/horticulturae8100950

Johnston, A. M., and Bruulsema, T. W. (2014). 4R Nutrient stewardship for improved nutrient use efficiency. *Proc. Eng.* 83, 365–370. doi: 10.1016/j.proeng.2014.09.029

Li, Y. C., Li, Z., Li, Z. W., Jiang, Y. H., Weng, B. Q., and Lin, W. X. (2016). Variations of rhizosphere bacterial communities in tea (*Camellia sinensis* L.) continuous cropping soil by high-throughput pyrosequencing approach. *J. Appl. Microbiol.* 121, 787–799. doi: 10.1111/jam.13225

Li, R. Y., Liu, K. Y., Liang, Z. W., Luo, H., Wang, T., An, J. S., et al. (2022). Unpruning improvement the quality of tea through increasing the levels of amino acids and reducing contents of flavonoids and caffeine. *Front. Nutr.* 9. doi: 10.3389/fnut.2022.1017693

Li, X., Qiao, L., Huang, Y. P., Li, D. C., Xu, M. G., Ge, T. D., et al. (2023). Manuring improves soil health by sustaining multifunction at relatively high levels in subtropical area. *Agric. Ecosyst. Environ.* 353, 108539. doi: 10.1016/j.agee.2023.108539

Liu, M. Y., Burgos, A., Ma, L. F., Zhang, Q. F., Tang, D. D., and Ruan, J. Y. (2017). Lipidomics analysis unravels the effect of nitrogen fertilization on lipid metabolism in tea plant (*Camellia sinensis* L.). *BMC Plant Biol.* 17, 165. doi: 10.1186/s12870-017-1111-6

Liu, N. F., Shen., S. S., Huang, L. F., Deng., G. J., Wei., Y. M., Ning., J. M., et al. (2023). Revelation of volatile contributions in green teas with different aroma types by GC–MS and GC–IMS. *Food Res. Int.* 169, 112845. doi: 10.1016/j.foodres.2023.112845

Liu, Y., Tian, J., Liu, B., Zhuo, Z. P., Shi, C., Xu, R. N., et al. (2022b). Effects of pruning on mineral nutrients and untargeted metabolites in fresh leaves of *Camellia sinensis* cv. Shuixian. *Front. Plant Sci.* 13. doi: 10.3389/fpls.2022.1016511

Liu, Y., Zhuo, Z. P., Tian, J., Liu, B., Shi, C., Xu, R. N., et al. (2022a). Directed accumulation of nitrogen metabolites through processing endows Wuyi Rock Tea with singular qualities. *Molecules* 27, 3264. doi: 10.3390/molecules27103264

Ma, L. F., Yang, X. D., Shi, Y. Z., Yi, X. Y., Ji, L. F., Cheng, Y., et al. (2021). Response of tea yield, quality and soil bacterial characteristics to long-term nitrogen fertilization in an eleven-year field experiment. *Appl. Soil Ecol.* 166, 103976. doi: 10.1016/j.apsoil.2021.103976

Manter, D. K., Delgado, J. A., Blackburn, H. D., Harmel, D., de León, A. A. P., and Honeycutt, C. W. (2017). Why we need a national living soil repository. *Proc. Natl. Acad. Sci. U S A.* 114, 13587–13590. doi: 10.1073/pnas.1720262115

Manzoor,, Ma, L. F., Ni, K., and Ruan, J. Y. (2024). Influence of organic and inorganic fertilizers on tea growth and quality and soil properties of tea orchards' top rhizosphere soil. *Plants* 13, 207. doi: 10.3390/plants13020207

Mishima, S., Endo, A., and Kohyama, K. (2010). Nitrogen and phosphate balance on crop production in Japan on national and prefectural scales. *Nutr. Cycl Agroecosys.* 87, 159–173. doi: 10.1007/s10705-009-9324-1

Morris, S. J., and Blackwood, C. B. (2023). *Soil Microbiology, Ecology and Biochemistry. Fifth edition* (Amsterdam: Elsevier). doi: 10.1016/B978-0-12-822941-5.00010-7

Ni, K., Liao, W. Y., Yi, X. Y., Niu, S. Y., MA, L. F., Shi, Y. Z., et al. (2019). Fertilization status and reduction potential in tea gardens of China. *J. Plant Nutr. Fertilizers* 25, 421–432. doi: 10.11674/zwyf.18078

Peng, W. T., Zhang, L. D., Zhou, Z., Fu, C., Chen, Z. C., and Liao, H. (2018). Magnesium promotes root nodulation through facilitation of carbohydrate allocation in soybean. *Physiol. Plant* 163, 372–385. doi: 10.1111/ppl.12730

Piyasena, K. N. P., and Hettiarachchi, L. S. K. (2023). Comparison of tea quality parameters of conventionally and organically grown tea, and effects of fertilizer on tea quality: A mini-review. *Food Chem. Adv.* 3, 100399. doi: 10.1016/j.focha.2023.100399

Qiu, Z. H., Liao, J. M., Chen, J. H., Li, A. S., Lin, M. Y., Liu, H. M., et al. (2024). Comprehensive analysis of fresh tea (*Camellia sinensis* cv. Lingtou Dancong) leaf quality under different nitrogen fertilization regimes. *Food Chem.* 439, 138127. doi: 10.1016/j.foodchem.2023.138127

Raza, A., Chen, C. Q., Luo, L., Asghar, M. A., Li, L., Shoaib, N., et al. (2024). Combined application of organic and chemical fertilizers improved the catechins and flavonoids biosynthesis involved in tea quality. *Scientia Hortic.* 337, 113518. doi: 10.1016/j.scienta.2024.113518

Ruan, L., Wang, L. Y., Wei, K., Cheng, H., Li, H. L., Shao, S. J., et al. (2019). Comparative analysis of nitrogen spatial heterogeneity responses in low nitrogen susceptible and tolerant tea plants (*Camellia sinensis*). *Scientia Hortic.* 246, 182–189. doi: 10.1016/j.scienta.2018.10.063

Saha, A., Basak, B. B., Gajbhiye, N. A., Kalariya, K. A., and Manivel, P. (2019). Sustainable fertilization through co-application of biochar and chemical fertilizers improves yi-eld, quality of *Andrographis paniculata* and soil health. *Ind. Crops Prod.* 140, 111607. doi: 10.1016/j.indcrop.2019.111607

Shaji, H., Chandran, V., and Mathew, L. (2020). *Controlled Release Fertilizers for Sustainable Agriculture* (Amsterdam: Elsevier). doi: 10.1016/B978-0-12-819555-0.00013-3

Shi, R., Wang, Y., Zhou, F., Hussain, S., Lei, X. Y., Chen, E. X., et al. (2024). Nitrogen fertilizer reduction based on bioorganic fertilizer improves the yield and quality of fresh leaves of alpine tea in summer. *Beverage Plant Res.* 4, 1–10. doi: 10.48130/bpr-0024-0024

Sönmez, O., Turan, V., and Kaya, C. (2016). The effects of sulfur, cattle, and poultry manure addition on soil phosphorus. *Turk J. Agric. For.* 40, 536–541. doi: 10.3906/tar-1601-41

Turan, V. (2021). Arbuscular mycorrhizal fungi and pistachio husk biochar combination reduces Ni distribution in mungbean plant and improves plant antioxidants and soil enzymes. *Physiol. Plant* 173, 418–429. doi: 10.1111/ppl.13490

Wang, Z. H., Gan, S., Sun, W. J., and Chen, Z. D. (2022a). Quality characteristics of Oolong tea products in different regions and the contribution of thirteen phytochemical components to its taste. *Horticulturae* 8, 278. doi: 10.3390/horticulturae8040278

Wang, Y., Liu, Y., Zhuo, Z. P., Xue, J. P., Xu., R. N., Sun., L. L., et al. (2022b). Effects of high nitrogen and low phosphorus medium potassium ratios on the yield and quality of Wuyi rock tea. *Jounral South. Agric.* 53, 391–400. doi: 10.3969/j.issn.2095-1191.2022.02.012

Wang, B., Wang, S., Li, G. Y., Fu, L. B., Chen, H., Yin, M., et al. (2025). Reducing nitrogen fertilizer usage coupled with organic substitution improves soil quality and boosts tea yield and quality in tea plantations. *J. Sci. Food Agric.* 105, 1228–1238. doi: 10.1002/jsfa.13913

Wei, K., Liu, M., Shi, Y., Zhang, H., Ruan, J., Zhang, Q., et al. (2022). Metabolomics reveal that the high application of phosphorus and potassium in tea plantation inhibited amino-acid accumulation but promoted metabolism of flavonoid. *Agronomy* 12, 1086. doi: 10.3390/agronomy12051086

Withers, E., Hill, P. W., Chadwick, D. R., and Jones, D. L. (2020). Use of untargeted metabolomics for assessing soil quality and microbial function. *Soil Biol. Biochem.* 143, 107758. doi: 10.1016/j.soilbio.2020.107758

Yan, P., Shen, C., Fan, L. C., Li, X., Zhang, L. P., Zhang, L., et al. (2018). Tea planting affects soil acidification and nitrogen and phosphorus distribution in soil. *Agric. Ecosyst. Environ.* 254, 20–25. doi: 10.1016/j.agee.2017.11.015

Yan, P., Wu, L. Q., Wang, D. H., Fu, J. Y., Shen, C., Li, X., et al. (2020). Soil acidification in Chinese tea plantations. *Sci. Total Environ.* 715, 136963. doi: 10.1016/j.scitotenv.2020.136963

Yang, X. D., Ni, K., Shi, Y. Z., Yi, X. Y., Zhang, Q. F., Fang, L., et al. (2018). Effects of long-term nitrogen application on soil acidification and solution chemistry of a tea plantation in China. *Agric. Ecosyst. Environ.* 252, 74–82. doi: 10.1016/j.agee.2017.10.004

Yang, T., Siddique, K. H. M., and Liu, K. (2020). Cropping systems in agriculture and their impact on soil health-A review. *Glob. Ecol. Conserv.* 23, e01118. doi: 10.1016/j.gecco.2020

Ye, J. H., Ye, Y., Yin, J. F., Jin, J., Liang, Y. R., Liu, R. Y., et al. (2022). Bitterness and astringency of tea leaves and products: Formation mechanism and reducing strategies. *Trends Food Sci. Tech.* 123, 130–143. doi: 10.1016/j.tifs.2022.02.031

Zhai, X. T., Zhang, L., Granvogl, M., Ho, C. T., and Wan, X. C. (2022). Flavor of tea (*Camellia sinensis*): A review on odorants and analytical techniques. *Compr. Rev. Food Sci. F.* 21, 3867–3909. doi: 10.1111/1541-4337.12999

Zhang, H., Li, C., Wei, K., Liu, M., Shi, Y., Yang, X., et al. (2023). The reduction of tea quality caused by irrational phosphate application is associated with anthocyanin metabolism. *Beverage Plant Res.* 3, 10. doi: 10.48130/BPR-2023-0010

Zhang, M. Y., Riaz, M., Zhang, L., El-desouki, Z., and Jiang, C. C. (2019). Biochar induces changes to basic soil properties and bacterial communities of different soils to varying degrees at 25 mm rainfall: More effective on acidic soils. *Front. Microbiol.* 10. doi: 10.3389/fmicb.2019.01321

Zheng, Y., Hu, Q., Wu, Z., Bi, W., Chen, B., Hao, Z., et al. (2022). Volatile metabolomics and coexpression network analyses provide insight into the formation of the characteristic cultivar aroma of oolong tea (*Camellia sinensis*). *Lwt* 164, 113666. doi: 10.1016/j.lwt.2022.113666

Zhou, B., Chen, Y., Zeng, L., Cui, Y., Li, J., Tang, H., et al. (2022). Soil nutrient deficiency decreases the postharvest quality-related metabolite contents of tea

(*Camellia sinensis* (L.) Kuntze) leaves. *Food Chem.* 377, 132003. doi: 10.1016/j.foodchem.2021.132003

Zhou, Z., Liu., Y., Zhang., L. M., Xu., R. N., Sun., L. L., and Liao, H. (2019). Soil nutrient status in Wuyi tea region and its effects on tea quality-related constituents. *Sci. Agric. Sinica.* 52, 1425–1434. doi: 10.3864/j.issn.0578-1752.2019.08.012

Zhu, J. C., Niu, Y. W., and Xiao, Z. B. (2021). Characterization of the key aroma compounds in Laoshan green teas by application of odour activity value (OAV), gas chromatography-mass spectrometry-olfactometry (GC-MS-O) and comprehensive two-dimensional gas chromatography mass spectrometry (GCxGC-qMS). *Food Chem.* 339, 128136. doi: 10.1016/j.foodchem.2020.128136

frontiers | Frontiers in Plant Science

TYPE Original Research
PUBLISHED 18 June 2025
DOI 10.3389/fpls.2025.1577962

Check for updates

OPEN ACCESS

EDITED BY
Amir Ali Khoddamzadeh,
Florida International University, United States

REVIEWED BY
Amarinder Singh Riar,
Guru Nanak Dev University, India
Jatinderpal Singh,
Indian Agricultural Research Institute (ICAR), India

*CORRESPONDENCE
Qiang Li
liqiangxj@163.com
Yun Ren
reny1989@sina.com

†These authors have contributed equally to this work

RECEIVED 17 February 2025
ACCEPTED 27 May 2025
PUBLISHED 18 June 2025

CITATION
Bao S, Chai X, Liao L, Li X, Shi L, Dong X, Long S, Li H, Wang H, Li Z, Wang M, Ren Y and Li Q (2025) Construction of nitrogen critical dilution curve and differences in nitrogen nutrition characteristics in different organs of maize varieties with contrasting nitrogen efficiencies.
Front. Plant Sci. 16:1577962.
doi: 10.3389/fpls.2025.1577962

COPYRIGHT
© 2025 Bao, Chai, Liao, Li, Shi, Dong, Long, Li, Wang, Li, Wang, Ren and Li. This is an open-access article distributed under the terms of the Creative Commons Attribution License (CC BY). The use, distribution or reproduction in other forums is permitted, provided the original author(s) and the copyright owner(s) are credited and that the original publication in this journal is cited, in accordance with accepted academic practice. No use, distribution or reproduction is permitted which does not comply with these terms.

Construction of nitrogen critical dilution curve and differences in nitrogen nutrition characteristics in different organs of maize varieties with contrasting nitrogen efficiencies

Shuqin Bao[1†], Xingying Chai[1,2†], Linzheng Liao[1†], Xiaoying Li[1], Lin Shi[1], Xixi Dong[1], Sida Long[1], Huifu Li[1], Hanyu Wang[1], Zhenghong Li[1], Mengting Wang[1], Yun Ren[1*] and Qiang Li[1*]

[1]Chongqing Key Laboratory for Germplasm Innovation for Special Aromatic Spice Plants, Institute of Special Plants, College of Landscape Architecture and Life Science, Chongqing University of Arts and Sciences, Chongqing, China, [2]College of Biology and Food Engineering, Chongqing Three Gorges University, Chongqing, China

Introduction: This study aimed to establish and verify a critical nitrogen dilution model for different organs of maize varieties with different nitrogen efficiencies and clarify differences in nitrogen nutritional characteristics.

Methods: Two maize varieties (nitrogen-efficient variety ZH 311 and nitrogen-inefficient variety XY 508) were grown under four nitrogen levels to evaluate N dynamics and dry matter accumulation.

Results: The results showed that the critical nitrogen concentration dilution curves based on root dry matter, stem-sheath dry matter, leaf dry matter, and plant dry matter, with coefficient of determination (R^2>0.90), all reached significant levels and could be used for nitrogen nutrition diagnosis of maize. However, a and b values of the critical nitrogen concentration models for different organs differed significantly; e.g., the root model had the lowest a value and the leaf model had the lowest b value. ZH 311 exhibited higher a values and lower b values (except in roots) than XY 508. The model established on ZH 311 based on stem-sheath had the highest stability, and the model established on XY 508 based on leaf had the highest stability. Relative yield (RY), nitrogen nutrition index (NNI), and cumulative nitrogen deficit (AND) were significantly correlated at different growth stages of different organs (R^2>0.80) using each critical nitrogen concentration dilution curve to predict yield.

Discussion: In the high-nitrogen efficiency variety ZH 311, roots, stem-sheath, leaves, and plants showed weaker responses to AND than those of the low nitrogen-efficiency variety ZH 311 with at all growth stages. ZH 311 roots

exhibited stronger responses to NNI at the early growth stage, and stem-sheath, leaves, and plants had stronger responses to NNI at the later growth stage, indicating that the high nitrogen-efficiency variety ZH 311 was not sensitive to nitrogen deficiency and was more efficient for nitrogen nutrition.

KEYWORDS

maize, nitrogen efficiency, different organs, nitrogen critical dilution curve, nitrogen nutrition index, nitrogen deficiency

1 Introduction

The global annual output of maize (*Zea mays* L.) exceeds 12×10^8 t, accounting for more than 40% of total global food production, making it the largest food crop globally (Sun et al., 2024). High and stable maize yields are crucial for global food security and animal husbandry (Ray et al., 2013). By 2050, global food production must increase by 100% to meet the needs of the global population; however, due to urbanization, farmland degradation, and environmental damage, the arable land area in China is decreasing at a rate of 2.67×10^5 ha/year, with a decrease of about 30% from 1986 to 2020 (Tilman et al., 2011; Li, 2017; Tu et al., 2024). China is the world 's second largest producer of maize; the area of maize planted and its yield in China represent 22% and 24% of the global total, respectively, and it thus makes significant contributions to global maize production (Tian et al., 2020). Therefore, effectively increasing the maize yield per unit area is crucial for ensuring global food security.

Nitrogen application is the simplest and most efficient way to increase crop yield per unit area; however, excessive nitrogen application leads to resource wastage, environmental pollution, and increased production costs (Ma and Diao, 2018). Therefore, diagnosing nitrogen nutrition in crop production and scientific and reasonable nitrogen fertilizer application according to the nitrogen requirement characteristics of different crops at different growth stages have important strategic significance for improving crop yield and nitrogen-use efficiency and realizing high agricultural efficiency, environmental protection, and sustainable development. The critical nitrogen concentration refers to the minimum nitrogen concentration when a crop or certain organ of a crop obtains the maximum biomass during a certain growth period (Li et al., 2015a), and is widely used to assess the nitrogen nutrition status of crops (Zhao et al., 2017; Yue et al., 2016). Tian et al. (2019) established a relationship between the wheat nitrogen nutrition index (NNI) and relative yield (RY) based on a critical nitrogen concentration curve, which can be used for accurate field nitrogen management of wheat. Xue et al. (2006) established a critical post-flowering nitrogen concentration dilution curve model for cotton that can be used to assess post-flowering nitrogen requirements and dynamically monitor nitrogen nutrition to guide timely and accurate fertilization (Wang et al., 2015). Various characteristics (nitrogen-efficiency differences), environmental changes (ecological points and management levels), and model optimization put forward higher requirements for the parameters of the critical nitrogen concentration dilution curve. Therefore, establishing critical nitrogen concentration dilution curves based on dry matter in different organs (rather than traditional plant dry matter) can not only clarify differences in nitrogen nutrition characteristics of various organs but can also help to investigate the physiological function differences of crop nitrogen dynamics resulting from the genotype and environment (Lu et al., 2007).

Breeding and promotion of nitrogen-efficient maize varieties are the most direct and effective means by which to increase maize yield per unit area and reduce nitrogen fertilizer use (Wang et al., 2012). There have been many reports on differences in dry matter accumulation, carbon and nitrogen metabolism, and yield formation of maize varieties with different nitrogen efficiencies; However, studies on differences in critical nitrogen dilution models and nitrogen nutrient characteristics of varieties with different nitrogen efficiency are limited, and current models have limitations, mainly reflected in the failure to consider differences in nitrogen uptake, distribution and metabolism among different maize varieties and their organs. In addition, most models assume a linear relationship between nitrogen concentration and biomass accumulation (Yang et al., 2014). It ignores the complex interactions between nitrogen, carbon and other nutrients. This indicates that the effect of nitrogen efficiency on the critical nitrogen concentration of crops (Nc) model has not been fully explored, and more targeted models need to be developed to accurately predict nitrogen dynamics and optimize nitrogen management, thereby improving crop yield and nitrogen use efficiency (Wang et al., 2019; Liu et al., 2020). Therefore, in this study, maize varieties with different nitrogen efficiencies were used, and critical nitrogen dilution curves were established and verified based on the relationship between the nitrogen concentration and dry matter mass of each organ to clarify differences in the critical nitrogen dilution models of various organs of maize varieties with different nitrogen efficiencies. On this basis, NNI and the cumulative nitrogen deficit (AND) were used to estimate maize yield at key growth stages. A critical nitrogen dilution model was used to calculate the nitrogen production capacity of maize varieties with different nitrogen efficiencies, and differences in their nitrogen nutrient characteristics were identified. This study systematically

compared the critical nitrogen dilution models and nitrogen nutrient characteristics of maize varieties with different nitrogen efficiencies for the first time, providing a comprehensive method for diagnosing plant nitrogen status and guidance for precise nitrogen management at each key maize growth stage.

2 Materials and methods

2.1 Study area and climate

The experiment was conducted at the experimental base of Chongqing University of Arts and Sciences, Wujian Town, Yongchuan District, Chongqing (29°21'N, 105°54'E, altitude 343.5 m), which has a subtropical monsoon climate.

2.2 Experimental details

The experimental materials were maize varieties with different nitrogen efficiencies selected from previous experiments: nitrogen-efficient variety Zhenghong 311 (ZH 311), and nitrogen-inefficient variety Xianyu 508 (XY 508). These two varieties have similar growth periods in southwestern China (i.e., approximately 120 d). The experiment was conducted during three consecutive maize seasons from April, 2019 to August, 2021 (Figure 1 shows the weather data of crop growth period). The previous crop was a vegetable, and the soil was purple (Regosols). Basic soil samples were collected from the 0–30 cm soil layer with organic matter content of 16.14 g·kg^{-1}, total nitrogen content of 1.63 g kg^{-1}, total phosphorus of 0.62 g kg^{-1}, total potassium content of 11.55 g·kg^{-1}, alkaline hydrolytic nitrogen content of 48.72 mg kg^{-1}, available phosphorus content of 2.68 mg kg^{-1}, available potassium content of 145.21 mg kg^{-1}, and pH of 7.92. The experiment followed a two-factor randomized design with two maize varieties (ZH 311 and XY 508) and four nitrogen fertilizer levels (N1: 0 kg·ha^{-1}, N2: 120 kg·ha^{-1}, N3: 240 kg·ha^{-1}, N4: 360 kg·ha^{-1}). Each treatment included 3 replicates, with a total of 24 (8×5 m=40 m^2) plots, the plant spacing is 25 cm. Maize was planted in wide and narrow rows (1.4 and 0.6 m, respectively) with a density of 52500 plants·ha^{-1}. According to the experimental treatment, nitrogen fertilizer was applied in equal amounts before seeding and V12, and phosphate (containing 12.0% P_2O_5) and potassium fertilizers (containing 60.0% K_2O) were used as base fertilizers; application amounts were 600 kg·ha^{-1} of superphosphate and 150 kg ha^{-1} of potassium chloride, respectively. Urea was used as the nitrogen fertilizer (containing 46.4% N).

Maize was sown on March 27, 2019, March 26, 2020, and March 28, 2021, and seedlings were set at the three-leaf stage; maize was harvested on July 29, 2019, July 30, 2020, and July 31, 2021, respectively. Standard field management practices (scheduled irrigation, balanced fertilization, and soil tillage) and integrated pest management strategies (combination of biological control agents and selective pesticides) were implemented in accordance with the Chongqing High-Yield Cultivation Technical Regulations.

2.3 Field measurement and index determination

In the V6, V12, R1, R3, and R6 stages (representing the maize jointing, large horn, silking, filling, and maturity stages, respectively), five representative plants with uniform growth were selected from each plot, and divided into roots (Specifically, a soil column with a length of 0.3 m, width of 0.1 m, and depth of 80 cm was excavated with an iron plate root picker centered on a single plant), stem-sheath, leaves, and ears. Samples were defoliated at 105°C for 30 min, then dried at 80°C to a constant weight and weighed, and dry matter accumulation in roots, stem-sheath, leaves, and individual plants was measured (Figure 2 shows the experiments and technical flowchart of this study). Samples were then crushed through a 60-mesh sieve and the nitrogen concentration in each organs was determined using the Kjeldahl method with reference to Li et al. (2023). The nitrogen concentration per plant was determined as total nitrogen accumulation per plant/total dry matter accumulation per plant.

At maturity, 30 consecutive ears were harvested from each plot for drying and threshing, and the yield of each treatment was calculated based on a water content of 14%.

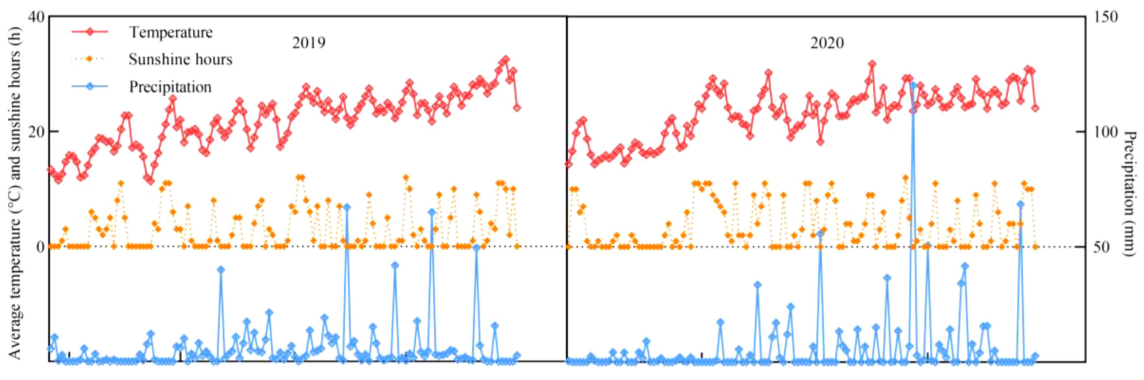

FIGURE 1
Meteorological factors during maize growth.

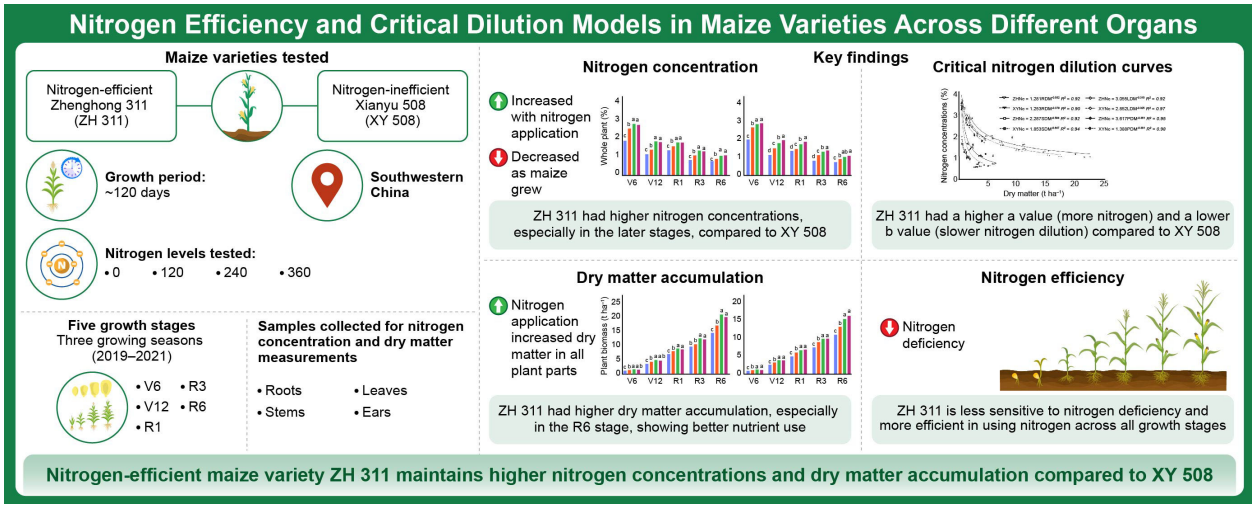

FIGURE 2
Experiments and technical flowchart of this study.

2.4 Critical nitrogen dilution model

2.4.1 Model construction

The critical nitrogen concentration dilution curve was modeled according to the methodology proposed by Justes et al. (1994). The specific steps applied in this study were as follows: (1) individual plant dry matter (root, stem-sheath, and leaf dry matter) treated with different nitrogen concentrations were divided into nitrogen-limited and non-nitrogen-limited nutrient groups using analysis of variance; (2) linear fitting of dry matter and the nitrogen concentration in the nitrogen-limited nutrient group was carried out, and the dry matter of the non-limited nitrogen nutrient group was averaged and the curve perpendicular to the horizontal axis. The intersection of the two lines corresponded to the critical nitrogen concentration.

Maize critical nitrogen concentration dilution curve model:

$$N_c = aDM^{-b} \tag{1}$$

Here, N_c represents the critical nitrogen concentration of crops; DM is the dry matter of each organ (t ha^{-1}); parameter a represents the critical nitrogen concentration corresponding to each part of maize when the dry matter of each part is 1 t, and; parameter b is the statistical parameter of the slope of the dilution curve of the critical nitrogen concentration.

2.4.2 Model verification

The root mean square error (RMSE) and normalized root mean square error (n-RMSE) (Yang et al., 2000) were adopted for model evaluation, These metrics were calculated using Equations 2, 3:

$$\mathrm{RMSE} = \sqrt{\frac{\sum_{i=1}^{n}(Oi - Pi)^2}{n}} \tag{2}$$

$$n - \mathrm{RMSE} = \frac{\mathrm{RMSE}}{\mathrm{S}} \times 100\,\% \tag{3}$$

where Oi and Pi are measured and simulated values of the critical nitrogen concentration, respectively; n is the sample size, and; S is the average value of the measured data. Model stability was measured according to the standard proposed by Jamieson et al. (1991), i.e., model stability is excellent if n-RMSE<10%; model stability is good if 10%<n-RMSE<20%; model stability is general if 20%<n-RMSE<30%, and; model stability is poor if n-RMSE>30%.

2.5 Correlation calculations

Referring to the NNI model described by Lemaire et al. (2008), Equation 4 defines the NNI:

$$\mathrm{NNI} = \frac{\mathrm{Na}}{Nc} \tag{4}$$

where NNI is the nitrogen nutrient index; Na is the measured nitrogen concentration, and; Nc is the critical nitrogen concentration. Nitrogen nutrition was optimal when NNI=1, excessive when NNI>1, and insufficient when NNI<1. Equation 5 calculates the absolute nitrogen deficit (AND):

$$\mathrm{AND} = N_{\mathrm{cna}} - N_{\mathrm{na}} \tag{5}$$

Here, AND is the nitrogen deficit (kg ha^{-1}); N_{cna} is the crop nitrogen accumulation under the critical nitrogen concentration (kg ha^{-1}), and; N_{na} is actual crop nitrogen accumulation (kg ha^{-1}). The nitrogen nutrition status was optimal when AND=0, and nitrogen accumulation was insufficient when AND>0 and excessive when AND<0.

According to the critical nitrogen dilution curve model, when a certain nitrogen concentration in a certain period is determined, the corresponding dry matter accumulation can be estimated and its level can determine the dry matter production capacity under the same nitrogen concentration. It is defined as the nitrogen dry matter production capacity (NDMP, t ha^{-1}) and was calculated using Equation 6:

$$NDMP = \sqrt[b]{\frac{a}{Nt}} \quad (6)$$

where Nt is the nitrogen concentration in each organ of the plant, and the a and b values are the same as those in Equation 1.

2.6 Data analysis

Excel 2013 was used for data sorting and analysis, and SPSS (version 26.0) was used for analysis of variance. Variance analysis was performed using the least significant difference for comparisons between treatments at $p<0.05$. Graphpad Prism 9.5 was used for drawing. Field data from 2019 and 2020 were used to build the model, while test data from 2021 were used to verify the model.

3 Results and analysis

3.1 Changes in nitrogen concentration in different growth periods of maize varieties with different nitrogen efficiencies

Nitrogen concentrations in maize roots, stem-sheath, leaves, and individual plants gradually decreased during growth (Figure 3). The root system area decreased from 1.81% in the V6 stage to 0.60% in the R6 stage. Stem-sheath thickness decreased from 3.39% in V6 stage to 0.23% in the R6 stage. The blade area decreased from 3.33% in the V6 stage to 0.81% in the R6 stage, and the rate per plant decreased from 2.83% in the V6 stage to 0.74% in the R6 stage. Nitrogen concentrations in the roots, stem-sheath, leaves, and individual plants of the N-treated maize significantly increased. Compared with N1, the roots of the two varieties increased by 51.92% in the V6 stage, 63.10% in the V12 stage, 43.87% in the R1 stage, 62.19% in the R3 stage, and 54.74% in the R6 stage. The results showed that nitrogen application had the greatest effect on root nitrogen concentrations in maize varieties in the V12 and R3 stages, with increases of>60%. The stem-sheath nitrogen concentration increased by 47.15%, 63.31%, 71.95%, 91.01%, and 42.62%, respectively, indicating that nitrogen application had the greatest effect on the concentration of stem-sheath nitrogen in the R1–R3 stages, with increases>70%. The leaf nitrogen concentration increased by 33.03%, 37.56%, 31.49%, 75.45%, and 32.40%, respectively, indicating that nitrogen application had the greatest effect on leaf nitrogen concentration during the R3 stage; the plant nitrogen concentration increased by 42.05%, 49.14%, 23.89%, 50.29%, and 32.10%, respectively, indicating that nitrogen application had the greatest effect on nitrogen concentration during the R3 stage.

On average, the root nitrogen concentration of ZH 311 (except in the V12 stage) was higher than that of XY 508; those in the V6, R1, R3, and R6 stages were 11.00%, 1.28%, 4.51% and 5.29% higher, respectively. The stem-sheath nitrogen concentration of ZH 311 was higher than that of XY 508 in all stages, and those in the V6, V12, R1, R3, and R6 stages were 1.58%, 3.08%, 5.22%, 15.29%, and 6.17% higher, respectively, than those of XY 508, indicating that ZH 311 maintained a higher stem- sheath nitrogen concentration than XY 508, particularly after the R3 stage. There was no significant difference in leaf nitrogen concentration between the two varieties in the V6-R3 stages, but at R6 stage, ZH 311 was significantly higher than XY 508 (13.94%), indicating that ZH 311 was more effective than XY 508 in maintaining leaf nitrogen concentration and delaying leaf senescence. The nitrogen concentration per plant in ZH 311 was lower than that in XY 508 in the V6 and V12 stages, but higher than that in XY 508 in the R1-R6 stages. The advantage of the nitrogen concentration per plant of ZH 311 was more obvious than that of XY 508 as the growth period was delayed, indicating that the nitrogen concentration per plant of ZH 311 had a certain advantage over XY 508 in the later growth period.

3.2 Changes in dry matter of maize varieties with different nitrogen efficiencies in different stages

Dry matter of maize root, stem-sheath, leaf, and individual plant increased gradually with growth, and the dry matter of maize root increased from 0.39 t ha^{-1} in the V6 stage to 1.98 t ha^{-1} in the R6 stage. Stem-sheath dry matter increased from 0.24 t ha^{-1} in the V6 stage to 5.30 t ha^{-1} in the R6 stage. Blade dry matter increased from 0.46 t ha^{-1} in the V6 stage to 2.38 t ha^{-1} in the R6 stage. Single plant dry matter increased from 1.09 t ha^{-1} in the V6 stage to 21.29 t ha^{-1} in the R6 stage (Figure 4). Roots, stem-sheath, leaves, and dry matter per plant in nitrogen-treated maize increased gradually. Compared with N1, the roots of the two varieties were 19.30% higher ($p<0.05$) in the V6 stage, 29.19% higher in the V12 stage, 14.77% higher in the R1 stage, 20.20% higher in the R3 stage, and 19.12% higher in the R6 stage. Stem-sheaths were 26.60% higher in the V6 stage, 29.59% higher in the V12 stage, 22.17% higher in the R1 stage, 21.59% higher in the R3 stage, and 44.25% higher in the R6 stage. The blades were 28.12% higher in the V6 stage, 24.90% higher in the V12 stage, 22.87% higher in the R1 stage, 18.88% higher in the R3 stage, and 38.95% higher in the R6 stage. Plants increased by 25.21% in the V6 stage, 27.68% in the V12 stage, 24.25% in the R1 stage, 22.78% in the R3 stage, and 34.58% in the R6 stage. Nitrogen application significantly promoted dry matter accumulation at different maize growth stages, and increases in the dry matter of the stem-sheath and whole plant were particularly significant in the R6 stage. These results indicated that appropriate nitrogen application could not only promote growth of each maize organ but also contribute to increasing dry matter with advancement of the growth cycle.

10.3389/fpls.2025.1577962

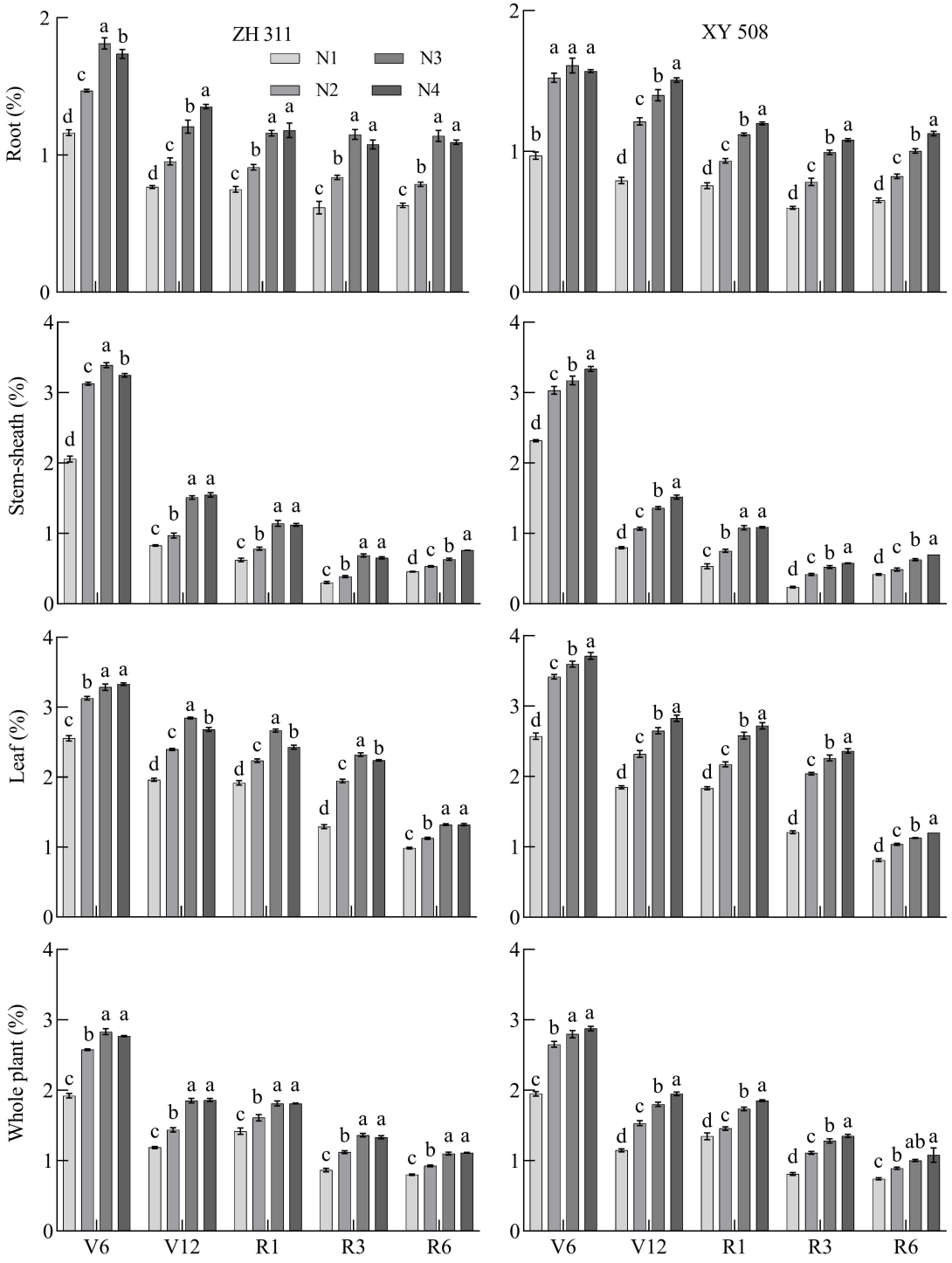

FIGURE 3
Changes in the nitrogen concentration in maize varieties with contrasting nitrogen efficiencies at different stages (Average data for 2019-2020). ZH 311–Zhenghong 311; XY 508–Xianyu 508; N1–0 kg·ha^{-1}; N2–120 kg·ha^{-1}; N3–240 kg·ha^{-1}; N4–360 kg·ha^{-1}; V6–jointing stage; V12–large horn stage; R1–silking stage; R3–filling stage; R6–maturity stage.

The average dry matter performance of the ZH 311 root system was significantly higher than that of XY 508 during the V6, V12, R1, R3, and R6 stages, during which the root dry matter quality was 12.22%, 16.09%, 18.70%, 10.63%, and 17.835 higher, respectively. ZH 311 roots had a stronger soil nutrient absorption capacity than XY 508 roots during the critical growth period. Similarly, the performance of ZH 311 in the stem-sheath and leaf was higher than that of XY 508 at all stages, particularly in the R6 stage; stem-sheath dry matter was 53.11% higher and leaf dry matter was 44.37% higher, indicating that ZH 311 had

10.3389/fpls.2025.1577962

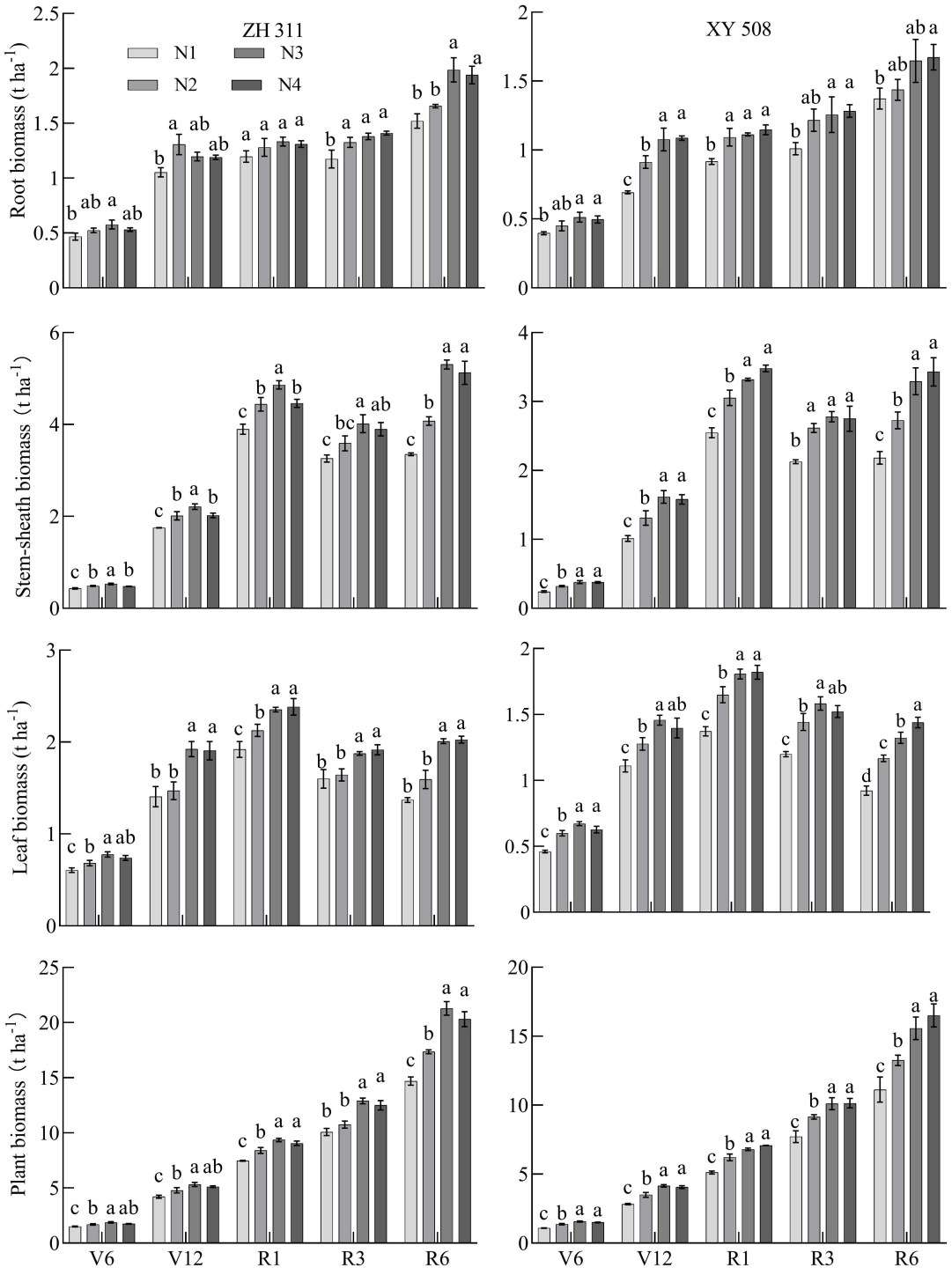

FIGURE 4
Changes of dry matter accumulation in maize cultivars with contrasting nitrogen efficiencies at different stages (Average data for 2019-2020). ZH 311–Zhenghong 311; XY 508–Xianyu 508; N1–0 kg·ha^{-1}; N2–120 kg·ha^{-1}; N3–240 kg·ha^{-1}; N4–360 kg·ha^{-1}; V6–jointing stage; V12–large horn stage; R1–silking stage; R3–filling stage; R6–maturity stage.

considerable advantages in nutrient absorption and resource utilization efficiency in the later growth period. The dry matter per plant of ZH 311 was higher than that of XY 508 from stages V6-R6, particularly in the R1 stage (35.41% higher), reflecting the comprehensive performance advantages of ZH 311 in late growth, particularly in terms of dry matter accumulation and nitrogen utilization, which have potential application value in improving crop yield and quality.

3.3 Construction of nitrogen critical dilution curve in different maize organs

The critical nitrogen concentration dilution curve (Figure 5) was established based on the relationship between the dry matter and nitrogen concentration of maize roots (RDM), stem-sheath (SDM), leaves (LDM), and plants (PDM); R^2 values of the critical nitrogen concentration dilution curve of each organ of the two varieties were>0.90. The critical nitrogen dilution curve parameters of the different maize organs differed significantly, among which plant dry matter had the highest a value (3.617 and 3.388), the root a value was the lowest (1.281 and 1.253), the stem-sheath a value was the highest (0.594 and 0.647), and the leaf a value was the lowest (0.315 and 0.325). There were also significant differences in critical nitrogen dilution curve parameters between the two maize varieties. The critical nitrogen concentration dilution curves for ZH 311 roots, stem-sheath, leaves, and plants (1.281, 2.287, 3.055, and 3.617, respectively) were higher than those for XY 508 (1.253, 1.853, 2.852, and 3.388, respectively). The critical nitrogen concentration dilution curve of the ZH 311 root system (0.552) was higher than that of the XY 508 root system (0.379), and those of the stem-sheath (0.594), leaf (0.315), and plant (0.361) were lower than those of XY 508 (0.647, 0.325, and 0.381, respectively).

3.4 Verification of critical nitrogen concentration dilution curve

The critical nitrogen concentration curve was verified using 2021 data. The results showed that the critical nitrogen concentration dilution curve could divide maize into growth conditions with and without nitrogen restriction. Under nitrogen restriction, all data points fell below the *Nc* dilution curve; whereas, without nitrogen restriction, all data points fell on or above the *Nc* dilution curve (Figure 6). Simultaneously, to verify the model accuracy, the measured dry matter data points were introduced into Equation 1 to calculate the simulated value of the critical nitrogen content, which was compared with the observed value (Table 1). Deviations based on the root and plant models of the two varieties were 10.85% and 9.50%, and 16.14% and 14.94%, respectively, and the stability of the<20% model was high; deviations based on the stem-sheath and leaf models were 6.77% and 8.64%, and 7.70%, and 5.15%, respectively, and the stability of the<10% model was excellent. Therefore, the critical nitrogen dilution curve model for different maize organs constructed in this study had high accuracy, indicating that the critical nitrogen concentration dilution curve for different organs of maize varieties with different nitrogen efficiencies constructed in this study can be used for nitrogen nutrition diagnosis of maize.

3.5 Relationship between NNI, AND, and RY

Relationships between NNI and RY and between RY and are shown in Figures 6 and 7. With an increase in NNI, RY exhibited a linear growth trend until it no longer increased with an increase in NNI, and its change trend presented a linear and stable mode. With an increase in AND, RY showed a trend of initially remaining constant and then decreasing linearly. Based on the critical nitrogen concentration dilution curve of root dry matter, the R^2 value

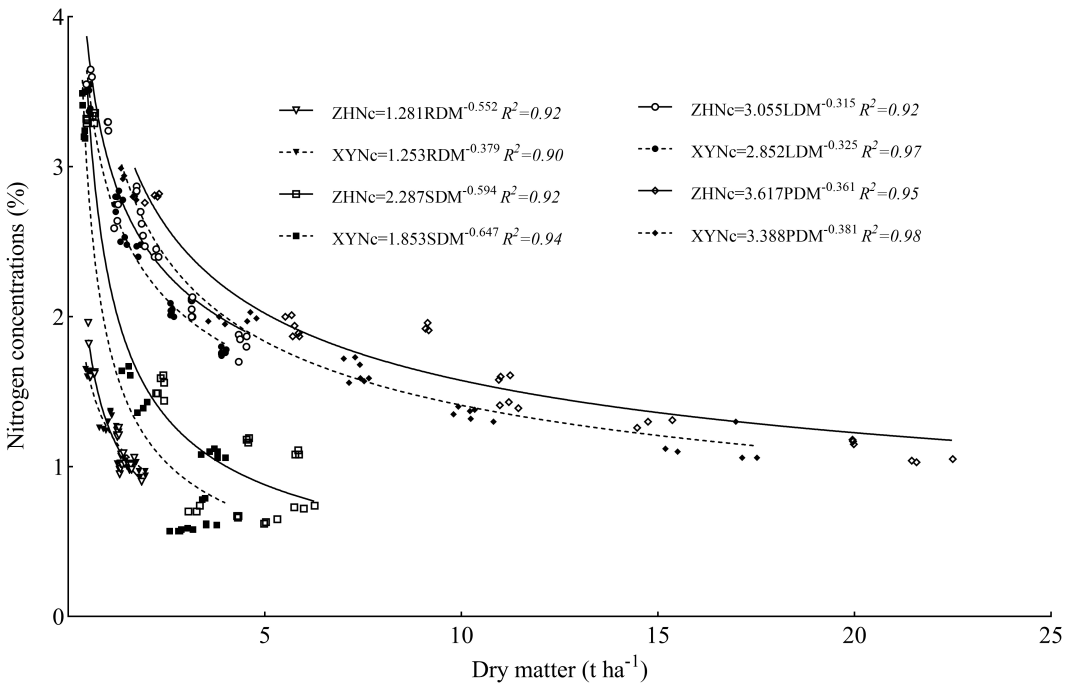

FIGURE 5
Nitrogen critical dilution curves in different maize organs.

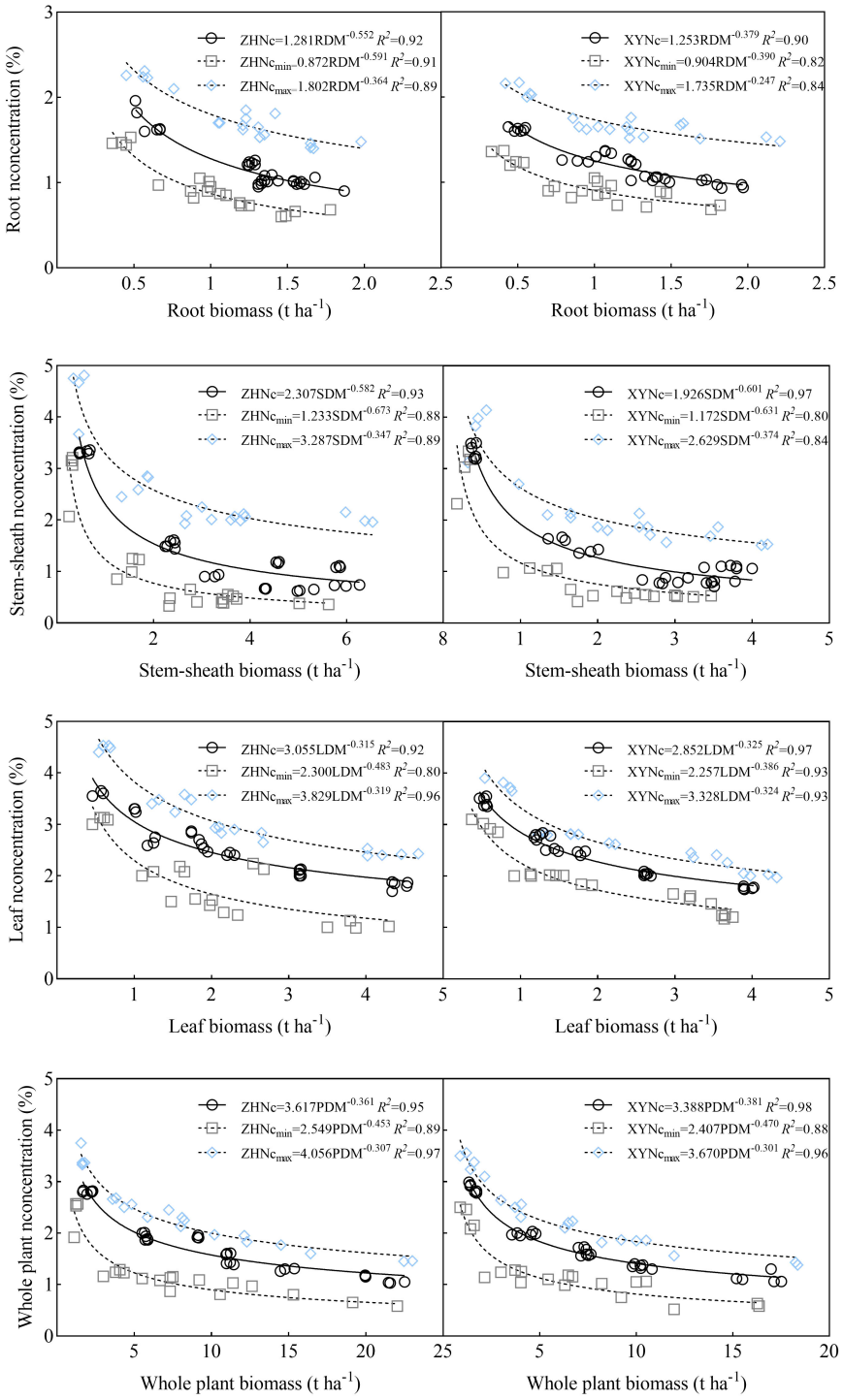

FIGURE 6
Critical nitrogen dilution curve validation.

between NNI, AND, and RY ranged from 0.815–0.984 and between AND and RY ranged from 0.818–0.988. Based on the critical nitrogen concentration dilution curve of the stem-sheath dry matter, the R^2 value between NNI and RY ranged from 0.852–0.985 and that between AND and RY ranged from 0.757–0.987. Based on the critical nitrogen concentration dilution curve of dry matter, the R^2 value between NNI and RY ranged from 0.853–0.994 and between AND and RY ranged from 0.735–0.991. Based on the critical nitrogen concentration dilution curve of plant dry matter, the R^2 value between NNI and RY ranged from 0.894–0.983 and that between AND and RY ranged from 0.890–0.984. Relationships among RY, NNI, and AND were determined based on the critical

TABLE 1 Observed and simulated values of critical nitrogen concentrations in maize.

Stage	Root				Stem-sheath				Leaf				Plant			
	ZH 311		XY 508		ZH 311		XY 508		ZH 311		XY 508		ZH 311		XY 508	
	OV	SV	OV	SV	OV	SV	OV	SV	OV	SV	OV	SV	OV	SV	OV	SV
V6	1.55	1.37	1.42	1.32	2.95	2.58	2.97	2.51	3.02	3.19	3.06	3.01	2.53	2.03	2.57	2.00
V12	1.07	1.34	1.23	1.29	1.22	1.28	1.19	1.26	2.13	1.68	2.05	1.88	1.64	1.11	1.55	1.12
R1	1.02	1.27	1.05	1.24	0.92	0.95	0.86	0.90	1.65	1.33	1.67	1.37	1.63	0.88	1.62	0.93
R3	0.92	1.23	0.88	1.22	0.51	0.52	0.44	0.48	1.51	1.23	1.51	1.25	1.18	0.76	1.13	0.83
R6	0.88	1.01	0.84	1.06	0.60	0.61	0.56	0.57	1.23	1.08	1.12	1.14	0.98	0.74	0.96	0.80
RMSE	0.118		0.103		0.084		0.104		0.147		0.097		0.257		0.234	
n-RMSE	10.85%		9.50%		6.77%		8.64%		7.70%		5.15%		16.14%		14.94%	

OV, Observed value; SV, Simulated value.

nitrogen concentration curves established for maize roots, stem-sheath, leaves, and plant dry matter. R^2 values of each organ of the two varieties were all > 0.70 in each stage; therefore, the effect on yield could be evaluated according to the nitrogen nutrient state (NNI and AND) of crop vegetative growth.

Further analysis showed that with an increase in NNI, maize RY first increased and then stabilized (Figure 7). At most growth stages, the RY of ZH 311 was higher than that of XY 508, and the curve of ZH 311 was generally steeper and had a higher slope than that of XY 508 (Figure 7), indicating that ZH 311 was able to use nitrogen more efficiently and convert it into biomass. The root difference between ZH 311 and XY 508 was greatest during the R1 stage, with ZH 311 showing higher RYs at an NNI of 1, suggesting that ZH 311 roots may be more efficient at absorbing nutrients when the nitrogen supply is adequate. The largest difference in stem-sheaths was during the R6 stage, when ZH 311 showed higher RYs at an NNI of 0.59, suggesting that ZH 311 stem-sheaths were more efficient in nutrient transport in the absence of nitrogen. The NNI yields of ZH 311 at different stages were higher than those of XY 508, and ranged from 0–1.5, indicating that ZH 311 leaves could photosynthesize more efficiently under deficient or sufficient nitrogen conditions. The largest difference in plant parts was observed between the V6 and V12 stages, and ZH 311 showed a higher RY at an NNI of 0.79, suggesting that whole ZH 311 plants could grow more efficiently in the absence of nitrogen. Overall, the yield advantage of ZH 311 over that of XY 508 was particularly significant, with higher nitrogen-use efficiency in R1 and R3 stages, better grain filling and ripening, and ultimately higher yields.

Differences were observed between ZH 311 and XY 508 in the root, stem-sheath, leaf, and plant yields depending on the crop growth stage (Figure 8). In roots and stem-sheaths, ZH 311 showed a high yield in both the V6 and V12 stages. This showed that ZH 311 had higher nitrogen-use efficiency and was able to use limited nitrogen resources more effectively to promote growth and development of organs such as roots and stem-sheaths. In leaves, ZH 311 and XY 508 showed the largest differences in yield during the R1 stage, and ZH 311 showed a smaller yield decline and higher R^2 value, indicating that it was better adapted to nitrogen deficiency and could reduce the effect on reproductive organ development through more efficient nitrogen use or distribution mechanisms. ZH 311 showed high yields in both the V6 and V12 stages, with the highest yield observed in the R6 stage. In summary, ZH 311 was more adaptable to nitrogen deficiency throughout the growth cycle, particularly during the reproductive growth phase; whereas, XY 508 showed high sensitivity to nitrogen deficiency during the early vegetative growth phase, which may affect its overall productivity. These results help elucidate the differences in nitrogen use and yield between the two varieties, as well as their performance at different growth stages and in different organs.

3.6 Differences in nitrogen dry matter production capacity of maize varieties with different nitrogen-use efficiencies

Nitrogen concentrations in maize roots, stem-sheaths, leaves, and individual plants gradually decreased with growth (Figure 3); whereas, dry matter gradually increased with growth (Figure 4). With a decrease in the nitrogen concentration, dry matter accumulation in maize roots, stem-sheaths, leaves, and individual plants increased significantly; however, there were significant differences among the varieties (Table 2). In ZH 311, root (except in R3 and R6 stages), stem-sheath, leaf, and single plant NDMP were significantly higher than those of XY 508, and NDMP was 55.17%, 33.33%, 13.33%, -6.38%, and -28.13% higher in V6, V12, R1, R3 and R6 stages, respectively; stem-sheath NDMP were 32.43%, 34.04%, 36.51%, 40.45%, and 46.04% higher, respectively; leaf NDMP were 22.64%, 23.26%, 26.0%, 32.22%, and 32.55% higher, respectively. Plant NDMP was 21.74%, 25.23%, 29.32%, 38.87%, and 43.13% higher, respectively, indicating that the nitrogen-efficient variety ZH 311 had stronger dry matter production capacity than the nitrogen-efficient variety XY 508 at the same nitrogen concentration, and that the differences in nitrogen dry matter production capacity of stem-sheath, leaves, and individual plants increased with decreases in the nitrogen concentration.

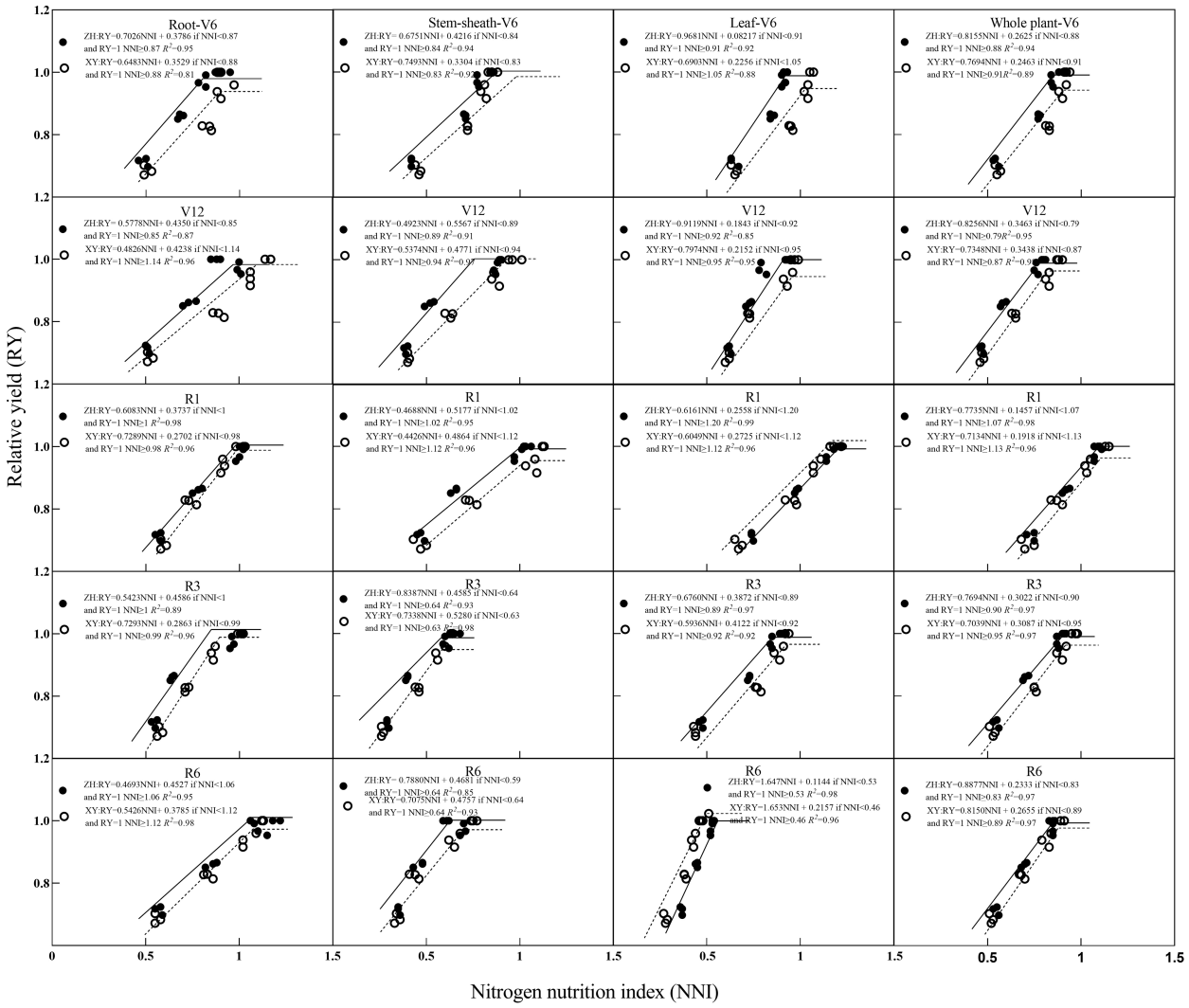

FIGURE 7
Relationships between relative yield (RY) and nitrogen nutrition index (NNI) obtained from critical nitrogen concentration curves. V6–jointing stage; V12–large horn stage; R1–silking stage; R3–filling stage; R6–maturity stage.

4 Discussion

4.1 Establishment of critical nitrogen concentration dilution curves for different maize organs

Nitrogen nutrition diagnosis and nitrogen nutrition status of crops can be determined by establishing a crop critical nitrogen concentration dilution curve (Cao et al., 2020; Li et al., 2015b). Previous studies have established and verified a series of critical nitrogen concentration dilution curves based on leaf (Jia and Fu, 2020), stem-sheath (Lu et al., 2019), ear (Li et al., 2015a), and leaf areas (Lu et al., 2021) of plants. However, because of the differences in nitrogen absorption, distribution, and utilization of various plant indices, models of critical nitrogen dilution curves for various organs differed significantly (An et al., 2019). In this experiment, the determination coefficients (R^2>0.90) of the critical nitrogen concentration dilution curves established based on RDM, SDM, LDM, and PDM all reached significant levels and had higher inter-year stability, which could be used for diagnosing maize nitrogen nutrition in Southwest China. Values of parameters a and b of the critical nitrogen concentration models based on RDM, SDM, LDM, and PDM differed significantly, among which the a value of the root model was the smallest, which is consistent with the results of Lan et al. (2022). Because the root biomass was significantly lower than that of other organs, and its nitrogen concentration in the early growth stage was also significantly lower than that of other organs, the dilution effect of nitrogen concentration was lower and sensitivity was higher. The b value based on the leaf model was the lowest, which was consistent with the results of Su et al. (2021) and Ata et al. (2017). Because leaves are the most important metabolic organs of plants, a large amount of nitrogen is transferred from plant roots and stem-sheath to leaves during growth to maintain their high nitrogen concentrations and ensure

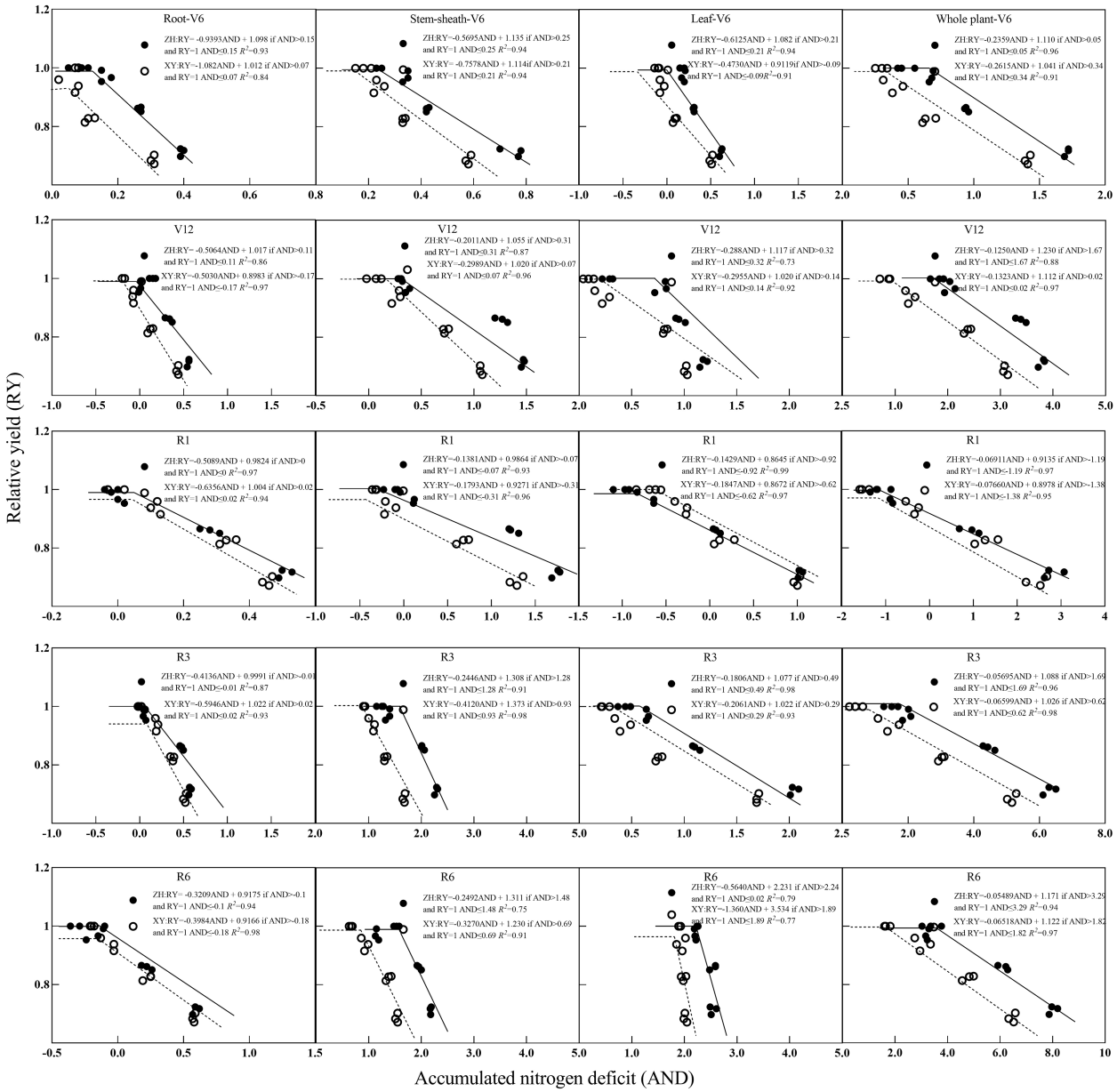

FIGURE 8
Relationships between relative yield (RY) and accumulated nitrogen deficit (AND) obtained from critical nitrogen concentration curves. V6–jointing stage; V12–large horn stage; R1–silking stage; R3–filling stage; R6–maturity stage.

efficient operation of photosynthesis; therefore, the reduction in the leaf nitrogen concentration was much lower than that of roots and stem-sheaths (Lu et al., 2024). The results of this experiment also showed that the nitrogen concentration in maize leaves at each stage was significantly higher than that in the roots and stem-sheaths, further confirming the above conclusion.

Further analysis showed that the a value of the critical nitrogen concentration dilution model for all organs of the nitrogen-efficient variety ZH 311 was higher than that of the nitrogen-inefficient variety XY 508, which was inconsistent with the results of An et al (An et al., 2019; Zhao et al., 2022), mainly because the nitrogen-efficient variety ZH 311 selected in this experiment was a nitrogen-efficient absorption type. The nitrogen concentration per unit biomass (parameter a) of ZH 311 was higher than that of XY 508, which was beneficial for maintaining a higher nitrogen concentration and delaying aging of various organs during later growth periods. Previous studies have found that ZH 311 has advantages over XY 508 in dry matter production, nitrogen accumulation, and yield, mainly because of the later growth period (Li et al., 2016a, Li et al., 2016b), which also supports this conclusion. Furthermore, the b value of the critical nitrogen concentration dilution model for all organs of the nitrogen-efficient variety ZH 311 (except roots) was lower than that of the nitrogen-inefficient variety XY 508, which is consistent with the results of Du et al. (2020). The nitrogen-efficient variety was able to absorb and utilize nitrogen more effectively, thereby slowing the

TABLE 2 Differences in nitrogen dry matter production capacity (NDMP) of maize varieties with contrast nitrogen efficiency.

Different stage	Nitrogen content (g kg^{-1})	Root (t ha^{-1})		Nitrogen content (g kg^{-1})	Stem-sheath (t ha^{-1})		Nitrogen content (g kg^{-1})	Leaf (t ha^{-1})		Nitrogen content (g kg^{-1})	Plant (t ha^{-1})	
		ZH	XY		ZH	XY		ZH	XY		ZH	XY
V6	2.0	0.45a	0.29b	3.5	0.49a	0.37b	3.5	0.65a	0.53b	3.0	1.68a	1.38b
V12	1.7	0.60a	0.45b	3.0	0.63a	0.47b	3.0	1.06a	0.86b	2.5	2.78a	2.22b
R1	1.4	0.85a	0.75b	2.5	0.86a	0.63b	2.5	1.89a	1.50b	2.0	5.16a	3.99b
R3	1.1	1.32b	1.41a	2.0	1.25a	0.89b	2.0	3.84a	2.98b	1.5	11.45a	8.49b
R6	0.8	2.35b	3.27a	1.5	2.03a	1.39b	1.5	9.57a	7.22b	1.0	35.21a	24.60b
	Mean	1.11 b	1.23a		1.05a	0.75b		3.40a	2.62b		11.26a	8.23b

nitrogen dilution rate and increasing its stem, leaf, and plant nitrogen concentrations compared to those of the nitrogen-inefficient variety. This is particularly consistent with the results of this experiment during the later growth period (Li et al., 2022). The root b value of the high nitrogen efficiency varieties was higher than that of the low nitrogen efficiency varieties, which was conducive to maintaining a higher nitrogen concentration in the early growth stage, improving nitrogen accumulation, and promoting morphogenesis; whereas, the nitrogen concentration decreased rapidly in the later growth stage, improving nitrogen transport and utilization. Therefore, the root nitrogen concentration of ZH 311 in the early growth stage was significantly higher than that of XY 508 in later growth stages. Consistent with the results of Du et al. (2020), this study demonstrated efficient nitrogen use in nitrogen-efficient varieties.

In addition, the *n*-RMSE evaluation model was used to prove that the nitrogen-efficient variety ZH 311 had the highest stability based on the stem-sheath (*n*-RMSE=6.77%), which was consistent with the results of Su et al. (2021) This was mainly because the difference in nitrogen efficiency was mainly caused by the difference in stems rather than those in leaves. This reflected the high nitrogen dilution rate (i.e., the highest b value) of the maize stem-sheath, which, on the one hand, is related to rapid dry matter accumulation in the stem-sheath of nitrogen-efficient varieties; on the other hand, it reflected the efficient post-flowering nitrogen transport of nitrogen-efficient varieties to the ear to maintain rapid grain growth, which is consistent with the higher nitrogen transport efficiencies of nitrogen-efficient maize varieties than those of nitrogen-inefficient varieties. The model stability of the nitrogen-inefficient variety XY 508 based on leaves was the highest (*n*-RMSE=5.15%), which is consistent with the results of Fu et al. (2020), where the low nitrogen-efficiency variety XY 508 had the highest leaf a value, highest demand for nitrogen concentration per unit biomass, lowest leaf b value, and lowest nitrogen dilution rate. Nitrogen was preferentially transferred to the leaves during the later growth period to maintain the nitrogen concentration during this period. Therefore, leaf senescence during the late growth period is key to limiting yield in nitrogen-inefficient varieties (Kosgey et al., 2013; Mu et al., 2015).

4.2 Differences in nitrogen nutrition characteristics in different maize organs

A relationship model between crop NNI, AND, and RY can be constructed to effectively evaluate the nitrogen nutrition status of crops and its effect on yield (Zhao et al., 2017; Yao et al., 2014; Zhang et al., 2024). Previous studies have established a series of relationship models between NNI, AND, and RY based on differences in nitrogen uptake and utilization of different crops or crops at different growth stages (Zhao et al., 2022; Wang et al., 2010) however, obvious differences exist in nitrogen uptake, distribution, and utilization of different crops or crops at different growth stages. Therefore, the applicability and accuracy of this model must be further verified (Zhao et al., 2018). In this experiment, the relationship models of NNI, AND, and RY established based on maize RDM, SDM, LDM, and PDM reached a significant determination coefficient (R^2>0.80), which is consistent with the results of Su et al. (2021), indicating that the relationship models of NNI, AND, and RY showed high stability at different growth stages and in different maize organs. The model can be used to evaluate the nitrogen nutritional status of maize; however, there are obvious differences between organs and varieties. The response of maize roots to NNI was strong in the early growth stage and AND gradually weakened in later growth stages; whereas, the response to AND was weak in the early growth stage and gradually enhanced in the later growth stage, which is consistent with the results of Guo et al. (2024) and Wang et al. (2011) Nitrogen absorbed by roots in the early growth stage was mainly used for root morphogenesis and maintenance of its physiological function; whereas, in the later growth stage, root nitrogen was rapidly transferred to the kernel, and the nitrogen content decreased rapidly. The response of yield to root NNI was weakened and the response to AND was enhanced (Ata et al., 2014; Peng et al., 2009; Chun et al., 2005; Gao et al., 2023). In the early growth stage, the responses of the stem-sheath to NNI and AND were weak and gradually increased in the later growth stage, which is consistent with

the results of Wang et al. (2010) In the early growth stages, plants preferentially allocate nitrogen to the roots and leaves to promote establishment of absorbing and photosynthetic organs. As an organ for nutrient and substance transport, the nitrogen status of the stem-sheath directly affects the grains. The response of leaves to NNI was strong in all stages; whereas, the response to AND was weak in the early stage and gradually increased in the later stage, which is consistent with the results of Su et al. (2021). As the most important photosynthetic organ of plants, plants preferentially distribute nitrogen to leaves during the vegetative growth stage, which not only contributes to chlorophyll synthesis but also improves photosynthetic efficiency. It can also significantly improve dry matter accumulation (Bian et al., 2019).

Further analysis of the relationship model of NNI, AND, and RY showed that ZH 311 roots, stem-sheath, leaves, and plants with high nitrogen efficiency were less responsive to AND than those of ZH 311 with low nitrogen efficiency at each growth stage; whereas, ZH 311 roots had a stronger response to NNI at the early growth stage, and stem-sheath, leaves, and plants had a stronger response to NNI at the later growth stage. The results showed that nitrogen-efficient varieties were not sensitive to nitrogen deficiency and were more efficient in nitrogen nutrition, which is consistent with the results of Qu et al. (2016) Nitrogen-efficient varieties have superior root structures, higher root biomass, and increased nitrogen uptake (Liu et al., 2019, Liu et al., 2022). Furthermore, these varieties have a stronger nitrogen transport capacity in the stem-sheath and leaves, which promotes efficient nitrogen use and results in each organ having a higher nitrogen concentration, which is insensitive to nitrogen deficiency (Hao et al., 2011; Du et al., 2024), has more efficient nitrogen nutrition, and can maintain higher dry matter accumulation and yield under nitrogen deficient conditions. We also found that under the same nitrogen concentration condition, the nitrogen dry matter production capacities (NDMP) of stem-sheath, leaves, and plants in different growth stages of the nitrogen-efficient variety ZH 311 were significantly higher than those of nitrogen-inefficient variety XY 508, which was consistent with the results of Ji et al (2014) in a study on rice. From another perspective, this study proved that the nitrogen efficient varieties were insensitive to nitrogen deficiency and efficient use of nitrogen nutrition.

5 Conclusion

In this study, critical nitrogen concentration dilution curves were established based on different organs of maize varieties with different nitrogen efficiencies, and the coefficients of determination (R^2>0.90) reached significance, which could be used for diagnosing maize nitrogen nutrition. The critical nitrogen dilution curves of the different organs of maize varieties with different nitrogen efficiencies differed significantly. The critical nitrogen concentration dilution model of each organ of the maize variety with high nitrogen efficiency, ZH 311, had a higher value than that of the maize variety with low nitrogen efficiency, XY 508, which was conducive to maintaining a higher nitrogen concentration in each organ during the later growth period and delayed aging of each organ. A lower b value (except for the roots) can slow the nitrogen dilution rate and maintain the nitrogen concentration in each organ. Further analysis showed that the nitrogen-efficient variety ZH 311 had the highest stability based on the stem-sheath, and XY 508 had the highest stability based on the leaves. RY, NNI, and AND were significantly correlated at different growth stages of different organs (R^2>0.80) using each critical nitrogen concentration dilution curve to predict yield. ZH 311 roots, stem-sheath, leaves, and plants with high nitrogen efficiency showed weaker responses to AND than those of ZH 311 with low nitrogen efficiency at all growth stages, and ZH 311 roots had stronger responses to NNI at the early growth stage, and the stem-sheath, leaves, and plants had stronger responses to NNI at the later growth stage, indicating that ZH 311 with high nitrogen efficiency was not sensitive to nitrogen deficiency and was more efficient for nitrogen nutrition. However, the research is limited by the singleness of varieties, the lack of analysis of environmental interaction and the lack of physiological mechanism. In the future, it is necessary to expand the universality of genetic and environmental diversity verification models and develop precise nitrogen diagnosis tools based on organ CNDCs to optimize maize nitrogen management strategies.

Data availability statement

The original contributions presented in the study are included in the article/supplementary material. Further inquiries can be directed to the corresponding authors.

Author contributions

SB: Project administration, Writing – original draft. XC: Supervision, Writing – review & editing. LL: Funding acquisition, Writing – review & editing. XL: Investigation, Supervision, Writing – review & editing. LS: Investigation, Methodology, Writing – review & editing. XD: Methodology, Project administration, Writing – review & editing. SL: Data curation, Methodology, Writing – review & editing. HL: Data curation, Software, Writing – review & editing. HW: Data curation, Software, Writing – review & editing. ZL: Formal analysis, Investigation, Methodology, Writing – review & editing. MW: Investigation, Software, Writing – review & editing. QL: Writing – review & editing, Funding acquisition. YR: Writing – review & editing, Supervision.

Funding

The author(s) declare that financial support was received for the research and/or publication of this article. This study was supported by the Scientific and Technological Research Program of the Chongqing Municipal Education Commission (KJQN202201305), Natural Science Foundation of Chongqing (cstc2019jcyj-msxmx0803), Projects for Innovative Research Groups of Chongqing Universities (CXQT21028), and Chongqing Talent Program for Zexiong Chen., the Science and Technology Program

of Sichuan Province: Research and Development of New Varieties of Cyathula officinalis and Enhancement of Key Industrial Technologies (Project Number: 2023YFS0341) and the Science and Technology Program of Xichang City(Grant No. NYKJ-2024-03), the Academician Expert Workstation of Yunnan Province (to Han Lan, Grant No. 202305AF150052).

Conflict of interest

The authors declare that the research was conducted in the absence of any commercial or financial relationships that could be construed as a potential conflict of interest.

Generative AI statement

The author(s) declare that no Generative AI was used in the creation of this manuscript.

Publisher's note

All claims expressed in this article are solely those of the authors and do not necessarily represent those of their affiliated organizations, or those of the publisher, the editors and the reviewers. Any product that may be evaluated in this article, or claim that may be made by its manufacturer, is not guaranteed or endorsed by the publisher.

References

An, Z. C., Huang, Y. F., Wang, Y., Zhao, Y. N., Yue, S. H., Shi, H. B., et al. (2019). Dilution model of critical nitrogen concentration and nitrogen nutrition diagnosis of summer maize with different nitrogen efficiency. *Plant Nutr. Fertilizer J.* 25, 123–133. doi: 10.11674/zwyf.18020

Ata, S. T., Zhu, Y., Liu, X., Cao, Q., Tian, Y., and Cao, W. (2017). Comparison of different critical nitrogen dilution curves for nitrogen diagnosis in rice. *Sci. Rep.* 7, 42679. doi: 10.1038/srep42679

Ata, S. T., Zhu, Y., Yao, X., and Cao, W. (2014). Determination of critical nitrogen dilution curve based on leaf area index in rice. *Field Crops Res.* 167, 76–85. doi: 10.1016/j.fcr.2014.07.010

Bian, S. N., Chang, P., Wang, N. H., Liu, Z. G., Zhang, M. R., Wu, J. S., et al. (2019). Leaf growth, chlorophyll fluorescence characteristics, and expression of photosystem-related genes in *Camptotheca acuminata* with different N forms'fertilization. *J. Zhejiang A F Univ.* 36, 908–916. doi: 10.11833/j.issn.2095-0756.2019.05.009

Cao, Q., Tian, X. S., Ma, J. F., Yao, X., Liu, X. J., Tian, Y. C., et al. (2020). Research progress in critical nitrogen dilution curve of three main grain crops in China. *J. Nanjing Agric. Univ.* 43, 392–402. doi: 10.7685/jnau.201907005

Chun, L., Chen, F. J., Zhang, F. S., and Mi, G. H. (2005). Root growth, nitrogen uptake and yield formation of hybrid maize with different N efficiency. *Plant Nutr. Fertilizer J.* 05), 615–619. doi: 10.11674/zwyf.2005.0508

Du, L. J., Li, Q., Li, L., Wu, Y. W., Zhou, F., Liu, B. X., et al. (2020). Construction of a critical nitrogen dilution curve for maize in Southwest China. *Sci. Rep.* 10, 13084. doi: 10.1038/s41598-020-70065-3

Du, K., Zhao, W. Q., Lv, Z. W., Xu, B., Zhou, Z. G., and Wang, Y. H. (2024). Optimal rate of nitrogen fertilizer improves maize grain yield by delaying the senescence of ear leaves and thereby altering their nitrogen remobilization. *Field Crops Res.* 310, 0378–4290. doi: 10.1016/j.fcr.2024.109359

Fu, J. P., Jia, B., Yang, W. W., Wei, X., Ma, C., Liu, G. H., et al. (2020). Development of critical nitrogen dilution curve based on leaf dry matter for maize under drip irrigation. *Chin. J. Appl. Ecol.* 31, 945–952. doi: 10.13287/j.1001-9332.202003.030

Gao, Y., Yan, Y. T., Zhao, G., Zhang, W. W., Dou, L. P., Li, K. F., et al. (2023). Regulation effects of nitrogen fertilizer management on grain yield formation and nitrogen transportation of spring maize in the Loess Plateau, China. *Chin. J. Soil Sci. Fertilizer* 06), 186–195. doi: 10.11838/sfsc.1673-6257.22328

Guo, C. X., Huang, G. J., Wang, Y. L., Guo, J. L., and Yang, Z. P. (2024). Construction and verification of critical nitrogen dilution curves for spring maize varieties with different nitrogen efficiencies. *Chin. J. Eco-Agriculture* 32, 1355–1365. doi: 10.12357/cjea.20240021

Hao, B. Z., Jiang, L., Fang, B. D., Zhang, Y. H., Zhang, H., Li, C. X., et al. (2011). Effect of different nitrogen supply on the temporal and spatial distribution and remobilization of canopy nitrogen in winter wheat under limited irrigation condition. *Acta Ecologica Sin.* 31, 4941–4951.

Jamieson, P. D., Porter, J. R., and Wilson, D. R. (1991). A test of the computer simulation model ARCWHEAT1 on wheat crops grown in New Zealand. *Field Crops Res.* 27, 337–350. doi: 10.1016/0378-4290%2891%2990040-3

Ji, L., Yang, H., Li, T. X., Zhang, X. Z., and Yu, H. Y. (2014). Dry matter production and nitrogen accumulation of rice genotypes with different nitrogen use efficiencies. *Acta Prataculturae Sin.* 3, 327–335. doi: 10.11686/cyxb20140639

Jia, B., and Fu, J. P. (2020). Critical nitrogen dilution curve of drip-irrigated maize at vegetativegrowth stage based on leaf area index. *Trans. Chin. Soc. Agric. Eng.* 36, 66–73. doi: 10.11975/j.issn.1002-6819.2020.06.008

Justes, E., Mary, B., Meynard, J. M., Machet, J. M., and Thelier-Huche, L. (1994). Determination of A critical nitrogen dilution curve for winter-wheat Crops. *Ann. Bot.* 74, 397–407. doi: 10.1006/anbo.1994.1133

Kosgey, J. R., Moot, D. J., Fletcher, A. L., and McKenzie, B. A. (2013). Dry matter accumulation and post-silking N economy of 'stay-green' maize (*Zea mays* L.) hybrids. *Eur. J. Agron.* 51, 43–52. doi: 10.1016/j.eja.2013.07.001

Lan, Y., Ji, L., Jia, B., Wei, X., Zhai, Y. Q., Yun, B. Y., et al. (2022). Construction of critical nitrogen dilution curve for maize under drip irrigation in Ningxia based on root biomass. *Chin. J. Ecol.* 41, 1448–1456. doi: 10.13292/j.1000-4890.202207.018

Lemaire, G., Jeuffroy, M. H., and Gastal, F. (2008). Diagnosis tool for plant and crop N status in vegetative stage: Theory and practices for crop N management. *Eur. J. Agron.* 28, 614–624. doi: 10.1016/J.EJA.2008.01.005

Li, Q. (2017). Response of maize varieties with different nitrogen efficiency to nitrogen fertilizer level and operation and differences in nitrogen uptake and utilization. *Sichuan Agric. University.*

Li, Z. P., Feng, H., and Song, M. D. (2015a). Critical nitrogen dilution curve and nitrogen nutrition index of winter wheat in guanzhong plain of winter wheat in guanzhong plain. *Trans. Chin. Soc. Agric. Machinery* 46, 177–183 + 273. doi: 10.6041/j.issn.1000-1298.2015.10.023

Li, X., Jiang, R., Hou, Y. P., He, P., Zou, G. Y., Xu, X. P., et al. (2023). Using DNDC model to study the potential of nitrogen fertilizer reduction in spring maize production under long-term straw return. *J. Plant Nutr. Fertilizers* 29, 2004–2017. doi: 10.11674 / zwyf.2023126

Li, Q., Ma, X. J., Cheng, Q. B., Dou, P., Yu, D. H., Luo, Y. H., et al. (2016a). Effects of nitrogen application on nitrogen utilization and nitrogen balance in fields of maize cultivars with different low nitrogen tolerance. *J. Soil Water Conserv.* 30, 7. doi: 10.13870/j.cnki.stbcxb.2016.03.030

Li, Q., Ma, X. J., Cheng, Q. B., Dou, P., Yu, D. H., Luo, Y. H., et al. (2016b). Effects of nitrogen fertilizer on post-silking dry matter production and leaves function characteristics of low-nitrogen tolerance maize. *Chin. J. Eco-Agriculture* 24, 17–26. doi: 10.13930/j.cnki.cjea.150744

Li, Q., Ren, Y., Fu, H., Li, Z. X., Kong, F. L., and Yuan, J. C. (2022). Cultivar differences in carbon and nitrogen accumulation, balance, and grain yield in maize. *Front. Plant Sci.* 13. doi: 10.3389/fpls.2022.992041

Li, Z. P., Song, M. D., and Feng, H. (2015b). Development and validation of critical nitrogen content curve for maize in Guanzhong area. *Trans. Chin. Soc. Agric. Eng.* 31, 135–141. doi: 10.11975/j.issn.1002-6819.2015.13.019

Liu, Z., Hao, Z., Sha, Y., Huang, Y. W., Guo, W. Q., Ke, L. H., et al. (2022). High responsiveness of maize grain yield to nitrogen supply is explained by high ear growth rate and efficient ear nitrogen allocation. *Field Crops Res.* 286, 0378–4290. doi: 10.1016/j.fcr.2022.108610

Liu, P. Z., Shi, Z. J., Ning, F., Wang, R., Wang, X. L., and Li, J. (2020). Critical nitrogen dilution curves and nitrogen nutrition diagnosis of spring maize under different precipitation patterns in Weibei dryland. *Acta Agronomica Sin.* 46, 1225–1237. doi: 10.3724/SP.J.1006.2020.03007

Liu, Z., Zhao, Y., Guo, S., Cheng, S., Guan, Y. J., Cai, H. J., et al. (2019). Enhanced crown root number and length confers potential for yield improvement and fertilizer reduction in nitrogen-efficient maize cultivars. *Field Crops Res.* 241, 0378–4290. doi: 10.1016/j.fcr.2019.107562

Lu, J. S., Geng, C. M., Cui, X. L., Li, M. Y., and Hu, T. T. (2021). Determination of summer maize leaf critical nitrogen dilution curve based on leaf area index. *Trans. Chin. Soc. Agric. Machinery* 52, 319–326. doi: 10.6041/j.issn.1000-1298.2021.04.034

Lu, X. J., Guo, X. Y., Wen, W. L., and Yu, Z. T. (2019). evelopment and validation of critical nitrogen dilution curve for spring maize in northeast China. *J. Agric. Sci. Technol.* 21, 77–83. doi: 10.13304/j.nykjdb.2018.0588

Lu, J. S., Hu, T. T., Li, Y., Cui, X. L., Cheng, M. H., Yan, S. C., et al. (2024). Effects of different water management strategies on critical nitrogen concentration dilution curves, nitrogen accumulation, and grain yield in winter wheat. *Agric. Commun.* 2, 2949–7981. doi: 10.1016/j.agrcom.2024.100052

Lu, Y. L., Lu, W. P., Liu, X. B., Wang, J. F., Liu, P., Lu, D. L., et al. (2007). The difference of nitrogen uptake and utilization in waxy corn III.Genetic differences in nitrogen distribution and translocation. *J. Plant Nutr. Fertilizers* 13, 86–92. doi: 10.11674/zwyf.2007.0115

Ma, K., and Diao, G. (2018). Research on the contribution rate of fertilizer to grain yield in China. *Plant Nutr. Fertilizer J.* 24, 1113–1120. doi: 10.11674/zwyf.17375

Mu, X. H., Chen, F. J., Wu, Q. P., Chen, Q. W., Wang, J. F., Yuan, L. X., et al. (2015). Genetic improvement of root growth increases maize yield via enhanced post-silking nitrogen uptake. *Eur. J. Agron.* 63, 55–61. doi: 10.1016/J.EJA.2014.11.009

Peng, Y. F., Zhang, W. P., and Li, C. J. (2009). Relationship between nitrogen efficiency and root architecture of maize plants: simulation and application. *Chin. J. Agric. Sci.* 42, 843–853. doi: 10.3864/j.issn.0578-1752.2009.03.011

Qu, J. W., Gao, J. L., Wang, Z. G., Yu, X. F., Hu, S. P., and Sun, J. Y. (2016). Genotype differences in root characteristics by maize and its relations to nitrogen uptake efficiency. *Maize Sci.* 24, 72–78. doi: 10.13597/j.cnki.maize.science.20160214

Ray, D. K., Mueller, N. D., West, P. C., and Foley, J. A. (2013). Yield trends are insufficient to double global crop production by 2050. *PloS One* 8, e66428. doi: 10.1371/journal.pone.0066428

Su, W. N., Xie, J., Han, J., Liu, T. N., and Han, Q. F. (2021). Construction of critical nitrogen dilution curve based on dry matter in diffe rent organs of summer maize and estimation of grain yield. *Acta Cropologica Sin.* 47, 16. doi: 10.3724/SP.J.1006.2021.03021

Sun, Z. N., Zhang, Y. B., Zhao, P., Pan, Y. J., Xun, L. F., and Kou, W. (2024). Preparation, characterization and adsorption performance of corn straw biochar. *Renewable Energy Resour.* 42, 1587–1593. doi: 10.13941/j.cnki.21-1469/tk.2024.12.015

Tian, E. K., Cheng, S. M., Wang, T., Wang, S. R., and Lin, X. S. (2020). Study on breeding and its supporting technology of a new maize variety 'Hemuyu 153'. *Seed* 39, 123–126. doi: 10.16590/j.cnki.1001-4705.2020.11.123

Tian, X. S., Li, S. Y., Zhang, Y., Liu, X. J., Tian, Y. C., Zhu, Y., et al. (2019). Estimation of nitrogen fertilizer requirement of winter wheat based on critical nitrogen dilution curve. *J. Wheat Crops* 39, 1112–1120. doi: 10.7606/j.issn.1009-1041.2019.09.12

Tilman, D., Balzer, C., Hill, J., and Befort, B. L. (2011). Global food demand and the sustainable intensification of agriculture. *Proceeding Natl. Acad. Sci. United States America* 108, 20260–20264. doi: 10.1073/pnas.1116437108

Tu, Y., Wu, S. B., Chen, B., Weng, Q. S., Bai, Y. Q., Yang, J., et al. (2024). A 30m annual cropland dataset of China from 1986 to 2021. *Earth System Sci. Data Discussions* 16, 20. doi: 10.5194/essd-16-2297-2024

Wang, L. M., Li, S. Q., and Shao, M. G. (2010). Effects of N and water supply on dry matter and N accumulation and distribution in maize (*Zea mays* L.) leaf and straw-sheat. *Chin. J. Agric. Sci.* 43, 2697–2705. doi: 10.3864/j.issn.0578-1752.2010.13.009

Wang, J. F., Liu, P., Zhao, B. Q., Dong, S. D., Zhang, J. W., Zhao, M., et al. (2011). Comparison of root characteristics and nitrogen uptake and use efficiency in different corn genotypes. *Scientia Agricultura Sin.* 44, 699–707.

Wang, X. C., Wang, X. H., Xiong, S. P., Ma, X. M., Ding, S. J., Wu, K. Y., et al. (2015). Differences in nitrogen efficiency and nitrogen metabolism of wheat varieties under different nitrogen levels. *Scientia Agricultura Sin.* 48, 2569–2579. doi: 10.3864/j.issn.0578-1752.2015.13.009

Wang, Y. H., Xu, H. T., Xu, B., Zhang, H. S., and Feng, X. X. (2010). Effect of N fertilizer applicationon yield components and root system growth of maize. *Chin. Soil Fertilizer* 03), 55–57. doi: 10.3969/j.issn.1673-6257.2010.03.014

Wang, L. M., Ye, X. X., Chen, F. J., and Shang, Y. F. (2012). Effect of nitrogen fertilization on maize yield and nitrogenefficiency of different maize varieties. *Chin. J. Eco-Agriculture* 20, 529–535. doi: 10.3724/SP.J.1011.2012.00529

Wang, X. R., Zhang, R. Z., Li, S. M., Xu, N., Mu, Y., and Zhang, C. Y. (2019). Simulation of dry matter accumulation and nitrogen absorption in a maize/soybean intercropping system supplied with different nitrogen levels. *Chin. J. Eco-Agriculture* 27, 1354–1363. doi: 10.13930/j.cnki.cjea.190075

Xue, X. P., Zhou, Z. G., Zhang, L. J., Wang, Y. L., Guo, W. Q., and Chen, B. L. (2006). Development and application of critical nitrogen concentration Dilution Model for cotton after flowering. *Acta Ecologica Sin.* 06), 1781–1791.

Yang, J., Greenwood, D. J., Rowell, D. L., Wadsworth, G. A., and Burns, I. G. (2000). Statistical methods for evaluating a crop nitrogen simulation model, N_ABLE. *Agric. Syst.* 64, 37–53. doi: 10.1016/S0308-521X(00)00010-X

Yang, H., Yang, J. P., Lv, Y. M., and He, J. J. (2014). SPAD values and nitrogen nutrition index for the evaluation of rice nitrogen status. *Plant Production Sci.* 17, 81–92. doi: 10.1626/pps.17.81

Yao, X., Ata, S. T., Zhu, Y., Tian, Y. C., Liu, X. J., and Cao, W. X. (2014). Development of critical nitrogen dilution curve in rice based on leaf dry matter. *Eur. J. Agron.* 55, 20–28. doi: 10.1016/j.eja.2013.12.004

Yue, S. H., Liu, C. Y., and Huang, Y. F. (2016). Simulating critical nitrogen dilution curve and modeling nitrogen nutrition index in winter wheat in central henan area. *Acta Cropologica Sin.* 42, 909–916. doi: 10.3724/SP.J.1006.2016.00909

Zhang, Y. X., Lü, N., Gao, Z. J., Li, Q. S., Zhang, Y. L., and Wang, G. D. (2024). Construction and verification of critical nitrogen concentration dilution curves for early maturing cotton under different water conditions. *Plant Nutr. Fertilizer Sci.* 30, 731–744. doi: 10.11674/zwyf.2023407

Zhao, B., Ata, S. T., Duan, A. W., Liu, Z. D., Wang, X. L., Xiao, J. F., et al. (2018). Determination of critical nitrogen concentration and dilution curve based on leaf area index for summer maize. *Field Crops Res.* 228, 195–203. doi: 10.1016/j.fcr.2018.09.005

Zhao, B., Ata, S. T., Liu, Z. D., Ning, D. F., Xiao, J. F., Liu, Z. G., et al. (2017). Development of a critical nitrogen dilution curve based on leaf dry matter for summer maize. *Field Crops Res.* 208, 60–68. doi: 10.1016/j.fcr.2017.03.010

Zhao, X. H., Zhang, Y. Y., Rong, Y. S., Duan, J. Z., He, L., Liu, W. D., et al. (2022). Study on critical nitrogen dilution model of winter wheat spike organs under different water and nitrogen conditions. *Chin. J. Agric. Sci.* 55, 3321–3333. doi: 10.3864/j.issn.0578-1752.2022.17.005

frontiers | Frontiers in Plant Science

TYPE Original Research
PUBLISHED 21 July 2025
DOI 10.3389/fpls.2025.1597198

Check for updates

OPEN ACCESS

EDITED BY
Maruthi Sridhar Balaji Bhaskar,
Florida International University, United States

REVIEWED BY
Xiaojuan Chen,
Guangxi University, China
Tianfu Han,
Zhengzhou University, China

*CORRESPONDENCE
Hongquan Liu
lhq@hebau.edu.cn

RECEIVED 20 March 2025
ACCEPTED 16 June 2025
PUBLISHED 21 July 2025

CITATION
Gao M, Wang X, Chen R, Gao H, Wang X and Liu H (2025) Optimization of water and fertilizer management on the intercropping system between maize and mung bean to improve photosynthetic characteristics & water use and to increase plant yield. *Front. Plant Sci.* 16:1597198. doi: 10.3389/fpls.2025.1597198

COPYRIGHT
© 2025 Gao, Wang, Chen, Gao, Wang and Liu. This is an open-access article distributed under the terms of the Creative Commons Attribution License (CC BY). The use, distribution or reproduction in other forums is permitted, provided the original author(s) and the copyright owner(s) are credited and that the original publication in this journal is cited, in accordance with accepted academic practice. No use, distribution or reproduction is permitted which does not comply with these terms.

Optimization of water and fertilizer management on the intercropping system between maize and mung bean to improve photosynthetic characteristics & water use and to increase plant yield

Mengfan Gao[1], Xinxin Wang[2,3,4], Renqiang Chen[1], Huiyan Gao[1], Xiaoling Wang[5] and Hongquan Liu[6,7]*

[1]College of Urban and Rural Construction, Hebei Agricultural University, Baoding, China, [2]Agricultural Technology Innovation Center in Mountainous Areas of Hebei Province, Hebei Agricultural University, Baoding, China, [3]Agricultural Engineering Technology Research Center, National North Mountainous Area, Baoding, China, [4]Hebei Mountain Research Institute, Hebei Agricultural University, Baoding, China, [5]College of Horticulture, Hebei Agricultural University, Baoding, China, [6]North China Water saving Agriculture Key Laboratory, Ministry of Agriculture and Rural Affairs, Baoding, China, [7]State Key Laboratory of North China Crop Improvement and Regulation, Hebei Agricultural University, Baoding, China

Intercropping has the advantages of improving the canopy environment and enhancing the productivity of farmland. However, the responses of photosynthetic physiological characteristics, canopy structure and yield to different water and fertilizer measures need to be further clarified. The study took the maize/mung bean intercropping as the cultivation mode, used organic fertilizer instead of chemical fertilizer, combined with the upper and lower limits of field water holding capacity to control the irrigation amount, and set up a two-factor field experiment. The research results show that the leaf area index and chlorophyll relative content of maize and mung beans increase first and then decrease with the emergence time of maize and mung beans. Compared with the treatment without organic fertilizer, the leaf area index of maize and mung beans increased by 5.99% - 36.70% and 27.43% - 28.72% respectively, and the chlorophyll relative content increased by 2.31% - 3.47% and 4.59% - 4.63% respectively. Compared with I_0, leaf area index increased by 9.73% - 33.42% and 6.60% - 17.39% respectively, and chlorophyll relative content increased by 2.75% - 12.68% and 4.14% - 9.12% respectively. The gas exchange parameters and absorbance(Ab) of maize and mung beans showed a trend of increasing first and then decreasing with the emergence time. The net photosynthetic rates of maize and mung beans increased by 5.04% - 47.12% and 11.29% - 26.60% respectively. Maize Pn was strongly positively correlated with chlorophyll relative content and Ab (R^2>0.5). The three-dimensional growth curves of Pn along with chlorophyll relative content and Ab were S-shaped. As the growth period progressed, the leaves would age, and the gradual decrease of chlorophyll relative content and Ab led to a gradual decrease in maize Pn. Within a certain range, with the increase of irrigation volume, the water use efficiency(WUE) of crops shows a trend of

increasing first and then decreasing. Organic fertilizer can significantly improve the WUE of maize/mung beans intercropping crops. In conclusion, optimizing the combination of organic fertilizers and irrigation practices is a win-win strategy that can enhance both grain output and quality.

KEYWORDS

intercropping, organic fertilizer, photosynthetic traits, water use efficiency, irrigation

1 Introduction

Maize (*Zea mays* L.), as a key staple crop, faces a rapidly widening gap between production and demand (Wu et al., 2024; Yang et al., 2024). Mung bean (*Vigna radiata* L.), as an economical crop with high nutritional content, exhibits stable market demand. However, the industry faces challenges of reduced yields due to decreasing planting areas and inadequate technical support (Huang et al., 2024). Intercropping of gramineous and legumes represents a typical intercropping system. By leveraging differences in biological characteristics, a scientifically designed composite spatial layout can be established to enhance light availability for crops and create an environment conducive to the harmonious coexistence of both crops in terms of light, nutrients, and water resources (Pelzer et al., 2012; Li et al., 2023; Yang et al., 2023a). Numerous qualitative studies (Bedoussac and Justes, 2011; Chimonyo et al., 2016; Kermah et al., 2017) and systematic reviews (Bedoussac et al., 2015; Du et al., 2018; Tilman, 2020) have demonstrated through practical applications worldwide that intercropping enhances nitrogen use efficiency, resource utilization efficiency, and soil ecosystem capacity by addressing factors such as growth physiology, interspecific competition, and agronomic practices. These findings suggest that intercropping serves as a viable approach to achieving sustainable intensive agricultural production.

Irrigation and nitrogen fertilization are critical factors in agricultural production, directly influencing crop growth and development (Liu et al., 2022; Ma et al., 2022). Water plays a pivotal role in enhancing fertilizer availability, while fertilizers are critical for unlocking the productivity of soil-water systems (Himmelstein et al., 2017). Because of the lack of scientific and efficient irrigation and fertilizer management among local farmers, the amounts of water and fertilizers applied in intercropping systems often exceed the actual crop demands, leading to resource waste and reduced efficiency (Zhang et al., 2011; Chen et al., 2023b). Organic fertilizers, as natural nutrient sources, not only supply multiple essential elements for crop growth but also improve photosynthetic characteristics, thereby enhancing product quality (Jannoura et al., 2014; Adetunji et al., 2020). To mitigate water scarcity in arid and semi-arid regions, understanding water-fertilizer interactions and their underlying physiological mechanisms is fundamental for optimizing water-saving irrigation systems (Xue et al., 2016). Studies demonstrate that appropriate water and fertilizer management helps maintain higher chlorophyll content, delays leaf senescence, and consequently enhances photosynthetic efficiency through sustaining stomatal openness, increasing transpiration rates, and promoting the transport and accumulation of photosynthetic products (Tian et al., 2019; Yang et al., 2023b). For instance, Wu et al. (2023) optimized water-nitrogen management to increase leaf number, improve canopy light conditions, and enhance cotton yield. Similarly, Luo et al. (2021) improved light environments and boosted biomass and yield in intercropped wheat through refined nitrogen application strategies.

Although irrigation and organic fertilizers are widely applied in agricultural practices, current research on optimizing water-fertilizer management to improve plant growth, physiological traits, light energy utilization, biomass, and yield responses in maize/mung bean intercropping systems remains limited. Existing studies predominantly focus on monoculture systems, failing to provide theoretical foundations for agricultural production under maize/mung bean intercropping (Yang et al., 2014; Liu et al., 2017; Luo et al., 2024). Furthermore, strategies to rationally design irrigation schedules (e.g., water volume and timing) based on crop water requirements, enhance coordination between crop water demand and supply, and maximize the systemic advantages of cereal-legume intercropping require further in-depth exploration.

Therefore, this study adopts a maize/mung bean intercropping system as the experimental model, with two independent variables: organic fertilizer application rate and irrigation volume. The objectives are to: 1) investigate the effects of varying organic fertilizer application rates and irrigation volumes on the yield of maize and mung beans; 2) explore the synergistic effects of water-fertilizer interactions on crop photosynthetic and physiological traits; 3) examine the regulatory roles of organic fertilizer application rate and irrigation volume in crop water consumption and water use efficiency (WUE).

2 Materials and methods

2.1 Site decription

The experiment was conducted from March 2023 to July 2024 at the Comprehensive Experimental Station of Hebei Agricultural University, located in Xingtai City, Hebei Province, China (37°34′N, 115°13′E). The region experiences a continental monsoon climate, characterized by

anaverage annual temperature of 14.8°C, annual precipitation of 748.5 mm, and 2235 hours of sunshine. The soil at the site is yellow loam, with a bulk density of 1.41 g cm^{-3}, pH 7.5, and the nutrient properties (0 – 30 cm depth): organic matter (12.09 g kg^{-1}), total nitrogen (0.73 g kg^{-1}), alkali-hydrolyzable nitrogen (131 mg kg^{-1}), available phosphorus (20.5 mg kg^{-1}), and available potassium (121 mg kg^{-1}). Meteorological data for temperature and precipitation during the experimental years (2023 and 2024) are provided in Figure 1.

The trial periods spanned 109 days (8 March – 25 June 2023) and 108 days (15 March – 1 July 2024). To ensure optimal growth conditions, maize and mung bean were cultivated under plastic film mulching, which was removed on 20 April 2023 and 30 April 2024, respectively. Pest management included foliar applications of cypermethrin (for maize) and bifenthrin (for mung bean) as required. Pre-emergence weed control was achieved through metolachlor application prior to seeding, supplemented by manual weeding during the growing season.

2.2 Experimental design

The farming habits of local farmers are applying compound fertilizer and urea at 1500 ~ 2000 kg·ha^{-1} for maize and 600 ~ 900 kg·ha^{-1} for mung beans The irrigation method was border irrigation, with each irrigation to field capacity (FC). Therefore, according to the local practice, the application of chemical fertilizer was reduced, organic fertilizer was used as part of the nitrogen source input, and border irrigation was changed to different irrigation levels controlled by the upper and lower limits of FC. Split plot design was adopt double factors, crack area for water level: $40\%\theta_{FC}<\theta<60\%\theta_{FC}$ (I0), $60\%\theta_{FC}<\theta<80\%\theta_{FC}$ (I1), $80\%\theta_{FC}<\theta<95\%\theta_{FC}$ (I2); The main area is the application amount of organic fertilizer: Organic fertilizer (F0, 0 kg·ha^{-1}) was not applied, the recommended application amount was reduced by 50% (F1, 3750 kg·ha^{-1}) and the recommended application amount (F2, 7500 kg·ha^{-1}). Organic fertilizer was consisted of locally sourced decomposed chicken manure (organic matter content 14.5 g·kg^{-1}, total nitrogen content 20 g·kg^{-1}). Total phosphorus content 18 g·kg^{-1}, total potassium content 9 g·kg^{-1}, water content 320 g·kg^{-1}). There were 9 treatments with 3 repetitions for each treatment, and a total of 27 spots with an area of 3.5 m × 6 m.

Maize and mung bean intercropping 4M6B (4 rows of maize: 6 rows of mung bean) as planting method, maize strip width 1.5 m, mung bean strip width 2.0 m, maize and mung bean belt spacing 0.6 m. The mung bean variety was Jilu 20, which came from the Grain and Oil Crops Research Institute of Hebei Academy of Agriculture and Forestry Sciences. The row spacing of mung bean plants was 0.1 m × 0.4 m, and the seeding density was 162,000 plants·ha^{-1}. The maize variety was Jinguan 220 (fresh maize) from Beijing Sihai Seed Industry Co., LTD., with row spacing of 0.2 m × 0.5 m and seeding density of 36,000 plants·ha^{-1}. Detailed water and nutrient inputs are shown in Table 1. Maize and mung bean were harvested on June 28 in both years.

Since the nitrogen content of organic fertilizer could not fully meet the growth demand of maize, quantitative chemical fertilizer was applied to maize sowing, including 375 kg·ha^{1}($N\text{-}P_2O_5\text{-}K_2O$: 16-16-16) compound fertilizer and 300 kg·ha^{1} urea (N≥46.0%), and only organic fertilizer was applied to mung bean sowing. After fertilizing maize and mung bean, rotary tillage was carried out, and the depth of rotary tillage was 0.3 m. Under the I0 irrigation level, there was no excess irrigation except effective precipitation in 2023 during the whole growth period of maize and mung bean, and one irrigation was carried out in 2024. At the I1 irrigation level, maize and mung bean were irrigated once in 2023 and twice in 2024. At the I2 irrigation level, maize and mung beans were irrigated twice in 2023 and three times in 2024. According to the formula of irrigation quota, the planned depth of wet layer for maize and mung bean during irrigation is 0.6 m (drawing stage) and 0.8 m (filling stage) respectively, and the planned depth of wet layer for mung bean is 0.2 m (branching stage) and 0.4 m

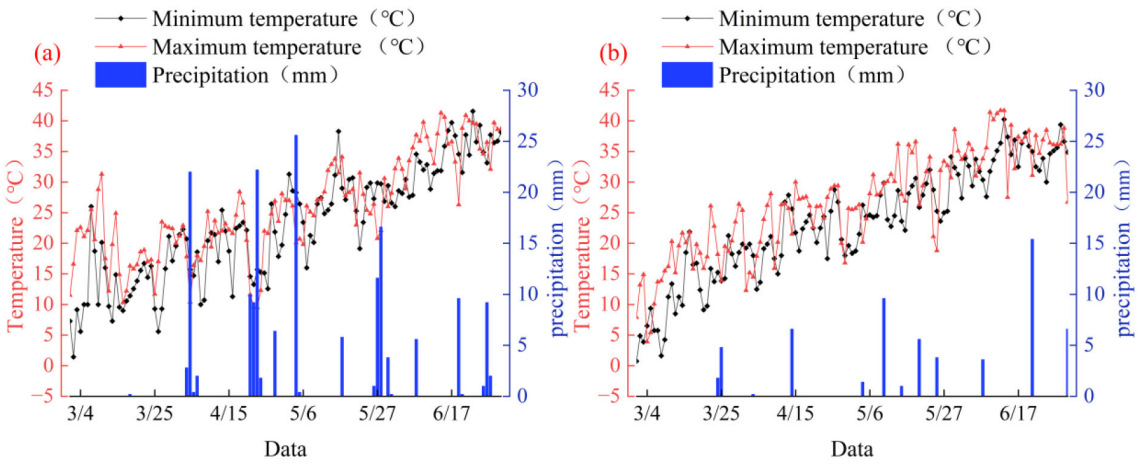

FIGURE 1
Weather patterns during the growing season of maize/mung bean in 2023 and 2024: weather patterns in 2023 **(a)**, weather patterns in 2024 **(b)**.

10.3389/fpls.2025.1597198

TABLE 1 Water and nutrient inputs of maize/mung bean under different treatments.

Treatment	Organic fertilizer (kg/hm²)	Inorganic fertilizer (kg/hm²)						Nutrient input (kg/hm²)						Field moisture capacity		Effective precipitation (mm)		Irrigating quota on each application (mm)				Irrigation water quantity (mm)			
		Maize			Mung bean			Maize			Mung bean							Maize		Mung bean		Maize		Mung bean	
		N	P_2O_5	K_2O	N	P_2O_5	K_2O	N	P_2O_5	K_2O	N	P_2O_5	K_2O	Upper limit	floor	2023	2024	2023	2024	2023	2024	2023	2024	2023	2024
F_0I_0	0	198	60	60	0	0	0	198	60	60	0	0	0	$\theta_{60\%}$	$\theta_{40\%}$	166.40	57.00	0	75.00	0	46.87	166.40	132.00	166.40	103.87
F_0I_1	0	198	60	60	0	0	0	198	60	60	0	0	0	$\theta_{80\%}$	$\theta_{60\%}$	166.40	57.00	194.24	178.12	113.56	78.12	360.64	235.12	279.96	135.12
F_0I_2	0	198	60	60	0	0	0	198	60	60	0	0	0	$\theta_{95\%}$	$\theta_{80\%}$	166.40	57.00	272.24	209.38	152.52	93.75	438.64	266.38	318.92	150.75
F_1I_0	3750	198	60	60	0	0	0	249	106	83	75	68	34	$\theta_{60\%}$	$\theta_{40\%}$	166.40	57.00	0	84.38	0	62.50	166.40	119.50	166.40	119.50
F_1I_1	3750	198	60	60	0	0	0	249	106	83	75	68	34	$\theta_{80\%}$	$\theta_{60\%}$	166.40	57.00	211.26	240.63	96.64	109.38	377.66	297.63	263.04	166.38
F_1I_2	3750	198	60	60	0	0	0	249	106	83	75	68	34	$\theta_{95\%}$	$\theta_{80\%}$	166.40	57.00	321.55	271.89	90.76	125.01	487.95	325.89	257.16	182.01
F_2I_0	7500	198	60	60	0	0	0	300	152	106	150	135	68	$\theta_{60\%}$	$\theta_{40\%}$	166.40	57.00	0	89.38	0	71.88	166.40	146.38	166.40	128.88
F_2I_1	7500	198	60	60	0	0	0	300	152	106	150	135	68	$\theta_{80\%}$	$\theta_{60\%}$	166.40	57.00	238.76	303.13	116.35	140.63	405.16	360.13	282.75	197.63
F_2I_2	7500	198	60	60	0	0	0	300	152	106	150	135	68	$\theta_{95\%}$	$\theta_{80\%}$	166.40	57.00	340.27	334.38	157.08	156.25	506.67	391.38	323.48	213.25

(flowering pod stage) respectively. The irrigation method is pipeline irrigation, and the irrigation quota is controlled by solenoid valves.

2.3 Measurements

2.3.1 Leaf area index

In 2023 and 2024, three maize and mung bean plants were randomly selected from each plot at 35, 55, 70, 85, and 102 d after maize emergence and at 40, 55, and 70 d after mung bean emergence, and the leaf area index (LAI) was calculated by determining the functional leaf length (L_{ij}) versus the maximum width (B_{ij}) of each plant using a straightedge.

$$\mathrm{LAI} = 0.75\rho\frac{\sum_{j=1}^{m}\sum_{i=1}^{n}(\mathrm{L}_{ij}\times \mathrm{B}_{ij})}{\mathrm{m}} \quad (1)$$

where n is the total number of leaves of plant j; m is the number of plants measured; and ρ is the planting density.

2.3.2 Chlorophyll relative content

A hand-held dual-wavelength chlorophyll meter (SPAD-502, Minolta Camera Co, Ltd,Japan) was used in 2023 and 2024 at 35, 55, 70, 85, and 102 d after seedling emergence of maize and at 40, 55, and 70 d after seedling emergence of mung bean. Three maize and mung bean plants in side rows were selected in each plot, and Chlorophyll relative content (SPAD) was measured and finally averaged for all leaves of the whole plant, excluding damaged or wilted leaves and avoiding large leaf veins. Measurements were taken at the same time as the photosynthetic parameters, between 9:00 and 11:00 a.m. in the field.

2.3.3 Indicators of photosynthetic parameters

Yaxin-1102g portable photosynthetic apparatus (Beijing Yaxin Riyi Technology Co., Ltd., Beijing, China) was used for 35, 55, 70, 85 and 102 d after maize emergence and 40, 55 and 70 d after mung bean emergence, 9:00 am to 11:00 am: Three maize and mung bean plants were selected from each plot to detect Pn ($\mu mol{\cdot}m^{-2}{\cdot}s^{-1}$), transpiration rate (Tr, $mmol{\cdot}m^{-2}{\cdot}s^{-1}$), stomatal conductance (Gs, $mmol{\cdot}m^{-2}{\cdot}s^{-1}$) and intercellular CO_2 concentration (Ci, $\mu mol{\cdot}mol^{-1}$). The photosynthetic performance of maize was measured by the first fully unfolded leaf from top to bottom from 35 d to 70 d, and by ear leaf from 70 d to 102 d. The first compound leaf was taken from Mung bean.

2.3.4 Absorbance

Yaxin-1201 Plant Canopy Meter (Beijing Yaxin Riyi Technology Co., Ltd., Beijing, China) is an effective tool for quantitatively describing the structural parameters of plant canopies. The image method was chosen to obtain the canopy structure image. And by borrowing the principle of Beer's law, the universally recognized semi-empirical and semi-theoretical mathematical modeling formulas were used to non-destructively profile the parameters such as LAI, scattered radiation coefficients, and canopy porosity of the canopy leaves. absorbance (Ab) of maize was photographed using Yaxin-1201 plant canopy meter at 35, 55,

70, 85 and 102 d after emergence of maize for monitoring in synchronization with photosynthetic parameters.

2.3.5 Soil water storage and evapotranspiration

Before seeding and at the end of each growth period, 3 points were randomly selected in each plot, and the sampling position was between the peer plants. Use a soil drill to take a soil sample every 10 cm in the 0 ~ 100 cm soil layer. The soil sample taken from the field is immediately stored in a closed aluminum box. The drying method was used to bake the soil in the oven at 105 °C for 48 hours to constant weight and then weighed it. The formula for calculating soil moisture content SWS and ET was as follows:

$$b_i = \frac{w_i - d_i}{d_i - v_i} \quad (2)$$

In the formula, b_i is the soil moisture content of layer i (%),w_i is the wet soil weight of layer i (g), ρ_i is the dry soil weight of layer i (g), v_i is the aluminum box weight of layer i (g).

$$SWS = \sum_1^n h_i \times \rho_i \times b_i \quad (3)$$

where *SWS* is the soil water storage (mm), h_i is the depth of the i soil layer (cm), ρ_i is the soil bulk density of the i soil layer ($g \cdot cm^{-3}$), b_i is the mass water content of the i soil layer (%), and n is the number of soil layers.

$$ET = P + I_i + (SWS_i - SWS_{i+1}) \quad (4)$$

In the formula, ET is evapotranspiration (mm), P is precipitation during growth period (mm), I_i is treated irrigation amount (mm), SWS_i is soil water storage in 0 - 100 cm soil layer at the end of the previous growth period (mm), SWS_{i+1} is soil water storage in 0 - 100 cm soil layer at the end of growth period (mm).

2.3.6 Yield water use efficiency

WUE was calculated as

$$WUE = \frac{Y}{ET} \quad (5)$$

where WUE is water us efficiency Y is plant yield ($kg \cdot ha^{-1}$) and ET is evapotranspiration (mm).

2.3.7 Dry matter accumulation and yield

For dry matter accumulation (DMA) measurements of maize and mung bean, three plants each were randomly selected from each plot after maize and mung bean harvest and brought back to the chamber. The maize and mung bean were placed in paper bags and dried in an oven at 80°C for 48 h to a constant weight. The dry weight of the plants was subsequently determined. Maize and mung bean yields were hand harvested for maize and mung bean seed yields on June 25, 2023 and July 1, 2024, respectively. When harvesting maize blocks, the actual effective number of plants and the actual number of ears per maize plant in each treated maize belt were investigated, and the maize plants without long ears were not counted as effective trees. Ten ears were randomly selected from each plot to investigate the fresh weight of maize ears, and the fresh food yield was calculated by multiplying the weight of fresh ears without bracts and the number of effective plants. For mung bean, 1 m × 1 m blocks were selected for each plot, and the number of plants, pods per plant, graminous per pod, and 100 - kernel weight of mung bean were examined and theoretical yields were calculated.

2.4 Statistical analysis

Microsoft Excel 2019 and SPSS 25.0 were used for statistical analysis. The effects of LAI, SPAD, photosynthetic characteristics, DMA, ET, WUE and yield on emergence time, organic fertilizer application amount, irrigation amount and planting years of maize and mung bean were investigated by multivariate analysis of variance. The least significant difference (LSD) was used for ANOVA and multiple comparison (P<0.05). The correlation between Pn, SPAD and Ab was firstly transformed into dimensionless numbers ranging from 0 to 1 by normalization, then curves were estimated by SPSS, nonlinear fitting was applied to solve equation parameters, and nonlinear curve fitting was performed by Origin 2024 regression analysis. All other graphics were mapped using Origin 2024 software.

3 Results

3.1 Effects of different water and fertilizer treatments on dry matter accumulation of corn and mung beans

Irrigation volume, organic fertilizer application rate, and their interactions significantly affected the DMAof both maize and mung bean (P<0.05), while planting year also exerted significant effects on DMA (P<0.05; Table 2). Over the two-year study, irrigation had a larger effect on DMA than organic fertilizer application for both crops (Figure 2). For mung bean, DMA under I1 and I2 irrigation levels (strip irrigation) was significantly higher than I0 (P<0.05), but no significant differences were observed between I1 and I2 (P>0.05). Similarly, DMA in F1 and F2 organic fertilizer treatments exceeded F0 (P<0.05), with no notable differences between F1 and F2 (P>0.05). In maize strips, DMA exhibited a progressive increase with elevated irrigation and organic fertilizer inputs (P<0.05), contrasting with mung bean strips where such trends were absent.

Quantitatively, mung bean DMA ranged from 26.47 to 31.36g·plant^{-1}. Relative to F0, F1 and F2 treatments increased DMA by 1.98 ~ 2.73% and 2.47 ~ 2.72%, respectively. Compared to I0, I1 and I2 irrigation levels enhanced DMA by 10.78 ~ 11.53% and 14.60 ~ 16.13%, respectively. Maize DMA varied between 179.99 and 294.30 g·plant^{-1}. F1 and F2 treatments elevated DMA by 3.91 ~ 33.34% and 7.45 ~ 31.47%, respectively, relative to F0, while I1 and I2 increased DMA by 13.91 ~ 18.00% and 21.71 ~ 28.07%, respectively, compared to I0 (Figure 2).

10.3389/fpls.2025.1597198

TABLE 2 Results of three-factor analysis of variance for photosynthetic physiological characteristics of maize/mung bean [planting age (Y), amount of organic fertilizer (F) and irrigation (I)].

Treatment	Pn		Tr		Gs		Ci		SPAD		LAI		Ab		DMA		Yield	
	Maize	Mung bean	Maize	Mung bean	Maize	Mung bean	Maize	Mung bean	Maize	Mung bean	Maize	Mung bean	Maize	Mung bean	Maize	Mung bean	Maize	Mung bean
Y	1.91ns	49.80**	12.08**	64.40**	6.27*	910.05**	0.24ns	18.83**	77.39**	81.21**	2.05ns	1.59ns	4.86*	–	991.30**	61.55**	0.11ns	27.74**
F	25.86**	35.80**	182.01**	114.18**	25.85**	45.30**	30.21**	15.61**	48.43**	43.41**	109.16**	5.75**	45.79**	–	247.48**	115.13**	3.66*	31.35**
I	263.67**	363.07**	1041.73**	852.69**	68.02**	1112.79**	81.01**	347.17**	190.60**	500.20**	789.30**	55.78**	24.53**	–	393.60**	116.02**	98.13**	156.15**
Y×F	0.67ns	3.19ns	3.98*	0.76ns	1.22ns	10.12**	1.51ns	2.84ns	0.50ns	1.23ns	0.74ns	0.17ns	0.13ns	–	93.91**	15.61**	0.12ns	0.14ns
Y×I	0.99ns	9.29**	4.11*	7.77*	3.37*	9.54**	0.13ns	0.36ns	1.02ns	0.94ns	33.36**	0.87ns	0.27ns	–	0.06ns	6.71**	0.19ns	2.02ns
F×I	7.95**	2.93*	19.22**	8.56**	1.76ns	8.46**	5.31*	7.41**	0.76ns	15.24**	1.79ns	0.12ns	2.24ns	–	2.66*	6.61**	0.26ns	4.56**
Y×F×I	0.64ns	1.37ns	0.63ns	3.71*	0.06ns	4.49**	0.06ns	0.92ns	0.86ns	0.20ns	1.16ns	0.12ns	0.20ns	–	5.55**	1.69ns	0.33ns	0.46ns

ns means no significant difference ($P>0.05$); * and ** means significant difference at $P<0.05$ level or at $P<0.01$ level, respectively.

3.2 Effects of different water and fertilizer treatments on yield of corn and mung beans

Both maize and mung bean yields were significantly influenced by irrigation volume and organic fertilizer application rate ($P<0.05$). A significant interaction effect between these factors was observed for mung bean ($P<0.05$), but not for maize ($P>0.05$). Planting year significantly affected mung bean yield ($P<0.05$), whereas no such effect was detected for maize ($P>0.05$; Table 2).

Over the two-year study, mung bean yield under the F0I0, F0I1, and F0I2 treatments exhibited significant differences ($P<0.05$), with yields progressively increasing alongside irrigation volume. In F1 and F2 treatments, I1 and I2 irrigation levels significantly surpassed I0 ($P<0.05$), yielding 16.23 ~ 21.27% and 23.55 ~ 27.49% increases, respectively. However, no significant differences were observed between I1 and I2 ($P>0.05$). Similarly, mung bean yields under F1 and F2 treatments significantly exceeded F0 ($P<0.05$), showing 8.78 ~ 9.10% and 9.51 ~ 10.47% enhancements, respectively.

For maize, yields in F1 and F2 treatments were 7.18 ~ 16.73% and 6.98 ~ 16.22% higher than F0, respectively. Irrigation treatments followed analogous trends: I1 and I2 levels increased yields by 6.89 ~ 13.25% and 10.33 ~ 16.48%, respectively, compared to I0 (Figure 3).

3.3 Effects of different water and fertilizer treatments on leaf area index of corn and mung beans

3.3.1 Maize

Maize LAI peaked between 70 and 85 days (d) after emergence ($P<0.05$), with no interannual differences ($P>0.05$; Table 3). Three-way ANOVA (Table 2) revealed significant main effects of irrigation volume and organic fertilizer application rate on LAI ($P<0.05$), whereas their interaction and planting year exhibited no significant impacts ($P>0.05$).

Specifically, compared to the control (F0), F1 and F2 organic fertilizer treatments increased LAI by 5.99 ~ 7.80% and 12.68 ~ 36.70%, respectively. F2 further enhanced LAI by 6.96 ~ 24.27% relative to F1. Irrigation treatments followed similar trends: I1 and I2 elevated LAI by 9.73 ~ 11.16% and 14.49 ~ 33.42%, respectively, compared to I0, with I2 surpassing I1 by 8.12 ~ 11.22% (Equation 1).

3.3.2 Mung bean

Table 2 indicates that the quantity of irrigation and organic fertilizer application significantly influenced the LAI of mung bean plants ($P<0.05$). However, the interaction between these two factors did not have a significant effect on the LAI of mung bean ($P>0.05$). Additionally, the influence of planting age on the LAI of mung bean was not significantly different ($P>0.05$). Over a two-year field experiment, the LAI of mung bean exhibited a gradual increase coinciding with the emergence of maize (Table 4), reaching its peak within 55 ~ 70 d after emergence ($P<0.05$). Compared to F0, F1 did not show a significant increase ($P>0.05$); F2 increased by 27.43% ~

10.3389/fpls.2025.1597198

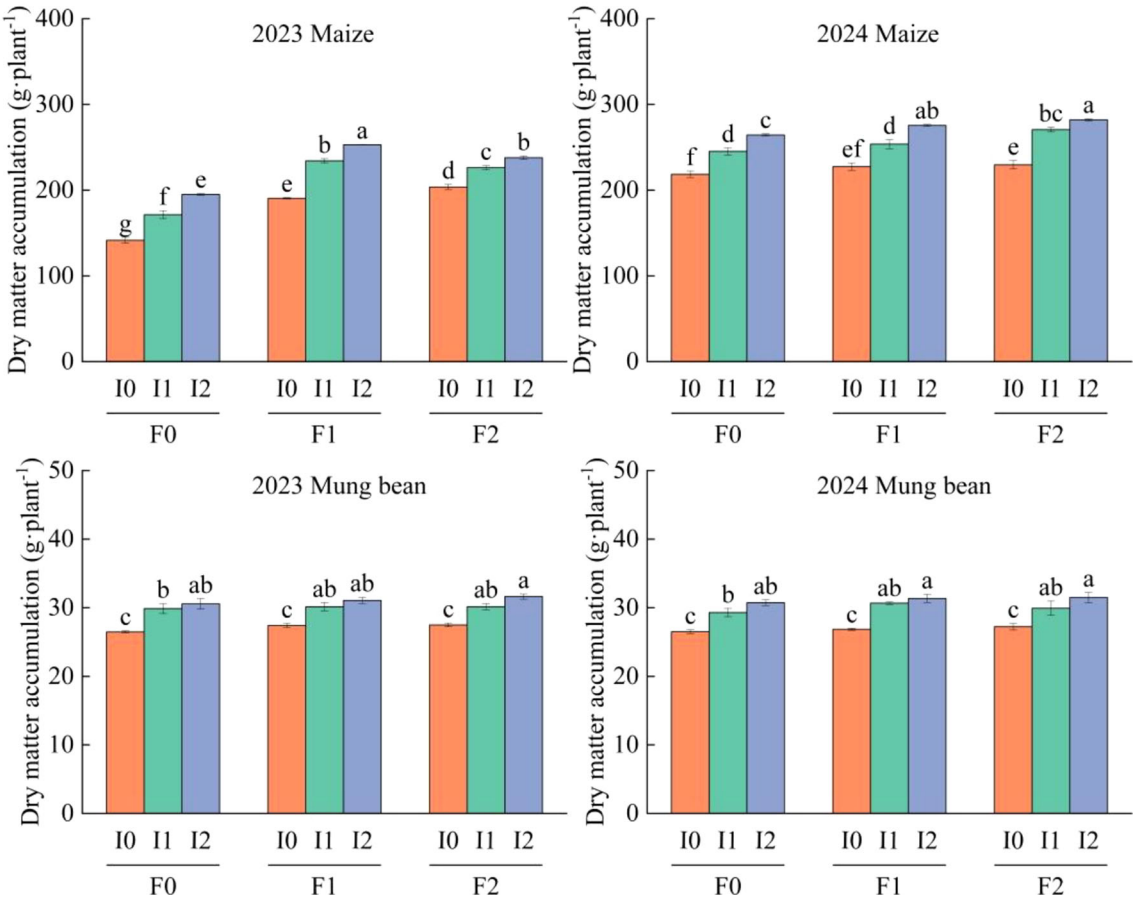

FIGURE 2
DMA of maize/mung bean under different organic fertilizer application and irrigation treatments in 2023 and 2024. F0 ~ F2 represents different organic fertilizer application rates, and I0 ~ I2 represents different irrigation rates. The two-factor analysis of variance method and post-test were performed using the LSD method; the lowercase letters on the column represent significant differences (P<0.05) under different organic fertilizer and irrigation water treatments.

28.72%, yet no significant difference was observed between F2 and F0 (P>0.05). Similarly, I2 showed an increase of 16.61% ~ 17.39% compared to I0, and there was no significant difference between I1 and I2 (P>0.05) (Figure 4; Table 3).

3.4 Effects of different water and fertilizer treatments on SPAD of corn and mung beans

3.4.1 Maize

Table 2 demonstrates that the quantity of water and organic fertilizer applied had a significant influence on maize SPAD values (P<0.05), while their interaction did not exhibit a significant effect (P>0.05). Under varying treatments, maize SPAD values progressively increased over time following crop emergence (P<0.05) (Table 5), ranging from 33.28 ~ 67.40 and reaching a peak between 35 and 70 dafter emergence. F1 exhibited an increase of 1.27% ~ 4.59% compared to F0, whereas F2 showed an increase of 0.55% ~ 4.63% relative to F0, with no significant difference observed between F1 and F2 (P>0.05). Maize SPAD values displayed a consistent increasing trend with increasing irrigation levels (P<0.05). Specifically, I1 was 0.81% ~ 8.99% higher than I0 from 35 ~ 102 d post-emergence, and I2 was 2.75% ~ 12.68% higher than I0 (Figure 5; Table 3).

3.4.2 Mung bean

The amount of irrigation, the application rate of organic fertilizer, and their interaction significantly influenced the SPAD values of mung bean (P<0.05), as did the planting age (P<0.05) (Table 2). Table 5 indicates that under various treatments, the SPAD values of mung bean increased initially and then decreased between 40 and 70 d after emergence (P<0.05). Under the main effect of irrigation, the SPAD values for treatments F1 and F2 were significantly higher than those for treatment F0 (P<0.05), with no significant difference observed between treatments F1 and F2 (P>0.05). Under the main effect of organic fertilizer application, SPAD values gradually increased with increasing irrigation levels. The SPAD values for treatments I2 and I1 were significantly higher than those for treatment I0 (P<0.05). Specifically, from 40 to 70 d after emergence, the SPAD values for I1 were 7.09% ~ 8.14% higher than those for I0, while those for I2 were 12.62% ~ 16.85% higher than those for I0, and I2 was 4.14% ~ 9.12% higher than I1 (Figure 5; Table 3).

10.3389/fpls.2025.1597198

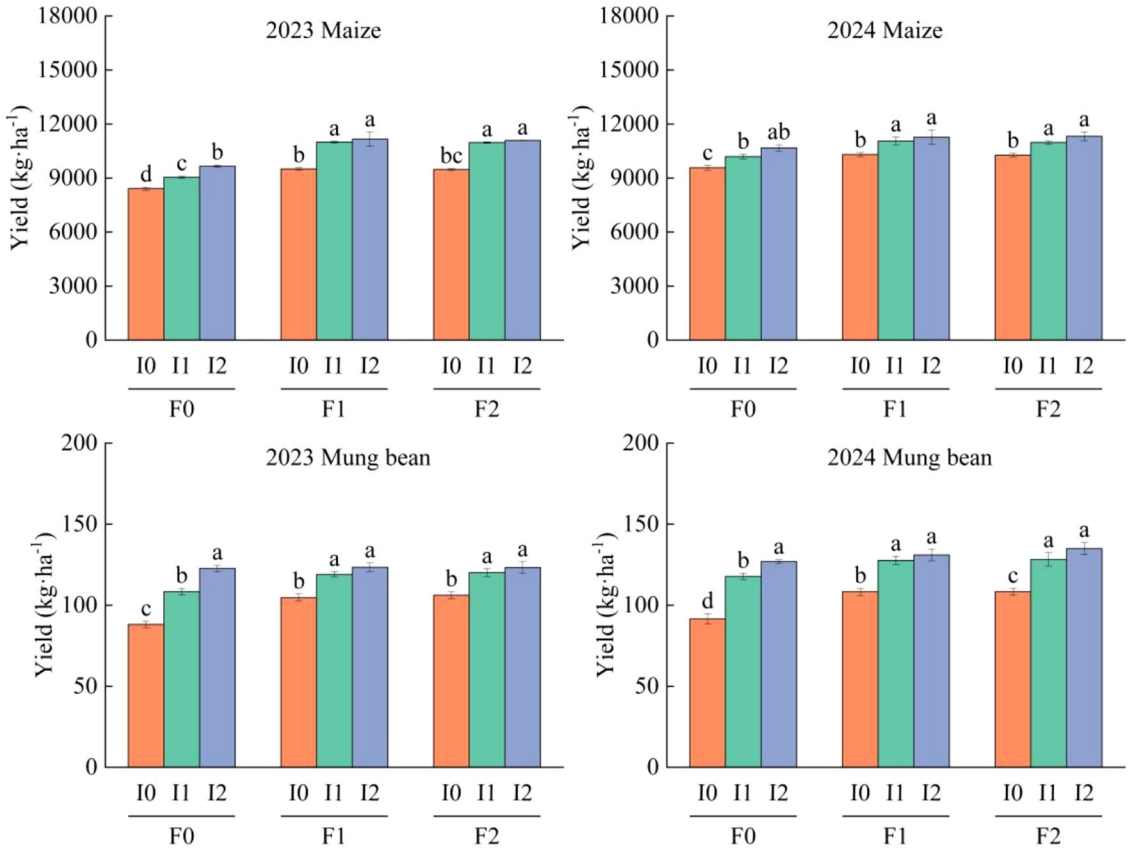

FIGURE 3
Yield of maize/mung bean under different organic fertilizer application rates and irrigation water treatments in 2023 and 2024. F0 ~ F2 represents different organic fertilizer application rates, and I0 ~ I2 represents different irrigation water rates. The two-factor analysis of variance method and post-test were performed using the LSD method; the lowercase letters on the column represent significant differences (P<0.05) under different organic fertilizer amounts and irrigation amounts.

TABLE 3 Results of the two-factor analysis of the photosynthetic physiological characteristics of maize with the emergence time and planting age, Lowercase letters indicate results with P<0.05 significance at different irrigation levels.

Planting year	Days after sowing	LAI	SPAD	Pn (μmol m^{-2} s^{-1})	Tr (mmol m^{-2} s^{-1})	Gs (mmol m^{-2} s^{-1})	Ci (μmol mol^{-1})	Ab
2023	35 d	1.06d	47.64c	22.22d	5.91c	261.73d	147.23d	0.68d
	55 d	1.90c	61.58a	42.38b	6.97b	313.49b	211.07b	0.89b
	70 d	2.46b	61.22a	45.92a	8.07a	338.56a	287.08a	1.01a
	85 d	3.07a	50.91b	31.56c	5.48c	332.76a	277.63a	0.78c
	102 d	3.05a	41.11d	17.50e	3.06d	200.46c	180.21c	0.62e
2024	35 d	1.11e	45.68d	21.39d	6.08c	263.57c	145.02d	0.68d
	55 d	1.89d	64.02a	42.40b	7.01b	302.39b	240.53b	0.91b
	70 d	2.57c	59.68b	45.36a	8.05a	329.76a	274.20a	1.04a
	85 d	2.93b	49.32c	30.64c	5.58d	304.06b	250.58b	0.79c
	102 d	3.13a	36.18d	18.30e	3.22e	218.06d	187.76c	0.64e
Year		0.22ns	26.75**	0.51ns	0.83ns	4.17*	0.11ns	3.96*
Time		372.88**	1221.61**	715.79**	260.03**	252.11**	269.36**	399.10**
Year×Time		1.33ns	21.33**	0.61ns	0.13ns	7.16**	9.88**	0.54ns

ns means no significant difference (P>0.05); * and ** means significant difference at P<0.05 level or at P<0.01 level, respectively.

10.3389/fpls.2025.1597198

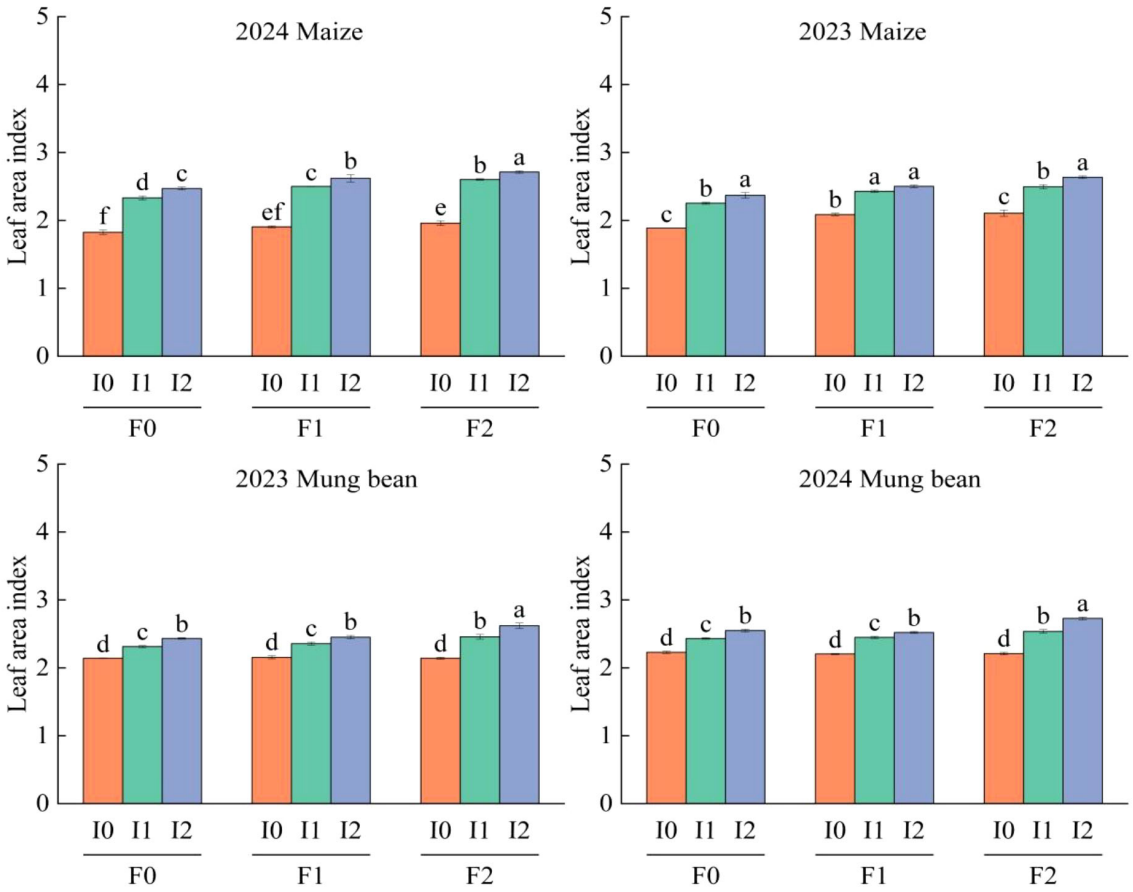

FIGURE 4
LAI of maize/mung bean under different organic fertilizer application rates and irrigation amounts in 2023 and 2024. F0 ~ F2 represents different organic fertilizer application amounts, I0 ~ I2 represents different irrigation amounts. LSD method was used to conduct two-factor analysis of variance and post-test. Lower case letters on the column represent significant difference under different organic fertilizer amount and irrigation amount (P<0.05).

TABLE 4 Results of the two-factor analysis of the photosynthetic physiological characteristics of mung bean with the emergence time and planting age, Lowercase letters indicate results with P<0.05 significance at different irrigation levels.

Planting year	Emergence time	LAI	SPAD	Pn (μmol m^{-2} s^{-1})	Tr (mmol m^{-2} s^{-1})	Gs (mmol m^{-2} s^{-1})	Ci (μmol mol^{-1})
2023	40 d	1.46c	34.25c	21.23a	2.66a	174.06a	325.07a
	55 d	2.56b	44.92a	14.08b	1.87b	161.93b	321.41a
	70 d	3.00a	41.57b	9.84c	1.35c	80.65c	240.97b
2024	40 d	1.57c	34.22c	22.24a	2.84a	193.05a	331.88a
	55 d	2.56b	44.09a	14.48b	2.21b	187.32b	324.48b
	70 d	3.16a	40.86b	10.07c	1.28c	82.26c	242.08c
Year		9.59*	0.87ns	6.41*	1.40ns	40.66**	2.85ns
Time		1056.45**	116.49**	1020.35**	55.60**	737.54**	672.29**
Year×Time		3.08*	0.20ns	1.20ns	1.18ns	8.73**	0.60ns

ns means no significant difference (P>0.05); * and ** means significant difference at P<0.05 level or at P<0.01 level, respectively.

TABLE 5 Water use characteristics of maize/mung bean.

Planting year	Treatment		ET (mm)		Water use effiency (kg ha^{-1} mm^{-1})	
			Maize	Mung bean	Maize	Mung bean
2023	F0	I0	371.09e	260.91c	22.67f	0.34d
		I1	382.66cd	266.14c	23.65ef	0.41bc
		I2	389.83b	271.66b	24.79cde	0.43ab
	F1	I0	378.26c	268.81b	25.14de	0.39c
		I1	386.19bc	271.72a	28.49cde	0.44a
		I2	393.11b	277.54a	28.38bc	0.44a
	F2	I0	380.23cd	275.54b	24.91bcd	0.39c
		I1	392.82b	280.46a	27.93ab	0.43ab
		I2	402.80a	284.60a	27.52a	0.45a
2024	F0	I0	353.77f	267.78e	27.06f	0.34c
		I1	360.85cde	274.64de	28.24ef	0.43a
		I2	363.82cd	281.72abcd	29.34cde	0.45a
	F1	I0	356.11ef	279.61bcd	28.93de	0.39b
		I1	363.87cd	282.51ab	30.39cd	0.45a
		I2	365.44bc	288.32a	30.82bc	0.45a
	F2	I0	359.44de	287.54cde	28.58bc	0.38b
		I1	369.24b	292.70abcd	29.72ab	0.44a
		I2	378.54a	296.71abc	29.90a	0.45a

The letters represent the results of multiple comparisons of the same column of data under $P<0.05$, ns means no significant difference ($P>0.05$); * and ** means significant difference at $P<0.05$ level or at $P<0.01$ level, respectively.

3.5 Effects of different water and fertilizer treatments on photosynthetic characteristics of corn and mung beans

3.5.1 Maize

Table 3 presents the two-factor significant analysis of maize photosynthetic characteristics with respect to emergence time. The emergence time significantly affects Pn, Tr, Gs, and Ci ($P<0.05$), which initially increase and then decrease with emergence time, peaking between 55 and 85 d after emergence. The amount of irrigation water, the application rate of organic fertilizer, and their interaction all significantly influence the photosynthetic characteristics of maize ($P<0.05$), except for Gs (Table 2). Under the main effect of irrigation water, the photosynthetic characteristics of treatments F1 and F2 are higher than those of treatment F0. Specifically, the photosynthetic characteristics of treatments I1 and I2 are significantly higher than those of treatment I0. The increases in Pn, Tr, Gs, and Ci for F1 and F2 are 1.09% ~ 9.72%, 0.24% ~ 28.33%, 1.16% ~ 17.33%, and 0.19% ~ 28.84%, respectively. Treatments I1 and I2 enhance photosynthetic characteristics by 5.04% ~ 47.12%, 5.80% ~ 33.33%, 1.97% ~ 25.08%, and 2.69% ~ 33.22%, respectively. Among these, the effect of irrigation on Tr shows a gradual increasing trend ($P<0.05$), whereas no significant differences are observed for Pn, Gs, and Ci. Additionally, there is no significant difference between treatments I1 and I2 ($P>0.05$) (Figure 6).

3.5.2 Factors influencing and related to Pn of maize

Ab could accurately estimate the radiation interception of the dominant crop in both single-crop and mixed-crop systems. Maize seedling emergence time, irrigation amount, organic fertilizer application, and their interactions had significant effects ($P<0.05$) on Ab (Table 2). Ab exhibited an increasing and then decreasing trend with advancing maize seedling emergence time, peaking at 55 ~ 80 d after emergence. Additionally, Ab showed a gradual increasing trend with both irrigation amount and organic fertilizer application (Table 3). Compared to the F0 treatment, Ab increased by 5.86% ~ 10.13% under F2 and F1 treatments, with an additional increase of 2.95% ~ 3.08% under F2 compared to F1. Similarly, Ab increased by 2.45% ~ 7.66% under I2 and I1 treatments compared to I0, with an additional increase of 3.72% ~ 3.84% under I2 compared to I1 (Figure 7).

Two-year observation data for Pn, SPAD, and Ab were normalized into dimensionless values between 0 and 1. Regression fitting using Origin 2024 software analyzed the relationships among these three variables, yielding the relationship model shown in Figure 8. A significant positive

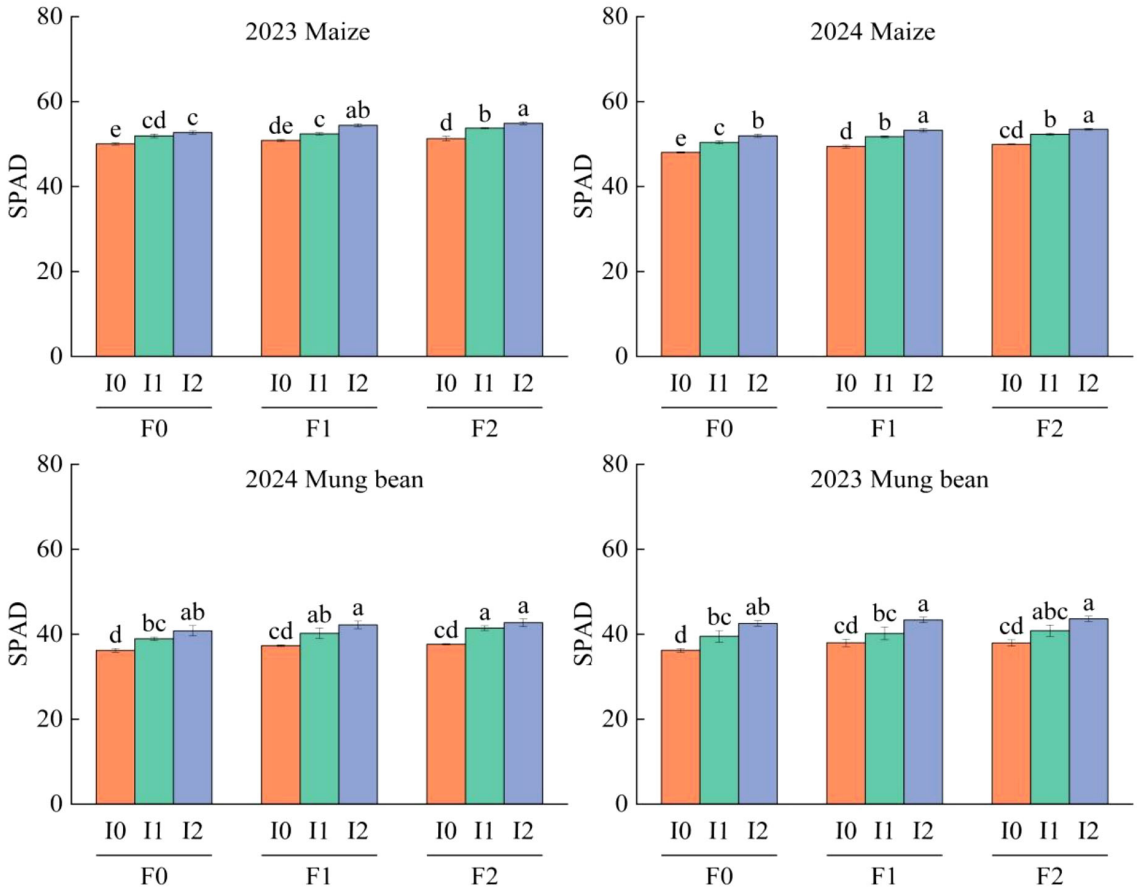

FIGURE 5
SPAD of maize/mung bean under different organic fertilizer application rates and irrigation amounts in 2023 and 2024. F0 ~ F2 represents different organic fertilizer application amounts, I0 ~ I2 represents different irrigation amounts. LSD method was used to conduct two-factor analysis of variance and post-test. Lower case letters on the column represent significant difference under different organic fertilizer amount and irrigation amount (P<0.05).

correlation was observed between Pn and SPAD, as well as between Pn and Ab (Figure 8; R^2>0.05), reaching a strong correlation level, with all fitted equations achieving significance (P<0.05). Among these, the strongest correlation was found between Pn and SPAD (R^2=0.839), while the correlations between Pn and Ab (R^2=0.565) and between SPAD and Ab (R^2=0.553) were relatively weaker. Therefore, SPAD had a stronger influence on Pn compared to Ab. Furthermore, a binary cubic regression model (b) was established for the effects of SPAD and Ab on Pn: $z = -0.011 + 0.615x + 1.503y - 3.016xy - 0.754x^2y + 2.163y^2x + 0.753x^3 - 0.289y^3$, where x and y represent the respective influence roles of SPAD and Ab on Pn indices.

3.5.3 Mung bean

The two-factor significant analysis of the photosynthetic characteristics of mung bean with respect to emergence time is presented in Table 4. The emergence time of mung bean significantly affects Pn, Tr, Gs, and Ci (P<0.05), which initially increase and then decrease with emergence time, peaking between 40 and 70 d after emergence. The amount of irrigation water, the application rate of organic fertilizer, and their interaction had significant effects on the photosynthetic characteristics of mung bean (P<0.05), except for Pn (Tables 2, 3). Compared with the F0 treatment, F1 and F2 treatments increased Pn, Tr, Gs, and Ci of mung bean by 0.70% ~ 3.60%, 16.36% ~ 28.93%, 1.98% ~ 5.44%, and 0.79% ~ 2.49%, respectively. However, no significant differences were observed between F1 and F2 treatments (P>0.05). The I1 and I2 treatments increased the photosynthetic characteristics of mung bean by 11.29% ~ 20.60%, 0.62% ~ 67.74%, 13.74% ~ 22.37%, and 5.17% ~ 9.61%, respectively, compared with the I0 treatment. The effect of irrigation on the photosynthetic characteristics of mung bean showed a gradual increasing trend (P<0.05), which differed from that observed in maize (Figure 9).

3.6 Effects of different water and fertilizer treatments on ET and WUE of corn and mung beans

3.6.1 Maize

According to the results of the three-factor ANOVA in Table 2, planting years, organic fertilizer application amount, and irrigation

10.3389/fpls.2025.1597198

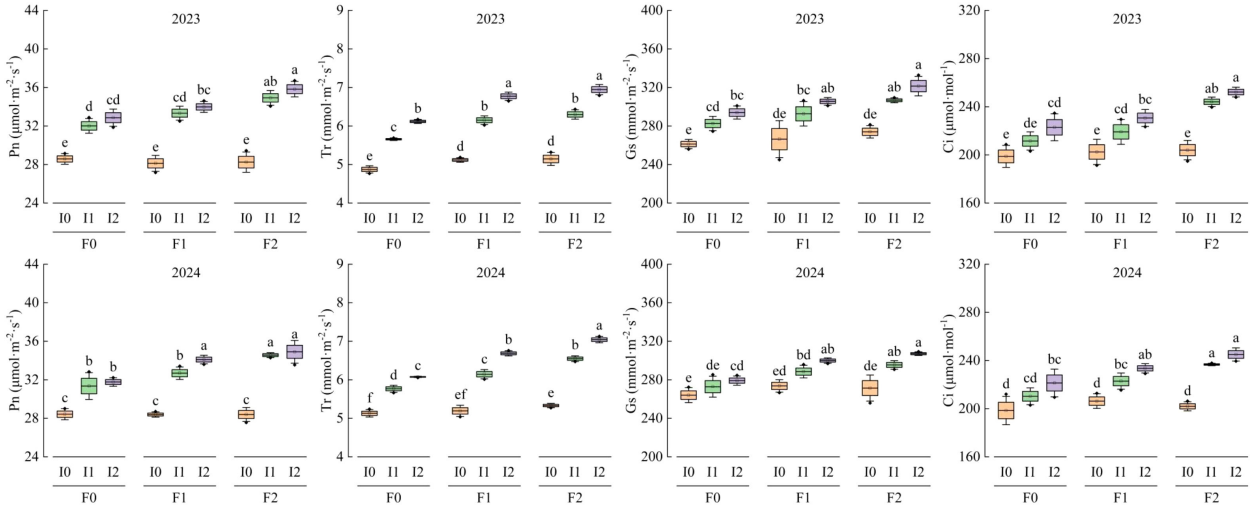

FIGURE 6
The photosynthetic characteristics of maize under different treatments in 2023 and 2024 with the change of emergence. The box plots show the mean, SD and SE, and the photosynthetic characteristics measured at different emergence times are normally distributed. The black origin represents the data distribution and value, the square box represents the SD, the whiskers represent the mean, and the error bars represent the SE of the total curve sum of the three repeated measurements. F0 ~ F2 represent different organic fertilizer application rates, and I0 ~ I2 represent different irrigation rates. Two-factor analysis of variance was performed using the LSD method and post-tests.

amount had significant effects on (Equation 4) and (Equation 6) of maize (P<0.05). The interaction between organic fertilizer application amount and irrigation amount significantly influenced ET (P<0.05), but did not significantly affect WUE (P>0.05). As shown in Table 5, with increasing levels of organic fertilizer application and irrigation, ET exhibited a gradually increasing trend (P>0.05). However, the pattern of WUE differed; no significant differences in WUE were observed between I1, I2, F1, and F2 treatments (P>0.05). Compared with the F0 treatment, ET increased by 0.93% ~ 27.45% under F1 and F2 treatments. Relative to the low irrigation level, ET increased by 2.57% ~ 4.29% under medium and high irrigation levels. Despite the increase in ET, WUE improved significantly: compared with the F0 treatment, WUE increased by 8.61% ~ 10.91% under F1 and F2 treatments. Similarly, relative to the low irrigation level, WUE increased by 7.29% ~ 8.73% under medium and high irrigation levels.

3.6.2 Mung bean

According to the results of three-factor ANOVA in Table 2, planting years, organic fertilizer application amount and irrigation amount had significant effects on ET and WUE of mung bean (P>0.05). The interaction of organic fertilizer application amount and irrigation amount had significant effects on WUE (P<0.05), but had significant effects on ET (P>0.05). This is the opposite of what happens with maize. According to Table 5, with the increase of organic fertilizer application amount and irrigation level, the effects

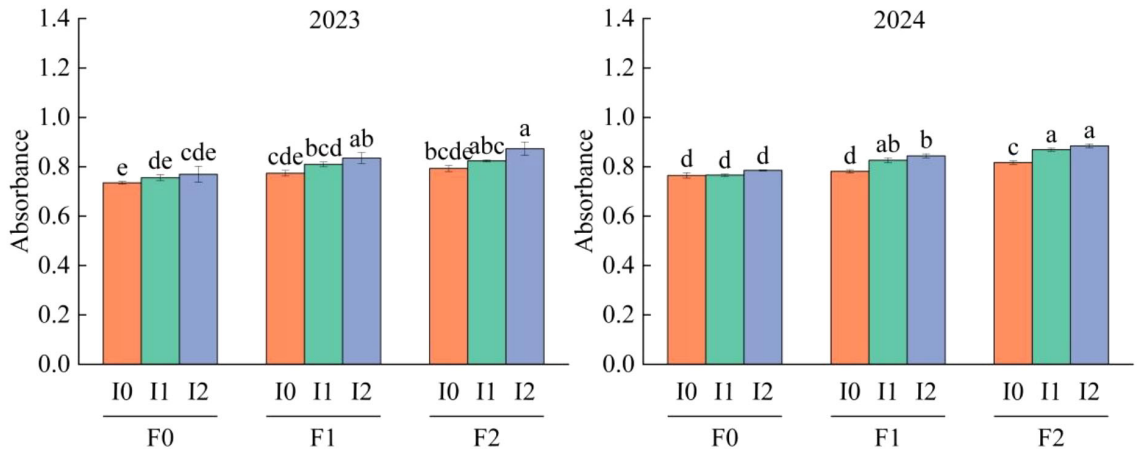

FIGURE 7
Changes of maize Ab with different organic fertilizer amount and irrigation amount at different seedling times in 2023 and 2024.

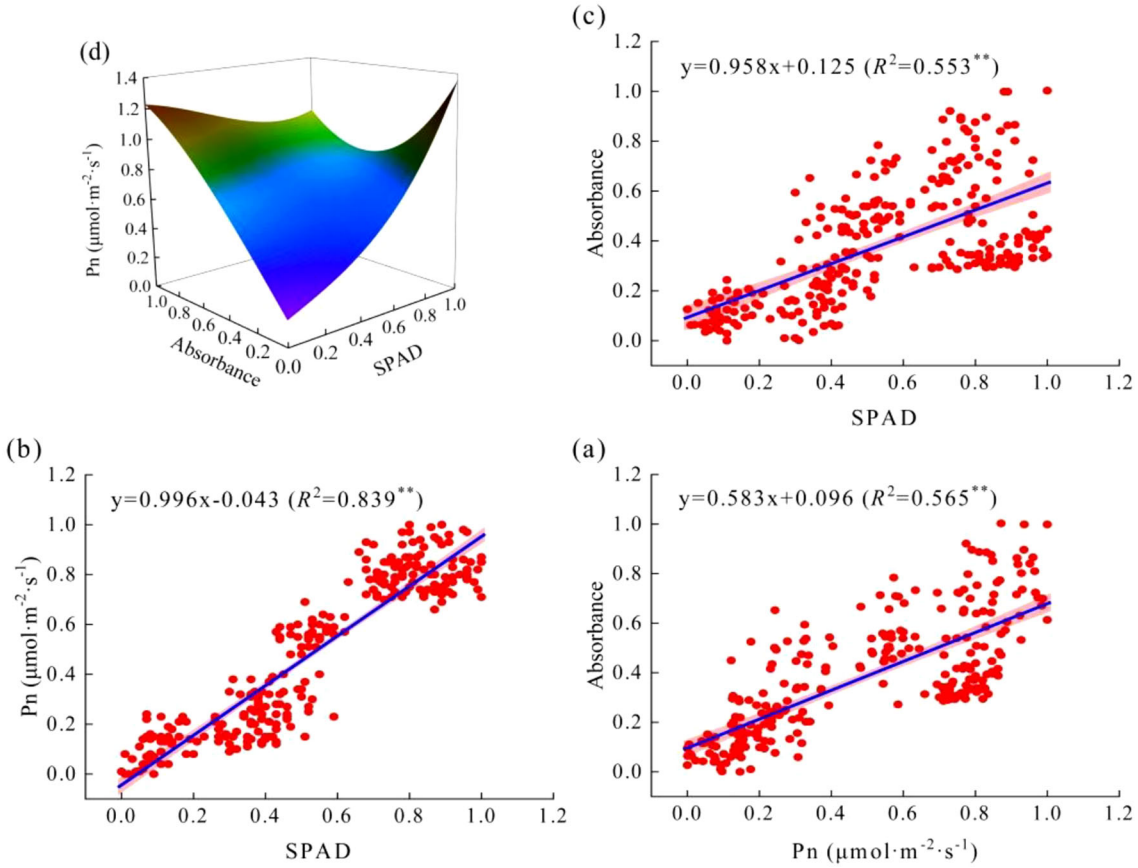

FIGURE 8
The correlation between Pn, SPAD and Ab of maize and the 3D function images among them. **(a)** is the linear fitting result of Ab and Pn, **(b)** is the linear fitting result of Pn and SPAD, **(c)** is the linear fitting result of Ab and SPAD, and **(d)** is the 3D function fitting image between Pn, SPAD and Ab. The red scatter in the 2D image represents the corresponding data, n=135, the blue line represents the regression equation, and the pink boundary represents the confidence interval, which provides a range of estimates for the population parameters.

on ET and WUE of mung bean were the same as those of maize. Compared with F0 treatment, ET in F1 and F2 treatment increased by 2.81% ~ 5.83%. Compared with low irrigation level, ET at medium and high irrigation level increased by 1.70% ~ 3.68%. Compared with F0 treatment, WUE of F1 and F2 treatment increased by 4.13% ~ 5.79%, while WUE of medium and high irrigation level increased by 16.60% ~ 19.74% compared with low irrigation level.

4 Discussion

4.1 Effect of organic fertilizer application rate and irrigation amount on maize/mung bean intercropping DMA and yield

Many studies have demonstrated that gramineous/legume intercropping exhibits greater potential than monocropping due to interspecies effects (Gao et al., 2024). The aim of this study is to investigate the impact of organic manure, a natural fertilizer, in combination with varying irrigation levels on crop growth and physiology, as well as to analyze the underlying patterns and causes. Consequently, this study did not include a monoculture treatment but directly implemented fertilizer and irrigation treatments. The rules and reasons were analyzed by comparing the effects of no application of organic fertilizer and low irrigation levels as a control.

Rational water-fertilizer combinations can effectively promote crop growth and enhance yield. Both irrigation volume, organic fertilizer application rate, and their interactions significantly influenced the DMA of maize and mung beans ($P<0.05$). Under the same irrigation regime, organic fertilizer application increased DMA and yield in both crops, with no significant differences observed between F1 and F2 treatments ($P>0.05$). Similarly, under the same organic fertilizer level, no significant differences were detected between I1 and I2 treatments ($P>0.05$). These findings align with previous studies (Li et al., 2022; Wu et al., 2023), which reported that optimized water-fertilizer management enhances plant DMA and yield. However, excessive fertilizer application does not lead to further increases in DMA or yield. Additionally, Farooq et al. (2019) demonstrated that substituting

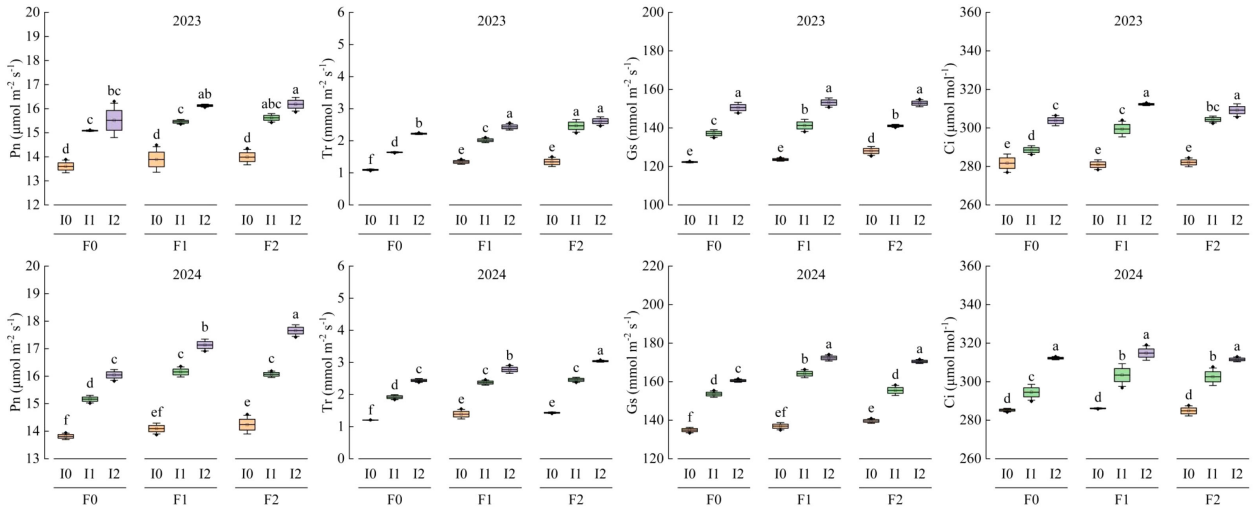

FIGURE 9
Changes of photosynthetic characteristics of mung bean with seedling emergence under different treatments in 2023 and 2024. The box plot shows the normal distribution of mean value, SD and SE and the photosynthetic characteristics data measured at different seedling emergence times, where the black origin represents the data distribution and value, the square box block represents SD, the required line represents the average value, and the error bar represents the SE of the sum of the total curves measured three times. F0 ~ F2 represents different organic fertilizer application amounts, I0 ~ I2 represents different irrigation amounts. LSD method was used to conduct two-factor analysis of variance and post-test.

chemical nitrogen fertilizers with organic fertilizers improves crop DMA and final yield. Comparing our results with existing literature, it is evident that appropriate organic fertilizer application combined with rational irrigation practices can optimize the growth of intercropped maize and mung beans, thereby increasing productivity.

4.2 Effect of organic fertilizer application rate and irrigation amount on LAI and SPAD of intercropped maize/mung bean

This study showed that irrigation amount and application of organic fertilizer had significant effects on LAI and SPAD of maize and mung bean (P<0.05), but their interaction had no significant effects on LAI and SPAD of maize and mung bean (P>0.05), but had significant effects on SPAD of mung bean (P<0.05) (Table 1). The LAI and SPAD of maize and mung bean were increased by increasing irrigation amount and applying organic fertilizer. This result is related to soil water content. When soil water is at a low level, plant leaf growth will be inhibited, chlorophyll degradation rate will be accelerated, resulting in leaf degreening and reduced photosynthetic rate; when soil water is at a high level, leaf growth and chlorophyll accumulation will be promoted (Yang et al., 2023b). LAI and SPAD of maize and mung bean showed a trend of increasing first and then decreasing gradually with the emergence time (Tables 3, 4), which was similar to previous results. After maize silk spinning and mung bean flowering, nitrogen in leaves would be transferred to seeds to meet the filling demand of seeds. In addition, with the advance of crop growth period, leaves will gradually age, resulting in a gradual decrease in leaf area index and SPAD, and a phenomenon of leaf greening (Osaki, 1995; Wang et al., 2023; Dosio et al., 2024).

4.3 Effect of organic fertilizer application rate and irrigation amount on the photosynthetic performance of intercropped maize/mung bean

The gas exchange parameters of maize gradually increased with higher irrigation levels and organic fertilizer inputs (P<0.05) (Figures 6, 9). Across growth stages, photosynthetic traits in maize exhibited a unimodal trend, peaking between 55 – 85 d after emergence (Table 3, Figure 7). Mung bean showed slightly different patterns: organic fertilization and increased irrigation significantly improved its photosynthetic characteristics (P<0.05), but no significant differences were observed between F1F2 or I1I2 treatments (P>0.05) (Figure 9), indicating that fertilized plants generally outperformed unfertilized ones in photosynthetic rate, though the incremental benefits of higher fertilizer/irrigation levels were marginal. Under low soil moisture, enhanced plant water loss induced stomatal closure to conserve water, consequently reducing Tr, Gs, and Ci (Efthimiadou et al., 2010).

In this study, the high water-fertilizer treatment (F2I2) maintained maize and mung bean photosynthesis in the stomatal limitation domain, characterized by unsaturated Gs, Tr, and Ci across treatments, with continuous Pn improvement. This eliminated non-stomatal limitations (e.g., decoupling of Ci and Pn observed in previous studies; Figure 6 and Figure 9), likely

because optimal water and nutrient supply ensured sufficient substrates and energy for photosynthesis. For example (Lo et al., 2019), showed that inadequate water supply reduces electron transport in the initial reaction, limiting CO_2 uptake and decreasing Pn. In such cases, moderate nitrogen fertilization can significantly enhance leaf SPAD values and Gs, promoting photosynthate accumulation and translocation (Yu et al., 2022). Low nitrogen availability may suppress root nutrient uptake, restricting plant growth and photosynthetic efficiency.

Organic fertilizer enhances leaf function through nutrient supply, while irrigation promotes stomatal opening and nutrient mobilization via stomatal regulation and water-fertilizer coupling, forming a positive feedback loop. Their synergistic effect stabilized photosynthetic performance across years in both crops, ensuring reproducible responses under varying environmental conditions. This study highlights the critical role of balanced water-nutrient management in sustaining photosynthetic efficiency and underscores the importance of distinguishing stomatal vs. non-stomatal limitations in crop physiology research.

4.4 The net photosynthetic rate of maize was controlled by absorbance and relative chlorophyll content

LAI, SPAD and available photosynthetic radiation are key factors affecting plant Pn (Tsubo and Walker, 2002; Munz et al., 2014; Bonelli and Andrade, 2020). Ab is a physical quantity used to measure the degree of light absorption, which can directly reflect the ability of the blade to absorb light (Chen et al., 2023a). In this study, only maize Ab was measured and analyzed, because mung bean plants were short and the distance from the surface was limited, and the measurement of Ab was inaccurate. maize Ab showed a single-peak trend with the advancement of maize growth period, and gradually increased with the increase of irrigation amount and organic fertilizer amount, which was similar to the change law of physiological characteristics of maize leaves in the previous paper. In the previous paper, we concluded that appropriate soil water management and increasing the application amount of organic fertilizer could promote LAI and SPAD, thus promoting the light utilization ability of leaves. Moreover, according to the correlation analysis results of Pn, Ab and SPAD, it can be seen that Pn, SPAD and Ab are positively correlated with each other, and all of them have reached a significant level ($P<0.05$). According to the three-dimensional function model established by Pn, Ab and SPAD, Namely $z = -0.011 + 0.615x + 1.503y - 3.016xy - 0.754x^2y + 2.163y^2x + 0.753x^3 - 0.289y^3$, It shows that Pn increases with the action of SPAD and Ab in S-shaped curve, which increases first and then decreases. This further confirms the above mentioned that LAI and SPAD of maize leaves decrease after silking with the advancement of the growth period, and the aging of maize leaves leads to the decrease of light absorption capacity of maize. With the increase of organic fertilizer amount and irrigation amount, LAI and SPAD of maize increased gradually, which resulted in the enhancement of light capture ability of maize.

4.5 Effects of organic fertilizer application rate and irrigation amount on water consumption and yield WUE of intercropping maize/mung bean

Current research on organic fertilizer-irrigation interactions for crop ET and WUE is predominantly confined to monocropping systems, leaving a critical gap in understanding their effects on intercropping—a practice inherently advantageous for resource-use efficiency. Our findings reveal that while crop water consumption in maize-mung bean intercropping increases with irrigation (I1 and I2 elevated ET by 2.57 ~ 4.29% and 1.70 ~ 3.68% vs. I0, respectively), organic fertilizer application significantly enhances WUE by 8.61 ~ 10.91% in maize and 16.60 ~ 19.74% in mung bean compared to unfertilized controls (Table 4). This synergy is theoretically grounded in resource-use complementarity and hydraulic-nutrient interactions, two mechanisms pivotal for optimizing productivity in water-scarce environments.

From a soil-plant hydraulics perspective, organic fertilizers improve soil structure by increasing organic matter content, thereby enhancing water retention and reducing gravitational drainage (Wang et al., 2023; Ning et al., 2024). In intercropping, this creates a "buffer zone" for water availability: maize (a tall, water-demanding crop) and mung bean (a short, drought-tolerant legume) exploit soil water at different depths, while organic matter reduces surface evaporation, directing more water to transpiration —a process directly linked to WUE. This aligns with the "hydraulic lift" hypothesis, where deeper-rooted maize may facilitate water redistribution to shallow-rooted mung bean under moderate irrigation, a phenomenon amplified by improved soil moisture storage from organic amendments (Tolimir et al., 2024).

The nutrient-water interaction effect further explains WUE gains. Organic fertilizers supply slow-release nutrients and bioactive compounds that stimulate root growth and photosynthetic apparatus development (Wang et al., 2021; Zhai et al., 2022; Xu et al., 2024). For instance, enhanced chlorophyll synthesis and stomatal regulation boost carbon assimilation per unit water loss, a mechanism corroborated by our earlier Photosynthetic characteristic data showing higher Pn under fertilized treatments. Critically, in water-limited systems, this nutrient-mediated improvement in "transpiration efficiency" offsets the ET increase from irrigation, creating a net gain in WUE (Sun et al., 2006). This tradeoff is absent in monocropping due to uniform root architecture and resource competition, highlighting intercropping's advantage in leveraging complementary niche differentiation (Chimonyo et al., 2016).

5 Conclusions

This study investigated the effects of organic fertilizer application amount and irrigation amount on leaf growth physiology, photosynthetic characteristics, ET, WUE, dry matter accumulation and yield under maize/mung bean intercropping mode, and the changes of leaf growth physiological characteristics with emergence time. The results showed that the leaf function of maize and mung bean

increased first and then decreased with emergence time. This is because when maize silks and mung beans bloom, nitrogen in the leaves is transferred to the seeds to meet the filling needs of the seeds. With the advancement of crop growth period, leaves will gradually age, resulting in a decline in leaf function. The application of organic fertilizer combined with different irrigation amounts can improve the utilization of light energy by maize/mung bean, significantly improve the leaf growth of maize and mung bean and the synthesis and accumulation of chlorophyll, affect the capture and absorption of light by plants, promote the accumulation of photosynthesis, and ensure the stability of yield. In the case of sufficient water, the application of appropriate reduction of organic fertilizer can ensure that the crop does not reduce production and enhance the yield stability of the plant. Secondly, with the increase of irrigation amount, ET of crops also increased correspondingly, and WUE showed a trend of increasing first and then decreasing. The right amount of water can meet the growth needs of crops, promote photosynthesis and dry matter accumulation, so as to improve WUE. However, when the amount of irrigation exceeds a certain limit, excessive water will lead to an increase in ineffective evaporation, which will reduce WUE.

Although this study explored the variation laws of photosynthetic characteristics, evapotranspiration and water use efficiency of crops in the corn-mung bean intercropping model under the coupling of water and fertilizer, as well as the interaction relationships among pn, spad and ab. However, it did not involve individual experiments or experimental designs in different geographical locations and climates. In subsequent studies, we will continue to set up long-term positioning experiments under different conditions for observation. Meanwhile, we are attempting to combine machine learning methods (such as random forest, neural network, etc.) to construct a relationship among water, fertilizer, photosynthetic characteristics and yield. Perhaps due to the influence of the experimental design, the current construction results are not ideal. Specifically, the constructed equation is somewhat monotonous in the setting of water and fertilizer gradients, which cannot be well visualized, and the coupling degree of the output results is insufficient. We will constantly try and explore its internal mechanism through further experiments.

Data availability statement

The original contributions presented in the study are included in the article/supplementary material. Further inquiries can be directed to the corresponding author.

Author contributions

MG: Data curation, Investigation, Methodology, Software, Validation, Visualization, Writing – original draft. XXW: Methodology, Software, Supervision, Writing – review & editing. RC: Methodology, Supervision, Writing – review & editing. HG: Supervision, Writing – review & editing. XLW: Supervision, Writing – review & editing, Project administration. HL: Project administration, Supervision, Writing – review & editing, Data curation, Funding acquisition.

Funding

The author(s) declare that financial support was received for the research and/or publication of this article. This work was supported by China Agriculture Research System of MOF and MARA-Food Legumes (CARS-08-G-22), Science and Engineering Foundation of Hebei Agricultural University (LG201813).

Conflict of interest

The authors declare that the research was conducted in the absence of any commercial or financial relationships that could be construed as a potential conflict of interest.

Generative AI statement

The author(s) declare that no Generative AI was used in the creation of this manuscript.

Publisher's note

All claims expressed in this article are solely those of the authors and do not necessarily represent those of their affiliated organizations, or those of the publisher, the editors and the reviewers. Any product that may be evaluated in this article, or claim that may be made by its manufacturer, is not guaranteed or endorsed by the publisher.

References

Adetunji, A. T., Ncube, B., Mulidzi, R., and Lewu, F. B. (2020). Management impact and benefit of cover crops on soil quality: A review. *Soil Tillage Res.* 204, 104717. doi: 10.1016/j.still.2020.104717

Bedoussac, L., Journet, E.-P., Hauggaard-Nielsen, H., Naudin, C., Corre-Hellou, G., Jensen, E. S., et al. (2015). Ecological principles underlying the increase of productivity achieved by cereal-grain legume intercrops in organic farming. A review. *Agron. Sustain. Dev.* 35, 911–935. doi: 10.1007/s13593-014-0277-7

Bedoussac, L., and Justes, E. (2011). A comparison of commonly used indices for evaluating species interactions and intercrop efficiency: Application to durum wheat–winter pea intercrops. *Field Crops Res.* 124, 25–36. doi: 10.1016/j.fcr.2011.05.025

Bonelli, L. E., and Andrade, F. H. (2020). Maize radiation use-efficiency response to optimally distributed foliar-nitrogen-content depends on canopy leaf-area index. *Field Crops Res.* 247, 107557. doi: 10.1016/j.fcr.2019.107557

Chen, D., Hu, X., Duan, X., Wei, X., Zhuo, L., Wang, X., et al. (2023a). Incorporating dynamic schemes of canopy light extinction coefficient improves transpiration model performance for fruit plantations. *J. Hydrology* 627, 130397. doi: 10.1016/j.jhydrol.2023.130397

Chen, X., Chen, J., and Cao, J. (2023b). Intercropping increases soil N-targeting enzyme activities: A meta-analysis. *Rhizosphere* 26, 100686. doi: 10.1016/j.rhisph.2023.100686

Chimonyo, V. G. P., Modi, A. T., and Mabhaudhi, T. (2016). Water use and productivity of a sorghum-cowpea-bottle gourd intercrop system. *Agric. Water Manage.* 165, 82–96. doi: 10.1016/j.agwat.2015.11.014

Dosio, G., Cicore, P., and Rizzalli, R. (2024). A time-window within the grain filling period accounted for early leaf senescence in maize under sink limitation. *Eur. J. Agron.* 152, 127027. doi: 10.1016/j.eja.2023.127027

Du, J. B., Han, T. F., Gai, J. Y., Yong, T. W., Sun, X., Wang, X. C., et al. (2018). Maize-soybean strip intercropping: Achieved a balance between high productivity and sustainability. *J. Integr. Agric.* 17, 747–754. doi: 10.1016/S2095-3119(17)61789-1

Efthimiadou, A., Bilalis, D., Karkanis, A., and Froud-Williams, B. (2010). Combined organic/inorganic fertilization enhance soil quality and increased yield, photosynthesis and sustainability of sweet maize crop. *Aust. J. Crop Sci.* 4, 722–729. doi: 10.2134/agronj2010.0122

Farooq, N., Iqbal, M., Farooq, M., and Zahir, Z. A. (2019). Interactive Effects of Synthetic Fertilizer and Organic Residue Inputs on Soil Fertility and Wheat Crop under Various Moisture Regimes. *Int. J. Agric. Biol.* 21, 244–250. doi: 10.17957/IJAB/15.0888

Gao, M. F., Wang, X. X., Chen, R. Q., Gao, H. Y., Chai, C. L., and Liu, H. Q. (2024). Research progress of water effient use in graminus-legume intercropping. *Water Saving Irrigation*. 6, 77–86. doi: 10.12396/jsgg.2023505

Himmelstein, J., Ares, A., Gallagher, D., and Myers, J. (2017). A meta-analysis of intercropping in Africa: impacts on crop yield, farmer income, and integrated pest management effects. *Int. J. Agric. Sustainability* 15, 1–10. doi: 10.1080/14735903.2016.1242332

Huang, Z. L., Li, Y., Fan, M. C., Qian, H. F., and Wang, L. (2024). Recent advances in mung bean protein: From structure, function to application. *Int. J. Biol. Macromolecules* 273, 133210. doi: 10.1016/j.ijbiomac.2024.133210

Jannoura, R., Joergensen, R. G., and Bruns, C. (2014). Organic fertilizer effects on growth, crop yield, and soil microbial biomass indices in sole and intercropped peas and oats under organic farming conditions. *Eur. J. Agron.* 52, 259–270. doi: 10.1016/j.eja.2013.09.001

Kermah, M., Franke, A. C., Adjei-Nsiah, S., Ahiabor, B. D. K., Abaidoo, R. C., and Giller, K. E. (2017). Maize-grain legume intercropping for enhanced resource use efficiency and crop productivity in the Guinea savanna of northern Ghana. *Field Crops Res.* 213, 38–50. doi: 10.1016/j.fcr.2017.07.008

Li, H., Fan, Z., Wang, Q., Wang, G., Yin, W., Zhao, C., et al. (2023). Green manure and maize intercropping with reduced chemical N enhances productivity and carbon mitigation of farmland in arid areas. *Eur. J. Agron.* 145, 126788. doi: 10.1016/j.eja.2023.126788

Li, Y. J., Ma, L. S., Wu, P. T., Zhao, X. N., Chen, X. L., and Gao, X. D. (2022). Impacts of interspecific interactions on crop growth and yield in wheat (*Triticum aestivum* L.)/maize (*Zea mays* L.) strip intercropping under different water and nitrogen levels. *Agronomy-Basel* 12, 951. doi: 10.3390/agronomy12040951

Liu, X., Rahman, T., Song, C., Su, B. Y., Yang, F., Yong, T., et al. (2017). Changes in light environment, morphology, growth and yield of soybean in maize-soybean intercropping systems. *Field Crops Res.* 200, 38–46. doi: 10.1016/j.fcr.2016.10.003

Liu, P. Z., Zhang, T., Zhang, F. Y., Ren, X. L., Chen, X. L., and Zhao, X. N. (2022). Ridge and furrow configuration improved grain yield by optimizing the soil hydrothermal environment and maize canopy traits in Northwest China. *Plant Soil* 499, 23–36. doi: 10.1007/s11104-022-05518-x

Lo, T. H., Rudnick, D. R., Krienke, B. T., Heeren, D. M., Ge, Y., and Shaver, T. M. (2019). Water effects on optical canopy sensing for late-season site-specific nitrogen management of maize. *Comput. Electron. Agric.* 162, 154–164. doi: 10.1016/j.compag.2019.04.006

Luo, C. S., Guo, Z. P., Xiao, J. X., Dong, K., and Dong, Y. (2021). Effects of Applied Ratio of Nitrogen on the Light Environment in the Canopy and Growth, Development and Yield of Wheat When Intercropped. *Front. Plant Sci.* 12, 719850. doi: 10.3389/fpls.2021.719850

Luo, K., Yuan, X. T., Zuo, J., Xue, Y. Y., Zhang, K. J., Chen, P., et al. (2024). Light recovery after maize harvesting promotes soybean flowering in a maize-soybean relay strip intercropping system. *Plant J.* 118, 2188–2201. doi: 10.1111/tpj.16738

Ma, S. T., Mei, F. J., Wang, T. C., Liu, Z. D., and Ma, S. C. (2022). Stereoscopic planting in ridge and furrow increases grain yield of maize (*Zea mays* L.) by reducing the plant's competition for water and light resources. *Agronomy-Basel* 12, 10–20. doi: 10.3390/agriculture12010020

Munz, S., Graeff-Hönninger, S., Lizaso, J. I., Chen, Q., and Claupein, W. (2014). Modeling light availability for a subordinate crop within a strip–intercropping system. *Field Crops Res.* 155, 77–89. doi: 10.1016/j.fcr.2013.09.020

Ning, D., Chen, H., Qin, A., Gao, Y., Zhang, J., Duan, A., et al. (2024). Optimizing irrigation and N fertigation regimes achieved high yield and water productivity and low N leaching in a maize field in the North China Plain. *Agric. Water Manage.* 301, 108945. doi: 10.1016/j.agwat.2024.108945

Osaki, M. (1995). Comparison of productivity between tropical and temperate maize.1. leaf senescence and productivity in relation to nitrogen nutrition. *Soil Sci. Planr Nutr.* 41, 439–450. doi: 10.1080/00380768.1995.10419606

Pelzer, E., Bazot, M., Makowski, D., Corre-Hellou, G., Naudin, C., Al Rifai, M., et al. (2012). Pea-wheat intercrops in low-input conditions combine high economic performances and low environmental impacts. *Eur. J. Agron.* 40, 39–53. doi: 10.1016/j.eja.2012.01.010

Sun, H.-Y., Liu, C.-M., Zhang, X.-Y., Shen, Y.-J., and Zhang, Y.-Q. (2006). Effects of irrigation on water balance, yield and WUE of winter wheat in the North China Plain. *Agric. Water Manage.* 85, 211–218. doi: 10.1016/j.agwat.2006.04.008

Tian, L. X., Li, J., Bi, W. S., Zuo, S. Y., Li, L. J., Li, W. L., et al. (2019). Effects of waterlogging stress at different growth stages on the photosynthetic characteristics and grain yield of spring maize (Zea mays L.) Under field conditions. *Agric. Water Manage.* 218, 250–258. doi: 10.1016/j.agwat.2019.03.054

Tilman, D. (2020). Benefits of intensive agricultural intercropping. *Nat. Plants* 6, 604–605. doi: 10.1038/s41477-020-0677-4

Tolimir, M., Gajić, B., Kresović, B., Životić, L., Gajić, K., Brankov, M., et al. (2024). Impact of deficit irrigation and planting density on grain yield and water productivity of maize grown under temperate continental climatic conditions. *Agric. Water Manage.* 302, 109009. doi: 10.1016/j.agwat.2024.109009

Tsubo, M., and Walker, S. (2002). A model of radiation interception and use by a maize–bean intercrop canopy. *Agric. For. Meteorology* 110, 203–215. doi: 10.1016/S0168-1923(01)00287-8

Wang, W., Li, M. Y., Zhou, R., Mo, F., Khan, A., Batool, A., et al. (2023). Leaf senescence, nitrogen remobilization, and productivity of maize in two semiarid intercropping systems. *Eur. J. Agron.* 150, 126943. doi: 10.1016/j.eja.2023.126943

Wang, X., Nie, J., Wang, P., Zhao, J., Yang, Y., Wang, S., et al. (2021). Does the replacement of chemical fertilizer nitrogen by manure benefit water use efficiency of winter wheat – summer maize systems? *Agric. Water Manage.* 243, 106428. doi: 10.1016/j.agwat.2020.106428

Wu, G., Huang, H.-M., Jia, B.-B., Hu, L.-L., Luan, C.-S., Wu, Q., et al. (2024). Partial organic substitution increases soil quality and crop yields but promotes global warming potential in a wheat-maize rotation system in China. *Soil Tillage Res.* 244, 106274. doi: 10.1016/j.still.2024.106274

Wu, B. J., Zuo, W. Q., Yang, P., and Zhang, W. F. (2023). Optimal water and nitrogen management increases cotton yield through improving leaf number and canopy light environment. *Field Crops Res.* 290, 107988. doi: 10.1016/j.fcr.2022.108745

Xu, Y., Liu, X., Yan, L., Huang, X., and Wang, J. (2024). The addition of organic fertilizer can reduce the dependence of dryland yield on rainfall-based on a 32-year long-term study. *Sci. Total Environ.* 915, 170152. doi: 10.1016/j.scitotenv.2024.170152

Xue, Y. F., Xia, H. Y., Christie, P., Zhang, Z., Li, L., and Tang, C. X. (2016). Crop acquisition of phosphorus, iron and zinc from soil in cereal/legume intercropping systems: a critical review. *Ann. Bot.* 117, 363–377. doi: 10.1093/aob/mcv182

Yang, F., Huang, S., Gao, R. C., Liu, W. G., Yong, T. W., Wang, X. C., et al. (2014). Growth of soybean seedlings in relay strip intercropping systems in relation to light quantity and red:far-red ratio. *Field Crops Res.* 155, 245–253. doi: 10.1016/j.fcr.2013.08.011

Yang, S., Li, H., Xu, Y., Wang, T., Hu, Y., Zhao, Y., et al. (2024). The yield performance of maize-soybean intercropping in the North China Plain: From 172 sites empirical investigation. *Field Crops Res.* 315, 109467. doi: 10.1016/j.fcr.2024.109467

Yang, L., Luo, Y., Lu, B., Zhou, G., Chang, D., Gao, S., et al. (2023a). Long-term maize and pea intercropping improved subsoil carbon storage while reduced greenhouse gas emissions. *Agriculture Ecosyst. Environ.* 349, 108444. doi: 10.1016/j.agee.2023.108444

Yang, Z. F., Tian, J. C., Wang, Z., Feng, K. P., Ouyang, Z., Zhang, L. X., et al. (2023b). Coupled soil water stress and environmental effects on changing photosynthetic traits in wheat and maize. *Agric. Water Manage.* 282, 108246. doi: 10.1016/j.agwat.2023.108246

Yu, N., Ren, B., Zhao, B., Liu, P., and Zhang, J. (2022). Optimized agronomic management practices narrow the yield gap of summer maize through regulating canopy light interception and nitrogen distribution. *Eur. J. Agron.* 137, 126520. doi: 10.1016/j.eja.2022.126520

Zhai, L., Wang, Z., Zhai, Y., Zhang, L., Zheng, M., Yao, H., et al. (2022). Partial substitution of chemical fertilizer by organic fertilizer benefits grain yield, water use efficiency, and economic return of summer maize. *Soil Tillage Res.* 217, 105287. doi: 10.1016/j.still.2021.105287

Zhang, F. S., Cui, Z. L., Fan, M. S., Zhang, W. F., Chen, X. P., and Jiang, R. F. (2011). Integrated Soil-Crop System Management: Reducing Environmental Risk while Increasing Crop Productivity and Improving Nutrient Use Efficiency in China. *J. Environ. Qual.* 40, 1051–1057. doi: 10.2134/jeq2010.0292

frontiers | Frontiers in Plant Science

TYPE Systematic Review
PUBLISHED 15 October 2025
DOI 10.3389/fpls.2025.1534702

Check for updates

OPEN ACCESS

EDITED BY
Maruthi Sridhar Balaji Bhaskar,
Florida International University, United States

REVIEWED BY
Amit Anil Shahane,
Central Agricultural University, India
Kailou Liu,
Jiangxi Institute of Red Soil, China
Ayesha Sadiqa,
University of Lahore, Pakistan

*CORRESPONDENCE
Long Zhao
hkdzhaolong@haust.edu.cn;
hkdzhaolong@163.com
Golam Jalal Ahammed
ahammed@haust.edu.cn

RECEIVED 26 November 2024
ACCEPTED 18 August 2025
PUBLISHED 15 October 2025

CITATION
Ding Y, Shang C, Zhao L, Jin S, Li C, Yin S and Ahammed GJ (2025) Effects of irrigation and fertilization management on kiwifruit yield, water use efficiency and quality in China: A meta-analysis.
Front. Plant Sci. 16:1534702.
doi: 10.3389/fpls.2025.1534702

COPYRIGHT
© 2025 Ding, Shang, Zhao, Jin, Li, Yin and Ahammed. This is an open-access article distributed under the terms of the Creative Commons Attribution License (CC BY). The use, distribution or reproduction in other forums is permitted, provided the original author(s) and the copyright owner(s) are credited and that the original publication in this journal is cited, in accordance with accepted academic practice. No use, distribution or reproduction is permitted which does not comply with these terms.

Effects of irrigation and fertilization management on kiwifruit yield, water use efficiency and quality in China: A meta-analysis

Yuehua Ding[1], Chunfeng Shang[1], Long Zhao[1*], Shanshan Jin[2], Chenyang Li[1], Shanshan Yin[3] and Golam Jalal Ahammed[1*]

[1]College of Horticulture and Plant Protection, Henan University of Science and Technology, Luoyang, China, [2]College of Agricultural Equipment Engineering, Henan University of Science and Technology, Luoyang, China, [3]College of Information Engineering, Henan University of Science and Technology, Luoyang, China

The water-saving and fertilizer-reduction strategies is important for sustainable agricultural development. However existing kiwifruit water-saving and fertilizer-reduction studies showed significant contradictions in the results of water and fertilizer management. Studies have reported conflicting findings on irrigation: some suggest over-irrigation increases yield and WUE, while others advocate low-volume irrigation. Consequently, this study offers a comprehensive meta-analysis encompassing 1038 observations, with the objective of evaluating the influence of water management and optimized fertilization on the yield, water use efficiency (WUE), and quality of kiwifruit. The results showed that the response of kiwifruit to water management was particularly significant in areas with annual average rainfall > 800 mm and field water holding capacity > 28%, and excessive irrigation had a greater negative impact on yield and WUE. With the increase of tree age, the yield-increasing effect of kiwifruit on water and fertilizer optimization gradually weakened. In terms of irrigation methods, drip irrigation has more advantages than traditional irrigation methods. Reducing super-optimal input (SOI) water input can increase kiwifruit yield by 16.24% and WUE by 20.06%. In terms of fertilization management, reducing the input of SOI nitrogen fertilizer can significantly increase the yield of kiwifruit by 32.76%, while reducing the input of SOI nitrogen, phosphorus and potassium can increase the yield by 3.45%. The contents of soluble sugar and vitamin C increased by 6.35% and 18.37%, respectively, but the contents of titratable acid and soluble solids decreased by 4.35% and 6.18%, respectively. In addition, the optimal nitrogen fertilizer level for kiwifruit varies from region to region, and it is generally recommended to be between 100 – 105 kg/ha per hectare. In summary,

scientific and reasonable water and fertilizer management can significantly improve the yield and quality of kiwifruit, optimize WUE, and reduce water and fertilizer waste, providing theoretical basis and practical guidance for sustainable agricultural development.

KEYWORDS

meta-analysis, *Actinidia chinensis*, fertilizer management, irrigation, fruit quality, yield, WUE

1 Introduction

Kiwifruit(Actinidia chinensis), renowned for its high nutritional content, is a widely cultivated fruit abundant in vitamin C, carbohydrates, proteins, and essential minerals (Zhao et al., 2023; Wu et al., 2023; Satpal et al., 2021). A marked increase in global kiwifruit production has been observed, rising from 3.622 million tons in 2014 to 4.518 million tons in 2020. Concurrently, the cultivation area expanded from 224,000 hectares to 280,000 hectares over the same period (Li, 2022). In China, kiwifruit production is predominantly concentrated in the central, southern, and southwestern regions, where both the planting area and total yield surpass those of other regions; however, the yield per unit area remains relatively modest (Lu et al., 2016).This phenomenon shows that while expanding the planting area helps to increase total yield, optimizing water and fertilizer management is urgently needed to improve yield per unit area.Water and fertilizer serve as foundational components of agricultural production, with fertilizer constituting approximately one-third of the overall management expenses in kiwifruit orchards. The prevalent practice of excessive fertilization and irrigation in China, aimed at mitigating the risk of yield loss, has led to significant resource wastage and environmental degradation, including the eutrophication of groundwater and leaching of soil nutrients (Wang et al., 2018a, 2018b; Lv et al., 2020; Cui and Shoemaker, 2018; Li et al., 2017; Davidson et al., 2015). As societal awareness of ecological issues and the economic implications of chemical fertilizers grows, the adoption of fertilizer- and water-saving strategies in agriculture has gained considerable momentum. Water and fertilizer serve as foundational components of agricultural production … the adoption of fertilizer- and water-saving strategies in agriculture has gained considerable momentum (Wang et al., 2019).

A study suggested that optimizing irrigation schedules based on soil water balance is an effective approach, particularly in arid regions, providing a solution for efficient water management in flood-irrigated maize fields (Yi et al., 2022).

Efficient use of water and fertilizer is critical for sustainable agricultural development, especially in arid and semi-arid regions where resource scarcity and environmental concerns are intensifying. The term super-optimal inputs refers to agricultural practices that exceed the optimal levels of water and nutrient application, often leading to resource wastage, reduced efficiency, and environmental degradation. In contrast, water-saving strategies aim to maximize crop productivity per unit of water applied, through techniques such as deficit irrigation or improved irrigation scheduling. Similarly, fertilizer-reduction refers to strategies that maintain yield while decreasing fertilizer input, often by optimizing nutrient timing, type, and dosage through data-driven approaches (Wu et al., 2025; Yi et al., 2022).

However, existing studies on irrigation and fertilization often show inconsistent results, particularly across different climates, cropping systems, and management scales. Many have focused on localized experiments with limited transferability to broader policy or regional planning. Gong et al. (2025) proposed a dynamic optimization of soil phosphorus status (DOP) approach that reduces phosphorus use by up to 47.4% in China without sacrificing yield, offering a model of nutrient management that integrates spatial heterogeneity, crop-specific requirements, and long-term planning (Gong et al., 2025).

These findings highlight the urgent need to integrate more regionally adaptive and resource-efficient management practices into irrigation scheduling and fertilization planning. In particular, flood-irrigated maize fields with varying cultivation histories require context-sensitive strategies to balance productivity with environmental sustainability.

.The previous section discussed the relationship between kiwifruit yield and water and fertilizer management, especially the effect of fertilization on yield. Plant nutrition plays a pivotal role in crop management, with nitrogen being an indispensable nutrient for both crop growth and agricultural yields (Kuypers et al., 2018; Wang et al., 2021; Yang et al., 2017; Tilman et al., 2011). The strategic application of nitrogen fertilizer is widely recognized as a key practice for enhancing crop productivity. However, it is crucial to note that the relationship between crop yield and nitrogen fertilizer input is not linear (Li Y. et al., 2019; Li M.F. et al., 2019; Gu et al., 2017; Hawkesford, 2014). As the amount of fertilizer gradually increases, reaching an optimal level, continuous fertilization beyond this point can lead to a decrease in yield.

Studies have indicated that excessive nitrogen application rates, surpassing 50 kg/ha, can adversely affect kiwifruit yield (Pinto et al., 2021). Over-application of nitrogen can result in the substantial accumulation of nitrate nitrogen in the soil profile, thereby altering the soil's physical and chemical properties (Edwards et al., 2018; Zhou et al., 2016). Nutrient elements are adjusted throughout the growth cycle of kiwifruit according to its growth needs and environmental conditions to ensure its healthy growth and improve yield and quality.

Furthermore, the balanced input of the primary nutrients—nitrogen, phosphorus, and potassium—is essential not only for manipulating yield but also for influencing the quality of kiwifruit. Optimal fertilizer application has been shown to yield the highest returns, with the application of nitrogen and potassium having minimal impact on fruit acidity and soluble solids, although it can compromise fruit firmness (Pacheco et al., 2008). The role of nitrogen and phosphorus in sustaining the yield and quality of 'Hayward' kiwifruit has been highlighted (Guarçoni and Ventura, 2011). The differential demands of kiwifruit for these nutrients suggest a propensity for efficient phosphorus utilization, with potentially lower soil phosphorus requirements and higher soil potassium demands (Liu et al., 2000). The impact of nitrogen and potassium application rates, ranging from 125 to 250 kg/ha for nitrogen and a fixed 200 kg/ha for potassium, on the mineral composition of kiwifruit has been significant (Santoni et al., 2016). Despite the existing body of research on the individual effects of nitrogen, phosphorus, and potassium on kiwifruit yield and quality, a comprehensive analysis of the combined application of these fertilizers and the implications of reducing their application rates on kiwifruit yield and quality is lacking. The optimal input (OI) levels of nitrogen (N), phosphorus (P) and potassium (K) in kiwifruit planting are determined according to the specific soil, climate and planting varieties in different regions. For example, the optimal nitrogen, phosphorus and potassium levels of Wuzhi No.3 kiwifruit planted in Heping County, Guangdong Province are: nitrogen (N) 100 – 105 kg/ha, phosphorus (P) 135 – 140 kg/ha, potassium (K) 170 – 175 kg/ha. These values can be regarded as the critical values of nitrogen, phosphorus and potassium in kiwifruit planting under certain conditions. It should be noted that these values are not fixed, but need to be adjusted according to specific soil test results, local climatic conditions and rootstock varieties. If the amount of fertilizer is insufficient, it can be adjusted by increasing the amount and frequency of fertilizer application; however, excessive fertilization should be avoided. If too much fertilizer is applied, the fertilizer concentration in the soil can be diluted by a large amount of water, and measures to remove damaged leaves and prune damaged roots can be taken. Therefore, a quantitative and systematic synthesis of how varying fertilization levels affect kiwifruit yield and quality is imperative for informed practical application.

Furthermore, research has shown that optimizing phosphorus fertilizer application can lead to a substantial reduction in phosphorus use. A dynamic optimization approach demonstrated a 47.4% reduction in phosphorus fertilizer use without any adverse effects on yield, offering a more sustainable solution for agricultural fertilizer management in China (Gong et al., 2025).

Water serves as a fundamental resource for agricultural productivity, with irrigation being a significant consumer of freshwater resources (Busschaert et al., 2022). In China, agriculture, particularly irrigation, is the primary user of water, and the scarcity of water resources poses a notable constraint on the agricultural sector's development (Li et al., 2020; Li et al., 2021). Research indicates that judicious application of deficit irrigation can often optimize crop water productivity (Wu et al., 2021; Khapte et al., 2019; Patanè and Cosentino, 2009). Kiwifruit, recognized for its substantial water requirements among deciduous fruit trees, necessitates the optimization of irrigation practices to curtail water usage while sustaining or enhancing yield (Gao et al., 2023). Observations reveal that within a specific range, an increase in irrigation volume correlates with elevated levels of reducing sugars and vitamin C in kiwifruit. However, beyond this threshold, a continued increase in irrigation can lead to a marked reduction in titratable acidity, soluble solids, and dry matter content (Wang et al., 2018a; Wang et al., 2018b). Additionally, excessive irrigation combined with high fertilization rates can exacerbate nutrient leaching, thereby impacting crop yields (Muhammad et al., 2022; Wang et al., 2021). Consequently, integrating irrigation and fertilization management at the field scale is deemed critical for the sustainability of agricultural systems (Dai et al., 2019).

However, there are some contradictions in the existing research on the effects of irrigation and fertilizer application. The existing research on water saving and weight loss of kiwifruit shows that there is a significant contradiction between water saving and fertilization management results. In light of this, a meta-analysis is warranted to synthesize the overarching findings from a broad spectrum of existing research (Hedges et al., 1999). The utility of meta-analysis lies in its capacity to account for the diverse water and fertilizer use efficiencies reported in various studies, and to provide a comprehensive examination of the effects of water and fertilizer optimization on kiwifruit trees, an area that has been previously understudied. It allows for the systematic dissection of a multitude of potential factors that could influence dependent variables, thereby enabling the extraction of meaningful conclusions from a body of literature (Stanley, 2001). Consequently, the present study undertakes a meta-analytic review of field trials related to kiwifruit production, with the following three objectives: (1) To evaluate the effects of fertilization and irrigation on kiwifruit yield in China, considering factors such as average annual rainfall, soil water retention capacity and irrigation techniques; (2) To analyze the effects of different irrigation and fertilization practices on water use efficiency (WUE) of kiwifruit; (3) To assess the effects of nitrogen, phosphorus and potassium fertilizers on the quality indexes of kiwifruit.

2 Materials and methods

2.1 Data acquisition

We searched the Web of Science, CNKI, Wanfang and Google Scholar databases for research literature published from May 2002

to February 2023 on the effects of irrigation and fertilization management on kiwifruit yield, WUE and quality. Our search strategy includes keywords such as ' kiwifruit ', ' fertilization ', ' irrigation ', ' nutrient ', ' yield ', ' WUE ' and ' quality ', which are not limited by publication date or language. In order to reduce the risk of data bias and ensure the reliability of the study, we have developed specific criteria for the selection of papers:

1. We included studies based on field trials, excluding those conducted in greenhouses or with potted plants.
2. Studies were required to present kiwifruit yield data, with water use efficiency(kg/m^3) defined as the ratio of yield to water consumption at the field level (WUE = yield/water consumption), which is also known as WUE.
3. We prioritized studies with a randomized block experimental design, favoring those with data repeated over at least two years. Studies lacking repetitive data were excluded. Observations from different years and locations within a single study were treated as independent experiments and included in our dataset.
4. The studies must have reported or allowed the calculation of specific nitrogen, phosphorus, and potassium fertilizer applications.
5. For all variables, studies had to present the mean, sample size (n), standard error (SE), or standard deviation (SD), either in tabular or graphical form. If only n and SE were provided, SD was calculated as SD = SE $\sqrt{n}$. In cases where SE and SD were not reported, SD was estimated as the mean value multiplied by 0.1. Data presented graphically were extracted using the WebPlotDigitizer-4.2.
6. We excluded data about the interaction between water and fertilization effects; the included data were categorized into water or fertilization subsets.

The literature screening process is depicted in Figure 1. Additional data not readily available in publications, such as annual average rainfall, were sourced from the National Meteorological Science Data Center. Considering the varying climatic, edaphic, and irrigation conditions in China's kiwifruit cultivation areas, we categorized the annual average rainfall into ≤ 800 mm and > 800 mm, the field water holding capacity into ≤ 28% and > 28%, and tree age into ≤ 8 years and > 8 years. These threshold values for annual rainfall (>800 mm) and field capacity (>28%) were determined based on the mean and interquartile range of the collected dataset. These cutoffs correspond to hydrological conditions where excessive water input can increase risks of nutrient leaching and root zone hypoxia, particularly in humid

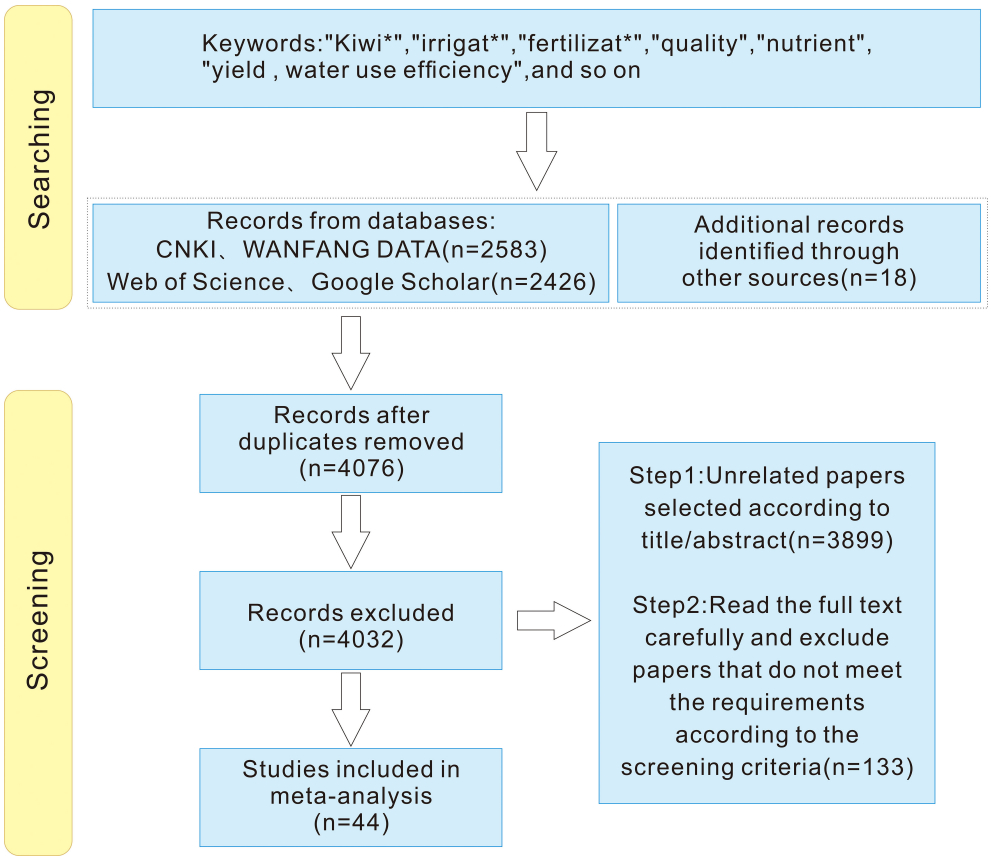

FIGURE 1
Database literature retrieval screening flow chart.

areas (Gao et al., 2023; Wang et al., 2018b). Irrigation systems were classified as drip irrigation and other systems, including small pipe outflow, micro-sprinkler irrigation, and combined drip and sprinkler systems. Ultimately, we amassed data from 44 publications comprising 1038 paired observations, which were categorized into 328 observations for kiwifruit yield, 624 for fruit quality, and 86 for WUE (kg/m^3) The geographical distribution of the experimental sites is illustrated in Figure 2. Details of the publications and data lists are given in Supplementary Materials.

2.2 Subgroup analysis

The term " OI of water and fertilizer" denotes the minimum amount required to achieve maximum yield. The optimum levels of nitrogen, phosphorus and potassium in kiwifruit cultivation should be determined according to local specific soil, climate and planting varieties, such as Wuzhi No.3 kiwifruit planted in Heping County, Guangdong Province. The optimum levels of nitrogen, phosphorus and potassium were N: 100 - 105kg/ha, P: 135 - 140kg/ha, K: 170 - 175kg/ha. The absence of fertilization is indicated as "None." The input of nitrogen fertilizer is categorized as "N" when it exceeds the sub-optimal input (SBI) level (N+) but is less than the SOI level (N-), with the inputs of phosphorus and potassium fertilizers held constant. Similarly, "P" and "K" represent the inputs of phosphorus and potassium fertilizers, respectively, which are above the sub-optimal (P+, K+) but below the SOI (P–, K–) levels. The combination "NK" signifies a scenario where the input of potassium fertilizer is below the optimal level, while the nitrogen fertilizer input is above (N+K-) but below (N-K-) the optimal nitrogen input. Conversely, "PK" indicates that with the potassium fertilizer input below the optimal level, the phosphorus fertilizer input is above (P+K-) but below (P-K-) the optimal phosphorus input. The acronym "NPK" refers to simultaneous changes in the ratios of nitrogen, phosphorus, and potassium fertilizers. It encompasses four combinations: N+P+K+, N+P+K-, N-P-K+, and N-P-K-. Here, N+P+K+ and N+P+K- imply nitrogen and phosphorus fertilizer inputs are above the optimal levels when the potassium input is either above or below the optimal level. N-P-K+ and N-P-K- indicate nitrogen and phosphorus fertilizer inputs are below the optimal levels when the potassium input is above or below the optimal, respectively. If the fertilizer input is insufficient, the amount and frequency of fertilization can be increased, but at the same time, too much fertilization should be avoided. If the fertilizer input is too much, the fertilizer concentration in the soil can be diluted by a large amount of water to remove the damaged leaves and trim the damaged roots. In each study included in the meta-analysis, the amount of fertilizer was adjusted according to the nutrient level in the soil. In the Supplementary Material, the data on nitrogen, phosphorus and potassium levels in the soil of the test site were supplemented. High water level (W+) and low water level (W–) are defined relative to the optimal water input, with high indicating above and low indicating below this benchmark. High water level (W+) and low water level (W –) are defined as water input higher and lower than the optimal water input, respectively. The optimum water level is the basis of water adjustment, which is determined by the growth stage, climatic conditions, soil type, soil moisture and root distribution range of

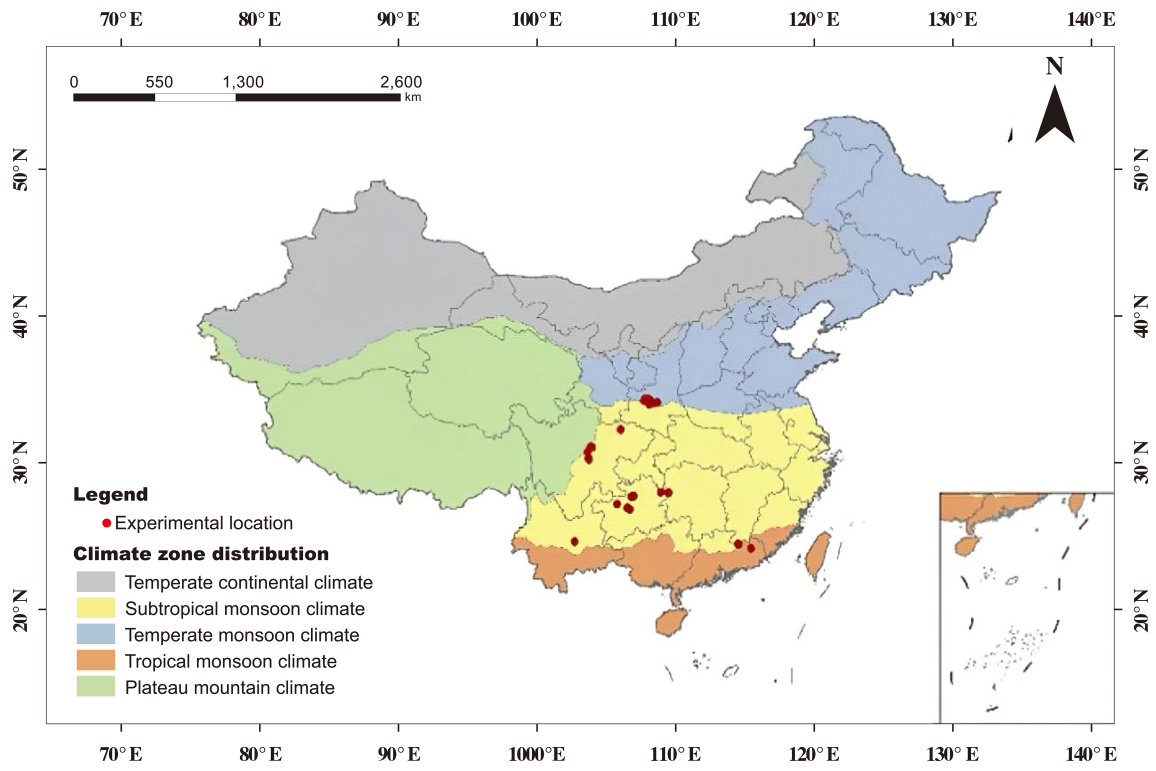

FIGURE 2
Field trial sites in China included in this meta-analysis.

kiwifruit. Inputs above and below these levels reduce yield and WUE. We compared the observed yield and maximum yield of each study to assess how much yield and WUE were reduced by non-optimal inputs. When performing subgroup analysis, if the number of subgroup data is less than two, the subgroup is not considered.For clarity, the following abbreviations were used throughout the figures and analysis: W+ (super-optimal water input), W− (sub-optimal water input), N+ (nitrogen input above optimal level), N− (nitrogen input below optimal level), and similarly for P+/P− and K+/K−.

2.3 Meta-analysis

To quantify the effects of non-optimal water and fertilizer inputs on different response variables (kiwifruit yield, quality, and WUE), the natural logarithm of the response ratio (RR) was used as a measure of the effect size in this meta-analysis, and the ratio of the given variable (X_{obs}) in the treatment group to the given variable (X_{max}) in the control group was used to calculate RR as follows:

Effect sizes were computed as log response ratios (Equation 1); the sampling variance (Equation 2) and study weights (Equation 3) were derived accordingly. The overall mean effect (Equation 4) and its 95% confidence interval (Equation 5) were estimated under a random-effects model, and heterogeneity was assessed using I^2 (Equation 6).

$$RR = \ln\left(\frac{X_{obs}}{X_{\max}}\right) = \ln(X_{obs}) - \ln(X_{\max}) \quad (1)$$

Among them, the average yield, quality, and WUE of kiwifruit under non-optimal water and fertilizer input are the quality and WUE values related to the optimal water and fertilizer input (the highest yield).

The variance (v) of the effect value can be calculated based on sample size, mean, and standard deviation (Luo et al., 2006):

$$v = \frac{S_{obs}^2}{n_{obs}X_{obs}^2} + \frac{S_{\max}^2}{n_{\max}X_{\max}^2} \quad (2)$$

Where, S_{obs}, n_{obs},and X_{obs},are the standard deviation, sample size and mean of the non-optimal input (treatment group), and S_{max}, n_{max}, X_{max},are the standard deviation, sample size and mean of the OI (control group), respectively. Due to the different statistical accuracy of the data in each study, the weighted response ratio (RR + +) was used to calculate the effect value of the treatment group and the control group to improve the accuracy of the effect value (Curtis et al., 1998). The calculation formula of the weighted response ratio and its weight is as follows:

$$RR++ = \frac{\sum_{i=1}^{m}\sum_{j=1}^{k} w_{ij}RR_{ij}}{\sum_{i=1}^{m}\sum_{j=1}^{k} w_{ij}} \quad (3)$$

$$w_{ij} = \frac{1}{v} \quad (4)$$

Among them, m is the number of comparison groups, and k is the comparison number of corresponding groups, and w_{ij} is the weight of the effect value of the item ij. The smaller the variance in the study, the greater the weight, indicating that the index is more important in the comprehensive evaluation process. For the convenience of explanation, all the analysis results in this study were expressed as the percentage change of the weighted response ratio RR + +=e^{RR++}-1×100%25 (Du et al., 2018).

The standard error of the weighted reaction ratio RR + + is calculated as follows:

$$S(RR++) = \sqrt{\frac{1}{\sum_{i=1}^{m}\sum_{j=1}^{k} w_{ij}}} \quad (5)$$

The 95% confidence interval (95% CI) was calculated as follows:

$$95\,\%\,\mathrm{CI} = RR++ \pm 1.96 \times S(RR++) \quad (6)$$

To ascertain the impact of reduced fertilizer application and water conservation on kiwifruit yield, quality, and water use efficiency (WUE), a meta-analysis was conducted utilizing R - 4.1.0 software. This analysis aimed to compute the average effect size and the corresponding 95% confidence interval. An effect is deemed significant if the 95% confidence interval does not overlap with the line of no effect. Heterogeneity among studies is suggested by a p-value greater than 0.1 in conjunction with an I^2 statistic exceeding 50%, necessitating the use of a random effects model; otherwise, a fixed effects model is appropriate. The meta-analytic outcomes for kiwifruit yield, quality, and WUE, as generated by R, indicated substantial heterogeneity across studies ($p > 0.1$ and $I^2 > 50\%$), thereby justifying the application of a random effects model. The presence of reporting bias could potentially skew the results of a meta-analysis, with publication bias being particularly influential (Rosenberg, 2005). Egger's test is a widely recognized quantitative technique for assessing funnel plot asymmetry, serving to identify the presence of publication bias (Egger et al., 1997). The results of this study for kiwifruit yield (fertilization: $p = 0.36$; irrigation: $p = 0.07$), WUE ($p = 0.24$), single fruit weight ($p = 0.08$), soluble sugar ($p = 0.73$), titratable acid ($p = 0.42$), soluble solids ($p = 0.83$), and vitamin C (VC) content ($p = 0.31$) suggested the absence of publication bias. Heterogeneity among studies was evaluated using the I^2 statistic and Cochran's Q-test. When $I^2 > 50\%$ and $p > 0.1$, the heterogeneity was considered substantial, and a random-effects model was applied. Otherwise, a fixed-effects model was used. Egger's regression test was applied to assess publication bias, with a p-value greater than 0.1 indicating low likelihood of bias (Egger et al., 1997). Additionally, effect sizes were weighted using inverse-variance weighting, which gives greater weight to studies with smaller standard errors and thus higher precision.

3 Results

3.1 Overview of the dataset

Variations in soil conditions, cultivar selection, and agricultural practices significantly influence the yield, quality, and water use efficiency (WUE) of kiwifruit. On average, non-optimal water input, as compared to the optimal level, has been observed to

reduce kiwifruit yield and WUE by 18.18% (95%CI: -21.20% to -15.05%) and 6.03% (95% CI: -11.23% to -0.53%) (Figure 3). The aggregate detrimental effects of sub-optimal fertilization on kiwifruit yield, single fruit weight, soluble sugar content, soluble solids, and vitamin C (VC) content were reductions of 23.04% (95% CI: -25.52% to -20.48%), 8.67% (95% CI: -10.82% to -6.46%), 2.74% (95% CI: -6.80% to 1.50%), 4.24% (95% CI: -6.78% to -1.63%), and 6.25% (95% CI: -10.93% to -1.32%), respectively. In contrast, the titratable acidity increased by 2.38% (95% CI: -0.08% to -4.90%) with non-optimal fertilization compared to the optimal condition (Figures 4, 5).

3.2 Response of kiwifruit yield and WUE to water and fertilizer input

The impact of sub-optimal fertilizer inputs on kiwifruit yield was examined, revealing significant reductions in yield compared to optimal levels. Specifically, the effects of low phosphorus and potassium (P-K+) and low nitrogen with high potassium (N-P-K+) on yield reduction were not significant. In contrast, non-optimal nitrogen, phosphorus, and potassium fertilizer inputs collectively led to a substantial decrease in kiwifruit yield (Figure 4). The most pronounced impact was observed with the absence of fertilization (-53.45%), followed by low potassium (K-) input (-48.27%), and low nitrogen (N-) input (-44.82%). The least effect on yield was attributed to the combination of low nitrogen, low phosphorus, and low potassium (N-P-K+) input (-0.15%), with the next highest effects being high nitrogen, high phosphorus, and high potassium (N+P+K+) input (-3.45%), and high nitrogen, high phosphorus, and low potassium (N+P+K-) input (-7.66%). It is important to note that the effect of the N-P-K+ combination should be further verified due to the small sample size (n=3). When nitrogen, phosphorus, and potassium were applied sub-optimally (N-, P-, K-), the rate of yield reduction was significantly higher than when applied super-optimally (N+, P+, K+). Furthermore, the mixed application of nutrients showed that the effect on yield from high nitrogen and low potassium (N+K-) input (-22.82%) was similar to that of high phosphorus and low potassium (P+K-) input (-20.88%), yet both were substantially less than the effects from low nitrogen and low potassium (N-K-) input (-42.94%) and from the combination of low nitrogen, low phosphorus, and low potassium (N-P-K-) input (-37.38%).

The impact of non-optimal water input on kiwifruit yield and WUE was found to be influenced by the annual average rainfall and the field's water holding capacity (Figures 6a, 7a). Irrespective of these factors, it was observed that super-optimal water input(W+) led to a significant reduction in both kiwifruit yield (by 14.19%) and WUE (by 18.48%). Conversely, sub-optimal water input (W-) resulted in a yield decrease of 18.52%, with its effect on WUE being negligible. When the annual average precipitation exceeded 800mm, the negative impact of super-optimal water input (W+) on kiwifruit yield and WUE was more pronounced, at 16.43% and 20.78%, respectively. In contrast, under conditions of sub-optimal water input (W-) and lower annual average precipitation (≤ 800 mm), the yield and WUE of kiwifruit decreased by 24.12% and 13.06%, respectively. Additionally, under the same field capacity, the sub-optimal water input (W-) had a more substantial effect on kiwifruit yield across different water holding capacities (≤ 28%, by 16.54%; > 28%, by 20.28%), whereas its effect on WUE remained minimal and statistically insignificant.

The influence of non-optimal water input on kiwifruit yield and WUE is modulated by tree age and irrigation techniques (Figures 6b, 7b). The impact of both SOI and sub-optimal water input on kiwifruit yield and WUE attenuates with an increase in tree age. Specifically, SOI water input markedly diminished the yield and WUE of kiwifruit in trees less than 8 years old by 19% and 22.32%, respectively. In contrast, this level of water input did not exert a significant negative effect on trees older than 8 years. Drip irrigation, when applied with SOI water, had a more pronounced negative impact on kiwifruit yield (-16.24%) and WUE (-20.06%) than other irrigation methods. Conversely, under sub-optimal water input, while other irrigation methods could significantly enhance kiwifruit WUE by 17.10%, they generally led to a reduction in yield and WUE. It is noteworthy that

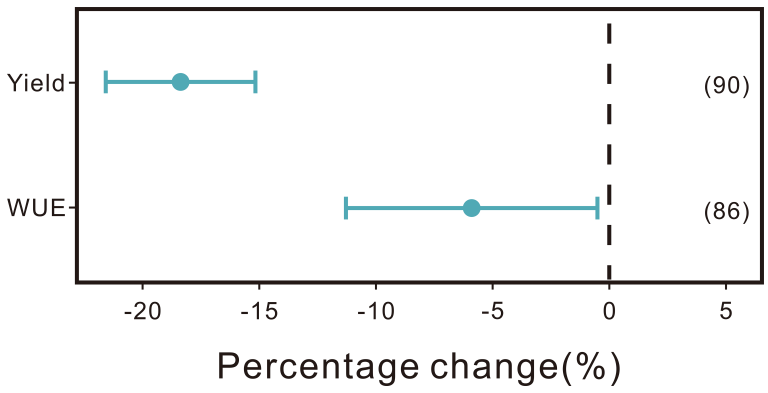

FIGURE 3
Comparison of the effects of non-optimal water input on kiwifruit yield and water use efficiency (WUE) relative to optimal water input levels. The point estimates and bar plots correspond to the mean effect size and the 95% confidence intervals, respectively. The figures encapsulated in parentheses indicate the number of comparative analyses incorporated within the meta-analytic framework.

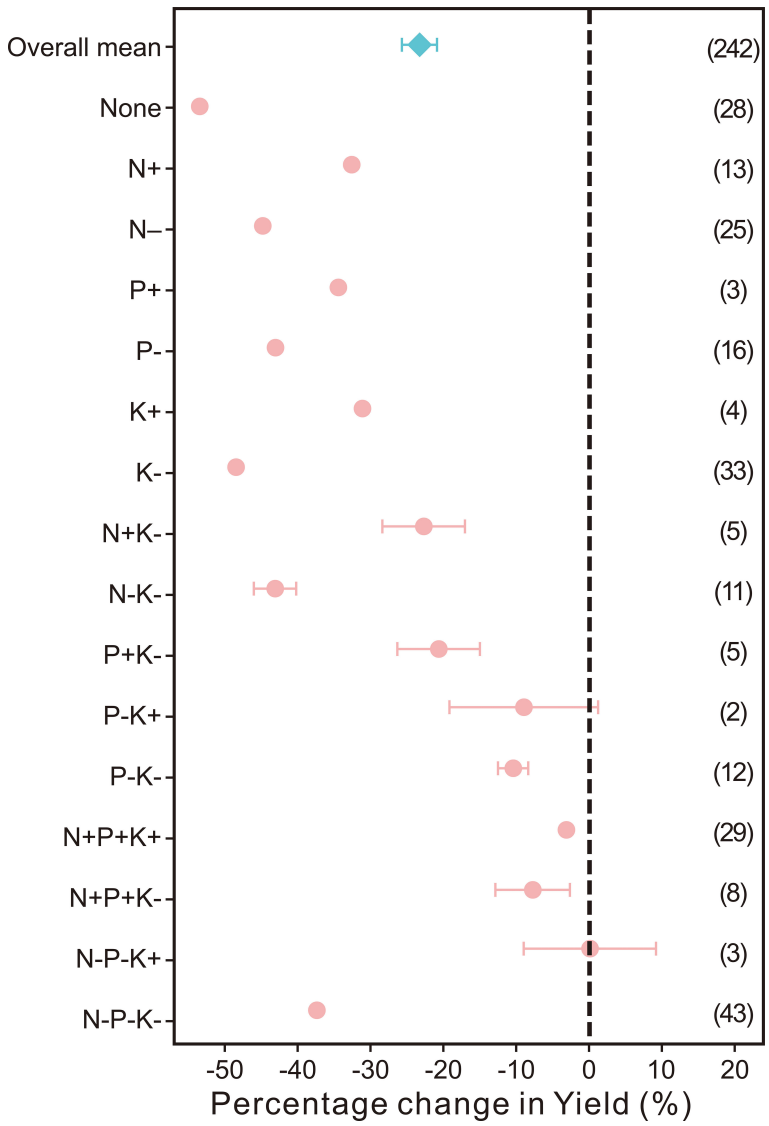

FIGURE 4
Comparison of the effects of non-optimal fertilization rates on kiwifruit yield relative to optimal fertilization rates. Points and bars represent the average effect and 95% confidence interval, respectively. The numbers in parentheses represent the number of comparisons used in the meta-analysis.

under the same irrigation method, the detrimental effect of insufficient irrigation on kiwifruit yield was more pronounced than that of over-irrigation, with the effect on WUE being inversely related.

3.3 Response of kiwifruit quality to nitrogen, phosphorus and potassium fertilizer input

3.3.1 Response of single fruit weight of kiwifruit to changes in nitrogen, phosphorus and potassium fertilizers

Except for a sole increase in phosphate fertilizer application, which marginally elevates the individual fruit weight of kiwifruit, alterations in other fertilizer combinations tend to result in a significant decrease in single fruit weight (Figure 5a). When juxtaposed with the optimal rate of fertilizer application, it is the variation in nitrogen fertilizer input (NK) that exerts the most substantial impact on kiwifruit's individual fruit weight, with a reduction of 16.91%. This effect notably surpasses the influence of phosphorus fertilizer input adjustments (PK), which results in a 9.44% decrease. Furthermore, the modulation of nitrogen fertilizer input (N) alone, either increased or decreased, has a slightly more pronounced effect on the single fruit weight of kiwifruit, at a 6.44% reduction, compared to the potassium fertilizer input (K), which yields a 4.12% reduction. The combined application of nitrogen, phosphorus, and potassium fertilizers generally has a more substantial effect on the single fruit weight of kiwifruit than does the application of a single type of fertilizer.

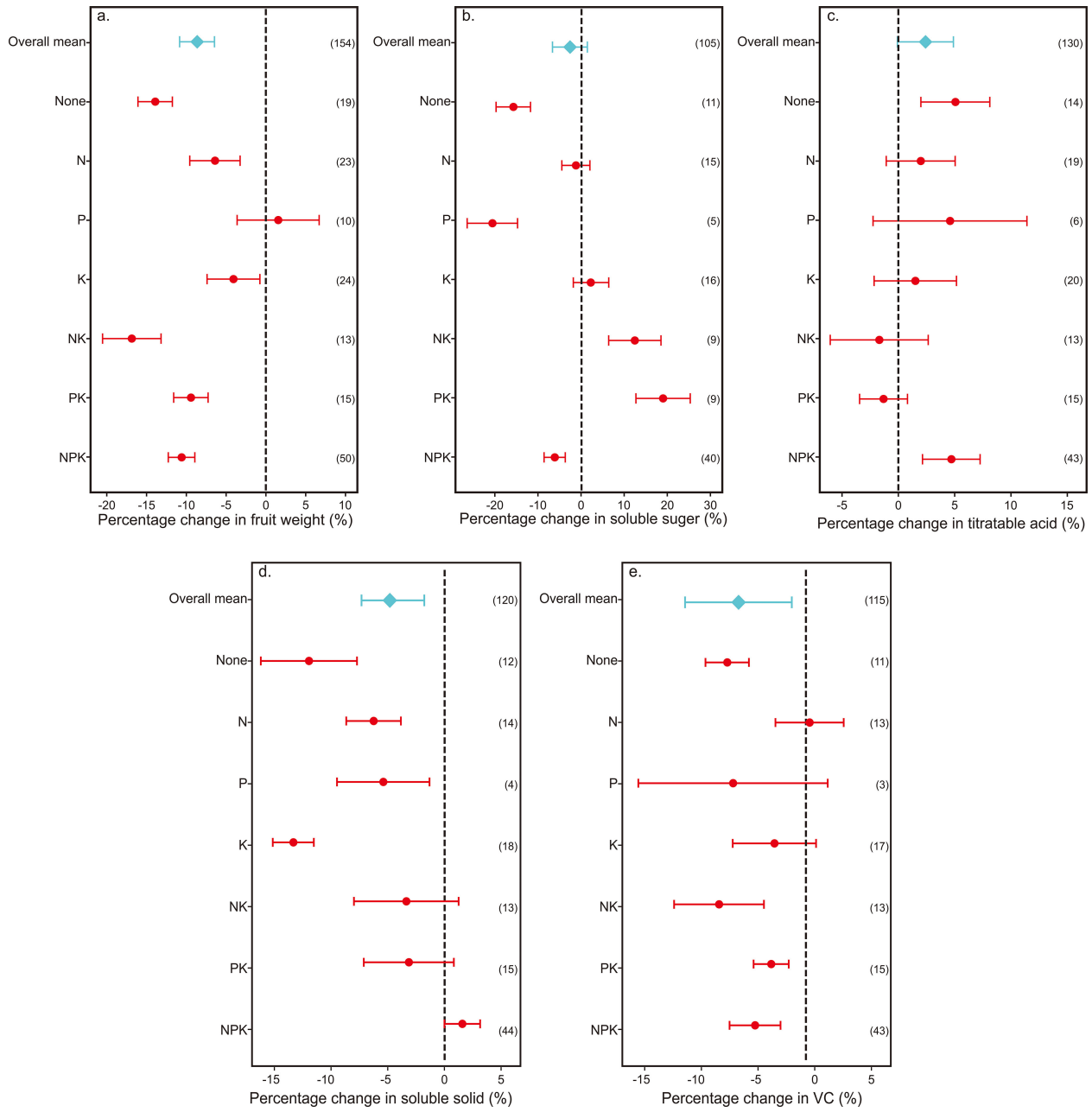

FIGURE 5
Comparison of the effects of non-optimal fertilization rate on different fruit quality indexes relative to the optimal fertilization rate in kiwifruit. Effects of fertilizer treatments on fruit quality parameters: **(a)** fruit weight; **(b)** soluble sugar; **(c)** titratable acid; **(d)** soluble solids; **(e)** vitamin C. The point and bar plots represent the average effect and the 95% confidence interval, respectively. The numbers in parentheses represent the number of comparisons used in the meta-analysis.

3.3.2 Response of soluble sugar in kiwifruit to changes in nitrogen, phosphorus and potassium fertilizers

The soluble sugar content in kiwifruit was found to be significantly diminished by 6.35% due to the application of SOI levels of nitrogen, phosphorus, and potassium fertilizers. Specifically, alterations in the phosphate fertilizer input (P) exerted the most pronounced effect on kiwifruit's soluble sugar levels, causing a reduction of 20.59% (Figure 5b). However, given the small sample size of n=5, these results warrant further verification. Additionally, the absence of fertilizer treatment had a notably negative impact, decreasing the soluble sugar content by 15.83%. While adjustments to potassium fertilizer input (K) slightly elevated the soluble sugar content of kiwifruit, this effect was not statistically significant. In contrast, when nitrogen or phosphorus fertilizer inputs were modified in conjunction with a reduced potassium fertilizer application, the soluble sugar content of kiwifruit experienced a significant increase of 12.44% for the

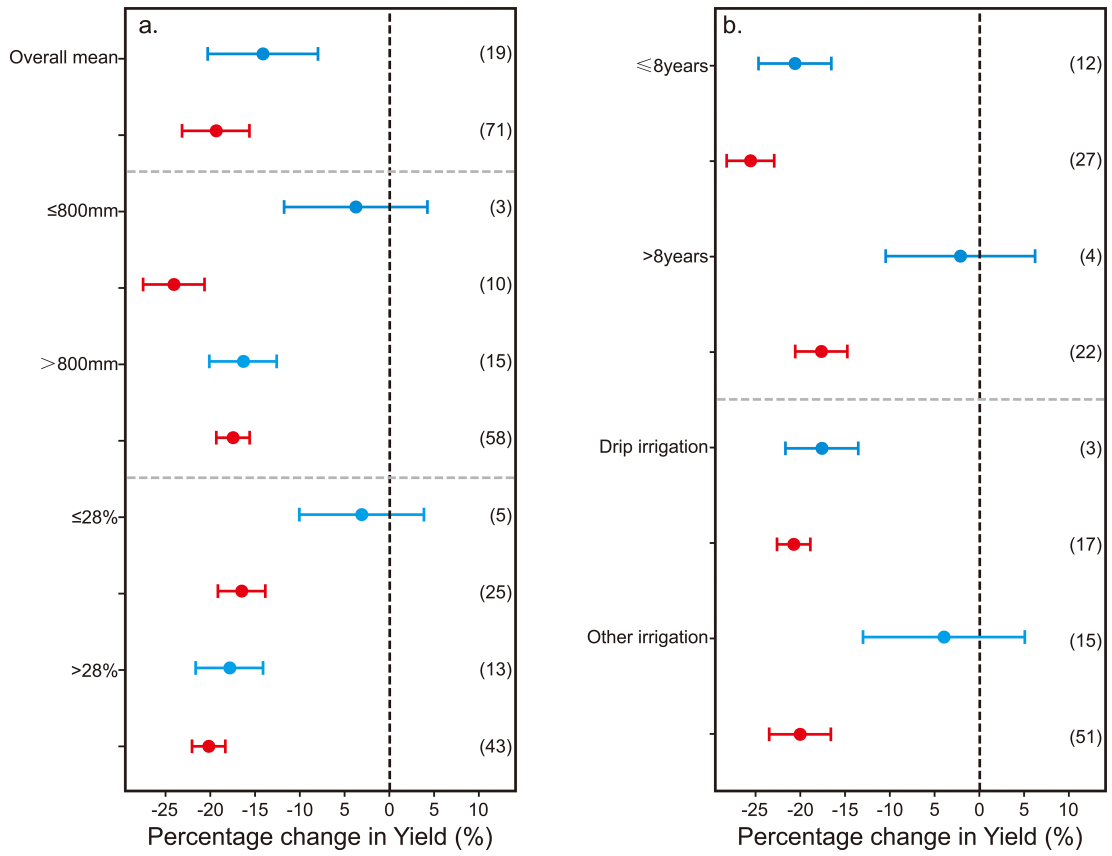

FIGURE 6
Percentage change in yield across conditions: **(a)** rainfall and slope; **(b)** orchard age and irrigation method.

nitrogen and potassium combination (NK) and 18.87% for the phosphorus and potassium combination (PK), respectively. Furthermore, changes in the combined nitrogen, phosphorus, and potassium (NPK) fertilizer input led to a significant reduction in kiwifruit's soluble sugar content by 6.1%.

3.3.3 Response of kiwifruit titratable acid to changes of nitrogen, phosphorus and potassium fertilizers

Among the various fertilization treatments, the sole exception to an increase in titratable acidity of kiwifruit was observed when potassium fertilizer was diminished alongside alterations in nitrogen (NK) or phosphorus (PK) fertilizer inputs, resulting in a minor decrease. Conversely, the remaining treatments were associated with an increase in titratable acidity (Figure 5c). In contrast to the optimal fertilization rate, both the absence of fertilization and the application of an NPK fertilizer mixture notably elevated the titratable acidity levels in kiwifruit, with comparable variation ranges (No Fertilization: 5.00%; NPK: 4.68%). Adjusting solely the input levels of nitrogen, phosphorus, or potassium fertilizers marginally affects the titratable acidity of kiwifruit, yet the impact is statistically insignificant. The application of fertilizers in quantities exceeding the optimal levels for nitrogen, phosphorus, and potassium notably augmented the titratable acidity of kiwifruit by 4.35%.

3.3.4 Response of soluble solids of kiwifruit to changes in nitrogen, phosphorus and potassium fertilizers

Among the various fertilizer inputs, the alteration in potassium fertilizer input had the most pronounced impact on the soluble solids content of kiwifruit. Adjustments to potassium fertilizer input, whether increases or decreases, resulted in a 12.49% reduction in the percentage change of kiwifruit's soluble solids (Figure 5d). Similarly, no fertilization treatment also significantly reduced the soluble solids content of kiwifruit by 11.25%. The effect of changing the input of nitrogen fertilizer or phosphorus fertilizer on the soluble solids of kiwifruit was similar when the potassium fertilizer was reduced, which decreased by 3.24% (NK) and 2.99% (PK), respectively. Among all fertilization treatments, solely the variation in the NPK fertilizer mixture input demonstrated a positive, albeit minor and statistically insignificant, impact on the soluble solids of kiwifruit. Conversely, the application of fertilizers at levels exceeding the optimal rates for nitrogen, phosphorus, and potassium notably elevated the soluble solids content of kiwifruit by 6.18%.

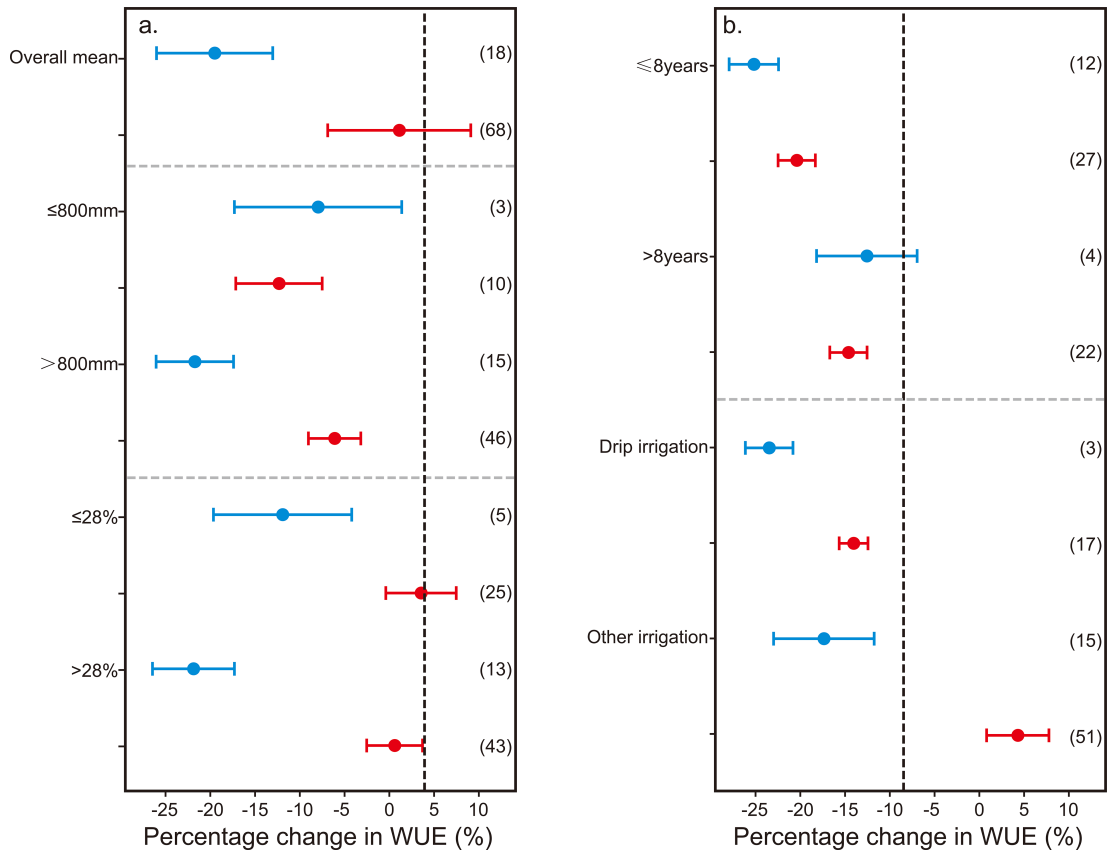

FIGURE 7
Comparison of the effect of non-optimal water input on the water use efficiency (WUE) of kiwifruit relative to the optimal water input under different annual average rainfall (≤ 800 mm and > 800 mm) **(a)**, field water holding capacity (≤ 28% and > 28%) **(a)**, tree age (≤ 8years and > 8 years) **(b)** and irrigation methods (drip irrigation and other irrigation) **(b)**. The effect of non-optimal water input on the WUE of kiwifruit. Blue (•) indicates SOI water input, and orange (•) indicates sub-optimal water input. The point and bar plots represent the average effect and the 95% confidence interval, respectively. The numbers in parentheses represent the number of comparisons used in the meta-analysis.

3.3.5 Response of VC content in kiwifruit to changes in nitrogen, phosphorus and potassium fertilizers

The input of SOI NPK fertilizer significantly reduced the VC content of kiwifruit by 18.37%. Compared with only changing the amount of nitrogen fertilizer input, there was almost no effect on the VC content of kiwifruit; however, various fertilization treatments resulted in a reduction of VC content in kiwifruit (Figure 5e). The variation range of VC content in kiwifruit was similar without fertilization and only changing the input of phosphate fertilizer (None: -7.25%; p: -7.06%), but the sample size of the treatment only changing the input of phosphate fertilizer was small (n = 3), and thus the results need to be further verified. Compared with the optimal amount of fertilizer, increasing or decreasing the amount of potassium fertilizer input (K) had little effect on the VC content of kiwifruit (-2.97%), but changing the amount of nitrogen fertilizer input (NK) when the amount of potassium fertilizer decreased would reduce the VC content of kiwifruit by 8.08%, which was higher than the effect of changing the amount of phosphorus fertilizer input (PK) on the VC content of kiwifruit when the amount of potassium fertilizer decreased (-3.23%).

4 Discussion

Based on existing literature, this study conducted a systematic and quantitative analysis of the impact of water conservation and fertilizer reduction on the yield and quality of kiwifruit. Based on the meta-analysis of this study, it was found that inappropriate water and fertilizer management significantly reduced kiwifruit yield and water use efficiency (WUE).The meta-analysis revealed that suboptimal fertilization practices led to a decrease in kiwifruit yield, individual fruit weight, soluble sugar content, soluble solids, and vitamin C content by 23.04%, 8.67%, 2.74%, 4.24%, and 6.25%, respectively, while the titratable acidity increased by 2.38% (Figures 4, 5). This outcome is primarily attributed to the fact that excessive fertilization raises the soil's hydrogen ion concentration, causing soil acidification by decreasing pH (Cui et al., 2013). This, in turn, hinders the complete absorption and utilization of nutrients such as nitrogen, phosphorus, and potassium by plants, thereby adversely affecting the yield and quality of kiwifruit. Furthermore, nitrogen, phosphorus, and potassium are essential nutrients required for plant growth and

development (Ahammed et al., 2022). An inadequate supply of nitrogen, phosphorus, and potassium fertilizers can restrict the growth and development of kiwifruit plants, consequently diminishing their yield and quality (Chu et al., 2021).

Reducing the application of SOI levels of nitrogen fertilizer and combined nitrogen, phosphorus, and potassium fertilizers to optimal levels can enhance kiwifruit yield by 32.76% and 3.45%, respectively (Figure 4). Studies have indicated that nitrogen application in excess of what is supported by soil, climate, and field management practices may result in yield losses (Zhang et al., 2015; Gao et al., 2012). The detrimental effect of insufficient application of individual nitrogen, phosphorus, and potassium nutrients on kiwifruit yield was found to be significantly greater than that of over-fertilization (Figure 4). This can be attributed to the high demand for nitrogen, phosphorus, potassium and other nutrients in kiwifruit. Although this study considered the effects of annual average rainfall and soil water holding capacity on kiwifruit yield and WUE, it may not fully consider the combined effects of other environmental factors (such as temperature, light, etc.). comparative analysis of the yield reduction rates associated with varying inputs of nitrogen, phosphorus, and potassium, particularly under conditions of low nitrogen and potassium (N-K-), revealed a significant decrease in kiwifruit yield by 42.94%. This suggests that kiwifruit has a relatively higher requirement for nitrogen and potassium, while the demand for phosphorus is comparatively lower, aligning with existing research findings. The disproportionate yield response to nitrogen alone *vs.* NPK combinations may be due to nutrient antagonism or dilution effects. Nitrogen promotes vegetative growth, which directly enhances yield, while excess phosphorus and potassium may interfere with nitrogen uptake or balance, reducing synergistic effects (Sardans and Peñuelas, 2021; Liu, 2021). This highlights kiwifruit's higher demand for N and K compared to P. In correlation with yield results, both excessive and insufficient applications of nitrogen and potassium fertilizers were found to significantly reduce the single fruit weight of kiwifruit (Figure 5a).

Conversely, adjusting the application amount of phosphate fertilizer increased the single fruit weight of kiwifruit by 1.32% compared to the optimal fertilization level, potentially due to variations in the number of fruits per plant among the sampled kiwifruit trees. The impact of combined nitrogen, phosphorus, and potassium fertilizer inputs on the single fruit weight of kiwifruit was generally more pronounced than that of single nutrient applications. This synergistic effect is attributed to the interactive relationships between these three essential nutrient elements (Chu et al., 2021). Potassium notably enhances the absorption and utilization efficiency of nitrogen by plants, facilitating its rapid conversion into protein, which in turn, contributes to an increase in the single fruit weight of kiwifruit (Liu, 2021)Although the effect of nitrogen (−16.91%) and phosphorus (−9.44%) fertilizer inputs on single fruit weight appeared notably different, the confidence intervals of these estimates partially overlap, indicating that the statistical significance of the difference between them may be limited. Further subgroup analyses by environmental factors such as tree age, rainfall, and soil capacity were constrained by limited sample size in the included studies. Nonetheless, the more pronounced effect of nitrogen may reflect its direct role in cell division and expansion during fruit development (Liu, 2021), whereas phosphorus primarily affects energy metabolism. These physiological differences might explain the observed magnitude gap.

Kiwifruit, known for its nutritional richness, exhibits varying responses in nutrient content to different fertilizer application rates. This study analyzed the impact of fertilization on kiwifruit quality, ensuring conditions were optimal for maximal yield. Relative to the optimal fertilization strategy, modifications in nitrogen fertilizer levels had minimal influence on the levels of soluble sugars, titratable acidity, and vitamin C (VC) in kiwifruit (Figures 5b, c, e). This insignificance may stem from the specific nitrogen requirements of kiwifruit, where an appropriate nitrogen input can notably enhance individual fruit weight without compromising fruit quality. Conversely, a reduction in soluble sugar, soluble solids, and VC content, and a rise in titratable acidity were observed in kiwifruit (Figures 5b–e). Phosphorus, integral to plant nutrition, is a constituent of key compounds including nucleic acids, proteins, and enzymes. Insufficient phosphorus can restrict plant growth, development, and metabolism (Poirier and Bucher, 2002; Sardans and Peñuelas, 2021). This study revealed that adjusting the levels of nitrogen, phosphorus, and potassium fertilizers to match the application rates at the peak yield point could markedly elevate the soluble sugar and VC content in kiwifruit by 6.35% and 18.37% (Figures 5b, e). Conversely, the titratable acidity and soluble solids content were significantly lowered by 4.35% and 6.18%(Figures 5c, d). The role of potassium in plant cells includes osmotic regulation and maintaining ionic balance. An excessive application of potassium fertilizer may lead to competition between potassium ions and other ions, such as Ca2+, Mg2+, NH4+, etc., for entry into fruit cells (Srivastava et al., 2020; Sustr et al., 2019; Xu et al., 2020; Panda et al., 2012; Sangha et al., 2023), potentially inhibiting VC synthesis. Furthermore, an overabundance of potassium can escalate the soluble solids content within the fruit, disrupting its acid-base equilibrium and elevating the fruit's pH value. This shift can accelerate fruit rancidity, thereby impairing fruit quality and flavor.

The yield and WUE of kiwifruit experienced respective increases of 14.19% and 18.48%, when SOI water input was adjusted to optimal levels. Conversely, augmenting sub-optimal water input to optimal levels resulted in yield and WUE increases of 18.52% and 1.57%, respectively (Figures 6a, 7a). These findings underscore the critical importance of precise water management. Over-irrigation may induce root hypoxia in kiwifruit and contribute to nutrient leaching from the soil, consequently diminishing yield and WUE (Li et al., 2014) Insufficient water supply, on the other hand, causes evident stress symptoms in plants, impeding normal growth and development (Yang et al., 2012; Pahalvi et al., 2021).

Subgroup analysis revealed that the impact of non-optimal water input on kiwifruit yield and WUE is contingent upon annual average rainfall and the field's water holding capacity (Figures 6a, 7a). In regions with an annual average rainfall exceeding 800 mm and a field water holding capacity above 28%, the adverse effects of SOI water input on kiwifruit yield and WUE were markedly more pronounced than in areas with lower rainfall and water holding capacity. This disparity may arise from the enhanced water holding capacity of soils

in regions with higher precipitation and water holding capacity. Excessive irrigation in such areas can lead to waterlogging and surface runoff, surpassing the water requirements of kiwifruit plants and thus reducing their WUE (Yang et al., 2012). Over-saturation of soil can impede oxygen circulation, degrade soil aeration, curtail microbial populations and activity, and adversely affect soil fertility and health (Wei et al., 2021).

Moreover, in low-lying areas with poor drainage, soil saturation can exacerbate salinization and potentially result in root death and decline of kiwifruit plants. The influence of non-optimal water input on kiwifruit yield and WUE is also moderated by tree age. The study confirmed that the negative effects of both SOI and sub-optimal water input on yield and WUE are mitigated with increasing tree age (Figures 6b, 7b). This outcome can be ascribed to the more extensive root systems of mature kiwifruit trees, which foster a more stable ecosystem, bolster environmental and soil adaptability, and confer greater resilience to drought and flood, thereby decreasing reliance on irrigation water.

Additionally, as kiwifruit trees age, their leaf area expands, escalating transpiration rates and influencing WUE. Appropriate irrigation methods are pivotal for enhancing crop yields. Meta-analysis results indicated that under drip irrigation, reducing SOI water input to optimal levels significantly increased kiwifruit yield and WUE by 16.24% and 20.06%, respectively—outperforming other irrigation techniques (Figures 6b, 7b). This superiority is largely attributed to the distinct soil water and salt transport characteristics associated with different irrigation methods (Yu et al., 2020). Drip irrigation delivers water directly to the root zone, enabling precise soil moisture management while minimizing surface evaporation and the risk of soil salinization. In contrast, other irrigation methods, such as tubular outflow, may lead to water pooling and localized hypoxia, which can significantly impede root respiration and the transport of water and nutrients. Nonetheless, other irrigation methods have been observed to enhance kiwifruit WUE under sub-optimal water input conditions (Figure 7b), possibly due to variations in irrigation water application across studies. Furthermore, micro-sprinkler irrigation and combined drip-sprinkler systems can more effectively manage water distribution, reducing deep percolation losses.

5 Conclusions

This paper presents a meta-analysis of field experimental data from kiwifruit production across various growth environments in China. This study demonstrates that optimizing nitrogen, phosphorus, and potassium (NPK) fertilizer levels, along with water input, can significantly improve kiwifruit yield and water use efficiency (WUE). In particular, reducing nitrogen fertilization to optimal levels enhances yield and quality, highlighting kiwifruit's higher demand for nitrogen and potassium compared to phosphorus. These findings provide valuable insights into water and fertilizer management for kiwifruit cultivation. These findings indicate that kiwifruit exhibits a relatively higher demand for nitrogen and potassium compared to phosphorus. Furthermore, by optimizing water input, both the yield and WUE of kiwifruit were increased by 14.19% and 18.48%, respectively. In regions with an annual average rainfall exceeding 800 mm and a field water holding capacity above 28%, the detrimental effects of SOI water input on kiwifruit yield and WUE were considerably more pronounced than in regions with lower rainfall and water holding capacity. The impact of both SOI and sub-optimal water input on kiwifruit yield and WUE was found to diminish with the increase in tree age. Drip irrigation, in particular, emerged as a superior water-saving technique in kiwifruit orchards, significantly boosting yield and WUE by 16.24% and 20.06%, respectively. Based on the results of this study, future research can further explore the changes in the response of kiwifruit to water and fertilizer reduction at different growth stages, and the best water and fertilizer management strategies under different climatic and soil conditions. In addition, the inclusion of economic cost analysis will help farmers and decision-makers to better balance resource utilization and economic benefits in practical applications. Future studies should integrate temperature and light conditions to further refine irrigation and fertilization recommendations tailored to local environments. In addition, these results highlight the importance of defining region-specific thresholds for water and nutrient inputs, as environmental factors such as rainfall and soil capacity vary widely across kiwifruit-producing areas. Future research should also incorporate economic input–output analysis, soil microbial community responses, and long-term sustainability modeling to develop more integrated and practical irrigation-fertilization strategies for farmers. Future studies should integrate temperature and light conditions to further refine irrigation and fertilization recommendations tailored to local environments.

Data availability statement

The original contributions presented in the study are included in the article/Supplementary Material. Further inquiries can be directed to the corresponding authors.

Author contributions

YD: Conceptualization, Data curation, Formal analysis, Methodology, Resources, Validation, Writing – review & editing. CS: Data curation, Formal analysis, Investigation, Resources, Software, Validation, Writing – original draft, Writing – review & editing. LZ: Conceptualization, Data curation, Formal analysis, Funding acquisition, Project administration, Resources, Supervision, Visualization, Writing – review & editing. SJ: Conceptualization, Data curation, Formal analysis, Methodology, Software, Validation, Writing – review & editing. CL: Investigation, Software, Validation, Writing – original draft. SY: Formal analysis, Investigation, Resources, Validation, Writing – original draft. GA: Writing – original draft, Writing – review & editing.

Funding

The author(s) declare financial support was received for the research and/or publication of this article. This work was supported by the National Natural Science Foundation of China (No. 52309050), Key R&D and Promotion Projects in Henan Province (Science and Technology Development) (No. 232102110264), and Key Scientific Research Projects of Colleges and Universities in Henan Province (No. 24B416001).

Conflict of interest

The authors declare that the research was conducted in the absence of any commercial or financial relationships that could be construed as a potential conflict of interest.

Generative AI statement

The author(s) declare that no Generative AI was used in the creation of this manuscript.

Any alternative text (alt text) provided alongside figures in this article has been generated by Frontiers with the support of artificial intelligence and reasonable efforts have been made to ensure accuracy, including review by the authors wherever possible. If you identify any issues, please contact us.

Publisher's note

All claims expressed in this article are solely those of the authors and do not necessarily represent those of their affiliated organizations, or those of the publisher, the editors and the reviewers. Any product that may be evaluated in this article, or claim that may be made by its manufacturer, is not guaranteed or endorsed by the publisher.

Supplementary material

The Supplementary Material for this article can be found online at: https://www.frontiersin.org/articles/10.3389/fpls.2025.1534702/full#supplementary-material

References

Ahammed, G. J., Chen, Y., Liu, C., and Yang, Y. (2022). Light regulation of potassium in plants. *Plant Physiol. Biochem.* 170, 316–324. doi: 10.1016/j.plaphy.2021.12.019

Busschaert, L., De Roos, S., Thiery, W., Raes, D., and De Lannoy, G. J. M. (2022). Net irrigation requirement under different climate scenarios using AquaCrop over Europe. *Hydrol. Earth Syst. Sci. Discuss.* 2022, 1–30. doi: 10.5194/hess-26-3731-2022

Chu, C., Wang, Y., and Wang, E. (2021). Research status and prospect of efficient utilization of nitrogen, phosphorus, and potassium in plants. *Chin. Sci.: Life Sci.* 51, 1415–1423. doi: 10.1360/SSV-2021-0163

Cui, S. H., Shi, Y. L., Groffman, P. M., Schlesinger, W. H., and Zhu, Y. G. (2013). Centennial-scale analysis of the creation and fate of reactive nitrogen in China, (1910 - 2010). *Proc. Natl. Acad. Sci.* 110, 2052–2057. doi: 10.1073/pnas.1221638110

Cui, K., and Shoemaker, S. P. (2018). A look at food security in China. *NPJ Sci. Food* 2, 4. doi: 10.1038/s41538-017-0016-2

Curtis, P. S., and Wang, A. (1998). A meta-analysis of elevated CO2 effects on woody plant mass, form, and physiology. *Oecologia* 113, 299–313. doi: 10.1007/s004420050381

Dai, Z. G., Fei, L. J., Huang, D. L., Zeng, J., Chen, L., and Cai, Y. H. (2019). Coupling effects of irrigation and nitrogen levels on yield, water and nitrogen use efficiency of surge-root irrigated jujube in a semiarid region. *Agric. Water Manage.* 213, 146–154. doi: 10.1016/j.agwat.2018.09.035

Davidson, E. A., Suddick, E. C., Rice, C. W., and Prokopy, L. S. (2015). More food, low pollution (Mo Fo Lo Po): a grand challenge for the 21st century. *J. Environ. Qual.* 44, 305–311. doi: 10.2134/jeq2014.09.0340

Du, Y. D., Niu, W. Q., Gu, X. B., Zhang, Q., Cui, B. J., and Zhao, Y. (2018). Crop yield and water use efficiency under aerated irrigation: A meta-analysis. *Agric. Water Manage.* 210, 158–164. doi: 10.1016/j.agwat.2018.07.038

Edwards, J. D., Pittelkow, C. M., Kent, A. D., and Yang, W. H. (2018). Dynamic biochar effects on soil nitrous oxide emissions and underlying microbial processes during the maize growing season. *Soil Biol. Biochem.* 122, 81–90. doi: 10.1016/j.soilbio.2017.12.017

Egger, M., Smith, G. D., Phillips, B. A., and &sidious, S. (1997). Bias in meta-analysis detected by a simple, graphical test. *BMJ* 315, 629–634. doi: 10.1136/bmj.315.7109.629

Gao, Q., Li, C., Feng, G., Wang, J., Cui, Z., Chen, X., et al. (2012). Understanding yield response to nitrogen to achieve high yield and high nitrogen use efficiency in rainfed corn. *Agron. J.* 104, 165–168. doi: 10.2134/agronj2011.0215

Gao, Z., Zhang, X., Chen, L., Lu, Y., Mao, J., Wang, X., et al. (2023). Study on the water consumption law of 'Jinguo' kiwifruit in hilly gentle slope. *Northern. Horticult.* 02, 17–24.

Gong, H., Yin, Y., Chen, Z., Zhang, Q., Tian, X., Wang, Z., et al. (2025). A dynamic optimization of soil phosphorus status approach could reduce phosphorus fertilizer use by half in China. *Nat. Commun.* 16, 976. doi: 10.1038/s41467-025-56178-1

Gu, X. B., Li, Y. N., and Du, Y. D. (2017). Optimized nitrogen fertilizer application improves yield, water and nitrogen use efficiencies of winter rapeseed cultivated under continuous ridges with film mulching. *Ind. Crops Products.* 109, 233–240. doi: 10.1016/j.indcr.2017.01.017

Guarçoni, M. A., and Ventura, J. A. (2011). Nitrogen, P, and K fertilization and the development, yield, and fruit quality of pineapple 'gold' (MD - 2). *Revista Brasileira de Ciência do Solo Uncited.* 35(4), 1367–1376. doi: 10.1590/S0100-06832011000400031

Hawkesford, M. J. (2014). Reducing the reliance on nitrogen fertilizer for wheat production. *J. Cereal Sci.* 59, 276–283. doi: 10.1016/j.jcs.2014.05.005

Hedges, L. V., Gurevitch, J., and Curtis, P. S. (1999). The meta-analysis of response ratios in experimental ecology. *Ecology* 80, 1150–1156. doi: 10.1890/0012-9658(1999)080[1150:TMAORR]2.0.CO;2

Khapte, P. S., Kumar, P., Burman, U., and Kumar, P. (2019). Deficit irrigation in tomato: Agronomical and physio-biochemical implications. *Sci. Hortic.* 248, 256–264. doi: 10.1016/j.scienta.2019.01.006

Kuypers, M. M., Marchant, H. K., and Kartal, B. (2018). The microbial nitrogen-cycling network. *Nat. Rev. Microbiol.* 16, 263–276. doi: 10.1038/s41579-018-0046-0

Li, Y. (2022). *Effects of branch traction on growth, yield and quality of kiwifruit and its mechanism* (Ya'an, China: Sichuan Agricultural University). doi: 10.27345/d.cnki.gsnyu.2022.001102

Li, J., Zhang, F. C., Fang, D., Li, Z., Gao, M., Wang, H., et al. (2014). Effects of water and nitrogen supply on cucumber growth and water use under drip fertigation. *Chin. Agric. Sci.* 47, 4475–4487. doi: 10.3864/j.issn.0578-1752.2014.22.013

Li, Y., Li, Z., Cui, S., Jagadamma, S., and Zhang, Q. P. (2019). Residue retention and minimum tillage improve physical environment of the soil in croplands: A global meta-analysis. *Soil Tillage. Res.* 194, 104292. doi: 10.1016/j.stres.2019.104292

Li, H. R., Mei, X., Wang, J., Huang, F., Hao, W., and Li, B. G. (2021). Drip fertigation significantly increased crop yield, water productivity, and nitrogen use efficiency with respect to traditional irrigation and fertilization practices: A meta-analysis in China. *Agric. Water Manage.* 244, 106534. doi: 10.1016/j.agwat.2020.106534

Li, Y. M., Sun, Y. X., Liao, S. Q., Zou, G. Y., Zhao, T. K., Chen, Y. H., et al. (2017). Effects of two slow-release nitrogen fertilizers and irrigation on yield, quality, and water-fertilizer productivity of greenhouse tomato. *Agric. Water Manage.* 186, 139–146. doi: 10.1016/j.agwat.2017.08.020

Li, M. F., Wang, J., Guo, D., Yang, R. R., and Fu, H. (2019). Effect of land management practices on the concentration of dissolved organic matter in soil: A meta-analysis. *Geoderma* 344, 74–81. doi: 10.1016/j.geoderma.2019.05.024

Li, Z., Zhang, Q., Wei, W., Cui, S., Tang, W., and Li, Y. (2020). Determining effects of water and nitrogen inputs on wheat yield and water productivity and nitrogen use efficiency in China: A quantitative synthesis. *Agric. Water Manage.* 242, 106397. doi: 10.1016/j.agwat.2020.106397

Liu, D. (2021). Root developmental responses to phosphorus nutrition. *J. Integr. Plant Biol.* 63, 1065–1090. doi: 10.1111/jipb.13090

Liu, Y., Shi, J., and Li, J. (2000). Miliang No.1, a delicious kiwifruit nutrient element and its seasonal variation. *J. Jishou. Univ.* 01, 6–10.

Lu, Y. L., Chen, Z. J., Kang, T., Zhang, X. J., Bellarby, J., and Zhou, J. B. (2016). Land-use changes from arable crop to kiwi-orchard increased nutrient surpluses and accumulation in soils. *Agricult. Ecosyst. Environ.* 223, 270–277. doi: 10.1016/j.agee.2016.04.017

Luo, Y. Q., Hui, D. F., and Zhang, D. Q. (2006). Elevated CO2 stimulates net accumulations of carbon and nitrogen in land ecosystems: A meta-analysis. *Ecology* 87, 53–63. doi: 10.1890/04-1724

Lv, H., et al. (2020). Conventional flooding irrigation and over fertilization drives soil pH decrease not only in the top-but also in subsoil layers in solar greenhouse vegetabe production systems. *Geoderma* 363, 114156. doi: 10.1016/j.geoderma.2020.114156

Muhammad, I., Yang, L., Ahmad, S., Farooq, S., Al-Ghamdi, A. A., Khan, A., et al. (2022). Nitrogen fertilizer modulates plant growth, chlorophyll pigments, and enzymatic activities under different irrigation regimes. *Agronomy* 12, 845. doi: 10.3390/agronomy12040845

Pacheco, C., Souza, L. C., Lemos, T. L., Pinheiro, J. C., and Gomes, R. C. (2008). Influence of nitrogen and potassium on yield, fruit quality, and mineral composition of kiwifruit. *Int. J. Energy Environ.* 2, 9–15.

Pahalvi, H. N., et al. (2021). "Chemical fertilizers and their impact on soil health," in *Ecofriendly tools for reclamation of degraded soil environs*, Cham, Switzerland: Springer. vol. 2. , 1–20. Microbiota and Biofertilizers.

Panda, B. B., Sharma, S., Mohapatra, P. K., and Das, A. (2012). Application of excess nitrogen, phosphorus, and potassium fertilizers leads to lowering of grain iron content in high-yielding tropical rice. *Commun. Soil Sci. Plant Anal.* 43, 2590–2602. doi: 10.1080/00103624.2012.716122

Patanè, C., and Cosentino, S. L. (2009). Effects of soil water deficit on yield and quality of processing tomato under a Mediterranean climate. *Agric. Water Manage.* 97, 131–138. doi: 10.1016/j.agwat.2009.08.021

Pinto, R., Brito, L. M., Rodrigues, J. R. O., Rego, R., and Moura, L. (2021). Influence of irrigation and nitrogen fertilization on kiwifruit production. *Agric. Eng.* 707, 2021–2021. doi: 10.1016/j.ageki.2021.100709

Poirier, Y., and Bucher, M. (2002). Phosphate transport and homeostasis in Arabidopsis. *Arabidopsis. Book.* 1, e0024. doi: 10.1199/tab.0024

Rosenberg, M. S. (2005). The file-drawer problem revisited: a general weighted method for calculating fail-safe numbers in meta-analysis. *Evolution* 59, 464–468. doi: 10.1111/j.0014-3820.2005.tb01004

Sangha, L., Shortridge, J., and Frame, W. (2023). The impact of nitrogen treatment and short-term weather forecast data in irrigation scheduling of corn and cotton on water and nutrient use efficiency in humid climates. *Agric. Water Manage.* 283, 108314. doi: 10.1016/j.agwat.2023.108314

Santoni, F., Petruccioli, M., Goni, F., Daolio, G., Dupont, J. M., and Motta, R. (2016). Influence of cultivation parameters on the mineral composition of kiwi fruit from Corsica. *Chem. Biodivers.* 13, 748–754. doi: 10.1002/cbdv.201500236

Sardans, J., and Peñuelas, J. (2021). Potassium control of plant functions: Ecological and agricultural implications. *Plants* 10, 419. doi: 10.3390/plants10020419

Satpal, D., Kaur, J., Bhadariya, V., and Sharma, K. (2021). Actinidia deliciosa (Kiwi fruit): A comprehensive review on the nutritional composition, health benefits, traditional utilization, and commercialization. *J. Food Process. Preserv.* 45, e15588. doi: 10.1111/jfpp.15588

Srivastava, A. K., Shankar, A., Nalini Chandran, A. K., Sharma, M., Jung, K. H., Suprasanna, P., et al. (2020). Emerging concepts of potassium homeostasis in plants. *J. Exp. Bot.* 71, 608–619. doi: 10.1093/jxb/erz458

Stanley, T. D. (2001). Wheat from chaff: Meta-analysis as quantitative literature review. *J. Econ. Perspect.* 15, 131–150. doi: 10.1257/jep.15.3.131

Sustr, M., Soukup, A., and Tylova, E. (2019). Potassium in root growth and development. *Plants* 8, 435. doi: 10.3390/plants8100435

Tilman, D., Cassman, K. G., Matson, P. A., Naylor, R. L., and Polasky, S. (2011). Global food demand and the sustainable intensification of agriculture. *Proc. Natl. Acad. Sci.* 108, 20260–20264. doi: 10.1016/j.croj.2015.05.001

Wang, G. Y., Hu, Y. X., Liu, Y. X., Ahmad, S., and Zhou, X. B. (2021). Effects of supplement irrigation and nitrogen application levels on soil carbon–nitrogen content and yield of one-year double crop maize in subtropical region. *Water* 13, 1180. doi: 10.3390/w13091180

Wang, L. L., Palta, J. A., Chen, W., Chen, Y. L., and Deng, X. P. (2018b). Nitrogen fertilization improved water-use efficiency of winter wheat through increasing water use during vegetative rather than grain filling. *Agric. Water Manage.* 197, 41–53. doi: 10.1016/j.agwat.2018.07.002

Wang, L. F., Sun, J. T., Zhang, Z. B., Xu, P., and Shangguan, Z. P. (2018a). Winter wheat grain yield in response to different production practices and soil fertility in northern China. *Soil Tillage. Res.* 176, 10–17. doi: 10.1016/j.still.2017.10.001

Wang, W., Zhuo, L., Li, M., Liu, Y. L., and Wu, P. T. (2019). The effect of development in water-saving irrigation techniques on spatial-temporal variations in crop water footprint and benchmarking. *J. Hydrol.* 577, 123916. doi: 10.1016/j.jhydrol.2019.123916

Wei, C. C., Ren, S. M., Yang, P. L., Wang, Y., He, X., Xu, Z., et al. (2021). Effects of irrigation methods and salinity on CO2 emissions from farmland soil during growth and fallow periods. *Sci. Total. Environ.* 752, 141639. doi: 10.1016/j.scitotenv.2020.141639

Wu, J., Song, Y., Wan, G.-Y., Sun, L.-Q., Wang, J.-X., Zhang, Z.-S., et al. (2025). Boosting crop yield and nitrogen use efficiency: the hidden power of nitrogen-iron balance. *New Crops* 2, 100047. doi: 10.1016/j.ncrops.2024.100047

Wu, H. B., Wang, L. C., Kang, L. A., Liu, C., and Li, M. W. (2023). Study on the effect of planting pattern adjustment on the growth of kiwifruit inter-root microorganisms and fruit quality. *Turkish. J. Agric. Forestry.* 47, 263–272. doi: 10.17766/tras.200002

Wu, Y., Zhang, X., Tang, X., Cheng, K., Fu, C., and Chen, X. (2021). Responses of growth, fruit yield, quality, and water productivity of greenhouse tomato to deficit drip irrigation. *Sci. Hortic.* 275, 109710. doi: 10.1016/j.scienta.2020.109710

Xu, X. X., Du, X., Wang, F., Sha, J. C., Chen, Q., Tian, G., et al. (2020). Effects of potassium levels on plant growth, accumulation and distribution of carbon, and nitrate metabolism in apple dwarf rootstock seedlings. *Front. Plant Sci.* 11, 534048. doi: 10.3389/fpls.2020.00904

Yang, A., et al. (2017). Optimising nitrogen fertilisation: A key to improving nitrogen-use efficiency and minimising nitrate leaching losses in an intensive wheat/maize rotation, (2008–2014). *Field Crops Res.* 206, 1–10. doi: 10.1016/j.fcr.2016.12.011

Yang, Q., Zhang, F., Liu, X., and Ge, Z. (2012). "Effects of drip irrigation mode and NaCl concentration on hydraulic resistance and water use of young apple tree," in *Transactions of the Chinese Society of Agricultural Engineering*, vol. 28. (Editorial Office of Transactions of the Chinese Society of Agricultural Engineering), 117–123.

Yi, J., Li, H., Zhao, Y., Shao, M., and Zhang, H. (2022). Assessing soil water balance to optimize irrigation schedules of flood-irrigated maize fields with different cultivation histories in the arid region. *Agric. Water Manage.* 266, 107543. doi: 10.1016/j.agwat.2022.107543

Yu, L. Y., Zhao, X. N., Gao, X. D., and Siddique, K. H. M. (2020). Improving/maintaining water-use efficiency and yield of wheat by deficit irrigation: A global meta-analysis. *Agric. Water Manage.* 228, 105906. doi: 10.1016/j.agwat.2019.105906

Zhang, S. L., Gao, P. C., Tong, Y. A., Norse, D., Lu, Y. L., and Powlson, D. (2015). Overcoming nitrogen fertilizer over-use through technical and advisory approaches: A case study from Shaanxi Province, northwest China. *Agricult. Ecosyst. Environ.* 209, 89–99. doi: 10.1016/j.agee.2015.03.002

Zhao, Y., Kang, Z., Chen, L., Guo, Y., Mu, Q., Wang, S., et al. (2023). Quality classification of kiwifruit under different storage conditions based on deep learning and hyperspectral imaging technology. *J. Food Measurement. Characterization.* 17, 289–305. doi: 10.1016/j.jfmc.2022.100824

Zhou, J. Y., Gu, B. J., Schlesinger, W. H., and Ju, X. T. (2016). Significant accumulation of nitrate in Chinese semi-humid croplands. *Sci. Rep.* 6, 25088. doi: 10.1038/srep25088

frontiers | Frontiers in Plant Science

TYPE Systematic Review
PUBLISHED 22 October 2025
DOI 10.3389/fpls.2025.1604686

Check for updates

OPEN ACCESS

EDITED BY
Maruthi Sridhar Balaji Bhaskar,
Florida International University, United States

REVIEWED BY
Jiawu Zhou,
Yunnan Academy of Agricultural Sciences, China
Gurjeet Singh,
Texas A&M University, United States

*CORRESPONDENCE
Wenfei Wang
wenfeiwang@fafu.edu.cn
Wenxiong Lin
wenxiong181@163.com

†These authors have contributed equally to this work

RECEIVED 02 April 2025
ACCEPTED 10 September 2025
PUBLISHED 22 October 2025

CITATION
Yang X, Ruan Z, Chen K, Gu S, Wang Y, Cai Q, Yao L-A, Boorboori MR, Yasir A, Chaiwanon J, Bessho-Uehara K, Shin K, Wu Y, Wang W and Lin W (2025) Meta-analysis reveals that grain quality is improved in ratoon season crop compared with main crop. *Front. Plant Sci.* 16:1604686. doi: 10.3389/fpls.2025.1604686

COPYRIGHT
© 2025 Yang, Ruan, Chen, Gu, Wang, Cai, Yao, Boorboori, Yasir, Chaiwanon, Bessho-Uehara, Shin, Wu, Wang and Lin. This is an open-access article distributed under the terms of the Creative Commons Attribution License (CC BY). The use, distribution or reproduction in other forums is permitted, provided the original author(s) and the copyright owner(s) are credited and that the original publication in this journal is cited, in accordance with accepted academic practice. No use, distribution or reproduction is permitted which does not comply with these terms.

Meta-analysis reveals that grain quality is improved in ratoon season crop compared with main crop

Xuelian Yang[1,2†], Zhijie Ruan[1†], Kezhi Chen[1], Shiting Gu[1], Yuchao Wang[1], Qiang Cai[1], Li-Ang Yao[1], Mohammad Reza Boorboori[3], Arafat Yasir[4], Juthamas Chaiwanon[5], Kanako Bessho-Uehara[6], Kihye Shin[7], Yunfei Wu[8], Wenfei Wang[1,2*] and Wenxiong Lin[1,2*]

[1]Fujian Provincial Key Laboratory of Agroecological Processing and Safety Monitoring, College of Juncao Science and Ecology, Fujian Agriculture and Forestry University (FAFU), Fuzhou, China, [2]Key Laboratory of Crop Ecology and Molecular Physiology (FAFU), Fujian Province University, Fuzhou, China, [3]College of Environment and Surveying and Mapping Engineering, Suzhou University, Suzhou, China, [4]State Key Laboratory of Desert and Oasis Ecology, Xinjiang Institute of Ecology and Geography, Chinese Academy of Sciences, Urumqi, China, [5]Center of Excellence in Environment and Plant Physiology, Department of Botany, Faculty of Science, Chulalongkorn University, Bangkok, Thailand, [6]Graduate School of Life Sciences, Tohoku University, Sendai, Japan, [7]Department of Microbiology and Immunology, Jeju National University College of Medicine, Jeju, Republic of Korea, [8]Jiangsu Key Laboratory of Crop Genetics and Physiology/Co-Innovation Center for Modern Production Technology of Grain Crops/Joint International Research Laboratory of Agriculture andAgri-Product Safety, Yangzhou University, Yangzhou, China

Rice ratooning cultivation refers to secondary production from the stubble left after the harvest of the main crop (MC). Besides providing additional yield, ratooning is known to affect grain quality. Here, we conducted a meta-analysis of grain quality traits between ratoon season crop (RC) and MC. The results showed that the overall grain quality of RC was higher than that of MC. Ratooning improved milling traits by increasing the milled rice rate (MRR) and head rice rate (HRR) and enhanced grain appearance by reducing chalkiness. Furthermore, ratooning had a positive impact on alkali spreading value (ASV) and amylose content (AC) but a negative influence on gel consistency (GC), which markedly affects cooking and sensory quality. Subgroup analysis showed that stubble height influenced the AC of RC, while planting region was a major factor regulating most grain properties. Meta-regression analysis suggested that latitude, precipitation, and temperature played important roles in rice quality, particularly in relation to milling parameters. In addition, we compared the grain quality of RC and the late-season crop (LC) with synchronized heading time. Negative trends were observed in brown rice rate (BRR) and protein content (PC), while planting region and rice variety were revealed as factors influencing

chalkiness and HRR. Overall, our findings indicate that ratooning has positive impacts on grain quality and uncover the relationships between environmental and agronomic factors and their effects on quality traits, which will lay the foundation for future breeding strategies and optimize cultivation management across growth regions.

KEYWORDS

ratoon season crop (RC), main crop (MC), rice quality, meta-analysis, milling traits, chalkiness

Introduction

Ratoon rice, a second rice production system generated from the stubble left after harvesting the main crop (MC), is considered an ideal cropping system in regions where light and temperature resources are sufficient for one seasonal crop but insufficient for two (IRRI, 1988). Rice ratooning is an ancient cultivation technique, with a history of more than 1,700 years since the West Jin Dynasty (AD 265–316) in China (Guo, 1993). It is now fairly widespread in many countries, including Japan, Korea, India, Thailand, Vietnam, the Philippines, Indonesia, the United States, and Nigeria (IRRI, 1988; Calendacion et al., 1992; Munda et al., 2009; Sanni et al., 2009; Wang et al., 2020b; Deng et al., 2021).

The main advantages of rice ratooning are promising high grain yield, high economic efficiency, and environmental friendliness (Lin et al., 2015). More recently, several studies have reported another potential advantage—grain quality of the ratoon crop (RC) may be better than that of the MC (Alizadeh and Habibi, 2016; Huang et al., 2020; Wang et al., 2020b). However, other studies found that the cooking quality of rice decreased after ratooning (Shin et al., 2015; Wang et al., 2020a). Thus, the impact of ratooning on grain quality appears to vary among studies.

Rice quality is determined by multiple traits, and quality perception varies across consumers and countries (Custodio et al., 2019). Several traits are widely used to evaluate rice quality, including milling properties, appearance, nutritional value, and cooking and sensory quality (Fitzgerald et al., 2009). Milling quality refers to the final yield of edible rice and the proportion of unbroken kernels, which is mainly evaluated by brown rice rate (BRR), milled rice rate (MRR), and head rice rate (HRR). Appearance is a crucial property after milling, commonly assessed by chalky rice rate (CRR), chalkiness degree (CD), and length–width ratio (LWR). Previous studies have reported significant reductions in chalkiness degree and CRR in ratoon-season grains (Alizadeh and Habibi, 2016; Cai et al., 2019; Lin et al., 2022). Cooking and sensory quality are usually predicted by alkali spreading value (ASV), gel consistency (GC), and amylose content (AC). Some studies showed that ratoon-season grains had higher AC and significantly lower transition gelatinization temperatures (Shin et al., 2015; Kuang et al., 2021). In addition, consumers are concerned about nutritional value, which mainly refers to the amounts of protein, vitamins, minerals, and lipids in the grain.

Rice quality can be influenced by cultivar, management practices, and environmental conditions during grain filling. Ratooning ability, yield, and quality vary among different types of varieties (Negalur et al., 2017). Recent studies have revealed that environmental factors, including precipitation, temperature, fertilizer application, and biotic and abiotic stresses, play key roles in ratooning production and quality (Wang et al., 2020b). For example, the cooking and eating quality of ratoon rice was higher in lower-latitude regions (Kuang et al., 2021). Crop management practices such as stubble height, irrigation, and nitrogen fertilization also affect ratoon rice (Jones, 1993; Chen et al., 2021; Yang et al., 2021). However, how these factors influence final grain quality remains largely unclear.

Meta-analysis, a quantitative synthesis of research results, allows assessment of overall trends (Gurevitch et al., 2018). Given the variability in findings regarding ratooning and grain quality, we used meta-analysis to integrate results across studies. We summarized and interpreted 59 studies to assess overall rice quality and quantify the effects of ratooning. Our results suggest that ratoon-season grain quality is generally better than that of the MC, with improvements in milling properties, reductions in chalkiness, and modifications in cooking and nutritional traits. Subgroup and meta-regression analyses further revealed relationships between grain quality and cultivar, management, and environmental factors. These findings provide a basis for future breeding strategies and optimization of cultivation management across different growth regions.

Abbreviations: RC, Ratoon season crop; MC, Main crop; LC, Late season main crop; BRR, Brown rice rate; MRR, Milled rice rate; HRR, Head rice rate; CRR, Chalky rice rate; CD, Chalkiness degree; LWR, Length-width ratio; ASV, Alkali spreading value; CI, Confidence interval; GC, Gel consistency; AC, Amylose content; ΔPrecipitation, Average precipitation per day; ΔTavg, Average temperature per day; ES, Effective size.

Materials and methods

Definitions of comparison groups

Two comparisons were conducted in this meta-analysis: (a) RC grain quality vs. MC grain quality, and (b) RC grain quality vs. late-season crop (LC) grain quality.

After harvesting the MC, the second rice crop generated from the stubble was defined as the RC. The LC refers to the late-season main crop with heading time synchronized with the RC, meaning that grains from both crops were obtained under the same weather conditions.

Literature selection

A systematic search was conducted to identify peer-reviewed studies describing the grain quality of ratoon rice, the main crop, and the late season crop. Ten grain quality parameters, including brown rice rate, milled rice rate, head rice rate, chalky rice rate, chalkiness degree, length-width ratio, alkali spreading value, gel consistency, amylose content, and protein content, were selected to conduct the meta-analysis.

Articles were collected through PubMed (https://pubmed.ncbi.nlm.nih.gov), Google Scholar (https://scholar.google.com), Web of Science (https://www.webofknowledge.com), Science Direct (https://www.sciencedirect.com), SpringerLink (https://link.springer.com), Wiley Online Library (https://onlinelibrary.wiley.com/), Scientific Information Database (https://www.sid.ir/), Taylor & Francis (https://www.tandfonline.com/), CNKI database (https://www.cnki.net/), Wanfang database (https://www.wanfangdata.com.cn/index.html), CQVIP database (http://www.cqvip.com/), Huayi Database (http://www.airitilibrary.cn/), CiNii research (https://cir.nii.ac.jp/) and AGRIS (https://agris.fao.org). Data collection was restricted to field studies; studies conducted in laboratories, greenhouses, or pots. The following four selection criteria were applied:

Criterion 1: We included studies that recorded rice quality data for either "ratoon rice vs. main crop" or "ratoon rice vs. late-season main crop." Studies reporting only general conclusions on rice quality without specific index data were excluded.

Criterion 2: The rice quality index data that we accepted only contained brown rice rate, milled rice rate, head rice rate, chalky grain rate, chalkiness degree, length-width ratio, alkali spreading value, gel consistency, amylose content, and protein content. Articles with grain length and width data, which allowed us to calculate the length-width ratio, were included.

Criterion 3: Studies with only one dataset and those on overwintering cultivated rice (a specific cropping practice in the low latitude zone with adapted local varieties) were excluded.

Criterion 4: Duplicate datasets from the same study were excluded after careful comparison.

Study selection followed the PRISMA protocol (Liberati et al., 2009; Moher et al., 2009) (Supplementary Figure S1). From August 2021 to May 2023, we used combinations of keywords to search for relevant literature. The keywords included ("ratoon rice" OR "ratooning" OR "ratoon" OR "double season rice" OR "double cropping") AND ("quality" OR "appearance" OR "milling properties" OR "milling" OR "cooking and sensory quality" OR "cooking" OR "sensory" OR "nutrient" OR "nutrition" OR "brown rice" OR "milled rice" OR "head rice" OR "chalky" OR "chalkiness" OR "milk white grain" OR "chalk white" OR "floury endosperm" OR "length-width ratio" OR "alkali spreading value" OR "gel consistency" OR "amylose content" OR "amylose" OR "protein content" OR "protein") without restriction on publication year. A total of 1,479 articles were initially identified. With the help of international researchers, 28 additional foreign-language articles were selected. After excluding duplicates, 1,422 articles remained for screening. During the second screening, 246 papers were retained after reviewing titles, keywords, and abstracts. The full texts of these papers were then assessed for suitability. Finally, 56 articles were included for RC vs. MC comparison, and 9 articles for RC vs. LC comparison (see Supplementary Database).

All data were integrated into a world map (Figure 1), generated using resources from the Resource and Environment Science and Data Center in China (https://www.resdc.cn/Default.aspx).

Risk of bias assessment

The Cochrane system was used to assess the risk of bias in all studies included in the meta-analysis. The assessment was conducted in six areas: "Sequence generation (selection bias)," "Blinding of participants (performance bias)," "Blinding of outcome assessment (detection bias)," "Incomplete outcome data (attrition bias)," "Selective outcome reporting (reporting bias)," and "Other potential threats to validity (other bias)," to detect deficiencies in study design, implementation, analysis, and reporting integrity (Source Data Supplementary Figure S2B). Due to the objectivity of the agricultural experiment process, in the 'Selection bias', we only adopted the assessment of "Sequence generation" while excluding "Allocation concealment" (Higgins et al., 2017). For performance bias, the evaluation criterion was whether the experimental field areas were managed uniformly to prevent staff from knowing which interventions the experimental subjects received. For detection bias, the criterion was whether the study provided a detailed explanation of the rice quality testing methods and strictly adhered to them to avoid testing bias caused by interventions from testers. Following the guidance of the Cochrane Handbook for Systematic Reviews of Interventions, we classified and evaluated each article as having "low risk of bias," "unclear risk," or "high risk of bias" (Source Data Supplementary Figure S2A) (Saric et al., 2019). Figures were generated using the "ggplot" package in R software (version 4.3.1).

Study quality assessment

Because no standardized system exists for evaluating the quality of the studies included, we applied "21 quality checklist questions" concerning the rationality of the experimental design and the strength of evidence for improvement of rice quality indicators through ratooning (Su et al., 2021) (Source Data Supplementary Figure S3).

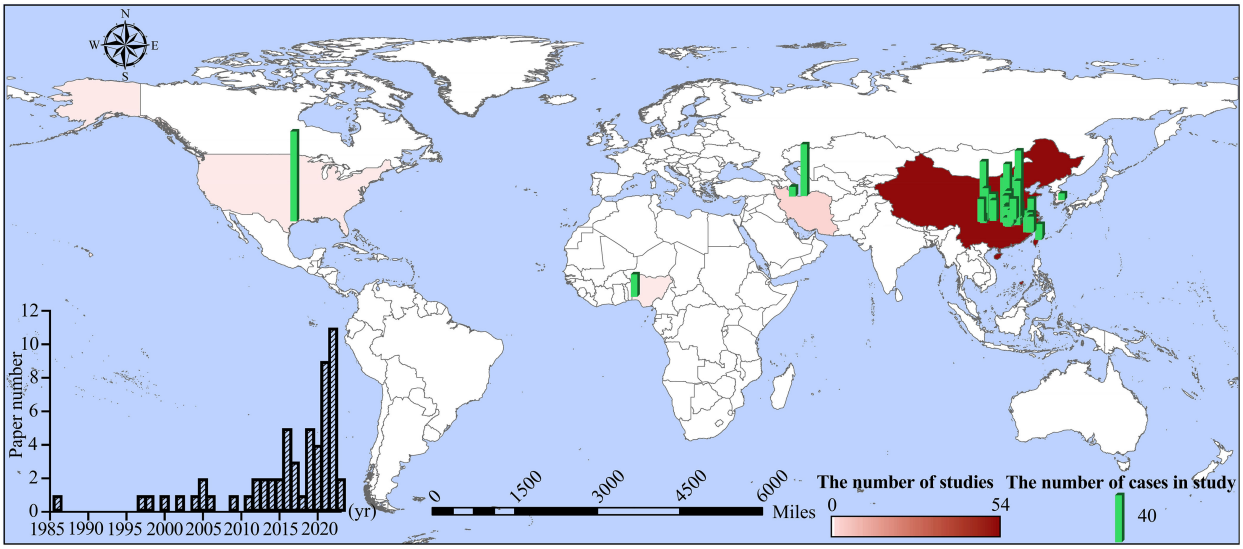

FIGURE 1
Distribution of reviewed studies related to grain quality of ratoon rice. The world map shows ratoon rice studies located around the world. Country color indicates the number of studies, and column height indicates the number of experimental cases in each study. The inset column plot in the lower left shows the number of reviewed articles per year (from 1986 to 2023). The horizontal bar with gradient red colors shows the number of studies. The vertical bar shows the number of cases in each study. For detailed figure information, see Supplementary Data and source data.

According to the classification criteria of Su et al., study quality was categorized as very strong evidence (score >75%), strong evidence (score 50%–74%), moderate evidence (score 25%–49%), or weak evidence (score <24%). For this meta-analysis, we included only studies with very strong (score >75%) and strong (score 50%–74%) evidence.

Meta-analysis

From each study, we extracted rice quality data, including BRR, MRR, HRR, CRR, CD, LWR, ASV, GC, AC, and PC. For the "RC vs. MC" comparison, data were included only when they came from the same year, in the same experimental field, and with the same variety. For the "RC vs. LC" comparison, data were included only when matched for the same variety and heading time.

The standardized mean difference (SMD; Cohen's d) was used as the effect size, calculated as the difference in means between two groups divided by the standard deviation. When comparing RC with MC or LC, the SMD value reflected whether grain quality increased or decreased (Lachenbruch, 1989). Meta-analysis was performed using a random-effects model with the constrained maximum likelihood (CML) method. The 95% confidence interval (CI) in the forest plots indicated significant positive or negative changes (Nakagawa and Cuthill, 2007; Borenstein et al., 2010). Heterogeneity was tested using the Q test and quantified with the I^2 statistic; generally, $I^2 > 50\%$ indicated significant heterogeneity among studies (Hedges and Olkin, 1985; Higgins et al., 2003). All analyses were performed in Stata version 16, following published guidelines for biological meta-analysis (Koricheva et al., 2013; Chaimani et al., 2014; Nakagawa et al., 2017).

Grain quality was evaluated according to the Chinese national standard for high-quality paddy (GB/T 17891-2017) (Supplementary Database). Grains were first classified as either *indica*-type rice or *japonica*-type rice. *Indica* rice, *indica*-type hybrids, and *indica–japonica* hybrids were evaluated under the "indica-type rice" standard, while *japonica* rice and *japonica*-type hybrids were grouped under "*japonica*-type rice." The *indica* group was further subdivided into "long grain", "medium grain", and short-grain categories based on reported grain length.

Grain quality was assessed using three parameters: HRR, CD, and AC. According to the standard, grain was scored as Grade 1 (score = 4), Grade 2 (score = 3), or Grade 3 (score = 2). If quality was lower than Grade 3, it was classified as Grade 4 (score = 1).

Subgroup analysis

Subgroup analyses were conducted for (a) stubble heights after the main rice harvest (more than 20 cm and below 20 cm), (b) rice varieties (*indica* rice, *japonica* rice, and hybrid rice), and (c) the geographical regions of study (e.g., South China Plain Hilly, Jiangnan Hilly Plain, Middle-lower Yangtze Plain, Sichuan Basin, Northern Iran, southern United States, Korea). These subgroup analyses were used to determine the source of heterogeneity among different studies by calculating effect sizes within each subgroup and analyzing their differences (Thompson and Higgins, 2002).

Meta-regression analysis

Factors with continuous data were used as variables for meta-regression analysis, including (a) latitude of the experimental area (all are in the Northern Hemisphere), meteorological factors in the grain-filling period (two months), including (b) average

precipitation per day (ΔPrecipitation), (c) average temperature per day (ΔTavg), (d) nitrogen (N) application, (e) planting density, (f) study year, and (g) average global surface solar radiation per year compared RC and MC. The application of nitrogen fertilizer described in the article during the main crop cutting period was converted into total nitrogen amount as "kilograms per hectare". Planting density was measured as "thousands of hills per hectare," which was recalculated according to the data from each study. The year of study was the trial time described in each study, not the article publication time. Global historical climate datasets are provided by the "National Centers for Environmental Information" (https://www.ncei.noaa.gov/). Global surface solar radiation datasets are provided by the "National Tibetan Plateau Data Center" (http://data.tpdc.ac.cn) and "Geographic remote sensing ecological network" platform (www.gisrs.cn). All the data were extracted from the articles to be categorized and recalculated. Bubble plots were used to present the results of regression analyses on correlations between effect sizes and variables (Cameron and Windmeijer, 1997).

Tests of publication bias

Egger's regression was performed to evaluate publication bias and presented as funnel plots, with parameters set as default (Egger et al., 1997).

Results

General literature description

Different methods were used to search articles about grain quality of MC, RC, and LC, in which rice heading time was synchronized with ratoon rice. A total of 1,507 articles from multiple databases were found to be relevant to rice grain quality (Supplementary Figure S1). After removing papers with duplicated data (N = 85) and unqualified data (N = 1,361), 59 articles met our criteria and were selected for analysis (Supplementary Database "list of publication"). The studies comparing RC and MC numbered 56, while studies referring to RC and LC numbered only 9 (Supplementary Database "RC vs MC" and "RC vs LC"). Six studies included grain quality data for RC, MC, and LC. The PRISMA flow diagram for the studies selected and included in our meta-analysis is shown in Supplementary Figure S1. The geographical distribution of the studies spanned 5 countries: China (53 studies), Iran (3 studies), Korea (1 study), the United States (1 study), and Nigeria (1 study) (Figure 1). The first article comparing grain quality between RC and MC was published in China in 1986. A rapid increase in publications occurred after 2010 (Figure 1, lower left chart), as governments and researchers devoted greater attention to ratoon rice over the past ten years.

The risk of bias and study quality assessments were performed to evaluate study reliability. According to the *Cochrane Handbook* for systematic reviews of interventions, six factors were assessed to qualify risk of bias (Supplementary Figure S2). The results showed that all assessment factors represented low risk of bias. Study quality was further assessed using "21 quality checklist questions." Based on the scores, the studies included in this analysis provided strong evidence (>60%) (Supplementary Figure S3).

All detailed figure information and values are provided in the Supplementary Material ("source data").

Effects of ratooning on the grain quality

Ten parameters from four primary quality traits were investigated in this study, covering milling properties (BRR, MRR, HRR), appearance properties (CRR, CD, LWR), cooking and sensory quality (ASV, GC, AC), and nutritional value (PC). All 10 grain traits were compared between RC and MC and collected for meta-analysis (using standardized mean difference (SMD; Cohen's d) as the effect size (ES)). In total, 1,138 observations met the inclusion criteria (Supplementary Database "RC vs MC" and "RC vs LC").

Compared with MC, the milling properties MRR and HRR of RC increased, with ES values of 0.61 (95% CI = 0.07 to 1.15) and 1.41 (95% CI = 0.90 to 1.92), respectively, which was considered a significant improvement (Figure 2A). For appearance traits, CRR and CD showed negative trends in RC compared with MC, with ES values of –1.68 (95% CIs = -2.12 to -1.24) and -1.78 (95% CIs = -2.27 to -1.29), respectively (Figure 2A), indicating improved appearance quality in ratoon rice.

Ratooning also had positive effects on ASV (ES = 0.90, 95% CI = 0.48 to 1.31) and AC (ES = 0.39, 95% CI = 0.02 to 0.76) (Figure 2A). In contrast, GC—an important parameter of eating quality—was reduced by ratooning (ES = –0.59, 95% CI = –0.97 to –0.11).

The overall grain quality was also evaluated according to the Chinese national standard for high-quality paddy (GB/T 17891-2017) (Supplementary Database), which is widely used in Chinese rice research and markets. Taking into account cooking and sensory parameters, as well as milling and appearance traits, rice grains were rated into four grades. Comparison of RC and MC grades showed that overall grain quality improved after ratooning, in both *indica* and *japonica* rice types (Figure 2B).

It is noteworthy that the funnel plots of five grain traits—HRR, CRR, CD, ASV, and AC—were asymmetric (Supplementary Figure S4), indicating potential publication bias in the relevant literature, marked with stars in Figure 2A. All potential publication biases were corrected using the trim-and-fill method, and the results did not change the conclusions (Supplementary Figure S4, Supplementary Table 4).

Taken together, comparison of grain qualities between RC and MC showed that ratooning improved overall grain quality across multiple traits.

Subgroup analysis of the categorical factors

Significant heterogeneity (I^2 ≥50%) appeared among studies in all grain traits (Figure 2A), suggesting that various factors may

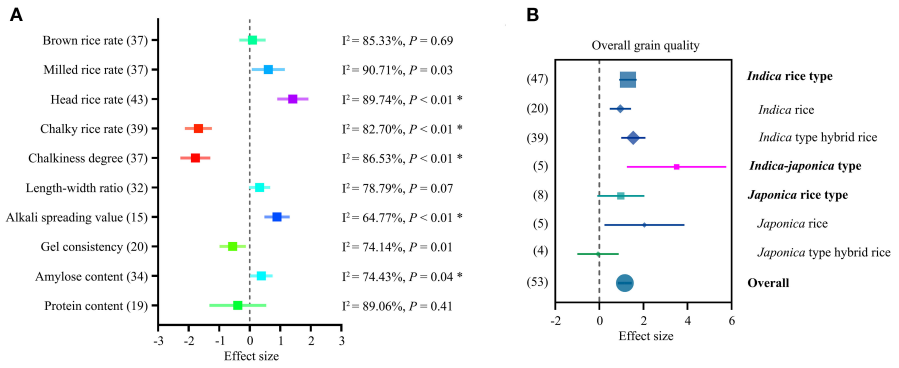

FIGURE 2
Mean effect sizes (ES) for the grain quality compared RC to MC. **(A)** ES of rice quality traits by ratooning (RC vs. MC). Heterogeneity value (I^2) and the *P* value are presented on the right. Asterisks indicate that publication bias was detected. **(B)** ES on overall grain quality comparing RC to MC. Grain quality was evaluated by the Chinese national standard of high-quality paddy (GB/T 17891-2017). ES is plotted as SMD (Cohen's d). Bars around the means denote 95% CIs. The bracketed numbers in A and B represent the number of accepted studies.

contribute to grain quality. Thus, to identify the potential influencing factors on the heterogeneity of the pooled ES, the following subgroup and meta-regression analyses were performed. Stubble height, rice variety, and study region were analyzed as categorical moderators for their contributions to grain quality change between RC and MC (Figure 3A).

Stubble height was divided into two groups: less than 20 cm and more than 20 cm. Our subgroup analysis showed that ratooning significantly promoted AC in the "less than 20 cm" group but not in the "more than 20 cm" group (Figure 3B). The influence of ratooning on CD, LWR, and ASV varied between cultivars (Figures 3C–E). *Japonica*, *indica*, and hybrid rice are three major planting cultivars today. Our subgroup analysis showed that CD decreased most in hybrid rice, although all three cultivars had lower CD in RC compared with MC (Figure 3C). Indica grain also showed slight increases in LWR (ES = 0.41, 95% CI = −0.04 to 0.87) and ASV (ES = 0.93, 95% CI = 0.49 to 1.37) (Figures 3D, E).

Planting region was found to be a major influencing factor on grain quality parameters, including BRR, MRR, HRR, CRR, ASV, GC, and PC (Figure 3A). Based on geographical and weather conditions, all tested cases were divided into six planting regions: South China Plain Hilly, Jiangnan Hilly Plain, Middle–Lower Yangtze Plain, Sichuan Basin, Northern Iran, southern United States, and Korea (Figures 3F–L). With ratooning, milling properties (BRR and MRR) especially increased in the Middle–Lower Yangtze Plain but decreased in South China (Figures 3F, G). HRR of ratoon rice was promoted in most parts of China (Figure 3H).

The effects on appearance parameters also varied across geographical regions. Significantly negative trends for CRR were observed in all study cases from China (Figure 3I). For other traits such as ASV, GC, and PC, most studies were conducted in the Jiangnan Hilly Plain; however, no obvious changes were observed after ratooning (Figures 3J–L). In other planting regions, fewer cases were available, making it difficult to draw firm conclusions about grain quality changes.

Regression analysis of the continuous factors

Besides the above categorical factors, associations between grain trait trends and six hypothesized continuous factors were estimated, including latitude, the difference in "average precipitation per day" (Δprecipitation), the difference in "average temperature per day" (ΔTavg), application of nitrogen (N) fertilizer in the studies, planting density, study year, and solar radiation between RC and MC (Figure 4A). All collected studies were conducted in the Northern Hemisphere, ranging from N 22° to N 42°.

Meta-regression analysis revealed that latitude had a moderate positive relationship with BRR and ASV (Figures 4B, C) but a negative relationship with GC (Figure 4D). HRR was positively correlated with a decrease in precipitation in the ratoon season (Figure 4E), while all three milling properties (BRR, MRR, and HRR) were positively correlated with a decrease in average temperature in the ratoon season (Figures 4F–H). For N fertilizer application, PC was positively related to the amount of nitrogen applied (Figure 4I). Planting density was also found to have an absolute negative relationship with ASV (R^2 = 100%) and a clearly positive relationship with GC (Figures 4J, K). With increasing study years, positive correlations were observed for all milling properties, including BRR, MRR, and HRR (Figures 4L–N).

Comparison of grain qualities between RC and LC

Previous studies suggested that the improvement of rice quality in RC was mainly due to relatively lower temperatures during the filling period compared with MC (Liu et al., 2002), which was also supported by our subgroup analysis of ΔTavg. To further investigate the potential factors affecting grain quality, we performed a meta-analysis comparing RC and LC, since LC was grown under the same environmental conditions as ratoon rice. In total, 112 observations met our criteria.

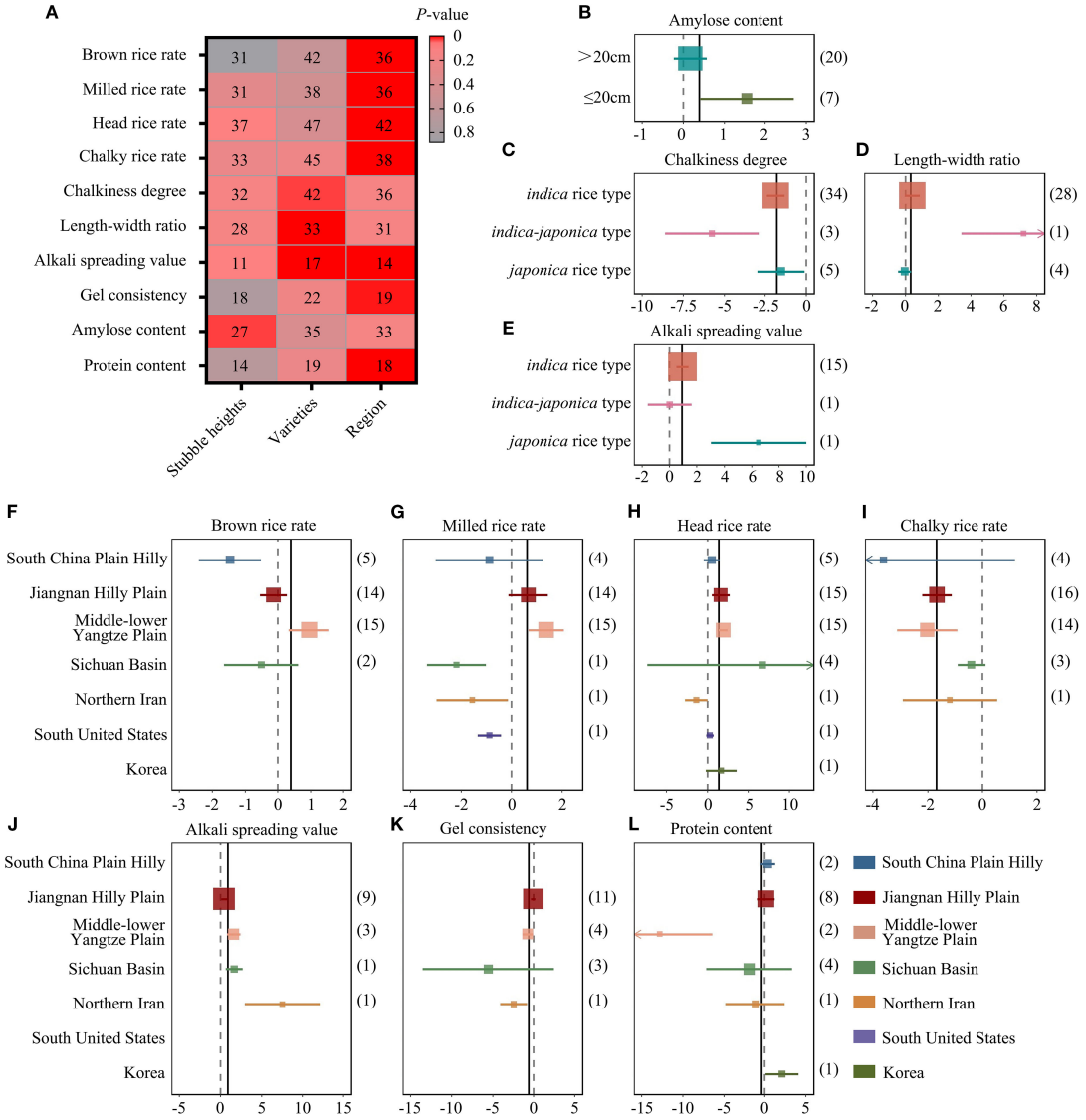

FIGURE 3
Subgroup analysis of categorical factors. **(A)** Heatmaps of correlations between grain quality traits and categorical factors (stubble heights, rice varieties, and study region). Gradient red color indicates *P*-values of correlations. Numbers in boxes represent the number of research cases included in the analysis. **(B)** Effects of stubble height on AC. **(C–E)** Effects of rice varieties on CD, LWR, and ASV. **(F–L)**. Effects of geographical regions on grain quality parameters [**(F)** BRR; **(G)** MRR; **(H)** HRR; **(I)** CRR; **(J)** ASV; **(K)** GC; **(L)** PC]. In **(B–L)**, ES is plotted as SMD (Cohen's d) comparing RC to MC. Bars around the means denote 95% CIs. For milling properties, if the means fall on the positive side and do not intersect with zero, BRR, MRR, and HRR are considered to increase relative to MC; the opposite applies if means fall on the negative side of the forest plot. For appearance properties (CD and CRR), negative means indicate decreases in RC compared with MC. All seven analyzed regions are shown in different colors. The vertical black line indicates the pooled ES of all categorical factors. Bracketed numbers represent the numbers of accepted study cases. For Q statistic tests, see Supplementary Table 1. For detailed SMD values, (Cohen's d), see "Source data".

Compared with LC, the appearance properties of RC were also improved. CRR decreased with an ES of –1.20 (95% CI = –2.29 to –0.11). BRR and PC also decreased, with ES values of -1.11 (95% CIs = -1.76 to -0.47) and -1.59 (95% CIs = -2.51 to -0.67), respectively (Figure 5A). Other grain traits showed no significant differences between RC and LC (P>0.05).

Considering the heterogeneity among studies, subgroup analysis was also performed. Ratooning increased HRR especially in South China but decreased it in Central China (Figure 5B). In addition, CRR decreased only in South China during the ratoon season, while no obvious differences were observed in Central China (Figure 5B). For CD, some decreases were observed in South China and the Jiangnan Hilly Plain. Furthermore, the effect on CRR varied between cultivars: CRR decreased in hybrid rice but not in *indica* cultivars (Figure 5C).

Discussion

Impacts of ratooning to grain quality

In our meta-analysis, milling properties were dramatically improved in RC compared with MC, especially in China.

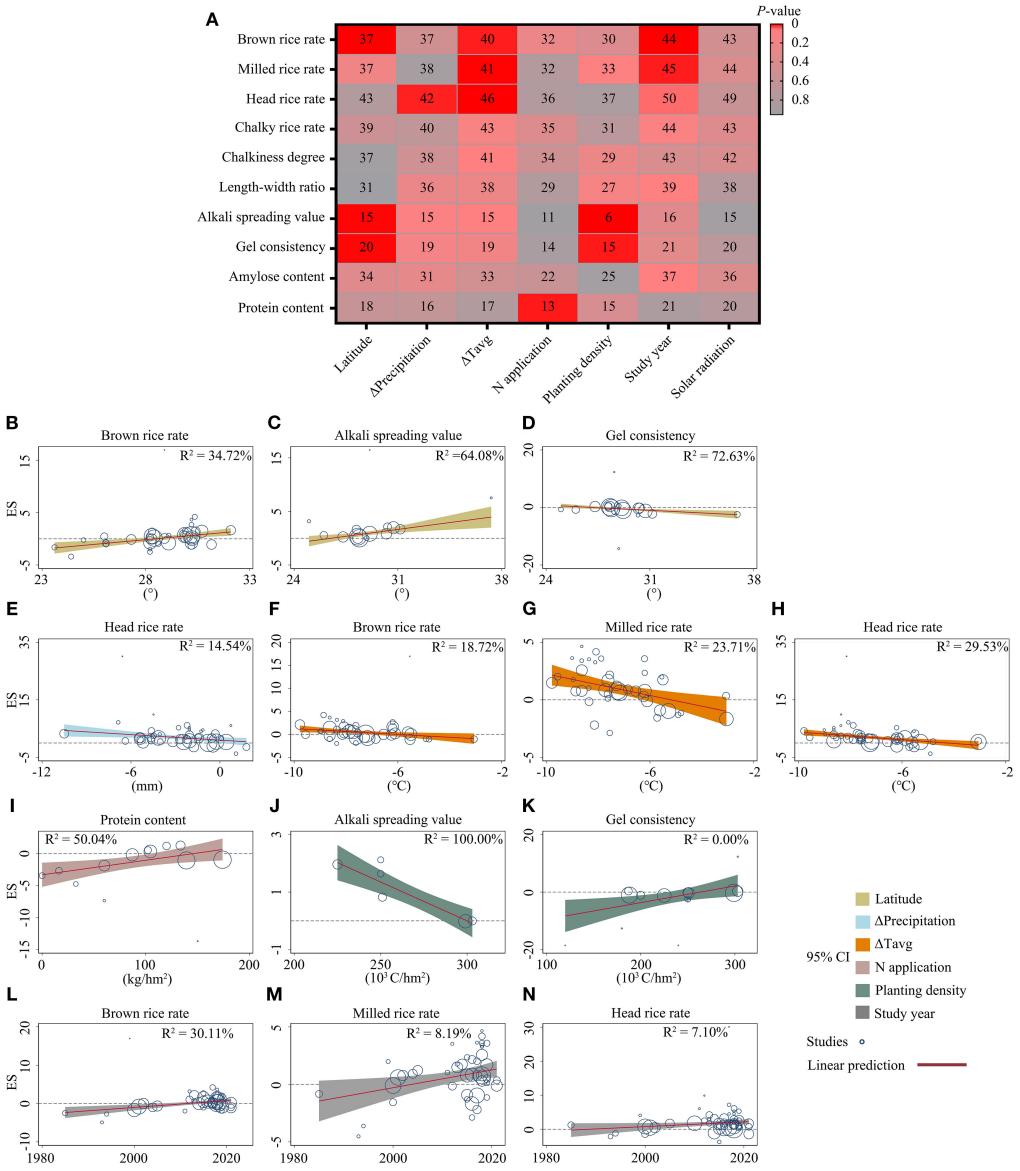

FIGURE 4
Regression analysis of continuous factors. **(A)** Heatmaps of correlations between grain quality traits and continuous factors (latitude, the difference of "average precipitation per day" compared RC and MC (Δprecipitation), the difference of "average temperature per day" compared RC and MC (ΔTavg), application of nitrogen (N) fertilizer, planting density, study year, and solar radiation). Red color indicates *P*-values. Numbers in boxes represent the number of research cases included in the analysis. **(B–N)** Bubble plots showing predicted trends of continuous factors on grain quality traits. Bubble sizes reflect sample sizes in individual studies. R^2 values for meta-regression analysis are shown in Supplementary Table 3.

The observed increase in HRR is consistent with the decline in chalkiness, as chalky kernels are more susceptible to breakage during milling (Siebenmorgen et al., 2013). Chalkiness is a complex trait attributed to both genetic and environmental factors, particularly high temperature (Nevame et al., 2018). Ratooning clearly decreased the chalky rice rate, supported by studies in Iran and China. Interestingly, research from the Sichuan Basin reported minimal changes in CD, potentially attributable to localized climate conditions, cultivar selection, or management practices.

Based on the viscosity of 4.4% milled-rice paste, rice can be divided into three categories: soft (>60 mm), adhesive (40–60 mm), and hard (<40 mm) (Zhang et al., 2020). A significant decrease was found in GC, which was negatively correlated with increasing latitude and positively correlated with planting density. This aligns with Kuang et al. (2021), who observed a 15% reduction in GC for ratoon rice at higher latitudes (Xinyang, 32.1°N) compared with lower-latitude sites (Changsha, 28.2°N; Zhaoqing, 23.0°N).

ASV is generally considered to represent the gelatinization temperature, which is negatively correlated with the cooking temperature of rice (Graham, 2002). In contrast to the negative impact on GC, ASV increased in the ratoon season, consistent with previous studies showing that ASV is negatively related to GC in a recombinant inbred line population derived from a *japonica*/*indica* cross (Wang et al., 2007; Lu et al., 2022).

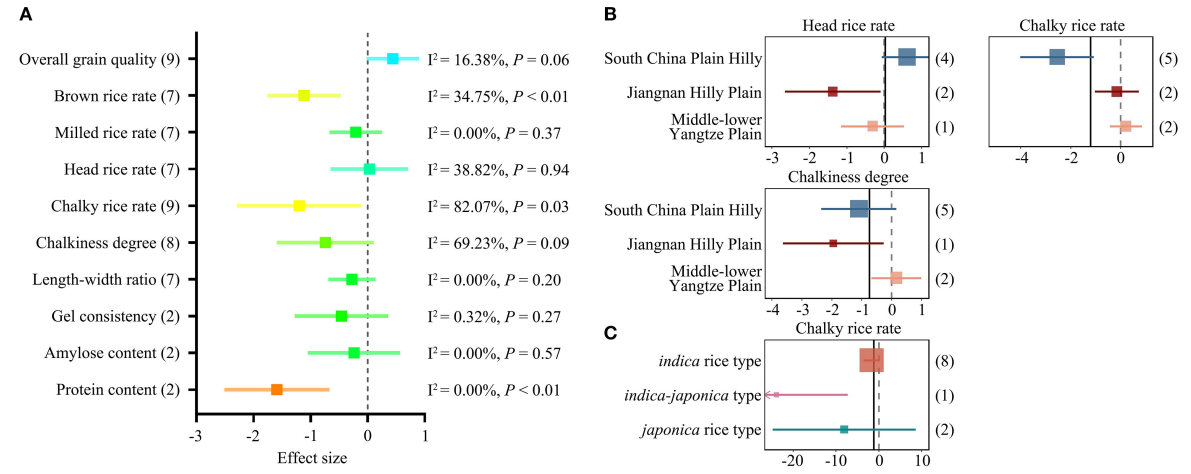

FIGURE 5
Mean ES for the grain quality compared RC and LC. **(A)** ES distribution is plotted as SMD (Cohen's d) comparing RC to LC. Bracketed numbers represent the number of accepted study cases. Heterogeneity value (I^2) and the *P* value are presented on the right. **(B)** Subgroup analysis of planting regions for grain quality traits comparing RC to LC. **(C)** Subgroup analysis of rice cultivar varieties for CRR comparing RC to LC. The vertical black line in **(B, C)** indicates the pooled ES of all categorical factors. Bars around the means denote 95% CIs. For Q statistic tests, see Supplementary Table 2.

In rice, AC is positively associated with hardness and negatively correlated with viscosity and water absorption High temperatures during grain filling substantially reduce AC by disrupting enzymatic processes required for consistent amylose synthesis (Yamakawa et al., 2007; Zhou et al., 2024). Thus, relatively lower temperatures during the grain-filling period may contribute to the increase in AC in the ratoon season. Furthermore, stubble height modulates these effects: lower stubble height prolongs the growth and grain-filling periods, potentially lowering grain-filling temperatures and thereby increasing AC in RC.

Mechanism underlying the regulation of ratooning on grain quality

Grain-filling temperatures critically modulate ratoon rice quality. The comparatively lower cumulative temperatures in RC versus MC likely drive observed grain quality variations. This thermal hypothesis is partially supported by our RC–LC comparison, where RC–MC quality patterns were absent (Figure 5), though the limited geographical scope and study numbers preclude definitive conclusions. Our findings align with recent multi-latitude analyses and likely reflect, at least in part, temperature effects on ratoon systems. For instance, in a recombinant inbred population of *indica–japonica* crosses grown across four regions, cooked rice hardness and stickiness increased with decreasing latitude, while springiness showed the opposite trend (Xu et al., 2019). Kuang et al. (2021) reported that differences in crystal structure and starch thermal properties between RC and MC were closely related to temperature during ripening. High temperature during kernel development can cause spikelet infertility, increase chalkiness, and decrease AC (Peng et al., 2004; Kadam et al., 2014), while lower temperature extends the grain-filling period, resulting in better milling and appearance parameters (Funaba et al., 2006). Recent molecular-level research reported that high temperature enhanced the expression and activity of α-amylase, leading to pitted and uneven starch granule surfaces (Liu et al., 2011).

Significant variation in grain quality traits exists among cultivars grown under identical conditions (Kang et al., 2006; Cameron et al., 2008). Generally, *japonica* varieties are considered to have better ratooning ability than *indica* varieties (Krishanamurthy, 1989). Hybrid varieties show enhanced ratooning ability and higher post-MC harvest dry weight relative to inbred varieties (Chen et al., 2018). Nevertheless, the roles of genetic factors and varietal differences in regulating post-ratooning grain quality remain poorly characterized.

Optimal agronomic practices are crucial to ensuring the productivity and quality of the ratoon rice system, including fertilizer application, planting density, and stubble height. N application at the grain-filling stage of MC was reported to have the most significant effects on tiller sprouting, growth, and yield of ratoon crops (Wang et al., 2021; Yang et al., 2021). However, elevated N fertilization increases endosperm PC, potentially improving grain hardness and milling resistance at the expense of eating and cooking quality (Leesawatwong et al., 2005; Gu et al., 2015; Zhou et al., 2018). Higher planting density enhances interception of photosynthetically active radiation and dry matter accumulation, thereby promoting tiller production, survival, and effective panicle formation (Bozorgi et al., 2011; Zheng et al., 2021). This practice also shows a strong positive correlation with GC but a negative correlation with ASV. Lowering MC stubble height increases ratoon yield by prolonging growth duration, reducing panicle number per unit area, and increasing spikelets per panicle, total spikelets, and leaf area index (Harrell et al., 2009; Yang et al., 2022), which subsequently affects milling parameters and AC.

Heterogeneity and limitation of our data

While rice ratooning studies have predominantly focused on grain yield, management practices, and varietal breeding, relatively few investigations have addressed grain quality. Quality assessment revealed high methodological standards across the literature, with most studies achieving high-quality scores and demonstrating minimal risk of bias. These findings substantiate the robustness of our analytical conclusions. However, the geographical distribution of research is uneven, with most studies located in Asia. In addition, substantial heterogeneity emerged in our meta-analysis. Rice quality represents a composite trait influenced by both genetic and environmental factors. This multifaceted nature inherently causes grain quality parameters to vary considerably across studies. In West Sumatra, Indonesia, a high-yield perennial rice cropping method called SALIBU involves three cropping cycles, but no grain quality data have been reported (Paiman et al., 2022). Using overwintering (OW) cultivated rice, Liang et al. (2021) reported that four grain quality traits (CRR, ASV, GC, and AC) showed relatively small but significant differences, except for CRR. However, the authors did not trace all cropping seasons, recording only four: RC of 2016, MC of both 2017 and 2018, and RC in 2019. The effects of multiple-harvest rice systems on grain quality require further study.

Conclusion

Our meta-analysis provides important insights into the benefits of ratooning on grain quality. Compared with MC, RC improved milling properties and appearance traits and altered cooking and sensory quality in a region-dependent manner. This study elucidates the interactive effects of thermal and light factors and agronomic practices on ratoon rice quality.

Future efforts should prioritize synergistic optimization of Genetics × Environment × Management to achieve premium grain quality. Our findings provide novel insights for optimizing ratoon rice production across diverse regions, including the development of region-specific agronomic protocols (e.g., dynamic adjustment of stubble height and planting density) and the screening and breeding of ratoon rice varieties with superior grain quality.

Data availability statement

The original contributions presented in the study are included in the article/Supplementary Material. Further inquiries can be directed to the corresponding authors.

Author contributions

WW: Conceptualization, Funding acquisition, Investigation, Project administration, Supervision, Writing – review & editing. XY: Conceptualization, Data curation, Formal analysis, Investigation, Supervision, Writing – original draft, Writing – review & editing. ZR: Data curation, Formal analysis, Investigation, Methodology, Software, Writing – original draft. KC: Data curation, Investigation, Writing – review & editing. SG: Data curation, Investigation, Writing – review & editing. YCW: Data curation, Investigation, Writing – review & editing. QC: Data curation, Investigation, Writing – review & editing. L-AY: Data curation, Investigation, Writing – review & editing. MB: Data curation, Investigation, Writing – review & editing. AY: Data curation, Investigation, Writing – review & editing. JC: Data curation, Investigation, Writing – review & editing. KB-U: Data curation, Investigation, Writing – review & editing. KS: Data curation, Investigation, Writing – review & editing. YFW: Data curation, Investigation, Writing – review & editing. WL: Conceptualization, Formal analysis, Funding acquisition, Supervision, Validation, Writing – review & editing.

Funding

The author(s) declare financial support was received for the research and/or publication of this article. This work was supported by grants from the Nature Science Foundation of Fujian Province (2023J01460) and the program of First-class Ecology Disciplines Construction of FAFU to WW, and the National Key Research and Development Project (2016YFD0300508) to WL.

Acknowledgments

We thank Dr. Zhenhua Liu (Shanghai Jiao Tong University) for critical reading of the manuscript. The datasets of global surface solar radiation (1985-2018) are provided by National Tibetan Plateau Data Center (http://data.tpdc.ac.cn). The data set of global surface solar radiation (2019-2021) is provided by Geographic remote sensing ecological network platform (www.gisrs.cn).

Conflict of interest

The authors declare that the research was conducted in the absence of any commercial or financial relationships that could be construed as a potential conflict of interest.

Generative AI statement

The author(s) declare that no Generative AI was used in the creation of this manuscript.

Any alternative text (alt text) provided alongside figures in this article has been generated by Frontiers with the support of artificial intelligence and reasonable efforts have been made to ensure accuracy, including review by the authors wherever possible. If you identify any issues, please contact us.

Publisher's note

All claims expressed in this article are solely those of the authors and do not necessarily represent those of their affiliated organizations, or those of the publisher, the editors and the reviewers. Any product that may be evaluated in this article, or claim that may be made by its manufacturer, is not guaranteed or endorsed by the publisher.

Supplementary material

The Supplementary Material for this article can be found online at: https://www.frontiersin.org/articles/10.3389/fpls.2025.1604686/full#supplementary-material

SUPPLEMENTARY FIGURE 1
PRISMA diagram for the studies selected and included in the meta-analysis.

SUPPLEMENTARY FIGURE 2
The risk of bias assessment in the literature. **(A)** A schematic representation of the risk of bias assessment in the literature. Risk of bias was assessed as "+" for low risk, "?" for unclear risk, and "−" for high risk. **(B)** The proportion of three kinds of risk of bias assessments in all the literature.

SUPPLEMENTARY FIGURE 3
Studies quality assessment. The numbers 1–21 on the left side of the bubble chart represent the 21 questions belonging to the "Quality checklist question." The histogram shows the score data with two Y-axes. The main Y-axis (left) shows the cumulative scores of all studies in the "Quality checklist question," and the right Y-axis shows the quality scores of all studies [C(Satisfied)/(C (Satisfied) + C(Dissatisfied)) (count)].

SUPPLEMENTARY FIGURE 4
Funnel plots of publication bias. All the tests with publication bias ($P < 0.05$) were indicated in red. Black dots represent individual studies, and the gray funnel area represents 95% CIs.

References

Alizadeh, M. R., and Habibi, F. (2016). A comparative study on the quality of the main and ratoon rice crops. *J. Food Qual.* 39, 669–674. doi: 10.1111/jfq.12250

Borenstein, M., Hedges, L. V., Higgins, J. P., and Rothstein, H. R. (2010). A basic introduction to fixed-effect and random-effects models for meta-analysis. *Res. synthesis Methods* 1, 97–111. doi: 10.1002/jrsm.12

Bozorgi, H. R., Faraji, A., Danesh, R. K., Keshavarz, A., Azarpour, E., and Tarighi, F. (2011). Effect of plant density on yield and yield components of rice. *World Appl. Sci. J.* 12, 2053–2057.

Cai, H., Tabien, R. E., Xu, D., Harper, C. L., Samford, J., Yang, Y., et al. (2019). Grain quality and yield of rice in the main and ratoon harvests in the. *J. Agric. Sci* 11. doi: 10.5539/jas.v11n15p1

Calendacion, A. N., Garrity, D. P., and Ingram, K. T. (1992). Lock lodging: A new technology for ratoon rice cropping. *Philipp J. Crop Sci.* 17, 1–10.

Cameron, D. K., Wang, Y.-J., and Moldenhauer, K. A. K. (2008). Comparison of physical and chemical properties of medium-grain rice cultivars grown in California and Arkansas. *J. Food Sci* 73, C72–C78. doi: 10.1111/j.1750-3841.2007.00631.x

Cameron, A. C., and Windmeijer, F. A. (1997). An R-squared measure of goodness of fit for some common nonlinear regression models. *J. econometrics* 77, 329–342. doi: 10.1016/S0304-4076(96)01818-0

Chaimani, A., Mavridis, D., and Salanti, G. (2014). A hands-on practical tutorial on performing meta-analysis with Stata. *R. Coll. Psychiatrists.* 17, 111–116. doi: 10.1136/eb-2014-101967

Chen, Q., He, A., Wang, W., Peng, S., Huang, J., Cui, K., et al. (2018). Comparisons of regeneration rate and yields performance between inbred and hybrid rice cultivars in a direct seeding rice-ratoon rice system in central China. *Field Crops Res.* 223, 164–170. doi: 10.1016/j.fcr.2018.04.010

Chen, Z., Li, P., Xiao, J., Jiang, Y., Cai, M., Wang, J., et al. (2021). Dry cultivation with ratoon system impacts rice quality using rice flour physicochemical traits,fatty and amino acids contents. *Food Res. Int.* 150, 110764. doi: 10.1016/j.foodres.2021.110764

Custodio, M. C., Cuevas, R. P., Ynion, J., Laborte, A. G., Velasco, M. L., and Demont, M. (2019). Rice quality: How is it defined by consumers, industry, food scientists, and geneticists? *Trends Food Sci Technol.* 92, 122–137. doi: 10.1016/j.tifs.2019.07.039

Deng, F., Yang, F., Li, Q., Zeng, Y., Li, B., Zhong, X., et al. (2021). Differences in starch structural and physicochemical properties and texture characteristics of cooked rice between the main crop and ratoon rice. *Food Hydrocolloids* 116, 106643. doi: 10.1016/j.foodhyd.2021.106643

Egger, M., Smith, G. D., Schneider, M., and Minder, C. (1997). Bias in meta-analysis detected by a simple, graphical test. *BMJ* 315, 629–634. doi: 10.1136/bmj.315.7109.629

Fitzgerald, M. A., Mccouch, S. R., and Hall, R. D. (2009). Not just a grain of rice: the quest for quality. *Trends Plant Sci* 14, 133–139. doi: 10.1016/j.tplants.2008.12.004

Funaba, M., Ishibashi, Y., Molla, A. H., Iwanami, K., and Iwaya-Inoue, M. (2006). Influence of low/high temperature on water status in developing and maturing rice grains. *Plant production Sci* 9, 347–354. doi: 10.1626/pps.9.347

Graham, R. (2002). A proposal for IRRI to establish a grain quality and nutrition research center. *IRRI Discussion Papers* 44, 1–24.

Gu, J., Chen, J., Chen, L., Wang, Z., Zhang, H., and Yang, J. (2015). Grain quality changes and responses to nitrogen fertilizer of japonica rice cultivars released in the Yangtze River Basin from the 1950s to 2000s. *Crop J.* 3, 285–297. doi: 10.1016/j.cj.2015.03.007

Guo, W. (1993). Brief discussion on the historical development of ratooning rice in China. *Agric. History China* 12, 1–6.

Gurevitch, J., Koricheva, J., Nakagawa, S., and Stewart, G. (2018). Meta-analysis and the science of research synthesis. *Nature* 555, 175–182. doi: 10.1038/nature25753

Harrell, D. L., Bond, J. A., and Blanche, S. (2009). Evaluation of main-crop stubble height on ratoon rice growth and development. *Field Crops Res.* 114, 396–403. doi: 10.1016/j.fcr.2009.09.011

Hedges, L. V., and Olkin, I. (1985). Statistical methods for meta-analysis. *New Dir. Program Eval.* 1984, 25–42.

Higgins, J. P. T., Altman, D. G., and Jac, S. (2017). "Chapter 8: Assessingrisk of bias in included studies," in *Cochrane Handbook for Systematic Reviews of Interventions version 5.2.0*Ed. C. M. S Cochrane. (The Atrium, Southern Gate, Chichester, England: John Wiley & Sons Ltd).

Higgins, J. P., Thompson, S. G., Deeks, J. J., and Altman, D. G. (2003). Measuring inconsistency in meta-analyses. *BMJ* 327, 557–560. doi: 10.1136/bmj.327.7414.557

Huang, J., Pan, Y., Chen, H., Zhang, Z., Fang, C., Shao, C., et al. (2020). Physiochemical mechanisms involved in the improvement of grain-filling, rice quality mediated by related enzyme activities in the ratoon cultivation system. *Field Crops Res.* 258, 107962. doi: 10.1016/j.fcr.2020.107962

IRRI (1988). *Rice ratooning* (Los BanOs, Philippines: Los BanOs, Philippines).

Jones, D. B. (1993). Rice ratoon response to main crop harvest cutting height. *Agron. J.* 85, 1139–1142. doi: 10.2134/agronj1993.00021962008500060008x

Kadam, N. N., Xiao, G., Melgar, R. J., Bahuguna, R. N., Quinones, C., Tamilselvan, A., et al. (2014). Agronomic and physiological responses to high temperature, drought, and elevated CO2 interactions in cereals. *Adv. Agron.* 127, 111–156. doi: 10.1016/B978-0-12-800131-8.00003-0

Kang, H.-J., Hwang, I.-K., Kim, K.-S., and Choi, H.-C. (2006). Comparison of the physicochemical properties and ultrastructure of *japonica* and *indica* rice grains. *J. Agric. Food Chem.* 54, 4833–4838. doi: 10.1021/jf060221+

Koricheva, J., Gurevitch, J., and Mengersen, K. (2013). *Handbook of meta-analysis in ecology and evolution* (Princeton, New Jersey, USA: Princeton University Press).

Krishanamurthy, K. (1989). "Rice ratooning as an alternative to double cropping in tropical Asia," in *Rice Ratooning, Bangalore* (IRRI, India).

Kuang, N., Zheng, H., Tang, Q., Chen, Y., Wang, X., and Luo, Y. (2021). Amylose content, morphology, crystal structure, and thermal properties of starch grains in main and ratoon rice crops. *Phyton-International J. Exp. Bot.* 90, 1119–1130. doi: 10.32604/phyton.2021.014637

Lachenbruch, P. A. (1989). Statistical power analysis for the behavioral sciences. *J. Am. Stat. Assoc.* 84, 1096–1097. doi: 10.2307/2290095

Leesawatwong, M., Jamjod, S., Kuo, J., Bell, B., and Rerkasem, B. (2005). Nitrogen fertilizer increases seed protein and milling quality of rice. *Cereal Chem.* 82, 588–593. doi: 10.1094/CC-82-0588

Liang, Y., Nan, W., Qin, X., and Zhang, H. (2021). Field performance on grain yield and quality and genetic diversity of overwintering cultivated rice (*Oryza sativa* L.) in southwest China. *Sci. Rep.* 11, 1846. doi: 10.1038/s41598-021-81291-8

Liberati, A., Altman, D. G., Tetzlaff, J., Mulrow, C., Gøtzsche, P. C., Ioannidis, J. P., et al. (2009). The PRISMA statement for reporting systematic reviews and meta-analyses of studies that evaluate health care interventions: explanation and elaboration. *J. Clin. Epidemiol.* 62, e1–e34. doi: 10.1016/j.jclinepi.2009.06.006

Lin, W., Chen, H., Zhang, Z., Xu, Q., Tu, N., Fang, C., et al. (2015). Research and prospect on physio-ecological properties of ratoon rice yield formation and its key cultivation technology. *Zhongguo Shengtai Nongye Xuebao/Chinese* 23, 392–401. doi: 10.13930/j.cnki.cjea.150246

Lin, F., Rensing, C., Pang, Z., Zou, J., Lin, S., Letuma, P., et al. (2022). Metabolomic analysis reveals differential metabolites and pathways involved in grain chalkiness improvement under rice ratooning. *Field Crops Res.* 283, 108521. doi: 10.1016/j.fcr.2022.108521

Liu, G., Deng, H., Chen, L., Xiao, Y., and Tang, W. (2002). Comparison of grain quality between main and ratooning crops of middle-season rice. *Hybrid Rice* 17, 45–47. doi: 10.3969/j.issn.1005-3956.2002.01.023

Liu, P., Guo, W., Jiang, Z., Pu, H., Feng, C., Zhu, X., et al. (2011). Effects of high temperature after anthesis on starch granules in grains of wheat (*Triticum aestivum* L.). *J. Agric. Sci* 149, 159–169. doi: 10.1017/S0021859610001024

Lu, X., Wang, L., Yunhuaxiao,, Wang, F., Guilianzhang,, Wenbangtang,, et al. (2022). Grain quality characterization of hybrid rice restorer lines with resilience to suboptimal temperatures during filling stage. *Foods* 11. doi: 10.3390/foods11213513

Moher, D., Liberati, A., Tetzlaff, J., Altman, D. G., and Prisma-Group (2009). Preferred reporting items for systematic reviews and meta-analyses: the PRISMA statement. *Ann. Internal Med.* 151, 264–269. doi: 10.7326/0003-4819-151-4-200908180-00135

Munda, G. C., Das, A., and Patel, D. P. (2009). Evaluation of transplanted and ratoon crop for double cropping of rice (*Oryza sativa* L.) under organic input management in mid altitude sub-tropical Meghalaya. *Curr. Sci* 96, 1620–1627.

Nakagawa, S., and Cuthill, I. C. (2007). Effect size, confidence interval and statistical significance: a practical guide for biologists. *Biol. Rev.* 82, 591–605. doi: 10.1111/j.1469-185X.2007.00027.x

Nakagawa, S., Noble, D. W., Senior, A. M., and Lagisz, M. (2017). Meta-evaluation of meta-analysis: ten appraisal questions for biologists. *BMC Biol.* 15, 1–14. doi: 10.1186/s12915-017-0357-7

Negalur, R. B., Yadahalli, G. S., Chittapur, B. M., Guruprasad, G. S., and Narappa, G. (2017). Ratoon rice: a climate and resource smart technology. *Int. J. Curr. Microbiol. Appl. Sci.* 6, 1638–1653. doi: 10.20546/ijcmas.2017.605.179

Nevame, A. Y. M., Emon, R. M., Malek, M. A., Hasan, M. M., Alam, M. A., Muharam, F. M., et al. (2018). Relationship between high temperature and formation of chalkiness and their effects on quality of rice. *BioMed. Res. Int.* 2018, 1–18. doi: 10.1155/2018/1653721

Paiman,, Isnawan, B. H., Aziez, A. F., Subeni,, and Salisu, M. A. (2022). The role of agronomic factors in Salibu rice cultivation. *Open Agric. J.* 16, e187433152112170. doi: 10.2174/18743315-v16-e2112170

Peng, S., Huang, J., Sheehy, J. E., Laza, R. C., Visperas, R. M., Zhong, X., et al. (2004). Rice yields decline with higher night temperature from global warming. *Proc. Natl. Acad. Sci.* 101, 9971–9975. doi: 10.1073/pnas.0403720101

Sanni, K., Ojo, D., Adebisi, M., Sanni, K. A., Ojo, D. K., Adebisi, M. A., et al. (2009). Ratooning potential of interspecific NERICA rice varieties (*Oryza glaberrima× Oryza sativa*). *Int. J. Bot.* 112, 115. doi: 10.3923/ijb.2009.112.115

Saric, F., Barcot, O., and Puljak, L. (2019). Risk of bias assessments for selective reporting were inadequate in the majority of Cochrane reviews. *J. Clin. Epidemiol.* 112, 53–58. doi: 10.1016/j.jclinepi.2019.04.007

Shin, J.-H., Kim, S.-K., and Park, S.-G. (2015). The ratooning potential of several early-ripening rice cultivar in Korea. *Korean J. Crop Sci* 60, 139–145. doi: 10.7740/kjcs.2015.60.2.139

Siebenmorgen, T. J., Grigg, B. C., and Lanning, S. B. (2013). Impacts of preharvest factors during kernel development on rice quality and functionality. *Annu. Rev. Food Sci Technol.* 4, 101–115. doi: 10.1146/annurev-food-030212-182644

Su, J., Friess, D. A., and Gasparatos, A. (2021). A meta-analysis of the ecological and economic outcomes of mangrove restoration. *Nat. Commun.* 12, 5050.

Thompson, S. G., and Higgins, J. P. (2002). How should meta-regression analyses be undertaken and interpreted? *Stat Med.* 21, 1559–1573. doi: 10.1002/sim.1187

Wang, W., He, A., Jiang, G., Sun, H., Jiang, M., Man, J., et al. (2020b). Ratoon rice technology: A green and resource-efficient way for rice production. *Adv. Agron.* 159, 135–167. doi: 10.1016/bs.agron.2019.07.006

Wang, Y., Li, X., Lee, T., Peng, S., and Dou, F. (2021). Effects of nitrogen management on the ratoon crop yield and head rice yield in South USA. *J. Integr. Agric.* 20, 1457–1464. doi: 10.1016/S2095-3119(20)63452-9

Wang, L. Q., Liu, W. J., Xu, Y., He, Y. Q., Luo, L. J., Xing, Y. Z., et al. (2007). Genetic basis of 17 traits and viscosity parameters characterizing the eating and cooking quality of rice grain. *Theor. Appl. Genet.* 115, 463–476. doi: 10.1007/s00122-007-0580-7

Wang, H., Zhang, Q., Zhang, W., Li, S., Huang, J., Zhu, A., et al. (2020a). Advances in the effects of the ability of axillary bud germination on grain yield in ratoon rice. *Chin. J. OF Rice Sci* 34, 205. doi: 10.16819/j.1001-7216.2020.9097

Xu, X., Xu, Z., Matsue, Y., and Xu, Q. (2019). Effects of genetic background and environmental conditions on texture properties in a recombinant inbred population of an inter-subspecies cross. *Rice* 12, 1–11. doi: 10.1186/s12284-019-0286-x

Yamakawa, H., Hirose, T., Kuroda, M., and Yamaguchi, T. (2007). Comprehensive expression profiling of rice grain filling-related genes under high temperature using DNA microarray. *Plant Physiol.* 144, 258–277. doi: 10.1104/pp.107.098665

Yang, D., Peng, S., Zheng, C., Xiang, H., Huang, J., Cui, K., et al. (2021). Effects of nitrogen fertilization for bud initiation and tiller growth on yield and quality of rice ratoon crop in central China. *Field Crops Res.* 272, 108286. doi: 10.1016/j.fcr.2021.108286

Yang, D., Peng, S., Zheng, C., Xiong, Z., Yang, G., Deng, S., et al. (2022). Stubble height affects the grain yield of ratoon rice under rainfed conditions. *Agric. Water Manage.* 272, 107815. doi: 10.1016/j.agwat.2022.107815

Zhang, A., Gao, Y., Li, Y., Ruan, B., Yang, S., Liu, C., et al. (2020). Genetic analysis for cooking and eating quality of super rice and fine mapping of a novel locus qGC10 for gel consistency. *Front. Plant Sci* 11, 342. doi: 10.3389/fpls.2020.00342

Zheng, B., Zhang, X., Wang, Q., Li, W., Huang, M., Zhou, Q., et al. (2021). Increasing plant density improves grain yield, protein quality and nitrogen agronomic efficiency of soft wheat cultivars with reduced nitrogen rate. *Field Crops Res.* 267, 108145. doi: 10.1016/j.fcr.2021.108145

Zhou, R., Hu, Q., Meng, X., Zhang, Y., Shuai, X., Gu, Y., et al. (2024). Effects of high temperature on grain quality and enzyme activity in heat-sensitive versus heat-tolerant rice cultivars. *J. Sci Food ang Agric.* 104, 9729–9741. doi: 10.1002/jsfa.13797

Zhou, C., Huang, Y., Jia, B., Wang, Y., Wang, Y., Xu, Q., et al. (2018). Effects of cultivar, nitrogen rate, and planting density on rice-grain quality. *Agronomy* 8, 246. doi: 10.3390/agronomy8110246

Frontiers in
Plant Science

Cultivates the science of plant biology and its applications

The most cited plant science journal, which advances our understanding of plant biology for sustainable food security, functional ecosystems and human health.

Discover the latest Research Topics

See more →

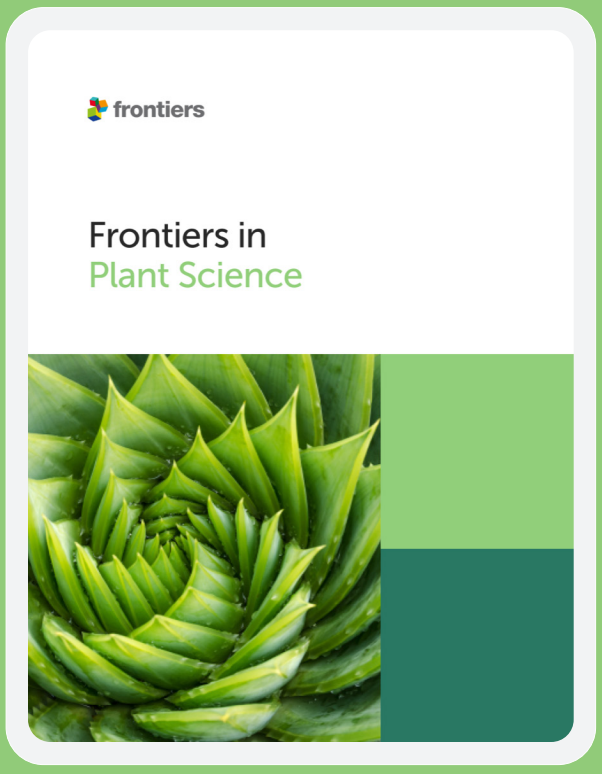

Frontiers

Avenue du Tribunal-Fédéral 34
1005 Lausanne, Switzerland
frontiersin.org

Contact us

+41 (0)21 510 17 00
frontiersin.org/about/contact